2019

STRUCTURAL STYLE AND STRATIGRAPHIC ARCHITECTURE OF THE NORTHEASTERN BROOKS RANGE, ALASKA

Benjamin G. Johnson
bgjohnson@mix.wvu.edu

STRUCTURAL STYLE AND STRATIGRAPHIC ARCHITECTURE OF THE NORTHEASTERN BROOKS RANGE, ALASKA

Benjamin G. Johnson

A dissertation submitted to the
Eberly College of Arts and Sciences at
West Virginia University

in partial fulfillment of requirements for the degree of

Doctor of Philosophy in
Geology

Jaime, Toro, Ph.D., Chair
Graham Andrews, Ph.D.
Kathleen Benison, Ph.D.
Amy Weislogel, Ph.D.
Jeffrey Benowitz, Ph. D.

Department of Geology and Geography

Morgantown, West Virginia
2019

Keywords: Brooks Range, Alaska, Plate tectonics, Structural geology, Sedimentology, Whale Mountain allochthon

ABSTRACT

STRUCTURAL STYLE AND STRATIGRAPHIC ARCHITECTURE OF THE NORTHEASTERN BROOKS RANGE, ALASKA

Benjamin G. Johnson

The Arctic Alaska–Chukotka microplate is a large Mesozoic–Cenozoic composite terrane that resides at the northern limit of the North American Cordillera. Although its Mesozoic origins are assuredly linked to the opening of the Amerasian Basin of the Arctic Ocean, its Paleozoic origins can be linked to at least three separate paleocontinents, including northern Laurentia, Baltica, and Siberia. Across the Arctic Alaska portion of the microplate, an internal, mid-Paleozoic suture zone presumably separates rocks of the North Slope subterrane (Laurentian affinity) from a collection of smaller subterranes in the southern Brooks Range and Seward Peninsula (Baltic affinity).

The mountains of the northeastern Brooks Range expose a thick assemblage of Neoproterozoic–Lower Cretaceous rocks that belong to the North Slope subterrane. New data from geological mapping, coupled with zircon U-Pb and muscovite $^{40}Ar/^{39}Ar$ radiometric ages, reveal that the Neoproterozoic–Ordovician rocks in the NE Brooks Range, assigned to the Firth River Group, Neruokpuk Formation, and the informal Leffingwell formation, record deep-water, slope- to basin-floor sedimentation along the ancient passive margin of northern Laurentia. Stata of the Ordovician–Lower Devonian(?) Clarence River Group (new name) disconformably overlie these passive margin units and record a major shift in the sedimentary source. Detrital zircon U-Pb ages from Clarence River Group strata closely resemble the deep-water, syn-orogenic strata exposed in the Franklinian Basin of northern Ellesmere Island, and are interpreted to reflect erosion and transport of sediment sourced from the Caledonian orogen.

A rootless thrust sheet places a Cambrian–Middle Ordovician structural complex of basalt, limestone and chert, herein named the Whale Mountain allochthon, above the upper strata of the Clarence River Group. Igneous geochemistry and trilobite paleontology suggest that the Whale Mountain allochthon formed as a series of remote volcanic islands or seamounts that established outboard the Laurentian margin. The emplacement of the allochthon occurred in concert with the locally-defined, Early–Middle Devonian Romanzof orogeny, and it may be linked to the closure of the Iapetus Ocean and the collision between Baltica and Laurentia in the Caledonian orogeny. This major collisional event is responsible for the assembly of the Arctic Alaska–Chukotka microplate, implicating the Whale Mountain allochthon as a potential relic to the suture zone that separates the North Slope subterrane from the rest of Arctic Alaska and Chukotka.

ACKNOWLEDGEMENTS

My time in the geology department a WVU is filled with many fond memories. Most notably, the relationship and mentorship I built with my advisor, Jaime Toro. He is a superb field geologist and outdoorsmen, but it is his sense of humor, his positive attitude, and his genuine curiosity that I admire most. At the end of our first field campaign together, after we had floated for 40 km down the Kongakut River in northern Alaska, I was utterly exhausted. While I was looking for an easy way to cross the river to reach our final take-out point, he told me to never take shortcuts and to embrace the hardships of life. We took the long way home, and this work is a testament to that.

Aside from the influence of Jaime, there are many other people at WVU that I am thankful to have known. My thesis committee members, Graham Andrews, Kathy Benison, and Amy Weislogel, provided a lot of helpful feedback to my research, and I enjoyed learning from them in the classroom. There are several other faculty members within the department that I need to acknowledge: Ryan Shackleton taught me more than I could ever know about structural geology; the late Helen Lang helped me distinguish between clinopyroxene and olivine in thin section; and Joe Donovan introduced me to the wonderful game of squash. I am also grateful to have been a member of a vibrant graduate student body, many of whom I spent countless Friday evenings with at the Brew Pub, resuscitating our soles with cold beer. My officemates, Patrick Frier, Greg Hammond, and Chantelle Parrish were my closest companions, serving as an initial sounding board to my early ideas.

There is an ever-growing list of coauthors, collaborators, and funding sources that I owe many thanks to. Sadly, I do not have the space to acknowledge them all here (see the acknowledgment sections at the end of Chapters 2, 3, and 4). There are a few, however, whose contributions are too great to go unmentioned. Jeff Benowitz, from the University of Alaska Fairbanks, served as an external member of my thesis committee. Not only did he let me borrow his truck in Fairbanks to help prepare for field work, but he provided radiometric ages in a timely fashion and helped me with their interpretation. John Taylor, from Indiana University of Pennsylvania, diligently identified and described all the trilobite specimens that field partners and I hauled from the mountains. His emails still make me smile. Tom Moore, from the

USGS in Menlo Park, California, is probably more critical of my research than anyone else I know. His insistent review of my first published manuscript, however, profoundly impacted my approach to science, and his >30 years of research serves as a foundation to my understanding of Brooks Range geology. And then there is my dear friend and closest collaborator Justin Strauss, who is now an assistant professor at Dartmouth College. Together, we waded through frigid rivers, climbed rugged mountains, and embraced the hardships of life in the Brooks Range, all in an effort to reconstruct our former world.

Above all others, I need to thank my wife, Patricia. She has been by my side since I started this journey. Through my greatest achievements and my biggest shortcomings, it was her adventurous spirit, her patience, and her unconditional support that kept me motivated to finish. Without her, none of this was possible.

.

TABLE OF CONTENTS

LIST OF FIGURES

CHAPTER 1

CHAPTER 2

CHAPTER 4

SUPPLEMENTAL MATERIAL

LIST OF TABLES

LIST OF PLATES

Chapter 1: Death of an ocean—birth of an orogen: An introduction to the tectonic history of the North Slope subterrane and its role in the assembly of the Arctic Alaska–Chukotka microplate

Closing an ocean basin requires subduction of dense oceanic lithosphere. The final phase of ocean closure often culminates in the collision between two continental blocks, or terranes, resulting in widespread deformation and metamorphism, uplift of an orogenic belt, and the deposition of a thick wedge of siliciclastic sediment. This is the process of accretionary tectonics. In most cases, the remnants of the subduction zone, and the intervening ocean basin that once separated the two blocks, are almost completely removed from the geological record. Nevertheless, these features are key to delineating accreted terrane boundaries and understanding the geodynamic and paleogeographic history of assembled orogens.

Preserved in the rock record of North America is a long-lived history of accretionary tectonics. The premier example is the North American Cordillera, a rugged chain of mountains that extend from southern Mexico to Arctic Alaska (Fig. 1.1). Recent tectonic reconstructions have proposed that several Cordilleran terranes have ties to the early Paleozoic Arctic realm, including the paleocontinents of northeastern (NE) Laurentia, northern Baltica, and/or Siberia. (e.g. Colpron and Nelson, 2011; Miller et al. 2011; Cocks and Torsvik, 2011; Metelkin et al., 2014; Strauss et al., 2017). Although no consensus among the models exists regarding the geodynamic pathways of individual terranes, or how these terranes were assembled into the Cordillera, most models call upon translation and/or deformation of terranes along the northern

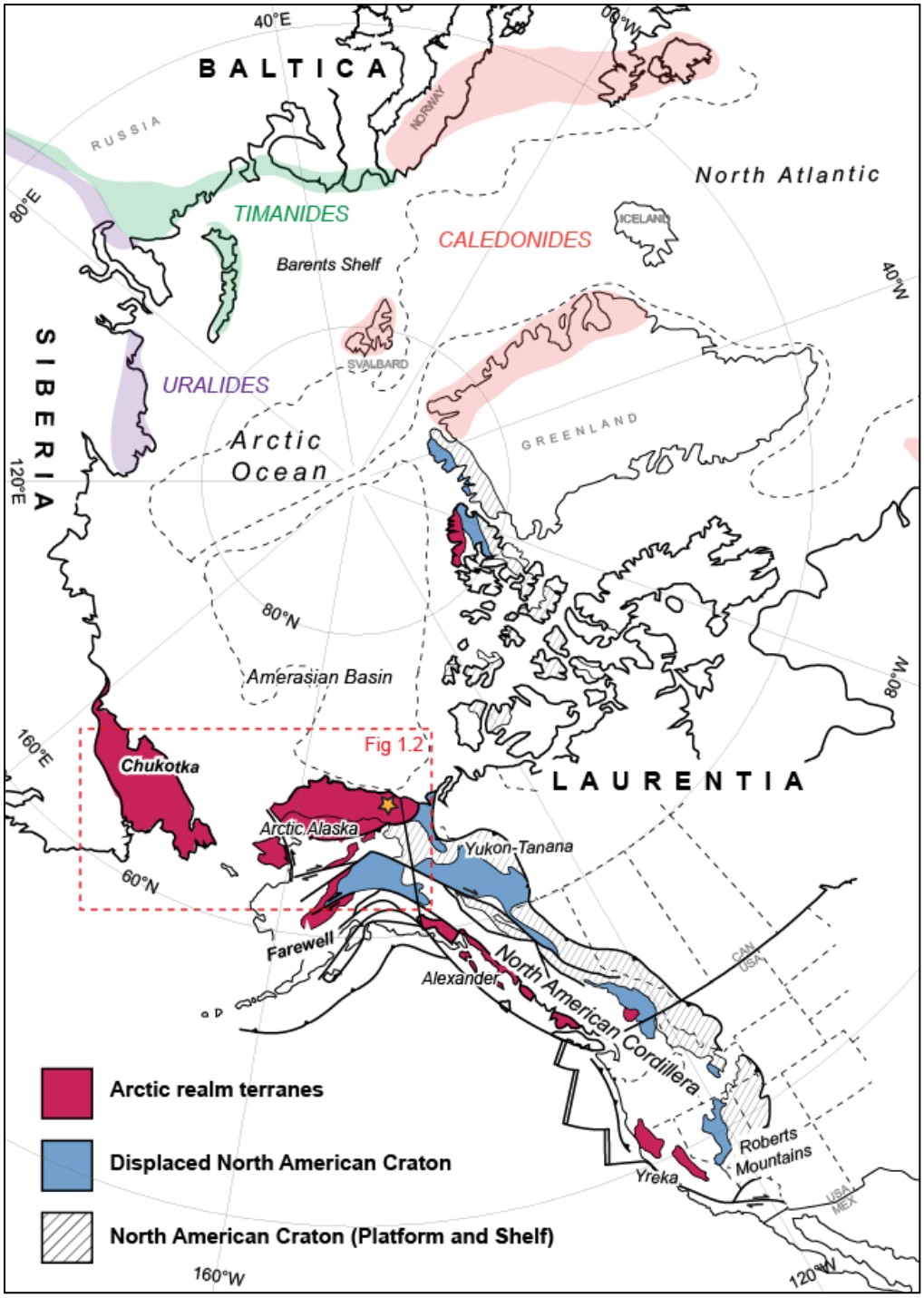

Figure 1.1: Simplified map of pertinent Proterozoic and Paleozoic orogenic belts, terranes, and cratons mapped onto the modern circum-Arctic continental margins and modified from Colpron and Nelson (2011) and Miller et al. (2011). Star indicates field area of this study.

(present coordinates) margin of Laurentia during the closure of the Iapetus Ocean and the onset of the Caledonian orogeny of East Greenland and Scandinavia (e.g. Colpron and Nelson, 2011).

Lower Paleozoic rocks from the composite Arctic Alaska–Chukotka microplate of northern Yukon, northern Alaska, and NE Russia (Fig. 1.2), preserve the most obvious link between the North American Cordillera and the Arctic realm. Its Mesozoic–Cenozoic configuration and geodynamic history is related to the southward (present coordinates) retreat of the paleo-Pacific margin and the opening of the Amerasian Basin of the Arctic Ocean (e.g., Moore et al., 1994; 2015 Miller et al., 2018), but the early Paleozoic origins of the Arctic Alaska–Chukotka microplate are less certain. A growing body of multidisciplinary evidence suggests that the Arctic Alaska–Chukotka microplate formed by suturing of previously independent terranes in a middle Paleozoic collisional event (e.g., Amato et al., 2009; Miller et al., 2011; 2006; Strauss et al., 2013; 2017). These independent terranes are recognized by their Neoproterozoic and lower Paleozoic affinities to different paleocontinents. Chukotka, the Seward Peninsula, and portions of the southern Brooks Range restore to the Barents Shelf (Fig. 1.1), where sedimentary and igneous rocks formed in response to the Neoproterozoic–Middle Cambrian Timanide orogeny, along the margins of Baltica or as peri-Siberian terranes (e.g. Patrick and McClelland 1995; Blodgett et al., 2002; Dumoulin et al., 2002, 2014; Miller et al., 2011, 2006; Amato et al., 2009, 2014; Till et al., 2014a, 2014b; Gottlieb et al., 2018; Hoiland et al., 2018). Conversely, rocks in the NE Brooks Range, Lisburne Peninsula, and North Slope subsurface (Colville Basin) are unequivocally linked to the northern margin of Laurentia (Dutro et al., 1972; Moore et al., 1994; MacDonald et al., 2009; Strauss et al. 2013; 2018a, 2018b; Cox et al., 2015; McClelland et al., 2015; Lane et al., 2016; Johnson et al., 2016, 2018; Colpron et al. 2018; Nelson et al., 2018). How and when these disparate terranes were assembled to form the

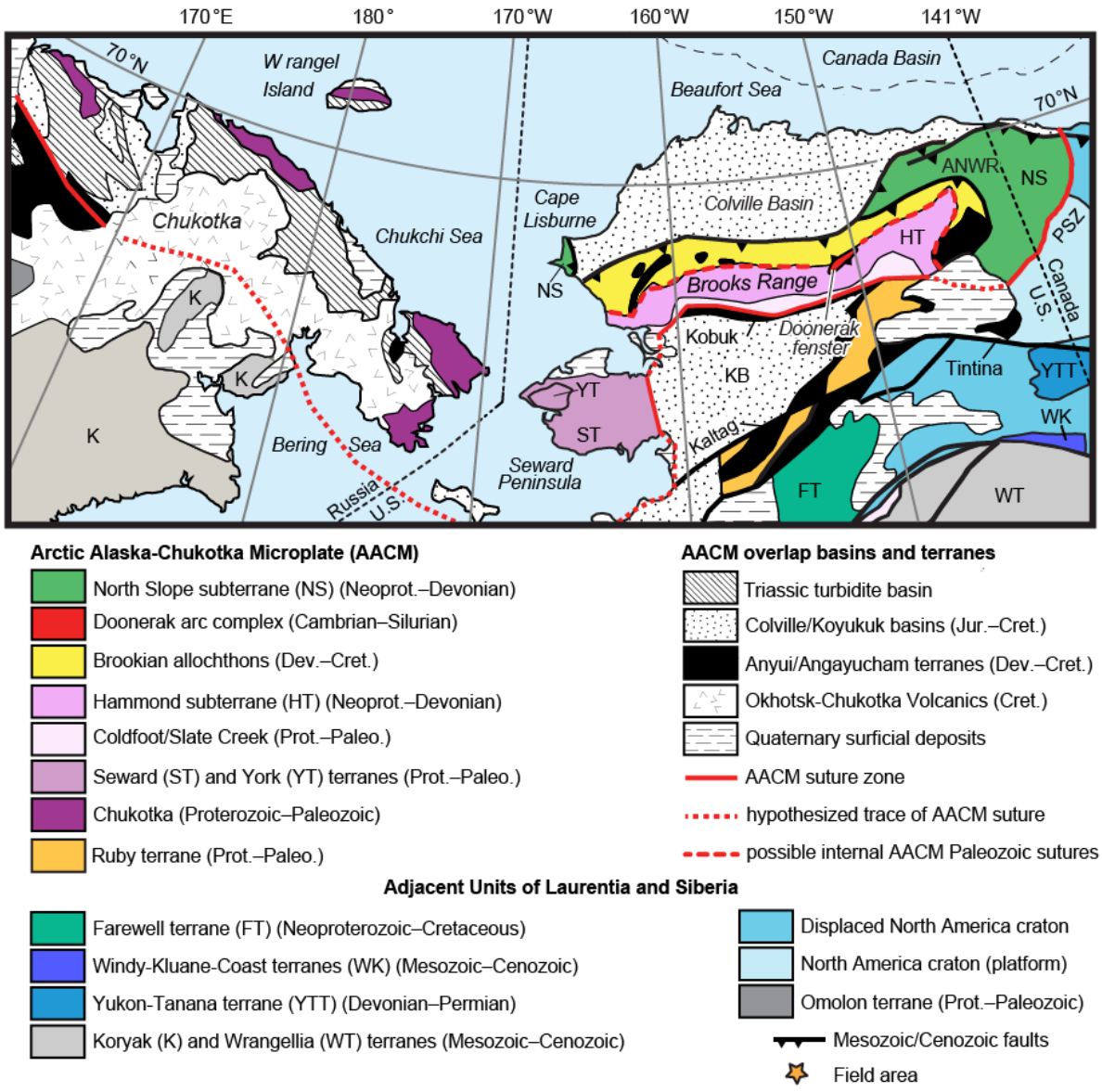

Figure 1.2: Simplified tectono-stratigraphic map of the composite Arctic Alaska–Chukotka microplate (AACM) after Mull (1982), Miller et al. (2006; 2011), Amato et al. (2009), Moore et al. (1994, 2015), and Strauss et al. (2017, 2018). Prot.—Proterozoic; PSZ—Porcupine Shear Zone; Paleo.— Paleozoic; ANWR—Arctic National Wildlife Refuge.

larger Arctic Alaska–Chukotka microplate remains uncertain because no definitive suture zones have been identified.

Strauss et al. (2013; 2017) and Hoiland et al. (2018) proposed that Neoproterozoic–lower Paleozoic rocks across Arctic Alaska are divided into two groups of crustal fragments, including (1) the North Slope subterrane and (2) the southwestern subterranes, and are separated by an east–west trending suture zone locally marked by the lower Paleozoic Doonerak arc complex in the central Brooks Range (Fig. 1.2). The continuation of this presumed suture zone, however, is unmapped, as it is either buried beneath Devonian–Cretaceous sedimentary rocks of the Brookian allochthons or it resides in the subsurface of the Colville Basin. The central argument of this study is that a relic of this suture zone, herein defined as the Whale Mountain allochthon, was thrusted onto the margin of the parautochthonous North Slope subterrane during the assembly of the Arctic Alaska–Chukotka microplate, perhaps in concert with the final closure of the Iapetus Ocean and the Caledonian orogeny.

What follows is a collection of field observations, radiometric ages, newly identified trilobite faunas, igneous geochemical data, and petrographical descriptions from rocks exposed in the Arctic National Wildlife Refuge of the NE Brooks Range. The data are presented in three standalone chapters, two of which have been published in peer-reviewed journals (Chapters 2 and 3), and the third (Chapter 4) will be submitted for future publication. All three chapters heavily rely on observations gathered over the course of four field campaigns in the NE Brooks Range, spanning from 2012 to 2015.

Chapter 2 (Johnson et al., 2016) presents detrital zircon U-Pb and muscovite 40Ar/39Ar radiometric ages from a Neoproterozoic–Upper Devonian(?), mixed carbonate and siliciclastic, basinal succession. The data support correlations to time-equivalent sedimentary units in the

Franklinian basin of Arctic Canada and record a pronounced provenance shift linked to the uplift and erosion of the Caledonian orogen of present-day Greenland. This chapter also introduces the Whale Mountain allochthon, a Cambrian–Middle Ordovician structural complex of igneous and marine sedimentary rocks that are in fault contact with the underlying Neoproterozoic–Upper Devonian(?) basinal succession.

Chapter 3 (Johnson et al., 2018) expands on the geological history of the Whale Mountain allochthon by coupling igneous petrology, U-Pb geochronology, and trilobite paleontology. It proposes that the allochthon formed as a series of volcanic islands that hosted unique, endemic trilobite faunas, which evolved in isolation, or with limited interchange with, the endemic faunas of the Laurentian platform. The proposed model aligns with the interpretations from Chapter 2, suggesting that the North Slope subterrane restores to the NE margin of Laurentia in the early Paleozoic and that the Whale Mountain allochthon represents an Arctic equivalent of the Iapetus suture observed in eastern North America and western Europe and Scandinavia.

The last chapter, Chapter 4 (unpublished), presents two 1:75,000 geological maps from the NE Brooks Range, which build on the findings from chapters 2 and 3 to elucidate the structural style and the stratigraphic architecture of the region. It also presents a collection of additional field observations and structural data not presented in the other chapters. The maps, cross sections, and structural data show that the Whale Mountain allochthon was emplaced in concert with the locally-defined Romanzof orogeny in the Early-Middle Devonian and was subsequently deformed by Cenozoic phases of the Brookian orogeny.

REFERENCES

Amato, J.M., Aleinikoff, J.N., Akinin, V.V., McClelland, W.C., and Toro, J., 2014, Age, chemistry, and correlations of Neoproterozoic –Devonian igneous rocks of the Arctic Alaska–Chukotka terrane: An overview with new U-Pb ages, *in* Dumoulin, J.A., and Till, A.B., eds., Reconstruction of a Late Proterozoic to Devonian Continental Margin Sequence, Northern Alaska: Its Paleogeographic Significance and Contained Base-Metal Sulfide Deposits: Geological Society of America Special Paper, v. 506, p. 29–57, doi: 10.1130/2014.2506(02).

Amato, J.M., Toro, J., Miller, E.L., Gehrels, G.E., Farmer, G.L., Gottlieb, E.S., and Till, A.B., 2009, Late Proterzoic-Paleozoic evolution of the Arctic Alaska-Chukotka terrane based on U-Pb igneous and detrital zircon ages: Implications for Neoproterozoic paleogeographic reconstructions: Bulletin of the Geological Society of America, v. 121, no. 9, p. 1219–1235, doi: 10.1130/B26510.1.

Blodgett, R.B., Rohr, D.M., and Boucot, A.J., 2002, Paleozoic links among some Alaskan accreted terranes and Siberia based on megafossils, in Miller, E.L., Grantz, A., and Klemperer, S.L. eds., Tectonic Evolution of the Bering Shelf–Chukchi Sea–Arctic Margin and Adjacent Landmasses, Geological Society of America Special Paper 360, p. 272–290.

Colpron, M., McClelland, W.C., and Strauss, J.V., 2018, Detrital zircon U-Pb geochronological and Hf isotopic constraints on the geological evolution of North Yukon, in Piepjohn, K., Strauss, J.V., Reinhardt, L., and McClelland, W.C., eds., Circum-Arctic Structural Events: Tectonic Evolution of the Arctic Margins and Trans-Arctic Links with Adjacent Orogens: Geological Society of America Special Paper 541, doi: 10.1130/2018.2541(19).

Colpron, M., and Nelson, J.L., 2011, A Palaeozoic NW Passage and the Timanian, Caledonian and Uralian connections of some exotic terranes in the North American Cordillera, *in* Spencer, A.M., Embry, A.F., Gautier, D.L., Stoupakova, A. V., and Sørensen, K. eds., Arctic Petroleum Geology, Geological Society of London Memoir 35, p. 463–484.

Cocks, L.R.M., and Torsvik, T.H., 2011, The Palaeozoic geography of Laurentia and western Laurussia: A stable craton with mobile margins: Earth-Science Reviews, v. 106, p. 1–51, doi: 10.1016/j.earscirev.2011.01.007.

Dumoulin, J. A, Harris, A.G., Gagiev, M., Bradley, D.C., Repetski, J.E., and Anonymous, 2002, Lithostratigraphic, conodont, and other faunal links between lower Paleozoic strata in northern and central Alaska and northeastern Russia; Tectonic evolution of the Bering Shelf-Chukchi Sea-Arctic margin and adjacent landmasses, *in* Miller, E.L., Grantz, A., and Klemperer, S.L. eds., Special Paper - Geological Society of America, Geological Society of America Special Paper 360, Boulder, Colorado, p. 291–312.

Dumoulin, J.A., Harris, A.G., and Repetski, J.E., 2014, Carbonate rocks of the Seward Peninsula, *in* Dumoulin, J.A., and Till, A.B., eds., Reconstruction of a Late Proterozoic to Devonian Continental Margin Sequence, Northern Alaska: Its Paleogeographic Significance and Contained Base-Metal Sulfide Deposits: Geological Society of America Special Paper 506, p. 59–110.

Cox, G.M., Strauss, J.V., Halverson, G.P., Schmitz, M.A., McClelland, W.C., Stevenson, R.S., and Macdonald, F.A., 2015, Kikiktat volcanics of Arctic Alaska–Melting of harzburgitic mantle associated with the Franklin large igneous province: Lithosphere, v. 7, no. 3, p. 275–295.

Dutro Jr., J.T., Brosgé, W.P., and Reiser, H.N., 1972, Significance of recently discovered Cambrian fossils and reinterpretation of Neruokpuk Formation, northeastern Alaska: American Association of Petroleum Geologists Bulletin, v. 56, p. 808–815.

Gottlieb, E. S., Pease, V., Miller, E. L., & Akinin, V. V., 2018, Neoproterozoic basement history of Wrangel Island and Arctic Chukotka: integrated insights from zircon U–Pb, O and Hf isotopic studies, *in* Pease, V.L. and Coakley, B.J. eds., Circum-Arctic Lithosphere Evolution, Geological Society, London, Special Publications, 460, p. 183-206

Hoiland, C.W., Miller, J.J., Pease, V., and Hourigan, J.K., 2018, Detrital zircon U–Pb geochronology and Hf isotope geochemistry of metasedimentary strata in the southern Brooks Range: constraints on Neoproterozoic–Cretaceous evolution of Arctic Alaska, *in* Pease, V.L. and Coakley, B.J. eds., Circum-Arctic Lithosphere Evolution, Geological Society, London, Special Publications, 460, p. 121-158

Johnson, B.G., Strauss, J.V., Taylor, J.F., Ward, W.P., Colpron, M., McClelland, W.C., and Toro, J., 2018, The Whale Mountain allochthon: A relic of the Iapetus Ocean preserved in the northeastern Brooks Range of Alaska and Yukon, *in* Piepjohn, K., Strauss, J.V., Reinhardt, L., and McClelland, W.C., eds., Circum-Arctic Structural Events: Tectonic Evolution of the Arctic Margins and Trans-Arctic Links with Adjacent Orogens: Geological Society of America Special Paper 541, https://doi.org/10.1130/2018.2541(20).

Johnson, B.G., Strauss, J. V., Toro, J., Benowitz, J.A., Ward, W.P., and Hourigan, J.K., 2016, Detrital geochronology of pre-Mississippian strata in the northeastern Brooks Range, Alaska: Insights into the tectonic evolution of northern Laurentia: Lithosphere, v. 8, p. 649–667, doi: 10.1130/L533.1.

Lane, L.S., Gehrels, G.E., and Layer, P.W., 2016, Provenance and paleogeography of the Neruokpuk Formation, northwest Laurentia: An integrated synthesis: Geological Society of America Bulletin, v. 129, p. 239−257, doi: 10.1130/B31234.1.

MacDonald, F. a., McClelland, W.C., Schrag, D.P., and MacDonald, W.P., 2009, Neoproterozoic glaciation on a carbonate platform margin in Arctic Alaska and the origin of the North slope subterrane: Bulletin of the Geological Society of America, v. 121, no. 3, p. 448–473, doi: 10.1130/B26401.1.

McClelland, W.C., Colpron, M., Piepjohn, K., von Gosen, W., Ward, W.P., and Strauss, J.V., 2015, Preliminary detrital zircon geochronology of the Neruokpuk Formation in the Barn Mountains, Yukon, *in* MacFarlane, K.E., Nordling, M.G., and Sack, P.J., eds., Yukon Exploration and Geology 2014: Yukon Geological Survey, p. 123–143.

Metelkin, D.V., Vernikovsky, V. a., and Matushkin, N.Y., 2015, Arctida between Rodinia and Pangea: Precambrian Research, v. 259, p. 114–129, doi: 10.1016/j.precamres.2014.09.013.

Miller, E.L., Kuznetsov, N., Soboleva, a., Udoratina, O., Grove, M.J., and Gehrels, G.E., 2011, Baltica in the Cordillera? Geology, v. 39, no. 8, p. 791–794, doi: 10.1130/G31910.1.

Miller, E.L., Meisling, K.E., Akinin, V.V., Brumley, K., Coakley, B.J., Gottlieb, E.S., Hoiland, C.W., O'Brien, T.M., Soboleva, A., and Toro, J., 2018, Circum-Arctic Lithosphere Evolution (CALE) Transect C: displacement of the Arctic Alaska–Chukotka microplate towards the Pacific during opening of the Amerasia Basin of the Arctic, *in* Pease, V. and Coakley, B., eds., Circum-Arctic Lithosphere Evolution: Geological Society of London, Special Publications, v. 460, p. 57–120

Miller, E.L., Toro, J., Gehrels, G.E., Amato, J.M., Prokopiev, A., Tuchkova, M.I., Akinin, V.V., Dumitru, T.A., Moore, T.E., and Cecile, M.P., 2006, New insights into Arctic paleogeography and tectonics from U-Pb detrital zircon geochronology: Tectonics, v. 25, TC3013, doi: 10.1029/2005TC001830.

Moore, T.E., O'Sullivan, P.B., Potter, C.J., and Donelick, R.A., 2015, Provenance and detrital zircon geochronologic evolution of lower Brookian foreland basin deposits of the western Brooks Range, Alaska, and implications for early Brookian tectonism: Geosphere, v. 11, p. 93–122, doi: 10.1130/GES01043 .1.

Moore, T.E., Wallace, W.K., Bird, K.J., Karl, S.M., Mull, C.G., and Dillon, J.T., 1994, Geology of northern Alaska, *in* Plafker, G. and Berg, H.C. eds., The Geology of Alaska, Geological Society of America, The Geology of North America, v. G-1, Boulder, Colorado, p. 49–140.

Mull, C.G., 1982, Tectonic evolution and structural style of the Brooks Range: an illustrated summary, *in* Powers, R.B. ed., Geological studies of the Cordilleran thrust belt, Rocky Mountain Association of Geologists, Denver, Colo., p. 1–45.

Nelson, L.L., Strauss, J.V., Crockford, P.W., Cox, G.M., Johnson, B.G., Ward, W., Colpron, M., McClelland, W.C., and Macdonald, F.A., 2018, Geochemical constraints on the provenance of pre-Mississippian sedimentary rocks in the North Slope subterrane of Yukon and Alaska, *in* Piepjohn, K., Strauss, J.V., Reinhart, L., and McClelland, W.C., eds., Circum-Arctic Structural Events: Tectonic Evolution of the Arctic Margins and Trans-Arctic Links with Adjacent Orogens: Geological Society of American Special Paper 541, doi: 10.1130/2018.2541(24).

Patrick, B.E., and McClelland, W.C., 1995, Late Proterozoic granitic magmatism on Seward Peninsula and a Barentian origin for Arctic Alaska – Chukotka: Geology, v. 23, no. 1, p. 81–84.

Strauss, J. V., Hoiland, C.W., Ward, W.P., Johnson, B.G., Nelson, L.L., and McClelland, W.C., 2017, Orogen transplant: Taconic–Caledonian arc magmatism in the central Brooks Range of Alaska: Geological Society of America Bulletin, v. 129, no. 5-6, p. 649–676, doi: 10.1130/B31593.1.

Strauss, J.V., Johnson, B.G., Ward, W.P., Nelson L.L., McClelland, W.C., 2018a, Pre-Mississippian stratigraphy and provenance of the North Slope subterrane of Arctic Alaska II: Basinal sediments of the northeastern Brooks Range and their significance in circum-Arctic evolution *in in* Piepjohn, K., Strauss, J.V., Reinhardt, L., and McClelland, W.C., eds., Circum-Arctic Structural Events: Tectonic Evolution of the Arctic Margins and Trans-Arctic Links with Adjacent Orogens: Geological Society of America Special Paper 541

Strauss, J.V., Macdonald, F.A., and McClelland, W.C., 2018b, Pre-Mississippian stratigraphy and provenance of the North Slope subterrane of Arctic Alaska I: Platformal rocks of the northeastern Brooks Range and their signifi cance in circum-Arctic evolution, *in* Piepjohn, K., Strauss, J.V., Reinhardt, L., and McClelland, W.C., eds., Circum-Arctic Structural Events: Tectonic Evolution of the Arctic Margins and Trans-Arctic Links with Adjacent Orogens: Geological Society of America Special Paper 541, doi: 10.1130/2018.2541(22).

Strauss, J. V., MacDonald, F.A., Taylor, J.F., Repetski, J.E., and McClelland, W.C., 2013, Laurentian origin for the North Slope of Alaska: Implications for the tectonic evolution of the Arctic: Lithosphere, v. 5, p. 477–482, doi: 10.1130/L284.1.

Till, A.B., Amato, J.M., Aleinikoff, J.N., and Bleick, H.A., 2014a, U-Pb detrital zircon geochronology as evidence for the origin of the Nome Complex, northern Alaska, and implications for regional and trans-Arctic correlations, *in* Dumoulin, J.A., and Till, A.B., eds., Reconstruction of a Late Proterozoic to Devonian Continental Margin Sequence, Northern Alaska: Its Paleogeographic Significance and Contained Base-Metal Sulfide Deposits: Geological Society of America Special Paper 506, p. 111–131.

Till, A.B., Dumoulin, J.A., Ayuso, R.A., Aleinikoff, J.N., Amato, J.M., Slack, J.F., and Shanks, W.C.P., III, 2014b, Reconstruction of an early Paleozoic continental margin basin on the nature of protoliths in the Nome Complex, Seward Peninsula, Alaska, *in* Dumoulin, J.A., and Till, A.B., eds., Reconstruction of a Late Proterozoic to Devonian Continental Margin Sequence, Northern Alaska: Its Paleogeographic Significance and Contained Base-Metal Sulfide Deposits: Geological Society of America Special Paper 506.

Chapter 2: Detrital geochronology of pre-Mississippian strata in the northeastern Brooks Range, Alaska: Insights into the tectonic evolution of northern Laurentia

Ben G. Johnson[1], Justin V. Strauss[2], Jaime Toro[1], Jeff A. Benowitz[3], William P. Ward[4], Jeremy K. Hourigan[5]

[1]Department of Geology and Geography, West Virginia University, Morgantown, West Virginia, 26506 USA

[2]Department of Earth Sciences, Dartmouth College, Hanover, New Hampshire 03755, USA

[3]Geophysical Institute, University of Alaska Fairbanks, Fairbanks, Alaska 99775, USA

[4]Department of Earth and Environmental Sciences, University of Iowa, Iowa City, Iowa 52242, USA

[5]Department of Earth and Planetary Sciences, University of California–Santa Cruz, Santa Cruz, California 95064, USA

ABSTRACT

The Arctic Alaska terrane of northern Alaska and Yukon is one of several exotic terranes in the North American Cordillera with putative early Paleozoic connections to the northern Caledonian–Appalachian orogen. The U-Pb and $^{40}Ar/^{39}Ar$ isotopic data from detrital minerals in pre-Mississippian sedimentary units of the northeastern Brooks Range are presented here to investigate the consequences of Caledonian orogenesis on sediment dispersal trends and the paleogeography of northern Laurentia. Neoproterozoic–Cambrian siliciclastic rocks of the informal Firth River group and the Neruokpuk Formation were most likely deposited along a passive margin that sourced Archean and Paleoproterozoic basement rocks of the Canadian

shield and reworked Mesoproterozoic and younger sedimentary units. These strata are overlain by a Lower Ordovician–Lower Devonian succession of fine-grained siliciclastic turbidites, herein referred to as the Clarence River group, which records a prominent shift in provenance most likely associated with the onset of the Caledonian-Appalachian orogeny in northeast Laurentia. U-Pb detrital zircon age populations of ca. 470–420 and 990–820 Ma, along with $^{40}Ar/^{39}Ar$ detrital muscovite ages of ca. 470–430 Ma, support provenance connections with the East Greenland Caledonides, Pearya, and Svalbard. Partially reset $^{40}Ar/^{39}Ar$ ages in these sedimentary successions are linked to low-grade metamorphism associated with the Early–Middle Devonian Romanzof orogeny, a poorly understood tectonic event in the Brooks Range that is possibly associated with the emplacement of an allochthonous oceanic assemblage, herein named the Whale Mountain allochthon.

INTRODUCTION

The expansion of continental margins typically occurs through the process of accretionary tectonics, whereby crustal fragments, or terranes, composed of intraoceanic island arcs, ophiolites, rifted continental fragments, microcontinents, and accretionary complexes are progressively sutured to the edge of a continent (e.g., Dewey and Horsfield, 1970; Coney et al., 1980; Moores, 1982; Saleeby, 1983; Schermer et al., 1984; Şengör et al., 1993). During the Phanerozoic, the Laurentian continent expanded along two major accretionary plate margins: the Caledonian-Appalachian orogen and the North American Cordillera. Numerous plate restorations link these two orogens by proposing that several exotic terranes (e.g., Arctic Alaska, Farewell, Alexander, Klamath-Sierra, and Pearya), now within the North American Cordillera and Canadian Arctic (Fig. 2.1A), were displaced from the northern Caledonian or paleo-Arctic realm

and translated along the northern margin of Laurentia (e.g., Colpron and Nelson, 2011; Cocks and Torsvik, 2011; Miller et al., 2011).

The Arctic Alaska terrane encompasses the Brooks Range, North Slope, and Seward Peninsula of northern Alaska, all of which contain several independent pre-Mississippian and Mesozoic crustal fragments, or subterranes, that host unique stratigraphic sequences (see review in Moore et al., 1994). During the Jurassic and Early Cretaceous, the south-facing passive margin of the Arctic Alaska terrane collided with the Koyukuk arc; this suture zone is marked by the Angayuchum terrane (Fig. 2.1B), a Devonian–Jurassic assemblage of ophiolitic fragments and pelagic sedimentary deposits (Moore et al., 1994). Some suggest that this suture zone extends westward across the Bering Sea to connect with the South Anyui suture zone of the Chukotka Peninsula, Arctic Russia, forming the composite Arctic Alaska–Chukotka microplate (e.g., Hubbard et al., 1987; Miller et al., 2006; Amato et al., 2009; Moore et al., 2015); however, distinct contrasts in structural styles along both the South Anyui and Angayuchum suture zones may imply different pre-Cretaceous histories for Arctic Alaska and Chukotka (Amato et al., 2015; Till, 2016).

Most Arctic plate models restore the northern edge of Arctic Alaska terrane as the conjugate margin to the Canadian Arctic Islands in Mesozoic time (e.g., Lawver and Scotese, 1990; Grantz et al., 2011). This is achieved by closing the Canada Basin by way of ~60° rotation of Arctic Alaska about a pole located near the Mackenzie Delta during the Early Cretaceous (Gottlieb et al., 2014, and references therein), but many issues remain unresolved regarding the evolution of the Canada Basin (e.g., Lane, 1997; appendix of Lane et al., 2016). A lasting subject of contention also involves the early Paleozoic position of the North Slope of Arctic Alaska at the time of the Caledonian-Appalachian orogeny (ca. 470–350 Ma). A commonly accepted

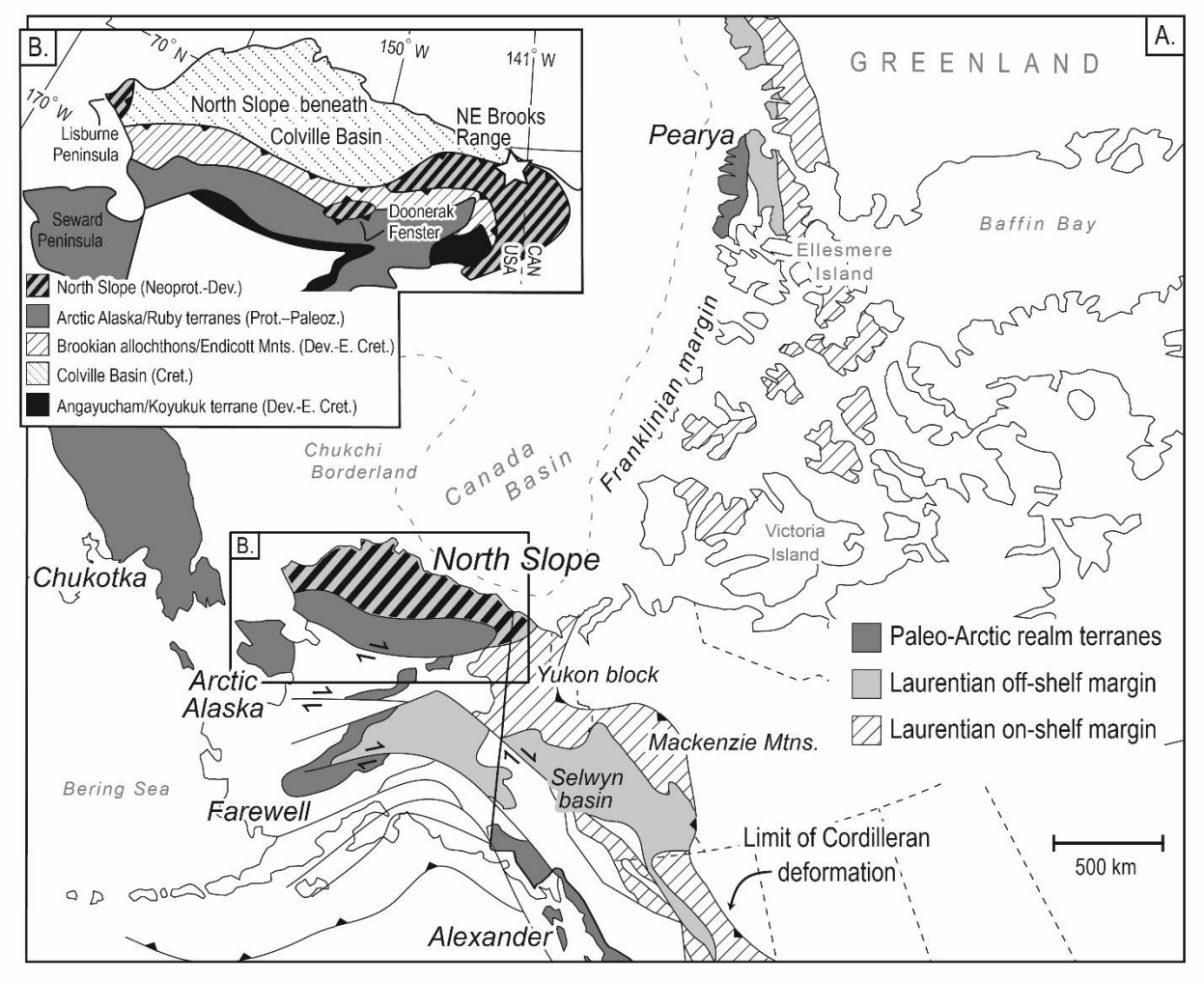

Figure 2.1: Generalized location maps. (A) The distribution of paleo-Arctic terranes in the northern Cordillera (modified from Colpron and Nelson, 2011). (B) Simplified tectonostratigraphic terrane map of northern Alaska (modified from Moore et al., 1994; 2015). Star indicates study area. NE—northeastern; Prot.—Proterozoic; Dev.—Devonian; E. Cret.—Early Cretaceous

model is that pre-Mississippian strata of the northeastern (NE) Brooks Range were deposited along a Neoproterozoic–Early Devonian passive margin that developed north (in present coordinates) of the Yukon block of northwest Laurentia (Fig. 2.1), before being deformed in the Early–Middle Devonian Romanzof orogeny (e.g., Lane, 1991, 2007; Moore et al., 1994; Cecile et al., 1999; Colpron and Nelson, 2011; Beranek et al., 2010; Lane et al., 2016). In contrast, others have argued that the North Slope has pre-Mississippian origins in northeast Laurentia, and that it did not attain its pre-Canada Basin position until sometime before the Late Devonian or Early Mississippian (Sweeney, 1982; Dumoulin et al., 2000; Macdonald et al., 2009; Strauss et al., 2013; Cox et al., 2015). Resolving these conflicting interpretations has broad implications for Neoproterozoic–Paleozoic plate reconstructions of the circum-Arctic region and Caledonian-Appalachian orogeny (Strauss et al., 2013); thus, our objective is to present new data pertaining to the structural and stratigraphic evolution of pre-Mississippian rocks in the NE Brooks Range to directly address these competing models.

GEOLOGICAL FRAMEWORK

Pre-Mississippian Stratigraphy of the NE Brooks Range

Pre-Mississippian strata of the North Slope of Arctic Alaska are well exposed in a series of east-west–trending antiforms that compose the NE salient of the Brooks Range (Fig. 2.2). These units are typically referred to as pre-Mississippian because of their regional truncation by a prominent sub-Mississippian unconformity, a characteristic feature of the NE Brooks Range and North Slope subsurface (Moore et al., 1994). A thick (1000–2000 m) succession of moderately to highly deformed quartzite, phyllite, and argillite called the Neruokpuk Formation (Leffingwell, 1919; Reed, 1968; Lane, 1991; Lane et al., 2016) is widely distributed in the Franklin, Romanzof, British, and Barn Mountains (Fig. 2.2). The exact age of the Neruokpuk

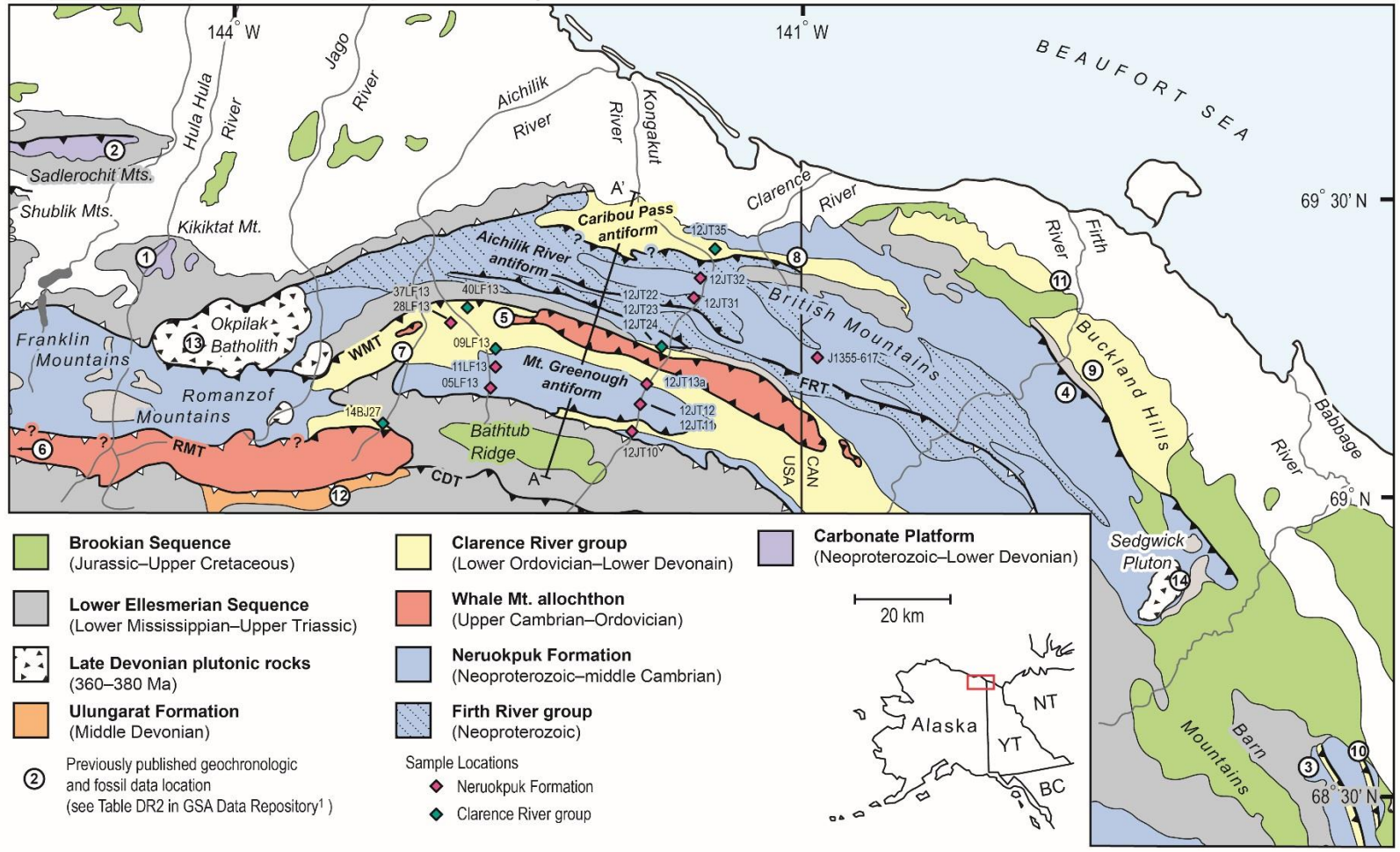

Figure 2.2: Simplified geologic map of the eastern half of the northeastern Brooks Range. Geology compiled after Reiser et al. (1980), Norris (1981a, 1981b), and Lane et al. (1995). Key structures: WMT—Whale Mountain thrust; RMT—Romanzof Mountain thrust; CDT—Continental Divide thrust (includes the Aichilik Pass thrust of Anderson et al., 1994); FRT—Firth River thrust. Solid teeth on thrust faults indicate disruption of stratigraphic section (old on young); open teeth indicate detachment surfaces along which there has been slip but no disruption of the stratigraphic section (young on old). Abbreviations: Mts.—mountains; YT—Yukon; NT—Northwest Territories; BC—British Columbia.

Formation is not well known, but previously it was suggested that it ranges from Neoproterozoic to middle Cambrian(?) based on the occurrence of *Oldhamia* ichnofossils in the northern British and Barn Mountains of Yukon (Hofmann and Cecile, 1981; Lane and Cecile, 1989; Lane, 1991; Hofmann et al., 1994; Lane et al., 2016; see Table SM2.1 in the Supplemental Material section for a summary of age constraints on pre-Mississippian units of the NE Brooks Range). The Neruokpuk Formation overlies a highly deformed and poorly studied mixed carbonate-siliciclastic succession (Fig. 2.3), now recognized as the informal Firth River group in the northern British Mountains of Yukon (Lane et al., 2016). In Alaska, the Firth River group includes sequence D and E of Dutro et al. (1972), Domain III of Mull and Anderson (1991), and various carbonate and fine-grained siliciclastic units of Reiser et al. (1980).

In the southern British Mountains of Alaska, a highly deformed and imbricated sequence of predominately fine-grained siliciclastic units, situated below the rocks of the Whale Mountain allochthon, disconformably overlies the Neruokpuk Formation. In the Demarcation Point quadrangle, Reiser et al. (1980) divided these deposits into the following four map units: chert and phyllite (Ccp), calcareous siltstone and sandstone (Css), dark gray to black shale locally metamorphosed to phyllite (map unit Cp), and a subordinate lithic sandstone unit (Cs). These map units were all assigned a Cambrian age based on a single locality of poorly preserved echinoderm debris and their assumed stratigraphic position beneath the trilobite-bearing limestone beds of the Whale Mountain volcanic rocks (Fig. 2.3; Reiser et al., 1980). Similar packages of interbedded chert, argillite, and lithic sandstone are broadly distributed throughout northern Yukon, particularly near the Alaska-Yukon border along the Clarence and Malcolm Rivers (Kelley et al., 1994; Lane et al., 1995), in the Buckland Hills region along the Firth River (Lane and Cecile, 1989), and in the Barn Mountains (Cecile, 1988; Cecile and Lane, 1991). Age

constraints for these strata are provided by a limited number of fossil localities that include Lower Ordovician–upper Silurian (Pridoli) graptolites (Lenz and Perry, 1972; Reiser et al., 1980; Lane and Cecile, 1989; Lane et al., 1995; Norford, 1997). The upper age limit of this sequence is locally constrained by two conodont localities: an upper Silurian (Pridoli)–Lower Devonian (earliest Pragian) fauna collected along the Clarence River in Alaska (Lane et al., 1995) and a Lower Devonian (Emsian?) fauna collected at the very northern limit of the British Mountains (Norris, 1986). Both of these samples were collected from isolated talus slopes, so their stratigraphic positions within the greater pre-Mississippian succession remain somewhat ambiguous.

Lane et al. (2016) split these early Paleozoic units of northern Yukon into two general lithostratigraphic successions: a lower graptolitic-bearing succession of interbedded chert and argillite, and an upper dark gray shale and sandstone turbidite package with subordinate chert-pebble conglomerate and limestone. The base of the lower succession is marked by a ridge-forming chert interval that contains Lower Ordovician graptolites (Lane and Cecile, 1989). A similar interval is mapped in the Barn Mountains of Yukon (Cecile, 1988; Cecile and Lane, 1991) and southern British Mountains of Alaska (unit Ccp of Reiser et al., 1980), where it presumably disconformably overlies the Neruokpuk Formation (Dutro et al., 1972). The base of the upper succession is uncertain. Geological mapping in the Buckland Hills region suggests that its contact with the lower succession is discordant (Lane and Cecile, 1989), whereas along the Clarence River and Barn Mountains the boundary between upper and lower succession is gradational (Kelley et al., 1994; Lane et al., 1995) or absent (Cecile, 1988; Cecile and Lane, 1991), respectively. Lane et al. (2016) referred to the lower succession as the Road River Group

following correlations with equivalent strata in the Yukon block (Gordey and Anderson, 1993) and the upper succession as the informal Buckland Hills succession.

Because we view many of the map relationships as uncertain and the correlations with coeval strata in the Yukon block as suspect, we propose that this entire stratigraphic package should be consolidated into a single lithostratigraphic group, which we informally name the Clarence River group based on a possible type area near the headwaters of Clarence River in the northern British Mountains (Fig. 2.2). The motivation behind this consolidation is because the recognition and documentation of definitive lithostratigraphic boundaries within the different successions have not been established. Moreover, the group designation allows for subsequent separation of distinct formations with type sections when more geological, geochronological, and biostratigraphic data become available. We tentatively propose that the Buckland Hills succession of Lane et al. (2016) constitutes the uppermost formation of the Clarence River group. The base of the Clarence River group is marked by the prominent Ordovician chert interval that is distributed throughout Yukon and Alaska.

In the Romanzof Mountains and along a linear belt in the southern British Mountains, a thick (>700 m) structural complex composed of basalt flows, discontinuous carbonate beds, and an imbricated package of bedded chert, phyllite, and lithic tubidites structurally overlie the pre-Mississippian sedimentary successions. In a broad sense the basalt flows, informally named the Whale Mountain volcanic rocks, geochemically resemble ocean-island basalt, showing enrichment in incompatible, large-ion lithophile, and high-field-strength elements (Moore, 1987; Goodfellow et al., 1995). The age of these volcanic rocks is constrained by upper Cambrian (Furongian) trilobites of Laurentian affinity discovered within the discontinuous carbonate beds that locally interfinger with the basalt flows (Dutro et al., 1972). The imbricated and folded

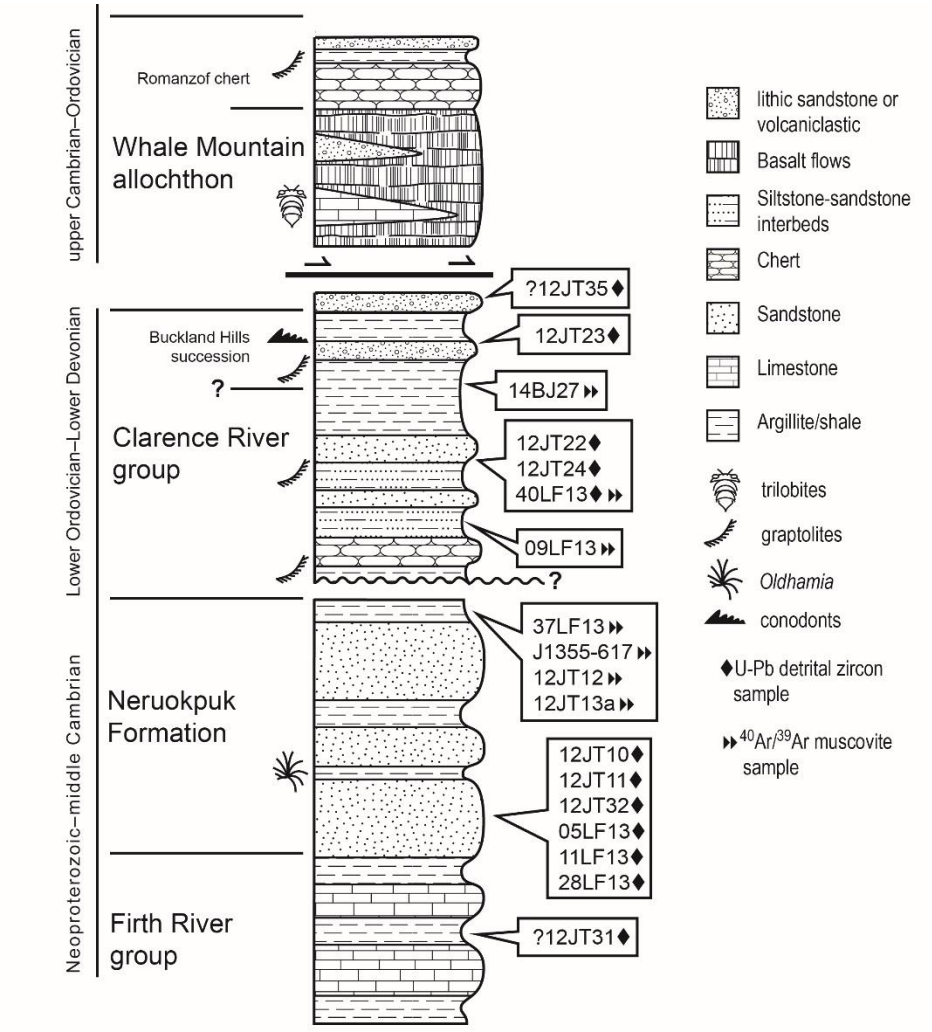

Figure 2.3: Schematic stratigraphic column of pre-Mississippian units in the eastern half of the northeastern (NE) Brooks Range (modified from Kelley et al., 1994). Stratigraphic positions of samples, indicated with sample number and conducted analysis, are approximated, and fossil constraints are from the Yukon side of the NE Brooks Range and may not correlate with sampled units in this study.

package of bedded chert, phyllite, and lithic turbidite units is widely distributed in the Romanzof Mountains, particularly near the headwaters of the Jago and Aichilik Rivers (Fig. 2.2). Mull and Anderson (1991) informally named these units the Romanzof chert, and along strike in the southern Franklin Mountains, a lithologically similar succession of argillite and radiolarian-bearing chert units contains upper Ordovician and possible lower Silurian (Llandovery) graptolite fossils (Moore and Churkin, 1984). The tectonic setting and structural relationships of these rocks are not well understood, and because we have yet to document any depositional and/or conformable relationships, we propose that their incorporation into the pre-Mississippian stratigraphy of the NE Brooks Range be ascribed to the emplacement of a now-dismembered thrust sheet, herein named the Whale Mountain allochthon (Figs. 2.3 and 2.4).

The pre-Mississippian rocks of the NE Brooks Range are crosscut by a suite of Late Devonian intrusive bodies (e.g., Okpilak batholith and Sedgwick pluton; Fig. 2.2), which yield U-Pb zircon ages of ca. 380–360 Ma (Dillon et al., 1987; Mortensen and Bell, 1991; Lane, 2007). These intrusive rocks share mineralogical and compositional similarities to S-type granites, implying that they were derived from the partial melting of lower crustal rocks (Sable, 1977; Newberry et al., 1986). Contact relationships with the older country rock, mainly the Neruokpuk Formation, are abrupt with a limited metamorphic aureole, possibly indicating shallow levels of emplacement and/or a shortage of hydrothermal fluids (Sable, 1977). In many places throughout the field area, the Mississippian Kekiktuk Conglomerate, the basal unit of the lower Ellesmerian sequence (e.g., Moore et al., 1994), overlies with angular unconformity on the pre-Mississippian sedimentary units and Late Devonian intrusive rocks. At the southern edge of the field area, near the headwaters of the Kongakut River (Fig. 2.2), the Kekiktuk Conglomerate also truncates the Middle Devonian Ulungarat Formation of Anderson et al. (1994), formerly

unit Ds of Reiser et al. (1980). The Ulungarat formation consists of a >300-m-thick, coarsening-upward succession of shallow-marine and terrigenous deposits that unconformably overlie the complexly deformed Romanzof chert of the Whale Mountain allochthon; however, this contact relationship is obscured by displacements along a major south-dipping Cenozoic thrust fault (the Aichilik Pass thrust of Anderson et al., 1994).

Deformation in the NE Brooks Range

The NE Brooks Range was affected by at least two major deformational events. Pre-Mississippian rocks throughout the NE Brooks Range are highly strained into tight, east-trending folds that display a combination of subhorizontal and steeply dipping penetrative fabrics (e.g., Oldow et al., 1987; Lane, 2007). The fabrics are not present in the Middle Devonian Ulungarat formation, implying a regional pre–Middle Devonian phase of deformation (Anderson et al., 1994), now widely known as the Romanzof orogeny (Lane, 2007). The paleogeographic and tectonic setting of this pre–Middle Devonian deformation are not well constrained, although Lane (2007) inferred from field and subsurface data that deformation was localized along the ancestral margin of northwest Laurentia, where a continent-scale terrane encroached from the north (present coordinates) and progressively accreted to the margin in the Early–Middle Devonian. It is critical that this assumes a fixed position of the North Slope with respect to northwest Laurentia throughout the Paleozoic.

The latest phase of deformation in the NE Brooks Range relates to the Late Jurassic(?) to Miocene Brookian orogeny, which is considered to have evolved through two distinct episodes of north-directed contractional deformation (Moore et al., 1994, 2004, 2015). In the NE Brooks Range, Brookian deformation was accommodated by the formation of several regionally spaced antiforms (e.g., Mount Greenough and Aichilik River antiforms; Fig. 2.2). These are typically

interpreted as a stacked duplex thrust system, with a floor thrust deep within the pre-Mississippian sequence and a roof thrust in the Kayak Shale of the lower Ellesmerian sequence (e.g., Wallace and Hanks, 1990).

In our cross section through the eastern portion of the NE Brooks Range (Fig. 2.4), we illustrate the Brookian style of deformation as a series of large imbricated fault-bend folds that culminate to a detachment between 8 and 15 km below the surface, which is derived from previous structural studies in the region (Hanks, 1989; Peapples et al., 1997; Cole et al., 1999; Moore, 1999; O'Sullivan and Wallace, 2002). The ramps of the fault-bend folds are often represented by major thrust faults that are as much as 100 km in length, including the Whale Mountain and Romanzof Mountain thrusts (WMT and RMT; Fig. 2.2). Apatite fission-track and $^{40}Ar/^{39}Ar$ thermochronological data indicate that many of these basement-involved thrusts underwent significant Cenozoic displacement (Hanks, 1993; O'Sullivan, 1994; Peapples et al., 1997; O'Sullivan and Wallace, 2002).

Differentiating between Brookian and Romanzof deformation fabrics in the NE Brooks Range represents a significant challenge to the understanding of the regional structural architecture. Most structural models collectively treat pre-Mississippian units as rigid thrust panels that undergo no internal shortening in response to Brookian contraction (Hanks, 1989; Wallace and Hanks, 1990; Cole et al., 1999; Moore, 1999; O'Sullivan and Wallace, 2002); however, these assumptions are oversimplified and problematic. For example, in the Mount Greenough antiform, the primary study area for this research, the classical north-directed fault-bend fold model (e.g., Wallace and Hanks, 1990; Moore, 1999) predicts that most of the structures and bedding planes should dip to the south (Fig. 2.4). In contrast, our field observations show that most of the pre-Mississippian units dip to the north, as illustrated in our

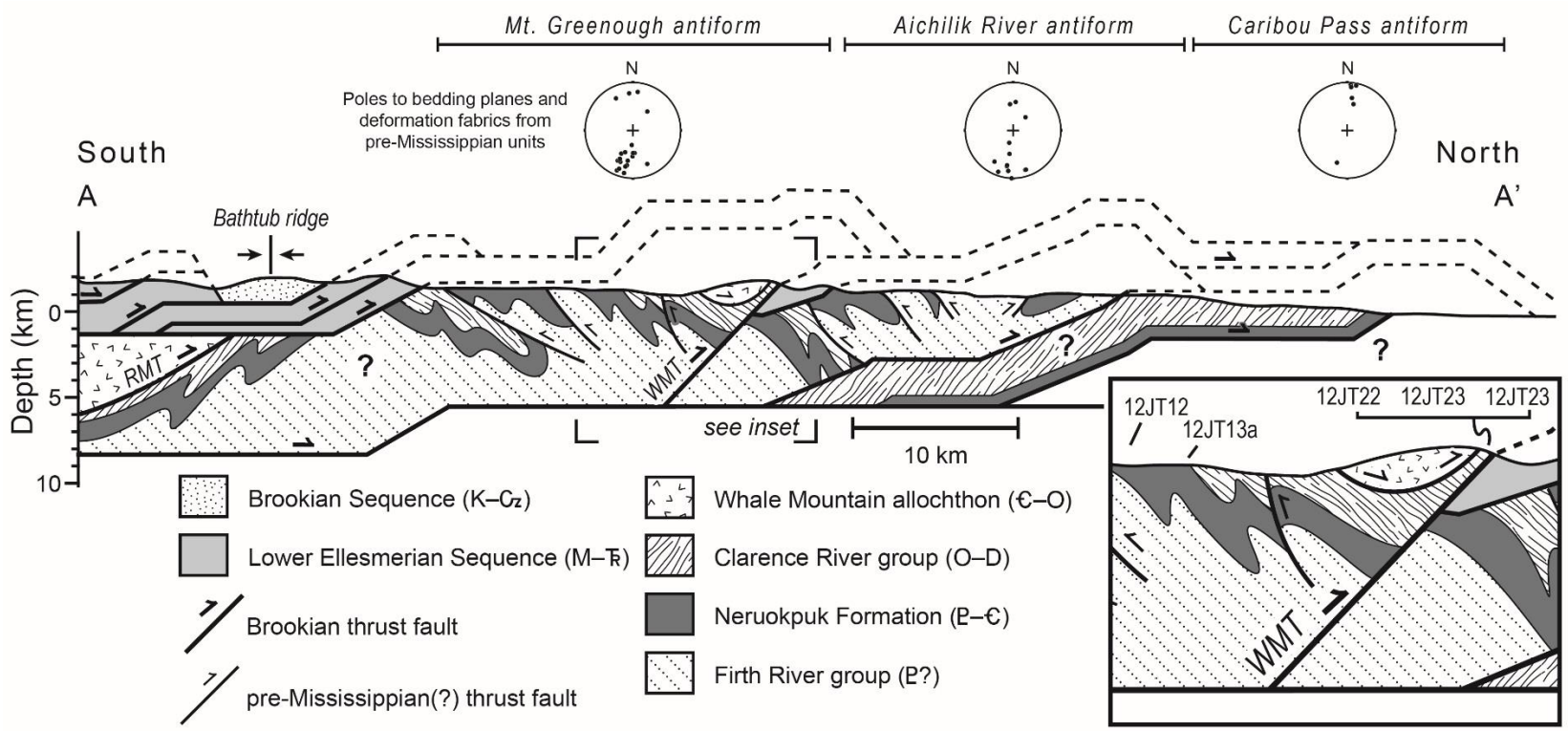

Figure 2.4: Cross section through the eastern half of the northeastern Brooks Range illustrating the major structural features and deformation trends with no vertical exaggeration (modified from Hanks, 1989; Wallace and Hanks, 1990; Moore, 1999). Approximate location of the section is shown in Figure 2.2. Pre-Mississippian structural features are constrained by field data along the Kongakut River, Alaska. Depth of detachment in the pre-Mississippian units is adopted from Hanks (1989) and Peapples et al. (1997). WMT—Whale Mountain thrust.

schematic cross section along the Kongakut River (Fig. 2.4). These structural simplifications also fail to explain the structural relationship between rocks of the Whale Mountain allochthon and Clarence River group, which cannot be restored by simple line-length restorations of a single fault-bend fold as modeled by Moore (1999). Although these issues are largely beyond the scope of this contribution, we highlight important issues brought to light by our new geochronological data that will guide future structural studies in the region.

METHODS AND RESULTS

U-Pb Detrital Zircon Geochronology

We analyzed 11 samples of sandstone from the NE Brooks Range for U-Pb detrital zircon geochronology by laser ablation–inductively coupled plasma–mass spectrometry (LA-ICPMS) at the University of California–Santa Cruz following the procedures outlined by Sharman et al. (2013). An additional sample (40LF13) was analyzed by combining LA-ICP-MS at Stockholm University with secondary ion mass spectrometry (SIMS) at the NordSIM facility at the Swedish Museum of Natural History following procedures outlined by Beranek et al. (2013a). The samples are separated into two distinct groups based on their major pre-Mississippian lithostratigraphic associations: (1) the Neoproterozoic–middle Cambrian Neruokpuk Formation (Leffingwell, 1919) and the Firth River group (Lane et al., 2016), and (2) the Lower Ordovician–Lower Devonian Clarence River group, including the Buckland Hills succession of Lane et al. (2016). The sample descriptions, raw geochronologic data, and procedures for collecting and interpreting the data are provided in the Supplemental Material section. The individual ages from each sample were filtered on the basis of concordance between 206Pb/207Pb and 206Pb/238U ratios, U and Th concentrations, and degree of uncertainty in the calculated ages (for a detailed

discussion, see Supplemental Material section). These filtered subsets of the data are presented as stacked normalized age-probability plots (Figs. 2.5 and 2.6).

Neruokpuk Formation and Firth River Group

The majority of the Neruokpuk Formation samples were collected from a broad belt of predominately north-dipping strata exposed within the core of the Mount Greenough antiform in the southern British Mountains (Fig. 2.2). These samples generally consist of coarse- to fine-grained, subrounded, quartz and sublithic arenites, with occasional feldspar, chert fragments, muscovite, and other accessory minerals. Most of these samples contain a complex assemblage of clay minerals that occupy interstitial space or compose the supporting matrix, and some samples have undergone intense deformation resulting in authigenic mica growth and pronounced strain shadows around individual quartz grains (Fig. SM2.1). Beds range between 0.5 and 2 m thick, are typically interbedded with intensely foliated green-gray argillite, and occasionally show flutes, scours, and Bouma A–D cycles. Two additional samples were collected from within the Aichilik River antiform in the northern British Mountains (Fig. 2.2). One sample (12JT32) was collected from an outcrop of units lithologically similar to the Neruokpuk samples collected in the southern British Mountains and to those described by Lane et al. (2016) in the northern British Mountains of Yukon. Another sample (12JT31) was collected from the phyllite and quartzite of Old Gungy Mountain (map unit pCpq of Reiser et al., 1980), which we assign to the Firth River group because of its inferred lower stratigraphic position with respect to the Neruokpuk Formation (Fig. 2.2). This sample was collected from an outcrop of subvertical, intensely foliated green to gray argillite and interbedded fine-grained quartzite, which is cut by numerous quartz veins that have undergone rotation from left-lateral, east-west shear.

Samples from the Neruokpuk Formation and Firth River group yield populations of well-rounded to elongate zircon. All seven samples show similar U-Pb age distributions with prominent Paleoproterozoic and Neoarchean peaks that are between ca. 2000 and 1700 Ma, 2400 and 2200 Ma, and 2600 and 2400 Ma (Fig. 2.5). Mesoproterozoic zircons only constitute subordinate populations in most samples that range between ca. 1500 and 1100 Ma. The Firth River group sample (12JT31) is mostly indistinguishable from the other Neruokpuk samples, with a slightly more prominent population of Mesoproterozoic zircon grains ca. 1300 Ma. Sample 12JT10 is the only sample that contains young zircons, represented by two single-grain ages of 632 ± 29 Ma and 936 ± 43 Ma (2σσ).

Clarence River Group

Sandstone samples from the Lower Ordovician–Lower Devonian(?) Clarence River group are texturally and compositionally immature. Individual sample descriptions and photomicrographs are provided in the Supplemental Material section. Four of the samples (12JT22, 12JT23, 12JT24, and 40LF13) were collected from outcrops along the northern edge of the Mount Greenough antiform (Figs. 2.2 and 2.4) in map units Cp and Cs of Reiser et al. (1980). Three of these samples (12JT22, 12JT24, and 40LF13) consist of medium- to fine-grained, angular quartz grains with occasional feldspar and coarse-grained detrital muscovite (Fig. SM2.2). These samples have an abundant (>25%) clay matrix, dominated by very fine mica, calcite, quartz, chlorite, and other clay minerals. Sample 12JT23 contains a variety of medium- to coarse-grained and angular clasts of monocrystalline and polycrystalline quartz, plagioclase feldspar, and chert, with minor volcanic and sedimentary lithic fragments, devitrified glass, and opaque minerals. The stratigraphic positions of each sample with respect to one another are uncertain, as the outcrops in this region are highly folded and possibly imbricated by minor

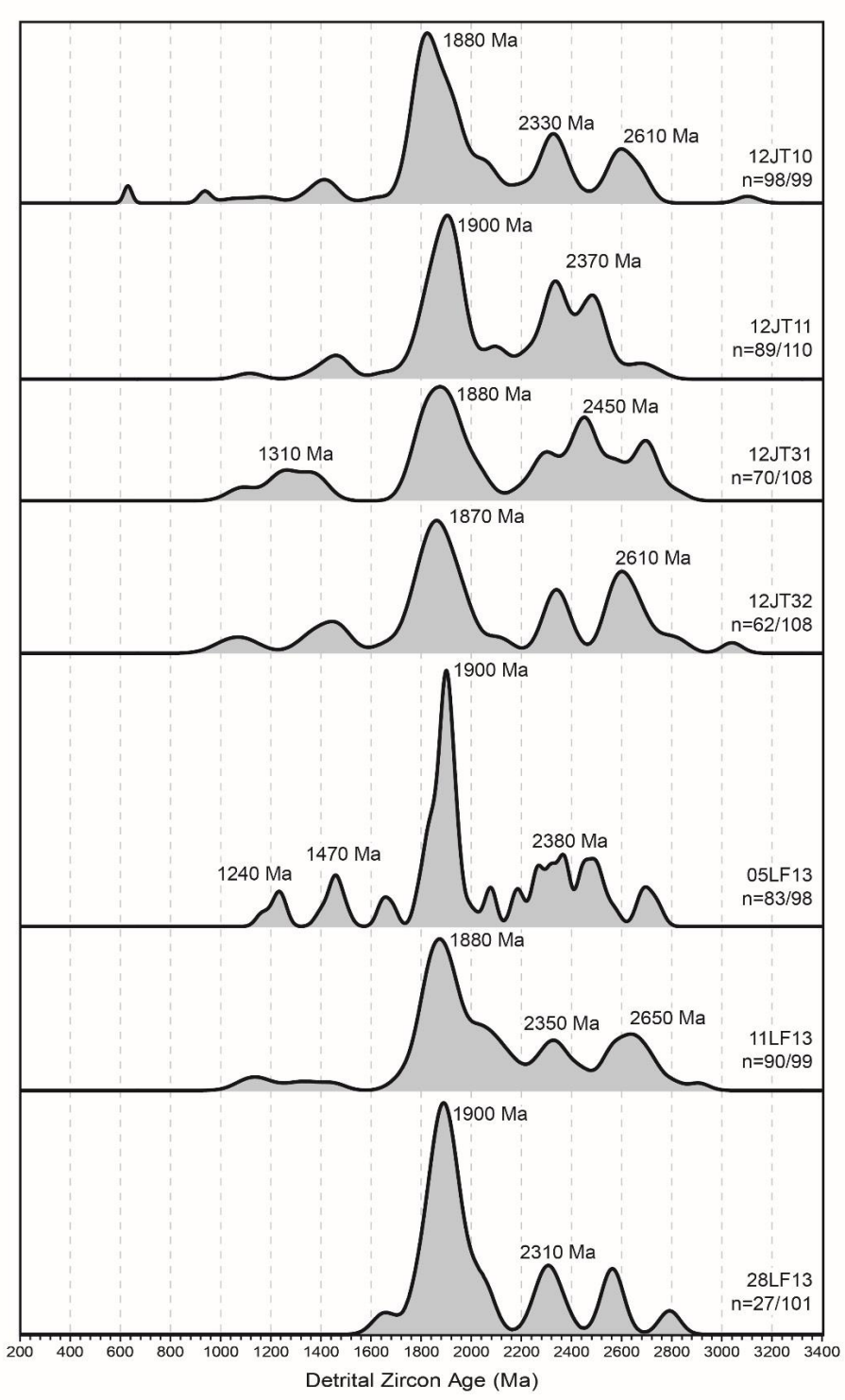

Figure 2.5: Normalized probability density plots of U-Pb detrital zircon ages from the Neruokpuk Formation. Ratio of analyses plotted versus total zircon analyzed is shown in upper right along with the sample number (see Fig. 2.2 for sample location). All analyses were conducted by laser ablation–inductively coupled plasma–mass spectrometry at the University of California Santa Cruz. The raw data and filtering methods are reported in Table SM2.3.

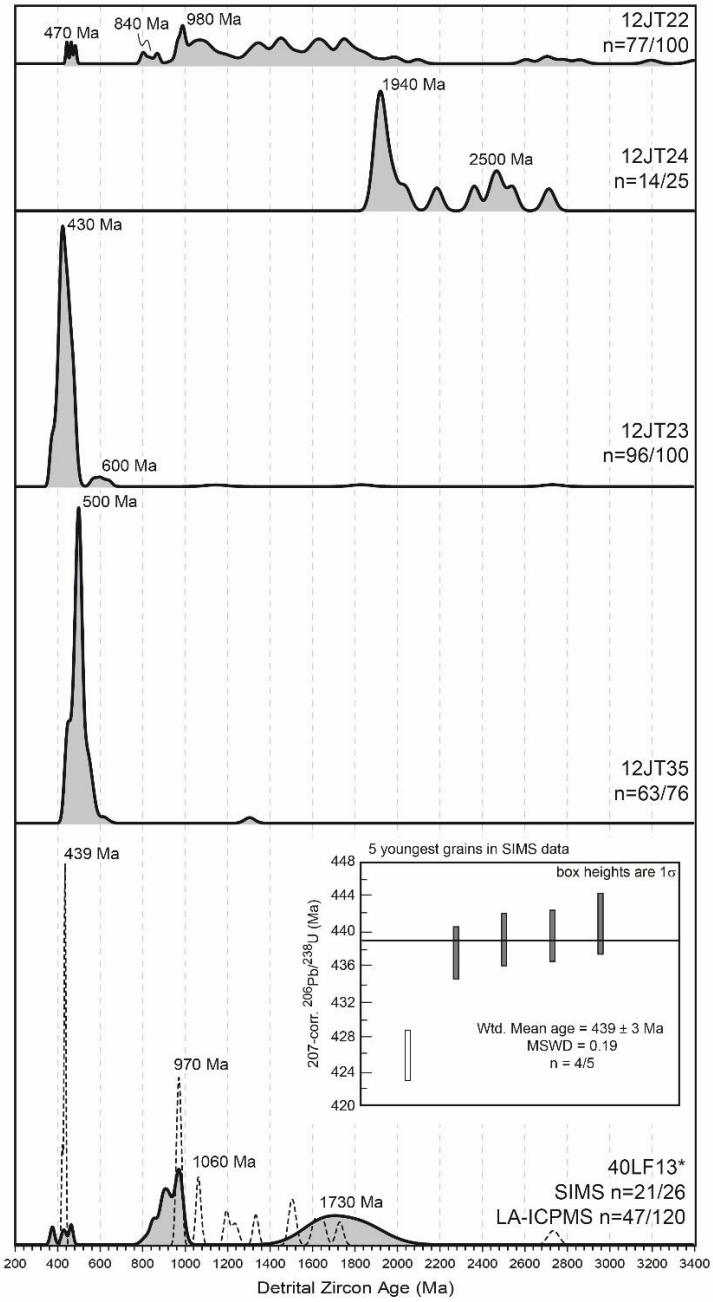

Figure 2.6: Normalized probability density plots of U-Pb detrital zircon ages from the Clarence River group and one sample (12JT35) from the Ovc map unit of Reiser et al. (1980). Ratio of analyses plotted versus total zircon analyzed is shown in upper right along with the sample number (see Fig. 2.2 for sample location). Samples 12JT22, 12JT23, 12JT24, and 12JT35 were analyzed by laser ablation–inductively coupled plasma–mass spectrometry (LA-ICP-MS) at the University of California Santa Cruz and are reported in Table SM2.3. Sample 40LF13 (bottom) was analyzed by LA-ICP-MS at Stockholm University (grayfilled black line) and by secondary ion mass spectrometry (SIMS) at the NordSIM facility, Swedish Museum of Natural History (dashed black line). These analyses are reported in Tables SM2.4 and SM2.5. Wtd.—weighted; MSWD—mean square of weighted deviates.

thrust faults. Beds range between 0.1 and 0.3 m thick, are typically interbedded with micaceous black siltstone or shale, and characterized by Bouma A–D cycles. A fifth sample (12JT35) was collected from a highly weathered outcrop of volcaniclastic and tuffaceous sandstone units in the northern British Mountains (map unit Ovc of Reiser et al., 1980), an area we refer to informally as the Caribou Pass antiform (Figs. 2.2 and 2.4). The sample contains medium- to fine-grained, subrounded to rounded opaque minerals, sericitized plagioclase, monocrystalline and polycrystalline quartz, volcanic rock fragments, and chert fragments in a clay-carbonate cement.

The distributions of U-Pb zircon ages among the Clarence River group samples are variable (Fig. 2.6). Sample 12JT22 is mostly composed of zircon older than 1000 Ma (~85%), with a broadly distributed population between ca. 2000 and 1300 Ma and a subordinate population between ca. 1200 and 1000 Ma. The younger population in this sample consists of three grains (~4%) that range between ca. 480 and 440 Ma and a second population of grains between ca. 990 and 800 Ma (~12%). Sample 12JT24 yields a small fraction of 25 zircon grains with age populations ranging between ca. 2000 and 1900 Ma (~57%) and 2700 and 2200 Ma (~43%). Zircon U-Pb ages from the lithic sandstone unit, sample 12JT23, comprise a nearly unimodal age population (~93%) between ca. 520 and 370 Ma (peak ca. 430 Ma; Fig. 2.6). This sample also contains two very small populations of older ages between ca. 650 and 560 Ma (~4%) and 2700 and 1150 Ma (3%). The volcaniclastic unit, sample 12JT35, also yields a unimodal age population between ca. 570 and 440 Ma (peak ca. 500 Ma, ~97% of grains; Fig. 2.6). Only two zircon grains yield ages outside of the main population: 620 ± 40 Ma and 1304 ± 44 Ma (2σ).

Sample 40LF13 was analyzed by LA-ICPMS at the Department of Geological Sciences at Stockholm University. Direct comparison of the zircon ages from this sample with other

Clarence River group samples should be done with caution because the isotopic measurements were conducted on different instruments with different sets of zircon standards (see Supplemental Material section). This sample yields three broad age populations between ca. 470 and 380 (~7%), 990 and 820 Ma (~40%), and 2000 and 1530 Ma (~53%). In addition to the LA-ICP-MS ages, 26 euhedral grains were selected and analyzed by SIMS. A filtered subset of 21 U-Pb ages is plotted along with the LA-ICP-MS data in Figure 2.6. The main age populations are between ca. 440 and 420 Ma (23%), 990 and 960 (23%), 1230 and 1000 (19%), 1510 and 1300 (14%), and 1726 and 1600 Ma (14%), with one Archean grain yielding a single-grain age of 2727 ± 5 Ma (1σ). The youngest single-grain age is 426 ± 3 Ma (1σ), and a cluster of four ages, which overlap in age at 1σ, yield a weighted mean age of 439 ± 3 Ma (1σ; Fig. 2.6). The ca. 1510–1000 Ma zircon ages observed in the SIMS distribution were filtered out from the LA-ICP-MS distribution because of substantial uncertainty (>10%) in the 206Pb/207Pb age, a typical phenomenon that occurs in LA-ICP-MS data sets at the crossover in precision between 206Pb/238U and 206Pb/207Pb ages caused by low intensity of the 207Pb signal.

^{40}Ar/^{39}Ar Muscovite Geochronology

Stepwise ^{40}Ar/^{39}Ar dating of single grains of muscovite from four samples from the Neruokpuk Formation and three samples from the Clarence River group was done at the University of Alaska Fairbanks following the procedures outlined by Martin et al. (2015). Step-heating experiments were conducted on one of the samples (12JT24) from an aggregate of very fine-grained muscovite (i.e., whole-rock chip). In another sample (14BJ27), we combined stepwise techniques with single-grain fusion ^{40}Ar/^{39}Ar geochronology (K-Ar equivalent ages) on 14 individual grains to investigate intrasample age variability.

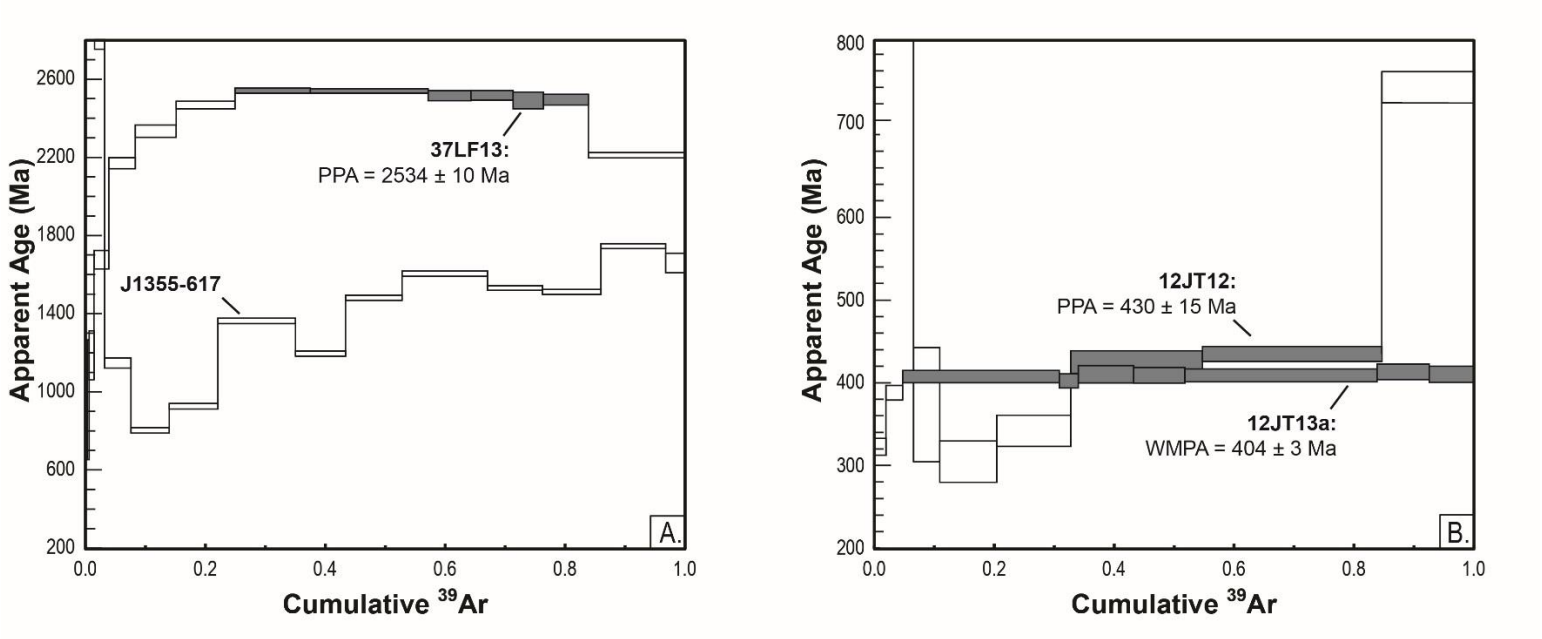

Figure 2.7: Stepwise $^{40}Ar/^{39}Ar$ age spectra of muscovite separates from the Neruokpuk Formation. (A) Samples that have retained detrital Ar (37LF13 and J1355–617). (B) Samples that have been partially or completely reset (12JT12 and 12JT13a). Analytical uncertainties are represented by vertical width of bars at the 1s level. Steps filled in dark gray were used for plateau age determinations. Weighted mean plateau ages (WMPA) are calculated using at least three contiguous steps that overlap in error at 1σ, and compose more than 60% of the ^{39}Ar release. Pseudo plateau ages (PPA) are calculated using the weighted mean age of two or more contiguous steps that overlap in error at 1σ, and compose 50%–60% of the ^{39}Ar released. Analyses are reported in Table SM2.6.

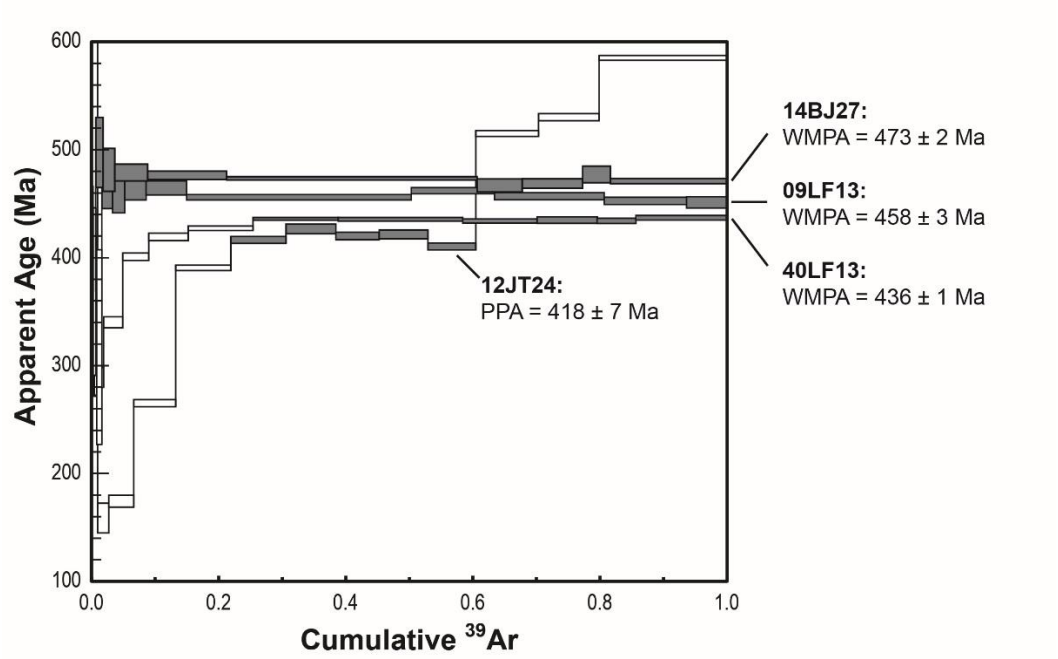

Figure 2.8: Stepwise $^{40}Ar/^{39}Ar$ age spectra on muscovite separates from the Clarence River group. Analytical uncertainties are represented by vertical width of bars at the 1s level. Steps filled in dark gray were used for plateau age determinations. Steps filled in dark gray were used for plateau age determinations. Weighted mean plateau ages (WMPA) are calculated using at least three contiguous steps that overlap in error at 1σ, and compose more than 60% of the ^{39}Ar release. Pseudo plateau ages (PPA) are calculated using weighted mean age of two or more contiguous steps that overlap in error at 1σ, and compose 50%–60% of the ^{39}Ar released. Analyses are reported in Table SM2.6.

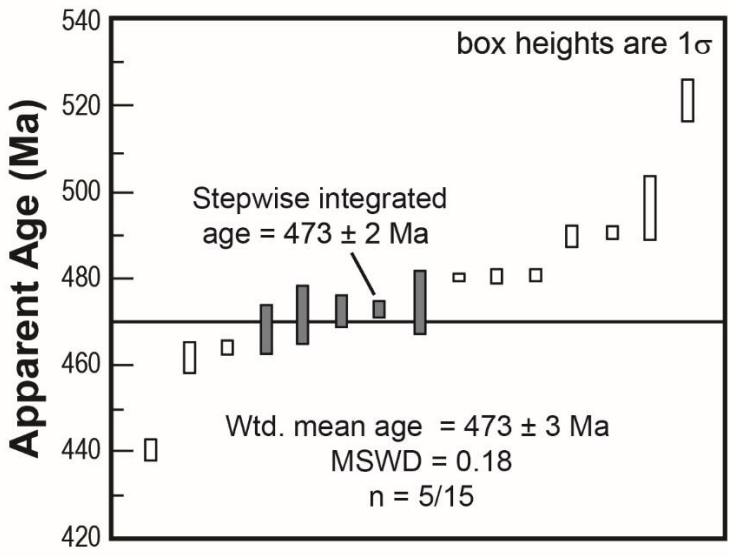

Figure 2.9: Distribution of the single-grain $^{40}Ar/^{39}Ar$ total fusion and stepwise integrated ages from sample 14BJ27 (Clarence River group). Analytical uncertainties are represented by the vertical width of bars at the 1σ level. The five ages filled in dark gray, composed of four total fusion ages and one stepwise integrated age, were used for weighted (Wtd.) mean age calculation (MSWD—mean square of weighted deviates). Analyses are reported in Table SM2.7.

The samples collected for the $^{40}Ar/^{39}Ar$ analyses have undergone thermal conditions above the diagenetic zone (>200 °C) and are within the range of anchizone to epizone metamorphic grades. All samples contain populations of coarse muscovite grains that are typically ~250–1000 μm in length, as well as fine-grained packets of interstitial muscovite that are ~10–100 □m thick. The sampled muscovite grains are typically situated within thin (<50 □m) disjunctive cleavage domains that envelop lens-shaped domains of quartz and other framework minerals. In most cases, we targeted the coarse-grained fraction of muscovite during the separation process. A summary of the $^{40}Ar/^{39}Ar$ ages from each sample are presented in Table 2.1 and the step-heating results are illustrated in Figures 2.7 and 2.8. The complete geochronological data, procedural methods, sample preparation techniques, and detailed petrographic descriptions are provided in the Supplemental Material section.

Results from the four Neruokpuk samples show complex and varied age spectra. Two of the samples (37LF13 and J1355–671) show significant scatter between heating steps, but most of the age steps from these samples are older than 800 Ma (Fig. 2.7A), indicating that the analyzed grains are clearly detrital. The other two samples (12JT12 and 12JT13b; Fig. 2.7B) are distinguished by having $^{40}Ar/^{39}Ar$ ages that are apparently younger than the depositional age of the Neruokpuk Formation. Sample 12JT13a shows a plateau release at 404 ± 3 Ma (Fig. 2.5B; 69% cumulative ^{39}Ar release). The stepwise results from sample 12JT12 show an irregular-shaped spectrum with 5 of the 12 steps (~77% cumulative ^{39}Ar release) yielding ages between ca. 430 and 372 Ma, where two consecutive steps yield a weighted mean age of 430 ± 15 Ma (Fig. 2.7B; 51% cumulative ^{39}Ar release).

TABLE 2.1: SUMMARY OF $^{40}Ar/^{39}Ar$ RESULTS

Sample	Biostratigraphic age*	Total fusion age (Ma)†	Plateau age (Ma)§	Remarks
Neruokpuk Formation				
12JT12	Neoproterozoic–middle Cambrian	1086 ± 11	430 ± 15	Pseudo plateau age from 2 of 12 fractions (52% 39Ar release), 77% 39Ar release is younger than fossil depositional age.
12JT13a	Neoproterozoic–middle Cambrian	402 ± 4	404 ± 3	Weighted mean plateau age from 7 of 9 fractions (69% 39Ar release), steps are younger than fossil depositional age.
37LF13	Neoproterozoic–middle Cambrian	2418 ± 9	2534 ± 10	Pseudo plateau age from 6 of 13 fractions (59% 39Ar release), all 13 fractions are older than fossil depositional age.
J1355-617	Neoproterozoic–middle Cambrian	1747 ± 13	NA	No plateau age, but all 13 fractions are older than fossil depositional.
Clarence River group				
12JT24	Lower Ordovician–Lower Devonian(?)	483 ± 2	418 ± 7	Pseudo plateau age from 5 of 13 fractions (39% 39Ar release), 40% 39Ar, release is older than the depositional age. Detrital zircon maximum depositional age comes from youngest graphical peak in sample 12JT23 collected nearby.
09LF13	Lower Ordovician–Lower Devonian(?)	455 ± 2	458 ± 3	Weighted mean plateau age from 9 of 13 fractions (97% 39Ar release), remaining 3% 39Ar release is younger than fossil depositional age.
40LF13	Lower Ordovician–Lower Devonian(?)	427 ± 2	436 ± 1	Weighted mean plateau age from 6 of 13 fractions (75% 39Ar release), remaining 25% 39Ar release is younger than depositional age. Detrital zircon maximum depositional age comes from the weighted mean age of the youngest 4 overlapping grains from sample 40LF13 secondary ion mass spectrometry data (Table SM2.5 in the Supplemental Material section).
14BJ27 stepwise	Lower Ordovician–Lower Devonian(?)	473 ± 2	473 ± 2	Weighted mean plateau age from 9 of 13 fractions (98% 39Ar release), remaining 2% 39Ar release is variable in age, fractions are both younger and older than fossil depositional age.
14BJ27 single-grain fusion (N = 14)	Lower Ordovician–Lower Devonian(?)	NA	NA	Total fusion single-grain ages range from 441 ± 2 to 521 ± 5 Ma; 4 ages are within error of the integrated age from the stepwise experiment, yielding a weighted mean age of 473 ± 3 Ma. All single-grain fusion ages are older than fossil depositional age.

*Biostratigraphic age (fossil age) is constrained by previous studies in Alaska and Yukon (Table SM2.1 in the Supplemental Material section).

†Total fusion age calculated by weighting the individual steps by the fraction of 39Ar released. This is analogous to an integrated age or conventional K-Ar age. NA indicates that integrated age is not applicable.

§Weighted mean plateau ages are calculated using at least three contiguous steps that overlap in error at 1σ, and comprise more than 60% of the ^{39}Ar release. Pseudo plateau ages are calculated using weighted mean age of 2 or more contiguous steps that overlap in error at 1σ, and comprise 50%–60% of the ^{39}Ar released. NA indicates that a plateau age could not be calculated or that a plateau age is not applicable.

Three of the four Clarence River group samples (09LF13, 40LF13, and 14BJ27) yield plateau release ages of 458 ± 3 Ma (97% of the ^{39}Ar), 436 ± 1 Ma (~75% cumulative ^{39}Ar release), and 473 ± 2 (~98% cumulative ^{39}Ar release), respectively (Fig. 2.8). The step-heating results from whole-rock chip sample (12JT24) shows significant scatter between heating steps, with a plateau release age of 418 ± 7 Ma constructed from four consecutive steps between ca. 420 and 421 Ma (~40% cumulative ^{39}Ar release) (Fig. 2.8). The ^{40}Ar/^{39}Ar single-grain fusion experiments on sample 14BJ27 produced a range of ages from 521 ± 5 Ma to 441 ± 2 Ma (Fig. 2.9). From this sample, we calculated a weighted mean age of 473 ± 2 Ma from five overlapping ages generated by four single-grain fusion ages and the integrated age (fusion age equivalent) from the step-heating experiments (Table 2.1).

DISCUSSION

The presence of Ordovician, Silurian, and Devonian zircon and muscovite from map units that were originally assigned to the Cambrian and Ordovician (e.g., Reiser et al., 1980) requires a reassessment of NE Brooks Range stratigraphy. Challenges associated with stratigraphic correlation across the Alaska-Yukon border in the NE Brooks Range have persisted because fossil localities are sparse and structural complexities disrupt the lateral continuity of major map units (e.g., Lane, 1991). In the following we incorporate our new radiometric ages to make inferences about the structural and stratigraphic architecture of the NE Brooks Range and then place our findings within the context of the early Paleozoic tectonic evolution of northern Laurentia.

Age and Provenance of the Neruokpuk Formation

As highlighted herein, the depositional age and depositional environment of the Neruokpuk Formation are still not well understood. At the most fundamental level, the sedimentological, petrological, and provenance characteristics are typical of a passive margin setting (e.g., Leffingwell, 1919; Reed, 1968; Dutro et al., 1972; Lerand, 1973; Lane, 1991; Lane et al., 2016); however, the structural complexity and unfossiliferous nature of these units impedes our current understanding of basin architecture, regional stratigraphic relationships, and correlations with age-equivalent units across the northern margin of Laurentia.

In addition to the new detrital zircon ages presented herein, abundant detrital zircon data are now available from coeval Neoproterozoic–middle Cambrian units in the NE Brooks Range (Fig. 2.10; Macdonald et al., 2009; Strauss et al., 2013; McClelland et al., 2015; Lane et al., 2016). We have compiled these data into five composite detrital zircon suites that represent distinct geographical localities. Suite 1 is compiled from samples dated by Macdonald et al. (2009) and Strauss et al. (2013). These were collected from sedimentary units that are exposed below Neoproterozoic–Ordovician carbonate platform rocks of the northern Sadlerochit Mountains (Fig. 2.2) and are thus older than the Neruokpuk Formation and possibly correlative to the Firth River group on the basis of age. Suite 2 is compiled from samples dated by Strauss et al. (2013) and this study (12JT31), which includes the mixed carbonate and siliciclastic strata of the Firth River group exposed in the northern British Mountains of Alaska (Aichilik River antiform). Suite 3 includes samples from the Neoproterozoic–middle Cambrian strata in the Barn Mountains of Yukon (McClelland et al., 2015), which are typically considered southeastern equivalents of the Neruokpuk Formation (e.g., Lane, 1991). Suite 4 represents the Neruokpuk Formation of the northern British Mountains and is constructed from one sample dated by

Strauss et al. (2013), three samples dated by Lane et al. (2016), and one sample from this study (12JT32). Suite 5 comprises the five samples dated in this study from the Neruokpuk Formation in the southern British Mountains of Alaska (Mount Greenough antiform).

The Neoproterozoic–middle Cambrian units as a whole contain populations of ca. 1200–1000, 1500–1300, 2000–1800, and 2800–2600 Ma zircon, but the relative abundances of individual populations, particularly the Mesoproterozoic populations, vary among the composite suites (Fig. 2.10). The zircon signatures from the Sadlerochit Mountains and the Firth River group have similar proportions of each of the major populations, but samples from the Sadlerochit Mountains contain a subpopulation of Neoproterozoic (ca. 980–760 Ma) grains that are not present in any of other composite suites of the NE Brooks Range. The composite Neruokpuk suite from the Barn Mountains also contains Mesoproterozoic populations, but these have slightly smaller proportions (Fig. 2.10B). The Neruokpuk units of the northern and southern British Mountains mostly lack the prominent Mesoproterozoic age populations and have nearly identical cumulative probability trends, indicating that detrital zircons from these two suites were likely shed from the same source region.

The proportional differences among the detrital zircon suites are likely an artifact of stratigraphic age. The samples from the northern Sadlerochit Mountains are stratigraphically below the ca. 720 Ma Kikiktat volcanics (Cox et al., 2015) and contain zircon grains as young as ca. 760 Ma, indicating that these units were deposited in the middle Cryogenian (Macdonald et al., 2009; Strauss et al., 2013). The Firth River group samples are typically assumed to be older than the units from the Neruokpuk Formation (e.g., Dutro et al., 1972; Reiser et al., 1980; Lane et al., 2016) and are possibly correlative with the units in the northern Sadlerochit Mountains (Macdonald et al., 2009; Strauss et al., 2013), indicating that they were likely deposited in the

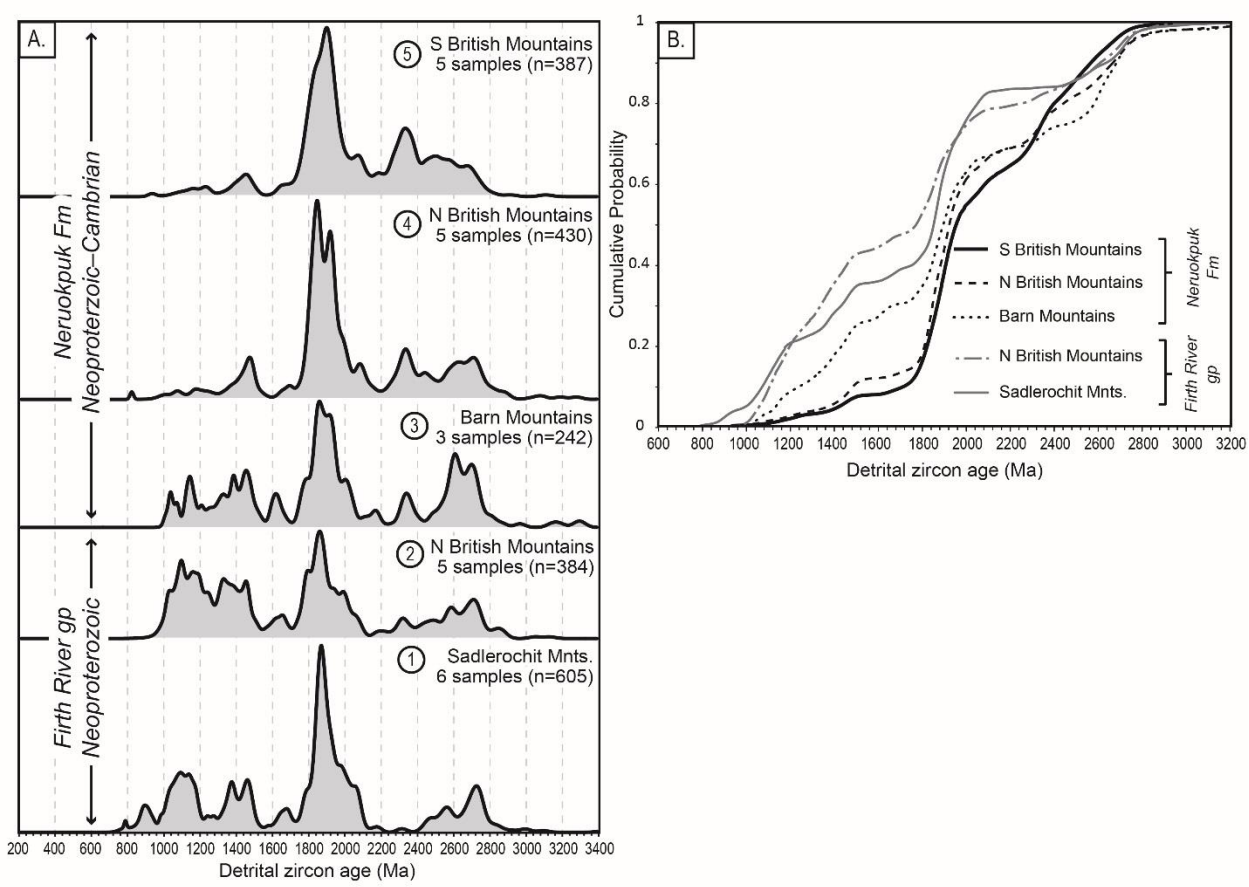

Figure 2.10: U-Pb detrital zircon ages from Neoproterozoic–Cambrian units throughout the northeastern Brooks Range. (A) Compared using normalized probability density plots. (B) Compared using cumulative probability plots. Data are from (1) Macdonald et al. (2009); (1, 2, and 4) Strauss et al. (2013); (3) McClelland et al. (2015); (4) Lane et al. (2016); (2, 4, and 5) this study. Fm—formation; gp—group.

Cryogenian or Ediacaran. The abundant populations of Mesoproterozoic zircon in these composite suites may have been sourced by recycling distal deposits of the Grenville foreland basin that blanketed much of the Laurentian continent in the Neoproterozoic (Rainbird et al., 1992, 1996, 2012). The Neruokpuk units of the northern and southern British Mountains may have been deposited later in the Ediacaran–middle Cambrian(?), by which time the Grenville foreland deposits had been extensively eroded from the source area, leaving mostly Paleoproterozoic and Archean crustal rocks exposed on the craton interior. The zircon signatures from the Barn Mountains could mark a transitional shift in the source region material, a slightly different age population, or a distinct drainage network separated from the one that fed the Neruokpuk units of the British Mountains.

Thick Neoproterozoic–Cambrian siliciclastic successions like the Neruokpuk Formation are widely distributed throughout northern Laurentia and constitute a period of prolific passive margin sedimentation following the breakup of the supercontinent Rodinia (e.g., Stewart, 1976; Bradley, 2008). Abundant detrital zircon studies have been conducted on these units, specifically from sedimentary successions of the surrounding basins of the Yukon block (Leslie, 2009; Hadlari et al., 2012; Lane and Gehrels, 2014; Gehrels and Pecha, 2014), the Canadian Arctic Islands (Anfinson et al., 2012; Hadlari et al., 2012, 2014; Beranek et al., 2013a; Malone et al., 2014), and northern Greenland (Kirkland et al., 2009; Morris et al., 2015). In all cases, like the units in the NE Brooks Range, variable proportions of Mesoproterozoic, Paleoproterozoic, and Archean zircon populations are observed. Nevertheless, recent studies (Lane et al., 2016) argue that zircon signatures from the Neruokpuk units share an affinity with age-equivalent units in northwest Laurentia, specifically the Cambrian strata of nearby Victoria Island (Hadlari et al., 2012). Alternatively, other studies (Strauss et al., 2013; McClelland et al., 2015) have noted that

the detrital zircon U-Pb signatures of the Neruokpuk Formation also closely match those from Ellesmere Island (Anfinson et al., 2012; Beranek et al., 2013a) and northern Greenland (Kirkland et al., 2009), indicating that paleogeographic correlation of the Neruokpuk Formation based solely on detrital zircon signatures is currently ambiguous.

The $^{40}Ar/^{39}Ar$ geochronology on muscovite can provide a complementary tool for assessing both the provenance and metamorphic and/or thermal conditions of sedimentary basins. Two of the Neruokpuk samples preserve their detrital Ar (Fig. 2.7). The dominant release from sample 37LF13 is ca. 2500 Ma, which overlaps with major thermomagmatic events from the Canadian shield (e.g., Bethune et al., 1999; Ernst and Bleeker, 2010). The complex age spectra in sample J1355–617 precludes any further interpretations, but it likely participated in multiple sedimentary cycles, undergoing various diagenetic and alteration events. Both of these samples were collected at the northern part of the field area, which suggests that sedimentary burial or the degree of pre-Mississippian deformation decreases northward.

The younger fractions released during the step-heating experiments may have also been influenced by partial degassing during Brookian tectonic and/or burial events. This was highlighted in one Neruokpuk sample in the northern British Mountains (Lane et al., 2016), where Ar loss as young as ca. 150 Ma was ascribed to the Jurassic to middle Cretaceous rifting and sedimentation associated with the opening of the Canada Basin. Much of this region is considered to have been unaffected by rifting events (Moore et al., 1994), so an alternative hypothesis is that rocks of the NE Brooks Range were significantly buried by the Late Cretaceous to Cenozoic foredeep deposits of the Brookian orogen. Color alteration of conodonts, vitrinite reflectance, and apatite fission track ages from Bathtub Ridge (Fig. 2.2) predict that the pre-Mississippian strata of the Mount Greenough antiform were buried below ~10 km of

sediment before being exhumed in the middle Cenozoic (O'Sullivan, 1994; Bird et al., 1999; Moore, 1999); however, an additional 4–7 km of overburden is needed to reach the ~425–400 °C muscovite closure temperature (assuming a normal geothermal gradient of ~30 °C/km). Therefore, given the significant releases of ^{39}Ar ca. 430 and 404 Ma, we ascribe most of the resetting and/or loss to a major Silurian–Early Devonian lowgrade metamorphic event that occurred during the Romanzof orogeny.

Age and Provenance of the Clarence River Group

As discussed here, the depositional age and stratigraphic architecture of the newly proposed Clarence River group remain unknown; however, it is clear from the regional stratigraphic architecture and from the U-Pb and ^{40}Ar/^{39}Ar data that these units not only overlie the older Neruokpuk Formation, but also record a prominent shift in provenance. A useful application of detrital zircon data is the ability to constrain the maximum depositional age of strata (Dickinson and Gehrels, 2009), especially where biostratigraphic constraints are limited (e.g., Kochelek et al., 2011); however, utilizing robust maximum depositional ages from the LA-ICP-MS data presented herein for the Clarence River group is difficult because of the large uncertainty (~4.5%) on many of the individual ages. Furthermore, determining the degree of discordance for grains generally younger than 700 Ma is challenging due to large uncertainties in the 207Pb/206Pb age, a common problem in most detrital zircon data sets (Nemchin and Cawood, 2005), and thus measurements compromised by Pb loss or inheritance cannot be ruled out. For these reasons, the most conservative estimate for the maximum depositional age from our LA-ICP-MS zircon ages is determined by using the center of the youngest graphical peak from the individual normalized probability distributions (Fig. 2.6).

Only one sample from the Clarence River group (12JT24) does not contain Paleozoic zircon, whereas the other four samples have maximum depositional peak ages that range between ca. 500 and 430 Ma (Fig. 2.6). Sample 12JT23 has the youngest graphical peak, ca. 430 Ma, and although this age is within the middle Wenlock (Gradstein et al., 2012), 19 single-grain ages have normal distributions centered in the Devonian (assuming each zircon age has a normal distribution using the age as the mean and uncertainty as the standard deviation). Despite this, clear clustering of the Devonian grains is not observed in the normalized probability distribution plot and there is no apparent trend in their U concentrations or U/Th ratios, suggesting that they simply represent the youngest ages from a continuous distribution that results from analytical uncertainty or Pb loss. This is also supported in the age distribution of sample 40LF13, where we combined LA-ICP-MS and SIMS techniques. The four overlapping SIMS ages yield a weighted mean age of 439 ± 3 Ma (Fig. 2.6), which nearly corresponds with the ca. 440 center of the youngest graphical peak in LAICP-MS age distribution, supporting the notion that these peaks conservatively represent maximum depositional ages.

Sample 12JT35 was collected from map unit Ovc of Reiser et al. (1980) in the Caribous Pass antiform (Fig. 2.2) of the northern British Mountains, and has a maximum depositional age of ca. 500 Ma (Furongian). This closely corresponds with the approximate age of the trilobite fossils from the Whale Mountain volcanic rocks and associated limestones in the Mount Greenough antiform (Dutro et al., 1972); this might imply that these volcaniclastic rocks were sourced from Whale Mountain allochthon.

The composite detrital zircon signature of the Clarence River group (Fig. 2.11) implies derivation from several different source areas. The subordinate Archean–Paleoproterozoic populations were likely derived from crystalline basement rocks of Laurentian craton and may

have been cycled through several sedimentary units prior to deposition. The early Neoproterozoic (ca. 990–820 Ma) age population of samples 12JT22 and 40LF13 is critical because original source regions within this age range are not widespread throughout Laurentia. Tonian magmatism is typically attributed to postorogenic collapse of the Grenville orogen, as recorded in the Central Gneiss Belt of Ontario, Canada (Ketchum et al., 1998), the East Greenland Caledonides (Kalsbeek et al. 2000; Watt et al., 2000), the Groswater Bay and Pinware terranes of eastern Labrador (Gower, 1996), and the Lewisian uplift in northwestern Scotland (Turnbull et al. 1996). Early Neoproterozoic magmatic rocks are also observed in the peri-Laurentian terranes of the northern Caledonides, including Pearya (e.g., Trettin, 1998) and the various terranes of Svalbard (e.g., Gee et al., 1995; Ohta et al., 2002; Johansson et al., 2004). These zircon grains may have also been recycled from older sedimentary units that contain prominent early Neoproterozoic populations, such as the late Neoproterozoic Succession II of Pearya (e.g., Malone et al., 2014) and the Eleonore Bay Supergroup of the East Greenland Caledonides (e.g., Watt et al., 2000).

Zircon from the ca. 470–420 Ma age population in the Clarence River group may have been sourced from magmatic rocks emplaced during the Caledonian-Appalachian orogeny, as similar U-Pb zircon ages are reported from magmatic rocks in the East Greenland Caledonides (e.g., Watt et al., 2000; Kalsbeek et al., 2001, 2008; Rehnström, 2010), Pearya (Trettin, 1987; McClelland et al., 2012), Svalbard (e.g., Johansson et al., 2004; Pettersson et al., 2009), New England and western Newfoundland (e.g., van Staal and Barr 2012, and references therein), and the northern British Isles (e.g., Oliver et al., 2008). Caledonian-age magmatism is also observed on various circum-Arctic terranes such as the Alexander terrane (Gehrels and Saleeby, 1987; Beranek et al., 2013b; White et al., 2016) and Klamath and Sierran terranes (Grove et al., 2008).

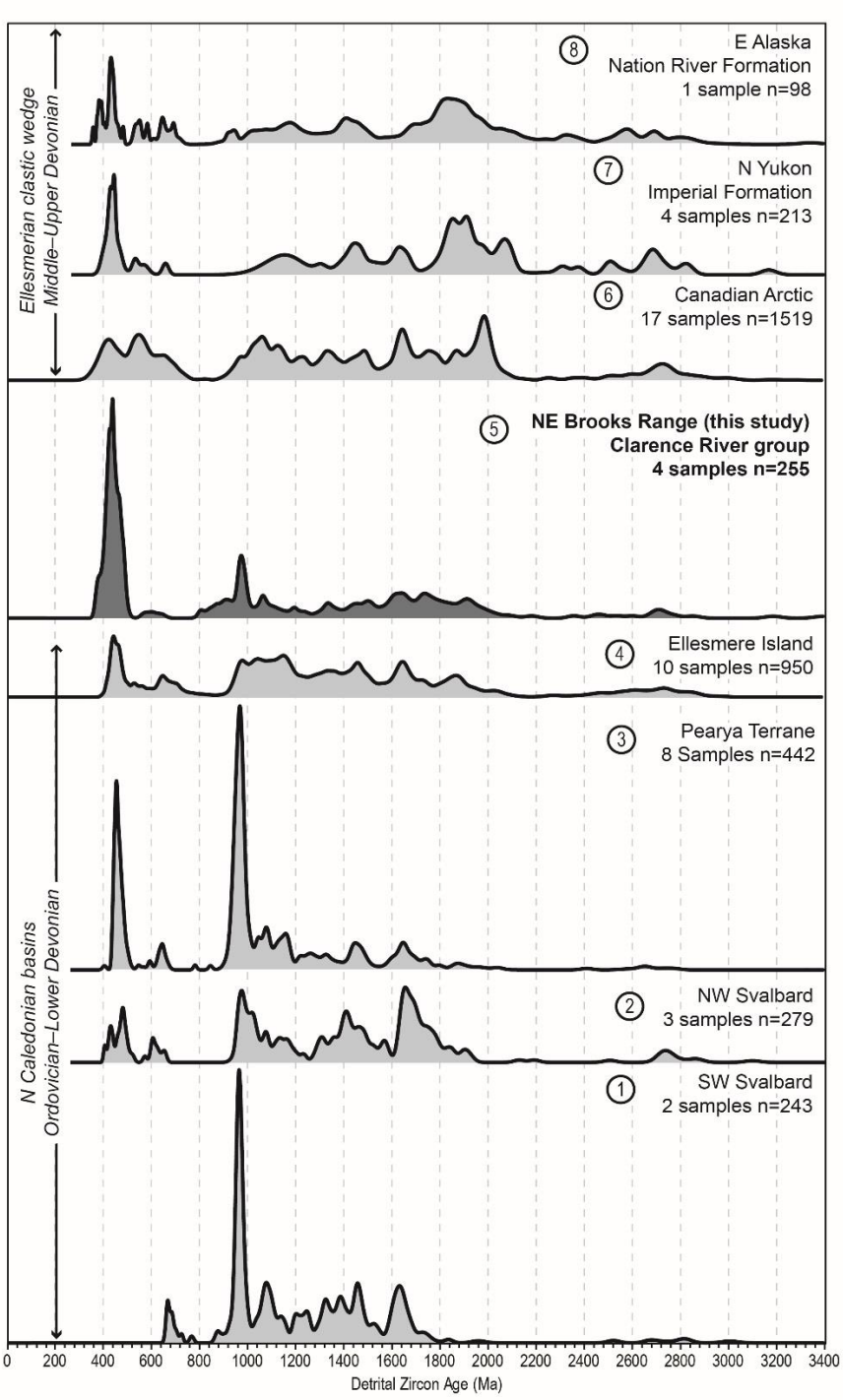

Figure 2.11: U-Pb detrital zircon ages from early Paleozoic sedimentary successions of northern Laurentia and associated Caledonian terranes, including: (1) southwestern Svalbard (Gasser and Andresen, 2013); (2) northwestern Svalbard (Pettersson et al., 2010); (3) Pearya terrane (Hadlari et al., 2014); (4) Ellesmere Island (Beranek et al., 2015); (5) northeastern Brooks Range (this study); (6) Ellesmerian clastic wedge in the Canadian Arctic Islands (Anfinson et al., 2012); (7) Ellesmerian clastic wedge in Yukon (Beranek et al., 2010); and (8) Ellesmerian clastic wedge in east-central Alaska (Gehrels and Pecha, 2014).

Note that magmatic rocks of this age group are rare in Arctic Alaska, although dredged samples of orthogneiss from the Chukchi Borderland (Fig. 2.1) yield U-Pb ages of ca. 430 Ma (Brumley et al., 2015) and volcanic rocks exposed in the Doonerak fenster of the central Brooks Range (Fig. 2.1B) have ages that range from ca. 470 to 370 Ma (Dutro et al., 1976). Because biostratigraphic constraints are limited for the samples dated in this study, we cannot exclude the possibility that this age population was recycled from an older sedimentary source; however, the compositional and textural immaturities of the Clarence River group samples, especially the presence of volcanic rock fragments and euhedral feldspar grains, imply direct sourcing from primary volcanic material.

The $^{40}Ar/^{39}Ar$ muscovite ages from the Clarence River group overlap with the prominent ca. 470–420 Ma detrital zircon population. Like the muscovite extracted from the Neruokpuk samples, we interpret the Clarence River group muscovite as detrital in origin because it is typically coarse grained, has a strong petrologic contrast with the surrounding clay matrix, and is commonly disaggregated into single sheets. Three of four samples analyzed yield robust weighted plateau ages (Fig. 2.8; Table 2.1) that reflect the highly retentive nature of coarse detrital grains. Therefore, we interpret these $^{40}Ar/^{39}Ar$ muscovite ages as records of the timing of cooling and/or crystallization of the respective source regions.

The 436 ± 1 Ma $^{40}Ar/^{39}Ar$ muscovite age of sample 40LF13 (Fig. 2.8) is within error of the 439 ± 3 Ma weighted-mean age calculated from the cluster of four U-Pb zircon ages (Fig. 2.6). Possible source regions for this detritus are nonexistent along the northwest margin of Laurentia, but are widely exposed in the East Greenland Caledonides, which host ca. 440–430 Ma muscoviterich, postorogenic S-type granites (Kalsbeek et al., 2001). This, along with the textural and compositional immaturities of the samples, implies that the Clarence River group

was deposited in proximity to the Caledonides during the collision between Baltica and Laurentia. The other plateau ages of ca. 473 and 458 Ma are significantly older than the S-type granites in the East Greenland Caledonides and were likely sourced from magmatic or metamorphic rocks that formed in the early phases of the Caledonian-Appalachian orogeny. A similar age distribution is recorded in southwestern Wales (UK), where detrital muscovite ages from the lower Silurian Old Red Sandstone record exhumation of the Northern and Central Highlands of Scotland during the Early–Middle Ordovician Grampian orogeny (Sherlock et al., 2002).

Unlike the other Clarence River group samples, sample 12JT24 has an irregular, staircaseshaped age spectrum (Fig. 2.8). The complex nature of this spectrum is likely a response to analyzing a fine aggregate of multiple grains in a single step-heating experiment (i.e., whole-rock analysis). The sample was most likely perturbed by a low-grade metamorphic event ca. 418 Ma, possibly in relation to the Romanzof orogeny. It is also possible that the sample contains newly formed (authigenic) muscovite that grew via the alteration of other fine-grained clay minerals like illite or kaolinite; this is a common process that occurs in the formation of low-grade metamorphic rocks (e.g., Hunziker et al., 1986; Verdel et al., 2012).

Paleogeography of the North Slope

The contact between the Neruokpuk Formation and Clarence River group marks a major shift in the dispersal of sediment in northern Laurentia. We postulate that this fundamental shift in provenance is linked to the closure of the northern tract of the Iapetus Ocean and the onset of the Caledonian orogeny. In this scenario, detritus was funneled from uplifted source regions in the East Greenland Caledonides, Pearya, Svalbard, and other circum-Arctic terranes, and transported axially along the Franklinian margin before filling the pre-Mississippian basin of the

North Slope (Fig. 2.12). A similar scenario is inferred from age-equivalent strata in the Clements Markham and Hazen fold belts of northern Ellesmere Island, which is supported by paleocurrent trends (Trettin, 1994, 1998), regional shifts in Nd isotopic values (Patchett et al., 1999), and detrital zircon studies (Anfinson et al., 2012; Hadlari et al., 2014; Beranek et al., 2015). Although the exact paleogeographic position of the North Slope with respect to northern Ellesmere Island and the Caledonian orogen is uncertain, the composite detrital zircon signature for the Clarence River group (Fig. 2.11) is remarkably similar to Silurian flysch deposits (e.g., Fire Bay, Lands Lokk, and Danish River formations) of Ellesmere Island (Beranek et al., 2015) and age-equivalent units in Pearya (Hadlari et al., 2014). In addition, the compositional and textural immaturity of the Clarence River group sandstone samples highlights proximity to the source region. These observations provide support for recent paleogeographic interpretations that restore the North Slope to northeast Laurentia in the early Paleozoic (e.g., Strauss et al., 2013; Malone et al., 2014; Cox et al., 2015).

An alternative scenario fixes the North Slope to northwest Laurentia throughout the Paleozoic (e.g., Lerand, 1973; Lane, 1991, 2007; Moore et al., 1994; Rainbird et al., 1996; Cecile et al., 1999; Lane et al., 2016). In this model, synorogenic detritus of the Clarence River group may have arrived by long-distance transport from the Caledonides or from the localized collision of an allochthonous terrane or terranes with the northwest Laurentian margin; the latter is the interpretation of Lane (2007) and Lane et al. (2016), who drew correlations between portions of the Clarence River group (i.e., the Buckland Hills succession) and the upper Devonian Imperial Formation of northern Yukon. The Imperial Formation was deposited in the Ellesmerian clastic wedge (Beranek et al., 2010; Lemieux et al., 2011), which blanketed much of the Canadian Arctic and northwest Laurentian margin during the Late Devonian and Early Mississippian.

Although the Ellesmerian clastic wedge units are lithologically similar and have comparable detrital zircon (e.g., Beranek et al., 2010; Anfinson et al., 2012; Gehrels and Pecha, 2014) and muscovite ages (Powell and Schneider, 2013), the deposition of the Clarence River group predates Ellesmerian clastic wedge sedimentation, as it was deformed in the Early–Middle Devonian Romanzof event (Anderson et al., 1994; Lane, 2007; Lane et al., 2016). Furthermore, the Clarence River group is crosscut by regional Late Devonian plutonic rocks, which are thought to be a principal source of detritus in Ellesmerian Clastic wedge units (Beranek et al., 2010; Anfinson et al., 2012).

Positioning the North Slope near northeast Laurentia in the Silurian–Early Devonian (Fig. 2.12) requires >1000 km of left-lateral displacement along the Franklinian margin of Arctic Canada prior to the Late Devonian–Early Mississippian to achieve a hypothesized pre–Canada Basin paleogeographic configuration (e.g., Gottlieb et al., 2014; Houseknecht and Connors, 2016). In this scenario, the Romanzof orogeny may represent a major transpressional event that occurred along strike with similar deformation associated with the docking of Pearya against the northeast margin of Laurentia (Trettin, 1998, and references therein). A strike-slip orogen along the northern margin of Laurentia in the early Paleozoic is favored by a number of paleogeographic models for the Arctic (e.g., Sweeney, 1982; Oldow et al., 1987; Colpron and Nelson, 2011), and previous studies in the NE Brooks Range have postulated strike-slip displacement along the Kaltag-Porcupine-Rapid fault array in severing stratigraphic ties between the NE Brooks Range and northwest Laurentia (Oldow et al., 1987; Norris, 1997; Strauss et al., 2013; von Gosen et al., 2015).

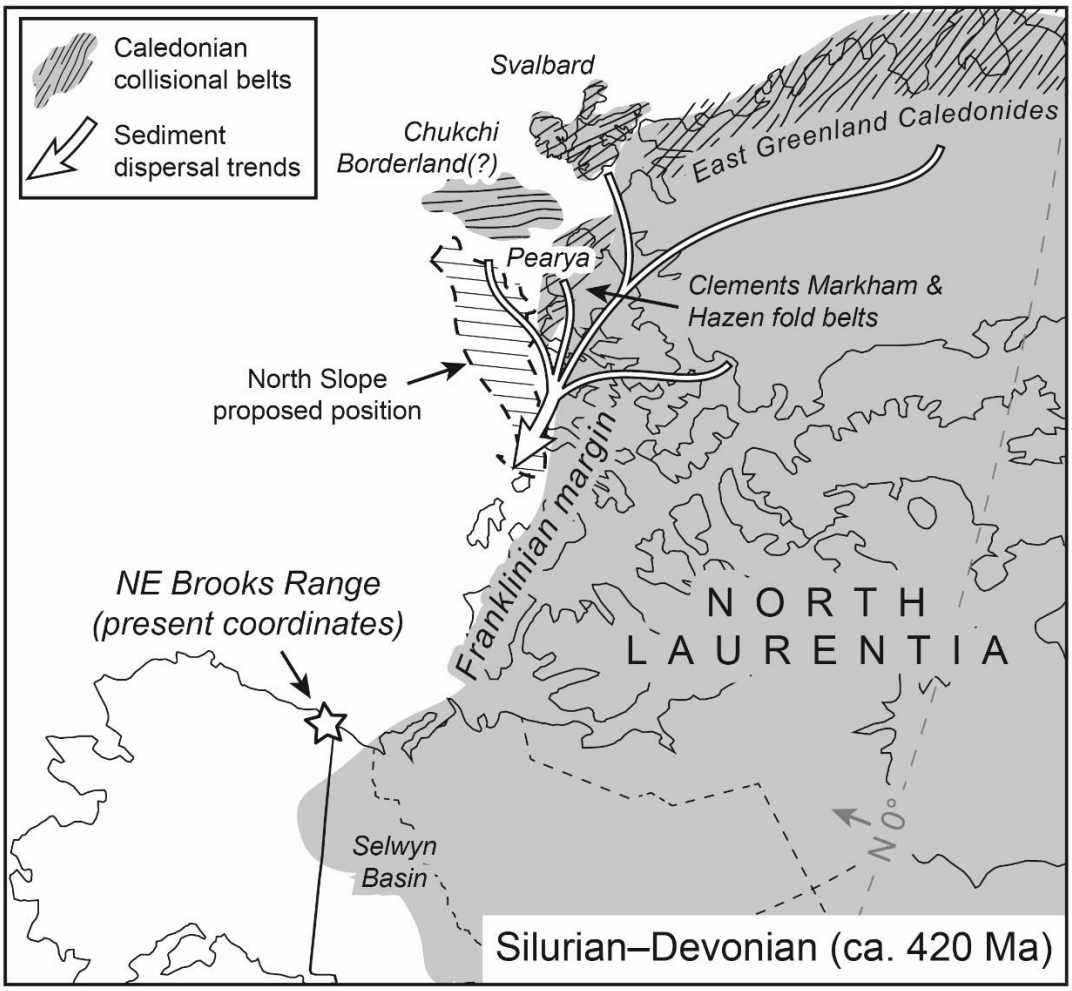

Figure 2.12: Paleogeographic position of terranes and sediment dispersal pathways along northern Laurentia during deposition of the Clarence River group (see text for discussion). Reconstruction is based on Trettin (1987, 1998), Patchett et al. (1999), McClelland et al. (2012), Gasser and Andresen (2013), Pettersson et al. (2010), Colpron and Nelson (2011), Anfinson et al. (2012), and Beranek et al. (2015). NE—northeastern.

Origin and Emplacement of the Whale Mountain Allochthon

The basic premise of the Whale Mountain allochthon model is that a structural complex composed of massive basalt flows, radiolarian chert, and limestone was emplaced onto the pre-Mississippian sedimentary units of the North Slope in the form of a single thrust sheet. Although previously researchers have interpreted the volcanic rocks as being in stratigraphic continuity with the other pre-Mississippian units (e.g., Dutro et al., 1972; Reiser et al., 1980; Lane, 1991; Lane et al., 2016), we observed the Clarence River group positioned below the volcanic rocks in almost all cases throughout the NE Brooks Range, indicating a major disruption in the stratigraphic sequence.

In the Mount Greenough antiform (Fig. 2.2), the volcanic rocks are juxtaposed above Clarence River group units by a low-angle thrust fault that was folded into a synform (Fig. 2.4). The age of this structure is unknown; however, along strike the thrust appears to juxtapose the volcanic rocks with the Lisburne Group of the Ellesmerian sequence (Reiser et al., 1980), indicating that some amount of Brookian displacement has occurred along the fault. If all of the displacement was a result of Brookian contraction, then shortening estimates across the NE Brooks Range are significantly underestimated. For example, an additional duplex or thrust panel would be required to retrodeform the Mount Greenough fault-bend fold in the model of Moore (1999) because it does not address the stratigraphic disruption observed between the Clarence River group and the overlying Whale Mountain volcanic rocks.

Alternatively, the emplacement of the Whale Mountain allochthon could have occurred in the Early–Middle Devonian Romanzof orogeny with subsequent reactivation during Brookian shortening. Lane (2007) interpreted the Romanzof orogen as a southward-verging (present coordinates) fold-thrust belt based largely on the lack of deformation in the Yukon block further

to the south. The northward dips of the structural fabrics and apparent south-directed imbrications of the stratigraphy across the Mount Greenough antiform (Fig. 2.4) both favor a south-vergent model. Conversely, the metamorphic gradient and the intensity of deformation appear to decrease in the northern British Mountains (Sable, 1977), and the pre-Mississippian deformation in the Aichilik River antiform appears to be north vergent along the Aichilik River (Hanks, 1989). These north to south discrepancies in structural style could be the result of the juxtaposition of different pre-Mississippian structural domains along east-west–trending strike-slip faults, supporting the notion that the Romanzof orogeny had a significant transpressional component. However, the relationships between the structural styles of the sedimentary units with those of the Whale Mountain allochthon are obscured by the strong contrast in mechanical competence of the rocks.

A multitude of paleogeographic scenarios are possible for emplacement of the Whale Mountain allochthon and the associated the Romanzof orogeny. We postulate that it occurred (1) from the accretion of an outboard terrane, possibly the southern subterranes of Arctic Alaska, (2) as the North Slope translated along the northern margin of Laurentia, or (3) some combination of both. Nevertheless, several outstanding challenges to the allochthon model remain. First, the source of the thrust sheet is unknown, largely because the fault that separates Whale Mountain allochthon from the Clarence River group is kinematically unconstrained. We prefer a northdirected sense of emplacement that restores the allochthon along a south-dipping thrust sheet to the Romanzof Mountain thrust exposed at the headwaters of the Jago River (RMT; Fig. 2.2). A second challenge is that the tectonic and/or depositional setting of the Whale Mountain allochthon can be interpreted in several ways from the available data. The geochemical signatures of the volcanic rocks are indicative of derivation from sublithospheric mantle (Moore,

1987; Goodfellow et al., 1995), which is typical for most basalts erupted in oceanic settings (e.g., Pearce, 2008), but continental flood basalts also have similar geochemical signatures (e.g., McKenzie and Bickle, 1988; Gallagher and Hawkesworth, 1992). It is important that these volcanic rocks are intimately associated with thick packages of radiolarian chert, slate and phyllite, and occasional lithic wacke of the Romanzof chert (Moore and Churkin, 1984; Mull and Anderson, 1991); this lends support to a deep marine origin. The structural and stratigraphic relationships of the volcaniclastic rocks exposed in the northern British Mountains, where sample 12JT35 was collected, may contradict the allochthon model. Detailed mapping by Kelley et al. (1994) placed these volcaniclastic rocks in stratigraphic continuity with Clarence River group, and suggested correlation with Whale Mountain volcanic rocks in the Mount Greenough antiform. However, outcrop exposure in northern British Mountains is relatively poor, and a scenario where these volcaniclastic rocks were deposited by reworking the Whale Mountain volcanic rocks and then subsequently imbricated with the Clarence River group units should not be eliminated from possible interpretations.

The Whale Mountain volcanic rocks are comparable to the continental flood basalts of the Selwyn basin on the basis of age (Leslie, 2009; MacNaughton et al., 2016) and geochemistry (Goodfellow et al., 1995), and correlation between the two volcanic suites is a critical component in models that prefer a fixed position of the North Slope with respect to northwest Laurentia (e.g., Lane et al., 2016). An allochthonous relationship between the Whale Mountain volcanic rocks and the pre-Mississippian sedimentary rocks of the North Slope permits the hybridization of the various paleogeographic models. For example, the paleogeographic model favored in this study (Fig. 2.12), with the North Slope originating near northeast Laurentia and translating along the Franklinian margin, could suggest that the Whale Mountain volcanic rocks erupted into an

oceanward extension of the Selwyn basin and were subsequently assembled with rest of the North Slope by strike-slip juxtapositioning. Alternatively, the rocks of the Whale Mountain allochthon could be correlative to similar-aged volcanic rocks at northern Ellesmere, implying that the emplacement could have happened closer to the main Caledonian collisional belt. Either interpretation is permissible if the allochthon model is considered.

CONCLUSIONS

The U-Pb and $^{40}Ar/^{39}Ar$ isotopic analysis on detrital minerals from 18 samples of pre-Mississippian strata in the NE Brooks Range of Alaska provide new constraints on the structural and stratigraphic architecture of the Arctic Alaska terrane. Two major sedimentary successions are now recognized in the British and Romanzof Mountains of Alaska: a Neoproterozoic–Cambrian passive margin succession that includes the Firth River group and the Neruokpuk Formation, and the newly identified Lower Ordovician–Lower Devonian Clarence River group. In addition to these sedimentary units, a late Cambrian–Ordovician structural complex composed of massive basalt flows, radiolarian chert, and limestone, herein named the Whale Mountain allochthon, is structurally juxtaposed with the underlying Clarence River group. When compared with the ages of igneous and metamorphic rocks in Laurentia and other circum-Arctic regions, the new detrital geochronological data presented herein shed light on the origin and dispersal of siliciclastic material along the northern margin of Laurentia throughout the Neoproterozoic and early Paleozoic. Specifically, detritus of Firth River group and Neruokpuk Formation was ultimately derived from Archean and Paleoproterozoic basement rocks in Canadian shield and possibly older sedimentary units of the Grenville foreland basin. The Clarence River group was most likely sourced from igneous and metamorphic rocks of Caledonian orogenic belt of northeast Laurentia.

The pre-Mississippian rocks of the NE Brooks Range were subsequently deformed and underwent low-grade metamorphism during the ill-defined Early–Middle Devonian Romanzof orogeny, which was closely associated with the emplacement of the Whale Mountain allochthon. How this event relates to the greater paleogeography of northern Laurentia and the circum-Arctic is unresolved, but future plate reconstructions should consider the possibility that the North Slope was positioned near northeast Laurentia during the closure of the Iapetus Ocean and Caledonian-Appalachian orogeny.

ACKNOWLEDGMENTS

Johnson and Toro thank West Virginia University's Faculty Senate Grant and the Circum-Arctic Lithosphere Evolution (CALE) project for providing financial support. Strauss thanks Francis Macdonald and the Department of Earth Sciences at Dartmouth College for support. Geological Society of America graduate student research fellowships also supplied additional funding to Johnson, Strauss, and Ward. We thank Blaze Budd, Patrick Frier, and Lyle Nelson for assistance in the field. Kirk Sweetsir from Yukon Air Service and the staff at Wright Air Service provided critical access to our remote field area. Permission to work in the Arctic National Wildlife Refuge was granted by Alfredo Soto at the United States Fish and Wildlife Service. Many of the ideas presented herein were conceived during discussions with Gil Mull, Bill McClelland, Francis Macdonald, Marwan Wartes, Elizabeth Miller, Victoria Pease, Eric Gottlieb, Carl Hoiland, and Tim O'Brien. The thoughtful and constructive reviews from Maurice Colpron, Tom Moore, and an anonymous reviewer greatly improved this manuscript.

REFERENCES CITED

Amato, J.M., Toro, J., Miller, E.L., Gehrels, G.E., Farmer, G.L., Gottlieb, E.S., and Till, A.B., 2009, Late Proterozoic–Paleozoic evolution of the Arctic Alaska-Chukotka terrane based

on U-Pb igneous and detrital zircon ages: Implications for Neoproterozoic paleogeographic reconstructions: Geological Society of America Bulletin, v. 121, p. 1219–1235, doi: 10.1130/B26510.1.

Amato, J.M., Toro, J., Akinin, V.V., Hampton, B.A., Salnikov, A.S., and Tuchkova, M.I., 2015, Tectonic evolution of the Mesozoic South Anyui suture zone, eastern Russia: A critical component of paleogeographic reconstructions of the Arctic region: Geosphere, v. 11, p. 1530–1564, doi: 10.1130/GES01165.1.

Anderson, A.V., Wallace, W.K., and Mull, C.G., 1994, Depositional record of a major tectonic transition in northern Alaska: Middle Devonian to Mississippian rift-basin margin deposits, upper Kongakut River region, eastern Brooks Range, Alaska, *in* Thurston, D.K., and Fujita, K., eds., 1992 Proceedings, International Conference on Arctic Margins: U.S. Department of the Interior Minerals Management Service, OCS (Outer Continental Shelf) Study MMS 94–0040, p. 71–76.

Anfinson, O.A., Leier, A.L., Embry, A.F., and Dewing, K., 2012, Detrital zircon geochronology and provenance of the Neoproterozoic to Late Devonian Franklinian Basin, Canadian Arctic Islands: Geological Society of America Bulletin, v. 124, p. 415–430, doi: 10.1130/B30503.1.

Beranek, L.P., Mortensen, J.K., Lane, L.S., Allen, T.L., Fraser, T.A., Hadlari, T., and Zantvoort, W.G., 2010, Detrital zircon geochronology of the western Ellesmerian clastic wedge, northwestern Canada: Insights on Arctic tectonics and the evolution of the northern Cordilleran miogeocline: Geological Society of America Bulletin, v. 122, no. 11, p. 1899–1911, doi: 10.1130/B30120.1.

Beranek, L.P., Pease, V.L., Scott, R.A, and Thomsen, T.B., 2013a, Detrital zircon geochronology of Ediacaran to Cambrian deep-water strata of the Franklinian basin, northern Ellesmere Island, Nunavut: Implications for regional stratigraphic correlations: Canadian Journal of Earth Sciences, v. 50, p. 1007–1018, doi: 10.1139/cjes-2013-0026.

Beranek, L.P., van Staal, C.R., McClelland, W.C., Israel, S., and Mihalynuk, M.G., 2013b, Baltican crustal provenance for Cambrian–Ordovician sandstones of the Alexander terrane, North American Cordillera: Evidence from detrital zircon U-Pb geochronology and Hf isotope geochemistry: Journal of the Geological Society [London], v. 170, p. 7–18, doi: 10.1144/jgs2012-028.

Beranek, L.P., Pease, V.L., Hadlari, T., and Dewing, K., 2015, Silurian flysch successions of Ellesmere Island, Arctic Canada, and their significance to northern Caledonian palaeogeography and tectonics: Journal of the Geological Society [London], v. 172, p. 201–212, doi: 10.1144/jgs2014-027.

Bethune, K.M., Villeneuve, M.E., and Bleeker, W., 1999, Laser $^{40}Ar/^{39}Ar$ thermochronology of Archean rocks in Yellowknife Domain, southwestern Slave Province: Insights into the cooling history of an Archean granite-greenstone terrane: Canadian Journal of Earth Sciences, v. 36, p. 1189– 206, doi: 10.1139/e99-006.

Bird, K.J., Burruss, R.C., and Pawlewicz, M.J., 1999, Thermal maturity, *in* ANWR Assessment Team, The oil and gas resource potential of the 1002 area, Arctic National Wildlife Refuge, Alaska: U.S. Geological Survey Open-File Report 98-34, Chapter VR, http://pubs.usgs.gov/of/1998/ofr-98-0034/VR.pdf64p.

Bradley, D.C., 2008, Passive margins through earth history: Earth-Science Reviews, v. 91, p. 1–26, doi: 10.1016 /j.earscirev.2008.08.001.

Brumley, K., Miller, E.L., Konstantinou, A., Grove, M., Meisling, K.E., and Mayer, L.A., 2015, First bedrock samples dredged from submarine outcrops in the Chukchi Borderland, Arctic Ocean: Geosphere, v. 11, p. 76–92, doi: 10.1130/GES01044.1.

Cecile, M.P., 1988, Corridor traverse through Barn Mountains, northernmost Yukon, *in* Current research part D: Interior plains and Arctic Canada: Geological Survey of Canada Paper 88–1D, p. 99–103.

Cecile, M.P. and Lane, L.S., 1991, Geology of the Barn uplift, northern Yukon: Geological Survey of Canada, Open File Map 2342, scale 1:50,000.

Cecile, M.P., Lane, L.S., Khudoley, A.K., and Kos'ko, M.K., 1999, Lower Paleozoic rocks around today's Arctic Ocean: Two ancestral continents and associated plates; Alaskan rotation unnecessary and unlikely: Polarforschung, v. 69, p. 235–241.

Cocks, L.R.M., and Torsvik, T.H., 2011, The Palaeozoic geography of Laurentia and western Laurussia: A stable craton with mobile margins: Earth-Science Reviews, v. 106, p. 1–51, doi:10.1016 /j.earscirev.2011.01.007.

Cole, F., Bird, K.J., Mull, C.G., Wallace, W.K., Sassi, W., Murphy, J.M., and Lee, M., 1999, A balanced cross section and kinematic and thermal model across the northeastern Brooks Range mountain front, Arctic National Wildlife Refuge, Alaska, *in* ANWR Assessment Team, The oil and gas resource potential of the 1002 area, Arctic National Wildlife Refuge, Alaska: U.S. Geological Survey Open-File Report 98-34, p. 60.

Colpron, M., and Nelson, J.L., 2011, A Palaeozoic NW Passage and the Timanian, Caledonian and Uralian connections of some exotic terranes in the North American Cordillera, *in* Spencer, A.M., et al., eds., Arctic petroleum geology: Geological Society, London, Memoir 35, p. 463–484, doi: 10.1144/M35.31.

Coney, P.J., Jones, D.L., and Monger, J.W.H., 1980, Cordilleran suspect terranes: Nature, v. 288, p. 329–333, doi: 10.1038/288329a0.

Cox, G.M., Strauss, J.V., Halverson, G.P., Schmitz, M.D., McClelland, W.C., Stevenson, R.S., and Macdonald, F.A., 2015, Kikiktat volcanics of Arctic Alaska—Melting of harzburgitic mantle associated with the Franklin large igneous province: Lithosphere, v. 7, p. 275–295, doi: 10 .1130 /L435 .1.

Dewey, J.F., and Horsfield, B., 1970, Plate tectonics, orogeny and continental growth: Nature, v. 225, p. 521–525, doi:10 .1038 /225521a0.

Dickinson, W.R., and Gehrels, G.E., 2009, Use of U-Pb ages of detrital zircons to infer maximum depositional ages of strata: A test against a Colorado Plateau Mesozoic database: Earth and Planetary Science Letters, v. 288, p. 115–125, doi:10.1016/j.epsl.2009.09.013.

Dillon, J.T., Tilton, G.R., Decker, J., and Kelley, M.J., 1987, Resource implications of magmatic and metamorphic ages for Devonian igneous rocks in the Brooks Range, *in* Tailleur, I.L., and Weimer, P., eds., Alaskan North Slope geology: Pacific Section, Society of Economic Paleontologists and Mineralogists Book 50, p. 713–723.

Dumoulin, J.A., Harris, A.G., Bradley, D.C., and De Freitas, T.A., 2000, Facies patterns and conodont biogeography in Arctic Alaska and the Canadian Arctic Islands: Evidence against juxtaposition of these areas during early Paleozoic time: Polarforschung, v. 68, p. 257–266.

Dutro, J.T., Jr., Brosgé, W.P., and Reiser, H.N., 1972, Significance of recently discovered Cambrian fossils and reinterpretation of Neruokpuk Formation, northeastern Alaska: American Association of Petroleum Geologists Bulletin, v. 56, p. 808–815.

Dutro, J.T., Jr., Brosgé, W.P., Lanphere, M.A., and Reiser, H.N., 1976, Geologic significance of Doonerak structural high, central Brooks Range, Alaska: American Association of Petroleum Geologists Bulletin, v. 60, p. 952–961.

Ernst, R., and Bleeker, W., 2010, Large igneous provinces (LIPs), giant dyke swarms, and mantle plumes: Significance for breakup events within Canada and adjacent regions from 2.5 Ga to the present: Canadian Journal of Earth Sciences, v. 47, p. 695–739, doi: 10.1139/E10-025.

Gallagher, K., and Hawkesworth, C., 1992, Dehydration melting and the generation of continental flood basalts: Nature, v. 358, p. 57–59, doi: 10.1038/358057a0.

Gasser, D., and Anderson, A., 2013, Caledonian terrane amalgamation of Svalbard: Detrital zircon provenance of Mesoproterozoic to Carboniferous strata from Oscar II Land, western Spitsbergen: Geological Magazine, v. 150, p. 1103–1126, doi: 10.1017 /S0016756813000174.

Gee, D.G., Johansson, Å., Ohta, Y., Tebenkov, A.M., Krasil'schikov, A.A., Balashov, Y.A., Larionov, A.N., Gannibal, L.F., and Ryungenen, G.I., 1995, Grenvillian basement and a major unconformity within the Caledonides of Nordaustlandet, Svalbard: Precambrian Research, v. 70, p. 215–234, doi: 10 .1016 /0301 -9268 (94)00041 -O.

Krasil'schikov, A.A., Balashov, Y.A., Larionov, A.N., Gannibal, L.F., and Ryungenen, G.I., 1995, Grenvillian basement and a major unconformity within the Caledonides of Nordaustlandet, Svalbard: Precambrian Research, v. 70, p. 215–234, doi: 10.1016/0301-9268(94)00041-O.

Gehrels, G.E., and Pecha, M., 2014, Detrital zircon U-Pb geochronology and Hf isotope geochemistry of Paleozoic and Triassic passive margin strata of western North America: Geosphere, v. 10, p. 49–65, doi: 10.1130/GES00889.1.

Gehrels, G.E., and Saleeby, J.B., 1987, Geologic framework, tectonic evolution, and displacement history of the Alexander Terrane: Tectonics, v. 6, no. 2, p. 151, doi: 10.1029/TC006i002p00151.

Goodfellow, W.D., Cecile, M.P., and Leybourne, M.I., 1995, Geochemistry, petrogenesis, and tectonic setting of lower Paleozoic alkalic and potassic volcanic rocks, northern Canadian Cordilleran miogeocline: Canadian Journal of Earth Sciences, v. 32, p. 2167, doi: 10.1139/e95-169.

Gordey, S.P., and Anderson, R.G., 1993, Evolution of the northern Cordilleran miogeocline, Nahanni map area (105-I), Yukon and Northwest Territories: Geological Survey of Canada Memoir 428, 214 p.

Gottlieb, E.S., Meisling, K.E., Miller, E.L., and Mull, C.G., 2014, Closing the Canada Basin: Detrital zircon geochronology relationships between the North Slope of Arctic Alaska and the Franklinian mobile belt of Arctic Canada: Geosphere, v. 10, p. 1366–1384, doi: 10.1130/GES01027.1.

Gower, C.F., 1996, The evolution of the Grenville Province in eastern Labrador, Canada, *in* Brewer, T.S., ed., Precambrian crustal evolution in the North Atlantic region: Geological Society, London, Special Publication 112, p. 197–218, doi: 10.1144/GSL.SP.1996.112.01.11.

Gradstein, F.M., Ogg, J.G., Smith, A.G., and Ogg, G., 2012, The geologic time scale 2012: Boston, Elsevier, 1176 p.

Grantz, A., Hart, P.E., and Childers, V.A., 2011, Geology and tectonic development of the Amerasia and Canada Basins, Arctic Ocean, *in* Spencer, A.M., et al., eds., Arctic petroleum geology: Geological Society, London, Memoir 35, p. 771–799, doi: 10.1144/M35.50.

Grove, M.J., Gehrels, G.E., Cotkin, S.J., Wright, J.E., and Zou, H., 2008, Non-Laurentian cratonal provenance of Late Ordovician eastern Klamath blueschists and a link to the Alexander terrane, *in* Wright, J.E., and Shervais, J.W., eds., Ophiolites, arcs, and batholiths: A tribute to Cliff Hopson: Geological Society of America Special Paper 438, p. 223–250, doi: 10.1130/2008.2438(08).

Hadlari, T., Davis, W.J., Dewing, K., Heaman, L.M., Lemieux, Y., Ootes, L., Pratt, B.R., and Pyle, L.J., 2012, Two detrital zircon signatures for the Cambrian passive margin of northern Laurentia highlighted by new U-Pb results from northern Canada: Geological Society of America Bulletin, v. 124, p. 1155–1168, doi: 10.1130/B30530.1.

Hadlari, T., Davis, W.J., and Dewing, K., 2014, A pericratonic model for the Pearya terrane as an extension of the Franklinian margin of Laurentia, Canadian Arctic: Geological Society of America Bulletin, v. 126, p. 182–200, doi: 10.1130/B30843.1.

Hames, W.E., and Cheney, J.T., 1997, On the loss of ^{40}Ar* from muscovite during polymetamorphism: Geochimica et Cosmochimica Acta, v. 61, p. 3863–3872, doi: 10.1016/S0016-7037(97)00207-X.

Hanks, C.L., 1989, Balanced cross sections of the Aichilik River and Okpilak Batholith regions, northeastern Brooks Range, Alaska: Alaska Division of Geological & Geophysical Surveys Public Data File 90-2A, 18 p., 2 sheets, scale 1:125,000, doi: 10.14509/1434.

Hanks, C.L., 1993, The Cenozoic structural evolution of a fold-and-thrust belt, northeastern Brooks Range, Alaska: Geological Society of America Bulletin, v. 105, p. 287–305, doi: 10.1130/0016-7606(1993)105<0287:TCSEOA>2.3.CO;2.

Harrison, T.M., Célérier, J., Aikman, A.B., Hermann, J., and Heizler, M.T., 2009, Diffusion of ^{40}Ar in muscovite: Geochimica et Cosmochimica Acta, v. 73, p. 1039–1051, doi: 10.1016/j.gca.2008.09.038.

Hofmann, H.J., and Cecile, M.P., 1981, Occurrence of Oldhamia and other trace fossils in Lower Cambrian(?) argillites, Niddery Lake map area, Selwyn Mountains, Yukon Territory, *in* Current research, Part A: Geological Survey of Canada Paper 81-1A, p. 281–289.

Hofmann, H.J., Cecile, M.P., and Lane, L.S., 1994, New occurrences of Oldhamia and other trace fossils in the Cambrian of the Yukon and Ellesmere Island, arctic Canada: Canadian Journal of Earth Sciences, v. 31, p. 767–782, doi: 10.1139/e94-070.

Houseknecht, D.W., and Connors, C.D., 2016, Pre-Mississippian tectonic affinity across the Canada Basin–Arctic margins of Alaska and Canada: Geology, v. 44, p. 507–510, doi: 10.1130/G37862.1.

Hubbard, R.J., Edrich, S.P., and Rattey, R.P., 1987, Geologic evolution and hydrocarbon habitat of the 'Arctic Alaska Microplate': Marine and Petroleum Geology, v. 4, p. 2–34, doi: 10.1016/0264-8172(87)90019-5.

Hunziker, J.C., Frey, M., Clauer, N., Dallmeyer, R.D., Friedrichsen, W., Hochstrasser, K., Roggwiler, P., and Schwander, H., 1986, The evolution of illite to muscovite: Mineralogical and isotopic data from the Glarus Alps, Switzerland: Contributions to Mineralogy and Petrology, v. 92, p. 157–180, doi: 10 .1007/BF00375291.

Johansson, Å., Larionov, A.N., Gee, D.G., Ohta, Y., Tebenkov, A.M., and Sandelin, S., 2004, Grenvillian and Caledonian tectono-magmatic activity in northeasternmost Svalbard, *in* Gee, D.G., and Pease, V.L., eds., The Neoproterozoic Timanide orogen of eastern Baltica: Geological Society, London, Memoir 30, p. 207–232, doi: 10.1144/GSL.MEM.2004.030.01.17.

Kalsbeek, F., Higgins, A.K., Jepsen, H.F., Nutman, A.P., Thrane, K., Nutman, A.P., and Jepsen, H.F., 2008, Granites and granites in the East Greenland Caledonides, *in* Higgins, A.K., et al., eds., The Greenland Caledonides: Evolution of the northeast margin of Laurentia: Geological Society of America Memoir 202, p. 227–249, doi: 10.1130/2008.1202(09).

Kalsbeek, F., Thrane, K., Nutman, A.P., and Jepsen, H.F., 2000, Late Mesoproterozoic to early Neoproterozoic history of the East Greenland Caledonides: Evidence for Grenvillian orogenesis?: Journal of the Geological Society [London], v. 157, p. 1215–1225, doi: 10.1144/jgs.157.6.1215.

Kalsbeek, F., Jepsen, H.F., and Nutman, A.P., 2001, From source migmatites to plutons: Tracking the origin of ca. 435 Ma S-type granites in the East Greenland Caledonian orogen: Lithos, v. 57, p. 1–21, doi: 10.1016/S0024-4937(00)00071-2.

Kelley, J.S., Wrucke, C.T., and Lane, L.S., 1994, Pre-Mississippian rocks in the Clarence and Malcolm rivers area, Alaska and Yukon Territory, *in* Thurston, D.K., and Fujita, K., eds., 1992 Proceedings, International Conference on Arctic Margins: U.S. Department of the Interior Minerals Management Service, OCS (Outer Continental Shelf) Study MMS 94–0040, p. 59–64.

Ketchum, J.W.F., Heaman, L.M., Krogh, T.E., Culshaw, N.G., and Jamieson, R.A., 1998, Timing and thermal influence of late orogenic extension in the lower crust: A U-Pb

geochronological study from the southwest Grenville orogen, Canada: Precambrian Research, v. 89, p. 25–45.

Kirkland, C.L., Pease, V.L., Whitehouse, M.J., and Ineson, J.R., 2009, Provenance record from Mesoproterozoic–Cambrian sediments of Peary Land, North Greenland: Implications for the ice-covered Greenland Shield and Laurentian palaeogeography: Precambrian Research, v. 170, p. 43–60, doi: 10.1016 /j.precamres.2008.11.006.

Kochelek, E.J., Amato, J.M., Pavlis, T.L., and Clift, P.D., 2011, Flysch deposition and preservation of coherent bedding in an accretionary complex: Detrital zircon ages from the upper Cretaceous Valdez Group, Chugach terrane, Alaska: Lithosphere, v. 3, p. 265–274, doi: 10.1130/L131.1.

Lane, L.S., 1991, The pre-Mississippian "Neruokpuk Formation," northeastern Alaska and northwestern Yukon: Review and new regional correlation: Canadian Journal of Earth Sciences, v. 28, p. 1521–1533, doi: 10.1139/e91-136.

Lane, L.S., 1997, Canada Basin, Arctic Ocean: Evidence against a rotational origin: Tectonics, v. 16, p. 363–387, doi: 10.1029/97TC00432.

Lane, L.S., 2007, Devonian–Carboniferous paleogeography and orogenesis, northern Yukon and adjacent Arctic Alaska: Canadian Journal of Earth Sciences, v. 44, p. 679–694, doi: 10.1139/e06-131.

Lane, L.S., and Cecile, M.P., 1989, Stratigraphy and structure of the Neruokpuk Formation, northern Yukon, *in* Current research, Part G: Frontier Geoscience program, Arctic Canada: Geological Survey of Canada Paper 89-1G, p. 57–62.

Lane, L.S., and Gehrels, G.E., 2014, Detrital zircon lineages of late Neoproterozoic and Cambrian strata, NW Laurentia: Geological Society of America Bulletin, v. 126, p. 398–414, doi: 10.1130/B30848 .1.

Lane, L.S., Kelley, J.S., and Wrucke, C.T., 1995, Stratigraphy and structure of the Clarence River area, Yukon–Alaska North Slope: A USGS-GSC co-operative project, *in* Current research, Part E: Geological Survey of Canada Paper 1995-E, p. 1–9.

Lane, L.S., Gehrels, G.E., and Layer, P.W., 2016, Provenance and paleogeography of the Neruokpuk Formation, northwest Laurentia: An integrated synthesis: Geological Society of America Bulletin, B31234.1, doi: 10.1130/B31234 .1.

Lawver, L.A., and Scotese, C.R., 1990, A review of tectonic models for the evolution of the Canadian Basin, *in* Grantz, A., et al., eds., The Arctic Ocean region: Boulder, Colorado, Geological Society of America, Geology of North America, v. L, p. 593–618.

Leffingwell, E.K., 1919, The Canning River region, northern Alaska: U.S. Geological Survey Professional Paper 109, 251 p.

Lemieux, Y., Hadlari, T., and Simonetti, A., 2011, Detrital zircon geochronology and provenance of Devono-Mississippian strata in the northern Canadian Cordilleran miogeocline: Canadian Journal of Earth Sciences, v. 48, p. 515–541, doi: 10.1139/E10-056.

Lenz, A.C., and Perry, D.G., 1972, The Neruokpuk Formation of the Barn Mountains and Driftwood Hills, northern Yukon: Its age and graptolite fauna: Canadian Journal of Earth Sciences, v. 9, p. 1129–1138, doi: 10.1139/e72-098.

Lerand, M., 1973, Beaufort Sea, *in* McCrossam, R.G., ed., The future petroleum provinces of Canada—Their geology and potential: Canadian Society of Petroleum Geology Memoir

1, p. 315–386. Leslie, C.D., 2009, Detrital zircon geochronology and rift-related magmatism: Central Mackenzie Mountains, Northwest Territories [M.S. thesis]: Vancouver, University of British Columbia, 224 p., doi: 10.14288/1.0052744.

Macdonald, F.A., McClelland, W.C., Schrag, D.P., and MacDonald, W.P., 2009, Neoproterozoic glaciation on a carbonate platform margin in Arctic Alaska and the origin of the North Slope subterrane: Geological Society of America Bulletin, v. 121, p. 448–473, doi: 10.1130/B26401 .1.

MacNaughton, R.B., Moynihan, D.P., Roots, C.F., and Crowley, J.L., 2016, New occurrences of Oldhamia in eastern Yukon, Canada: Stratigraphic context and implications for Cambrian deep-marine biostratigraphy: Ichnos, v. 23, p. 33–52, doi: 10.1080/10420940.2015.1127232.

Malone, S.J., McClelland, W.C., von Gosen, W., and Piepjohn, K., 2014, Proterozoic evolution of the North Atlantic–Arctic Caledonides: Insights from detrital zircon analysis of metasedimentary rocks from the Pearya terrane, Canadian High Arctic: Journal of Geology, v. 122, p. 623–647, doi: 10.1086/677902.

Martin, A.J., Copeland, P., and Benowitz, J.A., 2015, Muscovite $^{40}Ar/^{39}Ar$ ages help reveal the Neogene tectonic evolution of the southern Annapurna Range, central Nepal, *in* Mukherjee, S., et al., eds., Tectonics of the Himalaya: Geological Society, London, Special Publication 412, p. 199–220, doi: 10.1144/SP412 .5.

McClelland, W.C., Malone, S.J., von Gosen, W., Piepjohn, K., and Läufer, A., 2012, The timing of sinistral displacement of the Pearya terrane along the Canadian Arctic margin: Zeitschrift der Deutschen Gesellschaft für Geowissenschaften, v. 163, p. 251–259, doi: 10.1127/1860-1804/2012/0163-0251.

McClelland, W.C., Colpron, M., Piepjohn, K., von Gosen, W., Ward, W.P., and Strauss, J.V., 2015, Preliminary detrital zircon geochronology of the Neruokpuk Formation in the Barn Mountains, Yukon, *in* MacFarlane, K.E., et al., eds., Yukon exploration and geology 2014: Whitehorse, Yukon Geological Survey, p. 123–143.

McKenzie, D., and Bickle, M.J., 1988, The volume and composition of melt generated by extension of the lithosphere: Journal of Petrology, v. 29, p. 625–679, doi: 10.1093/petrology/29.3.625.

Miller, E.L., Toro, J., Gehrels, G.E., Amato, J.M., Prokopiev, A., Tuchkova, M.I., Akinin, V.V., Dumitru, T.A., Moore, T.E., and Cecile, M.P., 2006, New insights into Arctic paleogeography and tectonics from U-Pb detrital zircon geochronology: Tectonics, v. 25, TC3013, doi: 10.1029/2005TC001830.

Miller, E.L., Kuznetsov, N., Soboleva, A., Udoratina, O., Grove, M.J., and Gehrels, G.E., 2011, Baltica in the Cordillera?: Geology, v. 39, p. 791–794, doi: 10.1130 /G31910.1.

Moore, T.E., 1987, Geochemistry and the tectonic setting of volcanic rocks of the Frankinian assemblage, central and eastern Brooks Range, *in* Tailleur, I., and Weimer, P., eds., Alaskan North Slope geology: Pacific Section, Society of Economic Paleontologists and Mineralogists Publication 50, p. 691–710.

Moore, T.E., 1999, Balanced cross section, Bathtub syncline to Beaufort Sea through Niguanak structural high, Arctic National Wildlife Refuge (ANWR), northeastern Alaska: A balanced cross section and kinematic and thermal model across the northeastern Brooks Range mountain front, Arctic National Wildlife Refuge, Alaska, *in* ANWR Assessment Team, The oil and gas resource potential of the 1002 area, Arctic National Wildlife Refuge, Alaska: U.S. Geological Survey Open-File Report 98-34, 60 p.

Moore, T.E., and Churkin, M., Jr., 1984, Ordovician and Silurian graptolite discoveries from the Neruokpuk Formation (sensu lato), northeastern and central Brooks Range, Alaska, *in* Blodgett, R.B., ed., Paleozoic geology of Alaska and northwestern Canada newsletter: Alaska Geological Society, p. 21–23.

Moore, T.E., Wallace, W.K., Bird, K.J., Karl, S.M., Mull, C.G., and Dillon, J.T., 1994, Geology of northern Alaska, *in* Plafker, G., and Berg, H.C., eds., The geology of Alaska: Boulder, Colorado, Geological Society of America, Geology of North America, v. G-1, p. 49–140.

Moore, T.E., Potter, C.J., O'Sullivan, P.B., Shelton, K.L., and Underwood, M.B., 2004, Two stages of deformation and fluid migration in the west-central Brooks Range fold and thrust belt, northern Alaska, *in* Swennen, R., et al., eds., Deformation, fluid flow, and reservoir appraisal in foreland fold and thrust belts: American Association of Petroleum Geologists Hedberg Series no. 1, p. 157–186, doi: 10.1306/1025690H13116.

Moore, T.E., O'Sullivan, P.B., Potter, C.J., and Donelick, R.A., 2015, Provenance and detrital zircon geochronologic evolution of lower Brookian foreland basin deposits of the western Brooks Range, Alaska, and implications for early Brookian tectonism: Geosphere, v. 11, p. 93–122, doi: 10.1130/GES01043 .1.

Moores, E.M., 1982, Origin and emplacement of ophiolites: Reviews of Geophysics and Space Physics, v. 20, p. 735–760, doi: 10.1029/RG020i004p00735.

Morris, G.A., Kirkland, C.L., and Pease, V., 2015, Orogenic paleofluid flow recorded by discordant detrital zircons in the Caledonian foreland basin of northern Greenland: Lithosphere, v. 7, p. 138–143, doi: 10.1130/L420.1.

Mortensen, J.K., and Bell, R.T., 1991, U-Pb zircon and titanite geochronology of the Mount Sedgwick pluton, northern Yukon Territory, *in* Radiogenic age and isotope studies, Report 4: Geological Survey of Canada Paper 90-2, p. 19–24.

Mull, C.G., and Anderson, A.V., 1991, Franklinian lithotectonic domains, northeastern Brooks Range, Alaska: Alaska Division of Geological & Geophysical Surveys Public Data File 91-5, 40 p., doi: 10.14509/1472.

Nemchin, A.A., and Cawood, P.A., 2005, Discordance of the U-Pb system in detrital zircons: Implication for provenance studies of sedimentary rocks: Sedimentary Geology, v. 182, p. 143–162, doi: 10.1016/j.sedgeo.2005.07.011.

Newberry, R.J., Dillon, J.T., and Adams, D.D., 1986, Regionally metamorphosed, calc-silicate-hosted deposits of the Brooks Range, northern Alaska: Economic Geology and the Bulletin of the Society of Economic Geologists, v. 81, p. 1728–1752, doi: 10.2113/gsecongeo.81.7.1728.

Norford, B.S., 1997, Ordovician and Silurian, *in* Norris, D.K., ed., Geology and mineral and hydrocarbon potential of northern Yukon Territory and northwestern District of Mackenzie: Geological Survey of Canada Bulletin 422, p. 119–162.

Norris, D.K., 1981a, Geology, Blow River and Davidson Mountains, Yukon Territory-District of Mackenzie: Geological Survey of Canada, "A" Series Map 1516A, scale 1:250,000, 1 sheet, doi: 10.4095/119398.

Norris, D.K., 1981b, Geology, Herschel Island and Demarcation Point, Yukon Territory: Geological Survey of Canada, "A" Series Map 1514A, scale 1:250,000, 1 sheet, doi: 10.4095/109649.

Norris, D.K., 1986, Lower Devonian Road River Formation on the north flank of Romanzof uplift, northern Yukon Territory, *in* Current research, Part A: Geological Survey of Canada Paper 86-1A, p. 801–802.

Norris, D.K., 1997, Geological setting, *in* Norris, D.K., ed., The geology, mineral and hydrocarbon potential of the northern Yukon Territory and northwestern District of Mackenzie: Geological Survey of Canada Bulletin 422, p. 21–64.

Ohta, Y., Larionov, A.N., Tebenkov, A.M., Lepvrier, C., Maluski, H., Lange, M., and Hellebrandt, B., 2002, Single-zircon Pbevaporation and $^{40}Ar/^{39}Ar$ dating of the metamorphic and granitic rocks in northwest Spitsbergen: Polar Research, v. 21, p. 73–89, doi: 10.1111/j.1751-8369.2002.tb00068.x.

Oldow, J.S., Avé Lallemant, H.G., Julian, F.E., and Seidensticker, C.M., 1987, Ellesmerian(?) and Brookian deformation in the Franklin Mountains, northeastern Brooks Range, Alaska, and its bearing on the origin of the Canada Basin (USA): Geology, v. 15, p. 37–41, doi: 10.1130/0091-7613(1987)15<37:EABDIT>2.0.CO;2.

Oliver, G.J.H., Wilde, S.A., and Wan, Y., 2008, Geochronology and geodynamics of Scottish granitoids from the late Neoproterozoic break-up of Rodinia to Palaeozoic collision: Journal of the Geological Society [London], v. 165, p. 661–674, doi: 10.1144/0016-76492007-105.

O'Sullivan, P.B., 1993, Multiple phases of Tertiary uplift and erosion in the Arctic National Wildlife Refuge, Alaska, revealed by apatite fission track analysis: American Association of Petroleum Geologists Bulletin, v. 77, p. 359–385, doi: 10.1306/BDFF8C0E-1718-11D7-8645000102C1865D.

O'Sullivan, P.B., 1994, Timing of Tertiary episodes of cooling in response to uplift and erosion, northeastern Brooks Range, Alaska, *in* Thurston, D.K., and Fujita, K., eds., 1992 Proceedings, International Conference on Arctic Margins: U.S. Department of the Interior Minerals Management Service, OCS (Outer Continental Shelf) Study MMS 94-0040, p. 269–274.

O'Sullivan, P.B., and Wallace, W.K., 2002, Out-of-sequence, basement-involved structures in the Sadlerochit Mountains region of the Arctic National Wildlife Refuge, Alaska: Evidence and implications from fission-track thermochronology: Geological Society of America Bulletin, v. 114, p. 1356–1378, doi: 10.1130/0016-7606(2002)114 <1356:OOSBIS >2.0.CO;2.

Patchett, P.J., Roth, M.A., Canale, B.S., De Freitas, T.A., Harrison, J.C., Embry, A.F., and Ross, G.M., 1999, Nd isotopes, geochemistry, and constraints on sources of sediments in the Franklinian mobile belt, Arctic Canada: Geological Society of America Bulletin, v. 111, p. 578–589, doi: 10.1130/0016-7606(1999)111<0578:NIGACO>2.3.CO;2.

Peapples, P.R., Wallace, W.K., Hanks, C.L., Layer, P.W., and O'Sullivan, P.B., 1997, Style, controls, and timing of fold-and-thrust deformation of the Jago stock, northeastern Brooks Range, Alaska: Canadian Journal of Earth Sciences, v. 34, p. 992–1007, doi: 10.1139/e17-082.

Pearce, J.A., 2008, Geochemical fingerprinting of oceanic basalts with applications to ophiolite classification and the search for Archean oceanic crust: Lithos, v. 100, p. 14–48, doi: 10.1016/j.lithos.2007.06.016.

Pettersson, C.H., Tebenkov, A.M., Larionov, A.N., Andresen, A., and Pease, V., 2009, Timing of migmatization and granite genesis in the Northwestern terrane of Svalbard, Norway:

Implications for regional correlations in the Arctic Caledonides: Journal of the Geological Society [London], v. 166, p. 147–158, doi: 10.1144/0016-76492008-023.

Pettersson, C.H., Pease, V., and Frei, D., 2010, Detrital zircon U-Pb ages of Silurian-Devonian sediments from NW Svalbard: a fragment of Avalonia and Laurentia?: Journal of the Geological Society, v. 167, no. 5, p. 1019–1032, doi: 10.1144/0016-76492010-062.

Powell, J., and Schneider, D.A., 2013, Preliminary results of detrital muscovite $^{40}Ar/^{39}Ar$ geochronology from the eastern Mackenzie Mountains and Mackenzie Plain, Northwest Territories: Geological Survey of Canada Current Research 2013-18, 16 p., doi: 10 .4095 /292712.

Rainbird, R.H., Heaman, L.M., and Young, G., 1992, Sampling Laurentia: Detrital zircon geochronology offers evidence for an extensive Neoproterozoic river system originating from the Grenville orogen: Geology, v. 20, p. 351–354, doi: 10.1130/0091-7613(1992)020<0351:SLDZGO>2.3.CO;2

Rainbird, R.H., Jefferson, C.W., and Young, G.M., 1996, The early Neoproterozoic sedimentary Succession B of northwestern Laurentia: Correlations and paleogeographic significance: Geological Society of America Bulletin, v. 108, p. 454–470, doi: 10.1130/0016-7606 (1996)108 <0454:TENSSB>2.3.CO;2.

Rainbird, R., Cawood, P., and Gehrels, G., 2012, The Great Grenvillian sedimentation episode: Record of supercontinent Rodinia's assembly, *in* Busby, C., and Azor, A., eds., Tectonics of sedimentary basins: Recent advances: Chichester, John Wiley & Sons, Ltd., p. 583–601, doi: 10.1002/9781444347166.ch29.

Reed, B.L., 1968, Geology of the Lakes Peters area northeastern Brooks Range, Alaska: U.S. Geological Survey Bulletin 1236, 136 p.

Rehnström, E.F., 2010, Prolonged Paleozoic magmatism in the East Greenland Caledonides: Some constraints from U-Pb ages and Hf isotopes: Journal of Geology, v. 118, p. 447–465, doi: 10.1086/655010.

Reiser, H.N., Brosge, W.P., Dutro, J.T., Jr., and Detterman, R.L., 1980, Geologic map of the Demarcation Point quadrangle, Alaska: U.S. Geological Survey Miscellaneous Investigations Series Map 1133, scale 1:250,000.

Sable, E.G., 1977, Geology of the western Romanzof Mountains, Brooks Range, northeastern Alaska: U.S. Geological Survey Professional Paper 897, 84 p.

Saleeby, J.B., 1983, Accretionary tectonics of the North American Cordillera: Annual Review of Earth and Planetary Sciences, v. 11, p. 45–73, doi: 10 .1146 /annurev.ea.11.050183.000401.

Schermer, E.R., Howell, D.G., and Jones, D.L., 1984, The origin of allochthonous terranes: Perspectives on the growth and shaping of continents: Annual Review of Earth and Planetary Sciences, v. 12, p. 107–131, doi: 10.1146/annurev.ea.12.050184.000543.

Şengör, A.M.C., Natal'in, B.A., and Burtman, V.S., 1993, Evolution of the Altaid tectonic collage and Palaeozoic crustal growth in Eurasia: Nature, v. 364, no. 6435, p. 299–307, doi: 10.1038/364299a0.

Sharman, G.R., Graham, S.A., Grove, M., and Hourigan, J.K., 2013, A reappraisal of the early slip history of the San Andreas fault, central California, USA: Geology, v. 41, p. 727–730, doi: 10.1130/G34214.1.

Sherlock, S.C., Jones, K.A., and Kelley, S.P., 2002, Fingerprinting polyorogenic detritus using the laser microprobe $^{40}Ar/^{39}Ar$ ultraviolet: Geology, v. 30, p. 515–518, doi: 10.1130/0091-7613(2002)030<0515.

Stewart, J., 1976, Late Precambrian evolution of North America: Plate tectonics implication: Geology, v. 4, p. 11–15, doi: 10.1130/0091-7613(1976)4<11:LPEONA>2.0.CO;2

Strauss, J.V., MacDonald, F.A., Taylor, J.F., Repetski, J.E., and McClelland, W.C., 2013, Laurentian origin for the North Slope of Alaska: Implications for the tectonic evolution of the Arctic: Lithosphere, v. 5, p. 477-482, doi: 10.1130 /L284 .1.

Sweeney, J.F., 1982, Mid-Palaeozoic travels of Arctic Alaska: Nature, v. 298, p. 647–649, doi: 10.1038/298647a0.

Till, A.B., 2016, A synthesis of Jurassic and Early Cretaceous crustal evolution along the southern margin of the Arctic Alaska–Chukotka microplate and implications for defining tectonic boundaries active during opening of Arctic Ocean basins: Lithosphere, v. 8, p. 219–237, doi: 10.1130/L471.1.

Trettin, H.P., 1987, Pearya: A composite terrane with Caledonian affinities in northern Ellesmere Island: Canadian Journal of Earth Sciences, v. 24, p. 224–245, doi: 10.1139/e87 -025.

Trettin, H.P., 1994, Pre-Carboniferous geology of the northern part of the Arctic Islands, Hazen Fold Belt and adjacent parts of central Ellesmere Fold Belt, Ellesmere Island: Geological Survey of Canada Bulletin 430, 260 p., doi: 10.4095/194326.

Trettin, H.P., 1998, Pre-Carboniferous geology of the northern part of the Arctic Islands: Northern Heiberg Fold Belt, Clements Markham Fold Belt, and Pearya; northern Axel Heiberg and Ellesmere islands: Geological Survey of Canada Bulletin 425, 401 p., doi: 10.4095/209572.

Turnbull, M.J.M., Whitehouse, M.J., and Moorbath, S., 1996, New isotopic age determinations for the Torridonian, NW Scotland: Journal of the Geological Society [London], v. 153, p. 955–964, doi: 10.1144/gsjgs.153.6.0955.

van Staal, C.R., and Barr, S.M., 2012, Lithospheric architecture and tectonic evolution of the Canadian Appalachians and associated Atlantic margin, *in* Percival, J.A., et al., eds., Tectonic styles in Canada: The LITHOPROBE perspective: Geological Association of Canada Special Paper 49, p. 41–45.

Verdel, C., van der Pluijm, B.A., and Niemi, N., 2012, Variation of illite/muscovite $^{40}Ar/^{39}Ar$ age spectra during progressive low-grade metamorphism: An example from the US Cordillera: Contributions to Mineralogy and Petrology, v. 164, p. 521–536, doi: 10 .1007 /s00410 -012 -0751 -7.

von Gosen, W., Piepjohn, K., Murphy, D.C., Brandes, C., McClelland, W.C., and Colpron, M., 2015, Fault tectonics in the Rapid depression of the Yukon North Slope (Canadian Arctic)-Summary of preliminary results, *in* MacFarlane, K.E., and Nordling, M.G., eds., Yukon exploration and geology 2014: Whitehorse, Yukon Geological Survey, p. 157–165.

Wallace, W.K., and Hanks, C.L., 1990, Structural provinces of the northeastern Brooks Range, Arctic National Wildlife Refuge, Alaska: American Association of Petroleum Geologists Bulletin, v. 74, p. 1100–1118, doi: 10.1306 /0C9B2425-1710-11D7-8645000102C1865D.

Watt, G.R., Kinny, P.D., and Friderichsen, J.D., 2000, U-Pb geochronology of Neoproterozoic and Caledonian tectonothermal events in the East Greenland Caledonides: Journal of the Geological Society [London], v. 157, p. 1031–1048, doi: 10.1144 /jgs.157.5.1031.

White, C., Gehrels, G.E., Pecha, M., Giesler, D., Yokelson, I., McClelland, W.C., and Butler, R.F., 2016, U-Pb and Hf isotope analysis of detrital zircons from Paleozoic strata of the southern Alexander terrane (southeast Alaska): Lithosphere, v. 8, p. 83–96, doi: 10.1130/L475.1.

Chapter 3: The Whale Mountain allochthon: A relic of the Iapetus Ocean preserved in the northeastern Brooks Range of Alaska and Yukon

Benjamin G. Johnson[1], Justin V. Strauss[2], John F. Taylor[3], William P. Ward[4], Maurice Colpron[5], William C. McClelland[4], Jaime Toro[1]

[1]Department of Geology and Geography, West Virginia University, Morgantown, West Virginia, 26506 USA

[2]Department of Earth Sciences, Dartmouth College, Hanover, New Hampshire 03755, USA

[3]Department of Geoscience, Indiana University of Pennsylvania, Indiana, Pennsylvania 15705 USA

[4]Department of Earth and Environmental Sciences, University of Iowa, Iowa City, Iowa 52242, USA

[5]Yukon Geological Survey, Whitehorse, Yukon, Canada YIA 2C6

ABSTRACT

The Whale Mountain allochthon is a structural complex composed of lower Paleozoic mafic volcanic and marine sedimentary rocks that are exposed within three fault-bounded, east–west-trending belts in the northeastern Brooks Range of Alaska and Yukon. Each belt is characterized by a unique structural and stratigraphic architecture. Trace-element systematics from the volcanic rocks define distinctive suites that are geographically restricted to each belt. The volcanic rocks of the southern belt (the Marsh Fork volcanic rocks) have a tholeiitic character and rare earth element trends that resemble modern mid-ocean-ridge basalt. The volcanic rocks of the central belt (the Whale Mountain volcanic rocks) and northern belt

(Ekaluakat formation; new name) both have an alkaline character, but the northern belt rocks are significantly more enriched in the incompatible trace elements. New zircon U-Pb data from two volcaniclastic rock units, one from the southern belt and another from central belt, yield unimodal age populations that range from ca. 567 to 474 Ma, with weighted averages of 504 ± 11 and 512 ± 1.4 Ma for each sample. In the central and southern belts of the allochthon, basalt flows are interbedded with discontinuous limestone and dolostone units that contain trilobites and agnostoid arthropods. Three distinct trilobite faunas of late Cambrian (Furongian) age were recovered from widely separated localities. The scarcity of uniquely Laurentian genera, coupled with an abundance of distinctive species that could not be assigned to any established Furongian genus, argues against models that invoke extrusion of these volcanic rocks onto the autochthonous Laurentian shelf or slope. It is thus proposed that the Whale Mountain allochthon formed in a peri-Laurentian setting, possibly as disparate fragments of the northern Iapetus Ocean that were assembled in an ancient accretionary wedge and subsequently accreted to the northern margin of Laurentia during the early Paleozoic.

INTRODUCTION

Dense oceanic lithosphere is consumed by subduction at convergent margins, erasing most, if not all, evidence of the ancient seafloor from the geologic record. In rare cases, however, relics of ancient ocean basins are preserved within orogenic belts in the form of ophiolites or fragments of oceanic crust, scraped off a subducting plate and entrained into an accretionary wedge. The Iapetus Ocean, the early Paleozoic ancestor to the modern Atlantic Ocean, is a classic example of an ancient ocean basin where the geologic record has largely been destroyed by subduction and the suturing of several large paleocontinents (e.g., van Staal et al., 1998). Disconnected tracts of ophiolites and oceanic fragments scattered along the Northern

Appalachians (van Staal and Barr, 2012), the British Isles (Chew and Strachan, 2014), and the Scandinavian Caledonides (Corfu et al., 2014) mark the sparse remains of the Iapetus Ocean.

Paleogeographic reconstructions have postulated a continuation of the Iapetus suture into the paleo-Arctic realm (e.g., Lawver, et al., 2002; Colpron and Nelson, 2011; Miller et al., 2011; Pease, 2011; Beranek et al., 2013; Strauss et al., 2017; Hoiland et al., 2017). The composite Arctic Alaska terrane, sometimes grouped within the larger Arctic Alaska–Chukotka microplate (e.g., Miller et al., 2006), is prominently featured in the paleogeographic reconstructions of the Arctic. An abundance of recent geochronological and paleontological evidence suggests that the various subterranes that compose the greater Arctic Alaska terrane can be assigned to at least three separate paleogeographic affinities at the time of Iapetus closure. Southern Arctic Alaska includes the Seward, Hammond, Slate Creek, and Coldfoot subterranes of Moore et al. (1994). Recently, Hoiland et al. (2017) grouped these into a single southern Brooks Range terrane because they share early Paleozoic affinities with northern Baltica (e.g., Patrick and McClelland, 1995; Dumoulin et al., 2002; Amato et al., 2009, 2014; Miller et al., 2011). The northern half of the Arctic Alaska terrane is contained within the North Slope subterrane (herein simplified to the North Slope), which is unequivocally linked to Laurentia (Strauss et al., 2013; McClelland et al., 2015; Lane et al., 2016; Johnson et al., 2016). Residing along the boundary zone between the southern Brooks Range terrane and the North Slope is the Cambrian(?)–Silurian Doonerak arc complex, which was recently inferred by Strauss et al. (2017) to have formed contemporaneously with Taconic– Caledonian arc magmatism along the northeastern edge of Laurentia, thereby preserving a relic of the Iapetus suture within the Arctic Alaska terrane.

An enduring issue involving the paleogeographic restorations of Arctic Alaska relates to the early Paleozoic position of the North Slope along the northern margin of Laurentia. Some

researchers have argued that the North Slope restores to northeastern (NE) Laurentia, citing similarities between the rocks exposed in the NE Brooks Range (Fig. 3.1), which belongs to the North Slope, and Ellesmere Island in Arctic Canada (Sweeney, 1982; Strauss et al., 2013; Cox et al., 2015; Johnson et al., 2016). Others have argued that the North Slope remained fixed to northwestern (NW) Laurentia, calling for stratigraphic continuity between strata exposed in the NE Brooks Range and the Selwyn Basin of central Yukon and elsewhere in the Canadian Cordillera (Cecile et al., 1999; Lane, 2007; Lane et al., 2016).

A principal component in these debates relates to the tectonic and depositional setting of the upper Cambrian Whale Mountain volcanic rocks, exposed in the NE Brooks Range. Based on the alkaline geochemistry of the volcanic rocks and putative similarities with mafic volcanic rocks in northern Canada, Lane et al. (2016) argued that these volcanic rocks erupted within the continental margin of northwestern (NW) Laurentia. Conversely, Johnson et al. (2016) argued that the volcanic rocks in the NE Brooks Range were fault-bounded and instead belonged to an exotic Cambrian–Ordovician oceanic fragment, which they named the Whale Mountain allochthon. The interpretations of Lane et al. (2016) and Johnson et al. (2016), however, both fundamentally relied on sparse geochemical data from previous reconnaissance studies (Moore, 1987; Goodfellow et al., 1995), and the biostratigraphic data available to constrain the age and paleogeographic affinities of the Whale Mountain allochthon were limited and imprecise. The limited faunal control was particularly problematic, in that the endemic faunas that evolved on the Laurentian platform during the Cambrian provide the most definitive means of discriminating strata that originated on or adjacent to that paleocontinent from exotic packages that arrived subsequently through accretion. Here, we provide new field observations coupled with additional geochronological, geochemical, and paleontological data from the Whale Mountain volcanic

rocks and other associated units in the NE Brooks Range that support a peri-Laurentian oceanic origin for the Whale Mountain allochthon.

GEOLOGICAL SETTING

The high topography of the NE Brooks Range forms a structural salient that protrudes more than 100 km northward from the main front of the Brook Range and stretches from the Canning River in Alaska into northern Yukon (Fig. 3.1). It is a critical region for geological investigation because it exposes a prominent angular unconformity (Figs. 3.1 and 3.2) that separates Lower Mississippian quartz-rich siliciclastic units of the Endicott Group (Brosgéet al., 1962) from a thick (>2000 m) succession of tightly folded and weakly metamorphosed, Neoproterozoic to lower Paleozoic sedimentary and igneous rocks (pre-Mississippian sequence of Moore et al., 1994).

The sub-Mississippian rocks in the NE Brooks Range have been investigated using a variety of different map and stratigraphic schemes (see Strauss et al., this volume, Chapter 23, and references therein for a review). Initially, the Whale Mountain volcanic rocks were assigned to the "volcanic and carbonate member" of the broadly defined Neruokpuk Formation of Dutro et al. (1972). These workers split the Neruokpuk Formation into six regional sequences, lettered A through F, with the "volcanic and carbonate member" concentrated in parts of sequences A and C. Critically, Dutro et al. (1972) also recovered trilobite and brachiopod fossils from the "volcanic and carbonate member" at two localities, one along the Marsh Fork of the Canning River, and another along the Leffingwell Fork of the Aichilik River (Fig. 3.1). The Marsh Fork locality yielded olenellid trilobites of early Cambrian age, whereas the Leffingwell Fork locality yielded trilobites and brachiopods of late Cambrian age (middle Furongian).

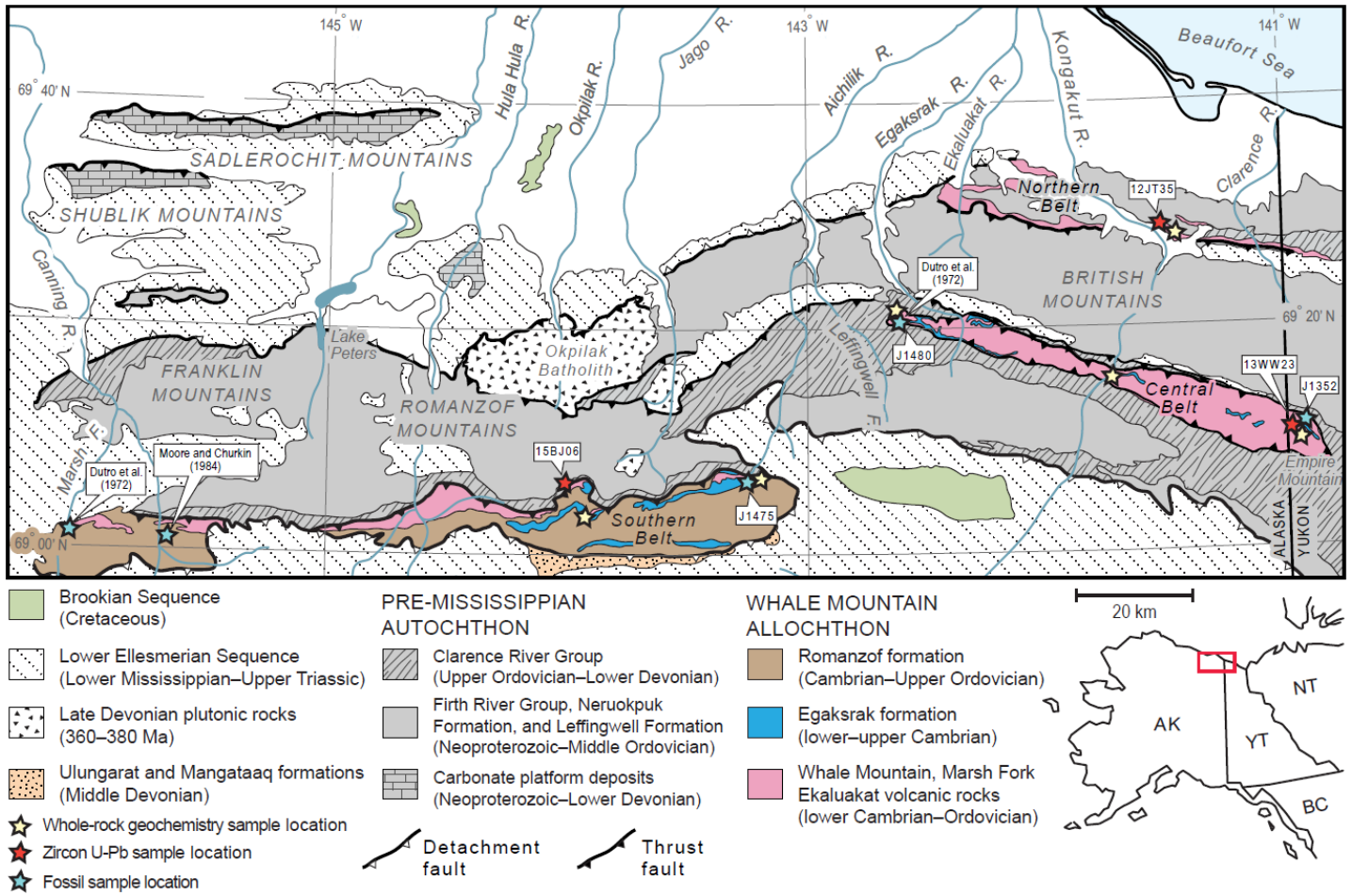

Figure 3.1: Simplified geologic map of the eastern half of the NE Brooks Range, Alaska, highlighting the distribution of rocks comprising the Whale Mountain allochthon and sample locations. The map is modified from Reiser et al. (1980), Wallace and Hanks, (1990), Mull and Anderson, (1991), Lane et al. (1995), and Johnson et al. (2016). Solid teeth on thrust faults indicate disruption of stratigraphic section (old-on-young); open teeth indicate detachment surfaces along which there has been slip but no disruption of the stratigraphic section (young-on-old). Sample numbers are described in the text and outlined in Supplemental Material (Table SM3.1). Sample 12JT35 in the northern belt is from Johnson et al. (2016), and sample 14BJ25 is from Strauss et al. (2018).

Although Dutro et al. (1972) treated the Neruokpuk Formation as a somewhat coherent stratigraphic package, they, along with an earlier study by Reiser (1970), recognized that a regional thrust fault disrupted parts of the stratigraphic order. The fault was mapped along the base of the volcanic rocks of sequence A in the headwaters of the Aichilik, Jago, Hulahula, and Canning rivers in the Romanzof Mountains, and it was inferred to be concealed by the sub-Mississippian unconformity. Later, during the compilation of the 1: 250,000 scale Demarcation Point geologic quadrangle by Reiser et al. (1980), the sequence nomenclature was abandoned, and the Neruokpuk name was reverted to the original usage of Leffingwell (1919), which restricts the Neruokpuk to the "quartzite and semischist member" of Dutro et al. (1972). The volcanic and carbonate member was also split into two map units: a "Cambrian volcanic and volcaniclastic" unit (Cv) and a "Cambrian limestone" unit (Cl).

Some of the thickest exposures of the volcanic and carbonate rocks occur at Whale Mountain in Alaska, where an ~100-km-long, E–W-trending synclinal exposure cuts perpendicularly across the middle reaches of the Kongakut River (Fig. 3.1). Moore (1987) informally named the volcanic rocks exposed along the ridge the "Whale Mountain volcanic rocks," which also included the volcanic rocks exposed at the Leffingwell Fork fossil locality of Dutro et al. (1972), where Moore (1987) analyzed three samples for whole-rock geochemistry. These data, along with a second suite of volcanic samples collected by Goodfellow et al. (1995) from the Yukon segment of the Whale Mountain ridge system, showed that the Whale Mountain volcanic rocks are enriched in incompatible elements (e.g., Ti, Zr, Nb) and resemble alkaline basalt. Moore (1987) also analyzed eight volcanic samples from exposures along strike at the Marsh Fork locality of Dutro et al. (1972), which were independently assigned to the Marsh Fork volcanic rocks. Moore (1987) showed that the Marsh Fork volcanic rocks had comparable levels

of incompatible element enrichment as the alkaline Whale Mountain volcanic rocks to the north; however, a few samples had more transitional and tholeiitic compositions.

A separate unit of volcanic rocks was delineated in the northern British Mountains on the map of Reiser et al. (1980). These volcanic rocks extend from the Ekaluakat River in Alaska to the Clarence River at the Alaska–Yukon border (Fig. 3.1). They were originally included in sequence E of Dutro et al. (1972) but were later reassigned to the "Ordovician volcaniclastic and volcanic rocks" (Ovc) map unit by Reiser et al. (1980). The Ordovician age was constrained by a graptolite locality in an adjacent "Ordovician black slate" (Os) map unit, which was tentatively mapped beneath the volcanic rocks. From mapping studies along the Alaska-Yukon border, the volcanic rocks exposed in the Clarence River region were correlated to the thick volcanic flows at Whale Mountain to the south on the basis of lithologic similarity and an apparent gradational contact with *Oldhamia*-bearing argillite beds (Lane, 1991; Kelley et al., 1994; Lane et al., 1995).

Two recent studies, one by Lane et al. (2016) and another by Johnson et al. (2016), have placed these previously described volcanic rocks of the NE Brooks Range into different stratigraphic positions. In the scheme of Lane et al. (2016), the volcanic rocks, which they named the informal "Whale Mountain formation" reside within a semiconformable succession of Neoproterozoic– Devonian strata. This agrees with previous interpretations from field work conducted in the Clarence River region and along the Alaska–Yukon border (Lane, 1991; Kelley et al., 1994; Lane et al., 1995). Lane et al. (2016) further argued that the volcanic rocks along the Alaska–Yukon border correlate to the Marsh Fork volcanic rocks of Moore (1987), and that these volcanic rocks are all paleogeographic equivalents of volcanic rocks exposed within the Selwyn Basin of central Yukon and elsewhere in the northern Canadian Cordillera (e.g., Goodfellow et al., 1995). Critically, this correlation fixes the North Slope to NW Laurentia in the

early Paleozoic, suggesting that the Whale Mountain volcanic rocks formed in response to periods of extension along the paleo-Pacific margin.

The scheme of Johnson et al. (2016) is different in that it places the volcanic rocks of the NE Brooks Range within a fault-bounded oceanic assemblage called the Whale Mountain allochthon. Based on mapping along the Kongakut River and Leffingwell Fork in Alaska, coupled with detrital zircon U-Pb and muscovite 40Ar/39Ar geochronology, Johnson et al. (2016) showed that the upper Cambrian Whale Mountain volcanic rocks of Moore (1987) overlie a Upper Ordovician–Lower Devonian(?) succession of interbedded shale, argillite, and lithic-rich sandstone. These sedimentary units were correlated to a similar succession of strata mapped in the Clarence River region along the Alaska–Yukon border (Lane, 1991; Kelley et al., 1994; Lane et al., 1995), which enabled Johnson et al. (2016) to apply the informal Clarence River group name (formalized to the Clarence River Group by Strauss et al., this volume, Chapter 23) to include all similar strata in the NE Brooks Range. This also included the siltstone, shale, sandstone, and lithic-rich pebble conglomerate units exposed in the Buckland Hills of northern Yukon, which Lane et al. (2016) originally assigned to the Lower Devonian "Buckland Hills succession" (updated to the Buckland Hills formation by Strauss et al., this volume, Chapter 23). Johnson et al. (2016) contended that detrital zircon signatures from the Clarence River Group closely resembled those of sedimentary units in the deep-water Franklinian Basin of Ellesmere Island, Arctic Canada (e.g., Beranek et al., 2015). In addition, Johnson et al. (2016) postulated that the emplacement of the Whale Mountain allochthon occurred in concert with protracted terrane accretion in NE Laurentia and the presumed closure of the northern Iapetus Ocean during the Caledonian orogeny.

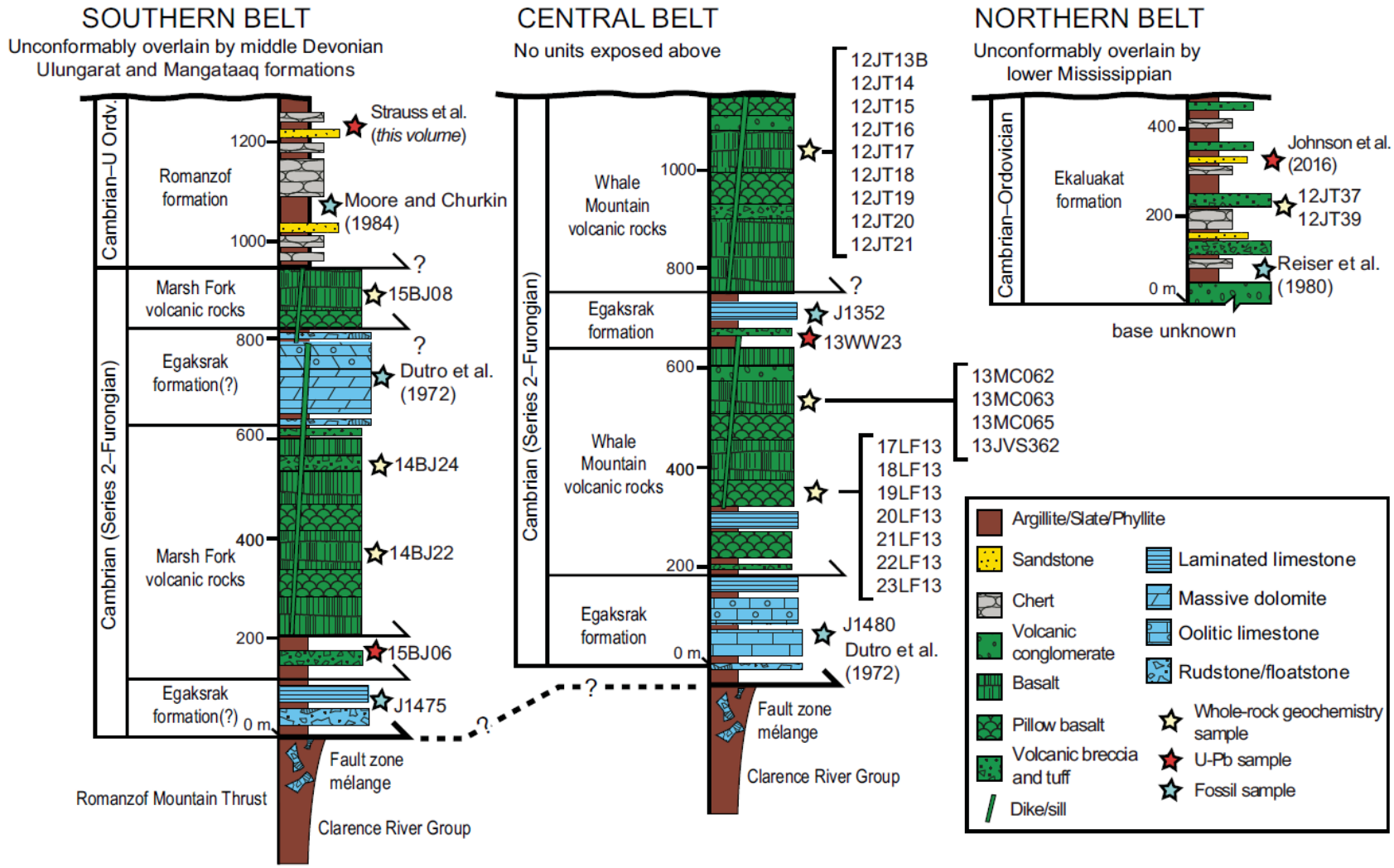

Figure 3.2: Schematic lithostratigraphy of the southern, central, and northern belts of the Whale Mountain allochthon. Thicknesses are approximated from generalized field observations. U. Ordv. stands for Upper Ordovician.

STRUCTURAL AND STRATIGRAPHIC ARCHITECTURE

Here, we provide updated lithological descriptions and field observations from the volcanic and sedimentary rocks of the Whale Mountain allochthon in the NE Brooks Range of Alaska and Yukon that were assembled during a series of field campaigns conducted over the course of 5 years (2011–2015). In addition, we put forth new informal terminology for previously unnamed map units (Egaksrak, Romanzof, and Ekaluakat forma¬tions), which are outlined in Figure 3.2. These rocks are exposed within three E–W-trending thrust sheets or belts, which we refer to as the southern, central, and northern belts (Figs. 3.1 and 3.2). These belts are separated by ~25 km, and each is defined by its own unique structural and stratigraphic architecture.

Southern Belt

The southern belt of the allochthon stretches across 100 km of the Romanzof Mountains, from the headwaters of the Aichilik River to the Marsh Fork of the Canning River (Fig. 3.1). Its stratigraphy consists of intensely imbricated assemblages of chert, phyllite, carbonate, and mafic volcanic and volcaniclastic rocks, which were all originally assigned to sequence A of Dutro et al. (1972). In the summer of 2014 and 2015, we conducted several traverses in the headwaters of the Aichilik and Jago Rivers, where we collected several samples for thin-section analysis, three samples for whole-rock igneous geochemical analysis (14BJ24, 14BJ22, and 15BJ08), and one volcaniclastic sample for zircon U-Pb geochronology (15BJ06). We also discovered one new fossil locality (J1475) along the Aichilik River (Figs. 3.1 and 3.3A).

The base of the southern belt section is marked by a south-dipping thrust fault (Fig. 3.3A), the Romanzof Mountain thrust of Johnson et al. (2016), which runs along the entire northern edge of the southern belt (Figs. 3.1 and 3.3A). Early mappers in the region (e.g., Dutro

et al., 1972; Reiser et al., 1980) recognized that the fault was truncated by the sub-Mississippian unconformity at the headwaters of the Aichilik River. During our traverses of the area in 2014 and 2015, we observed that in discrete locations, the Mississippian Kekiktuk Conglomerate (lower Endicott Group) is exposed in the footwall beneath the fault, indicating that some amount of post-Mississippian displacement has occurred along this structure. In other places, the volcanic and sedimentary rocks of the Whale Mountain allochthon are in direct contact with the Upper Ordovician–Lower Devonian(?) Clarence River Group (Fig. 3.3A).

The fault zone is >500 m wide in some places, and it contains a chaotic mix or mélange of different lithostratigraphic units. Along the Aichilik River, the mélange includes dark-maroon, gray, and green volcaniclastic argillite and phyllite that intertongue with discrete blocks of gray to tan-weathering dolostone and limestone. The carbonate blocks are heavily fractured and brecciated and range between ~10 and 200 m thick. Our new trilobite locality (J14745) was collected from an ~40-m-tall by 100-m-wide block within the fault zone along the western bank of the upper Aichilik River, just south of the Romanzof Mountain thrust (Fig. 3.3A). The rocks at the locality consist predominantly of recrystallized and locally dolomitized lime mudstone and wackestone with a pronounced volcaniclastic matrix. The fossils were recovered from an ~7-cm-thick bed of lime wackestone. Lithologically, these carbonate rocks resemble those from which *Olenellus* was recovered at the Marsh Fork locality of Dutro et al. (1972), but the fauna confirms a significantly younger age (see Paleontology section below), and the structural complexity of the J1475 locality obscures further stratigraphic comparisons.

Along strike of the Romanzof Mountain thrust, in the headwaters of the Jago River, the fault zone contains a similar succession of dark-maroon, gray, and green volcaniclastic argillite and phyllite, but it is intertongued or imbricated with an ~3-m-thick massive volcaniclastic

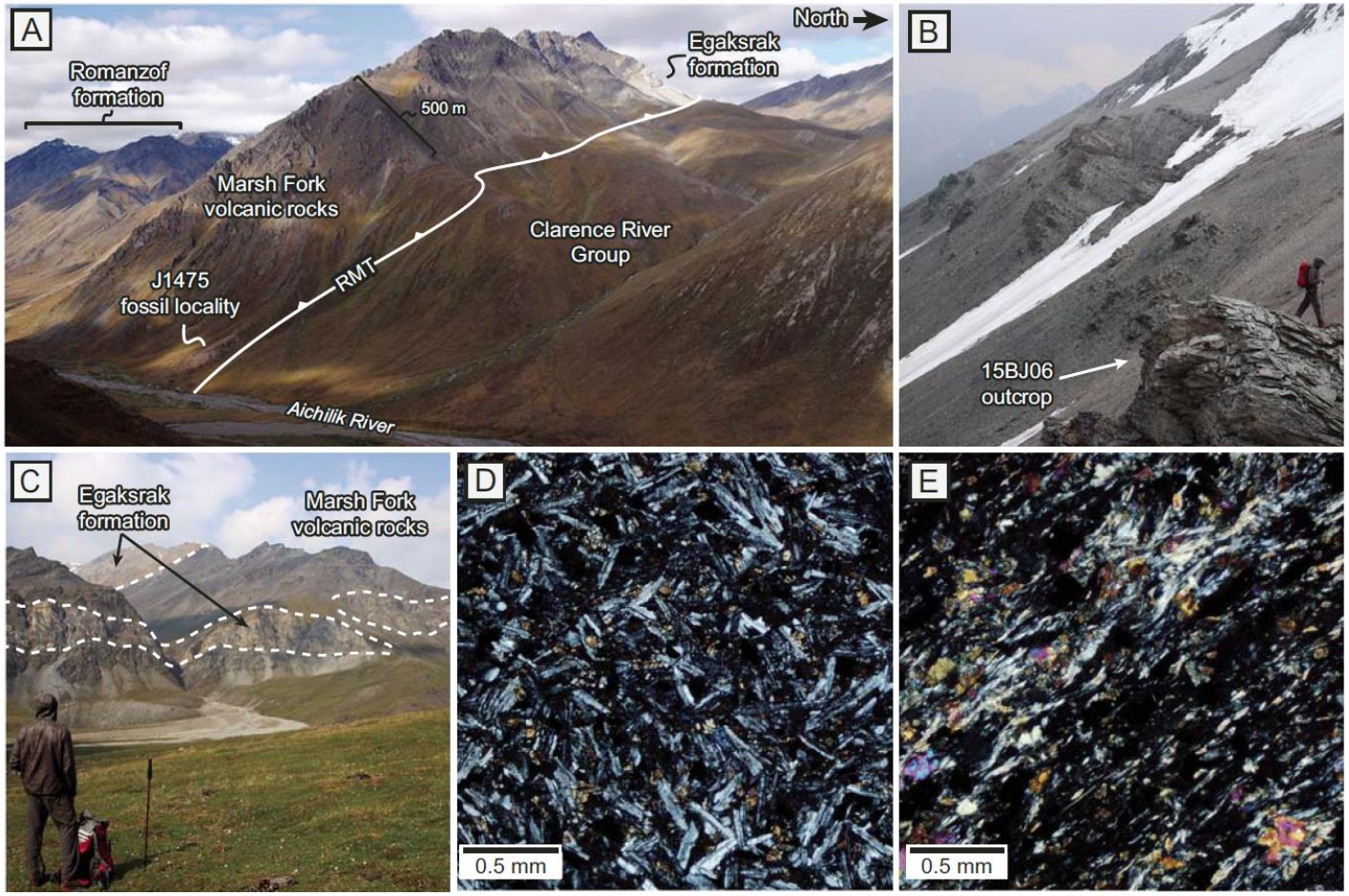

Figure 3.3: Field images and photomicrographs from rocks of the southern belt of the Whale Mountain allochthon in the NE Brooks Range, Alaska. (A) Looking southwest across the Romanzof Mountain Thrust (RMT) at the headwaters of the Aichilik River, showing the J1475 fossil location. (B) Looking east near the fault zone of the RMT at the headwaters of the Jago River, showing the outcrop of zircon U-Pb sample 15BJ06. (C) Looking southwest across intercalated Marsh Fork volcanic rocks and megablocks of the Egaksrak formation in the headwaters of the Jago River. (D) Cross-polarized view of sample 14BJ22 showing intergranular plagioclase phenocrysts with microcrystalline clinopyroxene. (E) Cross-polarized view of sample 15BJ08 showing aligned actinolite, epidote, plagioclase, and Fe- and Ti-oxide minerals.

sandstone unit (Fig. 3.3B), which we sampled for zircon U-Pb geochronology (15BJ06). The sample consists of sheared and angular volcanic detritus (mostly plagioclase) and volcanic rock fragments. The stratigraphic assignment of this unit is uncertain, but the predominance of angular volcanic material implies a close association to the volcanic flows exposed higher in the southern belt section.

Above the fault zone, the section transitions into an ~300–800-m-thick exposure of dark-greenish gray mafic amygdaloidal volcanic flows and subordinate beds of conglomerate, volcaniclastic argillite, and chert. The mafic flows typically show pillow structures or are brecciated, and they resemble the volcanic rocks described by Moore (1987) from the Marsh Fork area at the western limit of the southern belt. We therefore apply the Marsh Fork volcanic rocks name to these exposures. In many places, the volcanic rocks intertongue with large blocks of limestone and dolostone that sometimes exceed 200 m in thickness and cover areas as wide 10 km in length (Fig. 3.3C). These carbonate blocks consist of gray- and tan-weathering, massive, thickbedded oolitic and peloidal dolostone, as well as calcareous rudstone composed of angular carbonate and volcanic lithoclasts and lime mudstone horizons. Like the carbonate blocks near the fault zone, the megablocks have sharp contacts with the surrounding deformed volcanic units, which may be a product of imbrication by unmapped thrust faults or stratigraphic complexity derived through sediment-gravity flows. We tentatively assign the name Egaksrak formation to all the carbonate units in the southern belt because of lithological similarities to carbonate units in the type area between the Leffingwell Fork and the Egaksrak River (see Central Belt subsection below).

Two volcanic samples (14BJ22 and 14BJ24) were collected from the volcanic and carbonate section exposed along the Aichilik River. The samples are fi ne grained, sparsely

porphyritic (1%–5% phenocrysts) and dominated by plagioclase (>50 vol%). Plagioclase occurs as euhedral laths, both in the groundmass (<0.5 mm in length) and as phenocrysts (>1 mm in length). The plagioclase laths in sample 14BJ22 exhibit an intergranular texture with subhedral clinopyroxene and Fe- and Ti-oxide minerals (Fig. 3.3D). The uniform nature of the plagioclase and the intergranular texture in these samples suggest a cumulate origin in a thick lava fl ow or hypabyssal intrusion. Both samples are sparsely to moderately amygdaloidal (2–10 vol%). The amygdules typically have an elongate shape, range from 0.25 to 5 mm in diameter, and are fi lled with chlorite group minerals or calcite. A third volcanic sample (sample 15BJ08) was collected from a 3-m-thick outcrop of greenish-gray metabasalt in the headwaters of the Jago River. These units are heavily sheared and are crosscut by an extensive network of 1–3-cm-thick serpentinite veins. The dominant mineral phases include actinolite, chlorite, epidote, and opaque minerals. Actinolite occurs as elongate subhedral prismatic crystals, up to 1 mm in length, that define a moderate foliation (Fig. 3.3E). Epidote occurs as rounded, subhedral grains aligned along the actinolite grain boundaries, spatially associated with opaque minerals. The metamorphic mineral assemblage of actinolite, epidote, and chlorite indicates that these rocks were subject to greenschist metamorphic conditions.

Above the volcanic and carbonate units, there is an isoclinally folded package of undetermined thickness containing interbedded radiolarian chert and phyllite with minor beds of volcanic and lithic wacke. These rocks were originally designated as the “chert and phyllite member” by Dutro et al. (1972) and were later split into the “Ordovician–Cabrian chert and phyllite” (OCcp) and the “Ordovician volcanic wacke and tuffaceous sandstone” (OCw) map units of Reiser et al. (1980). Mull and Anderson (1991) referred to this package as the Romanzof chert, but we instead refer to this unit as the Romanzof formation due to its diversity of

lithofacies. Moore and Churkin (1984) collected Middle Ordovician graptolites from a phyllite and radiolarian chert interval within the Romanzof formation near the Marsh Fork of the Canning River.

The subordinate volcanic and lithic wacke units consist of centimeter- to meter-thick beds that occasionally exhibit erosional bases with channel-fill geometries in the surrounding chert and phyllite. The wacke is generally poorly sorted and composed of fi ne- to medium-grained, angular to subrounded, monocrystalline and polycrystalline quartz, plagioclase, opaque minerals, and chert and basalt lithic fragments. One detrital zircon sample was collected from these units by Strauss et al. (this volume, Chapter 23). The sample yielded 23 concordant U-Pb ages that define a unimodal population from ca. 494 to 436 Ma, with a peak at 452 Ma, suggesting that parts of the Romanzof formation are as young as Late Ordovician.

The Romanzof formation is overlain by sandstone, shale, and limestone of the Middle Devonian Ulungarat and Mangaqtaaq formations of Anderson et al. (1994). The contact relationships between these two units, however, are not well documented. Anderson et al. (1994) mapped the contact as a faulted unconformity (Aichilik Pass thrust). Because this contact is unconstrained, and because the region is structurally complex, the total estimated thickness of the southern belt section presented in Figure 3.2 should be treated as a structural thickness.

Central Belt

The central belt of the allochthon stretches from Empire Mountain in northern Yukon to the Leffingwell Fork of the Aichilik River in Alaska (Fig. 3.1). During the summers of 2012, 2013, and 2014, we traversed across three separate locations in the central belt, collecting >20 volcanic samples for thin section and geochemical analysis and one volcanic wacke sample (13WW23) for zircon U-Pb geochronology. We also discovered one new fossil locality in Yukon

(J1352) and resampled the fossils from the original locality of Dutro et al. (1972) between the Leffingwell Fork and Egaksrak River (Fig. 3.1).

The stratigraphy of the central belt consists predominantly of intercalated volcanic and carbonate rocks (Fig. 3.2), which were originally assigned to the upper parts the Neruokpuk sequence C of Dutro et al. (1972). The volcanic rocks have since been assigned to the Whale Mountain volcanic rocks by Moore (1987), and we assign the carbonate units to the Egaksrak formation, due to their prominent exposure along the ridge that separates the Leffingwell Fork and the Egaksrak River. The entire central belt appears to be folded into an ~10-km-wide by ~100-km-long synclinal ridge that is >1000 m thick where it crosses the Kongakut River in Alaska and that thins to <600 m thick along the Leffingwell Fork. Like the southern belt section, the base of the central belt section is marked by a complex fault zone mélange of Clarence River Group strata mixed with large slivers of the carbonate units that range from 5 to 200 m thick. This fault zone also appears to be broadly folded into a syn-form (Fig. 3.4A). The top of the central belt is not covered by any younger lithostratigraphic units, rendering its original stratigraphic thickness indeterminable.

At the western edge of the central belt, near the Leffingwell Fork fossil locality of Dutro et al. (1972), the fault zone becomes subhorizontal and is exposed along a broad saddle in the ridge that divides the Leffingwell Fork and the Egaksrak River (Fig. 3.4B). An ~200-m-thick, vertically dipping megablock of intensely sheared limestone is exposed between the black slate of the Clarence River Group and the Whale Mountain volcanic rocks higher in the section (Fig. 3.4B). The block includes contorted beds of discontinuous rudstone that contain angular to well-rounded, pebble- to sand-sized volcanic lithoclasts (Fig. 3.4C). This chaotic interval is bound to the north by a massive gray oolitic and peloidal grainstone unit that is interbedded with finely

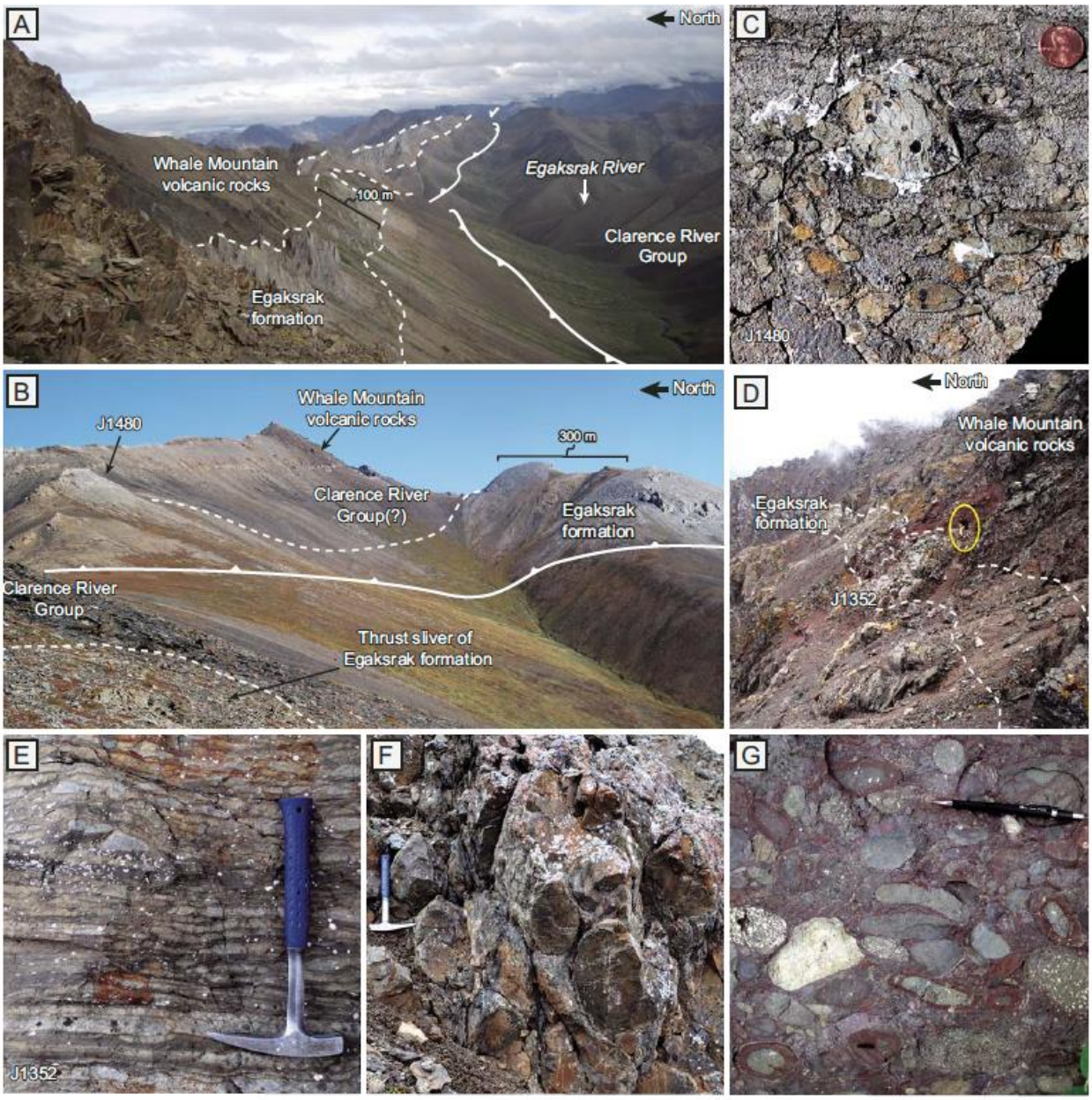

Figure 3.4: Field images from rocks of the central belt of the Whale Mountain allochthon in the NE Brooks Range, Alaska. (A) Looking east along the southern limb of synclinal ridge, showing interbedded Whale Mountain volcanic rocks and laminated lime mudstone units of the Egaksrak formation (B) Looking northeast at the Leffingwell Fork fossil locality (J1480), which shows the upper Cambrian limestone units above black slate units of the Middle Ordovician–Lower Devonian(?) Clarence River Group including thrust slivers of Egaksrak carbonate units. (C) Close-up of lime mudstone with abundant pebble- and cobble-sized clasts of basalt; penny for scale is 19 mm across. (D) Looking east at the J1352 fossil location in headwaters of the Malcom River, Yukon; person for scale is circled in yellow and is ~2 m tall. (E) Close-up of ribbon-bedded lime mudstone at the J1352 fossil location; hammer for scale is ~32 cm. (F) Pillow textures preserved within folded basalt flows; hammer for scale is 32 cm long. (G) Close-up of clast-supported conglomerate with well-rounded clast of basalt, diabase, and chert from the Kongakut River, Alaska; pencil for scale is ~15 cm.

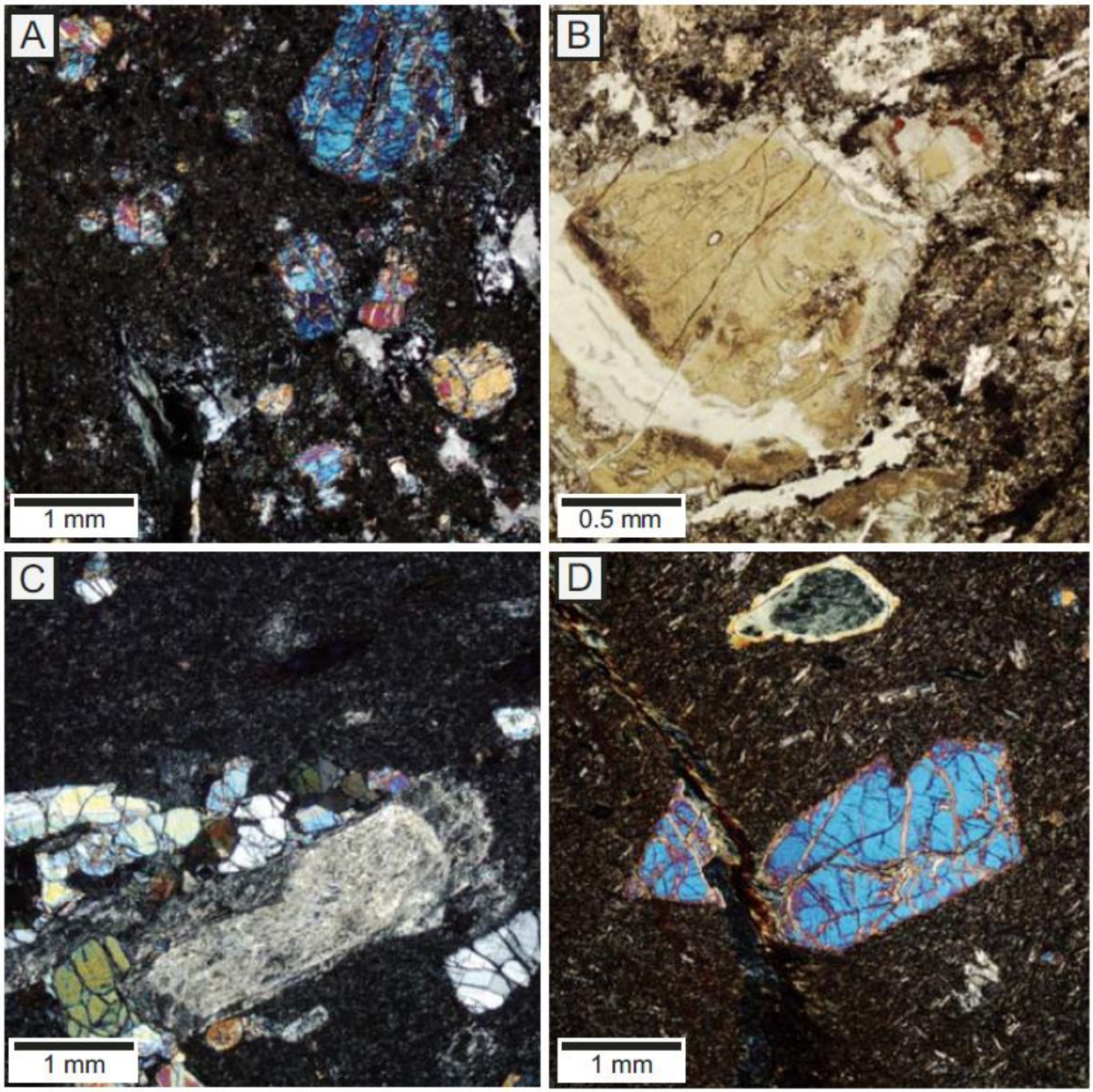

Figure 3.5: Photomicrographs of theWhale Mountain volcanic rocks. (A) Cross-polarized view of sample 12JT13B, showing fractured olivine phenocrysts in a groundmass composed of glass and Fe- and Ti-oxide minerals. (B) Plane-polarized view of sample 12JT20, showing complete iddingsite alteration of an olivine phenocryst. (C) Cross-polarized view of sample 12JT18 showing glomeroporphyritic olivine and plagioclase, sericitization of plagioclase phenocrysts, and chlorite amygdules that have been stretched. (D) Cross-polarized view of sample 20LF13 showing large fractured and altered olivine phenocryst.

laminated fossiliferous lime mudstone and wackestone. Our fossil locality J1480 was recovered from the laminated mudstone interval, which is likely the same location from which Dutro et al. (1972) collected their sample 6983-CO. Like the carbonate units in the southern belt, the stratigraphic context of these large carbonate blocks is unclear, but the contacts with the surrounding units are typically abrupt or marked by brecciated limestone and volcanic units, suggesting a structural or an olistostromal relationship.

In other locations along the central belt, the lime mudstone units of the Egaksrak formation occur as laterally extensive, ~150-m-thick beds that crop out for >10 km and are interbedded with the volcanic rocks (Fig. 3.4A). Near the headwaters of the Malcolm River in Yukon, the J1352 fossil locality was discovered in fossiliferous lime and volcaniclastic mudstone, grain-stone, and rudstone interbedded with pillowed Whale Mountain volcanic rocks (Fig. 3.4D). The fossiliferous strata include an ~15-m-thick lens of ribbon-bedded lime mudstone (Fig. 3.4E), fossiliferous wackestone, reworked meter-scale carbonate olistoliths and rudstone, and volcaniclastic conglomerate and sandstone within a dominantly maroon volcaniclastic mudstone matrix. Thin sections revealed that the carbonate units contain a prominent volcanic matrix composed of disseminated plagioclase laths and abundant chlorite, sericite, and calcite alteration products. Trilobites were recovered from ~2–3-cm-thick fossiliferous grainstone or wackestone horizons within the meter-scale carbonate olistoliths, as well as separate beds of fossiliferous grainstone outside the olistoliths.

The Whale Mountain volcanic rocks are prominently exposed where the middle reaches of the Kongakut River cut across the central belt (Fig. 3.1). They include dark-green basalt and diabase that weather dark olive brown and commonly crop out as fractured pillows (Fig. 3.4F), massive flows, or minor hypabyssal intrusions (sills and dikes). The basaltic flows typically

interfinger with various tuffaceous and volcaniclastic rocks, including lithic and volcanic wacke and conglomerate. The conglomerate is typically clast-supported and contains well-rounded, gravel- to cobble-sized clasts of weathered basalt, diabase, and chert (Fig. 3.4G).

In thin section, the basalt samples from the central belt dis-play a variety of microtextures (Figs. 3.5A–3.5D). Most samples are porphyritic, with textures that range from aphyric (<1% phenocrysts) to highly porphyritic (>10% phenocrysts). Olivine, clinopyroxene, and plagioclase are the dominant phenocrysts, although in some samples, olivine and clinopyroxene are the only phenocrysts present (e.g., 12JT13b; Fig. 3.5A). Many of the large olivine phenocrysts are crosscut by fractures and have undergone extensive serpentinization and iddingsite alteration, in some cases causing complete replacement of olivine by serpentine and other clay minerals (Fig. 3.5B). Plagioclase is commonly present as large (~1–4 mm) glomerocrysts forming aggregates with olivine (Fig. 3.5C). The plagioclase phenocrysts have undergone saussuritization, replacing the plagioclase with an assemblage of cryptocrystalline (<0.1 mm) epidote, clinozoisite, zoisite, and sericite. Amygdules are present in almost all samples and typically compose 1%–5% of the rock volume of each sample; they range from 0.25 to 5 mm in diameter and are semispherical to elongate in shape. The amygdules are typically filled with chlorite group minerals, microcrystalline quartz, calcite, or zeolites (Fig. 3.5C).

The composition and texture of the groundmass also vary from sample to sample. In some samples, the groundmass is composed of microcrystalline to fine-grained (0.1–1 mm) plagioclase, subhedral Fe- and Ti-oxide minerals, and cryptocrystalline pyroxene or olivine. In other samples, the groundmass is predominantly composed of altered glass and cryptocrystalline to microcrystalline subhedral Fe- and Ti-oxides. When plagioclase microlites are present in the

groundmass, they are typically aligned in a moderately to weakly developed trachytic texture (Fig. 3.5D).

The basaltic flows and volcaniclastic rocks are locally interbedded with a dark-maroon and gray argillite and phyllite, with minor beds of chert, which could be correlative units of the Romanzof formation in the southern belt. The stratigraphic relationships between the various volcanic and carbonate units throughout the central belt are also somewhat uncertain, but their intercalated nature, and the prevalence of volcanic debris within the carbonate units support a cogenetic relationship.

Northern Belt

The northern belt of the allochthon extends from the Malcolm River in northern Yukon to the Ekaluakat River in Alaska (Fig. 3.1). The stratigraphy of this belt predominantly consists of volcaniclastic and volcanic-rich sandstone units that interfinger with beds of chert, argillite, and black slate (Fig. 3.2). In Alaska, these units were originally assigned to sequence E of Dutro et al. (1972), and they were subsequently split by Reiser et al. (1980) into three separate Ordovician map units: a "volcaniclastic and volcanic" unit (Ovc), a "black slate" unit (Os), and a "gray phyllite and chert" unit (Opc). On the Yukon side of the international border, these units were mapped as part of a coherent basinal succession of Cambrian–Lower Devonian strata (e.g., Lane, 1991; Lane et al., 1995; Lane et al., 2016); however, we tentatively assign these sedimentary and volcanic rocks to a single informal lithostratigraphic unit, which we name the Ekaluakat formation due to its widespread exposure near the Ekaluakat River in Alaska.

Unlike the southern and central belts of the allochthon, the northern belt has a poorly defined base, where discrimination of the sedimentary rocks of the Ekaluakat formation from those of the Clarence River Group is largely hampered by poor exposure and repeated

imbrication. However, Reiser et al. (1980) mapped a distinct fault-related breccia unit along the Ekaluakat River that appears to separate volcanic and sedimentary rocks of the Ekaluakat formation from structurally(?) underlying rocks of the Neoproterozoic–Lower Cambrian(?) Firth River Group. Reiser et al. (1980) also reported a ca. 484 Ma K-Ar age on hornblende from a mafic intrusion near the breccia unit. Although we are unsure if the rocks of the Ekaluakat formation are unambiguously correlative with the volcanic and sedimentary rocks of the southern and central belts, this potential tectonic contact is similar to other boundaries with the Whale Mountain allochthon. The top of the Ekaluakat formation is also poorly constrained, because it is either truncated by the unconformity at the base of the overlying Lower Mississippian Endicott Group, or it is in thrust contact with older units (Reiser et al., 1980; Lane et al., 1995).

In the summer of 2012, we traversed along a north- trending ridge on the east bank of the lower Kongakut River, which exposes a steeply southward-dipping (~60°–75°) section of Ekaluakat rocks, with the top of the section concealed by the Lower Mississippian Kekiktuk Conglomerate. Below the unconformity and further north along the ridge, the section contains 0.5–1.5-m-thick beds of dark-brown and massive volcanic-rich pebble conglomerate. Similar outcrops were observed during a 2013 expedition on the Yukon side of the border, where clasts from the conglomerate consist of basalt and minor sedimentary lithics that are moderately rounded and range between 2 and 80 mm in diameter (Fig. 3.6A).

Further north along the Kongakut River section, the volcanic beds become thinner and more fine grained, and we collected two samples (12JT37 and 12JT39) for thin section and geochemical analysis. The two samples resemble tuffaceous breccia, consisting of a fine- to coarse-grained mixture of volcanogenic minerals, including rounded basalt clasts, loose grains of clinopyroxene and plagioclase, and fine-grained chert (Fig. 3.6B). The basalt clasts are

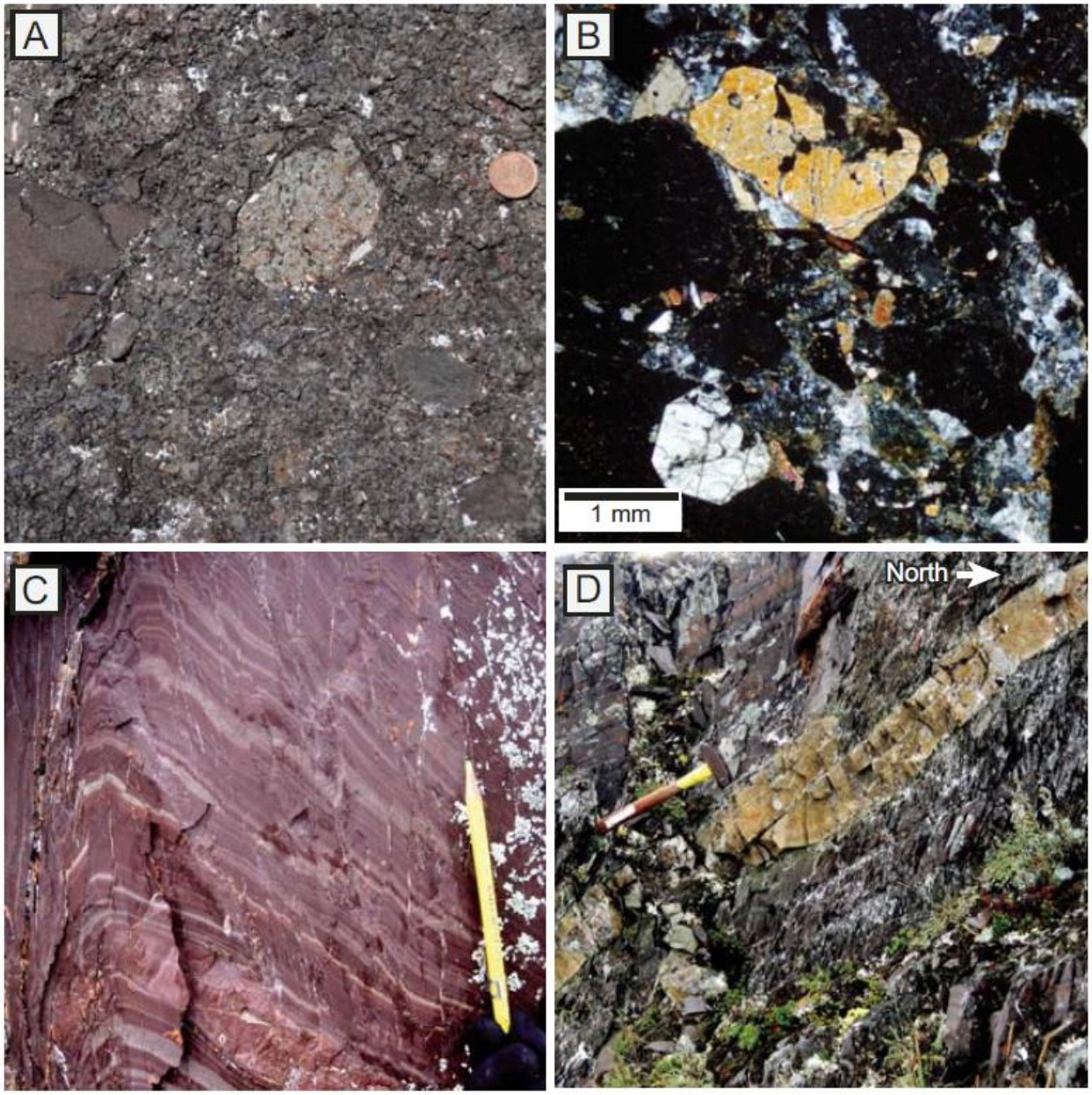

Figure 3.6: Field images of the Ekaluakat formation from the northern belt of the Whale Mountain allochthon in the NE Brooks Range, Alaska. (A) Close-up taken from volcanic breccia of the Ekaluakat formation exposed in northern Yukon; one-cent piece for scale is 1.9 cm in diameter. (B) Cross-polarized view of sample 12JT39 showing volcanic clast and clinopyroxene grains in a chert(?) and clay matrix. (C) Close-up of folded and laminated marron argillite, crosscut by steep micro-shear fractures; pencile for scale is ~13 cm. (D) Photo Looking west along the Kongakut River section of the northern belt showing laminated dark-maroon and gray argillite interbed with a faulted, tan-weathering tuff layer; hammer for scale in ~33 cm.

moderately porphyritic, containing 5%–10% clinopyroxene (augite) phenocrysts in a glassy to microcrystalline groundmass composed of plagioclase (<0.2 mm) and Fe- and Ti-oxide minerals. The clasts are generally fresh, showing little to no alteration from weathering or metamorphism, but in the surrounding groundmass, low-temperature alteration is common. Calcite, microcrystalline quartz, and clay minerals form veinlets in the groundmass and fill amygdules.

The northern parts of the Kongakut River section expose finely laminated, maroon, green, and dark-gray argillite that is crosscut by a steeply dipping network of microshear fractures that occur in the cores of small folds (Fig. 3.6C). The argillite is locally interbedded with a distinctive tan and greenish-gray tuff unit (Fig. 3.6D). A dark-gray, medium- to coarse-grained, volcanic-rich wacke is also occasionally interbedded with the argillite. The wacke consists mostly of reworked volcanic and detrital carbonate grains. Johnson et al. (2016) reported 63 concordant zircon U-Pb ages from this unit (sample 12JT35), 62 of which provided a broad unimodal age population ranging from ca. 602 to 440 Ma and centered at ca. 500 Ma.

ZIRCON U-Pb GEOCHRONOLOGY AND Hf ISOTOPE GEOCHEMISTRY

Zircon U-Pb geochronology and Hf isotope geochemistry from the two volcaniclastic samples (15BJ06 and 13WW23) pro-vide potential constraints on the age and magmatic setting of the volcanic rocks from Whale Mountain allochthon. Standard mineral separation and imaging procedures were followed at the University of Iowa, which included crushing, sieving, water density and magnetic separation, and heavy liquid density separation. The separated zircon grains were mounted in epoxy, ground to expose the grain interiors, and polished prior to cathodoluminescence (CL) and backscattered electron (BSE) imaging using a scanning electron microscope (SEM).

The mounted zircon grains were taken to the University of Arizona LaserChron Center in Tucson, Arizona, to measure the U-Pb and Lu-Hf isotopic ratios by laser ablation–inductively coupled plasma–mass spectrometry (LA-ICP-MS). The CL and BSE images were used to select spot locations for the in-situ measurement from each grain in order to avoid inherited cores, complex zoning, or zones of possible metamictization. The U-Pb isotopes were measured first using a 20-µm-diameter ablation site to determine the age of each grain following the methods of Gehrels et al. (2008). A subset of the measured grains from the same mounts was analyzed for Hf isotope geochemistry using high-resolution-ICP-MS (HR-ICP-MS) following methods outlined by Gehrels and Pecha (2014). In each Hf isotope analysis, a 40-µm-diameter ablation site was centered over the previously excavated U-Pb analysis pit to help ensure that the initial Hf isotopic composition was measured from the same domain as the U-Pb age. The detailed analytical procedures and filtering methods, along with tables of the individual measurements, are included in the Supplemental Material section at the end of this dissertation.

U-Pb ages from each of the volcaniclastic samples are shown on the two concordia diagrams in Figures 3.7A and 3.7B, which were generated using Isoplot 4.1 software (Ludwig, 2012). Reported uncertainties for each U-Pb age are at the 1σ level and include only measurement errors. A "best age" (see Table SM3.2) for each grain was selected using a cutoff of 900 Ma from the calculated $^{206}Pb/^{238}U$ ages. For zircon grains with $^{206}Pb/^{238}U$ ages older than 900 Ma, we used the calculated $^{207}Pb/^{206}Pb$ ages instead. Several ages were excluded/rejected from the data plots or interpretations because of discordance between the $^{206}Pb/^{238}U$ and the $^{206}Pb/^{207}Pb$ ages calculated for each grain. Grains with >20% discordance were rejected, as were grains with >5% reverse discordance.

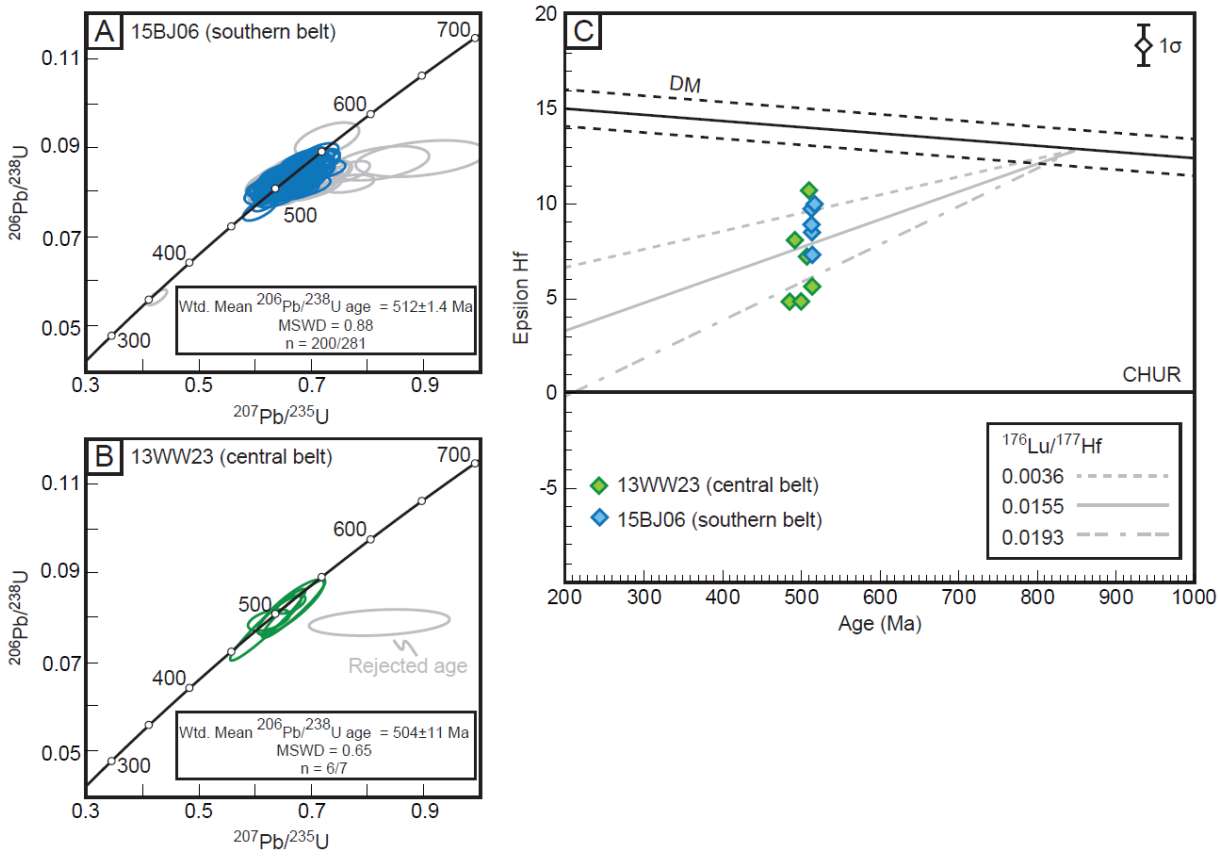

Figure 3.7: Zircon U-Pb ages and Hf isotopic values from laser ablation–inductively coupled plasma–mass spectrometry (LA-ICP-MS) of volcaniclastic rocks from the central and southern belts of the Whale Mountain allochthon. (B) Concordia plot of 274 grains from sample 15BJ06; gray ellipse represents an excluded measurement because of significant discordance. Inset shows calculated weighted (wtd.) mean age of the six concordant ages. (B) Concordia plot of seven grains from sample 13WW23. Inset shows calculated weighted (wtd.) mean age of the six concordant ages. (C) Hf evolution plot showing $\varepsilon Hf_{(t)}$ values for each sample (13WW23 and 15BJ06). The average measurement uncertainty for all analyses (upper right) is shown at the 1σ level. Reference lines on the Hf plot are as follows: DM—depleted mantle, calculated using $^{176}Hf/^{177}Hf_0$= 0.283225 and $^{176}Lu/^{177}Hf_0$ = 0.038512 (Vervoort and Blichert-Toft, 1999); CHUR—chondritic uniform reservoir, calculated using $^{176}Hf/^{177}Hf$ = 0.282785 and $^{176}Lu/^{177}Hf$ = 0.0336 (Bouvier et al., 2008); gray dashed show interpreted felsic crustal evolution trajectories assuming present-day $^{176}Lu/^{177}Hf$ = 0.0115 (Vervoort and Patchett, 1996; Vervoort et al., 1999). Full data tables are provided in the Supplemental Material section at the end of this dissertation.

U-Pb Geochronological Results

The two analyzed samples were composed of highly sheared and angular volcanic detritus (mostly plagioclase) and volcanic rock fragments set within an altered matrix of sericite and calcite. The southern belt sample (15BJ06) yielded more than 300 grains from the heavy mineral separation procedure. Nineteen of these grains analyzed by LA-ICP-MS yielded spurious isotopic ratios and were thus excluded from further data reduction. Using the CL images, we determined that these grains are not zircon because they lacked measurable luminescence (see Supplemental Material section). The remaining 281 grains consisted of light purple to clear angular grains that ranged from ~50 to 150 µm in length. Seventy-three of these grains showed discordance among the $2^{06}Pb/^{238}U$ and $^{206}Pb/^{207}Pb$ ages and were thus excluded from our "best age" filter. An additional five grains were excluded because they yielded $^{206}Pb/^{238}U$ ages younger than 200 Ma. These grains showed strong zonation in the CL images (see Supplemental Material section), and we infer that they were a result of sample contamination. The remaining 203 grains yielded ages from ca. 2578 to 354 Ma; however, most of the ages (n = 200) ranged from ca. 544 to 473 Ma and constituted a weighted mean age of 512 ± 1.4 Ma (1σ) with a mean square weighted deviation (MSWD) of 0.88 (Fig. 3.7A). A MSWD of 0.88 is close to 1.0, which implies that the observed scatter in the ages is consistent with precision, and that the analytical precision of the method employed is unable to resolve differences among the age populations (e.g., Wendt and Carl, 1991).

Sample 13WW23 was collected from the eastern edge of the central belt in Yukon at the same location as fossil locality J1352 (Fig. 3.1). Like sample 15BJ06, 13WW23 is predominately composed of angular volcanic material, and the separated zircon grains are angular and range from ~50 to 150 µm in length. The sample only yielded seven zircon grains, and one of the

grains was excluded from further discussion because of discordance among the $^{206}Pb/^{238}U$ and $^{206}Pb/^{207}Pb$ ages. The other six grains had ages ranging from ca. 514 to 485 Ma, with a $^{206}Pb/^{238}U$ weighted mean age of 504 ± 11 Ma (Fig. 3.7B) and MSWD of 0.65, which could indicate that the observed scatter among the ages is less than that predicted by the analytical uncertainties.

Hf Isotope Geochemistry

Hafnium isotopic measurements were performed on 11 individual grains: five from sample 15BJ06 and six from sample 13WW23. We specifically targeted grains with ages in the 544–475 Ma range because we inferred that those grains would represent the time at which the volcanic rocks erupted. The data are presented on a Hf-evolution diagram (Figs. 3.7C) that shows εHf(t) values at the time of crystallization. The εHf(t) values were determined by comparing the measured Hf isotopic values of an individual grain relative to the known Hf values of a chondritic uniform reservoir (CHUR; Bouvier et al., 2008) at the time of crystallization.

The Hf data from the two samples are similar, with εHf(t) values that range from 4.8 to 10.7. These values are considered as intermediate and juvenile in composition because they plot just below the depleted mantle trajectory. Several different interpretations can explain these values. One possible explanation is that the extracted melts from which the zircon grains crystallized were produced by melting of Neoproterozoic crust. This is inferred from the Hf evolution trajectories of felsic crust (gray lines in Fig. 3.8C), which are based on the average present-day $^{176}Lu/^{177}Hf$ ratio of 0.0115 (Vervoort and Patchett, 1996; Vervoort et al., 1999). A second explanation is that melts were derived from the depleted mantle but experienced contamination from enriched sources, such as old (>1000 Ma) crustal rocks or possibly enriched reservoirs in the mantle.

IGNEOUS GEOCHEMISTRY

Twenty-five whole-rock basalt samples were collected from outcrops in the British and Romanzof Mountains of the NE Brooks Range (Fig. 3.1), including three samples from the southern belt, 20 samples from the central belt, and two samples from the northern belt. The samples were subsequently trimmed to exclude visible alteration and weathering, crushed using a mortar and pestle, and powdered in a SPEX 8515 Shatterbox. The sample powders were shipped to Activation Laboratories LTD (Actlabs) in Ontario, Canada, where they were mixed with a flux of lithium metaborate and lithium tetraborate and fused into glass beads using an induction furnace. The major-element oxides (e.g., SiO2, MgO, etc.) and a subset of trace elements (Sr, Ba, Sc, V, Y, and Zr) were determined by inductively coupled plasma–optical emission spectrometry (ICP-OES) using a Thermo Jarrell-Ash ENVIRO II ICP or a Varian Vista 735 instrument. The remaining trace elements were determined by ICP-MS using a Perkin Elmer Sciex ELAN 9000 instrument. The calibration of the results was performed using prepared USGS and CANMET certified standard reference materials.

The major- and trace-element compositions of the basalt samples are given in Tables 3.1 and 3.2, with the major-element compositions expressed in weight percent (wt%), and the trace element compositions described in parts per million (ppm). The geochemical data were used to distinguish and classify different volcanic suites from each belt. The low to moderate levels of alteration observed in thin section were supported by the moderate (2–7 wt%) loss on ignition (LOI) values. Alteration likely caused some element mobility, especially for the large ion lithophile elements (LILEs). Several samples had K2O concentrations that were lower than the ICP-OES detection limits (0.01 wt%), and many of the samples showed large variations in Rb and Ce concentrations. Because of this, most of our classifications and interpretations are based

TABLE 3.1: MAJOR-ELEMENT CHEMISTRY OF THE WHALE MOUNTAIN ALLOCHTHON

Sample number	SiO_2 (wt. %)	TiO_2 (wt. %)	Al_2O_3 (wt. %)	$Fe_2O_3(T)$* (wt. %)	MnO (wt. %)	MgO (wt. %)	CaO (wt. %)	Na_2O (wt. %)	K_2O (wt. %)	P_2O_5 (wt. %)	LOI (wt. %)	Total
Southern Belt												
14BJ22	45.02	2.865	15.11	13	0.218	8.5	7.3	2.88	0.25	0.28	4.01	99.44
14BJ24	54.72	1.777	12.58	13.21	0.18	4.28	4.71	3.9	0.4	0.22	4.63	100.6
15BJ08	43.64	3.055	14.25	16.11	0.229	6.57	10.63	2.58	0.13	0.32	3.25	100.8
Central Belt												
12JT13B	42.07	1.814	13.03	11.21	0.206	12.21	13.56	0.16	0.001	0.18	6.36	100.8
12JT14	46.72	2.782	14.48	11.81	0.162	6.53	10.96	1.66	0.01	0.32	3.84	99.29
12JT15	46.33	2.336	16.39	9.36	0.234	6.6	11.25	2.14	0.21	0.26	5.53	100.7
12JT16	45.45	3.118	14.47	15.72	0.202	6.54	5.22	3.88	0.02	0.37	4.76	99.74
12JT17	42.87	2.586	15.2	12	0.173	7.97	12.16	1.93	0.03	0.32	4.26	99.48
12JT18	48.02	2.841	16.16	10.22	0.198	8.07	6.18	4.09	0.36	0.32	4.15	100.6
12JT19	49.52	2.749	13.55	11.99	0.141	6.09	10.1	0.51	0.001	0.32	5.74	100.7
12JT20	41.24	1.951	14.56	11.72	0.14	9.89	13.46	0.09	0.001	0.21	5.85	99.13
12JT21	49.91	3.23	13.2	14.44	0.209	5.12	7.63	3.26	0.07	0.32	3.41	100.8
17LF13	48.85	2.789	16	11.33	0.14	6.38	3.31	4.08	0.95	0.31	5.15	99.29
18LF13	54.97	3.373	16.27	7.63	0.064	4.24	2.69	1.87	4.3	0.41	4.14	99.96
19LF13	47.4	2.938	13.88	12.03	0.199	8.2	8.44	3.59	0.46	0.34	3.15	100.6
20LF13	48.78	2.443	13.67	12.53	0.17	8.19	6.85	3.96	0.41	0.27	3.56	100.8
21LF13	49.07	2.721	13.8	11.45	0.158	7.13	7.88	3.98	0.66	0.32	3.74	100.9
22LF13	49.26	3.045	14.59	12.55	0.181	6.45	4.01	4	0.61	0.34	5.06	100.1
23LF13	46.72	3.211	14.43	11.26	0.152	6.75	5.6	3.15	1.12	0.37	6.77	99.51
13MC-062	47.76	2.604	13.35	12.94	0.163	8.21	7.85	4.42	0.06	0.31	3.21	100.9
13MC-063	50.33	2.317	14.98	9.19	0.219	6.51	6.3	5.21	0.06	0.28	4.15	99.56
13MC-065	46.43	2.552	14.5	12.19	0.185	6.91	10.56	3.11	0.21	0.28	2.41	99.35
13JVS-362	46.82	3.066	14.91	13.34	0.181	6.15	9.11	3.69	0.41	0.38	2.11	100.2
Northern Belt												
12JT37	39.85	5.199	9.55	15.77	0.202	9.8	10.52	2.27	1.31	0.77	4.41	99.66
12JT39	45.49	4.266	12.06	12.2	0.192	5.45	11.1	4.49	0.3	0.87	4.1	100.5

Note: LOI—loss on ignition

*All Fe is converted and reported as ferric because oxidation state was not determined prior to heating during LOI measurements.

TABLE 3.2: TRACE-ELEMENT CHEMISTRY OF THE WHALE MOUNTAIN ALLOCHTHON

Sample number	Rb (ppm)	Sr (ppm)	Cs (ppm)	Ba (ppm)	Cr (ppm)	Co (ppm)	Ni (ppm)	Cu (ppm)	Zn (ppm)	Sc (ppm)	V (ppm)	Y (ppm)	Zr (ppm)	Nb (ppm)	Hf (ppm)	Ta (ppm)	Th (ppm)	U (ppm)
Southern Belt																		
14BJ22	5	186	2.3	92	270	50	130	150	100	50	426	47	204	6	5.0	0.5	0.7	0.20
14BJ24	6	156	1.1	51	210	36	100	30	70	37	268	33	126	4	3.1	0.3	0.4	< 0.1
15BJ08	2	223	< 0.5	62	150	47	60	160	110	43	485	38	191	9	4.5	0.7	0.8	0.30
Central Belt																		
12JT13B	< 2	950	< 0.5	17	980	62	400	90	80	39	256	14	99	17	2.4	1.2	1.2	0.40
12JT14	< 2	1341	< 0.5	36	160	40	110	170	100	31	313	22	173	25	4.3	1.8	2.1	0.60
12JT15	4	1307	< 0.5	82	190	45	130	180	80	32	291	16	134	19	3.4	1.4	1.6	0.40
12JT16	< 2	191	< 0.5	28	60	43	70	40	110	33	349	25	187	27	4.7	2.0	2.2	0.50
12JT17	< 2	515	< 0.5	54	140	44	100	90	90	34	323	20	161	28	4.0	2.1	2.2	0.60
12JT18	7	321	< 0.5	118	190	79	120	380	120	33	322	26	175	26	4.5	1.8	2.1	0.50
12JT19	< 2	66	< 0.5	24	130	39	90	80	90	30	291	23	185	25	4.3	1.8	2.0	0.50
12JT20	< 2	944	< 0.5	34	800	65	400	110	80	37	260	14	105	17	2.6	1.2	1.3	0.40
12JT21	< 2	68	< 0.5	63	30	47	60	60	130	28	417	20	158	28	4.0	2.0	2.2	0.70
17LF13	8	217	1.5	1643	90	42	50	100	110	30	334	21	168	26	4.0	1.8	2.0	0.60
18LF13	53	54	1.6	896	150	97	140	110	160	32	329	25	209	30	5.2	2.2	2.5	0.60
19LF13	4	430	< 0.5	577	190	44	150	40	100	31	322	21	185	32	4.3	2.2	2.4	0.80
20LF13	6	221	3.8	391	220	45	150	20	90	29	304	17	132	22	3.3	1.5	1.6	0.50
21LF13	7	399	1.9	697	230	39	130	30	80	31	307	20	176	29	4.1	2.1	2.2	0.70
22LF13	9	524	4.9	607	150	39	110	170	100	30	328	22	192	28	4.6	2.0	2.3	0.70
23LF13	12	191	0.8	439	190	42	120	30	90	32	310	21	199	33	4.9	2.4	2.5	0.70
13MC-062	< 1	160	< 0.1	59	490	51	210	30	90	36	337	24	151	26	3.6	1.6	1.6	0.42
13MC-063	< 1	203	< 0.1	83	160	43	70	30	100	29	265	24	160	24	4.0	1.8	2.0	0.64
13MC-065	2	485	0.4	134	220	47	110	120	90	34	337	23	141	23	3.6	1.8	1.5	0.47
13JVS-362	6	465	0.3	169	60	46	60	50	120	34	389	26	184	30	4.4	2.0	2.0	0.45
Northern Belt																		
12JT37	22	228	2.5	521	590	56	260	70	140	29	354	27	401	68	9.9	4.6	4.6	1.30
12JT39	6	659	1.0	3357	30	36	100	90	140	23	366	33	361	59	8.4	3.9	5.0	1.60

Note: Measurements with < before the number indicate that the elemental proportions are below the detection limit of the Inductively Coupled Plasma-Mass Spectrometry (ICP-MS).

TABLE 3.2 CONT'D

Sample number	La (ppm)	Ce (ppm)	Pr (ppm)	Nd (ppm)	Sm (ppm)	Eu (ppm)	Gd (ppm)	Tb (ppm)	Dy (ppm)	Ho (ppm)	Er (ppm)	Yb (ppm)	Lu (ppm)
Southern Belt													
14BJ22	7.9	24.5	4.13	21.7	7.30	2.56	8.70	1.50	9.50	1.90	5.40	5.10	0.76
14BJ24	4.8	15.0	2.49	13.8	4.80	1.63	5.80	1.00	6.50	1.30	3.80	3.70	0.55
15BJ08	11.0	28.2	4.16	19.5	5.90	2.31	7.00	1.30	7.70	1.50	4.30	4.00	0.59
Central Belt													
12JT13B	14.6	33.0	4.18	17.3	3.80	1.39	3.80	0.60	3.10	0.60	1.50	1.20	0.18
12JT14	22.8	52.8	6.56	27.6	6.30	2.29	5.90	1.00	5.00	0.90	2.50	2.00	0.29
12JT15	15.9	38.6	4.96	20.6	4.70	1.83	4.60	0.70	3.60	0.70	1.70	1.30	0.19
12JT16	24.0	54.6	7.00	29.0	6.90	2.39	6.90	1.10	5.90	1.10	2.90	2.20	0.31
12JT17	23.9	55.3	6.79	27.9	6.00	2.06	5.50	0.90	4.70	0.80	2.20	1.70	0.24
12JT18	18.9	46.4	5.85	24.6	5.90	2.02	5.60	1.00	5.60	1.10	2.90	2.50	0.38
12JT19	21.7	51.3	6.44	26.4	6.20	2.05	6.00	0.90	5.10	0.90	2.50	1.90	0.26
12JT20	16.1	36.0	4.33	17.3	3.90	1.56	3.80	0.60	3.30	0.60	1.60	1.20	0.17
12JT21	23.3	52.5	6.44	26.4	6.00	2.10	5.60	0.90	4.80	0.90	2.30	1.80	0.25
17LF13	20.8	48.7	6.11	25.2	6.00	2.34	6.00	0.90	4.80	0.90	2.30	1.70	0.24
18LF13	24.5	58.7	7.08	29.3	6.50	2.02	5.70	0.90	5.00	0.90	2.50	2.00	0.30
19LF13	26.6	59.5	7.14	28.7	6.40	2.10	5.90	0.90	4.80	0.90	2.30	1.70	0.24
20LF13	17.5	41.6	5.27	21.9	4.80	1.81	4.70	0.70	3.80	0.70	1.80	1.40	0.21
21LF13	24.5	57.3	6.98	28.5	6.10	2.16	5.80	0.90	4.60	0.80	2.20	1.80	0.26
22LF13	23.2	56.2	7.13	31.0	6.90	2.48	6.40	1.00	5.00	0.90	2.30	1.70	0.23
23LF13	20.9	52.0	6.72	29.1	6.50	2.30	6.00	1.00	5.00	0.90	2.40	1.80	0.24
13MC-062	21.0	46.0	6.13	23.1	5.92	1.86	5.27	0.81	4.62	0.84	2.23	1.93	0.27
13MC-063	16.9	41.0	5.60	24.5	5.38	1.79	5.06	0.80	4.44	0.80	2.22	1.81	0.26
13MC-065	15.7	36.9	5.02	20.6	5.41	1.84	5.14	0.81	4.27	0.77	2.08	1.81	0.25
13JVS-362	22.8	51.6	6.94	27.2	6.64	2.19	6.09	0.97	5.19	0.90	2.38	2.04	0.29
Northern Belt													
12JT37	51.5	119.0	14.70	59.6	12.60	4.07	10.70	1.50	6.90	1.10	2.70	1.80	0.26
12JT39	55.4	123.0	14.80	60.5	12.40	3.86	10.90	1.50	7.50	1.30	3.20	2.30	0.31

Note: Measurements with < before the number indicate that the elemental proportions are below the detection limit of the Inductively Coupled Plasma-Mass Spectrometry (ICP-MS).

on the relative abundances of incompatible and rare earth elements (REEs), which typically remain stable during alteration and metamorphism (e.g., Winchester and Floyd, 1977; Shervais, 1982; Pearce, 1996).

Geochemical Results

Southern Belt

The three samples from the Marsh Fork volcanic rocks of the southern belt have major-element oxide concentrations that resemble average basalt (Table 3.1), although one sample (14BJ24) has elevated SiO2 (~55 wt%) and depleted MgO (~4 wt%) concentrations, resembling andesite rather than basalt. All three samples, however, plot within the tholeiitic basalt field on the Nb/Y–Zr/Ti plot (Fig. 3.8), showing Nb/Y ratios <1 and Zr/Ti ratios ~0.01. On the Ti-V plot (Fig. 3.9A), the samples fall within the mid-ocean-ridge basalt (MORB) field and have constant Ti/V ratios of ~40. The nearly constant Ti/V ratios among the samples imply that clinopyroxene was not a fractionating melt phase or a refractory mantle phase during the generation of the melt. In support of this assertion, the petrographic work shows that clinopyroxene is only present as an intergranular phase with larger plagioclase (Fig. 3.3B).

The southern belt samples show pronounced depletions of the most incompatible elements, yielding relatively fl at to slightly positive slopes on the normalized variation diagrams (Fig. 3.10). The samples also show depletions in the high field strength elements Th, U, Nb, Ta, and La, enrichment in the heavy rare earth elements Dy, Yb, Y, and Lu, and relatively flat slopes on the chondrite-normalized REE diagram (Fig. 3.10A). This is supported by the chondrite-normalized LaN/SmN ratios, which range from 0.6 to 1.2, representing the lowest ratios among all the samples in the data set.

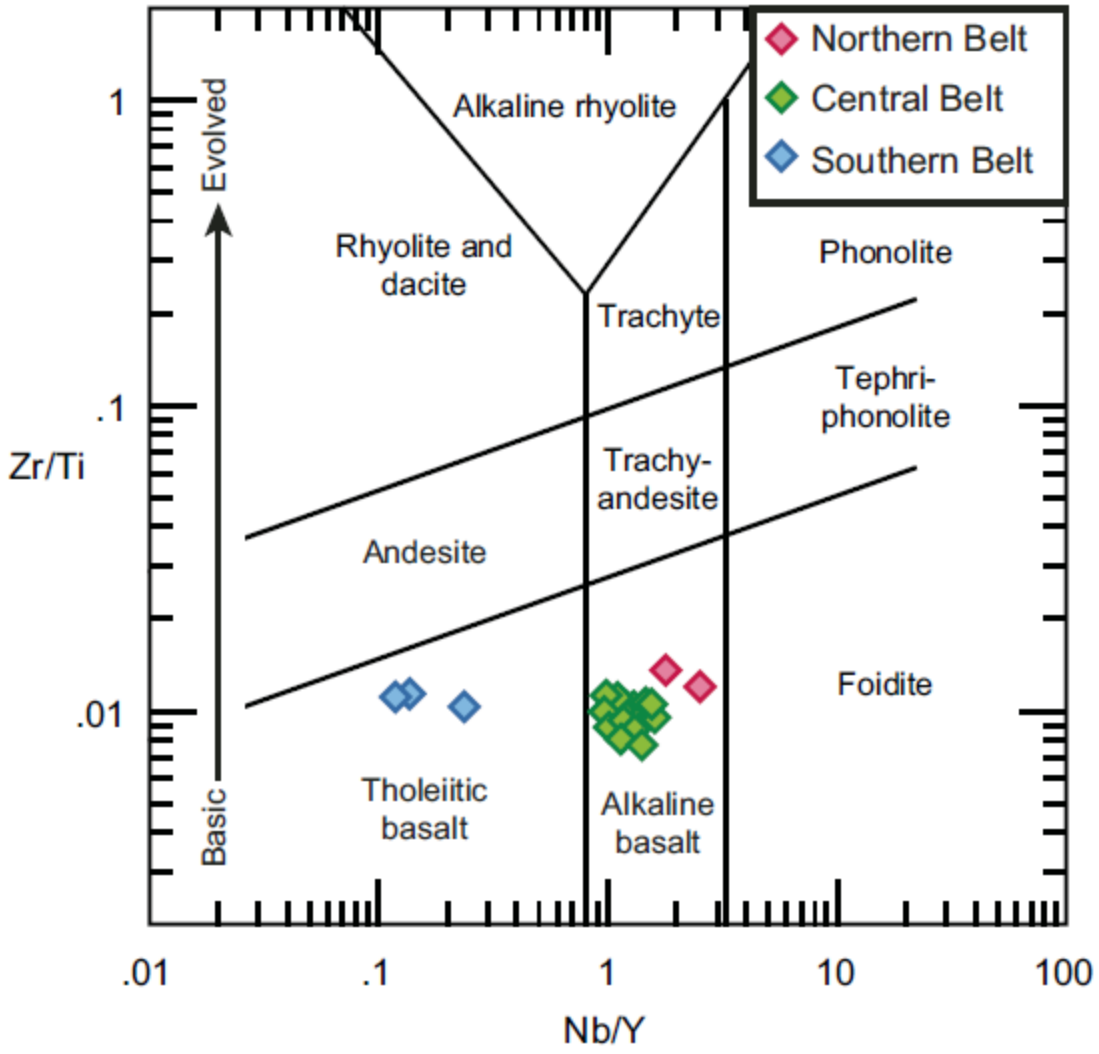

Figure 3.8: The Nb/Y–Zr/Ti discrimination plot of Pearce (1996). Zr/Ti ratio is used as an index of differentiation, and the Nb/Y is used as an alkalinity index.

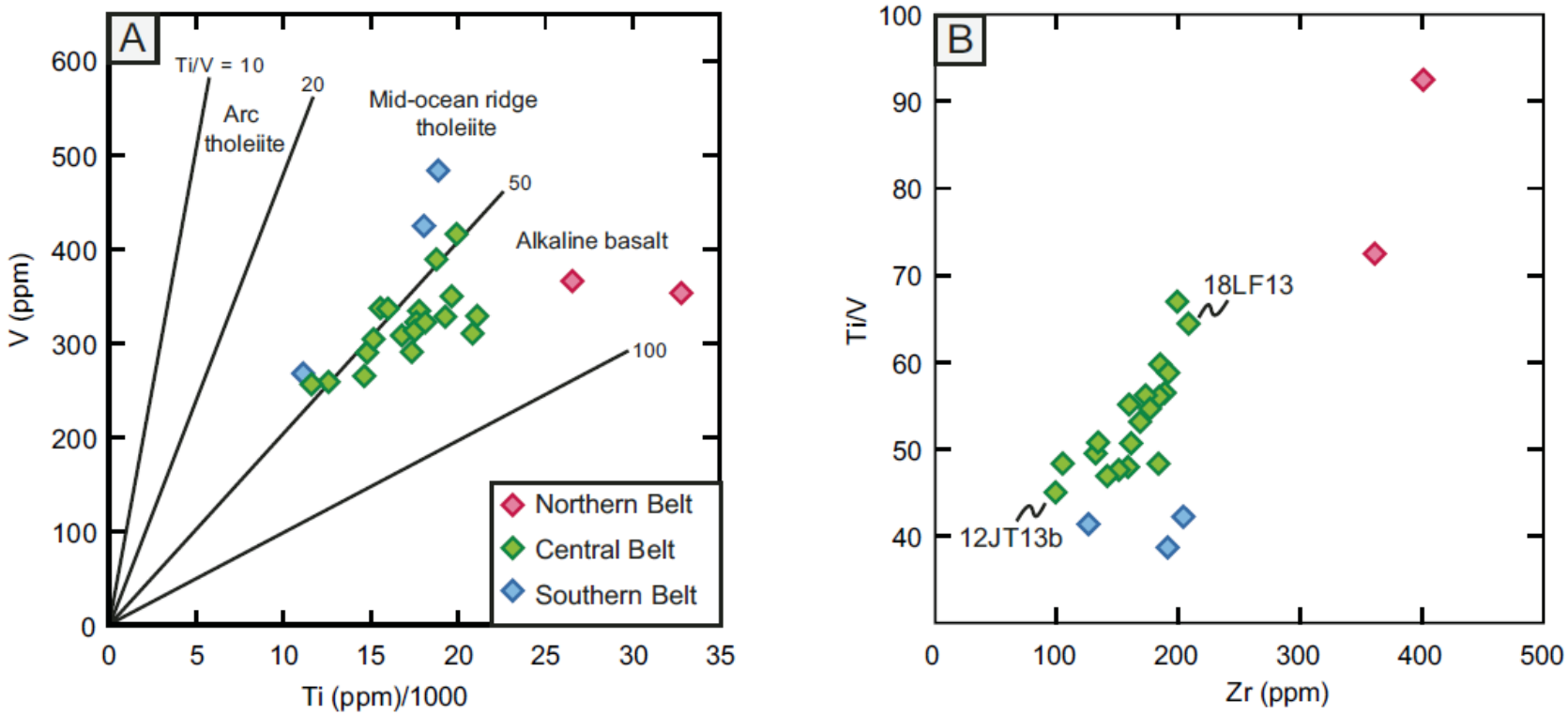

Figure 3.9: (A) Ti–V plot after after Shervais (1982) showing the fields of Low-Ti island arc tholeiite, island arc tholeiite, mid-ocean ridge tholeiite (includes back-arc basin basalt), and alkaline basalt. Solid lines represent constant Ti/V ratios of 10, 20, 50, and 100 (B) Zr–Ti/V plot showing the changes in the Ti/V ratio (controlled by clinopyroxene fractionation) with respect to Zr (a commonly used differentiation index for altered basalt).

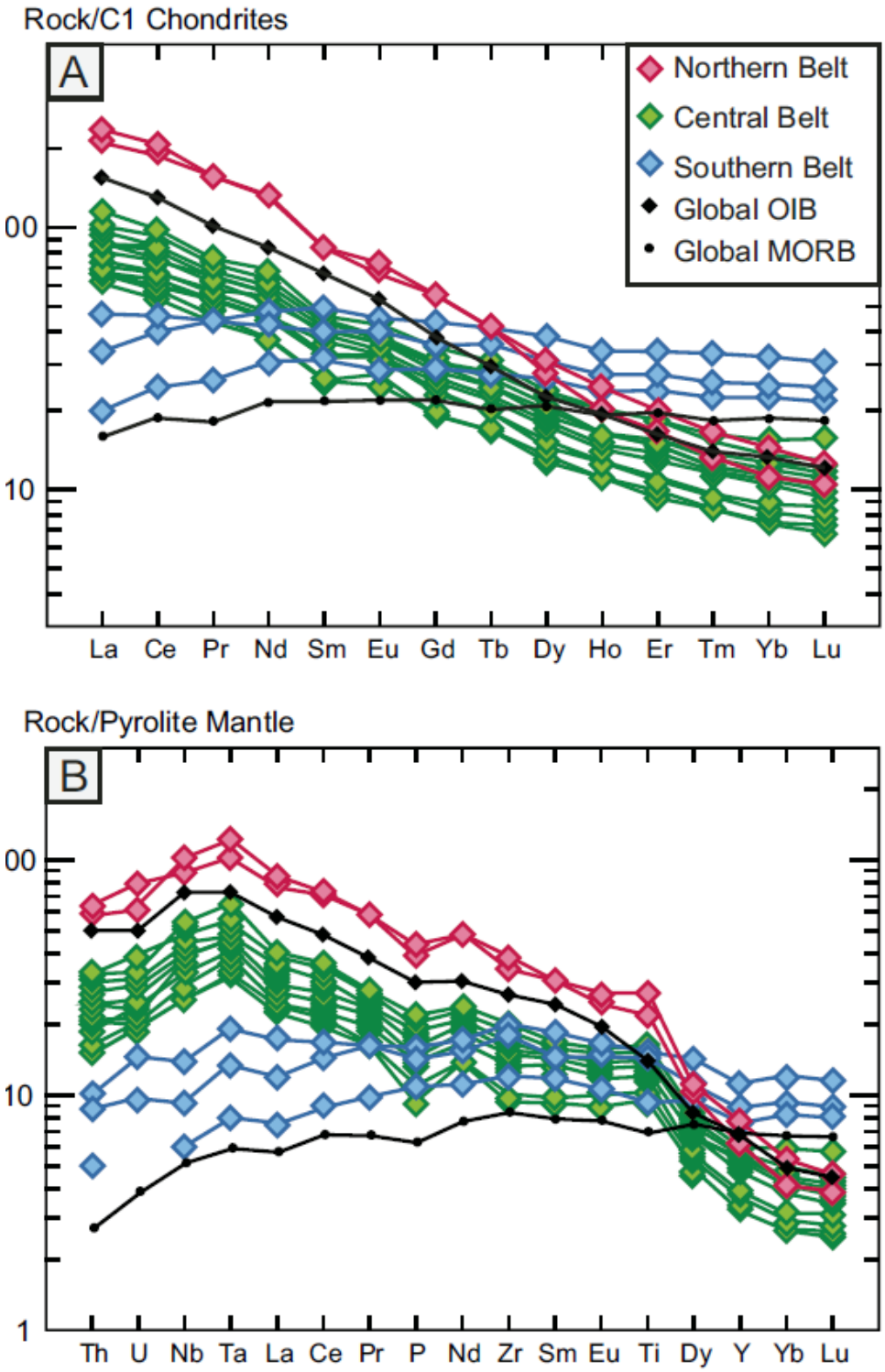

Figure 3.10: Trace-element variation diagrams. (A) Rare earth elements (REE) normalized to average C1 chondrite compositions from McDonough and Sun (1995). (B) selected trace element variations that are normalized to average pyrolite mantle compositions of McDonough and Sun (1995).

Central Belt

The 20 Whale Mountain volcanic samples collected from the central belt show significant variation among most major- element compositions (Table 3.1), but they are all within typical compositions of basalt. In general, correlation among element pairs is weak, but MgO, which is a common index of differentiation in basalts, is weakly correlated with SiO_2, TiO_2, CaO, and P_2O_5. All the samples from the central belt plot within the alkaline basalt field on the Nb/Y-Zr/Ti plot (Fig. 3.8) and have Nb/Y ratios that are generally >1. On the Ti-V discrimination plot (Fig. 3.9A), the samples plot along a linear trend that crosses the 50 Ti/V ratio line at a low angle. This is likely an effect of clinopyroxene fractionation, which causes an increase in the Ti/V ratio as the melt evolves because clinopyroxene preferentially takes on V3+ over Ti during crystallization. This is supported by an increase in the Ti/V ratio with respect to Zr concentration (Fig. 3.9B).

Much of the intrasample variation for central belt samples can be explained by crystal fractionation. Using Zr, another common fractionation index, sample 18LF13, which has the highest concentration of Zr (209 ppm) among the suite, plots at the extreme end of the evolution trend line on the Zr-Ti/V plot (Fig. 3.9B). In thin section, sample 18LF13 shows almost no recognizable primary phenocrysts, which is likely due to the extensive sericite alteration of plagioclase. Remnants of olivine or clinopyroxene are also absent. At the other end of the evolution trend line, two samples (12JT13b and 12JT20) have low Zr concentrations (<110 ppm) and low Ti/V ratios, which could be the result of little to no fractionation of clinopyroxene. The two samples are distinguished by high concentrations of MgO (>10%) and high concentrations of the compatible trace elements Ni (400 ppm each) and Cr (>800 ppm). This, along with the high abundances of olivine phenocrysts in thin section (Figs. 3.5A and 3.5B), favors

classification of these two samples as picrites, which could have formed by the accumulation of olivine in a fractionating magma chamber. Samples with more intermediate compositions (Zr = 140–190 ppm) typically show a greater variety of phenocrysts, including clinopyroxene and plagioclase. In some cases, olivine occurs as inclusions within larger plagioclase phenocrysts (Fig. 3.5C), suggesting that plagioclase crystallized after olivine.

The normalized variation diagrams (Fig. 3.10) support incompatible element enrichment. The steep negative slopes on the REE diagram (Fig. 3.10A), along with the 1.8–2.6 La_N/Sm_N ratios, indicate that partitioning of the most incompatible REEs into the melt occurred by low degrees of partial melting or by melting of an enriched mantle source. In the pyrolite-normalized diagram (Fig. 3.10B), the slopes drastically drop off after Ti due to the low concentrations of Dy, Y, Yb, and Lu. This is likely an indication of refractory garnet in the mantle source, because these elements, although highly incompatible with most minerals, are strongly partitioned into garnet and withheld from the melt (see Discussion section).

Northern Belt

The two volcanic samples from the Ekaluakat formation (12JT37 and 12JT38) collected from the northern belt are characterized by high concentrations of incompatible elements. Both samples show elevated concentrations of TiO_2 (>4 wt%), P_2O_5 (>0.75 wt%), and Zr (>350 ppm). Additionally, the two samples have noticeably lower concentrations of Al_2O_3 (9.55 and 12.06 wt%) and SiO_2 (39.85 and 45.49 wt%) but show a wide range in MgO concentrations (5.45 and 9.8 wt%). Both samples plot within the alkaline basalt fields on the Zr/Ti-Nb/Y plot (Fig. 3.8) of Pearce (1996) and the Ti-V plot (Fig. 3.9) of Shervais (1982). The significant differences between the two Ti/V ratios, 92.5 for 12JT37 and 72.5 for 12JT39, could be caused by the fractionation of clinopyroxene. Like the central belt samples, the northern belt samples have

steep negative slopes on the normalized variation diagrams (Fig. 3.10), although the northern belt samples show even greater incompatible element enrichment. They have La_N/Sm_N ratios >2.5 and low concentrations of Dy, Y, Yb, and Lu, reflecting the signature of refractory garnet in the mantle source.

PALEONTOLOGY

Dutro et al. (1972) were the first to report Cambrian fossils from the rocks here included in the Whale Mountain allochthon. From exposures of their sequence along the Marsh Fork of the Canning River (Fig. 3.1), they recovered a trilobite fauna from their "volcanic and carbonate member," strata assigned here to the Egaksrak formation. The trilobites from the Marsh Fork locality were assigned without reservation to the genus *Olenellus*, which confirmed an early Cambrian age and "North American affinities" for these rocks of the southern belt. A second collection, recovered from exposures of the same member near the Leffingwell Fork of the Aichilik River in the central belt, contained trilobites, agnostoid arthropods, and calcitic brachiopods. It also was interpreted as a "North American" fauna, but of late Cambrian age. Both the continental affinity and the age were based on identification of one trilobite in the collection as *Saratogia*. Here, we detail the findings from two new fossil localities and a resampled collection from the Leffingwell Fork locality of Dutro et al. (1972).

Fossil Locality J1475 (Southern Belt)

The Marsh Fork locality was not resampled in our study, but reconnaissance sampling did yield a new fossil locality near the eastern end of the southern belt in the eastern Romanzof Mountains (Figs. 3.1 and 3.3A). The faunal collection from this locality, designated J1475, includes at least three agnostoid arthropod species, four or five trilobite species, and phosphatic brachiopods. The agnostoids and trilobites, illustrated in Figure 3.11, are identified as:

(1) *Pseudagnostus aff. P. parvus Shergold,* 1980;

(2) *Pseudagnostus josepha*?;

(3) *Neoagnostus*? sp.;

(4) *Aplotaspis* new species;

(5) *Stenopilus*? sp.;

(6) genus species indeterminate 75A;

(7) genus species indeterminate 75B; and

(8) genus species indeterminate 75C.

Details on the morphology and taxonomic assignments are provided in Appendix 3.1. It is unknown whether genus species indeterminate (gen. sp. indet.) 75C is the pygidium of gen. sp. indet. 75A, gen. sp. indet. 75B, or a fifth trilobite species. The agnostoids and trilobites confirm an age significantly younger than the Marsh Fork fauna and suggests that some of the Egaksrak units in the southern belt are assigned to the upper Cambrian (Furongian Series), although an uppermost middle Cambrian assignment (Guzhangian Stage of the Miaolingian Series) cannot be ruled out entirely.

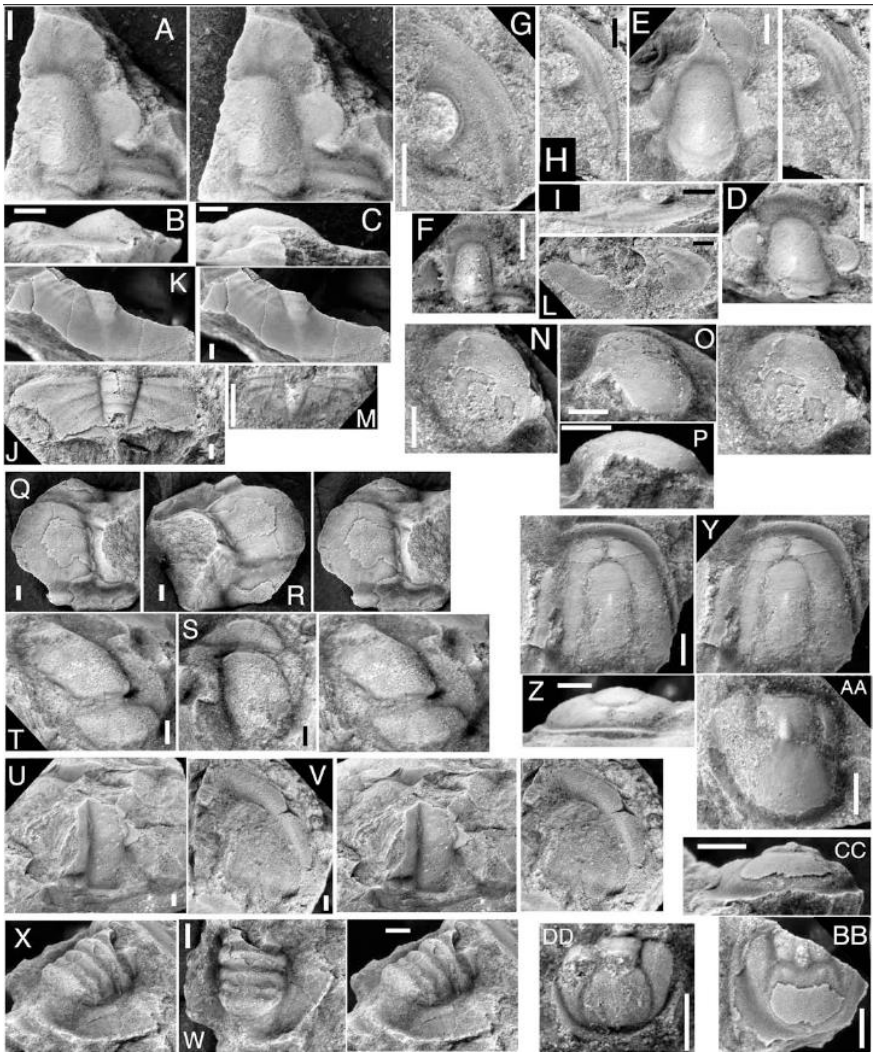

Figure 3.11: Trilobites and agnostoid arthropods from the Egaksrak formation at locality J1475. View is dorsal (palpebral for cranidia) unless indicated otherwise. White or black scale bar in each photo is ~1 mm in length. A–M: *Aplotaspis* new species; (A–C) dorsal stereopair, anterior, and lateral views of large cranidium, CM59287; (D–F) small CM59288, medium CM59289, and very small CM59290 cranidia; (G) large, fragmentary librigena, CM59291; (H–I) stereopair and exterior view of small librigena, CM59292; (J) large, fragmentary pygidium, CM59293; (K) stereopair of large, fragmentary pygidium CM59294; (L) small, fragmentary pygidium CM59295; (M) very small pygidium CM59296. N–P: *Stenopilus*? sp., dorsal stereopair, anterior oblique, and lateral views of fragmentary small cranidium CM59297. Q–T: Genus species indeterminate 75A, fragmentary large cranidia; (Q–R) dorsal stereopair and anterior oblique views of CM59298; (S–T) dorsal view and anterior-oblique stereopair of CM59299. U–V: Genus species indeterminate 75B; (U) stereopair of large, fragmentary cranidium CM59300; (V) stereopair of large, fragmentary librigena CM59301. W–X: Genus species indeterminate 75C, dorsal and posterior oblique stereopair of fragmentary medium pygidium CM59302. Y–AA: *Pseudagnostus* cf. *P. parvus*; (Y–Z) dorsal stereopair and anterior view of fragmentary large cephalon CM59303; (AA) fragmentary large pygidium CM59304. BB–CC: *Neoagnostus*? sp.; dorsal and posterior views of fragmentary small pygidium CM59305. DD: *Pseudagnostus josepha*?, fragmentary very small pygidium CM59306

Fossil Locality J1480 (Central Belt)

The exposures at the Leffingwell Fork locality were resampled in 2014. The new collection, referred to here as J1480, significantly expanded the number of trilobite and agnostoid specimens available to critically evaluate the taxonomic assignments of Dutro et al. (1972). One agnostoid and six trilobites are represented (Fig. 3.12), including:

(1) *Micragnostus* sp.;

(2) *Plethopeltis*? sp.;

(3) idahoiid new genus, new species 1;

(4) idahoiid new genus, new species 2;

(5) idahoiid?, genus and species indeterminate;

(6) genus species indeterminate 80A; and

(7) genus species indeterminate 80B.

The dominance of the fauna by idahoiids, and the similarity of the agnostoid species to specimens of *Microagnostus chiushuensis* (Kobayashi) illustrated by Westrop (1995) from lower Sunwaptan strata in northwestern Canada support the "mid- Franconian" age assigned to this fauna by Dutro et al. (1972). In modern terms, this equates to the mid-Furongian (Jiangshanian Stage). The idahoiids also link the fauna to Laurentia, but the absence of *Saratogia* and several other genera that occur in most *Saratogia* or *Idahoia* zone faunas across North America (see Discussion) suggests a paleogeographic location somewhat removed from the Laurentian platform itself.

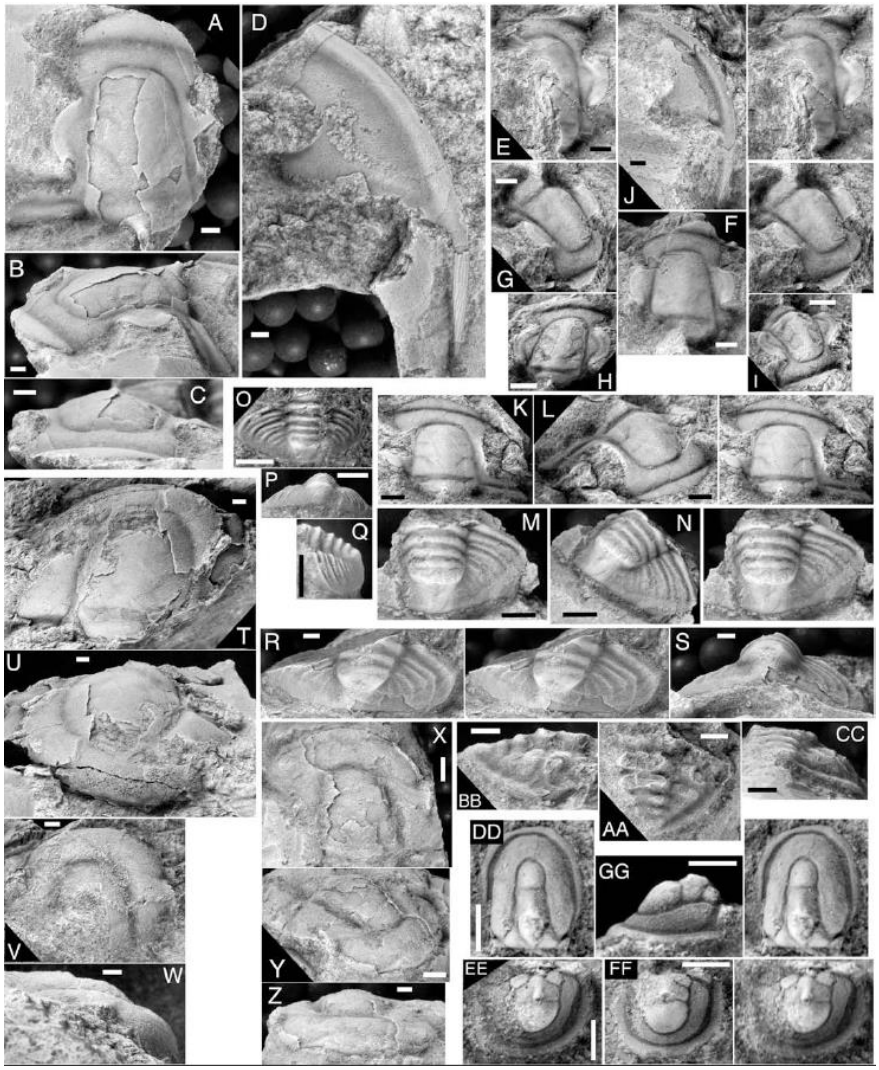

Figure 3.12: Trilobites and agnostoid arthropods from the Egaksrak formation at locality J1480. View is dorsal (palpebral for cranidia) unless indicated otherwise. White or black scale bar in each photo is ~1 mm in length. A–D: Idahoiid new genus new species 1; (A–C) dorsal, anterior oblique, and anterior views of cranidium CM59307; (D) large librigena CM59308. E–J: Idahoiid new genus new species 2; (E) stereopair of medium cranidium CM59309; (F–G) dorsal view and anterior oblique stereopair of medium cranidium CM59310; (H–I) dorsal and anterior oblique views of small cranidium CM59311; (J) large librigena CM59312. K–L: Genus species indeterminate 80B, dorsal stereopair and anterior oblique view of medium cranidium CM59320. M–Q: idahoiid pygidium 2; (M–N) dorsal stereopair and posterior oblique view of medium pygidium CM59314; (O–Q) dorsal, posterior, and lateral views of small pygidium CM59315. R–S: Idahoiid pygidium 1, stereopair and posterior view of large pygidium CM59313. T–W: *Plethopeltis*? sp.; (T–U) dorsal and anterior oblique views of large cranidium CM59316; (V–W) dorsal and lateral views of medium cranidium CM59317. X–Z: Genus species indeterminate 80A; dorsal, anterior oblique, and anterior views of large cranidium CM59318. AA–CC: Genus species indeterminate 80C; dorsal, lateral, and posterior views of fragmentary medium pygidium CM59321. DD–GG: *Micragnostus* sp.; (DD) stereopair of medium cephalon CM59322; (EE) stereopair of medium pygidium CM59323; (FF–GG) dorsal and lateral views of medium pygidium CM59324.

Fossil Locality J1352 (Central Belt)

A new fossil locality (J1352) in the central belt, ~70 km along strike from the Leffingwell Fork locality, yielded a sizable collection (127 specimens) of trilobites and agnostoids. This collection is the most unequivocally synvolcanic sample extracted from the Egaksrak formation. Unlike J1480, which was collected from a carbonate megablock within the mélange at the base of the central belt (Fig. 3.4B), J1352 was recovered from an interval dominated by thinly laminated volcaniclastic wackestone and lime mudstone interstratified with pillow basalt and volcaniclastic strata (Fig. 3.4C). The fossils were recovered from thin lenses and laminae of bioclastic grainstone (Fig. 3.4D), which attest to a shallow environment of deposition, as does the scarcity of agnostoids, which account for only 4 of the 127 specimens. The following taxa are represented and illustrated in Figure 3.13:

(1) agnostoid genus species indeterminate;
(3) genus species indeterminate 52A;
(4) genus species indeterminate 52B;
(5) genus species indeterminate 52C;
(6) genus species indeterminate 52D;
(7) genus species indeterminate 52E; and
(8) genus species indeterminate 52F.

The fauna is assigned an early Furongian age (Paibian Stage) on the presence of a single cranidium with granular texture assigned with slight reservation to *Cheilocephalus* (see Appendix 3.1). The presence of that genus suggests a linkage to Laurentia, although there have been a few reports of the genus from non-Laurentian successions in Siberia and North China (Westrop et al., 2008).

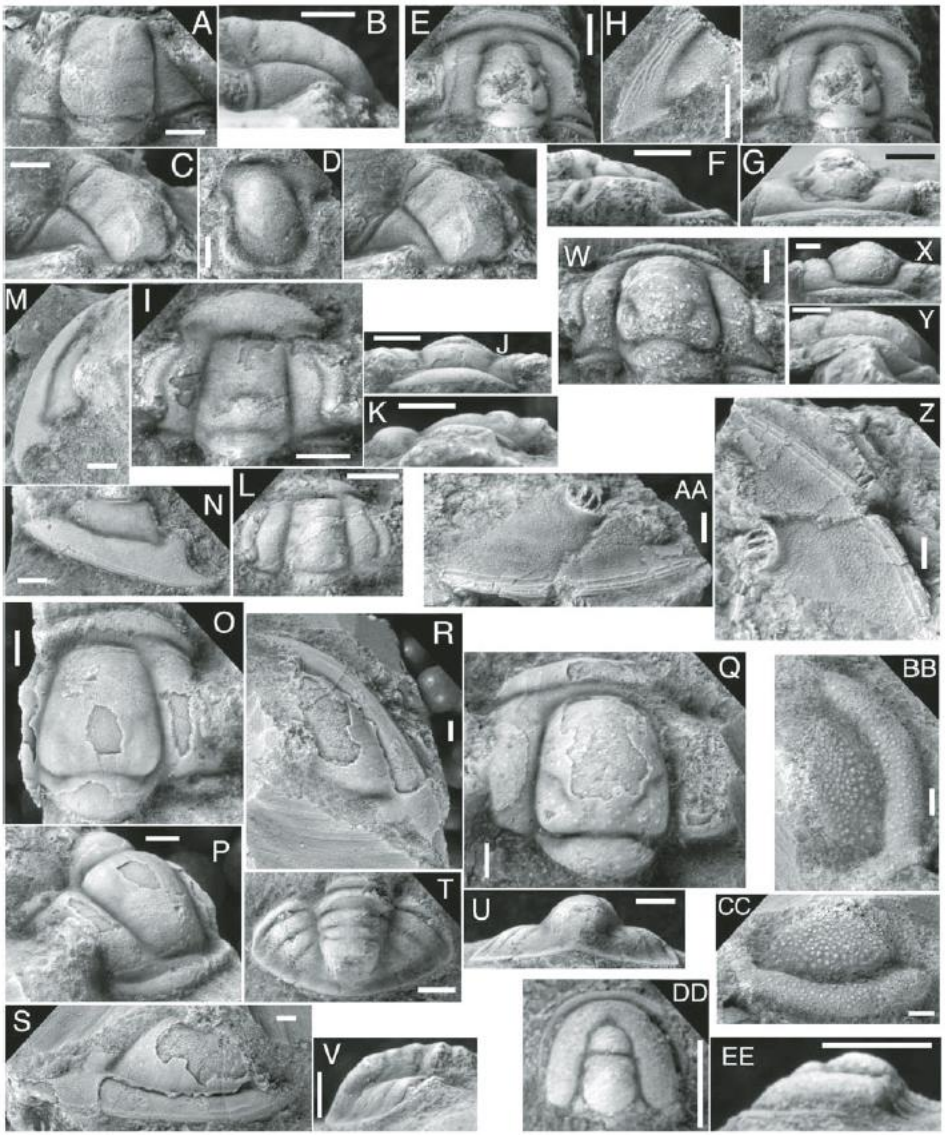

Figure 3.13: Trilobites from the Egaksrak formation at locality J1352. View is dorsal (palpebral for cranidia) unless indicated otherwise. White or black scale bar in each photo is approximately 1 mm in length. A–D, *Cheilocephalus*? sp.; A–C, dorsal and lateral views, and anterior oblique stereopair of medium cranidium CM59325; D, posterior-dorsal view of right posterolateral projection showing "shoulder". E–H, Genus species indeterminate 52A; E–G, dorsal stereopair, lateral, and anterior views of medium cranidium CM59326; H, fragmentary medium librigena CM59327. I–N, Genus species indeterminate 52B; I–K, dorsal, anterior, and lateral views of medium, slightly crushed cranidium CM59328; L, small cranidium CM59329; M–N, dorsal and exterior views of large librigena CM59330. O–V, Genus species indeterminate 52C; O–P, dorsal and anterior-oblique views of medium cranidium CM59331; Q, medium cranidium CM59332; R–S, dorsal and exterior views of large librigena CM59333; T–V, dorsal, posterior, and lateral views of medium pygidium CM59334. W–Y, Genus species indeterminate 52D, dorsal, anterior, and lateral views of medium cranidium CM59335. Z–AA, Genus species indeterminate 52E, dorsal and exterior views of large librigena CM59336. BB–CC, Genus species indeterminate 52F, dorsal and exterior views of fragmentary medium librigena CM59337. DD–EE, Agnostoid genus species indeterminate, dorsal and lateral views of small cephalon CM59338.

DISCUSSION

Age of the Whale Mountain Allochthon

The presence of *Olenellus* in the Egaksrak formation at the Marsh Fork locality (Dutro et al., 1972) assigns those strata to the Dyeran Stage of Laurentia (global Series 2; Fig. 3.14), confirming that extrusion of lavas in the southern belt had begun prior to the end of the early Cambrian (ca. 509 Ma; Gradstein et al., 2012). This is supported by the ca. 512 Ma weighted average zircon U-Pb age from the southern belt volcaniclastic sample 15BJ06 (Fig. 3.7A). The agnostoids and trilobites in collection J1475, however, assign other carbonate rocks of the southern belt to the upper Cambrian (Furongian Series). The presence of *Pseudagnostus* confirms that the collection is no older than Guzhangian (Miaolingian Series). The lowest occurrences of that genus reported from several continents (Shergold et al., 1990; Peng and Robison, 2000; Varlamov et al., 2006) all lie above the first appearance datum (FAD) of *Lejopyge laevigata*, the appearance of which marks the base of the Guzhangian Stage (ca. 500 Ma; Gradstein et al., 2012).

At the species level, the trilobites and agnostoids in J1475 more closely resemble younger species from Paibian to lower Jiangshanian strata, suggesting that the fauna is Furongian rather than Guzhangian. As noted in the detailed species comparisons provided in Appendix 3.1, *Aplotaspis* n. sp. is most similar to *Aplotaspis erugata* in the Idamean Stage (mid-Paibian) of Australia (Henderson, 1976), and it also resembles *Aplotaspis caelata* from the Jiangshanian *Plicatolina perlata* Zone of Siberia (Lazarenko et al., 2006) in pygidial morphology. The only evidence that J1475 could be younger than Jiangshanian, and instead represents Stage 10, is the tentative assignment of a single, poorly preserved cranidium (Figs. 3.11N–3.11P) to the upper Sunwaptan genus *Stenopilus*. That assignment is far from certain, however, and it would conflict

with the stratigraphic ranges established for *Aplotaspis* and the two species of *Pseudagnostus* that the agnostoids in J1475 most closely resemble (*Pseudagnostus josepha* and *Pseudagnostus parvus*), the youngest reported occurrences of which are from uppermost Jiangshanian (lower Sunwaptan *Taenicephalus* zone or equivalent) strata (Shergold, 1980; Westrop, 1995; Lazarenko et al., 2006; Chatterton and Gibb, 2016). Accordingly, the carbonate rocks containing the J1475 locality are assigned to either the Paibian or Jiangshanian, indicating that the volcanism in the southern belt continued through ca. 497 Ma, the approximate age determined for the base of the Paibian Stage (Gradstein et al., 2012).

The age constraints of the Romanzof formation are provided by a collection of biserial graptolites that Moore and Churkin (1984) recovered from a succession of argillite and chert (Romanzof formation) along the Canning River in Alaska. The collection included the genera *Climacograptus, Retiograptus,* and *Didymograptus,* which broadly occur in Lower–Middle Ordovician strata throughout parts of North America, Europe, and Asia (e.g., Jackson, 1964). The detrital zircon ages from a lithic- and volcanic-rich sandstone unit of the Romanzof formation suggest a ca. 452 Ma maximum depositional age (Strauss et al., this volume, Chapter 23), expanding the age constraints of the southern belt to potentially record a 60 m.y. history that ranges from the early Cambrian (ca. 512 Ma) to the Late Ordovician (ca. 452 Ma).

The rocks of the central belt span a much narrower range in age than those from the southern belt. The two faunas recovered from the Egaksrak formation are assigned to the Furongian, with the trilobites and agnostoid from the Leffingwell Fork locality (J1480) indicating a Jiangshanian age, and the probable *Cheilocephalus* in the new collection (J1352) placing it in the Paibian Stage or lowermost Jiangshanian Stage (Fig. 3.14). Despite reassignment of the agnostoid and idahoiid trilobites reported by Dutro et al. (1972) from the Leffingwell Fork

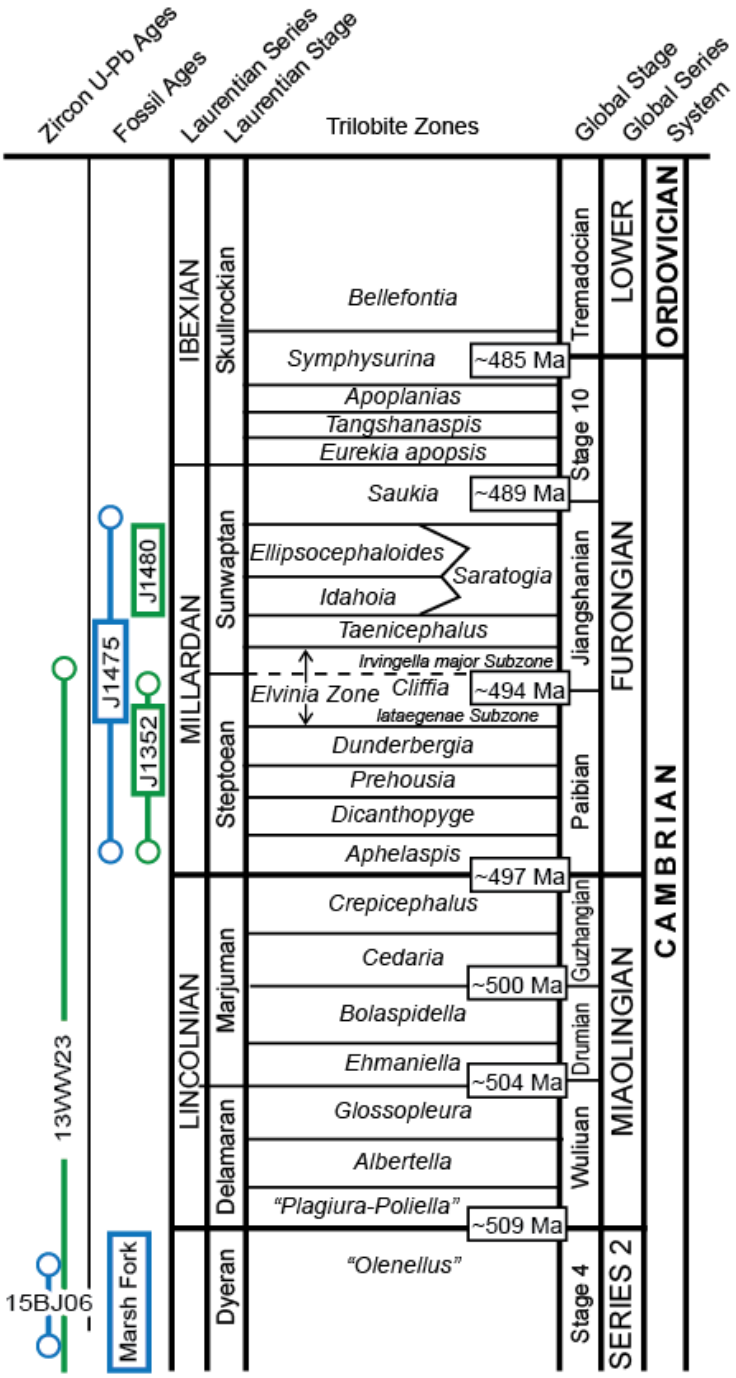

Figure 3.14: Chronostratigraphic chart showing probable positions of faunal and zircon collections from the Whale Mountain allochthon within the succession of upper Cambrian trilobite-based biochronozones, series, and stages established for Laurentia, and their relationship to global chronostratigraphic units (right-most columns). Chronostratigraphic units after Taylor et al. (2012). Numerical ages for the global stages are from Gradstein et al. (2012). Colors are used to differentiate southern belt collections (blue) from central belt (green) collections. Colored rectangles for fossil collections depict probable ranges; possible ranges shown with colored lines and white dots. Estimated ranges for the zircon U-Pb ages are taken from uncertainties depicted in the weight average age from each sample (Fig. 3.7).

locality to different genera (see Appendix 3.1), the new information provided by collection J1480 confirms their assessment of the fauna as "Franconian" (now lower Sunwaptan) in age. Like coeval faunas assigned to the *Saratogia* or *Idahoia* zones in various locations across North America, J1480 is dominated by idahoiid species. The close resemblance of Micragnostus sp. to specimens of *M. chiushuensis* illustrated by Westrop (1995) from the lower Sunwaptan *Noelaspis jeffreyi* fauna in the Rabbitkettle Formation of northwestern Canada reinforces this correlation.

The uniqueness of the fauna from locality J1352 makes correlation with previously described faunas difficult; however, the one small cranidium identified as *Cheilocephalus*? sp. probably does represent that primarily Steptoean genus. The generic assignment is tentative only because no pygidium or librigena is available to fortify it. *Cheilocephalus* is widely distributed across Laurentia in strata of Steptoean (Paibian) age, with a single occurrence in deep-water deposits of uppermost Marjuman (Guzhangian) age in Newfoundland (Westrop et al., 2008). However, that older species of *Cheilocephalus* lacks the granular sculpture displayed by the cranidium in J1352.

The Furongian fossil age of the central belt carbonate rocks is supported by the ca. 504 Ma weighted mean U-Pb age from the 13WW23 sample (Fig. 3.7B), which was taken from the same location as the J1352 fossil collection. The ~7–10 m.y. gap between the ca. 504 Ma zircon age and the ca. 497 Ma relative fossil age of the carbonate rocks could simply reflect uncertainty between all the ages, including those of the globally calibrated time scale (Fig. 3.14). Alternatively, the gap in ages could reflect transitions between volcanic eruptions and carbonate deposition, or that the zircon grains recovered from 13WW23 are of detrital origin and only constrain a maximum depositional age on the Egaksrak carbonate strata. In addition, the

structural complexity, in both the southern and central belts, obscures many of the stratigraphic and relative age relationships between the carbonate and volcanic rocks, however, is supported by the prevalence of volcanic material observed in outcrops and thin sections of the carbonate rocks in the southern and central belts of the allochthon.

The upper age limit of the central belt is constrained only by the Furongian age of the faunas from the Egaksrak formation. Reiser et al. (1980), however, did map equivalents of the Romanzof formation in the interior parts of the central belt. Although we never traversed those locations, we did observe several sequences of volcaniclastic phyllite beds with minor chert, which could correlate to the Romanzof formation in the southern belt. The presence of this formation implies that some of the central belt rocks can be assigned to the Upper Ordovician.

The rocks of the northern belt, assigned in this study to the Ekaluakat formation (Fig. 3.2), are the least constrained in terms of age, and correlation to the other belts of the allochthon is uncertain. The zircon U-Pb ages from a tuffaceous sandstone unit of the Ekaluakat formation, reported from sample 12JT35 of Johnson et al. (2016), have a nearly unimodal age distribution centered at ca. 500 Ma. This overlaps with the zircon U-Pb ages reported from the southern and central belts, and it implies that the volcanic and volcaniclastic rocks from all three belts formed at roughly the same time. The ca. 484 Ma K-Ar age reported by Reiser et al. (1980) also falls within the general ca. 512–452 Ma age range of rocks from the southern and central belts; however, the age is characterized by very low precision (±20 m.y.).

Several fossil localities, most of which include Ordovician and Silurian graptolite genera, have been reported from argillite and slate units in the northern belt (Reiser et al., 1980; Lane et al., 1995); however, most of these rocks are now considered part of the Cambrian–Ordovician Leffingwell formation or the Upper Ordovician–Lower Devonian(?) Clarence River Group

(Johnson et al., 2016; Nelson et al., this volume; Strauss et al., this volume, Chapter 23). Despite these potential geochronological connections and proposed stratigraphic revisions, it remains possible that rocks of the northern belt do not correlate with the other two belts and therefore are not part of the Whale Mountain allochthon. Johnson et al. (2016) speculated that the ca. 500 Ma volcaniclastic strata had formed by recycling of Whale Mountain allochthon rocks from the southern and/or central belts and that they belonged to the younger Clarence River Group. This may be supported by the fact that the volcanic and volcaniclastic rocks in the northern belt are imbricated with Clarence River Group strata along several small-scale, north-directed thrust faults (Kelley et al., 1994; Lane et al., 1995), whereas the central and southern belts are abruptly separated from the other rocks in the NE Brooks Range by large-scale thrust faults that cross the entire map area.

Paleogeographic Setting of the Whale Mountain Allochthon

Constraining the paleogeographic setting of the Whale Mountain allochthon is of fi rst-order significance to reconstructing the early Paleozoic history of the circum-Arctic region. Previous investigators (e.g., Lane, 1991; Cecile et al., 1999; Lane et al., 2016) linked the volcanic rocks in the NE Brooks Range, herein treated separately as the Marsh Fork, Whale Mountain, and Ekaluakat units, to lower Cambrian–Upper Ordovician rift-related alkaline basalt and ultrapotassic flows that are exposed within off-shelf areas of the ancestral NW Laurentian margin, including the Selwyn Basin, Kechika trough, and elsewhere in the Canadian Cordillera (Hart, 1986; Goodfellow et al., 1995; Cecile et al., 1997; Pyle and Barnes, 2003). The lithostratigraphic, geochemical, and paleontological evidence presented in this study reveals a more complex story of the Whale Mountain allochthon, making paleogeographic links between the allochthon and the Canadian Cordillera problematic. We argue that the Whale Mountain

allochthon represents a diverse assortment of oceanic rocks originating outboard of the Laurentian margin that were assembled into an ancient accretionary wedge that formed in front of an Iapetus subduction zone.

Constraints from Lithofacies and Biofacies

The lithofacies and biofacies of the sedimentary rocks from the allochthon record a variety of depositional settings, and the mixed stratigraphic relationships with the mafic volcanic rocks resemble the chaotic architecture of an accretionary complex. In the southern belt, lithofacies from individual blocks or outcrops of the Egaksrak formation reflect deposition in periplatformal carbonate slope, shallow-marine oolitic shoal, and peritidal shelf environments. In many ways, the Egaksrak blocks resemble the Oman Exotics of the Hawasina Nappes in eastern Oman (Searle and Graham, 1982; Pillevuit et al., 1997), or the Calera Lime-stone units of the Franciscan Complex in northern California (Tarduno et al., 1985). Similar to these analogs, the interlayered architecture of Egaksrak carbonate units and the Marsh Fork volcanic rocks likely resulted from several processes, including fi ne-grained pelagic settling of carbonate sediment on the basin floor, gravity sliding and mass transport of shallow-marine sediment, or repeated structural imbrication.

The faunal collections from the southern belt, including the early Cambrian fauna with *Olenellus* reported by Dutro et al. (1972) and the new collection from locality J1475, contain taxa that are common in deep-marine facies. *Olenellus*, while common in deeper-shelf and proximal off-shelf environments, was widely distributed across the facies belts that surrounded Laurentia (e.g., Palmer and Halley, 1979). The collection from locality J1475, however, unequivocally represents a deep-marine, off-platform fauna. Sclerites of the ceratopygid genus *Aplotaspis* make up more than 55% (30 of 54 specimens) of collection J1475. Ceratopygid

trilobites are dominant, or at least major components, of deep-marine faunas in the upper Cambrian sections of several paleocontinents. The lower Furongian *Proceratopyge rectispinata* fauna described by Pratt (1992) from the Rabbitkettle Formation in northwestern Canada is a good Laurentian example, as is the Franconian 2 fauna in the Hillard Limestone of eastern Alaska from which Palmer (1968) described *Yuepingia glabra*.

Many other non-Laurentian occurrences of ceratopygidrich, deep-marine biofacies have been reported from the Furongian and uppermost strata of Miaolingian in Asia and Australia. Aplotaspis and Proceratopyge are key elements of lower-slope biofacies described from Siberia (Pegel, 2000). They also abound in deep-marine deposits of the Georgina Basin of northeastern Australia (Henderson, 1976) and played a major role in zonation of the thick, deep-marine succession of the Jiangnan slope belt that bordered the Yangtze Platform in China (Peng, 1992). The high percentage of agnostoid arthropods in J1475, which make up 28% (12 out of 54) of the specimens recovered, is greater than that typically found in shallow-marine faunas but comparable to relative abundances of agnostoids reported for many collections that represent deeper-shelf to off-platform biofacies (e.g., Pratt, 1992; Westrop, 1995).

The Romanzof formation records hemipelagic sedimentation dominated by suspension rainout of fi ne-grained siliciclastic and biogenic detritus (Reiser et al., 1980; Moore, 1987; Mull and Anderson, 1991; Anderson et al., 1994; Nelson et al., this volume; Strauss et al., this volume, Chapter 23); furthermore, the lack of fi ne-grained pelagic carbonate deposits in the Romanzof formation most likely reflects deposition below the carbonate compensation depth. Fine-grained strata of the Romanzof formation are locally interbedded with lithic arenites and wackes that could represent trench-filling deposits, delivered by turbidity currents and sourced from an active volcanic margin (Strauss et al., this volume, Chapter 23).

The sedimentary rocks of the central and northern belts, although different in terms of their individual depositional settings, suggest sedimentation on or near a volcanic island. Similar to that described earlier from the southern belt, the Egaksrak formation of the central belt was most likely deposited in a combination of deep- and shallow-marine settings. The presence of interbedded volcanic matrix-supported lime rudstone, mudstone, and bioclastic grainstone at the J1352 locality reflects a combination of deep-marine suspension, sediment gravity, and turbidite sedimentation along a slope or steep-gradient setting. In contrast, the abundance of peloids, ooids, bioclasts, and rounded volcanic clasts (Fig. 3.4C) in some of the packstone and grainstone facies reflects some degree of reworking of shallow-marine carbonate sediment by wave action, as do the rounded clasts that compose the conglomeratic units that are interbedded with the basalt flows (Fig. 3.4G). The relative scarcity of agnostoids in faunal collections from sample localities J1352 and J1480 provides additional support for a shallow-water setting of the carbonate rocks in the central belt. Therefore, based upon the interstratification of shallow-water carbonates and alkaline basalt flows with ocean-island basalt (OIB) character, we interpret this belt to record deposition near an atoll or submerged volcanic island.

The Ekaluakat formation (Fig. 3.2) of the northern belt reflects deposition in a deep-marine basin, where the primary mode of deposition was pelagic and hemipelagic settling mixed with turbidity currents and possibly weak bottom currents. Notably, the sedimentary rocks of the Ekaluakat formation appear to lack abundant continental detritus. This is indicated by the near absence of detrital zircon grains older than 1 Ga from these units (Johnson et al., 2016) and by $\varepsilon Nd(t)$ values >+4 in the fine-grained units (Nelson et al., this volume). Several tuffaceous and volcaniclastic units are also interbedded throughout the sedimentary section (Fig. 3.6D), further supporting deposition along or at the base of a submerged volcanic slope.

Constraints from Igneous and Zircon Geochemistry

The geochemical and petrological characteristics of Marsh Fork volcanic rocks in the southern belt closely resemble MORB. Their tholeiitic character (Fig. 3.8), unfractionated concentrations of Dy, Y, Yb, and Lu, and the gentle slopes on the normalized variation diagrams (Fig. 3.10) imply that the volcanic rocks were derived from a shallow (<80 km), garnet-free mantle source that was depleted in incompatible elements (e.g., Salters and Stracke, 2004; Kushiro, 2001). Shallow melting conditions and the eruption of tholeiitic basalt are most commonly found along mid-ocean ridges, where the degree of partial melting is high and the flux of incompatible elements into the melt is diluted.

Although the southern belt samples show overall enrichment of most trace elements compared to the global average of MORB (Arevalo and McDonough, 2010), the trends on normalized variation diagrams are nearly parallel (Fig. 3.10). The enrichment was likely driven by postmelting crystallization of the magma. Some oceanic-island-arc suites have similar trace-element trends, but most of these suites also include negative Nb and Ta anomalies (e.g., Elliott, 2003). Furthermore, the >50 Ti/V ratios (Fig. 3.9A) are significantly higher than most island-arc suites (Shervais, 1982). Tholeiitic basalt is also common in oceanic and continental flood basalt provinces; however, these suites are typically more enriched in the incompatible elements with respect to MORB-type lavas (e.g., Hooper and Hawkesworth, 1993).

The volcanic rocks from the central and northern belts have petrological and geochemical characteristics that resemble alkaline basalt. Alkaline magmas are produced in a variety of tectonic settings, but empirical models show that alkaline magmas are typically generated under deep, high-pressure conditions that suppress the amount of partial melting and concentrate incompatible elements into the melt (e.g., Yoder and Tilley, 1962; Green and Ringwood, 1967;

Jaques and Green, 1980). A deep melting regime for the central and northern belt suites is supported by the relative depletions of Dy, Y, Yb, and Lu. These elements are typically withheld from the melt if the mantle source includes refractory garnet, which becomes stable at the expense of spinel below 85 km depth (Robinson and Wood, 1998). Deep melting conditions are further supported by the low oxygen fugacities inferred from the <50 Ti/V ratios (Shervais, 1982).

The enrichment of incompatible elements observed in the central and northern belt suites is also linked to melting of an enriched or fertile mantle source. There are several hypothesized types of fertile sources in the mantle (Hofmann, 2003), but melting of such sources typically requires a deep thermal anomaly or hotspot. Hotspot volcanism is commonly observed at intraplate oceanic-island settings or at off-axis seamounts, and the incompatible element trends of the central and northern belt suites follow the global OIB average (Sun and McDonough, 1989); however, similar trends have been observed from continental hotspots, including those found along the Cameroon line of western Africa (Fitton, 1987).

Isotopic compositions are particularly useful for determining mantle source geochemistry, because most isotopes do not fractionate during partial melting or crystallization processes. Although we did not measure any isotopes from our basalt samples, the εHf(t) zircon values of +4 to +11 from the two samples, 15BJ06 and 13WW23 (Fig. 3.7), present several implications. Notably, the εHf(t) values are slightly displaced from the depleted mantle trajectory of Vervoort and Blichert-Toft (1999). This could imply that the source material from which the zircon crystallized was derived from (1) isotopically fertile mantle sources, (2) melts of Neoproterozoic crust, or (3) mixed depleted mantle melts and older (Paleoproterozoic?) crustal contaminants. Given the prevalence of mafic melts recorded in our geochemical data set and the

absence of silicic melts, the volcanic rocks of the allochthon were not likely generated by crustal melting or assimilation. A cogenetic relationship between the melts that produced the volcanic rocks and those from which the zircon crystallized implies that the displaced εHf(t) values, like the OIB geochemical signatures, reflect derivation from an isotopically fertile mantle source. Future studies that directly measure the isotopic compositions of the volcanic rocks will test this interpretation.

The segregation of MORB-type rocks in the southern belt from OIB-type rocks in the central and northern belts is a perplexing issue. Plausibly, the rocks from all three belts could have formed in different tectonic settings, or each belt could reflect temporal changes in melting conditions. Although OIB- and MORB-type lavas can be found in continental rift settings, MORB-type rocks are typically subordinate, and none of samples analyzed in the study exhibited the ultra-alkaline character observed in many rift provinces (e.g., Kampunzu and Mohr, 1991). The volcanic rocks of the Whale Mountain allochthon thus either formed by conventional oceanic melting mechanisms, mid-ocean-ridge decompression or intraplate hotspots, or they formed by renewed extension along a previously attenuated segment of continental crust, such as the continent-ocean transition at the distal reaches of a passive margin.

Interpretations that link the volcanic rocks in the NE Brooks Range to extensional events along NW Laurentia typically cite similarities with the alkaline volcanic rocks exposed in the Selwyn Basin (e.g., Lane et al., 2016). These include the Old Cabin Formation and Nibbery volcanic rocks, which are characterized by pillowed basalt flows that are interbedded with the off-shelf carbonates of the Rabbitkettle Formation (Hart, 1986; Cecile, 2000; Goodfellow et al., 1995). The base of Old Cabin Formation is constrained by a 499 Ma zircon U-Pb age (MacNaughton et al., 2016), which overlaps with the zircon ages reported in this study.

Goodfellow et al. (1995), however, showed distinct geochemical differences between the Whale Mountain volcanic rocks and the volcanic rocks of the Selwyn Basin, suggesting that the Selwyn Basin volcanic rocks formed by partial melting of lithospheric mantle, whereas the Whale Mountain volcanic rocks formed by partial melting of enriched portions of the asthenosphere. In addition, the MORB-like basalt flows and imbricated chert units in the southern belt of the allochthon, which were not examined in the Goodfellow et al. (1995) geochemical study, are unlike anything exposed in the Selwyn Basin or the Canadian Cordillera.

In many ways, the Whale Mountains allochthon resembles the Franciscan Complex in northern California, which includes a wide array of both tholeiitic and alkaline volcanic rocks mixed with both deep-marine chert and shallow-marine limestone (e.g., Shervais and Kimbrough, 1987; Tarduno et al., 1985; MacPherson et al., 1990). The Hawasina Nappes in eastern Oman are another good analog, where chaotic mélanges of intercalated alkaline volcanic and shallow-marine carbonate rocks, the Oman Exotics, are imbricated with deep-marine sedimentary and subordinate tholeiitic volcanic rocks, all of which were thrusted onto passive-margin sequences of the Arabian Platform during the closure of the Tethys Ocean (e.g., Béchennec et al., 1990; Pillevuit et al., 1997).

Constraints from Paleobiogeography

The most unequivocal tie to Laurentia provided by the faunas from the Egaksrak formation is the *Olenellus* reported by Dutro et al. (1972) from their Marsh Fork locality. This uniquely Laurentian genus was widely distributed across the facies belts that surrounded Laurentia in the early Cambrian (e.g., Palmer and Halley, 1979), but it is particularly common in intermediate-and deep-marine facies that accumulated in open-shelf and off-shelf environments. If the cranidium from locality J1475 identified here as *Stenopilus*? sp. does represent that genus,

which is uncertain (see Appendix 3.1), it reinforces the evidence of proximity to Laurentia provided for the southern belt by *Olenellus*. *Stenopilus* is one of several plethopeltid genera closely associated with microbial reefs of the Laurentian platform (Ludvigsen and Westrop, 1983; Taylor et al., 2009), but it also occurs in deep-marine, toe-of-slope deposits sourced by downslope transport of sediment from reefs at the platform margin and upper slope (Ludvigsen et al., 1989). Like *Olenellus*, *Stenopilus* is uniquely Laurentian, and it requires at least proximity to that paleocontinent. However, having been reported from both platform and off-platform deposits, neither of these genera resolves whether the volcanic rocks of the southern belt were extruded on the Laurentian platform or were part of an oceanic volcanic succession outboard of the Laurentian margin.

Dutro et al. (1972) based their interpretation of the fauna at their Leffingwell Fork locality as one of North American (i.e., Laurentian) aspect on assignment of a single, fragmentary cranidium to the idahoiid genus *Saratogia*. This was a reasonable conclusion, given the prevalence of *Saratogia* and other idahoiids in early Sunwaptan faunas described previously from Montana and Wyoming (Grant, 1965), Texas (Longacre, 1970), and Oklahoma (Stitt, 1971). It was also reported in later studies of coeval faunas in Alberta (Westrop, 1986) and the Appalachians (Ludvigsen and Westrop, 1983; Taylor et al., 2009). However, the large collection (J1480) recovered in 2014 from the Leffing well Fork locality reveals that it is not a typical *Saratogia/Idahoia* zone fauna. As explained in detail in Appendix 3.1, J1480 is dominated by two new idahoiid species that cannot be assigned to any established genus. *Saratogia* is not represented, nor are other genera that characterize faunas of this age in various facies across Laurentia, such as *Drumaspis*, *Wilbernia*, and *Ptychaspis*.

Wilbernia is particularly widespread, occurring not only in most idahoiid-rich early Sunwaptan platform faunas, but even in coeval slope deposits in the Rabbitkettle Formation in NW Canada (Westrop, 1995). *Drumaspis* is similarly widespread in both shallow- and deep-marine faunas, the latter including the "Franconian 2" fauna described by Palmer (1968) from the Hillard Limestone, the off-platform equivalent of the Jones Ridge Formation in east-central Alaska. Although the dominance by idahoiids does suggest proximity to Laurentia, the absence of all characteristic and widespread *Saratogia*/*Idahoia* zone genera is difficult to reconcile with origination on or even directly adjacent to the Laurentian platform. The only specimens in J1480 that might represent a Laurentian genus are three cranidia assigned with considerable uncertainty to Plethopeltis (Figs. 3.12T–3.12W). These cranidia to some extent resemble *Plethopeltis saratogensis*, a species associated with *Saratogia* in the Appalachians (Ludvigsen and Westrop, 1983; Taylor et al., 2009), but they differ in some critical features (Appendix 3.1). Given these differences, the poor preservation, and lack of an associated pygidium or librigena, the assignment is quite tentative, and the link to Laurentia is equally tenuous.

The strongest evidence that the Egaksrak formation in the central belt did not originate on the Laurentian platform is provided by collection J1352, which consists of 127 specimens recovered from strata interstratified with pillow basalt and volcaniclastic rocks. Except for one cranidium, which probably represents *Cheilocephalus*, the fauna is remarkably unfamiliar. The species are distinct and specialized individually and collectively display a wide range of morphologies. Such differentiated faunas in the Laurentian platform succession characterize the middle to upper parts of the Cambrian stages, and the constituent genera and species are easily recognized as Laurentian taxa and diagnostic of their respective zones. The diverse faunas of the *Crepicephalus*, *Elvinia*, and *Saukia* zones at the tops of the Marjuman, Steptoean, and

Sunwaptan Stages, respectively, exemplify this, and at least a few of the endemic genera that characterize those zones are found consistently in coeval deep-marine deposits that accumulated along the Laurentian margin (Raymond, 1924; Rasetti, 1944; Palmer, 1968; Ludvigsen et al., 1989; Pratt, 1992; Westrop, 1995). None of the five to six genera in J1352 could be assigned to any established genus from Laurentia, or any other paleocontinent. For this reason, the paleogeographic model we favor for the rocks of the central belt is extrusion in an oceanic setting close enough to Laurentia for very limited interchange with the shallow-marine faunas of that paleocontinent, and hence the idahoiids and possible *Plethopeltis* in J1480 and *Cheilocephalus* in J1352, but sufficiently removed to allow for evolution of unique, endemic trilobite faunas in the shallow environments around the volcanic islands.

The data presented in this study do not directly address whether the Whale Mountain allochthon formed outboard NW or NE Laurentia. A peri-Laurentian origin for the allochthon, as recognized by the faunal collections from the Egaksrak formation, aligns with recent models that restore portions of the Arctic Alaska terrane to NE Laurentia in the early Paleozoic (e.g., Strauss et al., 2013, 2017, this volume, Chapter 23; Johnson et al., 2016). In the context of Mesozoic terrane boundaries, earlier studies grouped the pre-Mississippian rocks exposed in the NE Brooks Range and the Doonerak region of the central Brooks Range into the North Slope subterrane (e.g., Jones et al. 1987; Moore et al., 1994). The recent models of Strauss et al. (2017), however, severed the early Paleozoic ties between the Doonerak region and the North Slope, suggesting that the Ordovician–Silurian volcanic assemblages at Doonerak formed in response to subduction of Iapetus lithosphere outboard NE Laurentia, whereas the rocks of the North Slope had formed as a lateral continuation of the deep-marine, Franklinian Basin at northern Ellesmere Island in Arctic Canada (Johnson et al., 2016; Nelson et al., this volume;

Strauss et al., this volume, Chapter 23). This restoration calls for an ancient oceanic basin or marginal seaway that separated the North Slope from the Doonerak arc in the early Paleozoic. We contend that Whale Mountain allochthon is a relic of this basin, and it now marks the early Paleozoic suture between the North Slope and the Doonerak region.

The exact paleogeographic configuration of the basin remains unclear, because it is not possible, with the data presented in this study, to determine whether the rocks of the Whale Mountain allochthon formed in a true oceanic basin or in some type of marginal seaway that separated the Laurentian margin from outboard terranes. The faunal collections from the Egaksrak formation, particularly those of J1352, suggests that at least some portion of the allochthon formed in an open-ocean setting, allowing for faunal communities of the Egaksrak formation to evolve in isolation. The assembly and emplacement of the allochthon are also unclear. The allochthon's structural position above Upper Ordovician–Lower Devonian(?) strata of the Clarence River Group suggests that emplacement occurred in post–Early Devonian time (Johnson et al., 2016), but future work is needed to reconstruct the paleogeographic origins of each belt.

CONCLUSIONS

The general implications of this work reveal that the pre-Mississippian rocks of the NE Brooks Range cannot be assigned to a coherent stratigraphic architecture. The fault-bounded rocks of the Whale Mountain allochthon record a complex geological history, dating from Series 2 of the Cambrian (ca. 512 Ma) to the Late Ordovician (ca. 452 Ma). Field observations and igneous geochemistry show that the assorted igneous and sedimentary rocks formed in diverse depositional and tectonic settings, ranging from basin floor settings founded on MORB-type lavas to shallow platform settings that capped isolated volcanic islands. The new trilobite faunal

collections from the Egaksrak formation greatly expand the biostratigraphic record of the NE Brooks Range, with important implications for reconstructing the paleogeography of northern Laurentia. A few of the identified species have loose affinities to Laurentia, but all three collections are missing many of the diagnostic Laurentian platform species that are found throughout Upper Cambrian carbonate units from western to eastern North America. One of the fossil locations (J1352) yielded a collection of species that do not have a recognized affinity with any of the major late Cambrian paleocontinents.

We conclude that the rocks of the Whale Mountain allochthon did not form on the stable platforms that surrounded Laurentian in the late Cambrian, but instead formed in a peri-Laurentian setting, perhaps in the open waters of the Iapetus Ocean. The allochthon was later assembled when disparate rock assemblages were episodically scraped from a subducting oceanic plate into an ancient accretionary wedge and collectively emplaced onto the Laurentian margin at the time of basin closure.

APPENDIX 3.1: SYSTEMATIC PALEONTOLOGY

Illustrated specimens are reposited in the invertebrate paleontology collections at the Carnegie Museum of Natural History (prefix CM) in Pittsburgh, Pennsylvania, USA.

FAMILY AGNOSTIDAE M'COY, 1849

Genus *Micragnostus* Howell, 1935

Opinions vary widely regarding the relationships of several late Cambrian agnostoid genera, among them *Homagnostus*, *Micragnostus*, *Oncagnostus*, and *Trilobagnostus*. Recent discussions of the problem can be found in Choi et al. (2004) and Westrop and Eoff (2012). The approach taken by Choi et al. (2004) is adopted here, with the assignment of species with

relatively short and parallel-sided glabellae and pygidial axes, and weakly developed or absent median preglabellar furrows to the genus *Micragnostus*.

Micragnostus sp.

Illustrations: Figures 3.12DD–3.12GG.

Remarks: The agnostoids in collection J1480, originally identified by Dutro et al. (1972) as *Geragnostus* sp., resemble in all respects the specimens illustrated by Westrop (1995, his plate and figs. 14–16) for *Micragnostus chiushuensis* (Kobayashi). However, the deformed nature of the specimens from the Egaksrak formation renders detailed comparison difficult and precludes certain assignment to that species. Accordingly, they are left in open nomenclature as *Micragnostus* sp. The reassignment from *Geragnostus* does not reflect a disagreement with the initial identification in Dutro et al. (1972); it results from a widely accepted revision of that genus by Fortey (1980), who restricted it to species possessing a complex F3 glabellar furrow divided into three segments, with the glabellar node located barely behind the central segment. Species like the one in J1480, which display an undivided F3 and more posteriorly placed glabellar node, now fall within *Micragnostus.*

Genus *Pseudagnostus* Jaekel, 1909

***Pseudagnostus josepha*? (Fig. 3.11DD)**

Remarks: The morphology of the one, small pygidium in collection J1475 identified as *P. josepha*? falls within the broad concept used for *P. josepha* by Peng and Robison (2000). (See Westrop and Eoff [2012] for an alternate view of the range of variation that should be encompassed by this and other agnostoid species.) The Alaska pygidium is nearly identical to one of the small pygidia illustrated by Peng and Robison (2000, their fig. 10–5), differing only in displaying a slightly narrower border furrow and more firmly impressed axial furrow along the

posterior half of the posteroaxis. Westrop (1995) and Chatterton and Gibb (2016) reported similar species that they left in open nomenclature as *P.* cf. *P. josepha* from the Rabbitkettle Formation in the Northwest Territories and southeastern British Columbia, respectively.

***Pseudagnostus* aff. *P. parvus* Shergold, 1980 (Figs. 3.11Y–3.11AA)**

Remarks: This species in collection J1475 resembles *P. parvus* in its long, parabolic cephalon with a long and relatively narrow glabella, anteriorly placed glabellar node just behind a nearly obsolete F3, fairly narrow borders, and broad, deep border furrows. It differs in displaying a more transverse (less rounded) anterior margin, and a broader and less pointed anterior glabellar lobe.

Genus *Neoagnostus* Kobayashi, 1955

***Neoagnostus*? sp. (Figs. 3.11BB–3.11CC)**

Remarks: This single, fragmentary pygidium in collection J1475 resembles *N. canadensis* (Billings) in possessing well impressed but only weakly divergent axial furrows along the anterior half of the posteroaxis, and an exceptionally broad border furrow that is widest near the posterolateral corners. It resembles pygidia illustrated for this species by Shergold (1977, his plate 16 and fi g. 10) and Ludvigsen et al. (1989, his plate 4 and fig. 7) in these respects, but it differs in the shallowing of the axial furrows along the posterior half of the posteroaxis and resultant lack of elevation of the back of the axis above the border furrow.

Agnostoid gen. sp. undetermined (Figs. 3.13DD–3.13EE)

Remarks: This one cephalon in collection J1352 resembles a number of Furongian species in genera such as *Homagnostus*, *Micragnostus*, and *Oncagnostus* in its forwardly placed glabellar node, short and somewhat inflated posteroglabella, relatively small basal lobes, and partial

median preglabellar furrow. However, its small size and lack of an associated pygidium preclude certain assignment even to genus.

Class TRILOBITA

Family IDAHOIIDAE Lochman, 1956

Remarks: The dominant trilobites in J1480 are confidently assigned to the Idahoiidae based on their anteriorly truncate, subtrapezoidal glabellae, large, band-like palpebral lobes, faintly impressed palpebral furrows, prominent dorsally and ventrally directed occipital spines, and broad preglabellar and librigenal fields traversed by genal cecae. Two distinct idahoiid species are represented in the collection. The cephalon for each species could be reconstructed owing to a contrast in depth of border furrows and slope of genal/preglabellar fields, which allowed recognition of the corresponding librigena for each cranidium. Unfortunately, neither of the two pygidia displays any trait to link it with the appropriate cephalon, and they are treated separately below as Idahoiid pygidium 1 and 2.

Ludvigsen and Westrop (1983) significantly revised the Idahoiidae in a monograph describing a fauna from New York that included *Saratogia calcifera* (Walcott), the type species of *Saratogia*. Among the changes was reduction of *Idahoia* to a subgenus of *Saratogia*, with separation of the subgenera based on contrasting pygidial morphologies. A long axis extending to the posterior margin, and a narrow, convex border characterize the pygidium of *Saratogia* (*Saratogia*), while species of *Saratogia* (*Idahoia*) have pygidial axes that terminate well in front of the margin at the inner edge of a broad, gently concave border. Neither pygidium in collection J1480 displays the requisite features to justify assignment to either of these subgenera, nor to any other idahoiid genus such *Minkella*, *Meeria*, and *Psalaspis.* A single cranidium, here referred to

as Idahoiid? genus and species indeterminate, displays some of the characteristic features of *Minkella*, but it differs in too many respects to allow confident assignment to that genus.

Idahoiid new genus, new species 1 (Figs. 3.12A–3.12D)

Remarks: Although the basic form of the cranidium and librigenal of this species is quite similar to that of *Saratogia*, it is set apart by the weak impression of its axial, border, occipital, and lateral glabellar furrows, even where exfoliated. The gentle and even slope of the preglabellar field and broad, only moderately impressed anterior border furrow are also distinctive.

Idahoiid new genus, new species 2 (Figs. 3.12E–3.12J)

Remarks: This species differs from the other idahoiid species in J1480 in its more deeply incised furrows, especially the anterior, lateral, and posterior border furrows. Other differences include a steeply downsloping preglabellar field, slightly upturned anterior border, and S1 furrows that bifurcate distally and terminate well short of the axial furrow. The palpebral lobes are also elevated above the level of the narrow interocular fixigenae. It shares many of these features with some species of *Saratogia (*Idahoia), such as *Saratogia* (*I.*) *fria* Lochman and Hu (1959). However, as noted above, neither of the associated idahoiid pygidia in J1480 is consistent with assignment to that genus.

Idahoiid pygidium 1 (Figs. 3.12R–3.12S)

Remarks: A strongly convex axis comprising three rings and a terminal piece is elevated well above abaxially downsloping pleural fields marked by three pairs of pleurae. The axis ends well forward of the posterior margin at the inner edge of a fairly wide border, as is typical of *Saratogia* (*Idahoia*) pygidia. However, the border is flat to slightly dorsally convex, as opposed to strongly concave in that subgenus, and it makes up significantly less of the sagittal length of

the pygidium. The border also differs in being interrupted by a postaxial ridge and being traversed by the very narrow (exsagittal) posterior bands of the two anteriormost pleurae, for which intersection with the margin is marked by minute, inconspicuous terminal spines.

Idahoiid pygidium 2 (Figs. 3.12M–3.12Q)

Remarks: The axis, consisting of four axial rings and a terminal piece, is more parallel-sided and broader (transverse) at the posterior end than that of pygidium 1. The four pairs of pleurae display anterior and posterior bands of equal width (exsagittal) and pleural furrows that are relatively narrow and deeply incised. The pleural bands and furrows terminate at the inner margin of a gently convex border that is narrower (exsagittal) than that of pygidium 1, but much wider and less convex than that of *Saratogia* (*Saratogia*). The border ends adaxially at the sides of a broad postaxial ridge**.**

Idahoiid? genus and species indeterminate (Figs. 3.12K–3.12L)

Remarks: The small, thorn-like occipital spine and narrow anterior border on this single cranidium in J1480 resemble those of *Minkella*, but the palpebral lobes are longer than is characteristic of that genus, and the glabella is shorter relative to its width than that of any idahoiid. However, given the deformed condition of most sclerites in this collection, it is possible that the cranidium has experienced some anterior-posterior compression. Consequently, its assignment to the Idahoiidae is uncertain.

Genus *Plethopeltis* Ulrich in Bridge, 1931

***Plethopeltis?* sp. (Figs. 3.12T–3.12W)**

Remarks: The cranidia identified as *Plethopeltis*? sp. resemble in most respects those of *Plethopeltis saratogensis*, a species associated with *Saratogia* in the lower Sunwaptan of New York (Ludvigsen and Westrop, 1983). However, the occipital ring preserved on the most

complete cranidium (Figs. 3.12T–3.12U) does not expand posteriorly axially to produce a blunt occipital spine, as is characteristic of *P. saratogensis.* Instead, it displays a transverse posterior margin and remains fairly narrow (sagittal) across the axis. No species of *Plethopeltis* displays such an occipital ring. Given the atypical form of the occipital ring, and the absence of either a librigena or pygidium to reinforce or refute assignment to *Plethopeltis*, the generic assignment is questionable.

Genus *Stenopilus,* Clark, 1924

***Stenopilus?* sp. (Figs. 3.11N–3.11P)**

Remarks: A single, effaced (smooth) cranidium in collection J1475 is assigned with reservation to the genus *Stenopilus*, owing to its strong sagittal and transverse convexity, relatively short (exsagittal) posterior areas, and strongly convex, overhung posterior margin. Certain assignment to that genus is not possible, however, because tightly adhering matrix made it impossible to expose the anterior and lateral margins to confirm the presence of a strong anterior arch, and small eyes on the steeply sloping sides of the cranidium. These features set *Stenopilus* apart from other effaced genera.

Family CERATOPYGIDAE Linnarsson, 1869

Genus *Aplotaspis* Henderson, 1976

An anteriorly tapering glabella, narrow (exsagittal) posterolateral extensions, and a concave pygidial border identify the ceratopygid that dominates collection J1475 as a species of either *Aplotaspis* Henderson (1976) or *Yuepingia* Lu (1956). The eyes are larger than is typical of *Aplotaspis*, more closely resembling those of *Yuepingia*, but most cephalic and pygidial characteristics are more compatible with assignment to the former genus. *Yuepingia niobiformis* displays a concave pygidial border, but it is much narrower than the strongly convex pleural

fields, unlike the very broad border in *Aplotaspis*, which equals or exceeds the width of more restricted, flatly convex pleural fi elds. All other species of *Yuepingia* for which pygidia have been described have either a narrow, flat to gently convex border, or no border at all, with pleural furrows and the pygidial axis extending almost to the margin. The pygidial axis of *Aplotaspis* ends at the inner edge of the wide, concave border, and it is followed posteriorly by a faint, tapering postaxial ridge that extends to the margin. All but the most anterior pair of faintly impressed pleurae also terminate at or just beyond the inner edge of the border. A similarly broad, concave lateral border, equal in width to the genal field on the librigena of *Aplotaspis* n. sp. (Fig. 3.11G), also supports assignment to that genus, resembling that of the type species, *A. erugata* (Whitehouse), and contrasting with the relatively narrow, flat to convex borders that characterize species of *Yuepingia.*

A rigorous, parsimony-based reevaluation of these genera, and closely related taxa such as *Charchaqia* and *Pseudoyuepingia*, is badly needed but falls beyond the scope of the present study. At present, such an analysis would be severely hampered by the large number of species for which the pygidium and/or librigena remain unknown, and little if any information on ontogenetic variation is available. An example of such limitations can be found in Henderson (1976), wherein much smaller palpebral lobes were included among the primary characteristics that set *Aplotaspis* apart from *Yuepingia*. The deficiency in the comparison is that the single cranidium of *Yuepingia* illustrated (Henderson, 1976, his plate 48 and fig. 12), with palpebral lobes conspicuously larger than those shown for *Aplotaspis*, is a small sclerite only half the size of the figured *Aplotaspis* cranidia. As relative size of the palpebral lobes usually decreases through ontogeny (compare Figs. 3.11D and 3.11A herein), the size difference of the illustrated specimens exaggerates the contrast in the size of this feature between the genera. Future work

may ultimately confi rm that species of *Yuepingia* consistently display larger eyes than those of *Aplotaspis*, but that hypothesis is yet to be tested through quantitative comparison of collections large enough to account for ontogenetic variation.

Bao and Jago (2000) placed *Aplotaspis* in synonymy with *Charchaqia*, arguing that the width of the pygidial border is too variable within *Charchaqia* to justify placement of species with a longer border in a separate genus, i.e., *Aplotaspis*. As evidence, they noted variability in the width of the border on pygidia figured by Henderson (1976) for the type species of *Aplotaspis* (*A. erugata*), and on pygidia of *Charchaqia halli* that they illustrated from Tasmania. Unfortunately, two of the specimens of *C. halli* (Bao and Jago, 2000, their plate 2 and figs. 1 and 2) are internal molds on which the imprint of the pygidial doublure gives the false impression of a relatively broad, concave border. The two rubber casts made from external molds (Bao and Jago, 2000, their plate 2 and figs. 1 and 2) show that the convex pleural fields actually extend nearly to the margin, terminating at the inner edge of a very narrow, convex border. A quantitative comparison of border length/pygidial length ratios (discussed below) between the two genera, utilizing figured specimens of several species in both, does not support the claim of intergrading variation, and their synonymy is rejected. *Aplotaspis* is retained as a separate genus, and a broad, dorsally concave border on the librigena and the pygidium remains one of the primary features that distinguish it from *Charchaqia*, *Yuepingia*, and *Pseudoyeupingia*.

The pygidial border length used for comparison of these genera was obtained by measuring the distance along the axis from the posterior margin to the point on the axis in line with the inner edge of the border. That axial border length was divided by the axial length of the pygidium (excluding the articulating half ring) to obtain a border/length ratio that expresses the percentage of the pygidial length constituted by the border. Although border width does vary

somewhat in *Aplotaspis erugata*, measurements from the images of four pygidia illustrated by Henderson (1976) reveal that the concave border makes up at least a third of the axial length of the pygidium, and in some specimens accounts for nearly half. The ratios obtained for the four pygidia of *Aplotaspis erugata* ranged from 0.34 to 0.45. The border constitutes just over half (border/length ratio = 0.51) of the axial length of the pygidium figured for *Aplotaspis mucrora* (Henderson, 1976, his plate 48 and fig. 14). In contrast, species of *Charchaquia* display short (sagittal), flat to upwardly convex borders that constitute no more, and usually considerably less, than one fifth of the axial pygidial length. Pygidia illustrated by Peng (1992) for the type species of *Charchaqia*, *Charchaqia norini* (his fig. 53L), and for *Charchaqia glabrescens* (his fig. 55F) yielded border/length ratios of 0.19 and 0.125, respectively. The border/length ratio determined for *Charchaqia lata* Troedsson (Chien, 1961, his plate 5 and fig. 2) is 0.13. As previously noted, the concavity along the margin of the internal molds of *C. halli* illustrated by Bao and Jago (2000, their plate 2 and figs. 1 and 2) is the imprint of the pygidial doublure. The true border, visible on their figure 3, is an extremely narrow, convex rim that yields a border/length ratio less than 0.05.

***Aplotaspis* new species (Figs. 3.11A–3.11M)**

Aplotaspis n. sp. is most similar to *A. erugata* in displaying an ellipsoidal pygidium that is much wider (transverse) than long, with a transverse margin behind the axis, as opposed to the subcircular pygidia of *A. mucrora* and *A. caelata*, and subtriangular pygidium of *A.* ex. gr. *erugata* Varlamov et al. (2006). It also resembles the genotype in its very narrow (exsagittal), strap-like posterolateral projections, unequally divided by a well-impressed border furrow into wider posterior borders and exceptionally narrow posterior fixigenae. It differs from *A. erugata* in having more gently concave cephalic and pygidial borders, the inner boundaries of which are

marked by faint ridges rather than distinct furrows, and significantly larger palpebral lobes. In both species, the back of the palpebral lobe sits approximately in line with the glabellar node. The palpebral lobes in *A. erugata* and *A. mucrora* extend forward only approximately halfway to the front of the glabella from the glabellar node. Those of *Aplotaspis* n. sp. extend more than two thirds of the way, resembling species of *Yuepingia*, such as *Y. niobiformis* Lu and *Y. glabra* Palmer, in this regard. It is distinguished from those species by the greater length of the frontal area, broad and concave lateral and pygidial borders, and much wider (transverse) and less convex pygidium. The only species of *Yuepingia* that displays a frontal area as long (sagittal), and librigena as broad (transverse) as *Aplotaspis* n. sp. is *Yuepingia brevica* Lu and Zhu (1980), for which only two poorly preserved cranidia and one librigena are illustrated. The cranidia display more parallel-sided glabellae than *Aplotaspis* n. sp., and the librigena is unequally divided by a shallow border furrow into a broad genal field and much narrower, dorsally convex border. With no associated pygidium to assist in generic assignment, it is uncertain whether *Y. brevica* is properly placed in *Yuepingia.* Although the material available for *Aplotaspis* n. sp. is adequate to confirm that it is a new species, the specimens are too few and fragmentary to allow complete description and naming of the new taxon.

FAMILY CHEILOCEPHALIDAE SHAW, 1956

Genus *Cheilocephalus* Berkey, 1898

***Cheilocephalus*? sp. (Figs. 3.13A–3.13D)**

Remarks: A single, small cranidium in collection J1352 displays most of the diagnostic features of this genus. Small, forwardly placed palpebral lobes are centered opposite weakly impressed S2 furrows, creating large triangular posterior areas. Short (exsagittal) and narrow, dorsally concave anterior fixigenae lie between faint eye ridges and a very narrow, convex,

anterior border. It also displays (Figs. 3.13C–3.13D) the characteristic sharp downward flexure and slight inflation of the posterior border directly behind the palpebral lobe, referred to by Palmer (1965) as a "shoulder" and analyzed in greater detail by Westrop et al. (2008). This species is left in open nomenclature, rather than being assigned to *Cheilocephalus* without reservation, only because there is no associated pygidium or hypostome to fortify such assignment. Of the Laurentian species that display similar granular sculpture, *Cheilocephalus*? sp. most closely resembles *Cheilocephalus brachyops* Palmer (1965), especially the small cranidium (Palmer, 1965, his plate 1 and fig. 14) illustrated from Shingle Pass, Nevada. Like that small (axial length ~2 mm) cranidium of *C. brachyops*, the small (3.2-mm-long) cranidium in J1352 displays a short, nearly quadrate glabella and extremely short frontal area. The J1352 cranidium differs in having less strongly divergent posterior branches of the facial suture, narrower (transverse) and more steeply downsloping posterior areas, more distinct and slit-like S2 furrows, and a less transverse anterior margin that is curved backward strongly in front of the eye ridges. The weakly divergent posterior facial sutures set the Alaska species apart from all other species of *Cheilocephalus.* However, no comparably small cranidia have been illustrated for *Cheilocephalus granulosus* Palmer, nor for *Cheilocephalus buttsi* Resser, a species from the Ore Hill limestone in Pennsylvania (Wilson, 1951), in which unusually narrow (transverse) anterior fixigenae resemble those of *Cheilocephalus*? sp.

Family UNCERTAIN

The collections from the Egaksrak formation include at least 10 additional species for which no suitable genus could be found. These are left in open nomenclature as genus species indeterminate (gen. sp. indet.) with a number and letter designation, where the number is the last

two digits of the collection number. Eight of these species are represented by only one or two fragmentary sclerites.

Genus species indeterminate 52A (Figs. 3.13E–3.13H)

Remarks: This species, represented by a single cranidium and fragmentary librigena, resembles some Steptoean (Paibian) genera such as *Drabia* and *Sulcocephalus.* It resembles *Drabia* in the basic form of the cephalon, and *Sulcocephalus* in its more rounded glabella and deep S1 furrow isolated from the axial furrow. Neither of those genera, however, has the elevated occipital ring (LO), discontinuous occipital furrow (SO), and relatively broad and heavily terraced cephalic border displayed by gen. sp. indet. 52A.

Genus species indeterminate 52B (Figs. 3.13I–3.13N)

Remarks: This species resembles *Croixana* Nelson, 1951, in its subtrapezoidal, anteriorly truncated glabella and inflated frontal area, with the anterior border furrow expressed only at the anterolateral corners. However, it lacks the characteristic pits created by deepening of the axial furrow at the anterior corners of the glabella. It also differs from all known species of *Croixana* (see Westrop, 1986) in its exceptionally long palpebral lobes (>2/3 the length of the glabella), centered well behind instead of opposite the 2S furrows, and wide interocular fixigenae, which are nearly half the width of the glabella at its midlength. The anterior border furrow also differs in trending laterally and slightly anteriorly inward from margin, rather than being directed posterolaterally toward the anterior corners of the glabella as in *Croixana*.

Genus species indeterminate 52C (Figs. 3.13O–3.13V)

Remarks: Distinctive features of this common species in J1352 include a gently anteriorly tapering glabella with sigmoid S1 furrows that bifurcate distally without reaching the deep and narrow axial furrows; a moderately convex cephalic border of constant width separated

from slightly inflated genal fields by a narrow well-impressed furrow, and from the glabella by a narrow, slightly depressed preglabellar field; an inflated occipital ring with an ellipsoidal shape created by strong curvature of its posterior margin; an SO that is shallow and bowed forward over the axis, deepening and broadening behind L1; and widely spaced, coarse granules covering the glabella and genal fields. Fine, closely spaced granules cover the librigenal spine and pleural bands and axial rings of the pygidium. A broad border furrow that narrows behind the axis separates moderately convex pleural fields crossed by narrow, well-impressed pleural furrows from a very narrow convex border. The posterior margin rises adaxially to create a shallow notch behind the axis.

Genus species indeterminate 52D (Figs. 3.13W–3.13Y)

Remarks: The two cranidia in J1352 that represent this species display many of the features that characterize gen. sp. indet. 52C, but they differ in being wider than long and more strongly convex (sagittal and transverse), and having a much narrower anterior border that is more tapered and more strongly directed abaxially.

Genus species indeterminate 52E (Figs. 3.13Z–3.13AA)

Remarks: No associated cranidium, or established Furongian genus, was found to be compatible with the broad, flat to gently concave genal field, dense granular sculpture, long and inwardly curved anterior facial suture, and prominently terraced border of this single librigena in J1352.

Genus species indeterminate 52F (Figs. 3.13BB–3.13CC)

Remarks: The dense texture of coarse granules and broad, convex border of this single librigena in J1352 confi rm that it has no corresponding cranidium in the collection. No genus

was found with librigenae displaying those features and a minute, cylindrical, laterally directed librigenal spine.

Genus species indeterminate 75A (Figs. 3.11Q–3.11T)

Remarks: Two fragmentary cranidia in collection J1475 represent this granulose species, which has an inflated anterior border that tapers rapidly abaxially behind a strongly curved anterior margin, and in front of a transverse border furrow that shallows over the axis in front of a narrow, sunken preglabellar field.

Genus species indeterminate 75B (Figs. 3.11U–3.11V)

Remarks: A single librigena and fragmentary cranidium in collection J1475 represent this species. They are readily matched by a long, strongly divergent anterior branch of the facial suture, a relatively short (exsagittal) and elevated palpebral lobe, and scattered coarse granules on the fixigenae and steeply downsloping genal field, which terminates distally at the inner edge of a broad (transverse) gently convex lateral border.

Genus species indeterminate 75C (Figs. 3.11W–3.11X)

Remarks: This single, fragmentary pygidium in collection J1475 displays a broad, strongly convex, parallel-sided axis elevated above flat to slightly concave pleural fields with prominent depressed areas near the posterior margin in line with the sides of the axis.

Genus species indeterminate 80A (Figs. 3.12X–3.12Z)

Remarks: This species is represented by several poorly preserved cranidia in collection J1480 that resemble those of *Plethopeltis*? sp. In basic form, but they display a narrow (sagittal), laterally tapering anterior border and a prominent eye ridge.

Genus species indeterminate 80B (Figs. 3.12AA–3.12CC)

Remarks: This single, fragmentary, triangular pygidium in collection J1480 displays a posteriorly tapering, flat-topped axis with narrow (sagittal) axial rings separated by deep ring furrows, narrow and similarly incised pleural fields, and a steeply downsloping, gently convex, and terraced border that narrows adaxially and might disappear entirely at the axis where the deeply notched posterior margin reaches its highest point.

ACKNOWLEDGMENTS

Johnson and Toro thank West Virginia University's Faculty Senate Grant and the Circum-Arctic Lithosphere Evolution (CALE) project for providing financial support. Strauss was supported by a National Science Foundation (NSF) Graduate Research Fellowship and a grant from the NSF Tectonics Division (EAR-1624131). Financial support for study of the faunas was provided through a NSF Sedimentary Geology and Paleobiology grant (award 1325333) to Taylor, who also acknowledges invaluable assistance from fellow paleontologists J.R. Laurie and S.R. Westrop in evaluating the taxonomic and paleogeographic affinities of the trilobites and agnostoid arthropods of the Egaksrak formation. Indiana University of Pennsylvania students W.T. Kamerer and J.D. King assisted in the analysis of the faunas through senior research projects on the agnostoids and trilobites, respectively. The Geological Society of America Graduate Student Research Fellowships also supplied additional funding to Johnson, Strauss, and Ward. Field work in 2013 was conducted through the Circum-Arctic Structural Events (CASE) 13 expedition to northern Yukon, which was graciously supported by the Bundesanstalt für Geowissenschaften und Rohstoffe (BGR) and Yukon Geological Survey. We thank Karsten Piepjohn of BGR for funding the CASE 13 expedition, and Blaze Budd, Patrick Frier, and Lyle Nelson for assistance in the field. Kirk Sweetsir from Yukon Air Service and the staff at Wright Air Service provided critical access to our remote field area. Permission to work

in the Arctic National Wildlife Refuge was granted by Alfredo Soto at the U.S. Fish and Wildlife Service. Many of the ideas presented herein were conceived during spirited discussions with Tom Moore, Gil Mull, Francis Macdonald, Marwan Wartes, Tyrone Rooney, Elizabeth Miller, Eric Gottlieb, and Tim O'Brien. Finally, we are grateful to Carl Hoiland and Brian Pratt, who provided thoughtful reviews that drastically improved the manuscript, and we appreciate the editorial handling by Christian Koeberl and Karsten Piepjohn.

REFERENCES CITED

Amato, J.M., Aleinikoff, J.N., Akinin, V.V., McClelland, W.C., and Toro, J., 2014, Age, chemistry, and correlations of Neoproterozoic–Devonian igneous rocks of the Arctic Alaska–Chukotka terrane: An overview with new U-Pb ages, *in* Dumoulin, J.A., and Till, A.B., eds., Reconstruction of a Late Proterozoic and Early Paleozoic Continental Margin—Seward Peninsula and Correlative Rocks of the Arctic Alaska–Chukotka Terrane: Geological Society of America Special Paper 506, p. 29–57, https://doi.org/10.1130/2014.2506(02).

Amato, J.M., Toro, J., Miller, E.L., Gehrels, G.E., Farmer, G.L., Gottlieb, E.S., and Till, A.B., 2009, Late Proterozoic–Paleozoic evolution of the Arctic Alaska–Chukotka terrane based on U-Pb igneous and detrital zircon ages: Implications for Neoproterozoic paleogeographic reconstructions: Geological Society of America Bulletin, v. 121, p. 1219–1235, https://doi.org/10.1130/B26510.1.

Anderson, A.V., Wallace, W.K., and Mull, C.G., 1994, Depositional record of a major tectonic transition in northern Alaska: Middle Devonian to Mississippian rift-basin margin deposits, upper Kongakut River region, eastern Brooks Range, Alaska, *in* Thurston, D.K., and Fujita, K., eds., 1992 Proceedings of the International Conference on Arctic Margins:

Anchorage, Alaska, U.S. Department of the Interior, Minerals Management Service, OCS (Outer Continental Shelf) Study MMS 94–0040, p. 71–76.

Arevalo, R., and McDonough, W.F., 2010, Chemical variations and regional diversity observed in MORB: Chemical Geology, v. 271, p. 70–85, https://doi.org/10.1016/j.chemgeo.2009.12.013.

Bao, J.S., and Jago, J.B., 2000, Late late Cambrian trilobites from near Birch Inlet, south-western Tasmania: Palaeontology, v. 43, p. 881–917, https://doi.org/10.1111/1475-4983.00154.

Béchennec, F., Le Metour, J., Rabu, D., Bourdillon-de-Grissac, C., de Wever, P., Beurrier, M., and Villey, M., 1990, The Hawasina Nappes: Stratigraphy, palaeogeography and structural evolution of a fragment of the south- Tethyan passive continental margin, *in* Robertson, A.H.F., Searle, M.P., and Ries, A.C., eds., The Geology and Tectonics of the Oman Region: Geological Society, London, Special Publication 49, p. 213–223, https://doi.org/10.1144/GSL.SP.1992.049.01.14.

Beranek, L.P., van Staal, C.R., McClelland, W.C., Israel, S., and Mihalynuk, M.G., 2013, Detrital zircon Hf isotopic compositions indicate a northern Caledonian connection for the Alexander terrane: Lithosphere, v. 5, p. 163–168, https://doi.org/10.1130/L255.1.

Beranek, L.P., Pease, V.L., Hadlari, T., and Dewing, K., 2015, Silurian flysch successions of Ellesmere Island, Arctic Canada, and their significance to northern Caledonian palaeogeography and tectonics: Journal of the Geological Society [London], v. 172, p. 201–212, https://doi.org/10.1144/jgs2014-027.

Bouvier, A., Vervoort, J.D., and Patchett, P.J., 2008, The Lu-Hf and Sm-Nd isotopic composition of CHUR: Constraints from unequilibrated chondrites and implications for

the bulk composition of terrestrial planets: Earth and Planetary Science Letters, v. 273, p. 48–57, https://doi.org/10.1016/j.epsl.2008.06.010.

Brosgé, W.P., Dutro, J.T., Jr., Mangus, M.D., and Reiser, H.N., 1962, Paleozoic sequences in the eastern Brooks Range, Alaska: American Association of Petroleum Geologists Bulletin, v. 46, p. 2174–2198.

Cecile, M.P., 2000, Geology of the Northeastern Niddery Lake Map Area, East-Central Yukon and Adjacent Northwest Territories: Geological Survey of Canada Bulletin 553, 120 p., https://doi.org/10.4095/211664.

Cecile, M.P., Morrow, D.W., and Williams, G.K., 1997, Early Paleozoic (Cambrian to Early Devonian) tectonic framework, Canadian Cordillera: Bulletin of Canadian Petroleum Geology, v. 45, p. 54–74.

Cecile, M.P., Lane, L.S., Khudoley, A.K., and Kos'ko, M.K., 1999, Lower Paleozoic rocks around today's Arctic Ocean: Two ancestral continents and associated plates; Alaskan rotation unnecessary and unlikely: Polarforschung, v. 69, p. 235–241.

Chatterton, B.D.E., and Gibb, S., 2016, Furongian (Upper Cambrian) Trilobites from the McKay Group, Bull River Valley, near Cranbrook, Southeastern British Columbia, Canada: Palaeontographica Canadiana 35, 275 p.

Chew, D.M., and Strachan, R.A., 2014, The Laurentian Caledonides of Scotland and Ireland, *in* Corfu, F., Gasser, D., and Chew, D.M., eds., New Perspectives on the Caledonides of Scandinavia and Related Areas: Geological Society, London, Special Publication 390, p. 45–91, https://doi.org/10.1144/SP390.16.

Chien, Y.Y., 1961, Cambrian trilobites from Sandu and Duyan, southern Kweichow: Acta Palaeontologica Sinica, v. 9, p. 91–139.

Choi, D.K., Lee, J.G., and Sheen, B.C., 2004, Upper Cambrian agnostoid trilobites from the Machari Formation, Yongwol, Korea: Geobios, v. 37, p. 159–189, https://doi.org/10.1016/j.geobios.2003.02.004.

Colpron, M., and Nelson, J.L., 2011, A Palaeozoic NW Passage and the Timanian, Caledonian and Uralian connections of some exotic terranes in the North American Cordillera, *in* Spencer, A.M., Embry, A.F., Gautier, D.L., Stoupakova, A.V., and Sørensen, K., eds., Arctic Petroleum Geology: Geological Society, London, Memoir 35, p. 463–484, https://doi.org/10.1144/M35.31.

Corfu, F., Andersen, T.B., and Gasser, D., 2014, The Scandinavian Caledonides: Main features, conceptual advances and critical questions, *in* Corfu, F., Gasser, D., and Chew, D.M., eds., New Perspectives on the Caledonides of Scandinavia and Related Areas: Geological Society, London, Special Publication 390, p. 9–43, https://doi.org/10.1144/SP390.25.

Cox, G.M., Strauss, J.V., Halverson, G.P., Schmitz, M.D., McClelland, W.C., Stevenson, R.S., and MacDonald, F.A., 2015, Kikiktat volcanics of Arctic Alaska—Melting of harzburgitic mantle associated with the Franklin large igneous province: Lithosphere, v. 7, p. 275–295, https://doi.org/10.1130/L435.1.

Dumoulin, J.A., Harris, A.G., Gagiev, M., Bradley, D.C., and Repetski, J.E., 2002, Lithostratigraphic, conodont, and other faunal links between Lower Paleozoic strata in northern and central Alaska and northeastern Russia, *in* Miller, E.L., Grantz, A., and Klemperer, S.L., eds., Tectonic Evolution of the Bering Shelf–Chukchi Sea–Arctic Margin and Adjacent Landmasses: Geological Society of America Special Paper 360, p. 291–312, https://doi.org/10.1130/0-8137-2360-4.291.

Dutro, J.T., Jr., Brosgé, W.P., and Reiser, H.N., 1972, Signifi cance of recently discovered Cambrian fossils and reinterpretation of Neruokpuk Formation, northeastern Alaska: American Association of Petroleum Geologists Bulletin, v. 56, p. 808–815.

Elliott, T., 2003, Tracers of the slab, *in* Eiler, J., ed., Inside the Subduction Factory: American Geophysical Union Geophysical Monograph 138, p. 23–45, https://doi.org/10.1029/138GM03.

Fitton, J.G., 1987, The Cameroon line, West Africa: A comparison between oceanic and continental alkaline volcanism, *in* Fitton, J.G., and Upton, B.G.J., eds., Alkaline Igneous Rocks: Geological Society, London, Special Publication 30, p. 273–291, https://doi.org/10.1144/GSL.SP.1987.030.01.13.

Fortey, R.A., 1980, The Ordovician Trilobites of Spitsbergen III, Remaining Trilobites of the Valhallfonna Formation: Norsk Polarinstitutt Skrifter 171, 163 p.

Gehrels, G.E., and Pecha, M., 2014, Detrital zircon U-Pb geochronology and Hf isotope geochemistry of Paleozoic and Triassic passive margin strata of western North America: Geosphere, v. 10, p. 49–65, https://doi.org/10.1130/GES00889.1.

Gehrels, G.E., Valencia, V.A., and Ruiz, J., 2008, Enhanced precision, accuracy, efficiency, and spatial resolution of U-Pb ages by laser ablation–multicollector–inductively coupled plasma–mass spectrometry: Geochemistry Geophysics Geosystems, v. 9, Q03017, https://doi.org/10.1029/2007GC001805.

Goodfellow, W.D., Cecile, M.P., and Leybourne, M.I., 1995, Geochemistry, petrogenesis, and tectonic setting of Lower Paleozoic alkalic and potassic volcanic rocks, northern Canadian Cordilleran miogeocline: Canadian Journal of Earth Sciences, v. 32, no. 8, p. 1236–1254, https://doi.org/10.1139/e95-101.

Gradstein, F.M., Ogg, J.G., Smith, A.G., and Ogg, G., 2012, The Geologic Time Scale: Cambridge, UK, Cambridge University Press, 1176 p.

Grant, R.E., 1965, Faunas and Stratigraphy of the Snowy Range Formation (Upper Cambrian) in Southwestern Montana and Northwestern Wyoming: Geological Society of America Memoir 96, 171 p., https://doi.org/10.1130/MEM96-p1.

Green, D.H., and Ringwood, A.E., 1967, The genesis of basaltic magmas: Contributions to Mineralogy and Petrology, v. 15, p. 103–190, https://doi.org/10.1007/BF00372052.

Hart, C.J.R., 1986, The Geology of the Old Cabin Creek Massif, Selwyn Basin, Yukon Territory [B.S. thesis]: Hamilton, Ontario, Canada, McMaster University, 111 p.

Henderson, R.A., 1976, Upper Cambrian (Idamean) trilobites from western Queensland, Australia: Palaeontology, v. 19, p. 325–364.

Hofmann, A.W., 2003, Sampling mantle heterogeneity through oceanic basalts: Isotopes and trace elements, *in* Carlson, R.W., ed., Treatise on Geochemistry, Volume 2: The Mantle and Core: Oxford, Elsevier, p. 61–101.

Hoiland, C.W., Miller, E.L., Pease, V., and Hourigan, J.K., 2017, Detrital zircon U-Pb geochronology and Hf isotope geochemistry of metasedimentary strata in the southern Brooks Range: Constraints on Neoproterozoic–Cretaceous evolution of Arctic Alaska, *in* Pease, V.L., and Coakley, B.J., eds., Circum-Arctic Lithosphere Evolution: Geological Society, London, Special Publication 460, p. 121–158, https://doi.org/10.1144/SP460.16

Hooper, P.R., and Hawkesworth, C.J., 1993, Isotopic and geochemical constraints on the origin and evolution of the Columbia River Basalt: Journal of Petrology, v. 34, p. 1203–1246, https://doi.org/10.1093/petrology/34.6.1203.

Jackson, D.E., 1964, Observations on the sequence and correlation of Lower and Middle Ordovician graptolite faunas of North America: Geological Society of America Bulletin, v. 75, p. 523–534, https://doi.org/10.1130/0016-7606(1964)75[523:OOTSAC]2.0.CO;2.

Jaques, A.L., and Green, D.H., 1980, Anhydrous melting of peridotite at 0–15 Kb pressure and the genesis of tholeiitic basalts: Contributions to Mineralogy and Petrology, v. 73, p. 287–310, https://doi.org/10.1007/BF00381447.

Johnson, B.G., Strauss, J.V., Toro, J., Benowitz, J.A., Ward, W.P., and Hourigan, J.K., 2016, Detrital geochronology of pre-Mississippian strata in the northeastern Brooks Range, Alaska: Insights into the tectonic evolution of northern Laurentia: Lithosphere, v. 8, p. 649–667, https://doi.org/10.1130/L533.1.

Jones, D.L., Silberling, N.J., Coney, P.J., and Plafker, G., 1987, Lithotectonic Terrane Map of Alaska: U.S. Geological Survey Miscellaneous Field Studies Map MF-874, scale 1:2,500,000.

Kampunzu, A.B., and Mohr, P., 1991, Magmatic evolution and petrogenesis in the East African Rift System, *in* Kampunzu, A.B., and Lubala, R.T., eds., Magmatism in Extensional Structural Settings: Berlin, Springer, p. 85–136.

Kelley, J.S., Wrucke, C.T., and Lane, L.S., 1994, Pre-Mississippian rocks in the Clarence and Malcolm Rivers area, Alaska and Yukon Territory, *in* 1992 Proceedings of the International Conference on Arctic Margins: Anchorage, Alaska, U.S. Department of the Interior, Minerals Management Service, OCS (Outer Continental Shelf) Study MMS 94–0040, p. 59–64.

Kushiro, I., 2001, Partial melting experiments on peridotite and origin of midocean ridge basalt: Annual Review of Earth and Planetary Sciences, v. 29, p. 71–107, https://doi.org/10.1146/annurev.earth.29.1.71.

Lane, L.S., 1991, The pre-Mississippian "Neruokpuk Formation," northeastern Alaska and northwestern Yukon: Review and new regional correlation: Canadian Journal of Earth Sciences, v. 28, p. 1521–1533, https://doi.org/10.1139/e91-136.

Lane, L.S., 2007, Devonian–Carboniferous paleogeography and orogenesis, northern Yukon and adjacent Arctic Alaska: Canadian Journal of Earth Sciences, v. 44, p. 679–694, https://doi.org/10.1139/e06-131.

Lane, L.S., Kelley, J.S., and Wrucke, C.T., 1995, Stratigraphy and Structure of the Clarence River Area, Yukon–Alaska North Slope: A USGS-GSC Co-Operative Project: Current Research Part E: Geological Survey of Canada Paper 1995-E, p. 1–9, https://doi.org/10.4095/205183.

Lane, L.S., Gehrels, G.E., and Layer, P.W., 2016, Provenance and paleogeography of the Neruokpuk Formation, northwest Laurentia: An integrated synthesis: Geological Society of America Bulletin, v. 128, p. 239–257, https://doi.org/10.1130/B31234.1.

Lawver, L.A., Grantz, A., and Gahan, L.M., 2002, Plate kinematic evolution of the present Arctic region since the Ordovician, *in* Miller, E.L., Grantz, A., and Klemperer, S.L., eds., Tectonic Evolution of the Bering Shelf–Chukchi Sea–Arctic Margin and Adjacent Landmasses: Geological Society of America Special Paper 360, p. 333–358, https://doi.org/10.1130/0-8137-2360-4.333.

Lazarenko, N.P., Gogin, I.Y., Pegel, T.V., Sukhov, S.S., Abaimova, G.P., Egorova, L.I., Federov, A.B., Raevskaya, E.G., and Ushatinskaya, G.T., 2006, Cambrian stratigraphy of

the northeastern Siberian Platform and potential stratotypes of lower boundaries of the proposed Upper Cambrian Chekurovkian and Nelegerian stages in the Ogon'or Formation section at the Khos-Nelege River, *in* Rozanov, A.Y., and Varlamov, A.I., eds., The Cambrian System of the Siberian Platform, Part 2: North-east of the Siberian Platform, XIII International Field Conference of the Yakutia, Russia, Cambrian Stage Subdivision Working Group: International Commission on Cambrian Stratigraphy, p. 61–139.

Leffingwell, E. de K., 1919, The Canning River Region, Northern Alaska: U.S. Geological Survey Professional Paper 109, 251 p.

Longacre, S.A., 1970, Trilobites of the Upper Cambrian Ptychaspid Biomere, Wilberns Formation, Central Texas: Paleontological Society Memoir 4, 70 p.

Lu, Y.H., 1956, An Upper Cambrian trilobite faunule from eastern Kweichou: Acta Palaeontologica Sinica, v. 4, p. 365–380.

Lu, Y.K., and Zhu, Z.L., 1980, Cambrian trilobites from Chuxian-Quanjiao region, Anhui: Memoirs of the Nanjing Institute of Geology and Palaeontology, v. 16, p. 1–33.

Ludvigsen, R., and Westrop, S.R., 1983, Franconian Trilobites of New York State: New York State Museum Memoir 23, 83 p.

Ludvigsen, R., Westrop, S.R., and Kindle, C., 1989, Sunwaptan (Upper Cambrian) Trilobites of the Cow Head Group, Western Newfoundland, Canada: Palaeontographica Canadiana 6, 175 p.

Ludwig, K.R., 2012, User's Manual for Isoplot/Ex, Version 3.75: A Geochronological Toolkit for Microsoft Excel: Berkeley Geochronology Center Special Publication 5, 75 p.

MacNaughton, R.B., Moynihan, D.P., Roots, C.F., and Crowley, J.L., 2016, New occurrences of *Oldhamia* in eastern Yukon, Canada: Stratigraphic context and implications for Cambrian deep-marine biostratigraphy: Ichnos, v. 23, p. 33–52, https://doi.org/10.1080/10420940.2015.1127232.

MacPherson, G.J., Phipps, S.P., and Grossman, J.N., 1990, Diverse sources for igneous blocks in Franciscan mélanges, California Coast Ranges: The Journal of Geology, v. 98, p. 845–862, https://doi.org/10.1086/629457.

McClelland, W.C., Colpron, M., Piepjohn, K., von Gosen, W., Ward, W.P., and Strauss, J.V., 2015, Preliminary detrital zircon geochronology of the Neruokpuk Formation in the Barn Mountains, Yukon, *in* MacFarlane, K.E., Nordling, M.G., and Sack, P.J., eds., Yukon Exploration and Geology 2014: Whitehorse, Yukon Geological Survey, p. 123–143.

McDonough, W.F., and Sun, S.-s., 1995, The composition of the Earth: Chemical Geology, v. 120, p. 223–253, https://doi.org/10.1016/0009-2541(94)00140-4.

Miller, E.L., Kuznetsov, N., Soboleva, A., Udoratina, O., Grove, M.J., and Gehrels, G.E., 2011, Baltica in the Cordillera?: Geology, v. 39, p. 791–794, https://doi.org/10.1130/G31910.1.

Miller, E.L., Toro, J., Gehrels, G.E., Amato, J.M., Prokopiev, A., Tuchkova, M.I., Akinin, V.V., Dumitru, T.A., Moore, T.E., and Cecile, M.P., 2006, New insights into Arctic paleogeography and tectonics from U-Pb detrital zircon geochronology: Tectonics, v. 25, TC3013, https://doi.org/10.1029/2005TC001830.

Moore, T.E., 1987, Geochemistry and the tectonic setting of volcanic rocks of the Franklinian assemblage, central and eastern Brooks Range, *in* Tailleur, I., and Weimer, P., eds., Alaskan North Slope Geology: Pacifi c Section, Society of Economic Paleontologists and Mineralogists (SEPM) Publication 50, p. 691–710.

Moore, T.E., and Churkin, M., Jr., 1984, Ordovician and Silurian graptolite discoveries from the Neruokpuk Formation (sensu lato), northeastern and central Brooks Range, Alaska, *in* Blodgett, R.B., ed., Paleozoic Geology of Alaska and Northwestern Canada Newsletter 1: Anchorage, Alaska Geological Society, p. 21–23.

Moore, T.E., Wallace, W.K., Bird, K.J., Karl, S.M., Mull, C.G., and Dillon, J.T., 1994, Geology of northern Alaska, *in* Plafker, G., and Berg, H.C., eds., The Geology of Alaska: Boulder, Colorado, Geological Society of America, The Geology of North America, v. G-1, p. 49–140.

Mull, C.G., and Anderson, A.V., 1991, Franklinian Lithotectonic Domains, Northeastern Brooks Range, Alaska: Alaska Division of Geological & Geophysical Surveys Public Data File 91–5, 40 p., https://doi.org/10.14509/1472.

Nelson, L.L., Strauss, J.V., Crockford, P.W., Cox, G.M., Johnson, B.G., Ward, W., Colpron, M., McClelland, W.C., and Macdonald, F.A., 2018, this volume, Geochemical constraints on the provenance of pre-Mississippian sedimentary rocks in the North Slope subterrane of Yukon and Alaska, *in* Piepjohn, K., Strauss, J.V., Reinhart, L., and McClelland, W.C., eds., Circum-Arctic Structural Events: Tectonic Evolution of the Arctic Margins and Trans-Arctic Links with Adjacent Orogens: Geological Society of American Special Paper 541, Chapter 24, https://doi.org/10.1130/2018.2541(24).

Palmer, A.R., 1965, Trilobites of the Cambrian Pterocephaliid Biomere in the Great Basin, United States: U.S. Geological Survey Professional Paper 493, 105 p.

Palmer, A.R., 1968, Cambrian Trilobites of East-Central Alaska, United States: U.S. Geological Survey Professional Paper 559B, 115 p.

Palmer, A.R., and Halley, R.R., 1979, Physical Stratigraphy and Trilobite Biostratigraphy of the Carrara Formation (Lower and Middle Cambrian) in the Southern Great Basin: U.S. Geological Survey Professional Paper 1047, 131 p.

Patrick, B.E., and McClelland, W.C., 1995, Late Proterozoic granitic magmatism on Seward Peninsula and a Barentian origin for Arctic Alaska–Chukotka: Geology, v. 23, p. 81–84, https://doi.org/10.1130/0091-7613(1995)023<0081:LPGMOS>2.3.CO;2.

Pearce, J.A., 1996, A User's Guide to Basalt Discrimination Diagrams: Geological Association of Canada Short Course Notes 12, p. 79–113.

Pease, V.L., 2011, Eurasian orogens and Arctic tectonics: An overview, *in* Spencer, A.M., Embry, A.F., Gautier, D.L., Stoupakova, A.V., and Sørensen, K., eds., Arctic Petroleum Geology: Geological Society, London, Memoir 35, p. 311–324.

Pegel, T.V., 2000, Evolution of trilobite biofacies in Cambrian basins of the Siberian Platform: Journal of Paleontology, v. 74, p. 1000–1019, https://doi.org/10.1017/S0022336000017571.

Peng, S., 1992, Upper Cambrian Biostratigraphy and Trilobite Faunas of the Cili-Taoyuan Area, Northwestern Hunan, China: Association of Australasian Palaeontologists Memoir 13, 119 p.

Peng, S., and Robison, R.A., 2000, Agnostid Biostratigraphy across the Middle–Upper Cambrian Boundary in Hunan, China: Paleontological Society Memoir 53, 104 p.

Pillevuit, A., Marcoux, J., Stampfl i, G., and Baud, A., 1997, The Oman Exotics: A key to the understanding of the Neotethyan geodynamic evolution: Geodinamica Acta, v. 10, p. 209–238, https://doi.org/10.1080/09853111 .1997.11105303.

Pratt, B.R., 1992, Trilobites of the Marjuman and Steptoean Stages (Upper Cambrian), Rabbitkettle Formation, Southern Mackenzie Mountains, Northwest Canada: Palaeontographica Canadiana 9, 179 p.

Pyle, L., and Barnes, C., 2003, Lower Paleozoic stratigraphic and biostratigraphic correlations in the Canadian Cordillera: Implications for the tectonic evolution of the Laurentian margin: Canadian Journal of Earth Sciences, v. 40, p. 1739–1753, https://doi.org/10.1139/e03-049.

Rasetti, F., 1944, Upper Cambrian trilobites from the Levis Conglomerate: Journal of Paleontology, v. 18, p. 229–258.

Raymond, P.E., 1924, New Upper Cambrian and Lower Ordovician trilobites from Vermont: Proceedings of the Boston Society of Natural History, v. 37, p. 389–446.

Reiser, H.N., 1970, Northeastern Brooks Range—A surface expression of the Prudhoe Bay section, *in* Adkison, W.L., and Brosgé, W.P., eds., Proceedings of the Geological Seminar on the North Slope of Alaska: Los Angeles, California, Pacifi c Section, American Association of Petroleum Geologists, p. K1–K13.

Reiser, H.N., Brosge, W.P., Dutro, J.T., Jr., and Detterman, R.L., 1980, Geologic Map of the Demarcation Point Quadrangle, Alaska: U.S. Geological Survey Miscellaneous Investigations Series Map 1133, scale 1:250,000.

Robinson, J.A.C., and Wood, B.J., 1998, The depth of the spinel to garnet transition at the peridotite solidus: Earth and Planetary Science Letters, v. 164, p. 277–284, https://doi.org/10.1016/S0012-821X(98)00213-1.

Salters, V.J.M., and Stracke, A., 2004, Composition of the depleted mantle: Geochemistry Geophysics Geosystems, v. 5, Q05B07, https://doi.org/10.1029/2003GC000597.

Searle, M.P., and Graham, G.M., 1982, “Oman Exotics”—Oceanic carbonate build-ups associated with the early stages of continental rifting: Geology, v. 10, p. 43–49, https://doi.org/10.1130/0091-7613(1982)10<43:OECBAW>2.0.CO;2.

Shergold, J.H., 1977, Classifi cation of the trilobite *Pseudagnostus*: Palaeontology, v. 20, p. 69–100.

Shergold, J.H., 1980, Late Cambrian Trilobites from the Chatsworth Limestone, Western Queensland: Australian Bureau of Mineral Resources, Geology and Geophysics Bulletin 186, 111 p.

Shergold, J.H., Laurie, J.R., and Sun, X., 1990, Classifi cation and Review of the Trilobite Order Agnostida Salter, 1864: An Australian Perspective: Australian Bureau of Mineral Resources, Geology and Geophysics Report 296, 93 p.

Shervais, J.W., 1982, Ti-V plots and the petrogenesis of modern and ophiolitic lavas: Earth and Planetary Science Letters, v. 59, p. 101–118, https://doi.org/10.1016/0012-821X(82)90120-0.

Shervais, J.W., and Kimbrough, D.L.K., 1987, Alkaline and transitional subalkaline metabasalts in the Franciscan Complex mélange, California, *in* Morris, E.M., and Pasteris, J.D., eds., Mantle Metasomatism and Alkaline Magmatism: Geological Society of America Special Paper 215, p. 165–182, https://doi.org/10.1130/SPE215-p165.

Stitt, J.H., 1971, Late Cambrian and Earliest Ordovician Trilobites, Timbered Hills and Lower Arbuckle Groups, Western Arbuckle Mountains, Murray County, Oklahoma: Oklahoma Geological Survey Bulletin 110, 83 p.

Strauss, J.V., Macdonald, F.A., Taylor, J.F., Repetski, J.E., and McClelland, W.C., 2013, Laurentian origin for the North Slope of Alaska: Implications for the tectonic evolution of the Arctic: Lithosphere, v. 5, p. 477–482, https://doi.org/10.1130/L284.1.

Strauss, J.V., Hoiland, C.W., Ward, W.P., Johnson, B.G., Nelson, L.L., and McClelland, W.C., 2017, Orogen transplant: Taconic–Caledonian arc magmatism in the central Brooks Range of Alaska: Geological Society of America Bulletin, v. 129, p. 649–676, https://doi.org/10.1130/B31593.1.

Strauss, J.V., Johnson, B.G., Colpron, M., Nelson, L.L., Perez, J.L., Benowitz, J.A., Ward, W.P., and McClelland, W.C., 2018, this volume, Pre-Mississippian stratigraphy and provenance of the North Slope subterrane of Arctic Alaska II: Basinal rocks of the northeastern Brooks Range and their significance in circum-Arctic evolution, *in* Piepjohn, K., Strauss, J.V., Reinhardt, L., and McClelland, W.C., eds., Circum-Arctic Structural Events: Tectonic Evolution of the Arctic Margins and Trans-Arctic Links with Adjacent Orogens: Geological Society of America Special Paper 541, Chapter 23, https://doi.org/10.1130/2018.2541(23).

Sun, S.-s., and McDonough, W.F., 1989, Chemical and isotopic systematics of oceanic basalts: Implications for mantle composition and processes, *in* Saunders, A.D., and Norry, M.J., eds., Magmatism in the Ocean Basins: Geological Society, London, Special Publication 42, p. 313–345, https://doi.org/10.1144/GSL.SP.1989.042.01.19.

Sweeney, J.F., 1982, Mid-Palaeozoic travels of Arctic-Alaska: Nature, v. 298, p. 647–649, https://doi.org/10.1038/298647a0.

Tarduno, J.A., McWilliams, M., Debiche, M.G., Sliter, W.V., and Blake, M.C., 1985, Franciscan Complex Calera limestones: Accreted remnants of Farallon plate oceanic plateaus: Nature, v. 317, p. 345–347, https://doi.org/10.1038/317345a0.

Taylor, J.F., Brezinski, D.K., Repetski, J.E., and Welsh, N.M., 2009, The Adamstown submergence event: Faunal and sedimentological record of a late Cambrian (Furongian) transgression in the Appalachian region, *in* Laurie, J.R., ed., Cambro-Ordovician Studies IV: Association of Australasian Palaeontologists Memoir 37, p. 641–666.

Taylor, J.F., Repetski, J.E., Loch, J.D., and Leslie, S.A., 2012, Biostratigraphy and chronostratigraphy of the Cambrian–Ordovician Great American Carbonate Bank, *in* Derby, J.R., Fritz, R.D., Longacre, S.A., Morgan, W.A., and Sternbach, C.A., eds., The Great American Carbonate Bank: The Geology and Economic Resources of the Cambrian–Ordovician Sauk Megasequence of Laurentia: American Association of Petroleum Geologists Memoir 98, p. 15–35.

van Staal, C.R., and Barr, S.M., 2012, Lithospheric architecture and tectonic evolution of the Canadian Appalachians and associated Atlantic margin, *in* Percival, J.A., Cook, F.A., and Clowes, R.M., eds., Tectonic Styles in Canada: The LITHOPROBE Perspective: Geological Association of Canada Special Paper 49, p. 41–45.

van Staal, C.R., Dewey, J.F., Niocaill, C.M., and McKerrow, W.S., 1998, The Cambrian–Silurian tectonic evolution of the Northern Appalachians and British Caledonides: History of a complex, west and southwest Pacifi ctype segment of Iapetus: Geological Society, London, Special Publication 143, p. 197–242, https://doi.org/10.1144/GSL.SP.1998.143.01.17.

Varlamov, A.I., Pak, K.L., and Rosova, A.V., 2006, The Upper Cambrian of the Chopko River section, Norilsk region, northwestern Siberian Platform: Stratigraphy and trilobites: Palaeontological Journal, v. 40, Supplement 1, p. S1–S56.

Vervoort, J.D., and Blichert-Toft, J., 1999, Evolution of the depleted mantle: Hf isotope evidence from juvenile rocks through time: Geochimica et Cosmochimica Acta, v. 63, p. 533–556, https://doi.org/10.1016/S0016-7037(98)00274-9.

Vervoort, J.D., and Patchett, P.J., 1996, Behavior of hafnium and neodymium isotopes in the crust: Constraints from Precambrian crustally derived granites: Geochimica et Cosmochimica Acta, v. 60, p. 3717–3733, https://doi.org/10.1016/0016-7037(96)00201-3.

Vervoort, J.D., Patchett, P.J., Blichert-Toft, J., and Albarède, F., 1999, Relationships between Lu-Hf and Sm-Nd isotopic systems in the global sedimentary system: Earth and Planetary Science Letters, v. 168, p. 79–99, https://doi.org/10.1016/S0012-821X(99)00047-3.

Wallace, W.K., and Hanks, C.L., 1990, Structural provinces of the northeastern Brooks Range, Arctic National Wildlife Refuge, Alaska: American Association of Petroleum Geologists Bulletin, v. 74, p. 1100–1118.

Wendt, I., and Carl, C., 1991, The statistical distribution of the mean squared weighted deviation: Chemical Geology–Isotope Geoscience Section, v. 86, p. 275–285, https://doi.org/10.1016/0168-9622(91)90010-T.

Westrop, S.R., 1986, Trilobites of the Upper Cambrian Sunwaptan Stage, Southern Canadian Rocky Mountains, Alberta: Palaeontographica Canadiana 3, 179 p.

Westrop, S.R., 1995, Sunwaptan and Ibexian (Upper Cambrian–Lower Ordovician) Trilobites of the Rabbitkettle Formation, Mountain River Region, Northern Mackenzie Mountains, Northwest Canada: Palaeontographica Canadiana 12, 75 p.

Westrop, S.R., and Eoff, J.D., 2012, Late Cambrian (Furongian: Paibian, Steptoean) agnostoid arthropods from the Cow Head Group, western Newfoundland: BioOne, v. 86, p. 201–237, https://doi.org/10.1666/11-034.1.

Westrop, S.R., Eoff, J.D., Ng, T.-W., Dengler, A.A., and Adrain, J.M., 2008, Classifi cation of the late Cambrian (Steptoean) trilobite genera *Cheilocephalus* Berkey, 1898 and *Oligometopus* Resser, 1936 from Laurentia: Canadian Journal of Earth Sciences, v. 45, p. 725–744, https://doi.org/10.1139/E08-026.

Wilson, J.L., 1951, Franconian trilobites of the central Appalachians: Journal of Paleontology, v. 25, p. 617–654.

Winchester, J.A., and Floyd, P.A., 1977, Geochemical discrimination of different magma series and their differentiation products using immobile elements: Chemical Geology, v. 20, p. 325–343, https://doi.org/10.1016/0009-2541(77)90057-2.

Yoder, H.S., and Tilley, C.E., 1962, Origin of basalt magmas: An experimental study of natural and synthetic rock systems: Journal of Petrology, v. 3, p. 342–532, https://doi.org/10.1093/petrology/3.3.342.

Chapter 4: Geological mapping in the Arctic National Wildlife Refuge (ANWR), northeastern Brooks Range, Alaska

Benjamin G. Johnson[1], Justin V. Strauss[2], William P. Ward[3], Jaime Toro[1]

[1]Department of Geology and Geography, West Virginia University, Morgantown, West Virginia, 26506 USA

[2]Department of Earth Sciences, Dartmouth College, Hanover, New Hampshire 03755, USA

[4]Department of Earth and Environmental Sciences, University of Iowa, Iowa City, Iowa 52242, USA

ABSTRACT

Geological maps from the Arctic National Wildlife Refuge (ANWR) in the northeastern (NE) Brooks Range, Alaska, aid in the appraisal of hydrocarbon resources buried beneath the Arctic subsurface, but they also provide critical clues in reconstructing the tectonic history of the circum-Arctic region. Two 1:75,000 scale geological maps from the British and Romanzof mountains in the NE Brooks Range were created by integrating field-based observations with remote sensing data, such as the new 5-m ArcticDEM and satellite imagery from Google Earth. The maps include more than 20 distinct lithostratigraphic and lithodemic units and features a prominent sub-Mississippian unconformity, which truncates some of the thickest deposits of the lower Paleozoic strata in Arctic North America. Imbrication and folding of the unconformity, which is delineated by the Lower Mississippian Kekiktuck Conglomerate, is related to the late phases of Brookian contraction that occurred during the Cenozoic uplift of the NE Brooks Range. Below the unconformity, the rocks are deformed into tight to isoclinal, rotated folds, which are in strong discordance with the upright detachment folds that characterize overlying strata above the Kekiktuck Conglomerate, including the Kayak Shale and Lisburne Group. This earlier phase of deformation, the Romanzof orogeny, is attributed to the emplacement of the

Whale Mountain allochthon, an oceanic assemblage of Cambrian—Middle Ordovician volcanic and marine sedimentary rocks, and delineates an internal, middle Paleozoic suture within the greater Arctic Alaska—Chukotka microplate.

INTRODUCTION

The Brooks Range of Arctic Alaska and Yukon is one of the most sparsely mapped mountain ranges in North America. It is a steep and rugged region that extends more than 1,000 km in an east–west direction from northern Yukon to the Chukchi Sea (Fig. 4.1), reaching widths of up to 300 km and covering more than 50 million acres of largely uninhabited wilderness. The eastern portion of the Brooks Range is contained within the Arctic National Wildlife Refuge (ANWR) in Alaska and Ivvavik and Vuntut national parks in Yukon. The ANWR is the largest (>70,000 km^2) and wildest, publicly owned land in the United States. It is host to a fragile ecosystem, containing some 200 species of migratory birds, more than 35 different kinds of land mammals, and several species of fish and marine mammals, notably polar bears.

About 60 miles northwest of ANWR, along the northern edge of the North Slope, lies Prudhoe Bay (Fig. 4.1A), the site of North America's single largest oil discovery. In 2001, the United States Geological Survey estimated recoverable resources beneath subsurface of the coastal plain in ANWR (1002 Area; Fig. 4.1B) to contain about 10.4 billion barrels of oil (Bird and Houseknecht, 2001), making it an attractive target for future oil and gas development. This has led to tension between environmentalists and proponents of oil and gas drilling. The rocks in the subsurface of the ANWR coastal plain are exposed in the adjacent northeastern (NE) Brooks Range to the south (Fig. 4.1B). Geological mapping efforts in the Brooks Range portion of the ANWR and in Ivavvik National Park of Yukon have and continue to provide critical information to future assessments of the petroleum resources contained within ANWR (e.g., Reiser, 1970).

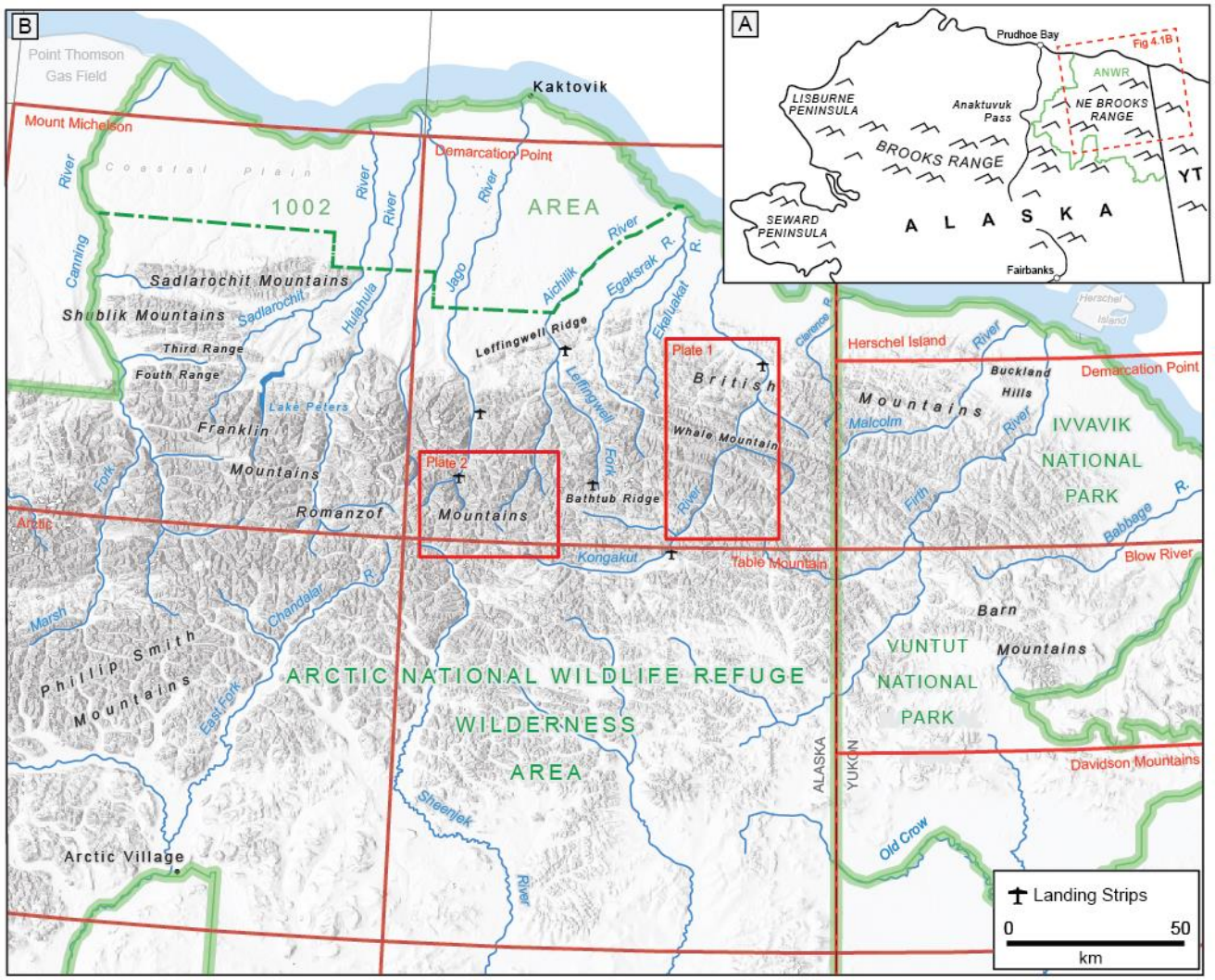

Figure 4.1: (A) Inset map of northern Alaska. (B) Shaded relief map of the northeastern Brooks Range of Alaska and Yukon showing the location of the two 1: 75,000 geological maps from this study (Plates 1 and 2). Previously published and open file 1: 250,000 geological quadrangles are labeled and outlined in light-red. R.–River.

Aside from their impact on natural resource assessments, geological maps from the NE Brooks Range provide clues to the geological and tectonic history of the circum-Arctic region. Late Mesozoic to Cenozoic deformation produced a broad structural salient that protruded the deformation front to within 35 km of the Arctic coastline and built the highest topography along the entire Brooks Range trend. The salient exposes a thick susseccsion of sedimentary, igneous, and metamorphic rocks that range in age from late Neoproterozoic to Cretaceous. Thick Pleistocene glacial and fluvial deposits also fill a network of narrow river valleys that run south to north, carrying snowmelt and rainwater from the high mountains of the continental divide to the Arctic coast. In this manuscript, observations made over the course of five field seasons (2011 to 2015) in the NE Brooks Range are assembled into two, 1: 75,000 scale geological maps (Plates 1 and 2), with an emphasis on the sub-Mississippian structural and stratigraphic architecture. We review nearly 100 years of geological investigation and provide some new observations to organize the various lithostratigraphic and lithodemic units in the NE Brooks Range into a coherent scheme that can be applied to future mapping efforts.

APPROACH

The 1:75,000 scale geological maps generated in this study (Plates 1 and 2) are focused in two key areas of the NE Brooks Range: along the Kongakut River (Plate 1), and in the headwaters of the Jago and Aichilik rivers (Plate 2). Field work was conducted in the summer, with individual campaigns lasting two to five weeks at a time. Access to our remote field area was achieved by bush plane, landing on gravel strips along major rivers (Fig. 4.1). Most of the observations included in this study were gathered during the 2012–2015 field campaigns, although J.V. Strauss and others explored the Elkaluakat River (Fig. 4.1) in the summer of 2011.

In the late summer of 2012, we traversed down the Kongakut River (Fig. 4.1) using a raft. In the following summer of 2013, we traversed the Leffingwell Fork of the Aichilik River (Fig. 4.1) also using a raft; however, much of the Leffingwell Fork was too shallow for paddling and we were forced to pull the raft with nylon ropes for most of the trip. Concurrently with the Leffingwell Fork expedition, a separate expedition was run in the Malcom and Firth river areas of northern Yukon (Fig. 4.1). This expedition was part of the Circum-Arctic Structural Events (CASE) project and was sponsored by the Federal Institute for Geosciences and Natural Resources in Germany (BGR) and the Yukon Geological Survey (YGS). The upper Jago and Aichilik drainages in Alaska were explored in the summer of 2014 and 2015, but the region was traversed by hiking with heavy (~100 lbs.) backpacks. Throughout these field seasons we collected >130 rock samples (Table 4.1) and made several hundred structural measurements. Many of the results and observations from this fieldwork were published in Johnson et al. (2016; 2018), Strauss et al., (2018a), and Nelson et al. (2018).

The observations and measurements from the field were assembled into a geographical information system (GIS) using a combination of ESRI ArcMap 10 and Google Earth software. We used previously published and unpublished geological maps of the region, including the maps of Sable (1977), Reiser et al. (1980), Hanks (1989, 1993), Homza (1991), Anderson (1993), Imm et al. (1993), Lane et al. (1995), and Peapples et al. (1997) as a reference for unit contacts. We then applied the stratigraphic nomenclature of Strauss et al. (2018a), specifically to illustrate the distribution and structure of the sub-Mississippian units. In addition, we integrated Landsat and DigitalGlobe © (2018) satellite imagery from Google Earth, in conjunction with the 5 m ArcticDEM created by the Polar Geospatial Center from DigitalGlobe © (2018) imagery, to interpolate and draw map lines between waypoints taken from the field.

TABLE 4.1: SAMPLE LIST FROM THE NE BROOKS RANGE

Sample Name	Latitude	Longitude	Map Unit	Analyses
Kongkut River, 2012				
12JT01	69.072	-142.204	Kk	TS
12JT02	69.044	-142.161	Kb	TS, DZ
12JT03	69.040	-142.069	₸Ps	TS
12JT04	69.052	-142.053	₸Ps	TS
12JT05	69.104	-141.919	Mky	TS, DZ
12JT06	69.107	-141.908	Mky	TS
12JT07	69.108	-141.907	Mky	TS
12JT08	69.108	-141.907	Mkt	TS, DZ
12JT09	69.108	-141.907	Mkt	TS, DZ
12JT10	69.110	-141.908	SOa	TS, DZ
12JT11	69.158	-141.865	€n	TS, DZ
12JT12	69.211	-141.849	€n	TS, AR
12JT13a	69.227	-141.831	€n,O€l, Soa	TS,AR
12JT13b	69.251	-141.729	€wv	TS,GC
12JT14	69.251	-141.729	€wv	TS,GC
12JT15	69.251	-141.729	€wv	TS,GC
12JT16	69.251	-141.729	€wv	TS,GC
12JT17	69.251	-141.729	€wv	TS,GC
12JT18	69.251	-141.729	€wv	TS,GC
12JT19	69.251	-141.729	€wv	TS,GC
12JT20	69.251	-141.729	€wv	TS,GC
12JT21	69.247	-141.724	€wv	TS,GC
12JT22	69.279	-141.727	Dbh	TS, DZ
12JT23	69.280	-141.747	Dbh	TS, DZ
12JT24	69.280	-141.747	Dbh	TS, DZ, AR
12JT25	69.276	-141.754	€wv	TS
12JT26	69.290	-141.753	O€l	TS
12JT29	69.328	-141.694	Z€fr	TS
12JT30	69.339	-141.643	Z€fr	TS
12JT31	69.387	-141.535	Z€fr	TS, DZ
12JT32	69.425	-141.508	€n	TS, DZ
12JT33	69.447	-141.452	Mkt	TS, DZ
12JT34	69.457	-141.453	O€e	TS
12JT35	69.468	-141.465	O€e	TS, DZ
12JT36	69.468	-141.465	O€e	TS
12JT37	69.469	-141.469	O€e	TS,GC
12JT38	69.469	-141.469	O€e	TS
12JT39	69.457	-141.451	O€e	TS,GC

Sample Name	Latitude	Longitude	Map Unit	Analyses
Leffingwell Fork, 2012				
01LF13	69.185	-142.602	Mky	TS
02LF13	69.192	-142.599	€n	TS
03LF13	69.182	-142.576	Mky	TS
04LF13	69.186	-142.662	Mkt	TS
05LF13	69.185	-142.664	€n	TS, DZ
06LF13	69.214	-142.666	€n	TS, DZ
07LF13	69.214	-142.666	€n	TS
08LF13	69.214	-142.666	€n	TS
09LF13	69.266	-142.658	€n,O€l, Soa	TS, AR
10LF13	69.264	-142.658	€n,O€l, Soa	TS
11LF13	69.263	-142.658	SOa	TS,DZ
12LF13	69.271	-142.684	SOa	TS
13LF13	69.583	-142.644	€e	TS
14LF13	69.346	-142.644	€e	TS
15LF13	69.346	-142.644	€e	TS
16LF13	69.347	-142.653	€e	TS
17LF13	69.348	-142.639	€wv	TS,GC
18LF13	69.348	-142.639	€wv	TS,GC
19LF13	69.348	-142.639	€wv	TS,GC
20LF13	69.348	-142.639	€wv	TS,GC
21LF13	69.348	-142.639	€wv	TS,GC
22LF13	69.348	-142.639	€wv	TS,GC
23LF13	69.348	-142.639	€wv	TS,GC
24LF13	69.314	-142.704	SOa	TS
25LF13	69.347	-142.853	SOa	TS
26LF13	69.352	-142.855	SOa	TS
27LF13	69.357	-142.858	€n	TS
28LF13	69.357	142.858-	€n	TS, DZ
29LF13	69.358	-142.858	€n,O€l, Soa	TS
30LF13	69.369	-142.871	Dbh	TS
31LF13	69.372	-142.875	Dbh	TS
32LF13	69.363	-142.919	Dbh	TS
33LF13	69.360	-142.921	O€l	TS
34LF13	69.360	-142.921	O€l	TS
35LF13	69.358	-142.922	O€l	TS
36LF13	69.358	-142.921	€n	TS
37LF13	69.357	-142.921	€n	TS, AR
38LF13	69.361	-142.884	Dbh	TS
39LF13	69.359	-142.884	Dbh	TS
40LF13	69.375	-142.912	Dbh	TS, DZ, AR
41LF13	69.388	-142.950	₸Ps	TS
42LF13	69.451	-143.009	Z€fr	TS
43LF13	69.467	-142.910	Z€fr	TS
44LF13	69.474	-142.827	Z€fr	TS, DZ
45LF13	69.474	-142.827	Z€fr	C

TABLE 4.1: SAMPLE LIST FROM THE NE BROOKS RANGE CONT'D

Sample Name	Latitude	Longitude	Map Unit	Analyses
Leffingwell Fork, 2012				
46LF13	69.474	-142.827	Z€fr	TS
47LF13	69.474	-142.827	Z€fr	TS
48LF13	69.474	-142.827	Z€fr	TS
Jago and Aichilik rivers, 2014				
14BJ01	69.098	-144.629	Qa	NA
14BJ02	69.314	-143.522	€n	TS
14BJ03	69.303	-143.456	Mky	TS
14BJ04	69.239	-143.714	Dbh, SOa	TS
14BJ05	69.239	-143.714	Dbh, SOa	TS
14BJ06	69.240	-143.715	Dbh, SOa	TS
14BJ05	69.241	-143.717	Dbh, SOa	TS
14BJ07	69.230	-143.681	Dgr	TS
14BJ08	69.272	-143.528	Dgr	TS
14BJ09	69.261	-143.510	Dgr	TS
14BJ10	69.261	-143.510	Mkt	TS
14BJ11	69.254	-143.508	Dgr	TS
14BJ12	69.254	-143.508	€n	TS
14BJ13	69.356	-143.539	PMl	TS
14BJ14	69.362	-143.653	Dgr	TS
14BJ15	69.360	-143.663	Dgr	TS
14BJ16	69.318	-143.551	Qa	TS
14BJ17	69.318	-143.551	Dgr	TS
14BJ18	69.303	-143.506	Da	TS
14BJ19	69.114	-142.707	Kb	TS
14BJ20	69.081	-143.068	O€r	TS, DZ
14BJ21	69.041	-143.132	Dmu	TS
14BJ22	69.117	-143.173	€mv	TS,GC
14BJ23	69.116	-143.175	€mv	TS,GC
14BJ24	69.117	-143.179	€mv	TS,GC, DZ
14BJ25	69.100	-143.112	O€r	TS, DZ
14BJ26	69.124	-143.218	Dbh	TS, DZ
14BJ27	69.125	-143.226	Dbh	TS, Ar
14BJ28	69.122	-143.169	€l	TS
14BJ29	69.339	-142.679	Dbh	TS, DZ
14BJ30	70.136	-143.591	€i	TS

Sample Name	Latitude	Longitude	Map Unit	Analyses
Jago and Chandalar rivers, 2015				
15BJ01	69.086	-143.576	€mv	NA
15BJ02	69.135	-143.782	Dgr	TS
15BJ03	69.135	-143.782	Dgr	TS
15BJ04	69.123	-143.825	€n	NA
15BJ05	69.109	-143.843	Z€fr	NA
15BJ06	69.109	-143.894	€mv	TS,DZ
15BJ07	69.086	-143.905	€n	NA
15BJ08	69.069	-143.908	€mv	NA
15BJ09a	69.060	-143.885	Dgr	TS
15BJ09b	69.060	-143.885	Dgr	TS
15BJ09c	69.060	-143.885	Dgr	TS
15BJ09d	69.060	-143.885	Dgr	TS
15BJ09c	69.060	-143.885	Dgr	TS
15BJ10	69.097	-143.583	Soa	TS,DZ,AR
15BJ11	69.097	-143.572	Dbh	TS,DZ,AR
15BJ12	68.996	-144.110	Di	NA
15BJ13	68.999	-144.105	Di	NA
15BJ14	69.106	-143.899	Dv	NA
15BJ15a	68.970	-144.369	Dv	NA
15BJ15b	68.970	-144.369	Dv	NA
15BJ15c	68.970	-144.369	Dv	NA
15BJ15d	68.970	-144.369	Dv	NA
15BJ15e	68.970	-144.369	Dv	NA

TS-Thin Section; DZ-Detrital zircon; Ar- $^{40}Ar/^{39}Ar$; GC-Geochemistry; NA-Not available

LITHOSTRATIGRAPHIC UNITS

The entire NE Brooks Range comprises more than 20 individual lithostratigraphic units. Their incorporation into the two 1:75,000 scale geological maps presented on Plates 1 and 2 is dependent a multitude of factors, including the degree of exposure, thickness, and how distinguishable they are in satellite imagery. We have excluded the Neoproterozoic to Devonian carbonate and volcanic units exposed in the Shublik and Sadlerochit mountains (Fig. 4.1) from the descriptions below because they are not included in our maps (Plates 1 and 2), and the reader is referred to Strauss et al. (2018b) and references therein for a more complete review of that region. What follows below is a description all the map units that are exposed in our map areas (Fig. 4.1; Plates 1 and 2). Their relative position and thicknesses are schematically illustrated in Figure 4.2.

Qa – Surface alluvium, undivided (Pleistocene–Holocene)

The river valleys in the NE Brooks Range are mostly covered by an ~1 to >100 m surface alluvium consisting of unconsolidated silt, sand, gravel, cobbles, and boulders. Much of this sediment is deposited in active channels and floodplains of rivers, streams, alluvial fans, piedmont slopes, and in the moraines of ancient and modern glaciers. The region records several alpine glacial events dating back to the Early Pleistocene (e.g., Detterman et al., 1958, Reed, 1968).

Kb – Bathtub Graywacke (Lower Cretaceous)

The type section of the Bathtub Graywacke is exposed on the north flank of Bathtub Ridge (Fig. 4.1), which stretches for 30 km east–west in the upper reaches of the Kongakut River (Detterman, et al., 1975). A second reference section is exposed along Sabbath Creek, a tributary of the lower Jago River, north of the Brooks Range front. The graywacke forms a resistive cap

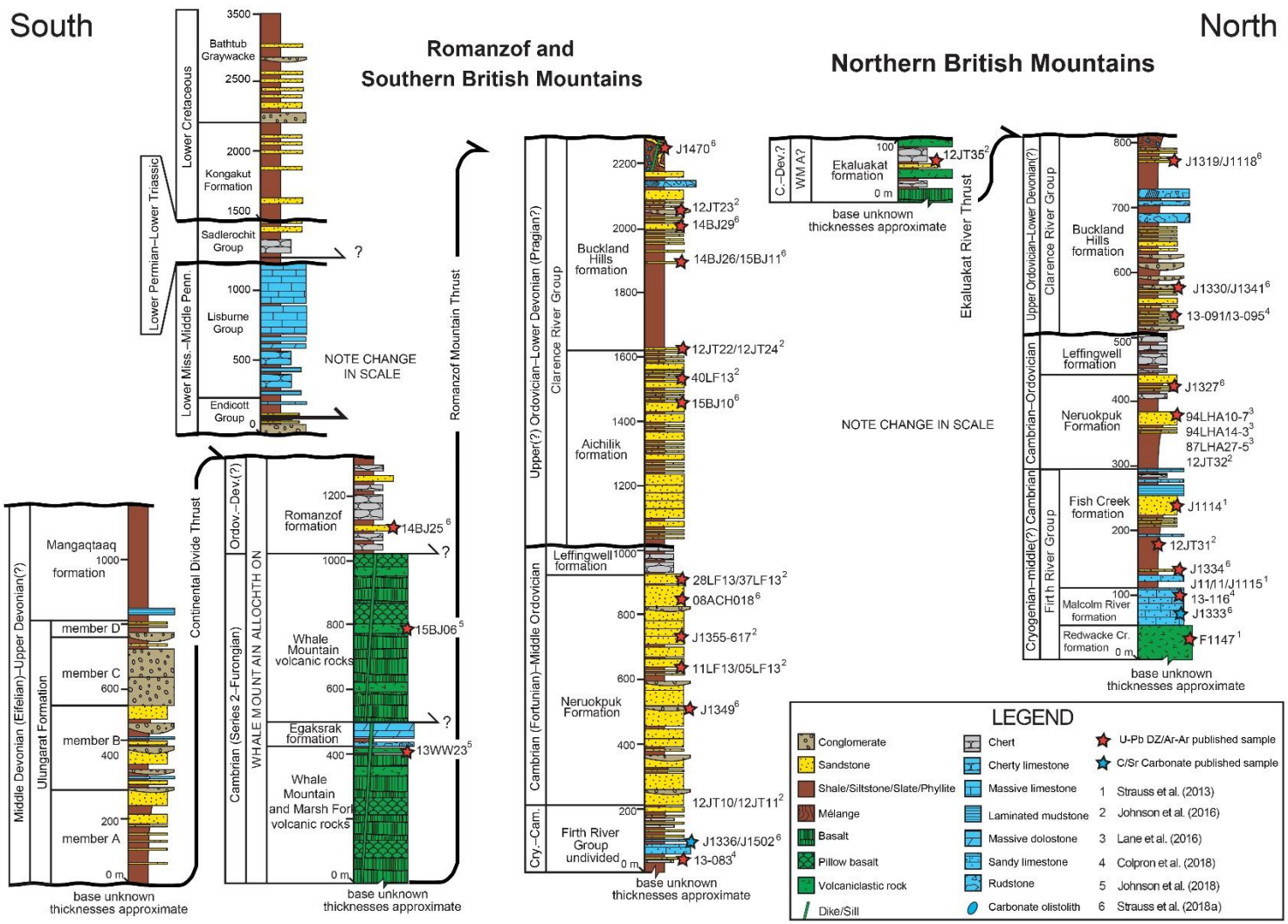

Figure 4.2: Simplified lithostratigraphic architecture of the northeasteastern Brooks Range, modified from Strauss et al. (2018a). These lithostratigraphic sections are based data published by Dutro et al. (1972), Sable (1977), Ditterman et al. (1975), Mamet and Armstrong (1972), Reiser et al. (1980), Lane (1991), Lane et al. (1995, 2016), Mull and Andersen (1991), Andersen et al. (1994; 1995), Kelley et al. (1994), Strauss et al. (2013; 2018a), and Johnson et al. (2016; 2018). Cry.–Cryogenian; C.–Cambrian; Cam.–Cambrian; Dev.–Devonian; Cr.–Creek; Miss.–Mississippian; Penn.–Pennsylvanian.

composed of up to 750 m of mainly subfeldspathic, lithic-rich, dark-grayish-green graywacke, with interbeds of siltstone, shale, and conglomerate. The contact with the underlying shale units of the Kongakut Formation appears conformable and is marked by the lowest exposure of massive greywacke.

The age of the Bathtub Graywacke is only constrained by the biostratigraphic ages from the units exposed above and below its boundaries (Detterman et al., 1975). The uppermost beds of the underlying Kongakut formation are assigned to the middle part of the Lower Cretaceous (Hauterivian–Berremian), and although no Aptian or Albian units have not been firmly identified in Brooks Range of Alaska, there are units assigned to the Upper Cretaceous (Cenomanian–lower Maastrichtian) and the Aptian–Albian stages that are exposed in the Yukon portion of the Brooks Range and in the Richardson Mountains (e.g., Norris, 1981a, 1981b; Dixon, 2004, Colpron et al., 2018). Detterman et al. (1975) therefore assigned the Bathtub Graywacke to the Albian, and suggested that it is equivalent, in part, to the Fortress Mountain Formation exposed in the foothills of the central Brooks Range if Alaska (Patton, 1956).

Kk – Kongakut Formation (Upper Jurassic(?)–Lower Cretaceous)

The Kongakut Formation includes four members: the informal clay shale, pebble shale, and siltstone members and the formal Kemic Sandstone Member (Dettermen et al., 1975). Other authors, working along the mountain front and costal plain of ANWR, raised the Kemic Sandstone and pebble shale members of the Kongakut Formation to formal formational rank and suggested that the Kongakut Formation name be geographically restricted to the rocks exposed at Bathtub Ridge (Mull, 1987; Molenaar et al., 1987). At its type locality along the flanks of Bathtub Ridge (Fig. 4.1), the Kongakut Formation is ~700 m thick. Its basal surface marks a unconformity that truncates the underlying Ivishak Formation of the Sadlerochit Group, which

represents the surface equivalent of the seismically imaged Lower Cretaceous Unconformity (LCU) in the subsurface at Prudhoe Bay and throughout other parts of northern Alaska (e.g., Molenaar et al., 1987). The basal part of the Kongakut section is marked by a nonresistant, saddle-forming, dark-gray fissile shale (clay shale member). The clay shale member grades into the Kemic Sandstone, which is composed of fine grained quartz arenite that forms resistant ledges along the northern part of Bathtub Ridge. Above the Kemic Sandstone, the section grades into the manganiferous pebbly shale and olive-gray siltstone members.

The age of the Kongakut Formation is constrained by a sparse collection of mega and microfauna, which assign most of the sedimentary intervals to the middle part of the Lower Cretaceous (Hauterivian–Berremian), but the lowermost section of the Kongakut Formation (clay shale member) is characterized by a mixed microfauna that suggests a lowermost Cretaceous–uppermost Jurassic assignment (Detterman et al., 1975; Reiser et al., 1980). This implies that the clay shale member at Bathtub Ridge is, in part, time correlative with the Kingak Shale, a Lower–Upper Jurassic sequence of dark, fissile shale exposed at the southeastern end of the Sadlerochit Mountains and in the North Slope subsurface (e.g., Leffingwell, 1919; Hubbard et al., 1987)

TrPs – Sadlerochit Group, undivided (Lower Permian–Lower Triassic)

The Sadlerochit Group includes two formal formations: a lower Echooka Formation and an upper Ivishak Formation, both of which are divided into several formal members (Ditterman et al., 1975). The group is named for its type area along the southern flank of Sadlerochit Mountains in the Mount Michelson 1:250,000 quadrangle, roughly 60 km to the northeast of our main study area (Fig. 4.1). A nearly complete section of Sadlerochit Group strata, however, is exposed at the base of Bathtub Ridge, which we examined in the field campaigns of 2012 and

2014. Collectively, the Sadlerochit Group ranges from ~200 to 500 m thick, and appears to be folded in concert with the underlying Lisburne Group (Fig 4.3A). Paleontological evidence indicates that the Sadlerochit Group is marked by unconformities on its upper and lower boundaries, separating it from the overlying Kongakut Formation and underlying Lisburne Group.

The lower half of the Sadlerochit Group, the Echooka Formation, comprises two members. The Joe Creek Member is in the lowest unit and is defined by a succession of dusky-yellow, thin to massively bedded dense chert, siliceous siltstone, and carbonate mudstone. The Joe Creek Member grades into the Ikiakpaurak Member, which consists of dark gray sandstone, predominantly composed of fine- to very-fine-grained quartz and chert fragments. The Ikiakpaurak Member grades into a recessive-weathering unit of siltstone and shale, defined by Detterman et al. (1975) as the Kavik Member, which forms the lower third of the Ivishak Formation. Above the Kavic Member lies the ~15 to 100 m thick Ledge Sandstone Member. Well known as the main oil-producing reservoir in the subsurface at Prudhoe Bay, the Ledge Sandstone is defined by the massive, resistive, and iron-stained sandstone unit that is locally conglomeratic. It is present in all outcrops of the Sadlerochit Group in the NE Brooks Range, but is thickest in the area near Ledge Creek, a tributary of the Sadlerochit River, where it forms numerous ledges or hogbacks along the east end of the Sadlerochit Mountains. In some parts of the NE Brooks Range, the Ledge Sandstone is conformably overlain by recessive-weathering shale and siltstone beds of the Fire Creek Member, but in other cases the Ledge Sandstone is truncated by the Lower Cretaceous unconformity.

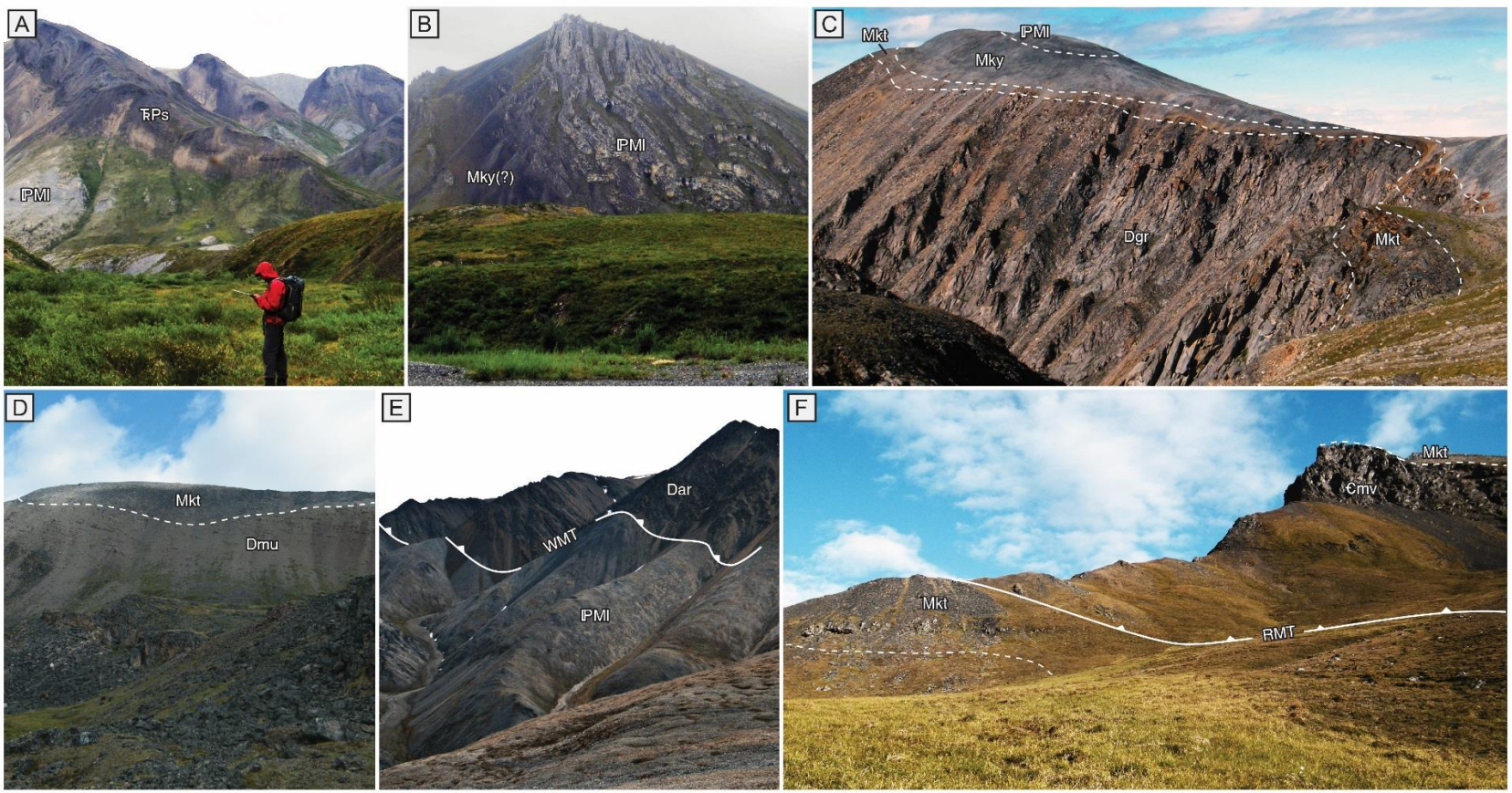

Figure 4.3: Selected field images from the northeastern Brooks Range, Alaska. (A) Looking southeast along the northern edge of Bathtub Ridge, showing folds in the Lisburne (PMl) and Sadlarochit (TrPs) groups. (B) Looking east across the Kongakut River at parasitic folds in the Lisburne Group (PMl) and Kayak Shale (Mky). (C) Looking north at the top of the Jago Stock, showing the gradational contact between the Devonian granitic rocks (Dgr) and the Kekiktuk Conglomerate (Mkt). (D) Looking northeast in the headwaters of the Kongakut River, showing the erosive contact between the Ulungarat Formation (DMu) and the Kekiktuk Conglomerate. (E) Looking southeast from the eastern wall of the Jago River valley at the Whale Mountain thrust (WMT). Units in the hanging wall are Devonian(?) altered rocks (Dar). (F) Looking southeast at the Romanzof Mountain thrust (RMT), in the headwaters of the Aichilik River, showing the Kekiktuk Conglomerate in foot wall with the Marsh Fork volcanic rocks (Cmv) overlain by Kekiktuk Conglomerate in the hanging wall.

IPMl – Lisburne Group, undivided (Lower Mississippian–Middle Pennsylvanian)

The Lisburne Group is divided into three formal limestone formations: Wachsmuth Limestone, Alpha Limestone, and Wahoo Limestone. The Lisburne name was originally assigned to limestone units exposed in the upper Anaktuvuk River valley of the central Brooks Range by Schrader (1902), who correlated the central Brooks Range units to a similar limestone and shale section exposed in the area of the Lisburne Peninsula along the NW coast of Alaska (Fig. 4.1B). Leffingwell (1919), who was working in the Canning River area, later applied the Lisburne name to many of the Paleozoic limestone units in the NE Brook Range. Later, Bowsher and Dutro (1957) identified several type sections in the Shanin Lake area just east of the Anaktuvuk River Valley, where they recognized two new formations, a lower Wachsmuth Limestone and an upper Alpha Limestone, and raised the Lisburne to group rank. A third formation, the Wahoo Limestone, was described by Brosgé et al. (1962) at Wahoo Lake near the Echooka River at the western edge of the Philip Smith Mountains, and it was assigned to the upper third of the Lisburne Group.

Most of the limestone units consist of massive, light-gray skeletal wackestone and packstone, with lesser amounts of carbonate mudstone, dolostone, and ooid grainstone. Intervals of dark-gray nobular and bedded chert and interbedded black carbonate mudstone are prevalent in the Wachsmuth Limestone and lower portions of the Alpha Limestone (Fig. 4.2). The stratigraphic boundaries that separate the three formations at the type sections are typically determined by biostratigraphy. The basal contact of the Lisburne Group with the underlying Kayak Shale, however, is typically picked by lithostratigraphic transition, and has been recognized to represent a time-transgressive surface throughout the region. The contact between the Wachsmuth Limestone and the Alpha Limestone in the Shanin Lake area is assigned to the

upper Visean (e.g., Bowsher and Dutro, 1957; Armstrong et al., 1970). Nearly all the limestone units in the NE Brooks Range, however, record deposition from the Serpukhovian to the middle Moscovian (e.g., Armstrong et al., 1970; Mamet and Armstrong, 1972; Armstrong and Mamet, 1977), indicating that the time-equivalent Wachsmuth Limestone units, exposed in the Shanin Lake area, are not recognized in our field area. The contact between the Alpha Limestone and the Wahoo Limestone is assigned to the Mississippian–Pennsylvanian boundary (Serpukhovian–Bashkirian), and it roughly corresponds to a gradational change in lithofacies, as the chert nodules and carbonate mudstone intervals of the Alpha Limestone grade into the skeletal packstone and wackestone-dominated intervals of the Wahoo Limestone.

The overall thickness of the Lisburne Group varies across entire Brooks Range, and because of the intense folding and the erosion across its upper surface, its absolute stratigraphic thickness is uncertain. Compyling the previously measured sections from the Franklin, Romanzof, and British Mountains (e.g., Mamet and Armstrong, 1972; Armstrong and Mamet, 1977), we use a thickness of 1000 m for the Lisburne Group in our cross sections (Plates 1 and 2).

Me – Endicott Group, undivided (Lower–Upper Mississippian)

The Endicott Group encompasses a thick siliciclastic-dominated succession of Upper Devonian–Lower Mississippian strata that are widely exposed throughout much of the Brooks Range and in the subsurface of the Colville Basin. It is named for its prominent exposure in the Endicott Mountains of the central Brooks Range, where it consists of, in ascending order, the Hunt Fork Shale, Kanayut Conglomerate, and Kayak Shale (Tailleur et al., 1967). In the northeastern Brooks Range, it includes the Kekiktuk Conglomerate, the Kayak Shale, and the locally defined Itkilyariak Formation of Mull and Magnus (1972). Below, we only describe the

Kekiktuk Conglomerate and Kayak Shale because they are the only two units from the Endicott Group exposed in our field area.

Mky – Kayak Shale (Lower–Upper Mississippian)

Like the limestone intervals of the Lisburne Group, the type section of the Kayak Shale was also described in the Shanin Lake area of the Endicott Mountains (Bowsher and Dutro, 1957). The section is predominantly composed of black shale with a quartzarenite or sublitharenite sandstone member at the base and a red-weathering carbonate mudstone and wackestone member at the top. Similar strata are exposed throughout parts of the NE Brooks Range. Brosgé et al. (1962) noted that structural complications restricted direct correlation to the type section at Shanin Lake, and they elected to use the name Kayak(?) Shale instead. Microfossil evidence indicates that the Kayak Shale, at its type section near Shanin Lake, is late Tournaisian in age (Armstrong et al., 1970). In the NE Brooks Range, however, the oldest limestone intervals in the upper part of the Kayak Shale(?) contain foraminifera that are late Viséan in age (Mamet and Armstrong, 1972; Armstrong and Mamet, 1977), whereas the Kayak Shale(?) intervals in the subsurface at Prudhoe Bay contain fauna as young as middle Serpukhovian age (Armstrong and Mamet, 1974). Nevertheless, the boundaries of the Kayak Shale are defined by lithostratigraphic changes described at Shanin Lake and the NE Brooks Range. We apply the name Kayak Shale to all the rocks positioned above the uppermost coal section of the Kekiktuk Conglomerate and below the black nodular and bedded chert and carbonate mudstone intervals of the lower Alpha Limestone.

Because of the intense deformation across the Kayak Shale interval, its stratigraphic thickness is hard to constrain. At its type section in the Shanin Lake area, the Kayak Shale is ~300 m thick (Bowsher and Dutro, 1957). In the NE Brooks Range, the Kayak Shale ranges

from <50 m to ~450 m thick (Brosgé et al., 1962; Mamet and Armstrong, 1972; Anderson, 1995), and is ~300 m in the subsurface at Prudhoe Bay (Armstrong and Mamet., 1974). At several locations within the NE Brooks Range, the Kayak Shale interval thins to <10 m or is completely absent. For example, on the southeast side of the Jago Stock (Plate 2), the Kayak Shale is only a few meters thick and is exposed as talus slope that separates limestone units of the Lisburne Group from the Kekiktuk Conglomerate. Along strike, the Kayak Shale pinches out, and the Lisburne Group rest directly on the Kekiktuk Conglomerate. In several other locations, the Kekiktuk Conglomerate is the only unit of the Endicott Group exposed. Some authors attribute these thickness variations to local basement highs that persisted throughout Early and Middle Mississippian time (e.g., Armstrong et al., 1974, LePlain et al., 1994). For the structural cross sections presented in this study (Plates 1 and 2) we use a uniform thickness of 200 m for the Kayak Shale in most parts of our field area. In the headwaters of the Kongakut River, however, Anderson (1993; 1995) prescribed a thickness of ~400 m for the Kayak Shale, which we apply to our cross sections in that specific area (Plate 2).

Mkt – Kekiktuk Conglomerate (Lower Mississippian)

The Kekiktuk Conglomerate defines the lower half of the Endicott Group (Tailleur et al., 1967). The formation was named by Brosgé et al. (1962) for the stream that drains Lake Peters in the Mount Michelson quadrangle (Fig. 4.1), and the type section was described at Whistler Creek (also near Lake Peters). The Kekikituk Conglomerate is found throughout many parts of the NE Brooks Range, as it typically forms ledges and ridges due to its strong resistance to weathering. It is an important marker bed because its base defines a prominent angular unconformity that truncates a highly deformed succession of Neoproterozoic to Devonian strata, what is often called the “pre-Mississippian sequence” (e.g., Moore et al., 1994) or the Franklinian sequence

(Lerand, 1973). Strauss et al. (2018a) revised much of the sub-Mississippian nomenclature (see below for further details).

At its type section, the Kekiktuk Conglomerate is consist of light- to dark-gray, conglomerate and coarse-grained sandstone that contains subangular to well-rounded sand grains, pebbles and cobbles of detrital chert fragments, quartz grains, and minor amounts of lithic fragments, such as polycrystalline quartz and siltstone. In the thicker sections of the Kekiktuk Conglomerate the sandstone and conglomerate intervals grade into dark-gray shale and siltstone that commonly contain wood fragments, thin (>0.5 m) coal seams and carbonate mudstone beds that have well-preserved bivalves. The age of the Kekiktuk Conglomerate is constrained only by the rare plant fossils found in sections that contain the coal seams, which assign the upper portions of the Kekiktuk Conglomerate to the Lower Mississippian (Dutro, 1987). In the headwaters of the Kongakut River, the basal unconformity of the Kekiktuk Conglomerate truncates Middle Devonian–Lower Mississippian strata of the Mangaqtaaq and Ulungarat formations (Fig. 4.3D; Anderson and Watt, 1992; Anderson et al., 1994; Anderson, 1995), further supporting the Lower Mississippian assignment of the Kekiktuk Conglomerate. The Kekiktuk intervals in the NE Brooks Range are time correlative, and in some cases, younger than the Kayak Shale intervals of the central Brooks Range (e.g., Dutro, 1987), exemplifying the time-transgress nature of these two units.

The Kekekiktuk Conglomerate is ~100 m thick at its type section (Brosgé et al., 1962), but its thickness varies across the field area, ranging from <10 m in some areas to ~180 m thick in the subsurface at Prudhoe Bay (Armstrong and Mamet, 1974). We use a uniform thickness of 100 m for the Kekiktuk Conglomerate in our cross sections (Plates 1 and 2). In most places throughout our field area, however, exposures of the Kekiktuk Conglomerate are <10 m thick.

Dmu – Mangaqtaaq and Ulungarat formations, undivided (Middle Devonian–Lower Mississippian(?))

The Mangaqtaaq and Ulungarat formations compose a southward thickening, siliciclastic-dominated, sedimentary wedge exposed in the headwater regions of the Kongakut, Sheenjek, and Chandalar rivers. Originally, these sedimentary units were collectively assigned to the "unnamed slate and sandstone unit" by Brosgé et al. (1962) and then the "Devonian sandstone" (Ds) map unit of Reiser et al. (1980). Later, the work of Anderson and Watts (1992), Anderson et al., (1994), and Anderson (1995) named the two formations and described their type sections. Since the detailed work of Anderson, however, the Mangaqtaaq and Ulungarat formations have received very little study, and many of the map relationships and regional correlations remain uncertain.

The Ulungarat Formation is represented by a coarsening upward succession of siliciclastic strata, which Anderson (1995) divided into four members (A, B, C, and D). Red and brown shale and siltstone intervals are more prevalent in the lower members (A and B), and they typically grade into channelized sandstone and conglomerate beds (member C), which are defined by erosional bases and cross stratification. Fossils recovered from the mudstone intervals of members A and B include inarticulate brachiopods identified as *Bicarinatina* n. Sp., which assign the lower parts of the succession to the Eifelian Stage (lower Middle Devonian). At the top of the Ulungarat succession, in member D, the thick, cliff-forming conglomerate beds of member C are overlain by mottled, red shale and siltstone with sparse, laterally discontinuous sandstone lenses. The overlying Mangaqtaaq Formation appears to onlap and truncate the upper members of the Ulungarat Formation, although the contact is typically concealed by vegetation (e.g., Anderson and Watt, 1992; Anderson, 1995). The Mangaqtaaq Formation includes algal

limestone, sandstone, pebbly sandstone, and black shale. Contacts between these lithologies are typically sharp, reflecting the cyclic character of the Mangaqtaaq Formation. Plant fossils were recovered from the black mudstone intervals at the base of the Mangaqtaaq type section (Anderson and Watt, 1992; Anderson, 1995). The fossils suggest a Lower Devonian–Lower Mississippian assignment.

From the measured sections described by Anderson (1995), the collective thickness of the Mangaqtaaq and Ulungarat formations ranges from ~100 to >400 m. In our cross section of the Jago–Aichilik map area (Plate 2), we draw the Ulungarat section as a southward-thickening wedge that reaches a thickness of ~400 m, although Brookian deformation has duplicated much of the section. Many of the map relationships in the southeastern quarter of the Jago–Aichilik map area were taken from the map of Anderson (1993). We also heavily relied on the satellite imagery, using the red and brown color as a marker for the distribution of the Ulungarat–Mangaqtaaq units and the gray and tan resistive unit as a marker for the Kekiktuk Conglomerate. In general, we drew thrust faults where the red and brown Ulungarat units overlie the younger tan Kekiktuk units. These relationships, however, are conjectural, as our traverse to the upper Kongakut River in 2014 revealed that distinguishing between the conglomerate beds of the upper Ulungarat Formation and the Kekiktuk Conglomerate is difficult.

DOcr – Clarence River Group, undivided (Upper Ordovician–Lower Devonian(?))

The Clarence River Group was defined by Johnson et al. (2016) using detrital zircon U-Pb and muscovite $^{40}Ar/^{39}Ar$ geochronology coupled with field evidence from the British and Romanzof mountains in Alaska. The group encompasses a succession of Ordovician–Lower Devonian(?), mostly fine-grained siliciclastic strata. No type section exists for the Clarence River Group, but its name is derived from the Clarence River region, near the Alaska–Yukon border in

the northern British Mountains (Fig. 4.2). The area was mapped in detail during a joint effort between the United States Geological Survey and the Geological Survey of Canada (Kelley et al., 1994; Lane et al., 1995). From that work, several fossil collections recovered graptolites that were assigned to the Upper Ordovician and the Lower Silurian, along with a single conodont that indicated a latest Silurian or earliest Devonian age. Johnson et al. (2016) showed overlap between the fossil ages from Clarence River region and the Ordovician–Early Devonian(?) detrital mineral ages recovered from strata as far south as the upper Aichilik River (~100 km to the southwest).

In the revised stratigraphic scheme of Strauss et al. (2018a), the Clarence River Group is partitioned into two lithostratigraphic units: the Aichilik and Buckland Hills formations (Fig. 4.2). These units have not been formalized because structural complexities generally preclude the measurement of detailed type sections, and the only place where we have definitively observed the contact between the two units is in the headwaters of the Aichilik and Jago River drainages, where brownish olive slaty phyllite and micaceous siltstone intervals of Aichilik formation grade into black to dark grey fine-grained slate, phyllite, and minor thin-bedded sandstone of the Buckland Hills formation. In the lower reaches of the Kongakut River (Plate 1), we have opted to simply map these units as "Clarence River Group, undivided" because of poor exposure and due to the limited time we spent in that area.

Dbh – Buckland Hills formation (Lower Devonian(?))

The name Buckland Hills formation derives from the work of Lane (2007) and Lane et al. (2016), who described a succession of dark grey siltstone and sandstone, locally interbedded with chert pebble conglomerate in the Buckland Hills of the Herschel Island 1:250,000 quadrangle of northern Yukon (Fig. 4.1). The expanded definition of Johnson et al. (2016) and

Strauss et al. (2018a) encompasses Reiser et al.'s (1980) "Cambrian phyllite" (Ꞓp) and "Cambrian sandstone" (Ꞓs) map units in the Romanzof and southern British Mountains and their "Ordovician black slate" (Os) and portions of the undifferentiated "phyllite" (ph) and "slate, argillite, quartzite, and chert" (sc) map units in the northern British Mountains of Alaska. Lane and Cecile (1989), Kelley et al. (1994), Lane et al. (1995, 2016), and Lane (2007) also singled out these strata from the older Firth River Group and Neruokpuk and Leffingwell formations in the northern British Mountains and mapped them as "Silurian argillite" (Sa), "Devonian(?) argillite and subordinate sandstone" (D?a), and "Paleozoic argillite" (Pza) map units, which they correlated with similar strata in the Barn Mountains (Fig. 4.1).

Fine-grained strata within the Buckland Hills formation are mainly composed of black to light green slate and phyllite with discrete zones of micaceous siltstone, all of which commonly contain a prominent penetrative cleavage that destroys primary sedimentary structures. In some local cases, however, the fine-grained intervals are less deformed and preserve trace fossils and/or poorly preserved graptolites, including a handful of Late Ordovician to late Silurian collections (Dutro et al., 1972; Reiser et al., 1980; Lane and Cecile, 1989; Kelley et al., 1994; Lane et al., 1995). Occasionally, these fine-grained intervals are disrupted by cm- to m-scale olistoliths or olistostromes, which are most commonly composed of subrounded boulders of orange- to white-weathering limestone and dolostone with poorly preserved internal textures (Johnson et al., 2018; Strauss et al., 2018a). Some of these carbonate olistoliths have a distinct mafic volcaniclastic matrix and contain unidentifiable trilobite and brachiopod fossil fragments, all of which resemble similar lithofacies to what is reported in the upper Cambrian Egaksrak formation of the Whale Mountain allochthon (Johnson et al., 2018).

Sandstone horizons in the Buckland Hills formation consist of thin- to medium-bedded, poorly to moderately sorted, lithic arenite and sublitharenite. These strata occasionally have a distinct orange-weathering hue and locally preserve abundant complex trace fossils (e.g., Lane et al., 1995), various sole marks, soft-sediment deformation structures, and distinct normal grading with several of the classic Bouma subdivisions. In thin section, sandstone horizons from the Buckland Hills formation contain angular to subrounded mono- and polycrystalline quartz, chert, plagioclase, various accessory minerals, and a wide variety of volcanic and sedimentary lithic fragments (Strauss et al., 2018a). Conglomerate horizons in the Buckland Hills formation are generally clast-supported, moderately to well sorted, medium- to thick-bedded, and composed of angular to subangular chert, plagioclase, monocrystalline quartz, and volcanic/plutonic lithic fragments.

The Buckland Hills formation either sits gradationally on strata of the Aichilik formation or rests disconformably on a variety of older strata (Reiser et al., 1980; Mull and Anderson, 1991; Kelley et al., 1994; Lane et al., 1995, 2016). Its upper boundary in the southern British Mountains and Romanzof Mountains is consistently marked by a major fault contact with overlying rocks of the Whale Mountain allochthon (Plates 1 and 2; Johnson et al., 2016, 2018). Where exposed, this contact is either marked by a sharp boundary with the overlying Whale Mountain volcanic rocks or it is represented by a discontinuous mélange, where cm- to decameter-scale blocks of Whale Mountain, Clarence River, and/or Neruokpuk lithologies are suspended in a black to dark gray shale matrix. Although poorly exposed, this mélange is potentially >100 m thick near Dutro et al.'s (1972) trilobite fossil locality along the Leffingwell Fork of the Aichilik River (Fig. 4.1), where >50 m thick blocks of fossiliferous and volcaniclastic limestone and minor mafic volcanic rocks are floating within a diffuse zone of

highly deformed black shale, slate, and phyllite. Like many of the other sub-Mississippian units in the area, the Buckland Hills formation is typically deformed into tight or isoclinal folds (Fig. 4.4) and imbricated by many unmapped faults. Therefore, its thickness is poorly constrained and roughly ranges from 300 to 1300 m thick. In our cross sections (Plates 1 and 2), the thickness of the Buckland Hill formation varies due to truncation by major thrust faults or the sub-Mississippian unconformity, but in some places, it is nearly 1000 m thick.

SOa – Aichilik formation (Upper Ordovician–Upper Silurian)

The informal Aichilik formation is named after the Aichilik River, which runs through the central part of the Demarcation Point 1:250,000 quadrangle in Alaska (Fig. 4.1). The name was originally proposed by Mull and Anderson (1991) and encompassed Reiser et al.'s (1980) "Cambrian calcareous siltstone and sandstone" (Css) map unit. The Cambrian age assignment, however, came from a single locality of poorly preserved echinoderm debris (Reiser et al., 1980) and its presumed stratigraphic position beneath the upper Cambrian Whale Mountain volcanic rocks (Dutro et al., 1972). Johnson et al. (2016) subsequently included these strata within the younger Clarence River Group because they appeared lithologically more akin to synorogenic deposits of the Buckland Hills succession. Strauss et al. (2018a) confirmed this correlation with Ordovician–Late Silurian detrital zircon U-Pb and muscovite $^{40}Ar/^{39}Ar$ ages.

Fine-grained strata within the Aichilik formation are mainly composed of brownish olive slaty phyllite and micaceous siltstone, which commonly contain a prominent penetrative cleavage that destroys the primary sedimentary fabrics. Sandstone horizons in the Aichilik formation are commonly thin- to medium-bedded, moderate to poorly sorted, and consist of micaceous and calcareous quartz and lithic wacke, lithic arenite, and sublitharenite. Locally, these strata preserve flute and other sole marks and display distinct normal grading with various

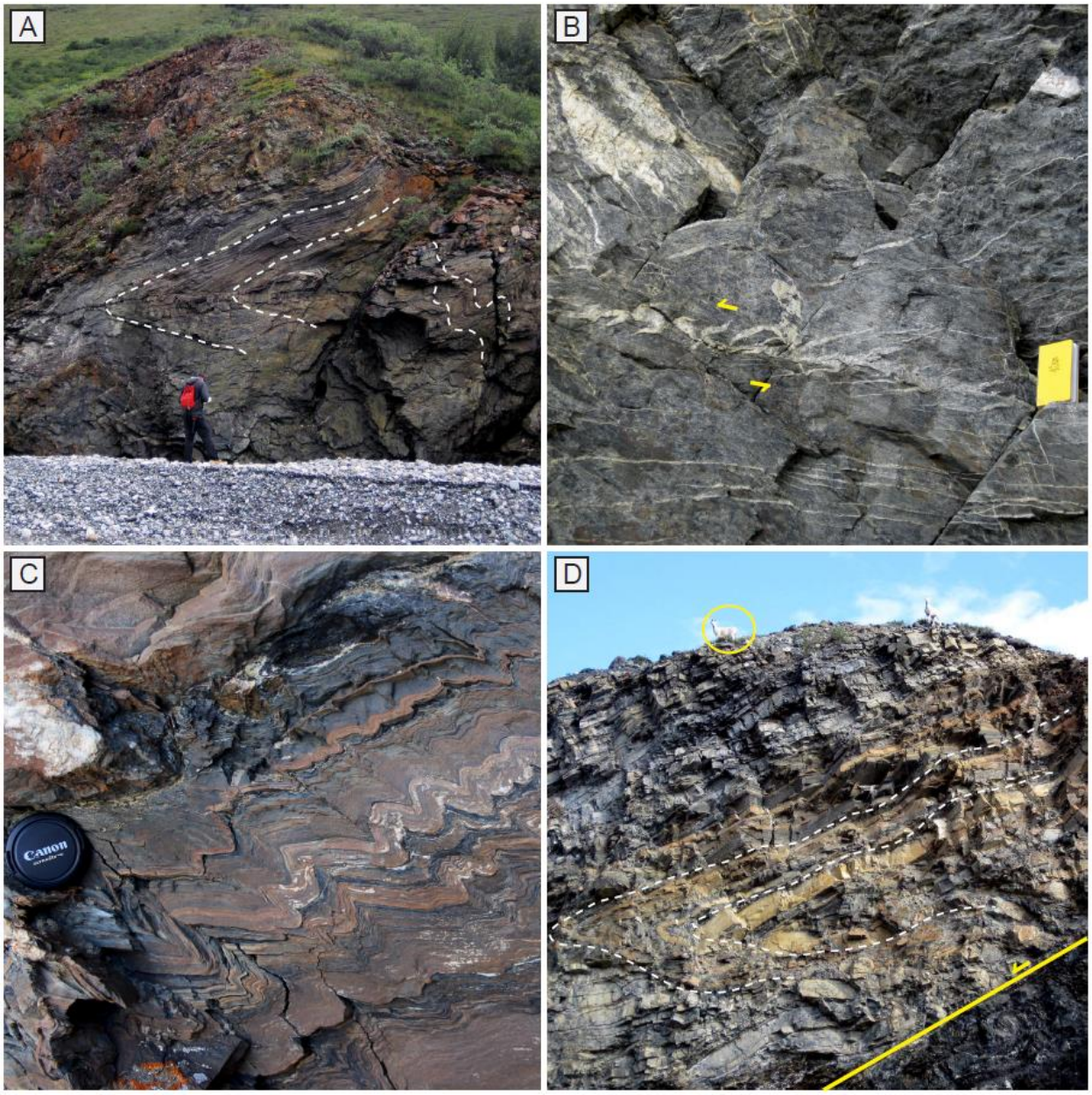

Figure 4.4 Selected field images of sub-Mississippian rocks in the northeastern Brooks Range, Alaska. (A) Looking east along the Kongakut River at sub-horizontal, tight to isoclinal, south-verging, class II folds in the Clarence River Group. (B) Looking west along the Kongakut River at sigmoidal veins in the Neruokpuk Formation, showing top-to-the-south shear. (C) Looking west in the upper Jago River, showing tight, north-verging, buckle (class I) folds in the Clarence River Group. (C) Looking northeast along the Kongakut River at sub-horizontal, south-verging, class II folds in Firth River Group strata; Dahl sheep (circled in yellow) are approximately 1.5 m tall for scale.

Bouma cycles, including well-developed ripple cross-stratification in Bouma C subdivisions, which in some outcrops are deformed into convolute bedding. Although primary sedimentary fabrics in this unit are commonly destroyed by penetrative cleavages and isoclinal folding, these strata do occasionally preserve indeterminate trace fossils, including *Nereites* and *Paleodictyon(?)*. In thin section, sandstone horizons from the Aichilik formation contain subangular to subrounded mono- and poly-crystalline quartz, plagioclase, muscovite, various unidentified opaques, and a wide variety of metamorphic, volcanic, and sedimentary lithic fragments. In particular, these strata contain abundant carbonate lithic fragments, most of which are highly recrystallized and therefore do not preserve primary microfacies (Strauss et al., 2018a). The matrix of the lithic wacke horizons consists of abundant sericite, carbonate, and clay mineral masses that may result from the breakdown of feldspar.

Similar to the Buckland Hills formation, the thickness of the Aichilik formation is uncertain. Its distribution and the reports on the thickness of this unit (e.g., Dutro et al., 1972; Reiser et al., 1980; Mull and Anderson, 1991) suggests that it ranges from ~300–1500(?) m. It is, however, repeatedly imbricated or tightly folded with the underlying Leffingwell formation in both of our map areas (Plates 1 and 2) and is characterized by significant internal deformation, thus the thickness estimates are likely overestimated due to structural thickening. Based on regional observations in the type area, Strauss et al. (2018a) estimated a thickness of ~600 m, which we have applied to our cross sections in Plates 1 and 2.

O€l – Leffingwell formation (Cambrian(?)–Middle Ordovician)

The informal Leffingwell formation was defined by Strauss et al., (2018a) as a <100 m thick package of maroon, purple, and green phyllite and slate interbedded with black, dark grey, and “bottle green” thin-bedded radiolarian chert that sits disconformably(?) between the lower-

middle Cambrian Neruokpuk Formation and the Upper Ordovician–Lower Devonian(?) Clarence River Group (Figs. 4.2). It is named after the Leffingwell Fork of the Aichilik River in the Demarcation Point 1:250,000 quadrangle of Alaska (Fig. 4.1), where the Leffingwell formation is well exposed in multiple imbricate thrust panels and folds with the Neruokpuk Formation and the Aichilik formation of the Clarence River Group.

Johnson et al. (2016) originally suggested that this chert-bearing interval marked the base of the Clarence River Group, and that it encompassed Reiser et al.'s (1980) Cambrian "chert and phyllite" (Ꞓcp) map unit. In the revised stratigraphic scheme of Strauss et al. (2018a), however, the Leffingwell formation was segregated from the Clarence River Group and assigned to an independent formation. Our maps also consider the Leffingwell formation separate from the Clarence River Group.

In the Firth River area of Yukon (Fig. 4.2), Lane and Cecile (1989) mapped an equivalent Ordovician "argillite and chert" unit (Oac or Oca), whose age designation came from a single Early Ordovician graptolite collection and by correlation with Lower Ordovician graptolitic strata of the Barn Mountains (Cecile, 1988). Strauss et al. (2018a) suggested that the chert-bearing strata in the Firth River area are correlative with the Leffingwell formation in Alaska. Direct stratigraphic correlations with the Barn Mountains strata, however, remain uncertain due to potential lithological and geochronological differences (McClelland et al., 2015; Colpron et al., 2018). In the Clarence River area of the northern British Mountains, Reiser et al. (1980), Kelley et al. (1994), and Lane et al. (1995, 2016) also mapped an Ordovician chert-bearing succession.

Stratigraphic relationships in the northern British Mountains are still unclear. The area is structurally complex, and exposure is generally poor. The work of Johnson et al. (2016; 2018),

Nelson et al. (2018), and Strauss et al. (2018a) suggests there are at least two distinct chert-bearing successions of somewhat similar lithological composition, one of which is most likely associated with fault-bounded rocks of the Whale Mountain allochthon and referred to as the informal Ekaluakat formation (see below) and the other of which occupies a similar stratigraphic position to the Leffingwell formation (Fig. 4.2). From our reconnaissance mapping along the northern reaches of the Kongakut River in 2012 (Plate 1), we could not definitively distinguish these two chert-bearing successions in the area, and, therefore, we place many of the units in the area under the umbrella of the Ekaluakat formation. Future mapping efforts in the area are needed to confirm correlations with the map units exposed along the Clarence River.

Ꞓn – Neruokpuk Formation (lower–middle Cambrian)

The Neruokpuk Formation gets its name from the "Neruokpuk Schist" of Leffingwell (1919), who described a thick succession dark-greenish gray to blueish gray quartzite and "semischist" in the Lake Peters area of the Mt. Michaelson 1:250,000 quadrangle (Fig. 4.1). Following this early work, the Neruokpuk Schist was renamed the Neruokpuk Formation (*sensu lato)*, and its definition was expanded to include nearly all the map units that resided below the sub-Mississippian unconformity (e.g., Brosgé et al., 1962; Reed et al., 1968; Dutro et al., 1972; Norris, 1985). The work of Reiser et al. (1980) in Alaska and Lane (1991) in Yukon, however, applied a more restricted definition to the Neruokpuk Formation (*sensu stricto),* which was akin to the original definition of Leffingwell (1919). Strauss et al. (2013; 2018a), along with other recent authors (e.g., Johnson et al., 2016; Lane et al., 2016), also applied the restricted definition of Neruokpuk Formation, and it is now defined as the thick succession of dark-greenish gray to brownish-black interbedded sandstone, siltstone, phyllite, slate, and semischist. These strata are

exposed in multiple east–west-trending antiformal and synformal belts throughout the Franklin, Romanzof, and British mountains (Fig. 4.1; Plates 1 and 2).

Thickness estimates for the Nerukpuk Formation range from >5 km (e.g., Leffingwell, 1919, Dutro et al., 1972; Norris, 1985) to <2500 m (Reiser et al., 1980; Johnson et al., 2016; Lane et al., 2016; Strauss et al., 2018a). Although true thickness differences certainly exist in different outcrop belts of the Neruokpuk Formation, these strata are commonly structurally thickened throughout the NE Brooks Range. Southern exposures of the Neruokpuk Formation (i.e., within the Franklin and southern British and Romanzof mountains) are commonly composed of interbedded thin- to very thick-bedded massive quartz arenite, wacke, and "semischist" with subordinate granule conglomerate and micaceous brown, maroon, and light-green phyllite, slate, and argillite. In thin section, the sandstone horizons are fine- to very coarse-grained, moderate to poorly sorted, and contain mono- and poly-crystalline quartz, potassium feldspar, and white mica with a wide variety of other accessory grains (Strauss et al., 2018a). The metamorphic grade appears to increase southward, as the Neruokpuk Formation becomes increasingly schistose in the Romanzof and Franklin mountains (e.g., Leffingwell, 1919; Reed, 1968; Sable, 1977).

In the northern part of the field area, in the northernmost British Mountains, the Neruokpuk Formation becomes thinner, and its character becomes difficult to distinguish from the underlying Fish Creek formation of the Firth River Group due to intense imbrication and similar lithofacies. The occurrence of *Oldhamia*-bearing maroon, green, and purple argillite/slate intervals also becomes more frequent (Lane, 1991; Lane et al., 1995; 2016; Strauss et al., 2018a). The *Oldhamia* trace fossils suggest that the Neruokpuk Formation is early to middle Cambrian in age (Herbosch and Verniers, 2011; MacNaughton et al., 2016). Oldhamia is also present in the

lithofacies that resemble the southern exposures of the Neruokpuk Formation (Strauss et al., 2018a), suggesting that the two facies belts can be correlated in terms of chronostratigraphy. Neruokpuk-equivalent units are also found as far south as the Barn Mountains in Yukon (Fig. 4.1; McClelland et al., 2015). Maximum depositional ages for sandstone intervals of the Neruokpuk Formation, constrained by detrital zircon U-Pb geochronology, range from ca. 600–800 Ma.

In our maps (Plates 1 and 2), we do not separate the southern and northern lithofacies of the Neruokpuk Formation. We apply a stratigraphic thickness of 1,800 m in our cross sections. This was taking from the measured sections provided by Sable (1977), who described the Neruokpuk Formation along the Jago River (Fig. 4.1). This thickness was confirmed during our investigation of the region in the summer of 2014.

€Zfr – Firth River Group, undivided (Cryogenian–Cambrian)

The Firth River Group was informally defined by Lane et al. (2016) as succession of Neoproterozoic to middle(?) Cambrian siliciclastic and carbonate strata that stratigraphically underlie the Neruokpuk Formation. Its name is derived from the Firth River, which cuts across much of the northern British Mountains in Yukon, where the strata are prominently exposed. In Alaska, these strata were previously referred to as "Sequences D and E" of Dutro et al. (1972), "Domain III" of Mull and Anderson (1991), and more than ten distinct pre-Cambrian carbonate-bearing map units of Reiser et al. (1980). The group was formalized by Strauss et al. (2018a) and organized into three informal formations, including the Fish Creek, Malcom River, and Redwacke Creek formations. Strauss et al. (2018a) also used C and Sr isotopic data to correlate the carbonate rocks of the Firth River Group to those exposed in the Shublik and Sadlerochit mountains (Strauss et al., 2018b) and infer a Cryogenian (middle Neoproterozoic) age. The Firth

River Group remains undivided in the southern British and Romanzof mountains due structural complexity and limited exposure (Plates 1 and 2). Our maps do not delineate the individual formations, but each formation is described sepertally below.

Fish Creek formation (no map units)

The informal Fish Creek formation was named by Strauss et al. (2018a) after Fish Creek, a tributary of the Malcolm River in the southern Demarcation Point 1:250,000 quadrangle of Yukon (Fig. 4.1). In this area, and throughout other parts of the northern British Mountains of Yukon and Alaska, these strata are well exposed along several tributaries and consists of a lithologically complex succession of calcareous slate, phyllite, and shale, with minor dolomitic sandstone and thin, fine-grained quartzite beds. In Alaska, Reiser et al. (1980) split these strata into individual "Precambrian" map units, including the "phyllite and quartzite of Old Grungy Mountain" (p€pq), "sandstone and dolomite" (p€sd), "brown-weathering limestone and shale" (p€lb), "grey and black slaty shale" (p€s), "limestone and calcareous sandstone" (p€ls), "argillite and limestone" (p€al or p€as), and "phyllite and argillite" (p€pa). The mapping in the Clarence River area by Kelley et al. (1994) and Lane et al. (1995) included these strata in their "Proterozoic or Cambrian limestone" unit (P€l).

The complex stratigraphic and structural architecture of these strata inhibit accurate thickness estimates, and their relative stratigraphic position is difficult to determine. They are seperated from the underlying Malcolm River formation because fine-grained intervals of shale, argillite, phyllite, and slate are more abundant (Strauss et al., 2018a). Lane et al. (1995, 2016) postulated that these strata may simply be a basinal facies of the more coarse-grained Neruokpuk Formation in the southern part of the field area. Our observations, however, align with those of other mappers in Alaska (e.g., Dutro et al., 1972; Sable, 1977; Reiser et al., 1980; Hanks 1989;

1993; Strauss et al., 2018a), placing the Firth River Group strata directly beneath the Neruokpuk Formation in the southern British and Romanzof mountains and suggesting the calcareous shale and limestone units grade into the basal sandstone-dominated strata of the Neruokpuk Formation and should therefore remain an independent unit.

Malcolm River formation (no map units)

The informal Malcolm River formation was named by Strauss et al. (2018a) after the Malcolm River, whose headwaters are in the southern Demarcation Point 1:250,000 quadrangle of Yukon (Fig. 4.1). The Malcolm River formation is widely exposed throughout the northern British Mountains and encompasses Reiser et al.'s (1980) Precambrian limestone-dominated map units (p€l, p€lr, and ls) in the Demarcation Point quadrangle of Alaska and Lane et al.'s (1995) "Proterozoic or Cambrian limestone" map unit (P€l) in adjacent Yukon. In district locations of the southern British and Romanzof Mountains, intensely deformed exposures of the Malcolm River formation are also present beneath the Neruokpuk Formation in the cores of a Brookian antiforms, specifically along a narrow stretch of the Kongakut River (Plate 1) and in the the headwaters of the Jago River (Plate 2), although we mapped these exposure as "Firth River Group undivided" because they were not examined in detail.

In its type area, the Malcom River formation is ~15 to 100 m thick and consists almost exclusively of medium- to thick-bedded, light grey to reddish black interbedded carbonate mudstone, packstone, wackestone, and rudstone with minor intervals of dolomitic wackestone and dark grey slate or phyllite. The Malcolm River formation is distinguished from the overlying Fish Creek formation by its typical gritty texture caused by the mixture of detrital quartz grains and carbonate material. Although many stratigraphic intervals of the Malcolm River formation are massive and/or partially recrystallized into coarse-grained spar, these strata locally display

normal grading, trough cross-stratification, cut/fill geometries with scour surfaces, and a wide variety of Bouma turbidite subdivisions, which suggest deposition in a deep-marine setting by carbonate-dominated gravity flows.

Redwacke Creek formation (no map units)

The informal Redwacke Creek formation is named after Redwacke Creek, a tributary of the Egaksrak River (Fig. 4.1), in the northwestern British Mountains of the Demarcation Point 1:250,000 quadrangle in Alaska and is equivalent to the Precambrian "volcaniclastic rocks of Redwacke Creek" (p€v) unit of Reiser et al. (1980). These strata are only exposed near the Redwacke Creek and have not been mapped in any other part of the field area. We examined outcrops of the Redwacke Creek formation ~5 km east of the Aichilik River during our traverse down the Leffingwell Fork in 2013, as did J.V. Strauss in 2011 during the Elkaluakat River traverse. Based on regional mapping relationships (Reiser et al., 1980; Hanks, 1989; 1993), Strauss et al. (2018a) proposed that the Redwacke Creek formation is the stratigraphically lowest unit in field area; however, the field relationships in the area are poorly constrained, and the Redwacke Creek could represent a lateral facies change or could be bounded by unmapped faults.

The base of the Redwacke Creek formation is not exposed and the overlying contact with the Malcolm River formation is covered by talus. The strata consist of interbedded rusty weathering, dark green medium- to thick-bedded volcaniclastic lithic arenite and wacke, pebble to cobble conglomerate, and minor dark green slate. A distinctive feature of the Redwacke Creek formation are the volcaniclastic sandstone and conglomerate intervals that weather rusty-brown. In thin section, these strata consist of an altered volcanogenic matrix of clay minerals with medium to coarse-grained and subrounded to subangular plagioclase, amphibole, clinopyroxene,

and monocrystalline and polycrystalline quartz (Strauss et al., 2018a). The overall thickness of the Redwacke Creek formation is unknown, but the main exposures in the northern British Mountains of Alaska range from ~50 to 200 m thick.

Whale Mountain Allochthon (lower Cambrian–Upper Ordovician)

The Whale Mountain allochthon is a fault-bounded, structural complex of lower Cambrian–Upper Ordovician mafic volcanic and marine sedimentary rocks (Johnson et al., 2016; 2018). Dutro et al. (1972) originally assigned many of these rocks to "sequences A, C, and E" of the expanded Neruokpuk Formation *(sensu lato*), which contained several members, including the "volcanic and carbonate" and "chert and phyllite" members. These three sequences, however, also included several other members that are now assigned to separate lithostratigraphic units, including the Clarence River Group, the redefined Neruokpuk Formation (*sensu stricto*), and parts of the Firth River Group (e.g., Johnson et al., 2016; Strauss et al., 2018a). In the stratigraphic scheme of Dutro et al. (1972), nearly all of the members in the NE Brooks Range were assigned to the Cambrian, largely because of two separate trilobite collections from the "volcanic and carbonate member" of "sequences A and C." Included in these collections, was an early Cambrian trilobite genus, *Ollenius*, which was recovered from carbonate rocks exposed along the Marsh Fork of the Canning River in the southeastern corner of the Mt. Michelson 1:250,000 quadrangle (Fig. 4.1) The second trilobite collection included a late Cambrian *Saratogia* genus, which was recovered from lithologically similar carbonate rocks exposed along a ridge between the Leffingwell Fork of the Aichilik River and the Egakserak River in the central part of the Demarcation Point 1:250,000 quadrangle in Alaska (see Johnson et al., 2018 and references therein for review).

Johnson et al. (2016) reported Ordovician–Early Devonian(?) detrital zircon U-Pb ages from strata below the volcanic and carbonate rocks exposed along the Kongakut River, in what are now assigned to the Buckland Hills formation of the Clarence River Group (Strauss et al., 2018a). With the upper Cambrian carbonate and volcanic rocks sitting on Ordovician–Early Devonian(?) strata, Johnson et al. (2016) contended that a major thrust fault separates the two lithostratigraphic domains. A similar relationship exists in the Romanzof Mountains (e.g., Dutro et al., 1972; Johnson et al., 2018; Strauss et al., 2018a). Although the age of the fault is unknown, Johnson et al. (2016; 2018) speculated that the emplacement of the Whale Mountain allochthon is linked to early Paleozoic tectonic events associated with the assembly of the North Slope subterrane of Moore et al. (1994). Rocks composing the Whale Mountain allochthon are defined by the five lithostratigraphic units (Fig. 4.2), but because structural complexities generally preclude the measurement of detailed type sections, the units have not been formalized.

Cmv – Marsh Fork Volcanic Rocks (lower–upper Cambrian)

The Marsh Fork volcanic rocks were originally defined as part of the "volcanic and carbonate member" of "sequence A" in the stratigraphic scheme of Dutro et al. (1972). The unit was later split into the "Cambrian volcanic and volcaniclastic rocks" (Cv) and the "Cambrian limestone" (Cl) of Reiser et al. (1980). In a geochemical and petrographic assessment of the volcanic rocks, Moore (1987) applied the Marsh Fork name to a series of basaltic flows that are prominently exposed along the Marsh Fork of the Canning River drainage (Fig. 4.1). The age of the flows was assigned to the lower Cambrian by the *Ollenius* trilobites collected by Dutro et al. (1972) from carbonate strata that are interlayered with the volcanic rocks. Johnson et al. (2018) used similar geochemical and petrographic techniques to correlate the Marsh Fork volcanic rocks

across the Romanzof Mountains to the headwaters of the Jago and Aichilik rivers, located in the southwestern corner of the Demarcation Point 1:250,000 quadrangle in Alaska (Fig. 4.1).

Along the Jago and Aichilik rivers, the volcanic rocks occur along an ~300 to 800 m thick exposure of greenish-gray, mafic amygdaloidal volcanic flows and subordinate beds of conglomerate, volcaniclastic argillite, and chert. The basalt flows are typically massive or pillowed and individually range from 1 to 10 m thick. The geochemical and petrographic data from Moore (1987) and Johnson et al. (2018) indicate that the Marsh Fork volcanic rocks have a tholeiitic composition and suggest that they may have erupted in a mid-ocean ridge setting.

Cmv – Whale Mountain Volcanic Rocks (lower–upper Cambrian)

The Whale Mountain volcanic rocks were also originally defined as part of the "volcanic and carbonate member" in the stratigraphic scheme of Dutro et al. (1972), but they formed the upper part of their "sequence C". Moore (1987) differentiated these volcanic rocks from those exposed along the Marsh Fork because of potential differences in age and because of the differences in their geochemical and petrographic character. The name comes from Whale Mountain, a prominent, east–west trending ridge that crosses the middle reaches of the Kongakut River in the Demarcation Point 1:250,000 quadrangle in Alaska (Fig. 4.1). The ridge crosses from the Alaska–Yukon boundary to the Leffingwell Fork of the Aichilik River. The age of the volcanic rocks was originally constrained by a single trilobite assigned to the genus *Saratogia*, which was recovered by Dutro et al. (1972) from a massive block of carbonate rock exposed at the base of large series of volcanic flows at the western limit of the Whale Mountain ridge, in the area between the Leffingwell Fork and the Egaksrak River (Fig. 4.1).

Like the Marsh Fork volcanic rocks, the Whale Mountain volcanic rocks are typically exposed as massive and pillowed flows of dark-greenish gray basalt that weather olive green and

are interbedded or interlayered with a variety of volcanic-rich conglomerate, argillite, and other volcaniclastic rocks. Their petrologic and geochemical characteristics, however, are significantly different from the Marsh Fork volcanic rocks. They are typically porphyritic, containing phenocrysts of olivine, clinopyroxene, and plagioclase (Johnson et al., 2018). Geochemically, the Whale Mountain volcanic rocks are enriched in the incompatible elements, including Ti, Nb, Nd, and Zr (Moore, 1987; Goodfellow et al., 1995; Johnson et al., 2018). The geochemical and petrological data suggests that the Whale Mountain volcanic rocks have a composition resembling alkaline basalt that potentially erupted in an ocean island setting (Johnson et al., 2018).

The overall thickness of the volcanic rocks is uncertain. Structural complications and the absence of clear marker beds preclude direct stratigraphic measurements. The same is true for the Marsh Fork volcanic rocks in the Romanzof Mountains. Along the central portion of Whale Mountain ridge, between the Kongakut and Egaksrak rivers, the volcanic rocks are between ~700 and 1000 m thick, as estimated from satellite imagery and field observations. These estimates, however, includes thickness additions from the intertongued Egaksrak formation and assumes that the section is not disrupted by unmapped faults.

Ce – Egaksrak Formation (lower–upper Cambrian)

The Egaksrak formation was defined by Johnson et al. (2018) to include the carbonate rocks that intertongue with the both the Marsh Fork and Whale Mountain volcanic rocks in the British and Romanzof Mountains. This designation replaced the “Cambrian limestone” (Cl) map unit of Reiser et al. (1980). The name was derived from the Egaksrak River in the Demarcation Point 1:250,000 quadrangle in Alaska (Fig. 4.1), which is near the site where Dutro et al. (1972) recovered the late Cambrian trilobites.

Exposures of the Egaksrak formation typically occur as 10 to 100 m thick megablocks or olistostromes entrained and deformed with the volcanic rocks. They also occur as discrete layers deposited between volcanic flows, which in some places are ~100 m thick and extend laterally for >10 km. The strata are highly variable, consisting of dark-gray- to tan-weathering, intensely sheared and contorted beds of rudstone, massive recrystallized pelloidal and oolitic grainstone and packstone, and finely laminated fossiliferous carbonate mudstone and wackestone. Many the rudstone intervals contain angular to well-rounded, pebble- to sand-sized volcanic lithoclasts. The occurrence of trilobite, agnostoid, and brachiopod fossils are typically found in the laminated, dark-brown and tan carbonate mudstone and wackestone intervals.

We visited the Leffingwell Fork fossil locality of Dutro et al. (1972) twice, once in the summer of 2013 and again in the summer of 2014. In the summer of 2014, we re-sampled the trilobite locality and confirmed the upper Cambrian (lower–middle Fuongian) assignment of the Egaksrak Formation with a collection that included a single agnostoid specimen and at least six individual trilobite specimens (Johnson et al., 2018). A separate collection was recovered in the summer of 2013 from similar exposures of the Egaksrak formation in the headwaters of the Malcolm River, along the Yukon portion of the Whale Mountain ridge. These fossils also confirmed an upper Cambrian assignment for the Egaksrak formation (Johnson et al., 2018). In the Marsh Fork area, Dutro et al. (1972) recovered a trilobite specimen that they identified as the genus *Ollenius*, indicating that parts of the Egaksrak formation may be assigned to the lower Cambrian. In the summer of 2014, we traversed across the major fault zone, in the headwaters of the Aichilik River, which separates the Whale Mountain allochthon from the underlying Clarence River group. In this location, we discovered a new trilobite locality. Although this locality is more-or-less along strike of Dutro et al.'s (1972) Marsh Fork lower Cambrian locality,

the recovered fossils at the upper Aichilik River locality more closely align with an upper Cambrian fauna recovered from the Egaksrak formation along the Whale Mountain ridge (Johnson et al., 2018). Johnson et al. (2018), thus suggested that the Egaksrak formation recorded early to late Cambrian carbonate deposition on a collection of volcanic islands that had formed outboard the ancient Laurentian margin.

O€r – Romanzof Formation (Cambrian(?)–Upper Ordovician)

The Romanzof formation was established in the work of Johnson et al. (2016; 2018) and Strauss et al. (2018a). It includes the "chert and phyllite" unit that was established in the mapping efforts of Brosgé et al. (1962), Dutro et al. (1972), and Reiser et al. (1980). Its name is derived from its widespread exposure across in the Romanzof Mountains, but also because Mull and Anderson (1991) applied the name "Romanzof chert" to the same succession of rocks. Johnson et al. (2016, 2018) and Strauss et al. (2018) updated the Romanzof chert to the Romanzof formation to include the "Cambrian–Ordovician volcanic wacke and tuffaceous sandstone" (O€w) map unit of Reiser et al. (1980), which appears sparsely interbedded or imbricated with chert and phyllite strata in the headwaters of the Jago and Aichilik rivers.

The Romanzof formation comprises a heterolithic succession of interbedded black, grey, white, and green thin-bedded radiolarian chert, dark-grey, green, and maroon phyllite and slate, and discrete intervals (<50 m thick) of channelized medium- to thick-bedded, dark-green to gray sandstone (Fig. 4.2). The sandstone intervals consist of poorly sorted, angular to subangular, fine- to very coarse-grained (and occasionally granular) massive lithic wacke. In thin section, these deposits are dominated by poorly sorted chert, volcanic lithic fragments, and rare mono- and poly-crystalline quartz set within an altered matrix of sericite, clay minerals, and calcite (Strauss et al., 2018a).

The Romanzof formation is frequently imbricated and deformed into upright isoclinal folds (e.g., Mull and Anderson, 1991). These structural complications preclude any reliable thickness estimates, but its extensive exposure throughout the southern Romanzof Mountains (Plate 2), suggests that it exceeds 500 m thick. The age of the Romanzof formation is constrained by a collection of Lower–Middle Ordovician biserial graptolites that Moore and Churkin (1984) recovered from the Canning River in the northwestern corner of the Arctic 1:250,000 quadrangle in Alaska (Fig. 4.1). Detrital zircon U-Pb ages from lithic wacke units of the Romanzof Formation, suggests a ca. 452 Ma (Late Ordovician) maximum depositional age (Strauss et al., 2018a).

O€e – Ekaluakat Formation (Cambrian(?)–Upper Ordovician)

The Ekaluakat formation was established in the work of Johnson et al. (2018) and Strauss et al. (2018a) to define a succession of mafic volcanic rocks, volcaniclastic breccia, tuff, chert, phyllite, and slate exposed in the northern British Mountains (Fig. 4.1). The Ekaluakat formation includes the "red and green phyllite" (ph), "Ordovician gray phyllite and chert" (Opc), "Ordovician volcaniclastic and volcanic rocks" (Ovc), and "Ordovician black slate" (Ovc) map units of Reiser et al. (1980). Many of these same map units were described in the Clarence River area along the Alaska–Yukon boundary by Kelly et al. (1994) and Lane et al., (1995). It is named for the Ekaluakat River in the central part of the Demarcation Point 1:250,000 quadrangle in Alaska, which J.V. Strauss visited in the summer of 2011. Rocks of the Ekaluakat formation are also well exposed along the northern bend of the Kongakut River (Plate 1), which we visited in the summer of 2012.

Johnson et al. (2018) and Strauss et al. (2018a) proposed a tentative correlation between the Ekaluakat and the Romanzof formations, suggesting that both formations represent deep-

marine sedimentary components in the upper parts of the Whale Mountain allochthon. However, some significant lithological differences exist between the two formations. For example, the Ekaluakat formation has a higher volcaniclastic component, including a distinctive, ~1 to 10 m thick unit of dark gray volcanic breccia with clasts consisting of both vesicular basalt and recycled sedimentary rocks. The geochemical character of these volcanic units is similar to the Whale Mountain volcanic rocks, although they are slightly more enriched in the incompatible elements (Johnson et al., 2018). Tuff is another common component of the Ekaluakat formation and forms it 10 cm to <1 cm thick horizons or lamination within a greater succession of red and green phyllite, argillite, and slate.

The age of the Ekaluakat formation is constrained by a single Late Ordovician graptolite collected from a succession of black slate that appears interbedded with the volcaniclastic and volcanic rocks along the Alaska–Yukon boundary (Reiser et al., 1980). As noted by Johnson et al. (2016; 2018), Strauss et al. (2018a), and Nelson et al. (2018), the stratigraphic assignment of this fossil locality is unclear, as the graptolite could have come from units now assigned to the Clarence River Group or the Leffingwell Formation. Because we have not spent much time in this area, and because of structural complications and poor exposure, our stratigraphic assignments remain poorly constrained. Johnson et al. (2016) reported 63 concordant detrital zircon U-Pb ages from a tuffaceous sandstone unit, containing a nearly unimodal age distribution centered at ca. 500 Ma, suggesting that the Ekaluakat formation was deposited no earlier than the late Cambrian and that some of the volcanic rocks are time correlative with the Whale Mountain and Marsh Fork volcanic rocks to the south.

LITHODEMIC UNITS

Dgr – Granitic Rocks (Upper Devonian)

In the central part of the field area, between the Jago and Hulahula rivers, the sedimentary rocks are crosscut by four individual intrusive bodies. The Okpilak Batholith is the largest intrusive body, covering an area of >400 km^2 and reaching surface elevations >3,000 m. South of the batholith, three smaller bodies or stocks are exposed along a north–south trend in the upper reaches of the Jago River (Plate 2). They are named the Jago, Romanzof, and Sheenjek stocks. The northern bodies were studied in detail by Sable (1977), whereas the southern bodies have not been closely studied. In fact, the southernmost intrusive body, the Sheenjek Stock, had not been discovered until we visited the area in the summer of 2015.

The northern most intrusive bodies, the Okpilak Batholith and the Jago Stock, consists of light- to medium gray, medium- to coarse-grained granite and quartz monazite, with a mineralogy of potassium feldspar, quartz, plagioclase feldspar, and biotite. In the southern intrusive bodies, the Romanzof and Sheenjek stocks, hornblende becomes abundant and potassium feldspar becomes sparse, shifting the rocks closer to diorite and tonalite compositions. The most reliable radiometric age from the intrusive rocks is the 381 ± 10 Ma, determined from the upper intercept on a U-Pb concordia plot of zircon grains collected from the Okpilak batholith and the Jago Stock (Dillon et al., 1987). Reiser et al. (1980) also reported a 432 ± 1 Ma K-Ar age from hornblende in the Romanzof Stock. Preliminary unpublished zircon U-Pb ages from rocks that we collected from the Romanzof and Jago stocks, however, align with the ca. 380 Ma U-Pb age from Dillion et al. (1987), as do the ca. 368–375 Ma zircon U-Pb ages from an intrusive suite in the Yukon portion of the NE Brooks Range (Ward et al., 2018), indicating that the K-Ar age of Reiser et al. (1980) is unreliable.

Dar – Alerted rocks (upper Devonian(?))

Contact metamorphism and alteration of the country rocks that surround the Devonian intrusive rocks were describe in detail by Sable (1977). In most places, especially at the northern and southern margins of the Okpilak Batholith, the contacts between the granitic rocks and the country rocks are concordant with the orientation of bedding planes of many of the lithostratigraphic units in the area, including the Clarence River Group, Neruokpuk Formation, Firth River Group, and units from the Whale Mountain allochthon. Along the southern margin of the Batholith, and along the southern margin of the Jago Stock (Plate 2), the contact with the Neruokpuk Formation and the Achilik formation coincides with a major thrust fault (Fig. 4.3E). In the map of Reiser et al. (1980), this fault is drawn as the westward continuation of the Whale Mountain thrust (see section of structural style below), which extends eastward into the Kongakut River area (Plate 1).

The granitic rocks do not exhibit definitive chilled margins, and contact metamorphism is rare, suggesting that the emplacement of the granitic rocks occurred at shallow depths and relatively dry conditions. Where contact metamorphism exists, it typically results in hornfels when intruding pelitic units and skarn when intruding impure carbonate units. In most places, however, the contact metamorphism projects no more than a 100 m into the surrounding country rocks. Along the northwest margin of the Jago Stock and southeast of the Okpilak Batholith, the Neruokpuk Formation is thermally metamorphosed into quartzite and banded gneiss that is repeatedly folded into m- to cm-scale isoclinal folds (Fig. 4.3). In other areas, Sable (1977) observed infiltration of granitic rocks into minute fractures that cross cut the country rocks, suggesting that the granitic rocks were emplaced by forceful injection.

The sub-Mississippian unconformity at the base of the Kekiktuk Conglomerate is well exposed in many areas surrounding the granitic rocks, especially on top of the Jago Stock, along the east wall of the Jago River (Fig. 4.3C). This contact is gradational or highly weathered, with fresh granite giving way to rocks with schistose a nd altered textures, and then conglomeratic rocks, which include abundant granitic rock clasts. This suggest that the granitic rocks were subaerially exposed at the time of Kekiktuk deposition (Early Mississippian), as the granitic rocks were reworked and deposited within the conglomerate.

STRUCTURAL STYLE

Brookian deformation (Mesozoic–Cenozoic)

Brookian deformation initiated during the Late Jurassic–Early Cretaceous (ca. 160–120 Ma), when the Koyukuk arc collided with the southern margin of the Arctic–Chukotka microplate (e.g., Mull, 1982; Mayfield et al., 1988; Moore et al., 1994; 2015). The collision resulted in high-grade metamorphism of Neoproterozoic–Devonian rocks in the southern Brooks Range and the emplacement of several allochthonous thrust wedges of Upper Devonian–Jurassic continental margin strata in the frontal part of the orogen, including the Endicott Mountains, Picnic Creek, Kelly River, Ipnavik River, and Nuka Ridge allochthons (e.g., Mull, 1982; Mayfield et al., 1988; Moore et al., 1994; 2015). Later phases of Brookian contraction deformed middle and Upper Cretaceous strata of the Colville foreland basin (e.g., Moore et al., 1994; 2004). Fission-track data indicate that these phases occurred during the early Cenozoic (ca. 60–45 Ma; e.g., O'Sullivan et al., 1997).

The NE Brooks Range is a prominent structural salient where the deformation front protrudes >80 km out from the main east–west axis of the Brooks Range. Like the deformation observed in the subsurface of the Colville basing, the NE Brooks Range salient formed in

response to late stages of Brookian contraction in the Cenozoic (Wallace and Hanks, 1990; Hanks and Wallace, 1990, Hanks, 1993). These late stages of uplift are also recorded in Cenozoic cooling ages from apatite fission-track data (O'Sullivan, 1993; O'Sullivan and Wallace, 1990).

Two major detachment zones, or décollements, which exist at different structural levels, control the northward propagation and accommodation of shortening in the NE Brooks Range (Wallace and Hanks, 1990). The upper detachment zone resides within the mechanically incompetent Kayak shale, and the competent units of the overlying Lisburne and Sadlerochit groups are repeatedly deformed into upright detachment folds of m- to km-scale wavelengths (e.g., Wallace and Hanks, 1990; Wallace, 1993; Homza and Wallace, 1997; Atkinson and Wallace, 2003; Jadamec and Wallace, 2014). A lower detachment zone links a series of breakthrough, high-angle thrust faults that originate deep below the sub-Mississippian unconformity and breach across or sole into the Kayak detachment zone.

Fold geometry above the Kayak detachment zone is largely controlled by competent and incompetent unit thicknesses, which vary throughout the field area. In some cases, the Lisburne Group and the lower Sadlerochit units (Echooka Formation) behave as a mechanically homogeneous unit and are folded in concert with one another, producing long wavelength folds (Fig 4.3A). In other parts of the NE Brook Range and at different structural levels, short wavelength, parasitic folds form, particularly where decimeter-scale beds of the lower Lisburne Group (Alpha Limestone) are rhythmically layered into competent and incompetent intervals (Fig 4.3B). The Kayak Shale also exhibits strong mechanical stratigraphy, as interbedded competent limestone intervals are deformed into cylindrical buckle folds and the shale intervals show pressure solution cleavage in the cores of larger Lisburne folds. Occasionally breakthrough

thrust faults originate in the Kayak shale cut the forelimbs of rotated Lisburne folds, particularly the where interlimb angle of the folds becomes >90° and/or where the Kayak Shale interval is thin (Jadamec and Wallace, 2014).

Because our study is focused on deformation of the sub-Mississippian rocks, and because many of the Lisburne detachment folds are below the resolution of our maps, the cross sections shown on Plates 1 and 2 do not account for the shortening and structural thickening of the detachment folds. Folds in Kekiktuk Conglomerate, however, have wavelengths and interlimb angles that are much larger than those in the Lisburne Group, and they define a set of first-order folds related to bending above the basement-derived high-angle thrust faults (reverse faults). In the Kongakut River area, Ellesmerian units appear folded about a subhorizontal, east–west trending axis, whereas in the Jago River area, the Ellesmerian fold axis is slightly rotated, trending at ~75° but also with a subhorizontal plunge (Fig. 4.5). The contrast between the east–northeast trends in the Jago River and and east–west trends in the Kongakut River could reflect oroclinal bending durning north-northwest tectonic transport during Cenozoic deformation. Also, uplift and bending associated with basement-derived thrust faults likely caused additional rotation of structures within the Ellesmerian sequence, as progressively deeper structural levels were involved in the later stages of Cenozoic contraction (e.g., Hanks, 1993).

The basement-derived thrust faults are drawn with steep dips (60–70°) that link to a deeper detachment zone and are akin to thick-skinned or “Lauramide” style reverse faults seen elsewhere along the North American Cordillera. These faults typically have low amounts of displacement, but they result in high amounts of structural relief. Some of the faults bring sub-Mississippian units in direct contact with strata of the Ellesmerian sequence. For example, The

Whale Mountain thrust, which cuts through the middle part of the Kongakut River cross section (Plate 1, A–A' cross section), juxtaposes the Clarence River Group strata and the Whale Mountain volcanic rocks units with Lisburne and Sadlerochit group strata. In the southern part of the Jago River area (Plate 2, cross section B–B'), the basement-derived faults become more closely spaced and they appear to splay, forming smaller synthetic faults as they cross cut the incompetent rocks of the Ulungarat and Mangaqtaaq formations.

Along the east wall of the Jago River valley, the Devonian(?) altered rocks, which are associated with the granitic rocks of the Jago Stock, are displaced by the Whale Mountain thrust and placed above the Lisburne Group strata (4.3E), implying that the granitic rocks were involved with Cenozoic thrusting, as previous authors have suggested (e.g., Hanks and Wallace, 1990; Peapples et al., 1997). The granitic rocks also deflect the northward propagation of Brookian contraction in the area. The major faults appear to bend and, in some cases, form tear faults around the intrusions. This is also supported by the westward rotation of fold axes observed in the Ellesmerian Sequence (Fig. 4.5). Our interpretation, however, differs from previous researches who interpreted the granitic rocks to be involved with a shallow, fold-and-thrust belt style of faulting, which resulted in long lateral transport distances of the granitic rocks (e.g., Wallace and Hanks, 1990; Hanks and Wallace; 1990; Peapples et al., 1997). Instead, we propose that the granitic rocks were also cross cut by the basement faults, but at high angles, with much of the shortening accommodated by vertical displacement.

Pre-Mississippian Deformation

Rocks below the sub-Mississippian unconformity are complexly deformed into tight and isoclinal, class II (similar) folds with inclined to sub-horizontal axial surfaces (Figs. 4.4 and 4.5). The geometry and structural style of the sub-Misissippian units is strongly discordant with the

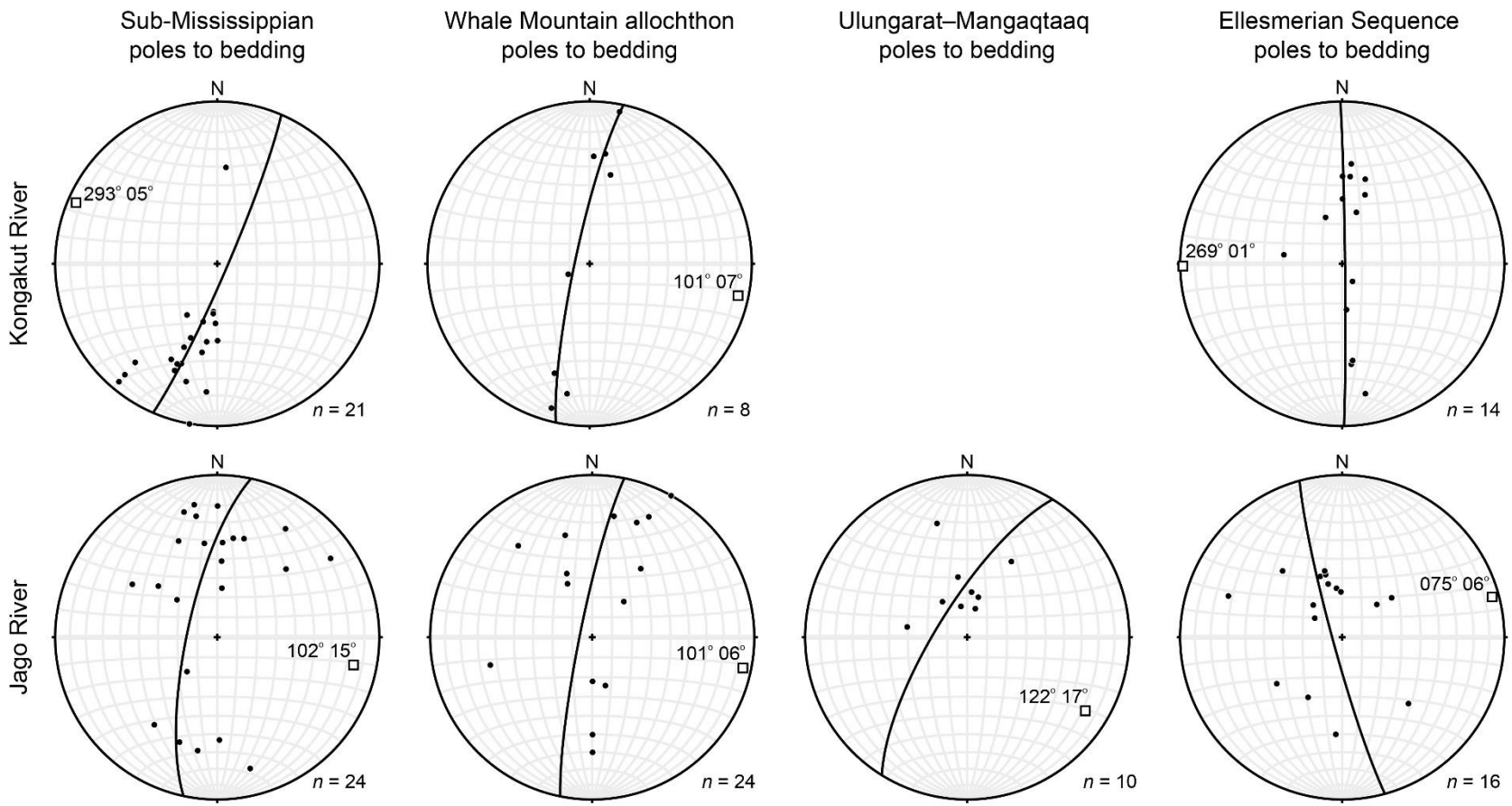

Figure 4.5: Lower-hemisphere, equal-area stereographic projections of poles to bedding planes from rocks in the Jago and Kongakut river areas. Filled circles represent poles to bedding planes, great circles represent calculated best-fit great circle to observed data, and open squares represent calculated fold axes of observed data.

upright detachment folds observed in the overlying Ellesmerian sequence, and the fabrics and fold trends are truncated by the sub-Mississippian unconformity. Past researches have thus concluded that an earlier phase of deformation is recorded in the sub-Mississippian rocks of the NE Brooks Range (e.g., Reed, 1968; Mull 1982; Oldow et al., 1987; Wallace and Hanks, 1990; Hanks, 1993; Moore et al., 1994; Lane, 2007; Johnson et al., 2016), yet the tectonic context and timing of this phase of deformation is still poorly understood.

Detailed mapping and structural measurements in the Franklin Mountains by Oldow et al. (1987), suggests that the pre-Mississippian deformation is recorded in mesoscopic and microscopic, south-verging, "D_1" folds that are overprinted by later Brookian phases of deformation (D_2 and D_3 phases). Along the lower reaches of the Aichilik River, in the western part of the British Mountains (Fig. 4.1), the work of Hanks et al. (1993) and Hanks (1989) showed that D_1 structure are predominantly south dipping and instead record north-vergent folding. From surface and subsurface mapping in northern Yukon, Lane (2007) showed that many of the sub-Mississippian folds and fabrics favore south vergence, but the folds are also cut series of north-directed thrust faults (backthrusts). Lane (2007) noted that the structures were intruded by the Late Devonian granitic rocks, indicating that deformation occurred in pre-Late Devonian time, and he named this the Romanzof orogeny.

A series of Brookian thrust faults at the southern limit of our field area expose Middle Devonian–Lower Carboniferous(?) strata of the Ulungarat and Manqataaq formations. These units are gently folded/tilted, and the bedding planes dip to the southeast and closely follow the structural trends in the overlying Ellesmerian Sequence (Fig. 4.5). They are not deformed into the tight and isoclinal folds that exemplify the sub-Mississippian rocks to the north, suggesting that Romanzof deformation may have actually initiated prior to the Middle Devonian. Despite

this age constraint, interpretations on the tectonic and depositional setting of the Ulungarat strata are uncertain, and it is plausible that these strata were deposited in a foreland basin that formed during the Romanzof orogeny. Conversely, Anderson (1995) interpreted the Ulungarat and Manqataaq formations as being deposited in a rift basin. How far these units have been transported by Brookian deformation is also unclear, but in the B–B' cross section of Plate 2, the Ulungarat and Manqataaq map unit (Dmu) is coupled with the underlying Romanzof formation (O€r) of the Whale Mountain allochthon.

The timing and kinematics of the Whale Mountain allochthon's emplacement are also unclear. As we mentioned above, the base of the allochthon is marked by a major fault zone that separates it from the rest of the sub-Mississippian rocks in the field area. In many places, the Upper Cambrian volcanic and carbonate rocks of the allochthon are juxtaposed with upper strata of the Clarence River Group, defined as the Lower Devonian(?) Buckland Hills formation of Lane et al. (2016) and Strauss et al. (2018a). This requires that emplacement occurred after or during Buckland Hills deposition. Rocks of the allochthon are also intruded by the granitic rocks of the Sheenjek Stock in the headwaters of the Jago River (Plate 2). Assuming that the age of the Sheenjek rocks parallel the ca. 380 Ma zircon U-Pb ages from the neighboring Okpilak Batholith and Jogo Stock (Dillon et al., 1987), the timing of emplacement narrows to an Early–Late Devonian window. Emplacement may have preceded the deposition of Ulungarat rocks in the Middle Devonian, but without further investigation of the contact relationships between the Ulungarat and Whale Mountain allochthon units, this time constraint cannot be confirmed.

We propose, as did Johnson et al. (2016, 2018), that the emplacement of the allochthon was related to, or directly the cause of, the Romanzof orogeny. Whether the emplacement resulted in south- or north-vergent folding of the underlying strata is uncertain. Our maps (Plates

1 and 2) suggests that fold vergence varies across the NE Brooks Range. In the Kongakut River area, the sub-Mississippian bedding planes and fold axes predominantly dip to the north and favor a south-vergent style of folding (Figs. 4.4 and 4.5). Conversely, most of the units in the Jago River area dip to the south and favor a north-vergent style of folding. The sub-Mississippian strata and related folds are also repeatedly disrupted by both north- and south-directed thrust faults. In addition, none of these structures appear to be significantly reoriented by Brookian deformation, as there is no correspondence between the breakthrough thrust faults and the orientations of the sub-Mississippian fold axes, and displacement on the Brookian thrust faults is relatively small (~500 m).

In our maps, we depict the Whale Mountain allochthon as a rootless thrust sheet that was emplaced from south to north. Remnants of the emplacing fault are marked by a mélange of blocks derived from the carbonate rocks of the Egaksrak formation, the Whale Mountain and Marsh Fork volcanic rocks, and intensely folded black slate and phyllite units of the Clarence River Group (Johnson et al., 2018; Strauss et al., 2018a). In both field areas, the fault zone is cross cut by the steeper Brookian thrust faults, namely the Romanzof Mountains and Whale Mountain thrust faults. This is particularly well showcased in the headwaters of the Aichilik River, where the Kekiktuk Conglomerate is exposed in both the hanging wall and footwall sides of the Romanzof Mountains thrust (Fig 4.3F), indicating that this is a Brookian fault. The basal thrust of the allochthon thus either merges with the Romanzof Mountains thrust at an angle or it has simply been reactivated by Brookian deformation. Again, the Brookian displacement on this fault is small (~500m), which is not enough to account for the emplacement of the allochthon.

The Whale Mountain allochthon should continue as a critical subject of future mapping efforts and research because these rocks potentially represent remnants of an ancient suture zone,

which separates the North Slope subterrane from the Doonerak arc complex and the southwestern subterranes of Arctic Alaska. Johnson et al. (2018) speculated that this suture zone is, in part, an Arctic equivalent of the Iapetus suture now exposed in parts of New England and the British Isles, which formed during the Caledonian orogeny when Baltica and Laurentia collided with one another. In turn, this suggests that the Romanzof orogeny of Lane (2007) is a local expression or extension of Caledonian deformation in the NE Brooks Range and is likely related to the assembly of the Arctic Alaska–Chukotka microplate.

CONCLUSIONS

The structural style and stratigraphic architecture of NE Brooks Range is preserved in more than 20 different map units that record two major orogenic events: one linked to Cenozoic phases of the Brookian orogeny and a second, poorly understood, Early–Middle Devonian event known as the Romanzof orogeny. The two 1:75,000 scale maps produced in this study are still a work in progress. Collectively, the recent work of Strauss et al. (2013, 2018a; 2018b), Lane et al. (2016), Colpron et al. (2018), Nelson et al. (2018), and Johnson et al. (2016; 2018) has greatly expanded the knowledge regarding the overall stratigraphy of the NE Brooks Range, but the structural style and architecture, especially that of the sub-Mississippian map units, remains poorly constrained. Future studies need to focus on building more detailed geological maps that incorporate balanced cross sections to illustrate the three-dimensional complexity of the region and address some of the uncertainties mentioned in this study.

ACKNOWLEDGMENTS

This study was supported by several different funding agencies, the Geological Society of America Student Research fund is one that we are especially thankful for. We would not have been able to haul all those rocks from our field area had we not had the assistance and

companionship from Blaze Budd, Patrick Frier, and Lyle Nelson. Kirk Sweetsir from Yukon Air Service and the staff at Wright Air Service got us home safely. The hard-working staff at United States Fish and Wildlife Service quickly granted us permission to work in the Arctic National Wildlife Refuge. DEMs were provided by the Polar Geospatial Center under NSF-OPP awards 1043681, 1559691, and 1542736. We are also greatly indebted to Gil Mull for sharing his knowledge and immaculate field notes from >20 years of field work in the Brooks Range of Alaska.

REFERENCES

Anderson, A.V., 1993, Variations in structural geometry across the continental divide thrust front, northeastern Brooks Range, Alaska: Alaska Division of Geological & Geophysical Surveys Public Data File 93-77, 45 p., 1 sheet, scale 1:25,000 doi: 10.14509/1616

Anderson, A.V., 1995, Stratigraphic variation across a Middle Devonian to Mississippian rift-basin margin and implications for subsequent fold and thrust geometry, northeastern Brooks Range, Alaska: unpublished PhD thesis, University of Alaska Fairbanks. 276 p.

Anderson, A.V., Wallace, W.K., and Mull, C.G., 1994, Depositional record of a major tectonic transition in northern Alaska: Middle Devonian to Mississippian rift-basin margin deposits, upper Kongakut River region, eastern Brooks Range, Alaska, in Thurston, D.K., and Fujita, K., eds., 1992 Proceedings of the International Conference on Arctic Margins: Anchorage, Alaska, U.S. Department of the Interior, Minerals Management Service, p. 71–76.

Anderson, A.V., and Watts, K.F., 1992, Mangaqtaag Formation lacustrine(?) deposits in the Endicott Group headwaters of the Kongakut River, eastern Brooks Range, Alaska: Public-data File 92-6, Alaska Division of Geological and Geophysical Surveys, 19 p.

Armstrong, A.K., and Mamet, B.L., 1974. Carboniferous Biostratigraphy, Prudhoe Bay State 1 to Northeastern Brooks Range, Arctic Alaska: American Association of Petroleum Geologists Bulletin v. 58, p. 646–660.

Armstrong, A.K., and Mamet, B.L., 1977, Carboniferous microfacies, microfossils, and corals, Lisburne Group, Arctic Alaska: U.S. Geological Survey Professional Paper 849, 144 p., 8 sheets.

Armstrong, A. K., Mamet, B. L., and Dutro, J, T., Jr., 1970, Foraminiferal zonation and carbonate facies of Carboniferous (Mississippian and Pennsylvanian) Lisburne Group, central and eastern Brooks Range, Arctic Alaska: American Association of Petroleum Geologists Bulletin, v. 54, p. 687-698.

Atkinson, P. K. and Wallace, W. K., 2003, Competent unit thickness variation in detachment folds in the Northeastern Brooks Range, Alaska: geometric analysis and a conceptual model. Journal of Structural Geology, v. *25*, p. 1751–1771.

Bird, K.J., and Houseknecht, D.W., 2001, Arctic National Wildlife Refuge, 1002 Area, petroleum assessment, 1998, including economic analysis: U.S. Geological Survey Fact Sheet 028–01

Bowsher, A. L., and Dutro, J. T., Jr., 1957, The Paleozoic section in the Shainin Lake area, central Brooks Range, Alaska: United States Geological Survey Professional Paper 303-A, 39 p.

Brosgé, W.P., Dutro, J.T., Jr., Mangus, M.D., and Reiser, H.N., 1962, Paleozoic sequence in eastern Brooks Range, Alaska: American Association of Petroleum Geologists Bulletin, v. 46, p. 174-198.

Cecile, M.P., 1988, Corridor traverse through Barn Mountains, northernmost Yukon: Geological Survey of Canada, Current Research, Part D, Paper 88-1D, p. 99–103.

Colpron, M., McClelland, W.C., and Strauss, J.V., 2018, Detrital zircon U-Pb geochronological and Hf isotopic constraints on the geological evolution of North Yukon, in Piepjohn, K., Strauss, J.V., Reinhardt, L., and McClelland, W.C., eds., Circum-Arctic Structural Events: Tectonic Evolution of the Arctic Margins and Trans-Arctic Links with Adjacent Orogens: Geological Society of America Special Paper 541, doi: 10.1130/2018.2541(19).

Detterman, R.L., Bowsher, A.L., and Dutro, J.T., Jr., 1958, Glaciation on the Arctic Slope of the Brooks Range, northern Alaska: Arctic, v. 11, p. 43–61.

Detterman, R.J., Reiser, H.N., Brosge, N.P. and Dutro, J.T., Jr. 1975. Post-Carboniferous stratigraphy, northeastern Alaska: United States Geological Survey, Professional Paper 886, 46 p.

Dillon, J.T., Jr., Tilton, G.R., Decker, J., and Kelly, M.J., 1987, Resource implications of magmatic and metamorphic ages for Devonian igneous rocks in the Brooks Range, in Tailleur, I., and Weimer, P., eds., Alaskan north slope geology: Society of Economic Paleontologists and Mineralogists (SEPM) and Alaska Geological Society, Book 50, p. 713–723.

Dixon, J., 2004, Lower Cretaceous (Albian) to Tertiary strata, Yukon Territory –Northwest Territories (a contribution to the Geological Atlas of the Northern Canadian Mainland Sedimentary Basin): Geological Survey of Canada, Open File 4633, 45 p.

Dutro Jr., J.T., 1987, Revised megafossil biostratigraphic zonation for the Carbonifereous of northern Alaska, *in* Tailleur, I., and Weimer, P., eds., Alaskan North Slope Geology: Pacific Section, Society of Economic Paleontologists and Mineralogists (SEPM)

Publication 50, p. 359-364

Dutro, J.T., Jr., Brosgé, W.P., and Reiser, H.N., 1972, Significance of recently discovered Cambrian fossils and reinterpretation of Neruokpuk Formation, northeastern Alaska: American Association of Petroleum Geologists Bulletin, v. 56, p. 808–815.

Goodfellow, W.D., Cecile, M.P., and Leybourne, M.I., 1995, Geochemistry, petrogenesis, and tectonic setting of lower Paleozoic alkalic and potassic volcanic rocks, Northern Canadian Cordilleran Miogeocline: Canadian Journal of Earth Sciences, v. 32, p. 2167–2167, doi: 10.1139/e95-169.

Hanks, C.L., 1989, Preliminary geology of the pre-Mississippian rocks of the Aichilik and Egaksrak River areas, northeastern Brooks Range, Alaska: Alaska Division of Geological and Geophysical Surveys, Public-date File 89-1a, 18 p.

Hanks, C.L., 1993, The Cenozoic structural evolution of a fold-and-thrust belt, northeastern Brooks Range, Alaska: Geological Society of America Bulletin, v. 105, p. 287–305, doi: 10.1130/0016-7606(1993)105<0287:TCSEOA>2.3.CO;2.

Hanks, C.L., and Wallace, W.K., 1990, Cenozoic thrust emplacement of a Devonian batholith, northeastern Brooks Range: Involvement of crystalline rocks in a foreland fold-and-thrust belt: Geology, v. 18, p. 395–398, doi: 10.1130/0091-7613(1990)018<0395:CTEOAD>2.3.CO;2.

Herbosch, A., and Verniers, J., 2011, What is the biostratigraphic value of the ichnofossil *Oldhamia* for the Cambrian?: A review: Geologica Belgica, v. 14, no. 3-4, p. 229–248.

Homza, T.X., 1991, Geologic map, cross section, and structural geology of an area southwest of Bathtub Ridge, northeastern Brooks Range, Alaska: Alaska Division of Geological &

Geophysical Surveys Public Data File 91-9, 21 p., 1 sheet, scale 1:25,000. http://doi.org/10.14509/1476

Homza, T.X., and Wallace, W.K., 1997, Detatchment Folds with Fixed Hinges and Variable Detatchment Depth, Norteastern Brookes Range, Alsaka, in Anastasio, D.J., Erslev, E.A., Fisher, D.M., and Evans, J.P. eds., Journal of Structural Geology, p. 337–354.

Imm, T.A., Dillon, J.T., and Bakke, A.A., 1993, Generalized geologic map of the Arctic National Wildlife Refuge, northeastern Brooks Range, Alaska: Alaska Division of Geological & Geophysical Surveys Special Report 42, 1 sheet, scale 1:500,000. http://doi.org/10.14509/2641

Jadamec, M.A., and Wallace, W.K., 2014, Thrust-breakthrough of asymmetric anticlines: Observational constraints from surveys in the Brooks Range, Alaska: Journal of Structural Geology, v. 62, p. 109–124, doi: 10.1016/j.jsg.2014.01.012.

Johnson, B.G., Strauss, J.V., Toro, J., Benowitz, J.A., and Ward, W.P., 2016, Geochronological constraints from synorogenic detritus and early Paleozoic accretionary tectonics in the NE Brooks Range: Lithosphere, v. 8, p. 649–667, doi: 10.1130/L533.1.

Johnson, B.G., Strauss, J.V., Taylor, J.F., Ward, W.P., Colpron, M., McClelland, W.C., and Toro, J., 2018, The Whale Mountain allochthon: A relic of the Iapetus Ocean preserved in the northeastern Brooks Range of Alaska and Yukon, in Piepjohn, K., Strauss, J.V., Reinhardt, L., and McClelland, W.C., eds., Circum-Arctic Structural Events: Tectonic Evolution of the Arctic Margins and Trans-Arctic Links with Adjacent Orogens: Geological Society of America Special Paper 541, doi: 10.1130/2018.2541(20).

Kelley, J.S., Wrucke, C.T., and Lane, L.S., 1994, Pre-Mississippian rocks of the Clarence and Malcolm Rivers area, in Thurston, D.K., and Fujita, K., eds., 1992 Proceedings of the International Conference on Arctic Margins, OCS Study, MMS 94-0040, p. 59–64.

Lane, L.S., 1991, The pre-Mississippian "Neruokpuk Formation," northeastern Alaska and northwestern Yukon: review and new regional correlation: Canadian Journal of Earth Sciences, v. 28, p. 1521–1533.

Lane, L.S., 2007, Devonian–Carboniferous paleogeography and orogenesis, northern Yukon and adjacent Arctic Alaska: Canadian Journal of Earth Sciences, v. 44, p. 679-694.

Lane, L.S., and Cecile, M.P., 1989, Stratigraphy and structure of the Neruokpuk Formation, northern Yukon: Geological Survey of Canada, Current Research, Part G, Paper 89-1G, p. 57–62.

Lane, L.S., Gehrels, G.E., and Layer, P.W., 2016, Provenance and paleogeography of the Neruokpuk Formation, northwest Laurentia: An integrated synthesis: Geological Society of America Bulletin, v. 129, p. 239−257, doi: 10.1130/B31234.1.

Lane, L.S., Kelley, J.S., and Wrucke, C.T., 1995, Stratigraphy and structure of the Clarence River area, Yukon-Alaska north slope: a USGS-GSC co-operative project: Geological Society of Canada Current Research 1995-E, p. 1–9.

Leffingwell, E. de K., 1919, The Canning River region, northern Alaska: U.S. Geological Survey Professional Paper 109, 251 p.

LePain, D. L., Crowder, R.K., and Wallace, W.K., 1994, Early Carboniferous transgression on a passive continental margin: Deposition of the Kekiktuk Conglomerate, northeastern Brooks Range, Alaska, American Association of Petroleum Geologists Bulletin, v. 78, p. 679–699.

Lerand, M., 1973, Beaufort Sea, *in* McCrossam, R.G., ed., The Future Petroleum Provinces of Canada —Their Geology and Potential: Canadian Society of Petroleum Geology Memoir 1, p. 315–386.

MacNaughton, R.B., Moynihan, D.P., Roots, C.F., and Crowley, J.L., 2016, New occurrences of *Oldhamia* in eastern Yukon, Canada: Stratigraphic context and implications for Cambrian deep-marine biostratigraphy: Ichnos, v. 23, p. 33–52, 1635 doi: 10.1080/10420940.2015.1127232.

Mamet, B. L., and Armstrong, A. K., 1972, Lisburne Group, Franklin and Romanzof Mountains, northeastern Alaska, *in* Geological Survey research 1972: United States Geological Survey Professional Paper 800-C, p. C127–C144.

Mayfield, C.F., Tailleur, I.L., and Ellersieck, I., 1988, Stratigraphy, structure, and palinspastic synthesis of the western Brooks Range, northwestern Alaska, *in* Gryc, George, ed., Geology and Exploration of the National Petroleum Reserve in Alaska, 1974 to 1982: U.S. Geological Survey Professional Paper 1399, p. 143–186.

McClelland, W.C., Colpron, M., Piepjohn, K., von Gosen, W., Ward, W.P., and Strauss, J.V., 2015, Preliminary detrital zircon geochronology of the Neruokpuk Formation in the Barn Mountains, Yukon, *in* MacFarlane, K.E., Nordling, M.G., and Sack, P.J., eds., Yukon Exploration and Geology 2014: Yukon Geological Survey, p. 123–143.

Molenaar, C. J., Bird, K. J., and Kirk, A. R. 1987, Cretaceous and Tertiary stratigraphy of northeastern Alaska, *in* Tailleur, I., and Weimer, P., eds., Alaskan North Slope Geology: Pacific Section, Society of Economic Paleontologists and Mineralogists (SEPM) Publication 50, p. 691–710.

Moore, T.E., 1987, Geochemistry and the tectonic setting of volcanic rocks of the Franklinian assemblage, central and eastern Brooks Range, *in* Tailleur, I., and Weimer, P., eds., Alaskan North Slope Geology: Pacific Section, Society of Economic Paleontologists and Mineralogists (SEPM) Publication 50, p. 691–710.

Moore, T.E., and Churkin, M., Jr., 1984, Ordovician and Silurian graptolite discoveries from the Neruokpuk Formation (sensu lato), northeastern and central Brooks Range, Alaska, *in* Blodgett, R.B., ed., Paleozoic Geology of Alaska and Northwestern Canada Newsletter 1: Alaska Geological Society, p. 21–23.

Moore, T.E., O'Sullivan, P.B., Potter, C.J., and Donelick, R.A., 2015, Provenance and detrital zircon geochronologic evolution of lower Brookian foreland basin deposits of the western Brooks Range, Alaska, and implications for early Brookian tectonism: Geosphere, v. 11, no. 1, p. 93–122, doi: 10.1130/GES01043.1.

Moore, T.E., Potter, C.J., O'Sullivan, P.B., Shelton, K.L., and Underwood, M.B., 2004, Two Stages of Deformation and Fluid Migration in the West-Central Brooks Range Fold and Thrust Belt, Northern Alaska, *in* Swennen, R., Roure, F., and Granath, J.W. eds., Deformation, fluid flow, and reservoir appraisal in foreland fold and thrust belts, AAPG Hedberg Series, no. 1, p. 157–186.

Moore, T.E., Wallace, W.K., Bird, K.J., Karl, S.M., Mull, C.G., and Dillon, J.T., 1994, Geology of northern Alaska, *in* Plafker, G., and Berg, H.C., eds., The Geology of Alaska: Boulder, Colorado, Geological Society of America, The Geology of North America, v. G-1, p. 49–140.

Mull, C.G., 1982, Tectonic evolution and structural style of the Brooks Range, Alaska: An illustrated summary, in Powers, R.B., ed., Geologic studies of the Cordilleran thrust belt, Volume 1: Denver, Colorado, Rocky Mountain Association of Geologists, p. 1-45.

Mull, C.G., 1987, Kemik sandstone, Arctic National Wildlife Refuge, northeastern Alaska, *in* Tailleur, I., and Weimer, P., eds., Alaskan North Slope Geology: Pacific Section, Society of Economic Paleontologists and Mineralogists (SEPM) Publication 50, p. 405-431

Mull, C.G., and Anderson, A.V., 1991, Franklinian Lithotectonic Domains, Northeastern Brooks Range, Alaska: Alaska Division of Geological & Geophysical Surveys Public Data File 91–5, 40 p., doi: 10.14509/1472.

Mull, C.G., and Mangus, M.D., 1972, Itkilyariak Formation: new Mississippian formation of Endicott Group, Arctic slope of Alaska: American Association of Petroleum Geologists Bulletin, v. 56, p. 1364–1369.

Nelson, L.L., Strauss, J.V., Crockford, P.W., Cox, G.M., Johnson, B.G., Ward, W., Colpron, M., McClelland, W.C., and Macdonald, F.A., 2018, Geochemical constraints on the provenance of pre-Mississippian sedimentary rocks in the North Slope subterrane of Yukon and Alaska, *in* Piepjohn, K., Strauss, J.V., Reinhart, L., and McClelland, W.C., eds., Circum-Arctic Structural Events: Tectonic Evolution of the Arctic Margins and Trans-Arctic Links with Adjacent Orogens: Geological Society of American Special Paper 541, doi: 10.1130/2018.2541(24).

Norris, D.K., 1981a, Geology, Blow River and Davidson Mountains, Yukon Territory -District of Mackenzie: Geological Survey of Canada, Map 1516A, 1:250,000.

Norris, D.K., 1981b, Geology, Hesrchel Island and Demarcation Point, Yukon Territory: Geological Survey of Canada, Map 1514A, 1:250,000.

Norris, D.K., 1985, The Neruokpuk Formation, Yukon Territory and Alaska: Geological Survey of Canada, Current Research, Part B, Paper 85-1B, p. 223–229.

Oldow, J.S., Avé Lallemant, H.G., Julian, F.E., and Seidensticker, C.M., 1987, Ellesmerian(?) and Brookian deformation in the Franklin Mountains, northeastern Brooks Range, Alaska, and its bearing on the origin of the Canada Basin (USA): Geology, v. 15, p. 37–41, doi: 10.1130/0091-7613(1987)15<37:EABDIT>2.0.CO;2.

O'Sullivan, P.B., 1993, Multiple phases of Tertiary uplift and erosion in the Arctic National Wildlife Refuge, Alaska, revealed by apatite fission track analysis: American Association of Petroleum Geologists Bulletin, v. 77, p. 359–385, doi: 10.1306/BDFF8C0E-1718-11D7-8645000102C1865D.

O'Sullivan, P.B., Murphy, J.M., and Blythe, A.E., 1997, Late Mesozoic and Cenozoic thermotectonic evolution of the central Brooks Range and adjacent North Slope foreland basin, Alaska: Including fission track results from the Trans-Alaska Crustal Transect (TACT): Journal of Geophysical Research, v. 102, no. 9, p. 20821, doi: 10.1029/96JB03411.

O'Sullivan, P.B., and Wallace, W.K., 2002, Out-of-sequence, basement-involved structures in the Sadlerochit Mountains region of the Arctic National Wildlife Refuge, Alaska: Evidence and implications from fission-track thermochronology: Geological Society of America Bulletin, v. 114, p. 1356–1378, doi: 10.1130/0016-7606(2002)114 <1356:OOSBIS >2.0.CO;2.

Patton, W.W., Jr., 1956, New and redefined formations of Early Cretaceous age, *in* Gryc, G., and others, American Association of Petroleum Geologists Bulletin, v. 40, p. 219–223.

Peapples, P.R., Wallace, W.K., Hanks, C.L., O'Sullivan, P.B., and Layer, P.W., 1997, Style, controls, and timing of fold-and-thrust deformation of the Jago stock, northeastern Brooks Range, Alaska: Canadian Journal of Earth Sciences, v. 34, p. 992–1007.

Reed, B. L., 1968, Geology of the Lake Peters area, northeastern Brooks Range, Alaska: U.S. Geological Survey Bulletin, v. 1236, p. 1–132.

Reiser, H.N., 1970, Northeastern Brooks Range–a surface expression of the Prudhoe Bay section, *in* Proceedings of the geological seminar on The north slope of Alaska, American Association of Petroleum Geologists Pacific Section, p. K1–K3.

Reiser, H.N., Brosgé, W.P., Dutro, J.T., and Detterman, R.L., 1980, Geologic map of the Demarcation Point quadrangle, Alaska: U.S. Geological Survey Map I-1133, 1:250,000 scale.

Sable, E.G., 1977, Geology of the western Romanzof Mountains, Brooks Range, northeastern Alaska: U.S. Geological Survey Professional Paper 897, 84 p.

Schrader, F. C., 1902, Geologic section of the Rocky Mountains in northern Alaska: Geological Society of America Bulletin, v. 13, p. 233–252.

Strauss, J.V., Johnson, B.G., Colpron, M., Nelson, L.L., Perez, J.L., Benowitz, J.A., Ward, W.P., and McClelland, W.C., 2018a,, Pre-Mississippian stratigraphy and provenance of the North Slope subterrane of Arctic Alaska II: Basinal rocks of the northeastern Brooks Range and their significance in circum-Arctic evolution, *in* Piepjohn, K., Strauss, J.V., Reinhardt, L., and McClelland, W.C., eds., Circum-Arctic Structural Events: Tectonic Evolution of the Arctic Margins and Trans-Arctic Links with Adjacent Orogens: Geological Society of America Special Paper 541, doi: 10.1130/2018.2541(23).

Strauss, J.V., Macdonald, F.A., and McClelland, W.C., 2018b, Pre-Mississippian stratigraphy and provenance of the North Slope subterrane of Arctic Alaska I: Platformal rocks of the northeastern Brooks Range and their signifi cance in circum-Arctic evolution, *in* Piepjohn, K., Strauss, J.V., Reinhardt, L., and McClelland, W.C., eds., Circum-Arctic Structural Events: Tectonic Evolution of the Arctic Margins and Trans-Arctic Links with Adjacent Orogens: Geological Society of America Special Paper 541, doi: 10.1130/2018.2541(22).

Strauss, J.V., Macdonald, F.A., Taylor, J.F., Repetski, J.E., and McClelland, W.C., 2013, Laurentian origin for the North Slope of Alaska: Implications for the tectonic evolution of the Arctic: Lithosphere, v. 5, p. 477–482, doi: 10.1130/L284.1.

Tailleur, I.L., Brosgé, W.P., and Reiser, H.N., 1967, Palinspastic analysis of Devonian rocks in northwestern Alaska, in International Symposium on the Devonian System: Alberta Society of Petroleum Geologists, v. 2, p. 1345–1361.

Wallace, W.K., 1993, Detachment folds and a passive-roof duplex: Examples from the northeastern Brooks Range, Alaska: *in* Solie, D.N., and Tannian, F., eds., Short notes on Alaskan Geology 1993, Alaska Division of Geological and Geophysical Surveys, Professional Report 113, p. 81–99.

Wallace, W.K., and Hanks, C.L., 1990, Structural provinces of the northeastern Brooks Range, Arctic National Wildlife Refuge, Alaska: American Association of Petroleum Geologists Bulletin, v. 74, p. 1100–1118.

Ward, W.P., Strauss, J.V., Johnson, B.G., McClelland, W.C., Colpron, M., von Gosen, W., Piepjohn, K., Cobble, M., Crockford, P.W., and Landis, J., 2018, Age, geochemistry and significance of Devonian felsic magmatism in the North Slope subterrane, Yukon, *in*

Piepjohn, K., Strauss, J.V., Reinhardt, L., and McClelland, W.C., eds., Circum-Arctic Structural Events: Tectonic Evolution of the Arctic Margins and Trans-Arctic Links with Adjacent Orogens: Geological Society of America Special Paper 541, doi: 10.1130/2018.2541(22).

SUPPLEMENTAL MATERIAL

Chapter 2 (supplemental material): Detrital geochronology of pre-Mississippian strata in the northeastern Brooks Range, Alaska: Insights into the tectonic evolution of northern Laurentia

Ben G. Johnson[1], Justin V. Strauss[2], Jaime Toro[1], Jeff A. Benowitz[3], William P. Ward[4], Jeremy K. Hourigan[5]

[1]Department of Geology and Geography, West Virginia University, Morgantown, West Virginia, 26506 USA

[2]Department of Earth Sciences, Dartmouth College, Hanover, New Hampshire 03755, USA

[3]Geophysical Institute, University of Alaska Fairbanks, Fairbanks, Alaska 99775, USA

[4]Department of Earth and Environmental Sciences, University of Iowa, Iowa City, Iowa 52242, USA

[5]Department of Earth and Planetary Sciences, University of California–Santa Cruz, Santa Cruz, California 95064, USA

SAMPLE DESCRIPTIONS

Reconnaissance scale mapping of the Demarcation Point Quadrangle by Reiser et al. (1980) is the most recent, continuous, and comprehensive geological map available in entire NE Brooks Range. The depositional environments, ages, and contact relationships among these rocks are poorly constrained. For these reasons, we rely on the mapping and unit descriptions of Reiser et al. (1980) from Alaska and of Lane (1991) and Lane et al. (1995; 2015) from Yukon to supplement these data with our own observations from multiple field seasons in the British and Romanzof mountains. All of the samples were collected from map units that are stratigraphically beneath the prominent sub-Mississippian unconformity, which spans most of Arctic Alaska (e.g.,

Moore et al., 1994). Our samples are generally grouped into two major lithostratigraphic successions exposed in the NE Brooks Range: the Neoproterozic–middle Cambrian siliclastic and carbonate units of the Firth River goup (Lane et al., 2016) and Neruokpuk Formation (Leffingwell, 1919; Lane, 1991); and a Lower Ordovician–Lower Devonian succession of turbidities herein referred to as the Clarence River group, which includes the Buckland Hills succession of Lane et al. (2016). A summery table (Table SM2.1) includes sample locations and type of analysis performed in this study. The age constraints from these units, along with age constraints from other pre-Mississippian units in the NE Brooks Range, are outlined in Table SM2.2.

Firth River group and Neruokpuk Formation Samples

12JT10 – Map unit of Css of Reiser et al. (1980), east side of the Kongakut River, just below the sub-Mississippian unconformity in the southern British Mountains (N 69.113734, W -141.903452): Very coarse- to fine-grained, subrounded, gray quartz arenite with abundant detrital muscovite and very fine-grained authigenic muscovite occupying the interstitial spaces. Sample is considered part of the Neruokpuk Formation based on its detrital zircon age distributions (see Table SM2.3) and was collected just below the sub-Mississippian unconformity.

12JT11 – Map unit of pCn of Reiser et al. (1980), east side of the Kongakut River, southern British Mountains (N 69.157950, W 141.864928): Moderatley-strained, coarse to medium-grained, green, subrounded quartz arenite. Surrounding the quartz grains are weakly developed, but prevalent, strain shadows (Fig. SM2.1A). Beds along the river are massive, up to a 1 m in thickness, and are tightly folded with with north-dipping axial surfaces.

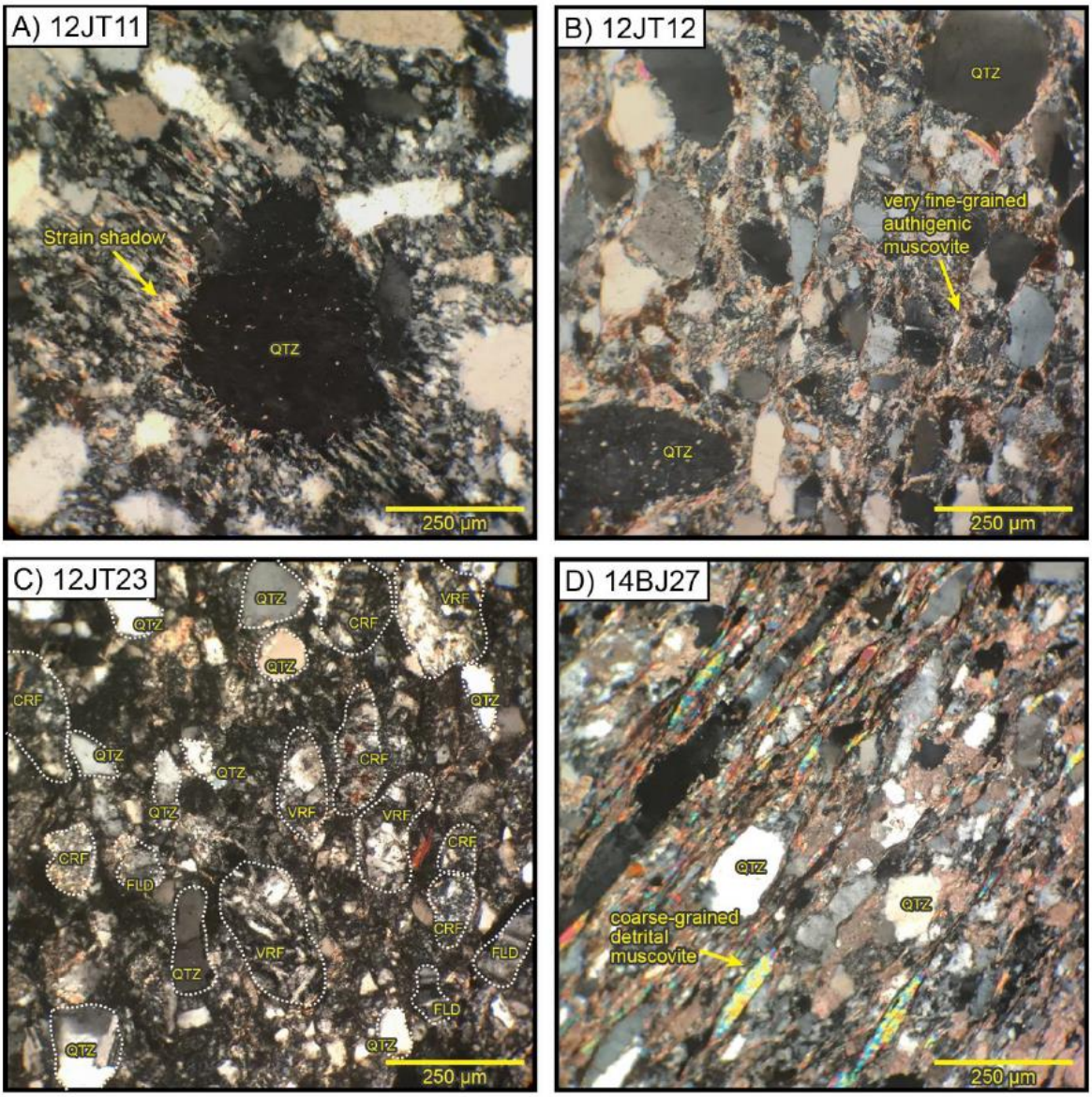

Figure SM2.1: Photomicrographs from the Neruokpuk Formation and the Clarence River Group. (A) Neruokpuk sample 12JT11 strain shadow around single quartz grain. (B) Neruokpuk sample 12JT12 showing fine-grained authigenic muscovite occupying interstitial spaces between quartz grains. (C) Clarence River Group sample 12JT23 showing various compositions of detrital grains, suggesting an immature composition. (D) Clarence River Group sample 14BJ27 showing coarse=grained detrital muscovite grains aligned within cleavage domains that surround larger quartz grains. Abbreviations: CRF–chert rock fragment; FLD–feldspar grain; QTZ–quartz grain; VRF–volcanic rock fragments

12JT12 – Map unit of pCn of Reiser et al. (1980), west side of the of the Kongakut River, southern British Mountains (N 69.192398, W 141.868887): Very coarse to fine-grained, subrounded gray lithic arenite, with >5% clay matrix. Sample contains small amounts of coarse-grained (250–800 μm) detrital(?) muscovite, 10-100 um thick packets of interstitial authigenic muscovite, and occasional feldspar grains (Fig. SM2.1B). Beds along the river are massive, up to a 1 m in thickness.

12JT13a – Map unit of pCn, Ccp, or Css of Reiser et al. (1980), east side of the of the Kongakut River, southern British Mountains (N 69.227013, W 141.831267): Moderately-strained, carbonate-cemented, fine- to very fine grained, subrounded, gray lithic arenite, with >5% clay matrix. Outcrop is interbedded with phyllite units which contain coarse-grained (250–800 μm) detrital(?) muscovite. Sample could be part of the Neruokpuk Formation or lower Clarence River group, as it was sampled near the contact.

12JT31 – Map unit pCpa, Old Grungy Mountain of Reiser et al. (1980), east side of the Kongakut River, northern British Mountains (N 69.387220, W 141.535461): Intensely foliated green-grey argillite cut by numerous quartz veins. Sample is considered part of the Firth River group because of its inferd lower stratigraphic position with respect to the Neruokpuk Formation and its along strike correlation to the carbonate units in the northern British mountains.

12JT32 – Map unit of pCn of Reiser et al. (1980) west side of the Kongakut River, northern British Mountains (N 69.424719, W 141.508195): Coarse to medium-grained, subrounded, gray lithic arenite with minor clay matrix. Beds are massive and up to 1 m in thickness.

05LF13 – Map unit of pCn of Reiser et al. (1980) east side of upper Leffingwell Fork of the Aichilik River, southern British Mountains (N 69.185356, W 142.664228): Moderately strained, coarse to very fine-grained, subangular, gray lithic-arenite. Lithic grains are predominantly chert.

11LF13 – Map unit of pCn of Reiser et al. (1980) east side of the Leffingwell Fork of the Aichilik River, southern British Mountains (N 69.263494, W 142.657930): Moderately strained, coarse- to very fine-grained, angular, green lithic-arenite. Lithic grains are predominantly chert

28LF13 – Map unit of pCn of Reiser et al. (1980) east side of the Leffingwell Fork of the Aichilik River, southern British Mountains (N 69.357533, W 142.858018): Coarse- to fine-grained, rounded, gray quartz arenite with <5% clay matrix. Beds are normally graded (Bouma-A sequence turbidites) and up to 0.5 m thick.

37LF13 – Map unit of pCn of Reiser et al. (1980), west side of the Leffingwell Fork of the Aichilik River, southern British Mountains (N 69.357257, W 142.921486): Coarse- to fine-grained, rounded to, gray lithic arenite with >5% clay matrix. Contains coarse- to medium-grained (250–800 µm) detrital muscovite, and lithic chert fragments.

J1355-617 – Map unit Css of Lane et al., (1995), upper Malcolm River, northern British Mountains in Yukon (N 69.219592, W 140.949294): Carbonate-cemented, medium- to very fine-grained, subrounded, brown quartz arenite. Contains coarse- to medium-grained (250–800 µm) detrital muscovite.

Clarence River Group Samples

12JT22 – Map unit Cp of Reiser et al. (1980), west side of the of the Kongakut River across from Whale Mountain, southern British Mountains (N 69.279048, W 141.727346):

Carbonate-cemented, coarse- to fine -grained, subrounded lithic arenite with a >5% clay matrix Contains lithic chert and metamorphic rock fragments and abundant fine- and coarse-grained (100-500 μm) detrital muscovite.

12JT23 – Map unit Cp or Cs of Reiser et al. (1980), west side of the of the Kongakut River across from Whale Mountain, southern British Mountains (N 69.279912, W 141.747478): Coarse- to medium -grained, angular to subangular, lithic or feldspathic arenite. Contains abundant chert, volcanic, and feldspar detrital grains (Fig. SM2.1C).

12JT24 – Map unit Cp of Reiser et al. (1980), west side of the of the Kongakut River across from Whale Mountain, southern British Mountains (N 69.279912, W 141.747478): Carbonate-cemented, fine- to very fine -grained, subangular, lithic arenite with a >5% clay matrix. Contains fine- and coarse-grained (100-500 μm) detrital muscovite separated for single-grain, stepwise 40Ar/39Ar analyses (Table SM2.6).

12JT35 – Map unit Ovc or Os of Reiser et al. (1980), east side of the Kongakut River, northern British Mountains along Caribou Pass (N 69.469365; W 141.469672): Carbonate-cemented, medium- to very fine-grained, subrounded, lithic arenite with abundant detrital carbonate, opaque minerals, and volcanic rock fragments.

09LF13 – Map unit Ccp or Css of Reiser et al. (1980), east side of the Leffingwell Fork of the Aichilik River, southern British Mountains (N 69.264435, W 142.657912): Moderately-strained, carbonate-cemented, subangular, fine-grained phyllite. Contains Medium- and fine-grained (100-800 μm) detrital muscovite, which occupy anastomosing cleavage domains.

40LF13 – Map unit Cp of Reiser et al. (1980), east side of the Leffingwell Fork of the Aichilik River, southern British Mountains (N 69.375307, W 142.912505): Medium- to

very fine -grained, subangular, lithic arenite with abundant detrital muscovite in a >5% clay matrix. Clay matrix composed of authigenic illite or muscovite. Contains coarse- and fine-grained (100-800 μm) detrital muscovite and occasional feldspar minerals.

14BJ27 – Map unit Cp or Css of Reiser et al. (1980), upper Aichilik River, Romanzof Mountains (N 69.117975, W 143.238008): Moderately-strained, carbonate-cemented, subangular, lithic arenite with abundant coarse- to fine-grained (100-800 μm) detrital muscovite occupying anastomosing cleavage domains (Fig. SM2.1D).

U–TH–PB GEOCHRONOLOGIC ANALYSES OF ZIRCON

Detrital zircon grains were extracted from ~2-3 kg of sample by traditional methods of crushing and grinding, followed by separation with a Gemini table, heavy liquids, and a Frantz magnetic separator at West Virginia University. After separation, the grains (generally hundreds of grains) were hand-picked and incorporated into a 2.5 cm epoxy mount together with the standards (see following sections for which standards were used). The mounts were polished using 1,500 grit sandpaper followed by 9 μm and then 3 μm down to a depth of ~20 microns, and then cleaned in 1% HNO_3 and rinsed in water prior to isotopic analysis.

LA-ICPMS: University of California Santa Cruz

Detrital zircon U-Pb geochronology conducted at the University of California Santa Cruz laser ablation inductively coupled plasma mass spectrometry (LA-ICPMS) laboratory (Table SM2.3) were analyzed using a single-collector Element XR high-resolution magnetic-sector ICP-MS and a Photon Machines Analyte.H 193 nm ArF excimer laser equipped with a Helex 2-volume laser ablation cell. Analytical procedures, tuning parameters, and data reduction techniques closely follow that of Sharman et al. (2013) and Dumitru et al. (2016). Mounted with the separated zircons, the R-33 zircon (419 Ma; Black et al. 2004) was used as a primary

standard and Plesovice (337 Ma; Sláma et al., 2008) was used as a secondary standard. Approximate concentrations of U and Th were calibrated relative to the concentrations from WF2 and Mudtank zircon standards (Woodhead and Hergt, 2005). A 26 µm spot diameter was used for all analyses. Each analysis consisted of 30 seconds of integrations with the laser off (for backgrounds), 30 seconds of integrations with the laser firing, and a 20 second delay to purge the previous sample and prepare for the next analysis.

Software used for data reduction included Iolite 2.2 (Paton et al., 2010), and VisualAge add-ons for Igor Pro. followed by an Excel spreadsheet (see below; Sharman et al., 2013). We used Iolite's exponential detrending algorithm, which calibrates to the observed down-hole fractionation of the standards. Iolite also permits efficient inspection of signal intensities, ratios, and ages as they evolved through the 30 seconds of integrations for each grain. Integration regions were generally resized if: (1) drill-through was observed based on a rapid decrease in total beam prior to the end of the integration; (2) erratic fluctuations of ^{204}Pb compared to values observed in the background-corrected ^{204}Pb signal; or (3) shallow levels within the pit exhibited substantially different ages compared to deeper levels. We did not apply a ^{204}Pb correction because average background-subtracted signals are typically less than a conservatively estimated limit of detection. Instead we utilized the ^{207}Pb-corrected ^{206}Pb/^{238}U age for ^{206}Pb/^{238}U ages <1000 Ma. This is calculated using Isoplot (version 4.15; Ludwig, 2012) based on a two-stage model of terrestrial lead isotope evolution to constrain initial Pb abundances (Stacey and Kramers, 1975; Table SM2.3). Analyses were rejected when the ^{207}Pb common lead correction is >2% of the uncorrected ^{206}Pb/^{238}U age, which excludes some grains with erratic fluctuations in ^{207}Pb/^{235}U apparent age (Dumitru et al., 2016). For grains with ^{206}Pb/^{238}U ages >1000 Ma, we use uncorrected ^{207}Pb/^{206}Pb ages because our strategy of truncating integration intervals with

detectable spikey, erratic, persistent fluctuations in ^{204}Pb above background greatly reduces the magnitude of any potential ^{204}Pb correction. Analyses with $^{206}Pb/^{238}U$ age > 600 Ma and with excessive discordance (>20% discordance or >5% reverse discordance) or high error (>10% uncertainty in $^{206}Pb/^{238}U$ or $^{207}Pb/^{206}Pb$ age) were rejected and not used for interpretation. Zircon ages <1000 Ma. For each sample, the rejected zircons are formatted with the strikethrough text (Table SM2.3).

LA-ICPMS: Stockholm University

Detrital zircon U-Pb geochronology for sample 40LF13 was conducted by LA-ICPMS techniques at the at the Department of Geological Sciences, Stockholm University laboratory (Table SM2.4) using a Thermo Scientific XSeries-2 single collector quadrupole ICP-MS and a New Wave Research 193UC excimer laser. A 40 μm spot diameter was used for all analyses. Analytical procedures, tuning parameters, and data reduction techniques closely follow that of Beranek et al. (2013). Mounted separately from the separated zircon grains, the Plesovice zircon (337 Ma; Sláma et al., 2008) was used as a primary standard and FC-52 zircon (1100 Ma; Paces and Miller, 1993) was used as a secondary standard. The synthetic glass standard, NIST 610, was used for calibration of U and Th concentrations. Total acquisition time for a single analysis included 50 seconds of integrations with the laser off (for backgrounds), 30 seconds of integrations with the laser firing, and a 50 second delay to purge the previous sample and prepare for the next analysis. The reduction methods, common Pb corrections, and filtering techniques implemented for sample 40LF13 are the same as those from the University of California Santa Cruz. For each sample, the rejected zircons are formatted with the strikethrough text (Table SM2.4).

Nordsim-laboratory

Twenty-six euhedral grains from sample 40LF13 were analyzed by secondary ion mass spectrometry (SIMS) at the NordSIMS facility, Swedish Museum of Natural History (Table SM2.5). The analyses were made using a CAMECA IMS 1280 ion-microprobe following the standardized procedures of Whitehouse et al. (1999) and Whitehouse and Kamber (2005). A 20μm spot size was used. U-Pb ages were calibrated relative to the 1065 Ma zircon standard 91500 (Wiedenbeck et al. 1995). The ^{207}Pb-corrected ^{206}Pb/^{238}U age for ^{206}Pb/^{238}U ages <1200 Ma is calculated using Isoplot (version 4.15; Ludwig, 2012) and based on a two-stage model of terrestrial lead isotope evolution to constrain initial Pb abundances (Stacey and Kramers, 1975; Table SM2.5).

^{40}AR/^{39}AR GEOCHRONOLOGIC ANALYSES OF MUSCOVITE

For ^{40}Ar/^{39}Ar analysis, eight samples were submitted to the Geochronology laboratory at University of Alaska Fairbanks where they were crushed, sieved, washed and hand-picked for muscovite mineral phases. The monitor mineral MMhb-1 (Samson and Alexander, 1987) with an age of 523.2 ± 0.9 Ma (Spell and McDougall, 2003) was used to monitor neutron flux (and calculate the irradiation parameter, J). The samples and standards were wrapped in aluminum foil and loaded into aluminum cans of 2.5 cm diameter and 6 cm height. The samples were irradiated in positions 5c (Sample 12JT13a) and 8b (all other samples) of the uranium enriched research reactor of McMaster University in Hamilton, Ontario, Canada for 20 to 150 megawatt-hours.

Upon their return from the reactor, the samples and monitors were loaded into 2 mm diameter holes in a copper tray that was then loaded in an ultra-high vacuum extraction line. The monitors were fused, and the samples heated and/or fused, using a 6-watt argon-ion laser

following the technique described in York et al. (1981), Benowitz et al. (2014) and Martin et al. (2014). Argon purification was achieved using a liquid nitrogen cold trap and a SAES Zr-Al getter at 400˚ C. The samples were analyzed in a VG-3600 mass spectrometer at the Geophysical Institute, University of Alaska Fairbanks. The argon isotopes measured were corrected for system blank and mass discrimination, as well as calcium, potassium and chlorine interference reactions following procedures outlined in McDougall and Harrison (1999). Typical full-system 8 min laser blank values (in moles) were generally 2×10^{-16} mol 40Ar, 3 × 10218 mol 39Ar, 9×10^{-18} mol 38Ar and 2×10^{-18} mol 36Ar, which are 10–50 times smaller than the sample/standard volume fractions. Correction factors for nucleogenic interferences during irradiation were determined from irradiated CaF2 and K2SO4 as follows: $(^{39}Ar/^{37}Ar)$ Ca = 7.06×10^{-4}, $(^{36}Ar/^{37}Ar)$ Ca = 2.79×10^{-4} and $(^{40}Ar/^{39}Ar)$ K = 0.0297. Mass discrimination was monitored by running calibrated air shots. The mass discrimination during these experiments was 0.8% per mass unit. While doing our experiments, calibration measurements were made on a weekly–monthly basis to check for changes in mass discrimination with no significant variation seen during these intervals.

The stepwise $^{40}Ar/^{39}Ar$ results for each smaple are presented in Table SM2.6 with all ages quoted to the ± 1 sigma level and calculated using the constants of Renne et al. (2010). The integrated age is the age given by the total gas measured and is equivalent to a potassium-argon (K-Ar) age. The spectrum results can be viewed in Figures 2.7 and 2.8, and the interpretations are summarized in Table 2.1 of the manuscript. A plateau age is provided when three or more consecutive gas fractions represent at least 60% of the total gas release and are within two standard deviations of each other (Mean Square Weighted Deviation less than 2.5; see Ludwig, 2012). Pseudo plateau ages (PPA) are reported when two or more consecutive gas fractions

represent at 50–60% of the total gas release and are within two standard deviations of each other.

Sample14BJ27 from the Clarence River group was analyzed, in addition to the stepwise techniques, with single-grain fusion $^{40}Ar/^{39}Ar$ geochronology on 14 grains to investigate intra-sample age variability. Argon was extracted by slowly increasing the power of a focused laser until total fusion of the target muscovite grain. These results are reported in Table SM2.7.

REFERENCES

Benowitz, J.A., Layer, P.W., and Vanlaningham, S., 2014, Persistent long-term (c. 24 Ma) exhumation in the Eastern Alaska Range constrained by stacked thermochronology, *in* Mark, F. and Verati, C. eds., Advances in 40Ar/39Ar Dating: from Archaeology to Planetary Sciences: Geological Society, London, Special Publications 378, p. 225–243.

Beranek, L.P., Pease, V.L., Scott, R. a, and Thomsen, T.B., 2013, Detrital zircon geochronology of Ediacaran to Cambrian deep-water strata of the Franklinian basin, northern Ellesmere Island, Nunavut: implications for regional stratigraphic correlations: Canadian Journal of Earth Sciences, v. 50, p. 1007–1018, doi: 10.1139/cjes-2013-0026.

Black, L.P., Kamo, S.L., Allen, C.M., Davis, D.W., Aleinikoff, J.N., Valley, J.W., Mundil, R., Campbell, I.H., Korsch, R.J., Williams, I.S., and Foudoulis, C., 2004, Improved 206Pb/238U microprobe geochronology by the monitoring of a trace-element-related matrix effect; SHRIMP, ID-TIMS, ELA-ICP-MS and oxygen isotope documentation for a series of zircon standards: Chemical Geology, v. 205, p. 115–140, doi: 10.1016/j.chemgeo.2004.01.003.

Blodgett, R.B., Rohr, D.M., and Boucot, A.J., 2002, Paleozoic links among some Alaskan accreted terranes and Siberia based on megafossils, *in* Miller, E.L., Grantz, A., and

Klemperer, S.L. eds., Tectonic Evolution of the Bering Shelf–Chukchi Sea–Arctic Margin and Adjacent Landmasses, Geological Society of America Special Paper 360, p. 272–290.

Cox, G.M., Strauss, J. V., Halverson, G.P., Schmitz, M.D., McClelland, W.C., Stevenson, R.S., and Macdonald, F. a., 2015, Kikiktat volcanics of Arctic Alaska--Melting of harzburgitic mantle associated with the Franklin large igneous province: Lithosphere, v. 7, no. 3, p. 275–295, doi: 10.1130/L435.1.

Dumitru, T.A., Elder, W.P., Hourigan, J.K., Chapman, A.D., Graham, S.A., and Wakabayashi, J., 2016, Four Cordilleran paleorivers that connected Sevier thrust zones in Idaho to depocenters in California, Washington, Wyoming, and, indirectly, Alaska: Geology, v. 44, no. 1, p. 75–78, doi: 10.1130/G37286.1.

Dutro Jr., J.T., Brosgé, W.P., and Reiser, H.N., 1972, Significance of recently discovered Cambrian fossils and reinterpretation of Neruokpuk Formation, northeastern Alaska: American Association of Petroleum Geologists Bulletin, v. 56, p. 808–815.

Hoffman, H.J., Cecile, M.P., and Lane, L.S., 1994, New occurrences of Oldhamia and other trace fossils in the Cambrian of the Yukon and Ellesmere Island, arctic Canada: Canadian Journal of Earth Sciences, v. 31, p. 767–782, doi: 10.1139/e94-070.

Lane, L.S., 1991, The pre-Mississippian "Neruokpuk Formation," northeastern Alaska and northwestern Yukon: review and new regional correlation: Canadian Journal of Earth Sciences, v. 28, no. 10, p. 1521–1533.

Lane, L.S., and Cecile, M.P., 1989, Stratigraphy and structure of the Neruokpuk Formation, northern Yukon, *in* Current Research, Part G: Frontier Geoscience program, Arctic Canada, Geological Survey of Canada, Ottawa, ON, Canada, p. 57–62.

Lane, L.S., Gehrels, G.E., and Layer, P.W., 2016, Provenance and paleogeography of the Neruokpuk Formation, northwest Laurentia: An integrated synthesis: Geological Society of America Bulletin, v. 1, p. 239-257, doi: 10.1130/B31234.1.

Lane, L.S., Kelley, J.S., and Wrucke, C.T., 1995, Stratigraphy and structure of the Clarence River area, Yukon–Alaska north slope: a USGS-GSC co-operative project: Current research: Part E: Geological Survey of Canada Paper 1995-E, p. 1–9.

Leffingwell, E. de K., 1919, The Canning River region, northern Alaska: U.S. Geological Survey Professional Paper 109, 251 p.

Lenz, A.C., and Perry, D.G., 1972, The Neruokpuk Formation of the Barn Mountains and Driftwood Hills, northern Yukon: Its age and graptolite fauna: Canadian Journal of Earth Sciences, v. 9, p. 1129–1138, doi: 10 .1139 /e72 -098.

Ludwig, K.R., 2012, User's Manual for Isoplot/Ex, Version 3.75: A Geochronological Toolkit for Microsoft Excel: Berkeley Geochronology Center Special Publication 5, Berkeley.

Moore, T.E., and Churkin Jr., M., 1984, Ordovician and Silurian graptolite discoveries from the Neruokpuk Formation (sensu lato), northeastern and central Brooks Range, Alaska, *in* Blodgett, R.B. ed., Paleozoic geology of Alaska and northwestern Canada newsletter, Alaska Geological Society, p. 21–23.

Moore, T.E., Wallace, W.K., Bird, K.J., Karl, S.M., Mull, C.G., and Dillon, J.T., 1994, Geology of northern Alaska, *in* Plafker, G. and Berg, H.C. eds., The Geology of Alaska, Geological Society of America, The Geology of North America, v. G-1, Boulder, Colorado, p. 49–140.

Martin, A.J., Copeland, P., and Benowitz, J.A., 2015, Muscovite 40Ar/39Ar ages help reveal the Neogene tectonic evolution of the southern Annapurna Range, central

Nepal, *in* Mukherjee, S., Carosi, R., van der Beek, P.A., Murkherjee, B.K., and Robinson, D.M. eds., Tectonics of the Himalaya, Geological Society of London, Special Publications 412, p. 199–220.

McDougall, I., and Harrison, M.T., 1989, Geochronology and Thermochronology by the 40Ar/39Ar method-2nd ed.: Oxford University Press, New York.

Norris, D.K., 1986, Lower Devonian Road River Formation on the north flank of Romanzof Uplift, northern Yukon Territory, *in* Current Research, Part A: Geological Survey of Canada Paper 86-1A, p. 801–802.

Paces, J.B., and Miller, J.D., 1993, Precise U-Pb ages of Duluth Complex and related mafic intrusions, northern Minnesota: geochronological insights to physical, petrogenic, paleomagnetic, and tectonomagmatic processes associated with the 1.1 Ga midcontinent rift system: Journal of Geophysical Research: Solid Earth, v. 98, p. 13,977–14,013, doi: 10.1029/9.

Paton, C., Woodhead, J.D., Hellstrom, J.C., Hergt, J.M., Greig, A., and Maas, R., 2010, Improved laser ablation U-Pb zircon geochronology through robust downhole fractionation correction: Geochemistry, Geophysics, Geosystems, v. 11, no. 3, doi: 10.1029/2009GC002618.

Reiser, H.N., Brouwers, E., Dutro Jr., J.T., and Detterman, R.L., 1980, Geologic map of the Demarcation Point Quadrangle, Alaska: U.S. Geological Survey Map I-1133, scale 1:250000, 1 sheet.

Renne, P.R., Mundil, R., Balco, G., Min, K.W., and Ludwig, K.R., 2010, Joint determination of K-40 decay constants and Ar-40*/K-40 for the Fish Canyon sanidine standard, and

improved accuracy for $^{40}Ar/^{39}Ar$ geochronology: Geochimica Et Cosmochimica Acta, v. 74, p. 5349–5367.

Samson, S.D., and Alexander, E.C., 1987, Calibration of the interlaboratory 40Ar39Ar dating standard, MMhb-1: Chemical Geology: Isotope Geoscience Section, v. 66, no. 1-2, p. 27–34, doi: 10.1016/0168-9622(87)90025-X.

Sharman, G.R., Graham, S.A., Grove, M., and Hourigan, J.K., 2013, A reappraisal of the early slip history of the San Andreas fault, central California, USA: Geology, v. 41, no. 7, p. 727–730, doi: 10.1130/G34214.1.

Sláma, J., Košler, I., Condon, D.J., Crowley, J.L., Gerdes, A., Hanchar, J.M., Horstwood, M.S.A., Morris, G.A., Nasdala, L., Norberg, N., Schaltegger, U., Schoene, B., Tubrett, M.N., and Whitehouse, M.J., 2008, Plešovice zircon - A new natural reference material for U-Pb and Hf isotopic microanalysis: Chemical Geology, v. 249, no. 1-2, p. 1–35, doi: 10.1016/j.chemgeo.2007.11.005.

Spell, T.L., and McDougall, I., 2003, Characterization and calibration of 40Ar/39Ar dating standards: Chemical Geology, v. 198, no. 3-4, p. 189–211, doi: 10.1016/S0009-2541(03)00005-6.

Stacey, J.S., and Kramers, J.D., 1975, Approximation of terrestrial lead isotope evolution by a two-stage model: Earth and Planetary Science Letters, v. 26, p. 207–221, doi: 10.1016/0012-821X(75)90088-6.

Whitehouse, M.J., and Kamber, B.S., 2005, Assigning dates to thin gneissic veins in high-grade metamorphic terranes: A cautionary tale from Akilia, southwest Greenland: Journal of Petrology, v. 46, no. 2, p. 291–318, doi: 10.1093/petrology/egh075.

Whitehouse, M.J., Kamber, B.S., and Moorbath, S., 1999, Age significance of U-Th-Pb zircon data from early Archaean rocks of west Greenland - a reassessment based on combined ion-microprobe and imaging studies: Chemical Geology, v. 160, no. 3, p. 201–224, doi: 10.1016/S0009-2541(99)00066-2.

York, D., Hall, C.M., Yanase, Y., and Hanes, J.A., 1981, $^{40}Ar/^{39}Ar$ dating of terrestrial minerals with a continuous laser: Geophysical Research Letters, v. 8, no. 11, p. 1136–1138.

TABLE SM2.1: SAMPLE LOCATIONS FROM THE NE BROOKS RANGE, AK

Sample Name	Latitude	Longitude	Predesignated Map Unit	Analysis
Neruokpuk Formation or Firth River group				
12JT10	N 69.157950	W 141.864928	Css*	U-Pb detrital zircon
12JT11	N 69.192398	W 141.868887	pCn*	U-Pb detrital zircon
12JT12	N 69.227013	W 141.831267	pCn*	40Ar/39Ar muscovite
12JT13a	N 69.387220	W 141.535461	pCn*	40Ar/39Ar muscovite
12JT31	N 69.387220	W 141.535461	pCpa*	U-Pb detrital zircon
12JT32	N 69.424719	W 141.508195	pCn*	U-Pb detrital zircon
05LF13	N 69.185356	W 142.664228	pCn*	U-Pb detrital zircon
11LF13	N 69.263494	W 142.657930	pCn*	U-Pb detrital zircon
28LF13	N 69.357533	W 142.858018	pCn*	U-Pb detrital zircon
37LF13	N 69.357257	W 142.921486	pCn*	U-Pb detrital zircon
J1355-617	N 69.219592	W 140.949294	Css**	U-Pb detrital zircon
Clarence River group				
12JT22	N 69.279048	W 141.727346	Cp*	U-Pb detrital zircon
12JT23	N 69.279912	W 141.747478	Cp*	U-Pb detrital zircon
12JT24	N 69.279912,	W 141.747478	Cp*	40Ar/39Ar muscovite & U-Pb detrital zircon
12JT35	N 69.469365	W 141.469672	Os or Ovc*	U-Pb detrital zircon
09LF13	N 69.264435	W 142.657912	Ccp or Css*	40Ar/39Ar muscovite
40LF13	N 69.375307	W 142.912505	Cp*	40Ar/39Ar muscovite & U-Pb detrital zircon
14BJ27	N 69.117975	W 143.238008	Cp or Css*	40Ar/39Ar muscovite

*Map units designated by Reiser et al. (1980)

**Map units designated by Lane et al. (1995)

TABLE SM2.2. GEOCHRONOLOGICAL AND FOSSIL AGE CONSTRAINTS

Formation/unit	Data localities (see Fig. 2)	Age/Biostratigraphy	Description	Reference
Kikiktat volcanics	1	Neoproterozoic (719.47 ± 0.29 Ma)	U-Pb age on detrital zircons by chemical abrasion–thermal ionization mass spectrometry (TIMS) from a volcanoclastic sample directly overlying basaltic flows of the Kikiktat volcanics	Cox et al., 2015
Nanook Limestone	2	Cambrian–Ordovician	Fossil collections: conodont *Clavohamulus densus* , trilobite *Plethopeltis armatus* , trilobite genus *Paraplethopeltis* , brachiopod and gastropod genera *Tcherskidium* n. sp. and *Eoconchidium*	Blodgett et al., 2002; 2002; Strauss et al., 2013
Neruokpuk Formation	3 and 4	Lower–Middle Cambrian	*Oldhamia* trace fossil assemblages from green and maroon argillite units in the British and Barn mountains of Yukon	Hoffman et al., 1994, Lane and Cecile, 1989
Whale Mountain volcanic rocks	5	Upper Cambrian (Furongian)	Fossil collections: trilobite genera *Geragnostus* sp., *Saratogia* sp. ; brachiopod genus *Billingsella* sp.	Dutro et al., 1972
Romanzof chert	6	Middle Ordovician–Llandovery	Fossil collections: graptolite genera *Climacograptus* sp, cf. *hughesi, Retiograptus geinitzlanus?, Orthograptus?, and Didymograptus?*	Moore and Churkin, 1984
Clarence River group	7	Cambrian(?)	Echinodem debris	Reiser et al., 1980
	8	Ordovician	Fossil collections: graptolite genera Orthograptus of the O. quadrium-cronatus type	Reiser et al., 1980
	9	Lower Ordovician and Silurian	Fossil collections: graptolite genera *Monograptus* sp., *Didymograptus* sp., *Goniograptus* sp., *Tetragraptus* sp.	Lane and Cecile, 1989

TABLE SM2.2. GEOCHRONOLOGICAL AND FOSSIL AGE CONSTRAINTS

Formation/unit	Data localities (see Fig. 2)	Age/Biostratigraphy	Description	Reference
	10	Ordovician and Silurian	Fossil collections: graptolite genera *Monograptus* sp., *Neodiversograptus* sp., *Dicellograptus* sp., *Paraglossograptus* sp., *Isograptus* sp., *Didymograptus* sp., *Goniograptus* sp., *Tetragraptus* sp.	Lenz and Perry, 1972
	11	Pridoli	Fossil collections: graptolite genera *Monograptus* cf., *M. transgrediens praecipuus*	Norford, 1997
Clarence River group	12	Early Devonian(?)	Conodont genus *Polygnathus* sp., with a Color Alteration Index of 5	Norris, 1986
Ulungarat Formation	13	Middle Devonian	Fossil collections: brachiopod genera *Warrenella(?)* sp., *Goniophoria* sp.; trilobite genus *Dechenella* sp.	Reiser et al., 1980
Devonian plutonic rocks	14 and 15	Late Devonian (380–360 Ma)	Pb-alpha, U–Pb zircon, and U–Pb titanite ages from the Mount Sedgwick pluton in northern Yukon and the Okpilak batholith in Alaska	Sable, 1977; Mortensen and Bell, 1991; Dillon et al., 1987

TABLE SM2.3: LA-ICPMS U-PB ISOTOPIC DATA (UC SANTA CRUZ LAB)

						Isotope ratios					Apparent ages (Ma)								
Analysis	U	U/Th	206Pb*	±	error	207Pb*	±	206Pb*	±	error	206Pb*	±	207Pb*	±	206Pb*	±	Best age	±	Conc
	(ppm)		207Pb*	(%)	corr.	235U*	(%)	238U	(%)	corr.	238U*	(Ma)	235U	(Ma)	207Pb*	(Ma)	(Ma)	(Ma)	(%)
12JT10; Neruokpuk Formation (N69.12, W141.90)																			
12JT10_83	166	1.5	0.066	0.360	0.2	0.93	6.7	0.103	0.5	0.24	632	29	664	35	790	120	632	29	80
12JT10_51	152	2.7	0.071	0.370	0.2	1.55	11.0	0.157	0.7	0.31	937	41	947	44	990	110	937	41	95
12JT10_87	90	1.3	0.075	0.410	0.3	1.73	13.0	0.168	0.8	0.34	1002	45	1016	48	1060	110	1060	110	95
12JT10_42	526	3.0	0.080	0.370	0.2	2.04	14.0	0.185	0.9	0.51	1095	47	1127	45	1183	91	1183	91	93
12JT10_82	307	1.4	0.086	0.400	0.3	2.58	17.0	0.216	1.0	0.51	1263	53	1294	48	1346	89	1346	89	94
12JT10_34	127	2.0	0.090	0.430	0.2	2.90	20.0	0.234	1.1	0.42	1358	57	1386	51	1413	93	1413	93	96
12JT10_99	143	2.2	0.090	0.450	0.4	3.19	22.0	0.256	1.2	0.23	1473	61	1462	52	1418	93	1418	93	104
12JT10_71	305	2.7	0.090	0.420	0.1	2.92	20.0	0.242	1.1	0.60	1396	58	1388	51	1424	88	1424	88	98
12JT10_73	223	2.4	0.090	0.430	0.2	2.95	20.0	0.237	1.1	0.39	1370	57	1395	52	1426	88	1426	88	96
12JT10_45	95	1.0	0.101	0.490	0.2	3.77	26.0	0.271	1.3	0.46	1543	65	1581	56	1626	92	1626	92	95
12JT10_64	66	1.3	0.108	0.540	0.3	4.52	31.0	0.309	1.5	0.40	1742	74	1730	57	1754	95	1754	95	99
12JT10_95	67	0.5	0.109	0.550	0.3	4.73	33.0	0.314	1.5	0.44	1759	74	1774	58	1760	91	1760	91	100
12JT10_80	242	1.8	0.108	0.500	0.3	4.58	30.0	0.303	1.4	0.58	1707	70	1745	55	1768	84	1768	84	97
12JT10_15	48	2.0	0.108	0.540	0.3	4.82	34.0	0.321	1.6	0.49	1797	77	1781	58	1770	92	1770	92	102
12JT10_56	114	1.7	0.109	0.520	0.3	4.58	31.0	0.298	1.4	0.48	1681	70	1746	56	1786	87	1786	87	94
12JT10_63	112	1.4	0.110	0.530	0.3	4.52	31.0	0.303	1.4	0.47	1708	72	1738	54	1792	88	1792	88	95
12JT10_79	141	0.7	0.110	0.510	0.3	4.66	31.0	0.299	1.4	0.49	1690	69	1758	56	1793	85	1793	85	94
12JT10_47	113	0.9	0.110	0.530	0.4	4.68	31.0	0.309	1.4	0.37	1734	72	1759	56	1796	87	1796	87	97
12JT10_43	329	1.9	0.110	0.500	0.2	4.58	30.0	0.304	1.4	0.56	1711	69	1746	55	1797	82	1797	82	95
12JT10_88	240	2.5	0.111	0.510	0.2	4.85	32.0	0.320	1.5	0.66	1790	73	1790	56	1805	84	1805	84	99
12JT10_66	195	3.7	0.111	0.520	0.3	4.61	31.0	0.315	1.5	0.49	1767	72	1753	56	1808	87	1808	87	98
12JT10_69	357	2.5	0.111	0.500	0.2	4.67	31.0	0.318	1.5	0.62	1779	72	1765	55	1808	83	1808	83	98
12JT10_25	111	1.7	0.111	0.530	0.3	4.69	32.0	0.304	1.4	0.41	1716	70	1767	57	1810	85	1810	85	95
12JT10_20	137	1.1	0.111	0.520	0.2	4.82	32.0	0.309	1.4	0.51	1737	72	1787	55	1813	86	1813	86	96
12JT10_30	240	1.7	0.111	0.510	0.2	4.81	32.0	0.304	1.4	0.63	1711	69	1783	56	1816	81	1816	81	94
12JT10_41	154	1.1	0.111	0.530	0.2	4.65	31.0	0.306	1.4	0.48	1724	72	1759	57	1816	88	1816	88	95

TABLE SM2.3: LA-ICPMS U-PB ISOTOPIC DATA (UC SANTA CRUZ LAB)

						Isotope ratios					Apparent ages (Ma)								
Analysis	U	U/Th	206Pb*	±	error	207Pb*	±	206Pb*	±	error	206Pb*	±	207Pb*	±	206Pb*	±	Best age	±	Conc
	(ppm)		207Pb*	(%)	corr.	235U*	(%)	238U	(%)	corr.	238U*	(Ma)	235U	(Ma)	207Pb*	(Ma)	(Ma)	(Ma)	(%)
12JT10_16	101	0.6	0.111	0.540	0.2	4.85	33.0	0.313	1.5	0.45	1753	72	1790	57	1818	86	1818	86	96
12JT10_17	137	1.8	0.111	0.520	0.3	4.64	31.0	0.297	1.4	0.57	1677	69	1756	55	1820	85	1820	85	92
12JT10_54	96	0.9	0.112	0.540	0.2	4.76	32.0	0.303	1.4	0.51	1707	71	1774	56	1820	86	1820	86	94
12JT10_53	357	2.8	0.111	0.510	0.4	4.69	31.0	0.301	1.4	0.55	1696	68	1766	55	1821	82	1821	82	93
12JT10_38	222	0.5	0.112	0.510	0.2	4.52	30.0	0.292	1.4	0.49	1652	67	1735	54	1822	84	1822	84	91
12JT10_28	281	3.9	0.112	0.510	0.3	4.66	31.0	0.298	1.4	0.56	1681	68	1759	54	1822	84	1822	84	92
12JT10_39	156	1.5	0.112	0.540	0.2	4.57	31.0	0.293	1.4	0.55	1657	69	1740	57	1823	89	1823	89	91
12JT10_8	111	1.3	0.112	0.530	0.2	4.95	33.0	0.328	1.5	0.46	1827	75	1814	58	1824	86	1824	86	100
12JT10_44	268	1.4	0.112	0.510	0.2	4.73	31.0	0.307	1.4	0.56	1723	70	1770	56	1832	83	1832	83	94
12JT10_40	68	0.8	0.112	0.560	0.3	4.64	32.0	0.297	1.4	0.43	1673	71	1755	58	1833	89	1833	89	91
12JT10_7	149	1.3	0.112	0.530	0.2	4.87	33.0	0.319	1.5	0.53	1787	72	1794	55	1838	84	1838	84	97
12JT10_96	88	1.3	0.112	0.550	0.3	5.01	34.0	0.322	1.5	0.36	1797	74	1828	56	1848	93	1848	93	97
12JT10_21	106	1.2	0.113	0.540	0.2	4.73	32.0	0.303	1.4	0.45	1702	70	1779	57	1849	88	1849	88	92
12JT10_62	130	2.2	0.113	0.520	0.2	4.73	32.0	0.306	1.4	0.58	1720	71	1770	56	1851	85	1851	85	93
12JT10_55	39	0.7	0.115	0.590	0.4	4.85	34.0	0.306	1.5	0.41	1726	75	1797	61	1854	99	1854	99	93
12JT10_75	59	1.2	0.115	0.570	0.2	5.08	35.0	0.314	1.5	0.51	1758	74	1829	59	1882	91	1882	91	93
12JT10_85	199	2.3	0.116	0.540	0.3	5.13	34.0	0.322	1.5	0.52	1797	74	1839	57	1893	84	1893	84	95
12JT10_26	253	2.4	0.116	0.530	0.1	5.20	34.0	0.316	1.5	0.59	1772	70	1849	56	1899	82	1899	82	93
12JT10_65	54	0.6	0.117	0.590	0.2	5.26	37.0	0.335	1.7	0.53	1861	79	1853	61	1903	92	1903	92	98
12JT10_48	251	1.2	0.117	0.540	0.4	5.20	34.0	0.325	1.5	0.52	1817	76	1855	57	1904	82	1904	82	95
12JT10_57	107	0.9	0.117	0.560	0.3	5.16	35.0	0.314	1.5	0.49	1758	72	1846	58	1906	86	1906	86	92
12JT10_46	75	2.2	0.117	0.570	0.1	5.03	35.0	0.312	1.5	0.51	1750	72	1828	61	1911	90	1911	90	92
12JT10_10	158	2.5	0.117	0.540	0.2	5.59	37.0	0.353	1.6	0.59	1946	78	1915	57	1911	83	1911	83	102
12JT10_94	239	1.3	0.117	0.540	0.3	5.41	36.0	0.333	1.5	0.55	1849	74	1885	57	1912	81	1912	81	97
12JT10_12	159	1.7	0.118	0.540	0.2	5.38	36.0	0.336	1.5	0.56	1866	76	1882	56	1917	85	1917	85	97
12JT10_77	277	1.9	0.119	0.540	0.3	5.40	36.0	0.321	1.5	0.56	1793	72	1886	57	1935	82	1935	82	93
12JT10_98	237	0.9	0.119	0.540	0.2	5.76	38.0	0.348	1.6	0.59	1926	78	1936	58	1936	85	1936	85	99
12JT10_86	113	2.0	0.119	0.560	0.2	5.15	35.0	0.317	1.5	0.55	1772	73	1848	59	1938	85	1938	85	91

TABLE SM2.3: LA-ICPMS U-PB ISOTOPIC DATA (UC SANTA CRUZ LAB)

						Isotope ratios					Apparent ages (Ma)								
Analysis	U	U/Th	206Pb*	±	error	207Pb*	±	206Pb*	±	error	206Pb*	±	207Pb*	±	206Pb*	±	Best age	±	Conc
	(ppm)		207Pb*	(%)	corr.	235U*	(%)	238U	(%)	corr.	238U*	(Ma)	235U	(Ma)	207Pb*	(Ma)	(Ma)	(Ma)	(%)
12JT10_74	105	1.1	0.120	0.590	0.2	5.34	37.0	0.320	1.5	0.38	1791	73	1873	57	1938	85	1938	85	92
12JT10_36	120	2.1	0.119	0.570	0.3	4.81	33.0	0.291	1.5	0.70	1644	73	1779	58	1939	87	1939	87	85
12JT10_6	80	0.7	0.119	0.580	0.4	5.75	39.0	0.353	1.7	0.36	1947	79	1937	58	1940	84	1940	84	100
12JT10_58	1021	1.9	0.121	0.540	0.2	5.01	33.0	0.295	1.4	0.74	1668	68	1821	55	1966	80	1966	80	85
12JT10_100	361	0.9	0.124	0.560	0.3	5.33	35.0	0.312	1.5	0.70	1751	72	1872	56	2004	81	2004	81	87
12JT10_81	73	1.5	0.126	0.620	0.3	5.97	41.0	0.342	1.7	0.52	1894	79	1969	57	2040	84	2040	84	93
12JT10_11	103	1.9	0.127	0.600	0.3	6.43	43.0	0.367	1.7	0.49	2020	82	2033	59	2048	82	2048	82	99
12JT10_13	68	0.6	0.127	0.870	0.1	5.07	43.0	0.297	1.6	0.48	1676	81	1814	72	2050	130	2050	130	82
12JT10_76	235	4.6	0.127	0.570	0.4	6.25	41.0	0.350	1.6	0.53	1935	78	2010	58	2051	81	2051	81	94
12JT10_19	372	2.6	0.127	0.580	0.3	6.38	42.0	0.358	1.7	0.53	1973	78	2028	57	2056	80	2056	80	96
12JT10_78	161	1.4	0.128	0.590	0.2	6.30	42.0	0.348	1.7	0.63	1924	79	2020	59	2069	82	2069	82	93
12JT10_37	157	2.8	0.130	0.610	0.4	6.03	40.0	0.338	1.6	0.50	1878	78	1982	56	2098	80	2098	80	90
12JT10_27	51	1.2	0.137	0.680	0.3	7.00	48.0	0.362	1.8	0.47	1993	82	2105	61	2179	87	2179	87	91
12JT10_61	319	4.8	0.138	0.660	0.2	6.11	41.0	0.321	1.5	0.35	1795	74	1990	59	2192	85	2192	85	82
12JT10_9	110	1.4	0.140	0.650	0.1	7.82	52.0	0.417	2.0	0.63	2248	89	2217	62	2220	81	2220	81	101
12JT10_29	59	0.9	0.145	0.700	0.2	8.20	56.0	0.403	2.0	0.59	2184	91	2253	63	2292	83	2292	83	95
12JT10_4	179	1.3	0.146	0.660	0.2	8.59	57.0	0.437	2.0	0.65	2336	91	2296	59	2294	79	2294	79	102
12JT10_22	248	3.2	0.145	0.660	0.2	8.04	53.0	0.393	1.8	0.67	2137	84	2238	60	2295	77	2295	77	93
12JT10_68	156	1.9	0.148	0.680	0.2	8.10	54.0	0.414	1.9	0.63	2235	87	2242	61	2318	78	2318	78	96
12JT10_93	64	1.1	0.147	0.710	0.3	8.65	59.0	0.428	2.1	0.54	2296	93	2303	63	2319	82	2319	82	99
12JT10_2	117	1.0	0.148	0.690	0.2	8.89	59.0	0.445	2.1	0.66	2369	93	2327	62	2323	80	2323	80	102
12JT10_23	108	0.7	0.149	0.690	0.2	8.59	58.0	0.409	1.9	0.61	2211	88	2294	60	2326	81	2326	81	95
12JT10_84	78	1.6	0.149	0.710	0.3	8.37	57.0	0.407	1.9	0.50	2207	88	2272	60	2327	81	2327	81	95
12JT10_33	119	1.6	0.149	0.690	0.3	8.04	54.0	0.388	1.8	0.54	2115	85	2235	60	2339	81	2339	81	90
12JT10_1	100	1.5	0.150	0.700	0.3	9.33	62.0	0.454	2.2	0.62	2413	95	2366	62	2342	81	2342	81	103
12JT10_50	132	1.2	0.150	0.690	0.4	8.38	56.0	0.406	1.9	0.51	2198	85	2272	60	2345	79	2345	79	94
12JT10_60	299	1.4	0.152	0.690	0.3	8.77	58.0	0.410	1.9	0.66	2217	87	2315	58	2371	76	2371	76	94
12JT10_31	131	1.4	0.154	0.710	0.3	8.48	57.0	0.393	1.9	0.53	2136	85	2284	60	2395	79	2395	79	89

TABLE SM2.3: LA-ICPMS U-PB ISOTOPIC DATA (UC SANTA CRUZ LAB)

						Isotope ratios					Apparent ages (Ma)								
Analysis	U	U/Th	206Pb*	±	error	207Pb*	±	206Pb*	±	error	206Pb*	±	207Pb*	±	206Pb*	±	Best age	±	Conc
	(ppm)		207Pb*	(%)	corr.	235U*	(%)	238U	(%)	corr.	238U*	(Ma)	235U	(Ma)	207Pb*	(Ma)	(Ma)	(Ma)	(%)
12JT10_59	84	1.5	0.154	0.730	0.2	8.85	60.0	0.408	1.9	0.64	2203	89	2318	63	2397	79	2397	79	92
12JT10_91	312	1.8	0.163	0.730	0.3	9.90	65.0	0.441	2.0	0.72	2353	92	2425	61	2483	77	2483	77	95
12JT10_70	313	3.8	0.170	0.760	0.3	10.69	70.0	0.477	2.2	0.73	2513	96	2495	61	2554	76	2554	76	98
12JT10_35	273	1.3	0.171	0.780	0.2	10.59	70.0	0.443	2.1	0.73	2367	94	2489	63	2569	76	2569	76	92
12JT10_90	169	2.8	0.172	0.780	0.4	11.08	73.0	0.473	2.2	0.61	2495	97	2532	60	2570	76	2570	76	97
12JT10_14	111	1.2	0.172	0.790	0.3	11.28	75.0	0.474	2.2	0.65	2500	96	2547	61	2576	77	2576	77	97
12JT10_92	229	1.9	0.174	0.780	0.1	11.40	75.0	0.475	2.2	0.76	2505	96	2556	60	2592	76	2592	76	97
12JT10_3	168	2.6	0.175	0.810	0.2	11.67	78.0	0.493	2.3	0.59	2580	100	2578	62	2599	78	2599	78	99
12JT10_49	211	3.6	0.175	0.800	0.3	11.20	74.0	0.465	2.2	0.66	2459	95	2540	61	2608	74	2608	74	94
12JT10_72	61	1.3	0.177	0.830	0.2	11.32	77.0	0.465	2.2	0.67	2458	99	2548	64	2616	77	2616	77	94
12JT10_24	432	0.6	0.178	0.800	0.2	11.16	73.0	0.444	2.1	0.79	2370	91	2535	62	2630	75	2630	75	90
12JT10_67	102	1.5	0.183	0.840	0.3	12.01	80.0	0.491	2.3	0.64	2580	100	2605	62	2674	75	2674	75	96
12JT10_5	109	1.0	0.182	0.830	0.3	12.52	83.0	0.509	2.4	0.66	2650	100	2643	63	2677	73	2677	73	99
12JT10_52	44	2.6	0.184	0.880	0.1	11.81	82.0	0.464	2.3	0.70	2454	99	2583	65	2680	80	2680	80	92
12JT10_97	54	1.8	0.183	0.860	0.2	13.13	90.0	0.517	2.5	0.71	2680	110	2685	64	2681	79	2681	79	100
12JT10_32	84	0.8	0.237	1.100	0.3	18.70	120.0	0.565	2.7	0.63	2890	110	3026	64	3103	73	3103	73	93
>20% Discordance																			
12JT10_89	1087	2.2	0.174	0.780	0.3	2.99	20.0	0.124	0.6	0.75	756	33	1405	49	2591	75	756	33	29
12JT11; Neruokpuk Formation (N69.16, W141.87)																			
12JT11_67	537	4.0	0.077	0.350	0.2	1.76	11.0	0.169	0.7	0.44	1008	41	1028	41	1115	92	1115	92	90
12JT11_71	89	2.0	0.087	0.440	0.3	2.47	17.0	0.206	1.0	0.36	1205	51	1260	50	1380	100	1380	100	87
12JT11_24	101	2.3	0.091	0.460	0.3	2.91	20.0	0.233	1.1	0.30	1349	55	1381	53	1420	100	1420	100	95
12JT11_4	319	3.0	0.092	0.420	0.3	3.13	20.0	0.251	1.1	0.49	1444	56	1441	48	1462	86	1462	86	99
12JT11_45	384	5.8	0.093	0.410	0.2	2.91	19.0	0.229	1.0	0.55	1330	53	1385	48	1474	84	1474	84	90
12JT11_31	248	1.8	0.093	0.420	0.3	3.15	20.0	0.244	1.1	0.47	1406	55	1447	49	1485	88	1485	88	95
12JT11_68	143	1.4	0.102	0.480	0.3	3.57	23.0	0.257	1.2	0.45	1477	60	1543	52	1649	87	1649	87	90
12JT11_36	271	2.2	0.107	0.480	0.2	4.52	29.0	0.302	1.3	0.53	1704	66	1735	52	1743	83	1743	83	98

TABLE SM2.3: LA-ICPMS U-PB ISOTOPIC DATA (UC SANTA CRUZ LAB)

						Isotope ratios					Apparent ages (Ma)								
Analysis	U	U/Th	206Pb*	±	error	207Pb*	±	206Pb*	±	error	206Pb*	±	207Pb*	±	206Pb*	±	Best age	±	Conc
	(ppm)		207Pb*	(%)	corr.	235U*	(%)	238U	(%)	corr.	238U*	(Ma)	235U	(Ma)	207Pb*	(Ma)	(Ma)	(Ma)	(%)
12JT11_40	76	1.9	0.109	0.550	0.3	4.68	32.0	0.310	1.4	0.41	1743	69	1763	55	1790	93	1790	93	97
12JT11_2	77	1.2	0.110	0.540	0.2	4.95	34.0	0.330	1.5	0.56	1836	73	1805	57	1800	90	1800	90	102
12JT11_1	206	1.7	0.111	0.500	0.2	4.94	32.0	0.324	1.4	0.53	1810	69	1805	55	1811	83	1811	83	100
12JT11_81	273	1.4	0.111	0.500	0.2	4.46	28.0	0.295	1.3	0.58	1664	65	1721	53	1823	80	1823	80	91
12JT11_39	102	1.4	0.113	0.540	0.3	4.95	33.0	0.317	1.4	0.48	1775	70	1803	56	1826	87	1826	87	97
12JT11_79	63	1.3	0.112	0.570	0.2	4.51	31.0	0.299	1.4	0.51	1683	68	1730	58	1828	91	1828	91	92
12JT11_26	292	2.4	0.112	0.500	0.2	4.96	32.0	0.317	1.4	0.58	1774	67	1811	54	1833	82	1833	82	97
12JT11_94	167	1.3	0.112	0.510	0.2	4.57	29.0	0.301	1.3	0.54	1694	66	1744	55	1837	84	1837	84	92
12JT11_16	244	1.9	0.113	0.530	0.3	5.16	34.0	0.329	1.5	0.54	1829	72	1849	56	1842	83	1842	83	99
12JT11_14	290	2.3	0.113	0.500	0.2	5.14	33.0	0.333	1.5	0.63	1850	71	1843	54	1846	79	1846	79	100
12JT11_3	93	1.0	0.114	0.540	0.2	5.37	35.0	0.347	1.6	0.47	1919	75	1880	55	1847	88	1847	88	104
12JT11_110	128	2.2	0.114	0.520	0.2	4.72	31.0	0.303	1.4	0.61	1706	67	1770	55	1857	83	1857	83	92
12JT11_89	188	1.4	0.115	0.530	-0.1	4.22	30.0	0.276	1.4	0.85	1574	71	1666	62	1863	84	1863	84	84
12JT11_101	470	3.4	0.115	0.500	0.3	4.79	30.0	0.304	1.3	0.61	1710	66	1782	53	1877	77	1877	77	91
12JT11_93	275	8.0	0.116	0.520	0.3	4.88	31.0	0.309	1.4	0.53	1737	66	1796	53	1888	81	1888	81	92
12JT11_15	127	2.8	0.117	0.540	0.4	5.36	35.0	0.336	1.5	0.32	1866	72	1876	56	1891	85	1891	85	99
12JT11_57	406	4.0	0.116	0.510	0.2	4.95	31.0	0.311	1.4	0.60	1748	68	1809	54	1899	78	1899	78	92
12JT11_109	51	1.7	0.117	0.600	0.3	5.14	36.0	0.320	1.5	0.48	1785	75	1837	59	1904	95	1904	95	94
12JT11_99	72	1.3	0.118	0.580	0.3	5.11	34.0	0.317	1.5	0.39	1773	72	1836	57	1907	92	1907	92	93
12JT11_37	100	1.0	0.117	0.550	0.3	5.43	36.0	0.340	1.5	0.47	1883	74	1894	56	1909	88	1909	88	99
12JT11_17	465	4.1	0.117	0.510	0.3	5.53	35.0	0.344	1.5	0.62	1905	72	1905	53	1909	78	1909	78	100
12JT11_61	200	2.7	0.117	0.530	0.4	5.18	33.0	0.324	1.4	0.49	1809	69	1847	54	1910	81	1910	81	95
12JT11_27	440	1.9	0.117	0.540	0.2	5.42	35.0	0.334	1.5	0.62	1856	73	1890	56	1913	82	1913	82	97
12JT11_73	220	0.6	0.118	0.530	0.3	4.87	31.0	0.309	1.4	0.49	1735	67	1799	52	1918	81	1918	81	90
12JT11_69	569	4.2	0.118	0.510	0.2	4.96	31.0	0.310	1.4	0.71	1741	66	1811	53	1920	79	1920	79	91
12JT11_49	228	3.3	0.118	0.520	0.4	5.20	33.0	0.323	1.4	0.48	1804	70	1854	54	1920	80	1920	80	94
12JT11_97	334	1.8	0.118	0.520	0.1	5.00	32.0	0.308	1.3	0.68	1734	67	1821	55	1924	80	1924	80	90
12JT11_46	240	2.2	0.118	0.530	0.3	5.09	32.0	0.314	1.4	0.62	1762	68	1833	54	1925	81	1925	81	92

TABLE SM2.3: LA-ICPMS U-PB ISOTOPIC DATA (UC SANTA CRUZ LAB)

						Isotope ratios					Apparent ages (Ma)								
Analysis	U	U/Th	206Pb*	±	error	207Pb*	±	206Pb*	±	error	206Pb*	±	207Pb*	±	206Pb*	±	Best age	±	Conc
	(ppm)		207Pb*	(%)	corr.	235U*	(%)	238U	(%)	corr.	238U*	(Ma)	235U	(Ma)	207Pb*	(Ma)	(Ma)	(Ma)	(%)
12JT11_13	97	1.0	0.118	0.620	0.3	5.63	40.0	0.349	1.7	0.48	1931	82	1916	60	1925	95	1925	95	100
12JT11_70	75	0.4	0.119	0.560	0.2	5.02	33.0	0.314	1.5	0.59	1761	70	1826	55	1929	86	1929	86	91
12JT11_75	210	0.6	0.119	0.540	0.3	4.97	32.0	0.310	1.4	0.52	1744	68	1812	54	1930	82	1930	82	90
12JT11_63	98	1.1	0.118	0.560	0.2	5.11	33.0	0.319	1.4	0.43	1784	69	1838	56	1930	83	1930	83	92
12JT11_91	136	0.5	0.119	0.540	0.3	5.04	32.0	0.311	1.4	0.45	1744	67	1822	54	1936	82	1936	82	90
12JT11_28	800	15.9	0.119	0.520	0.2	5.25	33.0	0.321	1.4	0.71	1793	69	1860	53	1936	78	1936	78	93
12JT11_9	111	0.7	0.120	0.560	0.2	5.58	36.0	0.342	1.5	0.45	1898	72	1915	57	1945	84	1945	84	98
12JT11_52	73	1.2	0.121	0.580	0.2	5.48	36.0	0.331	1.5	0.54	1842	73	1890	57	1958	86	1958	86	94
12JT11_106	423	3.6	0.121	0.530	0.2	4.80	30.0	0.288	1.3	0.71	1633	63	1784	54	1972	77	1972	77	83
12JT11_88	104	1.9	0.124	0.560	0.4	5.58	35.0	0.328	1.4	0.48	1829	71	1913	54	2024	79	2024	79	90
12JT11_54	122	2.1	0.128	0.590	0.3	6.28	40.0	0.359	1.6	0.48	1975	77	2013	56	2073	84	2073	84	95
12JT11_23	65	1.6	0.128	0.620	0.3	6.83	46.0	0.382	1.8	0.55	2080	83	2083	60	2082	87	2082	87	100
12JT11_80	132	1.3	0.130	0.600	0.2	5.88	38.0	0.335	1.5	0.54	1862	73	1961	56	2102	81	2102	81	89
12JT11_78	136	1.2	0.132	0.600	0.2	6.14	39.0	0.343	1.5	0.55	1899	73	1991	56	2114	79	2114	79	90
12JT11_66	91	2.1	0.131	0.610	0.3	5.92	38.0	0.333	1.5	0.52	1851	72	1962	56	2117	82	2117	82	87
12JT11_34	132	3.6	0.139	0.630	0.1	7.61	49.0	0.392	1.7	0.65	2131	81	2183	58	2201	78	2201	78	97
12JT11_100	200	1.4	0.139	0.620	0.1	7.04	45.0	0.369	1.6	0.68	2020	77	2114	56	2213	78	2213	78	91
12JT11_25	309	3.1	0.142	0.630	0.0	7.44	48.0	0.379	1.7	0.74	2070	79	2167	57	2244	77	2244	77	92
12JT11_76	157	3.5	0.142	0.640	0.3	7.05	45.0	0.367	1.6	0.52	2015	78	2116	57	2250	82	2250	82	90
12JT11_58	220	3.2	0.145	0.650	0.0	7.72	50.0	0.393	1.7	0.69	2137	79	2198	58	2289	77	2289	77	93
12JT11_30	522	4.1	0.147	0.640	0.2	8.49	54.0	0.416	1.8	0.74	2241	82	2284	56	2314	75	2314	75	97
12JT11_104	192	3.6	0.147	0.650	0.2	8.06	52.0	0.398	1.8	0.65	2162	80	2234	57	2319	78	2319	78	93
12JT11_42	124	1.2	0.149	0.680	0.2	8.12	53.0	0.402	1.8	0.64	2181	83	2243	60	2323	78	2323	78	94
12JT11_72	233	4.2	0.148	0.660	0.2	7.73	49.0	0.385	1.7	0.63	2099	79	2199	58	2325	77	2325	77	90
12JT11_51	104	2.9	0.149	0.670	0.3	7.93	51.0	0.392	1.8	0.61	2131	82	2221	59	2328	77	2328	77	92
12JT11_56	110	1.5	0.149	0.680	0.3	8.15	53.0	0.401	1.8	0.59	2177	84	2249	59	2332	77	2332	77	93
12JT11_18	257	2.9	0.149	0.660	0.3	8.57	54.0	0.414	1.8	0.68	2234	83	2292	59	2333	75	2333	75	96
12JT11_21	247	3.8	0.149	0.660	0.3	8.52	54.0	0.411	1.8	0.62	2222	82	2291	58	2334	74	2334	74	95

TABLE SM2.3: LA-ICPMS U-PB ISOTOPIC DATA (UC SANTA CRUZ LAB)

						Isotope ratios					Apparent ages (Ma)								
Analysis	U	U/Th	206Pb*	±	error	207Pb*	±	206Pb*	±	error	206Pb*	±	207Pb*	±	206Pb*	±	Best age	±	Conc
	(ppm)		207Pb*	(%)	corr.	235U*	(%)	238U	(%)	corr.	238U*	(Ma)	235U	(Ma)	207Pb*	(Ma)	(Ma)	(Ma)	(%)
12JT11_83	452	2.0	0.149	0.650	0.2	7.85	49.0	0.389	1.7	0.69	2119	78	2213	57	2337	74	2337	74	91
12JT11_38	283	2.4	0.150	0.650	0.3	8.44	53.0	0.407	1.8	0.68	2206	81	2279	56	2343	72	2343	72	94
12JT11_87	308	3.9	0.150	0.660	0.4	7.34	46.0	0.359	1.6	0.62	1979	74	2154	56	2345	74	2345	74	84
12JT11_102	343	1.4	0.152	0.660	0.3	8.59	54.0	0.406	1.8	0.65	2199	80	2293	57	2371	75	2371	75	93
12JT11_35	154	1.6	0.152	0.680	0.3	8.71	56.0	0.418	1.9	0.58	2250	84	2305	58	2371	76	2371	76	95
12JT11_8	295	2.4	0.153	0.670	0.3	9.19	58.0	0.439	1.9	0.68	2343	86	2356	58	2381	75	2381	75	98
12JT11_10	403	2.5	0.157	0.690	-0.1	8.42	55.0	0.393	1.8	0.87	2135	82	2270	59	2422	75	2422	75	88
12JT11_74	102	2.9	0.158	0.720	0.3	8.72	56.0	0.409	1.9	0.58	2207	84	2307	58	2430	76	2430	76	91
12JT11_64	422	3.1	0.158	0.690	0.0	8.08	52.0	0.374	1.7	0.84	2049	79	2241	59	2437	72	2437	72	84
12JT11_65	277	1.5	0.158	0.700	0.3	8.75	55.0	0.405	1.8	0.68	2192	81	2313	56	2440	75	2440	75	90
12JT11_48	346	2.8	0.161	0.700	0.2	9.35	59.0	0.423	1.9	0.74	2278	83	2372	58	2469	73	2469	73	92
12JT11_44	536	2.6	0.162	0.700	0.0	8.60	55.0	0.383	1.7	0.87	2092	81	2293	59	2479	72	2479	72	84
12JT11_86	119	1.8	0.162	0.730	0.2	9.11	58.0	0.419	1.9	0.62	2253	85	2348	59	2480	76	2480	76	91
12JT11_85	430	3.6	0.163	0.710	0.1	8.90	57.0	0.405	1.8	0.83	2188	83	2327	57	2484	72	2484	72	88
12JT11_29	93	1.9	0.164	0.750	0.3	10.65	68.0	0.465	2.1	0.52	2458	91	2488	59	2491	77	2491	77	99
12JT11_53	62	1.2	0.164	0.790	0.4	9.63	63.0	0.430	2.0	0.44	2300	91	2399	61	2496	80	2496	80	92
12JT11_20	166	1.8	0.164	0.730	0.2	10.96	70.0	0.482	2.1	0.70	2532	93	2521	59	2499	74	2499	74	101
12JT11_5	107	2.7	0.165	0.740	0.3	10.37	66.0	0.462	2.1	0.58	2444	92	2467	59	2503	76	2503	76	98
12JT11_92	203	1.5	0.166	0.730	0.2	9.86	63.0	0.434	1.9	0.65	2320	85	2418	58	2513	75	2513	75	92
12JT11_90	198	2.1	0.167	0.740	0.3	9.59	61.0	0.422	1.9	0.59	2272	85	2395	58	2523	74	2523	74	90
12JT11_11	130	2.0	0.167	0.750	0.3	11.02	70.0	0.479	2.1	0.62	2520	92	2521	59	2530	75	2530	75	100
12JT11_108	470	3.2	0.174	0.760	0.2	9.84	62.0	0.412	1.8	0.81	2222	83	2422	59	2593	72	2593	72	86
12JT11_19	91	1.1	0.179	0.820	0.3	11.90	77.0	0.478	2.2	0.53	2515	94	2595	61	2653	76	2653	76	95
12JT11_22	161	1.6	0.185	0.810	0.3	13.24	84.0	0.514	2.3	0.71	2673	96	2698	60	2690	73	2690	73	99
12JT11_96	33	1.8	0.191	0.920	0.3	12.15	83.0	0.474	2.3	0.67	2490	100	2611	64	2745	81	2745	81	91
>20% Discordance																			
12JT11_95	1291	1.8	0.132	0.580	0.1	2.03	13.0	0.113	0.5	0.86	688	30	1123	45	2116	76	688	30	33

TABLE SM2.3: LA-ICPMS U-PB ISOTOPIC DATA (UC SANTA CRUZ LAB)

						Isotope ratios					Apparent ages (Ma)								
Analysis	U	U/Th	206Pb*	±	error	207Pb*	±	206Pb*	±	error	206Pb*	±	207Pb*	±	206Pb*	±	Best age	±	Conc
	(ppm)		207Pb*	(%)	corr.	235U*	(%)	238U	(%)	corr.	238U*	(Ma)	235U	(Ma)	207Pb*	(Ma)	(Ma)	(Ma)	(%)
12JT11_47	1544	2.5	0.103	0.460	-0.5	1.77	15.0	0.123	0.8	0.96	749	45	1019	54	1678	81	749	45	45
12JT11_60	2035	7.5	0.112	0.490	-0.1	2.00	13.0	0.131	0.6	0.82	796	33	1115	43	1826	78	796	33	44
12JT11_84	984	2.2	0.104	0.460	-0.1	2.69	17.0	0.192	0.9	0.80	1134	45	1323	47	1691	82	1691	82	67
12JT11_107	536	4.9	0.113	0.500	-0.3	3.91	27.0	0.253	1.3	0.93	1449	67	1616	58	1844	79	1844	79	79
12JT11_103	187	1.3	0.124	0.570	0.3	4.75	31.0	0.282	1.3	0.46	1601	63	1774	54	2006	80	2006	80	80
12JT11_6	632	2.5	0.131	0.580	-0.1	3.93	26.0	0.220	1.0	0.82	1283	53	1615	53	2107	78	2107	78	61
12JT11_59	560	3.8	0.134	0.580	-0.1	5.30	35.0	0.290	1.4	0.91	1640	69	1865	57	2150	75	2150	75	76
12JT11_77	865	3.8	0.135	0.600	-0.1	3.58	23.0	0.197	0.9	0.87	1159	48	1550	52	2162	77	2162	77	54
12JT11_43	670	2.3	0.139	0.610	-0.2	5.35	35.0	0.280	1.3	0.90	1593	64	1880	57	2214	74	2214	74	72
12JT11_82	638	1.5	0.142	0.640	0.0	3.41	23.0	0.178	0.8	0.84	1057	46	1508	53	2248	77	2248	77	47
12JT11_62	531	2.5	0.144	0.640	-0.5	4.98	37.0	0.251	1.4	0.96	1440	70	1791	64	2281	75	2281	75	63
12JT11_41	66	4.6	0.181	1.100	0.4	8.94	71.0	0.365	2.3	0.66	1990	110	2327	76	2611	89	2611	89	76
12JT11_105	499	2.1	0.180	0.780	0.2	8.87	56.0	0.358	1.6	0.79	1974	75	2324	58	2654	72	2654	72	74
>5% Reverse Discordance																			
12JT11_98	22	3739.7	0.107	0.650	0.2	5.49	44.0	0.372	2.0	0.51	2036	94	1878	67	1730	110	1730	110	118
12JT11_32	38	3576.4	0.109	0.590	0.3	5.69	41.0	0.379	1.9	0.49	2070	88	1925	61	1760	100	1760	100	118
12JT11_50	11	11344.0	0.113	0.790	0.3	6.16	53.0	0.396	2.3	0.53	2130	100	1958	75	1780	130	1780	130	120
12JT11_55	51	6614.0	0.109	0.550	0.2	5.99	41.0	0.403	1.9	0.53	2187	88	1975	62	1786	92	1786	92	122
12JT11_33	42	1072.9	0.112	0.560	0.2	6.16	43.0	0.399	2.0	0.58	2155	90	1989	61	1814	95	1814	95	119
12JT11_12	48	12465.3	0.113	0.580	0.4	6.40	44.0	0.413	2.0	0.50	2232	89	2026	61	1839	93	1839	93	121
>1000 U ppm																			
12JT11_7	1375	3.5	0.078	0.340	0.2	1.85	12.0	0.172	0.8	0.60	1024	41	1062	41	1152	87	1152	87	89
12JT31; Neruokpuk Formation (N69.39, W141.53)																			
12JT31_108	124	0.9	0.076	0.400	0.3	1.90	14.0	0.179	0.9	0.32	1058	49	1076	49	1100	100	1100	100	96
12JT31_78	226	2.3	0.075	0.370	0.3	1.95	14.0	0.190	1.0	0.36	1122	51	1099	48	1070	100	1070	100	105

TABLE SM2.3: LA-ICPMS U-PB ISOTOPIC DATA (UC SANTA CRUZ LAB)

						Isotope ratios					Apparent ages (Ma)								
Analysis	U	U/Th	206Pb*	±	error	207Pb*	±	206Pb*	±	error	206Pb*	±	207Pb*	±	206Pb*	±	Best age	±	Conc
	(ppm)		207Pb*	(%)	corr.	235U*	(%)	238U	(%)	corr.	238U*	(Ma)	235U	(Ma)	207Pb*	(Ma)	(Ma)	(Ma)	(%)
12JT31_12	122	13.3	0.081	0.420	0.2	2.41	18.0	0.212	1.1	0.43	1236	56	1243	53	1230	100	1230	100	100
12JT31_103	126	2.0	0.082	0.410	0.2	2.38	17.0	0.211	1.0	0.40	1236	55	1240	51	1250	100	1250	100	99
12JT31_60	289	4.0	0.081	0.380	0.2	2.40	17.0	0.215	1.1	0.48	1254	55	1240	50	1228	94	1228	94	102
12JT31_67	265	1.8	0.083	0.400	0.2	2.59	18.0	0.226	1.1	0.37	1315	58	1297	50	1279	96	1279	96	103
12JT31_59	44	1.5	0.087	0.520	0.3	2.68	21.0	0.228	1.2	0.36	1320	62	1319	59	1330	120	1330	120	99
12JT31_54	253	2.0	0.089	0.420	0.1	2.88	20.0	0.238	1.2	0.50	1375	61	1375	52	1399	94	1399	94	98
12JT31_98	142	1.7	0.087	0.420	0.3	2.89	20.0	0.241	1.2	0.33	1390	62	1378	55	1359	95	1359	95	102
12JT31_49	308	4.5	0.088	0.420	0.3	3.04	21.0	0.250	1.2	0.55	1437	64	1414	52	1381	92	1381	92	104
12JT31_23	223	5.0	0.108	0.500	0.2	4.93	34.0	0.332	1.7	0.67	1847	81	1807	59	1762	84	1762	84	105
12JT31_81	484	5.1	0.108	0.500	0.3	4.33	30.0	0.293	1.4	0.48	1657	71	1699	56	1767	86	1767	86	94
12JT31_72	115	2.0	0.111	0.530	0.3	5.14	36.0	0.341	1.7	0.53	1889	82	1843	59	1804	89	1804	89	105
12JT31_101	71	0.7	0.111	0.550	0.1	4.96	36.0	0.320	1.6	0.50	1788	79	1814	63	1812	93	1812	93	99
12JT31_84	217	1.6	0.111	0.510	0.2	5.15	36.0	0.341	1.7	0.66	1892	82	1847	60	1813	86	1813	86	104
12JT31_79	233	2.2	0.111	0.520	0.2	5.23	36.0	0.344	1.7	0.52	1904	82	1857	60	1816	86	1816	86	105
12JT31_63	160	3.2	0.111	0.530	0.3	5.01	35.0	0.332	1.7	0.42	1844	80	1821	59	1817	88	1817	88	101
12JT31_88	447	1.2	0.112	0.510	-0.3	4.83	34.0	0.314	1.6	0.93	1762	80	1782	64	1822	84	1822	84	97
12JT31_95	456	2.5	0.112	0.520	0.2	4.43	31.0	0.286	1.4	0.68	1622	71	1720	58	1835	82	1835	82	88
12JT31_30	58	1.8	0.112	0.570	0.1	5.35	39.0	0.339	1.7	0.49	1880	83	1877	63	1843	99	1843	99	102
12JT31_104	90	1.8	0.114	0.550	0.3	5.09	36.0	0.323	1.6	0.49	1804	80	1832	60	1845	88	1845	88	98
12JT31_40	73	1.9	0.114	0.570	0.1	5.39	39.0	0.340	1.8	0.64	1886	85	1878	61	1863	91	1863	91	101
12JT31_44	287	2.0	0.115	0.530	0.1	5.60	39.0	0.352	1.8	0.71	1942	83	1914	60	1875	83	1875	83	104
12JT31_89	128	1.2	0.115	0.550	0.3	5.49	39.0	0.344	1.7	0.50	1909	82	1901	60	1878	88	1878	88	102
12JT31_38	89	2.3	0.116	0.570	0.1	5.68	41.0	0.353	1.9	0.66	1946	88	1925	59	1885	88	1885	88	103
12JT31_77	384	1.4	0.117	0.530	0.4	5.66	39.0	0.358	1.8	0.18	1970	83	1923	60	1903	89	1903	89	104
12JT31_46	114	0.4	0.117	0.560	0.2	5.78	41.0	0.362	1.8	0.56	1990	87	1940	60	1909	86	1909	86	104
12JT31_100	69	1.3	0.117	0.590	0.2	4.98	36.0	0.306	1.6	0.54	1729	81	1810	60	1916	90	1916	90	90
12JT31_33	370	2.8	0.117	0.540	0.1	5.95	41.0	0.365	1.8	0.76	2004	86	1967	62	1916	83	1916	83	105
12JT31_80	131	1.6	0.118	0.560	0.2	5.55	39.0	0.345	1.7	0.49	1909	82	1908	59	1919	85	1919	85	99

TABLE SM2.3: LA-ICPMS U-PB ISOTOPIC DATA (UC SANTA CRUZ LAB)

						Isotope ratios					Apparent ages (Ma)								
Analysis	U	U/Th	206Pb*	±	error	207Pb*	±	206Pb*	±	error	206Pb*	±	207Pb*	±	206Pb*	±	Best age	±	Conc
	(ppm)		207Pb*	(%)	corr.	235U*	(%)	238U	(%)	corr.	238U*	(Ma)	235U	(Ma)	207Pb*	(Ma)	(Ma)	(Ma)	(%)
12JT31_51	252	1.0	0.118	0.550	0.2	5.88	41.0	0.363	1.8	0.65	1999	88	1955	60	1926	85	1926	85	104
12JT31_93	474	4.1	0.119	0.540	0.2	5.11	35.0	0.313	1.5	0.67	1757	75	1837	58	1931	83	1931	83	91
12JT31_68	98	0.8	0.120	0.590	0.0	4.65	33.0	0.284	1.4	0.60	1612	72	1754	61	1944	89	1944	89	83
12JT31_35	51	1.1	0.121	0.620	0.2	6.18	45.0	0.366	1.9	0.55	2011	90	1996	63	1966	94	1966	94	102
12JT31_75	152	1.3	0.122	0.570	0.1	6.14	43.0	0.367	1.8	0.65	2016	87	1996	62	1988	84	1988	84	101
12JT31_5	684	3.4	0.124	0.560	-0.1	6.09	43.0	0.353	1.8	0.90	1949	86	1987	62	2006	81	2006	81	97
12JT31_91	151	3.0	0.126	0.600	-0.1	6.70	48.0	0.382	1.9	0.71	2080	89	2069	64	2042	85	2042	85	102
12JT31_94	368	16.1	0.126	0.580	0.2	6.33	44.0	0.362	1.8	0.63	1992	84	2024	58	2050	83	2050	83	97
12JT31_92	113	2.2	0.137	0.650	0.0	7.54	54.0	0.394	2.0	0.73	2141	92	2175	65	2185	82	2185	82	98
12JT31_69	194	1.4	0.141	0.660	0.0	8.21	57.0	0.425	2.1	0.75	2281	95	2258	64	2244	82	2244	82	102
12JT31_55	171	3.0	0.145	0.680	0.2	8.29	57.0	0.418	2.1	0.56	2252	94	2264	64	2283	81	2283	81	99
12JT31_1	94	1.2	0.146	0.700	-0.1	6.80	54.0	0.331	1.9	0.87	1838	94	2077	73	2290	83	2290	83	80
12JT31_57	166	1.6	0.146	0.670	0.1	8.76	61.0	0.440	2.1	0.64	2350	95	2311	62	2292	80	2292	80	103
12JT31_53	311	5.5	0.147	0.670	0.2	8.48	58.0	0.419	2.0	0.65	2255	93	2283	62	2311	78	2311	78	98
12JT31_82	77	0.9	0.149	0.720	0.3	9.04	63.0	0.446	2.2	0.47	2370	100	2341	63	2319	84	2319	84	102
12JT31_52	252	2.1	0.152	0.700	0.2	9.29	64.0	0.442	2.2	0.64	2358	97	2366	63	2367	76	2367	76	100
12JT31_76	147	1.5	0.154	0.720	0.2	9.24	64.0	0.440	2.2	0.61	2350	96	2361	62	2390	79	2390	79	98
12JT31_58	173	2.5	0.158	0.730	0.2	10.02	69.0	0.462	2.3	0.65	2450	100	2434	63	2430	79	2430	79	101
12JT31_85	34	1.6	0.158	0.820	0.4	10.18	74.0	0.468	2.4	0.36	2470	110	2452	66	2431	90	2431	90	102
12JT31_32	125	1.4	0.157	0.740	-0.1	9.69	69.0	0.445	2.3	0.85	2370	100	2402	66	2432	79	2432	79	97
12JT31_11	166	2.5	0.159	0.740	-0.1	10.76	79.0	0.483	2.7	0.91	2540	120	2491	72	2445	77	2445	77	104
12JT31_74	125	2.4	0.160	0.750	0.2	10.01	70.0	0.459	2.3	0.61	2440	100	2441	64	2447	78	2447	78	100
12JT31_65	145	1.2	0.160	0.740	0.1	9.93	69.0	0.455	2.2	0.70	2424	97	2427	64	2456	79	2456	79	99
12JT31_73	285	2.1	0.161	0.730	0.2	8.32	58.0	0.378	1.9	0.82	2062	89	2264	63	2466	77	2466	77	84
12JT31_102	101	2.9	0.162	0.760	0.3	10.39	72.0	0.463	2.3	0.56	2450	100	2467	63	2468	80	2468	80	99
12JT31_99	222	3.5	0.162	0.740	0.3	10.15	70.0	0.453	2.2	0.67	2408	99	2450	65	2479	78	2479	78	97
12JT31_56	80	1.5	0.164	0.780	0.2	10.78	75.0	0.481	2.4	0.60	2530	100	2503	66	2494	80	2494	80	101
12JT31_110	60	1.0	0.170	0.810	0.2	10.81	77.0	0.460	2.4	0.64	2430	100	2506	67	2556	81	2556	81	95

TABLE SM2.3: LA-ICPMS U-PB ISOTOPIC DATA (UC SANTA CRUZ LAB)

						Isotope ratios					Apparent ages (Ma)								
Analysis	U	U/Th	206Pb*	±	error	207Pb*	±	206Pb*	±	error	206Pb*	±	207Pb*	±	206Pb*	±	Best age	±	Conc
	(ppm)		207Pb*	(%)	corr.	235U*	(%)	238U	(%)	corr.	238U*	(Ma)	235U	(Ma)	207Pb*	(Ma)	(Ma)	(Ma)	(%)
12JT31_42	140	2.8	0.171	0.790	0.3	12.20	85.0	0.513	2.6	0.70	2670	110	2623	65	2560	77	2560	77	104
12JT31_34	114	2.3	0.172	0.800	0.1	12.13	86.0	0.506	2.6	0.80	2630	110	2611	67	2578	79	2578	79	102
12JT31_48	77	2.7	0.173	0.810	0.3	12.04	84.0	0.498	2.5	0.70	2610	110	2605	66	2583	78	2583	78	101
12JT31_62	77	1.6	0.179	0.850	0.2	11.96	84.0	0.498	2.5	0.61	2600	110	2597	66	2633	78	2633	78	99
12JT31_36	68	2.6	0.183	0.880	0.2	13.56	97.0	0.528	2.7	0.73	2740	110	2709	67	2679	81	2679	81	102
12JT31_43	216	1.8	0.184	0.840	0.3	13.89	96.0	0.541	2.7	0.81	2790	120	2740	65	2689	75	2689	75	104
12JT31_83	282	3.3	0.185	0.840	0.3	13.61	93.0	0.535	2.6	0.69	2760	110	2723	65	2696	76	2696	76	102
12JT31_19	31	1.0	0.188	0.990	-0.2	14.10	110.0	0.534	3.0	0.81	2750	120	2720	68	2699	84	2699	84	102
12JT31_50	114	1.2	0.186	0.860	0.2	13.86	98.0	0.540	2.7	0.77	2780	110	2737	65	2703	77	2703	77	103
12JT31_39	96	1.1	0.187	0.870	0.2	14.16	99.0	0.548	2.8	0.68	2820	120	2757	66	2716	78	2716	78	104
12JT31_97	32	1.8	0.190	0.950	0.3	13.63	99.0	0.513	2.7	0.67	2670	110	2724	68	2735	83	2735	83	98
12JT31_28	51	1.1	0.199	0.950	0.3	15.70	110.0	0.561	2.9	0.72	2870	120	2859	65	2820	78	2820	78	102
>20% Discordance																			
12JT31_66	1800	2.8	0.112	0.510	0.1	1.70	12.0	0.111	0.5	0.71	680	32	1009	44	1828	82	680	32	37
12JT31_61	1394	4.1	0.123	0.560	0.3	2.04	14.0	0.123	0.6	0.67	747	35	1130	47	1991	82	747	35	38
12JT31_107	1425	1.8	0.130	0.590	0.2	2.43	17.0	0.134	0.7	0.74	813	38	1250	49	2101	81	813	38	39
12JT31_13	546	2.0	0.085	0.400	-0.1	1.84	16.0	0.159	1.1	0.94	941	61	1041	56	1313	92	941	61	72
12JT31_70	998	2.0	0.096	0.440	0.2	2.15	15.0	0.164	0.8	0.61	979	44	1164	47	1555	88	979	44	63
12JT31_22	171	0.6	0.090	0.450	0.3	2.28	17.0	0.184	1.1	0.70	1088	57	1198	52	1440	94	1440	94	76
12JT31_90	462	1.8	0.105	0.490	0.0	2.93	22.0	0.204	1.1	0.89	1192	61	1379	57	1713	86	1713	86	70
12JT31_109	282	1.4	0.116	0.540	0.1	4.16	30.0	0.261	1.3	0.80	1492	68	1668	59	1890	84	1890	84	79
12JT31_37	461	1.5	0.116	0.540	-0.1	4.24	35.0	0.260	1.7	0.96	1484	86	1648	73	1893	83	1893	83	78
12JT31_16	164	0.8	0.120	0.580	0.2	4.58	36.0	0.276	1.7	0.88	1569	87	1745	67	1966	84	1966	84	80
12JT31_4	255	2.8	0.127	0.600	-0.2	4.18	33.0	0.235	1.3	0.90	1353	70	1659	65	2051	84	2051	84	66
12JT31_3	618	2.9	0.131	0.600	-0.1	4.03	29.0	0.220	1.2	0.92	1285	62	1630	58	2109	81	2109	81	61
12JT31_47	163	0.9	0.232	1.100	0.0	14.40	100.0	0.446	2.4	0.90	2380	110	2768	69	3069	73	3069	73	78
12JT31_10	68	0.7	0.737	3.400	0.1	56.30	400.0	0.553	2.9	0.89	2830	120	4103	68	4820	76	4820	76	59

TABLE SM2.3: LA-ICPMS U-PB ISOTOPIC DATA (UC SANTA CRUZ LAB)

						Isotope ratios					Apparent ages (Ma)								
Analysis	U	U/Th	206Pb*	±	error	207Pb*	±	206Pb*	±	error	206Pb*	±	207Pb*	±	206Pb*	±	Best age	±	Conc
	(ppm)		207Pb*	(%)	corr.	235U*	(%)	238U	(%)	corr.	238U*	(Ma)	235U	(Ma)	207Pb*	(Ma)	(Ma)	(Ma)	(%)
12JT31_87	52	1.0	0.764	3.500	0.4	78.10	550.0	0.746	3.9	0.87	3580	140	4433	71	4883	80	4883	80	73
>5% Reverse Discordance																			
12JT31_41	37	2.6	0.085	0.530	0.3	2.79	22.0	0.238	1.3	0.35	1371	68	1346	59	1270	120	1270	120	108
12JT31_17	199	4.4	0.107	0.500	0.2	4.91	34.0	0.334	1.7	0.63	1860	80	1802	60	1745	88	1745	88	107
12JT31_14	46	0.9	0.108	0.550	0.2	5.42	40.0	0.355	1.9	0.56	1952	88	1881	63	1760	95	1760	95	111
12JT31_2	41	0.7	0.111	0.600	0.1	5.43	41.0	0.354	1.9	0.57	1949	89	1885	65	1786	98	1786	98	109
12JT31_26	42	0.6	0.111	0.610	0.2	5.32	40.0	0.348	1.9	0.54	1921	88	1872	65	1808	97	1808	97	106
12JT31_96	67	93.7	0.111	0.540	0.3	5.99	43.0	0.386	2.0	0.63	2112	95	1970	63	1810	91	1810	91	117
12JT31_6	184	1.8	0.111	0.520	0.2	5.35	37.0	0.347	1.7	0.64	1919	83	1876	60	1812	85	1812	85	106
12JT31_25	196	1.6	0.111	0.520	0.4	5.36	37.0	0.350	1.8	0.68	1930	86	1877	60	1818	86	1818	86	106
12JT31_106	95	604.0	0.113	0.540	0.2	6.14	44.0	0.396	2.1	0.66	2149	95	1994	61	1837	91	1837	91	117
12JT31_86	97	6413.3	0.113	0.540	0.2	6.12	44.0	0.397	2.1	0.70	2150	96	1990	61	1838	87	1838	87	117
12JT31_20	138	3.8	0.113	0.530	0.2	5.49	39.0	0.353	1.8	0.62	1950	85	1900	61	1852	91	1852	91	105
12JT31_7	79	1.7	0.114	0.560	0.2	5.52	39.0	0.356	1.8	0.59	1961	86	1897	60	1856	91	1856	91	106
12JT31_29	170	1.5	0.115	0.540	0.3	5.76	40.0	0.360	1.8	0.67	1986	87	1942	60	1883	81	1883	81	105
12JT31_8	39	1.2	0.118	0.610	0.1	6.20	47.0	0.376	2.0	0.63	2050	93	1996	65	1919	94	1919	94	107
12JT31_27	86	0.8	0.118	0.570	0.1	6.04	44.0	0.371	1.9	0.67	2031	90	1974	64	1920	85	1920	85	106
12JT31_64	28	515.6	0.118	0.660	0.3	6.51	51.0	0.405	2.3	0.60	2180	100	2034	69	1930	100	1930	100	113
12JT31_24	45	0.5	0.138	0.680	0.4	8.26	59.0	0.436	2.3	0.54	2330	100	2262	65	2193	90	2193	90	106
12JT31_31	224	3.0	0.163	0.740	0.2	11.47	79.0	0.502	2.5	0.82	2620	110	2560	64	2487	77	2487	77	105
12JT31_18	122	3.3	0.164	0.760	0.2	11.47	80.0	0.506	2.6	0.73	2640	110	2561	65	2492	79	2492	79	106
12JT31_45	112	1.1	0.165	0.770	0.3	11.66	82.0	0.509	2.6	0.77	2650	110	2577	68	2505	80	2505	80	106
12JT31_15	93	1.6	0.171	0.800	0.2	12.53	87.0	0.532	2.7	0.69	2750	110	2648	67	2565	78	2565	78	107
12JT31_9	51	1.0	0.171	0.820	0.2	13.08	93.0	0.548	2.9	0.68	2820	120	2688	66	2568	81	2568	81	110
12JT31_21	83	1.9	0.174	0.820	0.2	13.08	92.0	0.548	2.8	0.71	2820	110	2684	67	2595	80	2595	80	109
12JT32; Neruokpuk Formation (N69.72, W141.51)																			

TABLE SM2.3: LA-ICPMS U-PB ISOTOPIC DATA (UC SANTA CRUZ LAB)

						Isotope ratios					Apparent ages (Ma)								
Analysis	U	U/Th	206Pb*	±	error	207Pb*	±	206Pb*	±	error	206Pb*	±	207Pb*	±	206Pb*	±	Best age	±	Conc
	(ppm)		207Pb*	(%)	corr.	235U*	(%)	238U	(%)	corr.	238U*	(Ma)	235U	(Ma)	207Pb*	(Ma)	(Ma)	(Ma)	(%)
12JT32_12	66	0.9	0.074	0.420	0.1	1.80	14.0	0.180	0.9	0.38	1063	51	1040	50	1030	120	1030	120	103
12JT32_40	47	2.0	0.076	0.450	0.2	1.96	16.0	0.184	1.0	0.46	1091	53	1087	55	1050	130	1050	130	104
12JT32_8	66	1.5	0.077	0.450	0.4	2.02	16.0	0.188	1.0	0.15	1108	53	1115	52	1120	110	1120	110	99
12JT32_71	91	3.7	0.086	0.450	0.2	2.81	21.0	0.241	1.2	0.49	1388	64	1356	54	1340	110	1340	110	104
12JT32_69	281	3.1	0.088	0.420	0.0	3.00	21.0	0.249	1.2	0.68	1435	64	1404	53	1381	91	1381	91	104
12JT32_32	20	1.7	0.092	0.660	0.3	3.10	28.0	0.241	1.4	0.42	1385	72	1426	68	1410	150	1410	150	98
12JT32_44	91	1.4	0.092	0.480	0.2	3.25	24.0	0.259	1.3	0.45	1483	68	1463	56	1460	100	1460	100	102
12JT32_84	37	1.2	0.091	0.540	0.3	3.37	26.0	0.268	1.5	0.40	1534	74	1496	63	1470	110	1470	110	104
12JT32_33	366	1.3	0.092	0.430	0.1	3.43	24.0	0.269	1.3	0.63	1536	68	1510	54	1470	88	1470	88	104
12JT32_31	123	0.7	0.103	0.510	0.2	3.93	28.0	0.283	1.5	0.62	1601	74	1623	58	1658	92	1658	92	97
12JT32_20	38	0.9	0.110	0.590	0.2	4.44	34.0	0.298	1.6	0.50	1683	78	1720	63	1764	98	1764	98	95
12JT32_80	56	1.8	0.110	0.570	0.3	4.94	36.0	0.333	1.7	0.41	1849	84	1807	61	1775	95	1775	95	104
12JT32_45	35	0.7	0.110	0.610	0.3	5.15	39.0	0.337	1.8	0.48	1869	86	1828	64	1790	100	1790	100	104
12JT32_26	95	1.8	0.111	0.550	0.2	4.92	36.0	0.323	1.6	0.56	1801	80	1803	62	1798	92	1798	92	100
12JT32_18	128	1.4	0.110	0.520	0.2	5.16	36.0	0.337	1.7	0.61	1868	81	1842	60	1798	88	1798	88	104
12JT32_46	27	1.5	0.112	0.650	0.2	5.08	39.0	0.333	1.8	0.59	1846	87	1813	65	1810	110	1810	110	102
12JT32_41	32	0.9	0.113	0.630	0.2	5.24	41.0	0.332	1.8	0.55	1847	85	1852	66	1840	100	1840	100	100
12JT32_62	25	0.6	0.115	0.670	0.3	5.29	41.0	0.335	1.9	0.40	1860	90	1868	67	1840	110	1840	110	101
12JT32_87	12	0.8	0.114	0.780	0.2	5.38	48.0	0.345	2.2	0.47	1890	100	1847	75	1840	120	1840	120	103
12JT32_9	193	1.9	0.113	0.530	0.2	5.36	37.0	0.345	1.7	0.63	1910	83	1874	60	1844	85	1844	85	104
12JT32_63	146	1.5	0.113	0.540	0.1	5.33	37.0	0.346	1.7	0.64	1925	86	1875	62	1846	86	1846	86	104
12JT32_99	16	0.8	0.114	0.730	0.3	5.42	46.0	0.342	2.0	0.46	1899	99	1861	72	1850	120	1850	120	103
12JT32_11	135	1.8	0.115	0.550	0.3	4.78	34.0	0.302	1.5	0.51	1702	76	1781	58	1868	85	1868	85	91
12JT32_55	25	0.8	0.115	0.680	0.1	5.55	45.0	0.345	1.9	0.51	1919	93	1891	71	1870	100	1870	100	103
12JT32_43	161	1.5	0.114	0.540	0.2	5.49	38.0	0.349	1.8	0.58	1932	83	1899	60	1870	86	1870	86	103
12JT32_48	39	2.0	0.115	0.610	0.3	5.64	42.0	0.351	1.9	0.51	1934	90	1921	63	1874	95	1874	95	103
12JT32_4	53	3.0	0.115	0.600	0.4	5.61	41.0	0.353	1.8	0.38	1948	87	1917	64	1878	97	1878	97	104
12JT32_56	62	0.9	0.114	0.590	0.2	5.57	41.0	0.358	1.8	0.53	1972	86	1911	64	1882	93	1882	93	105

TABLE SM2.3: LA-ICPMS U-PB ISOTOPIC DATA (UC SANTA CRUZ LAB)

						Isotope ratios					Apparent ages (Ma)								
Analysis	U	U/Th	206Pb*	±	error	207Pb*	±	206Pb*	±	error	206Pb*	±	207Pb*	±	206Pb*	±	Best age	±	Conc
	(ppm)		207Pb*	(%)	corr.	235U*	(%)	238U	(%)	corr.	238U*	(Ma)	235U	(Ma)	207Pb*	(Ma)	(Ma)	(Ma)	(%)
12JT32_57	26	1.2	0.116	0.670	0.2	5.77	46.0	0.363	2.0	0.45	1993	94	1936	70	1910	110	1910	110	104
12JT32_38	266	2.2	0.118	0.550	0.0	5.07	38.0	0.316	1.8	0.90	1771	87	1834	65	1923	83	1923	83	92
12JT32_37	23	0.5	0.118	0.690	0.2	5.67	45.0	0.343	1.9	0.42	1896	90	1911	70	1930	110	1930	110	98
12JT32_85	28	1.0	0.117	0.650	0.3	5.76	45.0	0.356	2.0	0.51	1955	93	1940	66	1930	100	1930	100	101
12JT32_81	210	1.5	0.119	0.560	0.2	5.61	39.0	0.349	1.7	0.61	1926	83	1914	60	1933	85	1933	85	100
12JT32_29	100	1.4	0.121	0.580	0.2	6.05	43.0	0.363	1.8	0.49	1996	85	1984	62	1968	89	1968	89	101
12JT32_35	54	1.2	0.122	0.610	0.3	5.90	43.0	0.352	1.8	0.51	1940	86	1963	63	1971	95	1971	95	98
12JT32_7	273	3.3	0.122	0.570	-0.1	5.59	39.0	0.332	1.6	0.68	1852	79	1910	59	1989	80	1989	80	93
12JT32_14	84	1.5	0.128	0.620	0.2	6.90	49.0	0.386	2.0	0.60	2105	91	2094	62	2076	86	2076	86	101
12JT32_2	142	1.2	0.132	0.620	0.3	7.30	51.0	0.400	2.0	0.57	2169	92	2148	61	2130	81	2130	81	102
12JT32_17	56	1.2	0.146	0.710	0.1	8.88	64.0	0.441	2.3	0.69	2350	100	2321	65	2303	83	2303	83	102
12JT32_3	174	2.2	0.148	0.690	0.2	7.65	53.0	0.374	1.9	0.68	2047	88	2189	63	2322	78	2322	78	88
12JT32_68	14	109.5	0.156	1.100	0.0	9.47	87.0	0.435	2.5	0.57	2320	110	2331	87	2330	130	2330	130	100
12JT32_53	131	3.2	0.149	0.700	0.2	9.40	66.0	0.459	2.3	0.64	2440	100	2378	64	2331	81	2331	81	105
12JT32_34	81	3.6	0.150	0.710	0.2	9.17	65.0	0.447	2.3	0.64	2380	100	2353	64	2337	79	2337	79	102
12JT32_42	51	1.6	0.151	0.740	0.2	9.63	69.0	0.463	2.4	0.61	2450	100	2399	65	2353	82	2353	82	104
12JT32_92	112	1.5	0.152	0.720	0.2	8.17	58.0	0.390	2.0	0.63	2119	92	2254	64	2368	82	2368	82	89
12JT32_50	60	0.8	0.153	0.740	0.2	9.83	70.0	0.468	2.4	0.65	2470	110	2422	65	2385	82	2385	82	104
12JT32_75	168	6.8	0.169	0.800	0.1	10.99	81.0	0.482	2.6	0.16	2530	110	2504	70	2545	76	2545	76	99
12JT32_13	116	2.8	0.170	0.790	0.3	11.85	82.0	0.505	2.5	0.59	2640	110	2597	62	2555	79	2555	79	103
12JT32_28	112	1.1	0.171	0.850	0.0	9.40	72.0	0.396	2.2	0.87	2160	110	2367	71	2563	82	2563	82	84
12JT32_39	127	1.5	0.172	0.800	0.3	11.67	82.0	0.492	2.6	0.80	2570	110	2574	67	2586	80	2586	80	99
12JT32_1	98	1.4	0.173	0.810	0.4	12.50	87.0	0.521	2.6	0.61	2700	110	2643	65	2587	78	2587	78	104
12JT32_10	75	1.5	0.173	0.820	0.3	12.31	86.0	0.513	2.6	0.66	2660	110	2629	66	2591	77	2591	77	103
12JT32_16	84	2.0	0.175	0.820	0.4	12.13	84.0	0.502	2.6	0.64	2630	110	2612	66	2608	79	2608	79	101
12JT32_36	69	5.1	0.177	0.840	0.2	12.35	87.0	0.506	2.6	0.73	2640	110	2630	65	2621	78	2621	78	101
12JT32_73	26	1.0	0.180	0.930	0.2	12.78	97.0	0.529	3.0	0.70	2730	120	2664	70	2649	86	2649	86	103
12JT32_76	22	2.4	0.182	0.940	0.2	13.01	99.0	0.536	3.0	0.61	2750	120	2669	71	2652	89	2652	89	104

TABLE SM2.3: LA-ICPMS U-PB ISOTOPIC DATA (UC SANTA CRUZ LAB)

						Isotope ratios					Apparent ages (Ma)								
Analysis	U	U/Th	206Pb*	±	error	207Pb*	±	206Pb*	±	error	206Pb*	±	207Pb*	±	206Pb*	±	Best age	±	Conc
	(ppm)		207Pb*	(%)	corr.	235U*	(%)	238U	(%)	corr.	238U*	(Ma)	235U	(Ma)	207Pb*	(Ma)	(Ma)	(Ma)	(%)
12JT32_47	172	1.9	0.180	0.830	0.2	11.94	83.0	0.480	2.4	0.75	2530	100	2597	66	2653	78	2653	78	95
12JT32_5	23	2.0	0.183	0.940	0.3	13.35	99.0	0.532	2.9	0.61	2740	120	2693	69	2675	81	2675	81	102
12JT32_6	50	1.6	0.187	0.900	0.2	13.90	99.0	0.534	2.7	0.68	2750	110	2745	67	2716	79	2716	79	101
12JT32_49	57	2.3	0.194	0.930	0.3	14.60	100.0	0.547	2.8	0.71	2820	120	2783	67	2782	80	2782	80	101
12JT32_65	32	1.9	0.203	0.990	0.4	16.40	120.0	0.587	3.1	0.66	2970	130	2893	68	2837	82	2837	82	105
12JT32_22	78	4.6	0.228	1.100	0.4	19.60	140.0	0.620	3.2	0.70	3110	120	3070	66	3041	73	3041	73	102
>20% Discordance																			
12JT32_88	486	2.0	0.138	0.630	0.2	4.60	32.0	0.245	1.2	0.77	1409	64	1750	58	2193	79	2193	79	64
12JT32_77	274	1.2	0.154	0.710	0.1	6.68	47.0	0.319	1.6	0.80	1784	80	2070	61	2385	79	2385	79	75
12JT32_98	193	1.6	0.155	0.730	-0.2	6.84	50.0	0.318	1.7	0.85	1781	83	2076	67	2395	80	2395	80	74
>5% Reverse Discordance																			
12JT32_23	86	391.9	0.077	0.460	0.3	2.35	18.0	0.219	1.2	0.28	1272	62	1224	54	1130	120	1130	120	113
12JT32_25	113	1.7	0.082	0.420	0.1	2.51	18.0	0.223	1.1	0.44	1294	59	1273	54	1226	98	1226	98	106
12JT32_90	13	0.8	0.089	0.670	0.3	3.09	29.0	0.253	1.6	0.45	1441	82	1411	70	1290	150	1290	150	112
12JT32_96	44	2.1	0.087	0.500	0.2	2.91	22.0	0.251	1.4	0.39	1440	70	1381	59	1340	110	1340	110	107
12JT32_100	56	2.1	0.090	0.500	0.4	3.23	24.0	0.260	1.4	0.22	1488	69	1455	58	1400	110	1400	110	106
12JT32_94	81	2.6	0.092	0.480	0.3	3.34	24.0	0.268	1.4	0.39	1528	70	1481	56	1440	100	1440	100	106
12JT32_61	26	4079.3	0.104	0.600	0.1	4.88	39.0	0.349	2.1	0.52	1911	97	1783	69	1660	110	1660	110	115
12JT32_64	15	1.5	0.111	0.740	0.3	5.15	44.0	0.342	2.0	0.38	1890	97	1819	74	1710	130	1710	130	111
12JT32_93	13	246.1	0.105	0.690	0.1	5.94	54.0	0.404	2.6	0.61	2160	120	1947	82	1710	130	1710	130	126
12JT32_51	10	318.0	0.111	0.790	0.3	5.87	53.0	0.380	2.6	0.48	2040	110	1933	79	1730	150	1730	150	118
12JT32_52	11	489.3	0.108	0.730	0.2	5.48	48.0	0.383	2.4	0.49	2070	110	1885	80	1730	130	1730	130	120
12JT32_27	25	2391.9	0.108	0.610	0.3	5.79	46.0	0.389	2.2	0.48	2110	100	1931	67	1740	110	1740	110	121
12JT32_67	8	660.0	0.111	0.880	0.3	5.75	56.0	0.395	2.6	0.46	2110	120	1941	83	1750	140	1750	140	121
12JT32_19	15	2127.1	0.109	0.690	0.3	5.83	48.0	0.389	2.4	0.45	2100	110	1933	72	1760	120	1760	120	119
12JT32_24	14	0.9	0.111	0.750	0.3	5.28	45.0	0.342	2.0	0.39	1880	97	1852	74	1770	130	1770	130	106

TABLE SM2.3: LA-ICPMS U-PB ISOTOPIC DATA (UC SANTA CRUZ LAB)

						Isotope ratios					Apparent ages (Ma)								
Analysis	U	U/Th	206Pb*	±	error	207Pb*	±	206Pb*	±	error	206Pb*	±	207Pb*	±	206Pb*	±	Best age	±	Conc
	(ppm)		207Pb*	(%)	corr.	235U*	(%)	238U	(%)	corr.	238U*	(Ma)	235U	(Ma)	207Pb*	(Ma)	(Ma)	(Ma)	(%)
12JT32_70	19	0.7	0.111	0.670	0.2	5.33	44.0	0.350	2.0	0.54	1925	95	1846	71	1820	110	1820	110	106
12JT32_86	72	1.5	0.113	0.570	0.3	5.41	39.0	0.351	1.8	0.51	1945	84	1889	61	1849	89	1849	89	105
12JT32_82	71	1.9	0.114	0.570	0.1	5.55	40.0	0.362	1.9	0.59	1988	89	1909	61	1850	90	1850	90	107
12JT32_91	19	4845.4	0.115	0.660	0.3	6.21	49.0	0.398	2.3	0.59	2150	100	1997	66	1860	100	1860	100	116
12JT32_15	114	3.2	0.114	0.550	0.2	5.72	40.0	0.360	1.8	0.48	1983	85	1934	60	1865	88	1865	88	106
12JT32_97	29	1.5	0.116	0.640	0.3	5.96	45.0	0.373	2.0	0.42	2042	94	1961	65	1870	100	1870	100	109
12JT32_89	72	1.6	0.116	0.570	0.2	5.92	43.0	0.368	1.9	0.61	2016	90	1957	61	1889	89	1889	89	107
12JT32_58	13	1684.3	0.116	0.760	0.3	6.66	56.0	0.419	2.6	0.56	2230	120	2036	75	1890	120	1890	120	118
12JT32_83	39	844.8	0.117	0.610	0.2	6.84	52.0	0.434	2.4	0.62	2310	110	2089	68	1909	95	1909	95	121
12JT32_54	29	3006.2	0.118	0.640	0.2	6.24	49.0	0.387	2.2	0.63	2100	100	1991	69	1911	96	1911	96	110
12JT32_21	5	22.5	0.133	1.300	0.3	7.43	81.0	0.427	3.5	0.51	2230	150	2060	100	1950	180	1950	180	114
12JT32_66	43	2.2	0.133	0.660	0.3	7.40	54.0	0.414	2.2	0.63	2244	99	2161	66	2126	87	2126	87	106
12JT32_60	116	4.4	0.144	0.690	0.0	9.14	67.0	0.463	2.5	0.81	2460	110	2342	67	2278	80	2278	80	108
12JT32_95	54	1.7	0.148	0.720	0.1	9.38	68.0	0.462	2.4	0.70	2440	110	2368	66	2314	83	2314	83	105
12JT32_59	60	1.7	0.152	0.730	0.3	9.77	70.0	0.472	2.5	0.68	2490	110	2405	65	2361	81	2361	81	105
12JT32_72	122	2.3	0.152	0.710	0.3	10.06	70.0	0.485	2.5	0.66	2550	110	2437	64	2363	79	2363	79	108
12JT32_30	7	0.8	0.164	1.100	0.4	11.70	100.0	0.517	3.5	0.70	2640	140	2551	82	2460	120	2460	120	107
12JT32_79	93	2.6	0.169	0.800	0.2	11.94	84.0	0.520	2.7	0.68	2700	110	2598	66	2551	83	2551	83	106
12JT32_78	59	1.8	0.173	0.820	0.3	12.72	90.0	0.537	2.8	0.71	2770	120	2652	67	2595	80	2595	80	107
12JT32_74	21	0.8	0.184	0.970	0.1	13.70	100.0	0.553	3.1	0.73	2810	120	2722	70	2671	89	2671	89	105
05LF13; Neruokpuk Formation (N69.18, W142.66)																			
05LF13_50	229	2.4	0.079	0.170	0.2	2.06	9.7	0.190	0.8	0.62	1118	46	1136	32	1165	45	1165	45	96
05LF13_58	354	3.3	0.081	0.180	0.1	2.24	10.0	0.202	0.9	0.76	1186	48	1194	33	1215	43	1215	43	98
05LF13_84	295	4.0	0.082	0.180	0.3	2.34	11.0	0.210	0.9	0.50	1229	50	1226	33	1236	44	1236	44	99
05LF13_85	126	4.1	0.082	0.190	0.3	2.51	12.0	0.224	1.0	0.49	1302	53	1274	34	1247	44	1247	44	104
05LF13_26	67	2.4	0.089	0.210	0.3	3.04	14.0	0.246	1.1	0.47	1419	58	1416	36	1398	45	1398	45	102
05LF13_87	85	3.0	0.091	0.210	0.2	3.23	15.0	0.261	1.2	0.52	1495	59	1463	36	1435	44	1435	44	104

TABLE SM2.3: LA-ICPMS U-PB ISOTOPIC DATA (UC SANTA CRUZ LAB)

						Isotope ratios					Apparent ages (Ma)								
Analysis	U	U/Th	206Pb*	±	error	207Pb*	±	206Pb*	±	error	206Pb*	±	207Pb*	±	206Pb*	±	Best age	±	Conc
	(ppm)		207Pb*	(%)	corr.	235U*	(%)	238U	(%)	corr.	238U*	(Ma)	235U	(Ma)	207Pb*	(Ma)	(Ma)	(Ma)	(%)
05LF13_43	504	1.8	0.091	0.190	0.0	2.72	13.0	0.215	1.0	0.81	1258	51	1335	34	1454	41	1454	41	87
05LF13_68	107	2.6	0.092	0.210	0.3	3.32	16.0	0.265	1.2	0.52	1515	60	1486	36	1460	42	1460	42	104
05LF13_60	178	2.2	0.092	0.200	0.2	3.12	15.0	0.245	1.1	0.60	1414	56	1435	36	1471	43	1471	43	96
05LF13_6	86	2.2	0.094	0.210	0.3	3.15	15.0	0.242	1.1	0.59	1398	57	1444	37	1500	43	1500	43	93
05LF13_39	152	1.2	0.101	0.220	0.4	4.07	19.0	0.290	1.3	0.56	1643	65	1648	38	1641	41	1641	41	100
05LF13_52	76	4.2	0.102	0.230	0.0	3.73	18.0	0.264	1.2	0.70	1509	60	1578	39	1658	43	1658	43	91
05LF13_13	197	2.9	0.104	0.230	0.0	4.15	20.0	0.289	1.3	0.84	1639	65	1664	38	1689	40	1689	40	97
05LF13_51	350	2.4	0.109	0.240	0.0	3.99	20.0	0.266	1.2	0.90	1520	63	1634	40	1784	40	1784	40	85
05LF13_21	83	1.1	0.110	0.250	0.2	4.61	22.0	0.304	1.4	0.67	1713	68	1752	38	1798	42	1798	42	95
05LF13_32	262	1.5	0.111	0.250	0.2	5.06	24.0	0.331	1.5	0.72	1843	72	1829	41	1815	40	1815	40	102
05LF13_93	148	1.8	0.112	0.240	0.2	4.99	23.0	0.326	1.4	0.58	1817	70	1818	39	1828	40	1828	40	99
05LF13_35	117	3.2	0.112	0.250	0.2	5.06	24.0	0.329	1.5	0.62	1832	72	1829	39	1828	41	1828	41	100
05LF13_8	42	1.3	0.112	0.270	0.2	5.14	25.0	0.331	1.5	0.58	1845	72	1840	41	1839	43	1839	43	100
05LF13_1	70	1.9	0.112	0.250	0.2	5.38	25.0	0.346	1.5	0.60	1913	74	1879	40	1840	40	1840	40	104
05LF13_61	100	2.6	0.113	0.250	0.3	4.82	22.0	0.312	1.4	0.56	1749	67	1788	39	1841	40	1841	40	95
05LF13_67	79	2.5	0.114	0.260	0.1	5.14	25.0	0.331	1.5	0.79	1843	74	1841	42	1852	41	1852	41	100
05LF13_71	87	3.6	0.115	0.250	0.3	4.98	23.0	0.319	1.4	0.76	1787	70	1813	40	1870	40	1870	40	96
05LF13_3	185	2.5	0.115	0.270	-0.3	4.98	27.0	0.310	1.6	0.94	1736	78	1809	47	1876	42	1876	42	93
05LF13_24	75	2.0	0.115	0.260	0.3	4.82	23.0	0.303	1.4	0.71	1705	69	1788	41	1878	42	1878	42	91
05LF13_65	92	2.8	0.115	0.250	0.2	5.13	24.0	0.324	1.4	0.64	1809	70	1842	40	1882	40	1882	40	96
05LF13_59	230	2.8	0.116	0.250	0.2	5.10	24.0	0.320	1.4	0.74	1788	69	1837	39	1887	39	1887	39	95
05LF13_15	92	2.3	0.115	0.260	0.2	4.66	22.0	0.293	1.3	0.68	1658	65	1760	39	1888	41	1888	41	88
05LF13_28	48	0.6	0.116	0.290	0.3	5.36	26.0	0.336	1.5	0.49	1869	73	1878	41	1888	44	1888	44	99
05LF13_38	49	0.5	0.116	0.270	0.1	5.30	25.0	0.328	1.5	0.64	1828	72	1867	41	1896	42	1896	42	96
05LF13_14	178	1.2	0.116	0.250	0.3	5.60	26.0	0.348	1.6	0.72	1924	74	1915	40	1896	39	1896	39	101
05LF13_72	65	1.3	0.116	0.260	0.3	5.72	27.0	0.360	1.6	0.55	1984	76	1934	40	1897	39	1897	39	105
05LF13_7	130	0.6	0.116	0.250	0.3	5.65	26.0	0.349	1.5	0.63	1932	73	1925	40	1900	39	1900	39	102
05LF13_94	128	1.2	0.117	0.250	0.2	5.47	25.0	0.342	1.5	0.59	1897	73	1899	40	1903	39	1903	39	100

TABLE SM2.3: LA-ICPMS U-PB ISOTOPIC DATA (UC SANTA CRUZ LAB)

						Isotope ratios					Apparent ages (Ma)								
Analysis	U	U/Th	206Pb*	±	error	207Pb*	±	206Pb*	±	error	206Pb*	±	207Pb*	±	206Pb*	±	Best age	±	Conc
	(ppm)		207Pb*	(%)	corr.	235U*	(%)	238U	(%)	corr.	238U*	(Ma)	235U	(Ma)	207Pb*	(Ma)	(Ma)	(Ma)	(%)
05LF13_45	72	0.7	0.117	0.270	0.3	5.31	25.0	0.330	1.5	0.60	1837	72	1872	40	1905	41	1905	41	96
05LF13_92	45	1.0	0.117	0.270	0.2	5.36	25.0	0.337	1.5	0.56	1872	72	1881	41	1905	42	1905	42	98
05LF13_49	128	0.6	0.117	0.260	0.2	5.59	26.0	0.346	1.5	0.72	1916	74	1915	41	1906	40	1906	40	101
05LF13_57	223	2.5	0.117	0.260	0.0	5.04	24.0	0.313	1.4	0.88	1755	71	1825	40	1907	39	1907	39	92
05LF13_66	143	2.6	0.117	0.250	0.2	5.71	26.0	0.356	1.6	0.65	1963	75	1932	40	1909	39	1909	39	103
05LF13_18	282	2.3	0.117	0.250	0.3	5.18	24.0	0.321	1.4	0.66	1792	69	1850	40	1913	38	1913	38	94
05LF13_2	287	7.0	0.117	0.250	0.2	5.43	25.0	0.335	1.5	0.69	1863	71	1890	40	1914	40	1914	40	97
05LF13_4	104	1.3	0.118	0.260	0.1	5.28	25.0	0.321	1.4	0.71	1794	70	1867	41	1931	39	1931	39	93
05LF13_100	69	0.8	0.119	0.270	0.1	5.79	27.0	0.356	1.6	0.71	1964	76	1945	42	1934	40	1934	40	102
05LF13_78	199	1.2	0.119	0.250	0.3	5.80	27.0	0.357	1.6	0.68	1970	75	1946	40	1936	38	1936	38	102
05LF13_11	164	0.8	0.119	0.260	0.1	5.28	25.0	0.320	1.4	0.78	1792	70	1865	40	1938	38	1938	38	92
05LF13_83	34	1.0	0.120	0.300	0.1	5.62	28.0	0.342	1.6	0.71	1892	76	1918	42	1950	45	1950	45	97
05LF13_10	71	2.2	0.121	0.300	0.0	5.55	27.0	0.336	1.5	0.46	1868	73	1903	40	1959	43	1959	43	95
05LF13_79	169	5.9	0.123	0.270	-0.4	5.52	27.0	0.331	1.5	0.90	1841	73	1904	41	2001	39	2001	39	92
05LF13_98	13	1.6	0.127	0.340	0.2	6.74	34.0	0.391	1.8	0.53	2124	84	2079	45	2060	48	2060	48	103
05LF13_55	220	1.4	0.129	0.290	-0.5	6.38	31.0	0.359	1.6	0.86	1978	76	2027	42	2078	40	2078	40	95
05LF13_34	174	1.2	0.129	0.280	0.2	6.94	33.0	0.389	1.7	0.78	2118	81	2104	41	2083	38	2083	38	102
05LF13_69	41	1.1	0.136	0.330	0.0	7.12	35.0	0.383	1.7	0.71	2091	82	2126	45	2172	42	2172	42	96
05LF13_33	115	1.9	0.136	0.300	0.1	7.62	36.0	0.403	1.8	0.71	2184	82	2186	42	2182	38	2182	38	100
05LF13_89	80	2.5	0.138	0.300	0.0	7.70	36.0	0.410	1.8	0.72	2215	84	2198	42	2203	38	2203	38	101
05LF13_91	42	1.0	0.142	0.320	0.3	8.03	38.0	0.415	1.9	0.63	2238	85	2234	44	2250	40	2250	40	99
05LF13_16	153	2.2	0.143	0.310	0.0	8.31	39.0	0.419	1.9	0.69	2256	85	2265	42	2265	38	2265	38	100
05LF13_54	206	1.7	0.143	0.310	0.2	7.93	37.0	0.400	1.8	0.74	2169	81	2222	42	2268	37	2268	37	96
05LF13_44	48	1.3	0.144	0.340	0.0	8.24	40.0	0.418	1.9	0.78	2253	88	2261	45	2270	40	2270	40	99
05LF13_70	75	0.5	0.147	0.320	0.2	8.68	41.0	0.432	1.9	0.75	2316	88	2304	43	2309	38	2309	38	100
05LF13_95	72	1.2	0.147	0.330	0.3	8.74	41.0	0.431	1.9	0.68	2311	88	2310	43	2310	38	2310	38	100
05LF13_23	215	2.0	0.148	0.320	0.3	8.14	38.0	0.396	1.8	0.81	2151	83	2246	42	2325	36	2325	36	93
05LF13_22	82	1.1	0.148	0.320	0.3	9.26	43.0	0.453	2.0	0.61	2412	91	2363	43	2325	37	2325	37	104

TABLE SM2.3: LA-ICPMS U-PB ISOTOPIC DATA (UC SANTA CRUZ LAB)

						Isotope ratios					Apparent ages (Ma)								
Analysis	U	U/Th	206Pb*	±	error	207Pb*	±	206Pb*	±	error	206Pb*	±	207Pb*	±	206Pb*	±	Best age	±	Conc
	(ppm)		207Pb*	(%)	corr.	235U*	(%)	238U	(%)	corr.	238U*	(Ma)	235U	(Ma)	207Pb*	(Ma)	(Ma)	(Ma)	(%)
05LF13_27	173	1.7	0.151	0.320	0.1	8.43	39.0	0.404	1.8	0.84	2187	83	2278	43	2356	37	2356	37	93
05LF13_62	115	1.4	0.152	0.330	0.2	7.22	34.0	0.346	1.5	0.69	1914	74	2140	42	2369	38	2369	38	81
05LF13_53	134	3.1	0.153	0.330	0.2	8.91	41.0	0.423	1.9	0.70	2273	84	2330	42	2374	37	2374	37	96
05LF13_42	164	1.0	0.153	0.330	0.3	9.42	44.0	0.444	2.0	0.74	2370	88	2380	43	2375	37	2375	37	100
05LF13_40	127	2.0	0.153	0.330	0.4	9.52	44.0	0.449	2.0	0.64	2389	89	2388	43	2378	37	2378	37	100
05LF13_82	42	2.0	0.159	0.370	0.1	9.78	47.0	0.452	2.1	0.69	2404	93	2415	43	2441	39	2441	39	98
05LF13_81	84	3.2	0.159	0.410	0.2	7.68	40.0	0.359	1.7	0.79	1979	81	2198	47	2442	43	2442	43	81
05LF13_25	298	2.3	0.159	0.340	0.1	9.34	43.0	0.425	1.9	0.84	2281	85	2373	43	2443	36	2443	36	93
05LF13_73	162	2.8	0.160	0.340	0.2	8.48	39.0	0.389	1.7	0.79	2116	81	2284	42	2452	36	2452	36	86
05LF13_47	78	1.5	0.163	0.350	0.2	10.32	48.0	0.459	2.0	0.70	2438	91	2464	44	2483	37	2483	37	98
05LF13_88	102	1.6	0.163	0.350	0.0	9.93	47.0	0.448	2.0	0.86	2387	89	2429	43	2484	37	2484	37	96
05LF13_19	96	1.5	0.164	0.360	0.1	9.92	47.0	0.435	2.0	0.80	2327	88	2429	44	2497	36	2497	36	93
05LF13_76	43	1.4	0.165	0.380	0.2	9.69	47.0	0.431	2.0	0.75	2308	90	2404	45	2508	39	2508	39	92
05LF13_99	126	1.1	0.166	0.360	-0.2	9.66	49.0	0.422	2.0	0.95	2264	93	2396	48	2514	37	2514	37	90
05LF13_86	25	1.2	0.168	0.420	0.1	8.99	46.0	0.392	1.9	0.77	2128	86	2335	47	2540	41	2540	41	84
05LF13_41	71	2.4	0.172	0.380	0.1	11.69	55.0	0.490	2.2	0.72	2570	94	2580	43	2576	36	2576	36	100
05LF13_31	34	1.3	0.182	0.410	0.3	12.95	61.0	0.517	2.3	0.63	2688	98	2677	46	2671	38	2671	38	101
05LF13_20	115	1.4	0.184	0.390	0.3	12.85	60.0	0.506	2.3	0.72	2637	97	2669	44	2689	36	2689	36	98
05LF13_77	121	1.4	0.185	0.390	0.2	13.28	62.0	0.527	2.3	0.83	2730	100	2700	45	2698	34	2698	34	101
05LF13_96	112	2.4	0.189	0.400	0.2	13.97	65.0	0.541	2.4	0.75	2790	100	2749	44	2729	35	2729	35	102
05LF13_30	149	2.2	0.191	0.420	0.1	12.65	60.0	0.481	2.2	0.84	2532	95	2655	45	2748	36	2748	36	92
>20% Discordance																			
05LF13_63	288	1.7	0.113	0.260	0.6	1.65	8.0	0.106	0.5	0.83	651	30	991	31	1844	41	651	30	35
05LF13_75	620	3.3	0.137	0.310	-0.5	2.42	13.0	0.130	0.6	0.97	787	36	1246	37	2185	40	787	36	36
05LF13_74	757	4.7	0.121	0.260	-0.3	2.73	13.0	0.165	0.8	0.92	984	42	1337	36	1963	39	984	42	50
05LF13_56	362	2.0	0.096	0.220	0.2	2.45	12.0	0.183	0.8	0.67	1082	45	1259	33	1544	43	1544	43	70
05LF13_48	232	0.9	0.114	0.330	-0.3	3.98	21.0	0.251	1.1	0.61	1442	58	1621	36	1856	46	1856	46	78

TABLE SM2.3: LA-ICPMS U-PB ISOTOPIC DATA (UC SANTA CRUZ LAB)

						Isotope ratios					Apparent ages (Ma)								
Analysis	U	U/Th	206Pb*	±	error	207Pb*	±	206Pb*	±	error	206Pb*	±	207Pb*	±	206Pb*	±	Best age	±	Conc
	(ppm)		207Pb*	(%)	corr.	235U*	(%)	238U	(%)	corr.	238U*	(Ma)	235U	(Ma)	207Pb*	(Ma)	(Ma)	(Ma)	(%)
05LF13_5	136	1.5	0.116	0.260	0.1	4.26	20.0	0.265	1.2	0.86	1517	62	1686	40	1901	39	1901	39	80
05LF13_80	288	3.6	0.132	0.340	-0.7	5.29	30.0	0.292	1.4	0.96	1648	70	1863	48	2131	44	2131	44	77
05LF13_12	585	0.9	0.150	0.320	-0.2	3.64	17.0	0.175	0.8	0.89	1038	43	1559	38	2351	36	2351	36	44
05LF13_90	322	1.8	0.162	0.350	0.1	7.86	37.0	0.356	1.6	0.89	1962	75	2214	43	2474	36	2474	36	79
05LF13_97	206	2.7	0.168	0.360	-0.1	7.73	37.0	0.335	1.5	0.91	1862	74	2199	43	2535	36	2535	36	73
05LF13_64	85	1.7	0.181	0.420	-0.2	9.65	50.0	0.384	1.9	0.92	2092	87	2397	49	2659	38	2659	38	79
05LF13_9	420	2.3	0.265	0.570	-0.5	9.57	47.0	0.261	1.2	0.95	1495	61	2395	46	3273	34	3273	34	46
>5% Reverse Discordance																			
05LF13_46	441	12.4	0.053	0.120	0.2	0.39	1.9	0.053	0.2	0.33	334	14	336	13	329	53	334	14	102
05LF13_37	74	1.0	0.106	0.250	0.2	4.98	24.0	0.338	1.5	0.65	1876	74	1814	41	1724	43	1724	43	109
05LF13_29	51	1.5	0.112	0.300	0.3	6.04	31.0	0.395	1.9	0.71	2143	87	1984	46	1824	47	1824	47	117
11LF13; Neruokpuk Formation (N69.26, W142.66)																			
11LF13_59	307	0.9	0.077	0.350	0.2	1.93	12.0	0.188	0.8	0.47	1109	46	1092	43	1102	95	1102	95	101
11LF13_43	64	4.0	0.076	0.450	0.3	2.10	16.0	0.196	0.9	0.27	1156	51	1143	51	1130	120	1130	120	102
11LF13_77	169	1.5	0.079	0.380	0.3	2.14	14.0	0.201	0.9	0.36	1181	49	1160	46	1172	95	1172	95	101
11LF13_92	97	3.5	0.084	0.430	0.3	2.36	16.0	0.208	1.0	0.41	1214	51	1228	50	1292	97	1292	97	94
11LF13_36	153	2.3	0.087	0.420	0.3	2.76	18.0	0.229	1.0	0.29	1329	54	1347	49	1364	95	1364	95	97
11LF13_93	531	1.4	0.092	0.400	0.2	3.09	20.0	0.252	1.1	0.65	1451	57	1428	49	1454	84	1454	84	100
11LF13_55	127	0.9	0.105	0.490	0.2	4.47	29.0	0.318	1.4	0.52	1781	70	1725	53	1709	88	1709	88	104
11LF13_53	103	1.7	0.106	0.500	0.2	4.52	30.0	0.315	1.4	0.57	1764	69	1734	54	1741	84	1741	84	101
11LF13_62	38	1.3	0.110	0.600	0.4	4.92	35.0	0.331	1.6	0.41	1836	79	1796	60	1790	100	1790	100	103
11LF13_72	194	2.9	0.110	0.490	0.3	4.77	31.0	0.322	1.4	0.59	1800	70	1777	54	1799	81	1799	81	100
11LF13_74	102	1.3	0.111	0.530	0.3	4.90	32.0	0.326	1.5	0.49	1818	72	1801	53	1810	86	1810	86	100
11LF13_7	275	1.5	0.111	0.500	0.3	4.48	29.0	0.294	1.3	0.57	1659	65	1729	53	1816	82	1816	82	91
11LF13_97	177	1.5	0.111	0.510	0.3	5.02	32.0	0.335	1.5	0.52	1862	72	1823	54	1821	82	1821	82	102
11LF13_99	81	2.7	0.112	0.530	0.3	4.91	32.0	0.329	1.5	0.56	1835	74	1801	57	1829	89	1829	89	100

TABLE SM2.3: LA-ICPMS U-PB ISOTOPIC DATA (UC SANTA CRUZ LAB)

						Isotope ratios					Apparent ages (Ma)								
Analysis	U	U/Th	206Pb*	±	error	207Pb*	±	206Pb*	±	error	206Pb*	±	207Pb*	±	206Pb*	±	Best age	±	Conc
	(ppm)		207Pb*	(%)	corr.	235U*	(%)	238U	(%)	corr.	238U*	(Ma)	235U	(Ma)	207Pb*	(Ma)	(Ma)	(Ma)	(%)
11LF13_64	63	0.7	0.112	0.550	0.2	5.00	34.0	0.325	1.5	0.52	1814	74	1807	58	1832	88	1832	88	99
11LF13_47	52	1.4	0.112	0.590	0.1	5.11	36.0	0.339	1.6	0.51	1881	77	1853	63	1837	99	1837	99	102
11LF13_3	209	1.9	0.113	0.510	0.3	5.09	33.0	0.329	1.5	0.57	1831	71	1832	54	1842	80	1842	80	99
11LF13_51	111	1.2	0.112	0.530	0.3	5.14	34.0	0.333	1.5	0.49	1851	73	1838	56	1843	87	1843	87	100
11LF13_89	36	0.7	0.113	0.500	0.3	5.06	32.0	0.330	1.5	0.59	1841	70	1828	53	1844	79	1844	79	100
11LF13_68	87	0.5	0.114	0.550	0.2	5.01	33.0	0.327	1.5	0.48	1822	72	1817	57	1848	89	1848	89	99
11LF13_84	90	1.7	0.114	0.550	0.3	4.87	32.0	0.323	1.5	0.39	1801	72	1796	56	1849	87	1849	87	97
11LF13_45	366	3.2	0.113	0.500	0.1	5.28	34.0	0.344	1.5	0.67	1906	72	1866	54	1849	79	1849	79	103
11LF13_19	115	1.7	0.113	0.530	0.2	5.21	34.0	0.332	1.5	0.53	1847	73	1852	55	1850	85	1850	85	100
11LF13_58	181	3.1	0.114	0.520	0.2	5.25	34.0	0.338	1.5	0.58	1882	72	1858	55	1856	83	1856	83	101
11LF13_17	156	1.6	0.114	0.520	0.3	5.49	35.0	0.354	1.6	0.55	1952	76	1906	58	1867	83	1867	83	105
11LF13_33	33	1.2	0.114	0.600	0.3	5.42	38.0	0.339	1.7	0.55	1879	83	1886	62	1868	96	1868	96	101
11LF13_9	332	4.4	0.115	0.620	0.2	5.19	37.0	0.331	1.6	0.41	1841	79	1852	61	1871	96	1871	96	98
11LF13_6	194	1.4	0.116	0.520	0.2	5.33	34.0	0.334	1.5	0.59	1861	72	1872	55	1886	78	1886	78	99
11LF13_11	63	0.8	0.117	0.590	0.3	5.51	37.0	0.343	1.6	0.41	1897	77	1897	58	1895	91	1895	91	100
11LF13_15	113	2.6	0.117	0.540	0.2	5.55	36.0	0.348	1.6	0.59	1923	76	1915	56	1900	83	1900	83	101
11LF13_95	53	0.8	0.118	0.590	0.2	5.43	38.0	0.342	1.6	0.56	1888	79	1883	60	1902	94	1902	94	99
11LF13_1	149	1.0	0.117	0.530	0.2	5.54	36.0	0.346	1.6	0.61	1912	75	1905	57	1905	84	1905	84	100
11LF13_91	54	1.2	0.117	0.570	0.2	5.29	36.0	0.333	1.6	0.52	1850	75	1865	57	1906	91	1906	91	97
11LF13_4	269	1.4	0.117	0.520	0.3	5.45	35.0	0.338	1.5	0.60	1877	73	1891	54	1912	80	1912	80	98
11LF13_98	218	1.9	0.117	0.520	0.3	5.48	35.0	0.351	1.6	0.58	1937	74	1898	55	1913	81	1913	81	101
11LF13_41	112	1.2	0.117	0.550	0.2	5.73	38.0	0.355	1.6	0.52	1961	77	1929	57	1913	84	1913	84	103
11LF13_78	302	3.0	0.118	0.520	0.3	5.47	35.0	0.342	1.5	0.61	1896	74	1896	54	1922	80	1922	80	99
11LF13_79	387	2.5	0.118	0.520	0.1	5.14	33.0	0.324	1.5	0.80	1807	72	1844	55	1923	79	1923	79	94
11LF13_57	57	0.8	0.120	0.630	0.1	5.23	37.0	0.327	1.6	0.53	1819	76	1849	59	1925	97	1925	97	94
11LF13_31	53	0.6	0.119	0.600	0.2	5.82	40.0	0.358	1.7	0.54	1965	80	1945	61	1929	87	1929	87	102
11LF13_46	71	1.0	0.118	0.570	0.2	5.81	39.0	0.358	1.7	0.52	1970	78	1944	59	1938	86	1938	86	102
11LF13_81	40	0.9	0.122	0.700	0.1	5.44	41.0	0.334	1.6	0.45	1857	77	1875	65	1960	100	1960	100	95

TABLE SM2.3: LA-ICPMS U-PB ISOTOPIC DATA (UC SANTA CRUZ LAB)

						Isotope ratios					Apparent ages (Ma)								
Analysis	U	U/Th	206Pb*	±	error	207Pb*	±	206Pb*	±	error	206Pb*	±	207Pb*	±	206Pb*	±	Best age	±	Conc
	(ppm)		207Pb*	(%)	corr.	235U*	(%)	238U	(%)	corr.	238U*	(Ma)	235U	(Ma)	207Pb*	(Ma)	(Ma)	(Ma)	(%)
11LF13_83	49	1.0	0.120	0.590	0.3	5.60	38.0	0.340	1.6	0.51	1888	77	1919	59	1965	89	1965	89	96
11LF13_29	85	0.9	0.122	0.580	0.2	6.22	41.0	0.371	1.7	0.56	2037	78	2004	57	1976	86	1976	86	103
11LF13_35	121	2.2	0.124	0.570	0.3	6.31	41.0	0.371	1.7	0.53	2032	79	2017	57	2007	85	2007	85	101
11LF13_52	101	0.6	0.124	0.580	0.2	6.34	42.0	0.377	1.7	0.60	2060	80	2023	57	2015	85	2015	85	102
11LF13_24	160	2.1	0.125	0.560	0.2	6.48	42.0	0.379	1.7	0.60	2072	79	2042	57	2022	77	2022	77	102
11LF13_94	145	1.0	0.125	0.580	0.3	5.18	34.0	0.309	1.4	0.62	1734	70	1848	57	2028	81	2028	81	86
11LF13_37	231	2.5	0.126	0.560	0.3	6.51	41.0	0.377	1.7	0.65	2057	79	2044	55	2044	81	2044	81	101
11LF13_56	295	2.7	0.126	0.560	0.3	6.49	41.0	0.379	1.7	0.66	2068	78	2045	56	2046	81	2046	81	101
11LF13_90	44	1.8	0.129	0.650	0.3	6.72	46.0	0.383	1.8	0.46	2093	85	2070	60	2072	89	2072	89	101
11LF13_50	80	0.9	0.130	0.610	0.2	6.70	44.0	0.381	1.8	0.59	2080	82	2069	59	2076	85	2076	85	100
11LF13_49	445	2.7	0.128	0.560	0.1	6.40	42.0	0.370	1.7	0.87	2030	82	2034	57	2077	79	2077	79	98
11LF13_63	582	4.5	0.130	0.570	0.1	6.11	39.0	0.347	1.5	0.82	1919	75	1989	55	2101	75	2101	75	91
11LF13_75	44	1.5	0.131	0.660	0.3	6.62	45.0	0.378	1.8	0.45	2063	84	2057	59	2113	86	2113	86	98
11LF13_10	394	1.7	0.133	0.580	0.0	6.79	44.0	0.372	1.7	0.87	2042	79	2083	56	2133	76	2133	76	96
11LF13_76	65	1.6	0.132	0.640	0.3	6.72	45.0	0.373	1.7	0.51	2041	81	2075	59	2135	84	2135	84	96
11LF13_21	189	1.3	0.136	0.610	0.3	7.91	51.0	0.419	1.9	0.57	2258	84	2218	57	2179	79	2179	79	104
11LF13_88	203	2.7	0.137	0.610	0.2	7.14	46.0	0.391	1.7	0.64	2128	81	2131	58	2180	76	2180	76	98
11LF13_67	90	1.1	0.142	0.690	0.3	7.73	52.0	0.398	1.9	0.56	2161	86	2197	60	2244	85	2244	85	96
11LF13_23	167	1.3	0.143	0.630	0.1	8.67	56.0	0.441	2.0	0.70	2357	86	2304	60	2264	78	2264	78	104
11LF13_70	228	1.0	0.144	0.640	0.1	6.72	45.0	0.342	1.6	0.88	1902	80	2077	58	2275	77	2275	77	84
11LF13_73	136	1.5	0.147	0.660	0.2	8.59	56.0	0.432	1.9	0.64	2315	88	2292	59	2310	79	2310	79	100
11LF13_61	215	14.8	0.148	0.660	0.3	8.79	56.0	0.442	2.0	0.64	2364	90	2313	58	2319	76	2319	76	102
11LF13_86	127	1.4	0.148	0.670	0.4	8.56	55.0	0.429	1.9	0.54	2302	87	2289	58	2329	79	2329	79	99
11LF13_28	46	3.4	0.149	0.720	0.3	8.95	60.0	0.439	2.1	0.54	2339	93	2331	64	2330	84	2330	84	100
11LF13_8	158	1.9	0.150	0.670	0.3	9.12	58.0	0.445	2.0	0.66	2371	88	2350	59	2340	74	2340	74	101
11LF13_54	97	1.3	0.151	0.680	0.3	9.17	59.0	0.450	2.0	0.60	2394	90	2355	59	2361	78	2361	78	101
11LF13_22	84	0.6	0.153	0.700	0.1	9.43	62.0	0.448	2.1	0.68	2395	90	2376	60	2372	77	2372	77	101
11LF13_34	275	2.1	0.157	0.690	0.2	9.85	62.0	0.458	2.0	0.72	2426	89	2419	59	2416	75	2416	75	100

TABLE SM2.3: LA-ICPMS U-PB ISOTOPIC DATA (UC SANTA CRUZ LAB)

						Isotope ratios					Apparent ages (Ma)								
Analysis	U	U/Th	206Pb*	±	error	207Pb*	±	206Pb*	±	error	206Pb*	±	207Pb*	±	206Pb*	±	Best age	±	Conc
	(ppm)		207Pb*	(%)	corr.	235U*	(%)	238U	(%)	corr.	238U*	(Ma)	235U	(Ma)	207Pb*	(Ma)	(Ma)	(Ma)	(%)
11LF13_5	35	1.4	0.159	0.770	0.3	10.06	69.0	0.465	2.3	0.58	2460	100	2439	65	2437	85	2437	85	101
11LF13_2	161	1.2	0.160	0.720	0.2	10.05	64.0	0.458	2.1	0.69	2430	91	2442	58	2457	74	2457	74	99
11LF13_25	117	2.2	0.168	0.780	-0.3	11.26	75.0	0.485	2.2	0.70	2543	96	2531	60	2531	74	2531	74	100
11LF13_100	207	1.7	0.170	0.750	0.3	11.22	71.0	0.493	2.2	0.76	2585	95	2540	61	2556	72	2556	72	101
11LF13_65	212	4.6	0.170	0.750	0.3	11.12	70.0	0.485	2.1	0.70	2548	94	2534	59	2561	74	2561	74	99
11LF13_85	43	0.8	0.171	0.830	0.2	11.13	76.0	0.478	2.3	0.61	2509	99	2523	64	2567	78	2567	78	98
11LF13_27	272	1.3	0.172	0.750	0.3	12.17	77.0	0.515	2.3	0.76	2678	97	2618	59	2572	73	2572	73	104
11LF13_16	111	2.0	0.175	0.780	0.3	12.59	81.0	0.526	2.4	0.72	2720	100	2647	60	2602	73	2602	73	105
11LF13_66	41	1.9	0.178	0.840	0.2	11.60	78.0	0.484	2.3	0.63	2544	98	2559	63	2627	78	2627	78	97
11LF13_18	47	1.0	0.179	0.840	0.3	12.52	83.0	0.509	2.4	0.65	2660	100	2641	63	2638	78	2638	78	101
11LF13_12	58	2.0	0.178	0.900	0.3	11.99	85.0	0.490	2.7	0.67	2560	120	2597	67	2639	82	2639	82	97
11LF13_26	318	5.7	0.179	0.780	0.3	12.82	81.0	0.517	2.3	0.76	2690	99	2666	59	2644	73	2644	73	102
11LF13_69	159	1.3	0.180	0.800	0.3	11.53	73.0	0.478	2.1	0.67	2518	93	2573	61	2645	74	2645	74	95
11LF13_48	176	3.7	0.184	0.810	0.3	12.63	80.0	0.510	2.3	0.73	2657	95	2657	59	2682	72	2682	72	99
11LF13_60	61	1.6	0.184	0.840	0.2	12.96	85.0	0.522	2.4	0.73	2710	100	2672	61	2684	77	2684	77	101
11LF13_71	83	1.9	0.185	0.840	0.3	13.15	85.0	0.522	2.4	0.66	2710	100	2686	60	2707	75	2707	75	100
11LF13_30	54	1.3	0.188	0.870	0.3	13.94	91.0	0.536	2.5	0.67	2770	100	2747	60	2723	78	2723	78	102
11LF13_80	111	1.9	0.189	0.840	0.3	13.48	86.0	0.527	2.4	0.71	2726	99	2715	59	2736	72	2736	72	100
11LF13_42	114	0.8	0.198	0.880	0.2	15.33	98.0	0.569	2.6	0.73	2900	110	2833	60	2807	71	2807	71	103
11LF13_32	62	1.1	0.211	0.960	0.2	17.00	110.0	0.582	2.7	0.70	2960	110	2928	61	2909	73	2909	73	102
>20% Discordance																			
11LF13_96	519	1.3	0.123	0.540	0.2	4.48	29.0	0.274	1.3	0.86	1557	66	1725	55	2000	76	2000	76	78
>5% Reverse Discordance																			
11LF13_82	42	3613.8	0.109	0.560	0.1	5.84	42.0	0.396	2.0	0.66	2147	90	1939	61	1762	95	1762	95	122
11LF13_87	142	1.5	0.110	0.500	0.3	5.11	33.0	0.342	1.6	0.58	1893	74	1833	55	1799	82	1799	82	105
11LF13_14	217	1.9	0.112	0.500	0.2	5.38	34.0	0.352	1.6	0.61	1943	73	1883	56	1822	79	1822	79	107

TABLE SM2.3: LA-ICPMS U-PB ISOTOPIC DATA (UC SANTA CRUZ LAB)

						Isotope ratios					Apparent ages (Ma)								
Analysis	U	U/Th	206Pb*	±	error	207Pb*	±	206Pb*	±	error	206Pb*	±	207Pb*	±	206Pb*	±	Best age	±	Conc
	(ppm)		207Pb*	(%)	corr.	235U*	(%)	238U	(%)	corr.	238U*	(Ma)	235U	(Ma)	207Pb*	(Ma)	(Ma)	(Ma)	(%)
11LF13_44	131	5.3	0.111	0.510	0.2	5.37	35.0	0.350	1.6	0.57	1932	74	1877	55	1824	81	1824	81	106
11LF13_38	50	0.8	0.113	0.600	0.2	5.60	40.0	0.357	1.8	0.58	1960	84	1909	61	1851	94	1851	94	106
11LF13_20	28	1.8	0.136	0.730	0.2	8.57	64.0	0.459	2.4	0.58	2430	110	2274	69	2153	97	2153	97	113
11LF13_39	85	2.1	0.169	0.760	0.3	12.11	79.0	0.517	2.3	0.65	2686	99	2612	61	2548	77	2548	77	105
11LF13_40	44	2.2	0.174	0.830	0.2	14.67	98.0	0.613	2.9	0.59	3070	120	2788	62	2583	79	2583	79	119
28LF13; Neruokpuk Formation (N69.36, W142.8)																			
28LF13_72	613	2.4	0.102	0.470	0.0	3.37	24.0	0.243	1.3	0.85	1399	65	1498	57	1653	85	1653	85	85
28LF13_1	45	1.3	0.110	0.580	0.2	4.96	37.0	0.328	1.7	0.47	1828	82	1803	63	1793	99	1793	99	102
28LF13_7	147	1.5	0.111	0.530	0.3	5.07	35.0	0.335	1.7	0.48	1865	79	1833	59	1808	87	1808	87	103
28LF13_33	513	1.5	0.111	0.520	-0.3	4.33	37.0	0.289	2.0	0.96	1610	100	1657	74	1820	85	1820	85	88
28LF13_10	56	1.3	0.115	0.570	0.3	5.37	39.0	0.339	1.8	0.59	1883	86	1878	60	1873	88	1873	88	101
28LF13_4	73	0.6	0.114	0.570	0.2	5.13	37.0	0.329	1.7	0.50	1830	80	1841	61	1877	89	1877	89	97
28LF13_9	72	1.3	0.115	0.570	0.3	5.50	39.0	0.347	1.8	0.51	1918	84	1893	60	1880	90	1880	90	102
28LF13_95	285	3.4	0.115	0.530	0.2	5.59	39.0	0.353	1.8	0.76	1944	86	1916	59	1883	86	1883	86	103
28LF13_39	321	3.1	0.116	0.570	0.7	4.98	35.0	0.310	1.7	0.53	1746	80	1813	60	1884	88	1884	88	93
28LF13_61	518	3.3	0.116	0.530	0.0	4.36	31.0	0.275	1.4	0.85	1570	72	1704	57	1891	82	1891	82	83
28LF13_29	50	1.1	0.115	0.610	0.3	5.53	40.0	0.356	1.8	0.36	1964	86	1895	63	1892	94	1892	94	104
28LF13_6	60	0.5	0.115	0.580	0.2	5.51	40.0	0.347	1.8	0.54	1922	85	1903	64	1895	91	1895	91	101
28LF13_2	87	1.6	0.117	0.580	0.4	5.54	39.0	0.344	1.7	0.41	1903	83	1903	61	1902	88	1902	88	100
28LF13_18	31	3.2	0.118	0.630	0.3	5.75	43.0	0.366	2.0	0.46	2008	94	1938	68	1923	97	1923	97	104
28LF13_19	202	2.4	0.120	0.560	0.2	5.99	41.0	0.372	1.8	0.60	2036	86	1976	61	1951	83	1951	83	104
28LF13_16	38	2.0	0.121	0.640	0.3	6.23	46.0	0.373	1.9	0.41	2040	91	2010	65	1956	93	1956	93	104
28LF13_64	23	2.3	0.123	0.770	0.2	5.25	43.0	0.316	1.8	0.50	1763	86	1861	73	1980	120	1980	120	89
28LF13_8	81	1.2	0.126	0.610	0.3	6.58	47.0	0.379	1.9	0.55	2071	90	2054	63	2042	88	2042	88	101
28LF13_65	287	1.9	0.127	0.590	-0.2	6.76	49.0	0.389	2.1	0.91	2117	98	2076	65	2057	80	2057	80	103
28LF13_14	42	0.5	0.144	0.750	0.1	8.54	63.0	0.434	2.2	0.52	2320	100	2293	68	2268	90	2268	90	102
28LF13_12	124	1.7	0.146	0.680	0.3	8.85	62.0	0.442	2.2	0.66	2358	98	2322	64	2296	79	2296	79	103

TABLE SM2.3: LA-ICPMS U-PB ISOTOPIC DATA (UC SANTA CRUZ LAB)

						Isotope ratios					Apparent ages (Ma)								
Analysis	U	U/Th	206Pb*	±	error	207Pb*	±	206Pb*	±	error	206Pb*	±	207Pb*	±	206Pb*	±	Best age	±	Conc
	(ppm)		207Pb*	(%)	corr.	235U*	(%)	238U	(%)	corr.	238U*	(Ma)	235U	(Ma)	207Pb*	(Ma)	(Ma)	(Ma)	(%)
28LF13_17	425	2.6	0.147	0.690	0.3	7.78	54.0	0.380	1.9	0.67	2080	87	2203	63	2315	80	2315	80	90
28LF13_76	136	2.1	0.152	0.730	-0.2	9.28	69.0	0.448	2.3	0.83	2390	100	2358	69	2362	83	2362	83	101
28LF13_82	154	2.0	0.169	0.780	0.2	11.77	82.0	0.510	2.6	0.76	2660	110	2587	65	2546	78	2546	78	104
28LF13_60	180	1.2	0.171	0.790	0.2	11.81	82.0	0.506	2.5	0.71	2640	110	2590	65	2570	77	2570	77	103
28LF13_56	105	0.7	0.173	0.810	0.2	11.87	85.0	0.506	2.7	0.79	2640	110	2592	67	2574	80	2574	80	103
28LF13_13	125	1.2	0.196	0.920	0.1	11.24	79.0	0.414	2.1	0.82	2233	99	2542	65	2792	75	2792	75	80
>20% Discordance																			
28LF13_3	2617	1.0	0.251	1.200	0.3	2.39	16.0	0.070	0.3	0.53	436	21	1239	49	3194	72	436	21	NA
28LF13_51	747	0.6	0.100	0.460	0.1	1.59	11.0	0.118	0.6	0.79	715	34	963	43	1627	82	715	34	44
12JT11_103	187	1.3	0.124	0.570	0.3	4.75	31.0	0.282	1.3	0.46	1601	63	1774	54	2006	80	2006	80	80
28LF13_69	489	0.8	0.145	0.660	0.0	5.43	37.0	0.275	1.4	0.74	1566	68	1888	59	2281	79	2281	79	69
28LF13_78	59	1.0	0.213	1.900	-0.7	10.40	140.0	0.317	1.8	0.91	1767	86	2272	96	2720	130	2720	130	65
>5% Reverse Discordance																			
28LF13_5	112	3.2	0.075	0.400	0.2	1.89	14.0	0.185	0.9	0.37	1092	51	1073	50	1030	110	1030	110	106
28LF13_26	192	1.9	0.083	0.400	0.2	2.64	19.0	0.236	1.2	0.47	1365	61	1313	52	1251	97	1251	97	109
28LF13_55	57	4.0	0.089	0.470	0.0	3.21	24.0	0.262	1.4	0.61	1498	73	1446	60	1380	110	1380	110	109
28LF13_31	231	3.3	0.105	0.490	0.2	4.98	35.0	0.350	1.7	0.65	1934	83	1815	59	1710	88	1710	88	113
28LF13_38	121	2.3	0.106	0.520	0.1	4.99	36.0	0.351	1.8	0.52	1943	85	1814	60	1716	90	1716	90	113
28LF13_66	13	1514.4	0.110	0.730	0.2	6.40	55.0	0.428	2.6	0.55	2290	120	2009	73	1760	120	1760	120	130
28LF13_94	17	2417.3	0.110	0.650	0.2	5.96	49.0	0.393	2.3	0.63	2120	110	1962	72	1770	110	1770	110	120
28LF13_20	19	3454.9	0.110	0.670	0.2	6.02	49.0	0.395	2.3	0.53	2150	100	1952	69	1770	110	1770	110	121
28LF13_92	17	5206.0	0.112	0.700	0.2	6.24	53.0	0.407	2.4	0.57	2190	110	1981	73	1790	120	1790	120	122
28LF13_25	91	1.0	0.110	0.540	0.1	5.53	40.0	0.369	1.9	0.63	2021	88	1898	62	1795	87	1795	87	113
28LF13_86	43	1.2	0.110	0.580	0.3	5.66	41.0	0.376	2.0	0.45	2052	93	1928	63	1797	96	1797	96	114
28LF13_67	104	1.1	0.110	0.530	0.1	5.80	41.0	0.383	1.9	0.62	2089	90	1941	61	1799	90	1799	90	116
28LF13_90	274	1.6	0.110	0.510	0.0	5.27	38.0	0.351	1.9	0.87	1935	90	1870	63	1802	82	1802	82	107

TABLE SM2.3: LA-ICPMS U-PB ISOTOPIC DATA (UC SANTA CRUZ LAB)

						Isotope ratios					Apparent ages (Ma)								
Analysis	U	U/Th	206Pb*	±	error	207Pb*	±	206Pb*	±	error	206Pb*	±	207Pb*	±	206Pb*	±	Best age	±	Conc
	(ppm)		207Pb*	(%)	corr.	235U*	(%)	238U	(%)	corr.	238U*	(Ma)	235U	(Ma)	207Pb*	(Ma)	(Ma)	(Ma)	(%)
28LF13_75	94	1.6	0.111	0.540	0.2	5.70	40.0	0.378	1.9	0.51	2065	91	1926	61	1803	89	1803	89	115
28LF13_15	38	0.9	0.110	0.600	0.3	5.20	39.0	0.348	1.9	0.47	1920	89	1844	65	1810	100	1810	100	106
28LF13_11	95	98.7	0.111	0.530	0.2	6.28	45.0	0.410	2.1	0.68	2208	96	2010	63	1813	88	1813	88	122
28LF13_93	81	9219.9	0.112	0.550	0.3	6.10	44.0	0.402	2.1	0.63	2176	94	1983	63	1826	87	1826	87	119
28LF13_57	55	1.2	0.113	0.570	0.1	5.85	43.0	0.378	2.0	0.58	2062	91	1953	63	1839	91	1839	91	112
28LF13_50	244	0.9	0.113	0.530	0.3	5.77	40.0	0.377	1.9	0.57	2067	90	1940	60	1840	85	1840	85	112
28LF13_74	10	0.2	0.116	0.830	0.2	6.19	56.0	0.397	2.4	0.52	2140	110	1964	78	1840	130	1840	130	116
28LF13_28	60	1.3	0.112	0.550	0.2	5.36	39.0	0.351	1.8	0.57	1937	86	1877	60	1842	93	1842	93	105
28LF13_84	38	1.4	0.113	0.600	0.3	5.89	44.0	0.378	2.0	0.52	2063	94	1954	66	1844	95	1844	95	112
28LF13_27	41	0.6	0.114	0.600	0.2	5.85	44.0	0.382	2.0	0.52	2093	95	1953	62	1844	93	1844	93	114
28LF13_52	101	1.5	0.113	0.550	0.2	5.55	39.0	0.359	1.8	0.59	1978	88	1902	62	1846	90	1846	90	107
28LF13_48	52	1.5	0.114	0.580	0.2	5.61	41.0	0.365	1.9	0.55	2003	89	1913	62	1849	91	1849	91	108
28LF13_77	22	7.1	0.113	0.650	0.2	6.53	52.0	0.425	2.4	0.46	2290	110	2046	73	1850	110	1850	110	124
28LF13_96	38	0.9	0.115	0.620	0.2	5.84	44.0	0.372	2.0	0.61	2028	95	1942	65	1852	99	1852	99	110
28LF13_47	72	1.4	0.114	0.570	0.2	5.78	42.0	0.374	2.0	0.63	2046	92	1938	64	1868	91	1868	91	110
28LF13_45	47	2.3	0.115	0.590	0.2	5.88	43.0	0.373	2.0	0.50	2047	91	1950	64	1876	94	1876	94	109
28LF13_35	116	1.3	0.116	0.550	0.1	5.66	40.0	0.363	1.8	0.58	1998	86	1925	61	1885	88	1885	88	106
28LF13_68	139	1.9	0.116	0.540	0.0	5.87	43.0	0.372	2.0	0.82	2043	91	1961	63	1888	85	1888	85	108
28LF13_99	83	1.4	0.116	0.570	0.1	5.95	43.0	0.372	1.9	0.55	2039	89	1965	61	1892	90	1892	90	108
28LF13_58	68	2.9	0.116	0.570	0.2	5.97	43.0	0.380	1.9	0.59	2073	91	1977	62	1892	85	1892	85	110
28LF13_81	47	0.9	0.118	0.600	0.3	6.22	45.0	0.390	2.1	0.55	2120	96	2005	64	1894	95	1894	95	112
28LF13_98	151	1.3	0.116	0.540	0.2	6.15	43.0	0.386	2.0	0.71	2102	92	1995	60	1899	83	1899	83	111
28LF13_62	179	1.4	0.117	0.550	0.2	6.00	42.0	0.377	1.9	0.59	2059	88	1973	59	1909	84	1909	84	108
28LF13_97	69	2.0	0.117	0.580	0.2	6.09	44.0	0.378	1.9	0.59	2068	91	1980	61	1909	91	1909	91	108
28LF13_63	38	0.9	0.118	0.640	0.2	5.94	44.0	0.371	2.0	0.52	2033	92	1962	68	1919	97	1919	97	106
28LF13_43	96	1.2	0.117	0.570	0.2	6.24	45.0	0.398	2.1	0.61	2156	95	2010	63	1919	87	1919	87	112
28LF13_23	112	2.0	0.117	0.560	0.1	5.92	42.0	0.370	1.8	0.62	2038	88	1966	62	1920	82	1920	82	106
28LF13_34	93	0.7	0.120	0.580	0.2	6.40	46.0	0.389	2.0	0.57	2117	91	2036	61	1951	89	1951	89	109

TABLE SM2.3: LA-ICPMS U-PB ISOTOPIC DATA (UC SANTA CRUZ LAB)

						Isotope ratios					Apparent ages (Ma)								
Analysis	U	U/Th	206Pb*	±	error	207Pb*	±	206Pb*	±	error	206Pb*	±	207Pb*	±	206Pb*	±	Best age	±	Conc
	(ppm)		207Pb*	(%)	corr.	235U*	(%)	238U	(%)	corr.	238U*	(Ma)	235U	(Ma)	207Pb*	(Ma)	(Ma)	(Ma)	(%)
28LF13_59	68	1.4	0.122	0.600	0.2	6.55	47.0	0.398	2.0	0.48	2155	93	2048	62	1963	89	1963	89	110
28LF13_89	45	12.9	0.123	0.630	0.1	6.45	49.0	0.385	2.1	0.68	2096	98	2041	67	1969	95	1969	95	106
28LF13_83	76	2.2	0.122	0.590	0.1	6.71	48.0	0.403	2.1	0.69	2179	95	2070	62	1975	88	1975	88	110
28LF13_37	31	0.7	0.125	0.670	0.3	7.08	53.0	0.429	2.3	0.44	2300	100	2123	67	2022	96	2022	96	114
28LF13_71	45	0.8	0.130	0.660	0.3	7.75	57.0	0.438	2.3	0.57	2340	100	2194	67	2088	89	2088	89	112
28LF13_22	75	2.2	0.130	0.640	0.1	7.32	53.0	0.409	2.1	0.63	2215	98	2142	65	2096	86	2096	86	106
28LF13_91	66	1.8	0.139	0.670	0.2	8.34	60.0	0.439	2.3	0.63	2340	100	2268	63	2198	85	2198	85	106
28LF13_21	133	3.1	0.143	0.670	0.2	8.73	61.0	0.451	2.3	0.68	2400	100	2308	63	2263	81	2263	81	106
28LF13_100	94	2.4	0.146	0.710	0.1	10.20	73.0	0.512	2.7	0.68	2660	120	2454	68	2299	82	2299	82	116
28LF13_49	120	1.6	0.149	0.690	0.0	10.11	71.0	0.502	2.5	0.80	2630	110	2445	63	2337	81	2337	81	113
28LF13_79	96	1.6	0.149	0.710	0.2	10.47	75.0	0.509	2.6	0.72	2660	110	2472	65	2337	78	2337	78	114
28LF13_54	27	1.7	0.151	0.780	0.1	9.90	75.0	0.482	2.6	0.64	2530	110	2414	69	2346	88	2346	88	108
28LF13_80	68	2.2	0.151	0.720	0.1	10.01	71.0	0.490	2.5	0.65	2570	110	2434	64	2352	81	2352	81	109
28LF13_73	61	2.0	0.151	0.740	0.2	10.05	72.0	0.486	2.5	0.63	2550	110	2444	66	2359	83	2359	83	108
28LF13_40	87	1.6	0.159	0.770	0.1	11.41	82.0	0.526	2.8	0.72	2720	110	2561	64	2445	80	2445	80	111
28LF13_42	129	2.7	0.160	0.740	0.2	11.13	77.0	0.513	2.6	0.69	2670	110	2533	66	2458	79	2458	79	109
28LF13_41	194	2.6	0.166	0.780	0.1	12.25	86.0	0.551	2.8	0.69	2840	120	2626	66	2509	79	2509	79	113
28LF13_85	72	1.5	0.174	0.830	0.2	12.65	89.0	0.537	2.8	0.70	2780	120	2654	66	2587	79	2587	79	107
28LF13_53	87	1.2	0.173	0.810	0.4	13.36	93.0	0.571	2.9	0.62	2910	120	2705	65	2587	78	2587	78	112
28LF13_70	135	1.8	0.174	0.800	0.2	12.71	90.0	0.544	2.8	0.80	2800	120	2657	66	2593	78	2593	78	108
28LF13_88	88	2.4	0.174	0.820	0.2	13.45	95.0	0.562	2.9	0.67	2870	120	2708	65	2597	79	2597	79	111
28LF13_32	211	2.7	0.175	0.800	0.3	13.00	89.0	0.549	2.7	0.71	2830	110	2681	67	2600	77	2600	77	109
28LF13_46	25	2.3	0.186	0.930	0.2	14.70	110.0	0.590	3.2	0.72	2980	130	2800	71	2688	85	2688	85	111
28LF13_36	39	2.5	0.184	0.920	0.1	14.40	100.0	0.579	3.0	0.63	2940	120	2768	67	2690	82	2690	82	109
28LF13_44	44	2.2	0.187	0.910	0.1	15.80	120.0	0.625	3.3	0.71	3130	130	2859	71	2712	82	2712	82	115
28LF13_24	23	0.4	0.189	0.950	0.2	14.50	110.0	0.567	3.1	0.70	2890	120	2776	66	2738	82	2738	82	106
28LF13_87	69	1.6	0.228	1.100	0.2	22.00	160.0	0.708	3.6	0.67	3450	130	3178	69	3034	76	3034	76	114

TABLE SM2.3: LA-ICPMS U-PB ISOTOPIC DATA (UC SANTA CRUZ LAB)

						Isotope ratios					Apparent ages (Ma)								
Analysis	U	U/Th	206Pb*	±	error	207Pb*	±	206Pb*	±	error	206Pb*	±	207Pb*	±	206Pb*	±	Best age	±	Conc
	(ppm)		207Pb*	(%)	corr.	235U*	(%)	238U	(%)	corr.	238U*	(Ma)	235U	(Ma)	207Pb*	(Ma)	(Ma)	(Ma)	(%)
>1000 U ppm																			
12JT11_7	1375	3.5	0.078	0.340	0.2	1.85	12.0	0.172	0.8	0.60	1024	41	1062	41	1152	87	1152	87	89
12JT22; Clarence River Group (N69.28, W141.73)																			
12JT22_8	327	2.6	0.057	0.160	0.3	0.57	1.7	0.072	0.1	0.27	449	8	456	11	495	64	449	8	NA
12JT22_64	227	1.5	0.056	0.160	0.3	0.57	1.8	0.075	0.1	0.23	467	9	460	12	424	66	467	9	NA
12JT22_89	159	1.7	0.055	0.170	0.3	0.59	1.9	0.078	0.2	0.41	486	10	474	12	417	69	486	10	NA
12JT22_13	543	3.1	0.068	0.190	-0.2	1.27	4.5	0.133	0.3	0.91	807	19	831	20	876	57	807	19	92
12JT22_65	331	2.8	0.071	0.200	-0.4	1.38	6.4	0.139	0.5	0.97	836	29	870	27	969	56	836	29	86
12JT22_82	371	4.8	0.071	0.190	-0.2	1.42	4.4	0.145	0.3	0.89	874	18	895	19	947	54	874	18	92
12JT22_68	286	1.6	0.071	0.200	0.3	1.59	4.6	0.162	0.3	0.46	966	17	967	18	964	54	966	17	100
12JT22_12	101	2.1	0.074	0.240	0.3	1.71	6.3	0.166	0.5	0.69	987	27	1008	24	1045	66	987	27	94
12JT22_57	569	14.0	0.072	0.190	0.2	1.64	4.7	0.166	0.3	0.76	988	18	986	18	976	54	988	18	101
12JT22_91	190	1.4	0.072	0.200	0.2	1.63	4.9	0.166	0.3	0.63	992	19	984	19	976	57	992	19	102
12JT22_95	701	0.6	0.071	0.190	0.3	1.64	4.6	0.168	0.3	0.54	1001	17	985	18	960	54	960	54	104
12JT22_98	302	4.4	0.072	0.200	-0.1	1.69	5.0	0.170	0.3	0.69	1013	18	1006	19	998	56	998	56	102
12JT22_62	401	7.2	0.074	0.200	-0.2	1.73	5.3	0.168	0.3	0.36	1002	18	1016	19	1029	55	1029	55	97
12JT22_55	239	2.9	0.074	0.200	0.2	1.79	5.2	0.176	0.3	0.48	1046	18	1040	19	1031	56	1031	56	101
12JT22_10	330	5.1	0.074	0.200	0.0	1.76	5.2	0.171	0.3	0.79	1015	19	1028	20	1038	55	1038	55	98
12JT22_37	307	4.9	0.074	0.200	0.1	1.75	5.1	0.170	0.3	0.70	1012	19	1027	19	1054	55	1054	55	96
12JT22_20	191	2.4	0.075	0.200	0.2	1.90	5.5	0.184	0.4	0.48	1088	19	1080	20	1057	55	1057	55	103
12JT22_30	85	0.9	0.076	0.220	0.1	1.97	6.3	0.188	0.4	0.53	1110	21	1106	21	1079	59	1079	59	103
12JT22_48	187	2.9	0.076	0.210	0.4	1.86	5.4	0.176	0.3	0.31	1046	19	1066	19	1086	56	1086	56	96
12JT22_93	105	1.3	0.076	0.220	0.1	1.97	6.1	0.189	0.4	0.53	1114	21	1104	22	1099	57	1099	57	101
12JT22_51	707	5.1	0.076	0.200	0.4	1.85	5.2	0.176	0.3	0.62	1046	18	1065	18	1104	52	1104	52	95
12JT22_46	388	2.6	0.077	0.210	0.2	1.84	5.4	0.173	0.4	0.73	1030	19	1060	19	1113	54	1113	54	93
12JT22_50	49	1.7	0.078	0.240	0.2	1.98	7.8	0.186	0.6	0.77	1098	32	1110	27	1137	63	1137	63	97
12JT22_71	312	1.7	0.079	0.220	0.2	2.05	6.2	0.188	0.4	0.47	1107	20	1131	20	1175	54	1175	54	94

TABLE SM2.3: LA-ICPMS U-PB ISOTOPIC DATA (UC SANTA CRUZ LAB)

						Isotope ratios					Apparent ages (Ma)								
Analysis	U	U/Th	206Pb*	±	error	207Pb*	±	206Pb*	±	error	206Pb*	±	207Pb*	±	206Pb*	±	Best age	±	Conc
	(ppm)		207Pb*	(%)	corr.	235U*	(%)	238U	(%)	corr.	238U*	(Ma)	235U	(Ma)	207Pb*	(Ma)	(Ma)	(Ma)	(%)
12JT22_76	33	1.0	0.080	0.270	0.2	2.04	7.2	0.188	0.4	0.32	1108	22	1128	24	1177	67	1177	67	94
12JT22_92	255	2.5	0.081	0.220	0.4	2.35	6.7	0.212	0.4	0.54	1239	22	1226	20	1219	54	1219	54	102
12JT22_58	67	1.4	0.085	0.320	-0.2	2.28	9.8	0.194	0.4	0.55	1145	21	1192	28	1279	71	1279	71	90
12JT22_52	237	2.1	0.085	0.230	0.1	2.50	7.3	0.214	0.4	0.74	1248	23	1272	22	1304	53	1304	53	96
12JT22_54	586	4.5	0.085	0.220	0.2	2.76	7.7	0.235	0.4	0.63	1358	23	1344	21	1313	51	1313	51	103
12JT22_16	252	3.7	0.086	0.230	0.1	2.84	8.7	0.240	0.5	0.81	1386	26	1368	23	1338	52	1338	52	104
12JT22_78	304	2.1	0.086	0.230	0.3	2.84	8.0	0.240	0.5	0.54	1385	23	1367	21	1345	51	1345	51	103
12JT22_7	138	3.7	0.087	0.240	0.2	2.65	8.1	0.223	0.5	0.60	1298	24	1315	23	1354	54	1354	54	96
12JT22_49	531	3.1	0.087	0.230	0.3	2.89	8.1	0.239	0.4	0.64	1382	23	1379	21	1364	50	1364	50	101
12JT22_38	700	2.6	0.088	0.230	-0.2	2.61	7.5	0.215	0.4	0.89	1257	22	1303	22	1370	51	1370	51	92
12JT22_18	666	4.2	0.090	0.240	0.1	2.92	8.6	0.235	0.5	0.78	1362	24	1387	22	1415	51	1415	51	96
12JT22_3	452	2.4	0.090	0.240	-0.4	2.67	8.4	0.213	0.4	0.93	1243	24	1318	24	1431	52	1431	52	87
12JT22_63	667	2.7	0.091	0.240	0.2	3.16	8.8	0.252	0.5	0.73	1451	24	1447	22	1440	50	1440	50	101
12JT22_2	783	4.0	0.091	0.240	-0.4	2.86	9.0	0.229	0.5	0.80	1327	25	1368	24	1444	51	1444	51	92
12JT22_99	353	4.1	0.091	0.240	-0.1	2.98	8.7	0.238	0.5	0.82	1376	24	1400	22	1454	51	1454	51	95
12JT22_59	140	2.1	0.092	0.250	0.2	3.15	9.1	0.250	0.5	0.52	1439	24	1444	22	1455	52	1455	52	99
12JT22_100	259	0.8	0.092	0.250	0.3	3.01	8.9	0.239	0.5	0.80	1382	27	1409	23	1474	50	1474	50	94
12JT22_85	318	2.8	0.092	0.240	0.1	3.20	9.3	0.253	0.5	0.78	1451	26	1456	23	1474	51	1474	51	98
12JT22_23	279	3.2	0.094	0.250	0.3	3.56	10.0	0.273	0.5	0.74	1556	27	1542	23	1509	50	1509	50	103
12JT22_74	386	2.6	0.095	0.250	-0.5	3.06	9.9	0.233	0.5	0.93	1348	27	1418	25	1533	50	1533	50	88
12JT22_31	63	2.3	0.096	0.270	0.3	3.41	10.0	0.257	0.5	0.42	1477	26	1509	24	1538	53	1538	53	96
12JT22_56	717	1.7	0.098	0.260	-0.3	3.89	12.0	0.287	0.6	0.95	1623	31	1610	25	1581	49	1581	49	103
12JT22_69	154	1.2	0.099	0.260	0.2	3.66	11.0	0.267	0.6	0.79	1525	28	1561	24	1601	50	1601	50	95
12JT22_47	99	1.8	0.099	0.270	0.2	3.78	12.0	0.276	0.6	0.75	1570	32	1587	26	1607	53	1607	53	98
12JT22_33	174	1.1	0.099	0.270	0.2	4.10	12.0	0.300	0.6	0.66	1690	29	1655	24	1612	49	1612	49	105
12JT22_45	209	1.8	0.100	0.270	0.2	3.38	10.0	0.244	0.5	0.79	1404	28	1500	24	1626	51	1626	51	86
12JT22_90	490	7.3	0.100	0.260	0.2	4.02	11.0	0.292	0.6	0.70	1652	27	1638	23	1629	48	1629	48	101
12JT22_60	339	2.7	0.102	0.270	0.2	4.07	11.0	0.291	0.5	0.59	1645	27	1649	23	1651	48	1651	48	100

TABLE SM2.3: LA-ICPMS U-PB ISOTOPIC DATA (UC SANTA CRUZ LAB)

						Isotope ratios					Apparent ages (Ma)								
Analysis	U	U/Th	206Pb*	±	error	207Pb*	±	206Pb*	±	error	206Pb*	±	207Pb*	±	206Pb*	±	Best age	±	Conc
	(ppm)		207Pb*	(%)	corr.	235U*	(%)	238U	(%)	corr.	238U*	(Ma)	235U	(Ma)	207Pb*	(Ma)	(Ma)	(Ma)	(%)
12JT22_19	91	1.0	0.102	0.280	0.3	3.86	11.0	0.274	0.6	0.64	1560	29	1605	24	1660	52	1660	52	94
12JT22_28	287	1.5	0.102	0.270	0.4	4.06	11.0	0.287	0.6	0.65	1628	28	1646	23	1662	48	1662	48	98
12JT22_25	273	0.7	0.104	0.310	0.1	3.38	14.0	0.232	0.7	0.52	1339	38	1487	32	1678	47	1678	47	80
12JT22_73	198	2.5	0.106	0.280	0.2	4.48	13.0	0.307	0.6	0.83	1726	31	1726	25	1731	48	1731	48	100
12JT22_32	855	2.7	0.106	0.280	0.1	4.38	12.0	0.298	0.6	0.90	1679	29	1708	24	1734	48	1734	48	97
12JT22_35	358	3.7	0.107	0.290	0.1	3.97	13.0	0.269	0.7	0.85	1536	33	1625	26	1740	49	1740	49	88
12JT22_17	283	1.6	0.107	0.280	0.1	4.84	14.0	0.327	0.6	0.83	1825	31	1791	24	1743	48	1743	48	105
12JT22_29	446	4.4	0.107	0.280	0.3	4.70	13.0	0.318	0.6	0.76	1781	30	1767	24	1748	48	1748	48	102
12JT22_83	405	2.5	0.108	0.280	0.0	4.52	13.0	0.306	0.6	0.89	1719	31	1734	25	1761	48	1761	48	98
12JT22_22	326	1.6	0.109	0.290	0.1	4.86	14.0	0.322	0.6	0.83	1797	30	1794	25	1785	47	1785	47	101
12JT22_97	86	2.1	0.110	0.300	0.2	5.04	15.0	0.335	0.7	0.67	1862	32	1826	25	1796	50	1796	50	104
12JT22_9	554	8.4	0.111	0.290	0.3	4.74	13.0	0.308	0.6	0.85	1732	28	1774	24	1814	47	1814	47	95
12JT22_15	242	2.6	0.113	0.300	0.1	5.44	18.0	0.347	0.9	0.93	1917	43	1884	30	1847	49	1847	49	104
12JT22_27	161	3.1	0.113	0.300	0.2	5.13	15.0	0.329	0.7	0.76	1833	34	1841	25	1851	49	1851	49	99
12JT22_72	146	1.1	0.117	0.310	0.3	5.53	16.0	0.344	0.7	0.70	1904	32	1905	25	1908	48	1908	48	100
12JT22_43	680	2.2	0.121	0.310	0.1	5.29	16.0	0.317	0.7	0.92	1772	32	1864	26	1964	47	1964	47	90
12JT22_77	190	2.5	0.123	0.320	0.3	6.36	18.0	0.378	0.7	0.64	2065	33	2027	25	2000	46	2000	46	103
12JT22_61	372	3.0	0.130	0.340	0.2	6.92	20.0	0.387	0.7	0.86	2109	34	2100	25	2092	46	2092	46	101
12JT22_80	401	1.3	0.174	0.450	0.3	11.38	32.0	0.474	0.9	0.81	2501	39	2555	26	2600	43	2600	43	96
12JT22_40	371	1.2	0.184	0.480	0.1	13.44	38.0	0.530	1.0	0.88	2741	43	2711	27	2684	43	2684	43	102
12JT22_81	229	1.5	0.187	0.490	0.3	14.04	39.0	0.547	1.0	0.80	2811	43	2752	27	2711	43	2711	43	104
12JT22_24	193	2.4	0.194	0.510	0.0	14.27	44.0	0.535	1.2	0.92	2757	52	2764	31	2774	44	2774	44	99
12JT22_53	56	2.5	0.203	0.540	-0.1	15.75	49.0	0.561	1.2	0.90	2866	50	2859	31	2852	44	2852	44	100
12JT22_6	152	2.6	0.250	0.660	-0.1	19.10	65.0	0.553	1.4	0.96	2834	57	3046	32	3185	42	3185	42	89
12JT22_75	64	1.2	0.285	0.750	0.3	28.38	81.0	0.723	1.4	0.77	3506	53	3432	28	3391	41	3391	41	103
>20% Discordance																			
12JT22_34	196	2.3	0.074	0.480	-0.1	0.17	1.5	0.016	0.1	0.70	101	7	155	13	880	120	101	7	NA

TABLE SM2.3: LA-ICPMS U-PB ISOTOPIC DATA (UC SANTA CRUZ LAB)

						Isotope ratios					Apparent ages (Ma)								
Analysis	U	U/Th	206Pb*	±	error	207Pb*	±	206Pb*	±	error	206Pb*	±	207Pb*	±	206Pb*	±	Best age	±	Conc
	(ppm)		207Pb*	(%)	corr.	235U*	(%)	238U	(%)	corr.	238U*	(Ma)	235U	(Ma)	207Pb*	(Ma)	(Ma)	(Ma)	(%)
12JT22_42	94	3.1	0.081	0.290	0.2	1.64	9.6	0.148	0.8	0.88	889	46	976	37	1205	71	889	46	74
12JT22_21	342	3.2	0.092	0.260	-0.8	2.47	13.0	0.192	0.7	0.98	1126	38	1239	38	1456	55	1456	55	77
12JT22_70	467	1.6	0.113	0.390	-0.8	3.95	17.0	0.251	0.5	0.94	1444	27	1607	24	1821	39	1821	39	79
12JT22_94	245	1.4	0.140	0.620	-0.8	7.11	42.0	0.361	0.8	0.94	1986	38	2073	36	2164	55	2164	55	92
12JT22_66	259	1.8	0.197	2.400	-1.0	21.80	580.0	0.432	5.0	1.00	2100	160	2280	140	2580	150	2580	150	81
>5% Reverse Discordance																			
12JT22_5	528	2.7	0.082	0.220	-0.5	2.54	8.0	0.224	0.5	0.91	1302	24	1280	23	1240	52	1240	52	105
12JT22_87	202	2.4	0.085	0.230	0.3	2.79	8.0	0.240	0.5	0.57	1387	24	1352	21	1315	52	1315	52	105
12JT22_88	323	3.5	0.087	0.230	0.2	3.00	8.5	0.251	0.5	0.69	1441	25	1407	22	1367	51	1367	51	105
12JT22_11	663	4.0	0.091	0.240	-0.1	3.44	11.0	0.274	0.6	0.97	1561	32	1513	25	1441	49	1441	49	108
12JT22_86	184	1.0	0.095	0.260	0.2	3.84	12.0	0.292	0.6	0.74	1650	32	1599	26	1534	51	1534	51	108
12JT22_1	103	1.6	0.101	0.270	0.1	4.45	13.0	0.319	0.6	0.73	1782	31	1720	25	1638	50	1638	50	109
12JT22_4	340	1.9	0.101	0.260	0.2	4.43	13.0	0.317	0.6	0.82	1775	30	1717	24	1640	49	1640	49	108
12JT22_79	323	1.7	0.106	0.280	0.3	4.89	14.0	0.336	0.6	0.73	1866	31	1800	24	1733	48	1733	48	108
12JT22_84	129	3.8	0.115	0.310	0.2	5.79	17.0	0.366	0.7	0.72	2012	34	1945	26	1874	48	1874	48	107
12JT22_96	81	1.4	0.184	0.490	0.0	13.80	41.0	0.551	1.1	0.87	2827	46	2735	29	2690	43	2690	43	105
>1000 U ppm																			
12JT22_41	3312	6.8	0.062	0.170	0.2	0.43	1.3	0.050	0.1	0.55	312	6	361	9	674	56	312	6	NA
12JT22_39	1612	2.7	0.079	0.300	0.0	1.26	4.7	0.118	0.3	0.28	717	18	824	21	1108	58	717	18	65
12JT22_44	2233	5.1	0.078	0.210	0.2	1.54	4.4	0.143	0.3	0.47	859	15	944	17	1137	52	859	15	76
12JT22_36	1531	17.1	0.078	0.220	-0.3	1.58	4.9	0.147	0.3	0.58	884	16	959	18	1141	50	884	16	77
12JT22_14	1501	10.7	0.070	0.180	-0.1	1.53	4.5	0.157	0.3	0.95	940	18	943	19	939	54	940	18	100
12JT22_67	1067	2.3	0.078	0.200	0.4	2.11	5.9	0.195	0.4	0.72	1146	19	1151	19	1156	52	1156	52	99
12JT22_26	1141	5.1	0.081	0.210	-0.3	2.04	6.7	0.182	0.4	0.95	1075	23	1127	23	1223	51	1223	51	88
12JT23; Clarence River Group (N69.28, W141.75)																			

TABLE SM2.3: LA-ICPMS U-PB ISOTOPIC DATA (UC SANTA CRUZ LAB)

						Isotope ratios					Apparent ages (Ma)								
Analysis	U	U/Th	206Pb*	±	error	207Pb*	±	206Pb*	±	error	206Pb*	±	207Pb*	±	206Pb*	±	Best age	±	Conc
	(ppm)		207Pb*	(%)	corr.	235U*	(%)	238U	(%)	corr.	238U*	(Ma)	235U	(Ma)	207Pb*	(Ma)	(Ma)	(Ma)	(%)
12JT23_100	371	1.9	0.056	0.290	0.2	0.46	3.2	0.060	0.3	0.26	373	17	380	22	410	110	373	17	NA
12JT23_99	731	1.9	0.056	0.270	0.3	0.46	3.1	0.060	0.3	0.25	374	17	384	21	440	110	374	17	NA
12JT23_108	247	1.4	0.056	0.300	0.2	0.47	3.4	0.060	0.3	0.18	375	17	388	24	400	110	375	17	NA
12JT23_105	592	1.6	0.055	0.280	0.3	0.47	3.3	0.061	0.3	0.18	382	17	389	23	380	110	382	17	NA
12JT23_110	447	3.7	0.055	0.280	0.2	0.48	3.3	0.062	0.3	0.24	385	17	397	23	430	110	385	17	NA
12JT23_66	263	2.2	0.059	0.360	0.2	0.50	3.8	0.063	0.3	0.20	392	18	406	25	480	120	392	18	NA
12JT23_46	367	1.6	0.054	0.290	0.3	0.47	3.3	0.063	0.3	0.18	392	18	389	23	350	110	392	18	NA
12JT23_92	486	1.7	0.055	0.280	0.2	0.50	3.5	0.064	0.3	0.23	397	18	411	23	390	110	397	18	NA
12JT23_94	327	1.7	0.056	0.300	0.1	0.50	3.6	0.064	0.3	0.28	399	18	416	24	400	110	399	18	NA
12JT23_104	423	2.6	0.054	0.270	0.3	0.49	3.4	0.065	0.3	0.23	403	18	404	23	380	110	403	18	NA
12JT23_98	555	4.8	0.056	0.280	0.3	0.51	3.5	0.065	0.3	0.17	407	18	417	23	430	110	407	18	NA
12JT23_96	837	1.8	0.055	0.260	0.2	0.51	3.4	0.065	0.3	0.41	408	18	418	23	420	110	408	18	NA
12JT23_106	79	3.5	0.058	0.430	0.2	0.53	4.6	0.066	0.3	0.19	412	20	428	31	460	150	412	20	NA
12JT23_107	131	2.8	0.057	0.360	0.2	0.52	4.1	0.066	0.3	0.17	413	19	428	27	470	130	413	19	NA
12JT23_97	319	1.7	0.055	0.300	0.3	0.50	3.6	0.066	0.3	0.14	413	19	411	24	380	110	413	19	NA
12JT23_26	137	2.2	0.052	0.310	0.2	0.50	3.9	0.066	0.3	0.26	414	19	406	26	280	120	414	19	NA
12JT23_27	621	1.9	0.055	0.270	0.2	0.52	3.5	0.066	0.3	0.27	414	19	424	24	390	110	414	19	NA
12JT23_28	401	2.0	0.053	0.270	0.2	0.51	3.6	0.067	0.3	0.24	415	19	415	24	320	110	415	19	NA
12JT23_77	498	1.7	0.055	0.270	0.2	0.51	3.5	0.066	0.3	0.27	415	19	420	24	380	110	415	19	NA
12JT23_29	173	2.5	0.054	0.330	0.3	0.50	3.9	0.067	0.3	0.12	417	19	415	27	300	120	417	19	NA
12JT23_88	148	4.2	0.052	0.330	0.2	0.48	3.9	0.067	0.3	0.19	418	20	402	26	300	130	418	20	NA
12JT23_58	748	1.3	0.056	0.270	0.2	0.50	3.4	0.067	0.3	0.23	418	19	415	23	420	110	418	19	NA
12JT23_36	960	1.5	0.057	0.300	0.2	0.51	3.7	0.067	0.3	0.33	418	19	419	25	460	120	418	19	NA
12JT23_55	383	1.7	0.054	0.280	0.2	0.50	3.5	0.067	0.3	0.23	420	19	409	24	350	110	420	19	NA
12JT23_18	842	1.7	0.055	0.260	0.3	0.50	3.3	0.067	0.3	0.18	420	19	411	23	420	110	420	19	NA
12JT23_2	343	2.0	0.058	0.310	0.3	0.55	3.9	0.068	0.3	0.09	422	19	448	26	500	110	422	19	NA
12JT23_73	421	1.8	0.056	0.280	0.2	0.53	3.7	0.068	0.3	0.29	422	19	433	25	410	110	422	19	NA
12JT23_44	472	1.5	0.055	0.280	0.2	0.52	3.7	0.068	0.3	0.35	423	19	425	24	430	110	423	19	NA

TABLE SM2.3: LA-ICPMS U-PB ISOTOPIC DATA (UC SANTA CRUZ LAB)

						Isotope ratios					Apparent ages (Ma)								
Analysis	U	U/Th	206Pb*	±	error	207Pb*	±	206Pb*	±	error	206Pb*	±	207Pb*	±	206Pb*	±	Best age	±	Conc
	(ppm)		207Pb*	(%)	corr.	235U*	(%)	238U	(%)	corr.	238U*	(Ma)	235U	(Ma)	207Pb*	(Ma)	(Ma)	(Ma)	(%)
12JT23_90	543	5.6	0.057	0.280	0.3	0.54	3.7	0.068	0.3	0.15	423	19	440	24	480	110	423	19	NA
12JT23_1	623	1.8	0.056	0.270	0.2	0.54	3.7	0.068	0.3	0.24	424	19	440	24	420	110	424	19	NA
12JT23_103	123	2.2	0.054	0.330	0.3	0.52	4.0	0.068	0.3	0.22	425	20	421	26	380	120	425	20	NA
12JT23_56	337	3.3	0.058	0.300	0.1	0.54	3.8	0.068	0.3	0.38	425	19	435	25	500	110	425	19	NA
12JT23_53	254	1.6	0.057	0.320	0.2	0.54	3.9	0.068	0.3	0.26	426	20	435	25	470	120	426	20	NA
12JT23_5	763	1.3	0.054	0.260	0.2	0.52	3.5	0.068	0.3	0.29	426	19	422	23	390	110	426	19	NA
12JT23_79	171	1.8	0.054	0.310	0.2	0.52	3.9	0.069	0.3	0.20	428	20	425	26	360	120	428	20	NA
12JT23_89	201	1.5	0.054	0.310	0.2	0.53	4.0	0.069	0.3	0.24	428	20	430	26	380	120	428	20	NA
12JT23_68	387	1.4	0.056	0.290	0.2	0.53	3.7	0.069	0.3	0.23	428	19	430	24	420	110	428	19	NA
12JT23_60	182	2.2	0.055	0.320	0.2	0.51	3.8	0.069	0.3	0.19	429	20	417	26	410	120	429	20	NA
12JT23_57	96	2.8	0.056	0.380	0.4	0.52	4.2	0.069	0.4	0.05	430	21	421	29	390	140	430	21	NA
12JT23_80	186	1.7	0.057	0.330	0.3	0.55	4.1	0.069	0.3	0.10	430	20	445	27	460	120	430	20	NA
12JT23_81	425	1.1	0.057	0.290	0.1	0.53	3.7	0.069	0.3	0.32	430	19	432	24	480	110	430	19	NA
12JT23_63	664	1.7	0.055	0.270	0.3	0.51	3.5	0.069	0.3	0.27	432	19	416	23	370	110	432	19	NA
12JT23_64	285	1.5	0.055	0.350	0.3	0.52	4.1	0.070	0.3	0.12	433	20	425	28	380	130	433	20	NA
12JT23_87	392	1.6	0.056	0.290	0.2	0.53	3.7	0.069	0.3	0.34	433	20	430	25	420	110	433	20	NA
12JT23_48	178	2.9	0.056	0.330	0.3	0.55	4.1	0.070	0.3	0.13	434	20	440	27	410	120	434	20	NA
12JT23_50	726	1.0	0.054	0.260	0.2	0.53	3.6	0.070	0.3	0.31	434	19	432	24	370	110	434	19	NA
12JT23_102	838	1.7	0.056	0.270	0.2	0.54	3.7	0.070	0.3	0.27	434	19	441	24	450	110	434	19	NA
12JT23_74	326	2.0	0.055	0.280	0.3	0.55	3.8	0.070	0.3	0.20	437	20	443	25	410	110	437	20	NA
12JT23_95	290	1.6	0.055	0.300	0.3	0.55	3.9	0.070	0.3	0.21	438	20	444	26	430	110	438	20	NA
12JT23_69	160	3.7	0.056	0.330	0.3	0.55	4.1	0.071	0.3	0.05	440	21	442	26	420	120	440	21	NA
12JT23_42	321	1.8	0.053	0.290	0.2	0.52	3.7	0.071	0.3	0.17	440	20	421	24	320	110	440	20	NA
12JT23_82	503	1.5	0.055	0.280	0.2	0.53	3.6	0.071	0.3	0.24	444	20	429	24	410	110	444	20	NA
12JT23_10	678	1.6	0.055	0.260	0.2	0.51	3.5	0.071	0.3	0.36	444	20	420	23	380	110	444	20	NA
12JT23_25	192	1.8	0.055	0.320	0.4	0.55	4.1	0.072	0.3	0.13	446	21	447	26	380	120	446	21	NA
12JT23_24	296	3.4	0.054	0.280	0.2	0.55	3.9	0.072	0.3	0.28	446	20	442	26	350	110	446	20	NA
12JT23_21	512	1.6	0.056	0.280	0.2	0.55	3.8	0.072	0.3	0.21	446	20	448	25	430	110	446	20	NA

TABLE SM2.3: LA-ICPMS U-PB ISOTOPIC DATA (UC SANTA CRUZ LAB)

						Isotope ratios					Apparent ages (Ma)								
Analysis	U	U/Th	206Pb*	±	error	207Pb*	±	206Pb*	±	error	206Pb*	±	207Pb*	±	206Pb*	±	Best age	±	Conc
	(ppm)		207Pb*	(%)	corr.	235U*	(%)	238U	(%)	corr.	238U*	(Ma)	235U	(Ma)	207Pb*	(Ma)	(Ma)	(Ma)	(%)
12JT23_33	571	2.8	0.056	0.280	0.3	0.55	3.8	0.072	0.3	0.12	446	20	445	25	430	110	446	20	NA
12JT23_41	720	2.8	0.054	0.270	0.1	0.54	3.7	0.072	0.3	0.39	446	20	437	24	370	100	446	20	NA
12JT23_12	250	2.5	0.056	0.310	0.2	0.53	3.8	0.072	0.3	0.19	449	21	432	25	420	120	449	21	NA
12JT23_59	570	3.1	0.057	0.280	0.3	0.55	3.8	0.072	0.3	0.13	450	20	446	24	460	110	450	20	NA
12JT23_75	250	4.3	0.055	0.310	0.3	0.56	4.1	0.072	0.4	0.15	451	21	449	26	370	110	451	21	NA
12JT23_30	285	3.0	0.055	0.290	0.2	0.58	4.0	0.073	0.3	0.22	453	20	460	26	420	110	453	20	NA
12JT23_40	178	1.7	0.055	0.340	0.4	0.54	4.1	0.073	0.4	0.04	454	21	442	27	380	120	454	21	NA
12JT23_91	218	3.0	0.060	0.330	0.3	0.63	4.6	0.073	0.4	0.20	454	21	497	29	580	120	454	21	NA
12JT23_67	245	3.2	0.058	0.300	0.2	0.58	4.1	0.073	0.3	0.25	455	21	461	26	490	110	455	21	NA
12JT23_39	131	3.1	0.055	0.330	0.1	0.55	4.3	0.073	0.4	0.31	456	21	441	27	390	120	456	21	NA
12JT23_72	133	2.9	0.054	0.330	0.1	0.55	4.4	0.073	0.4	0.26	456	21	444	28	340	120	456	21	NA
12JT23_3	237	3.4	0.056	0.300	0.2	0.57	4.1	0.073	0.4	0.11	456	21	459	27	420	110	456	21	NA
12JT23_37	337	2.4	0.055	0.290	0.2	0.55	3.9	0.073	0.4	0.29	456	21	445	25	420	110	456	21	NA
12JT23_20	153	2.3	0.056	0.340	0.3	0.55	4.2	0.074	0.4	0.11	458	21	444	27	410	120	458	21	NA
12JT23_23	367	4.6	0.054	0.270	0.3	0.56	3.9	0.074	0.3	0.13	458	21	448	25	340	110	458	21	NA
12JT23_65	459	2.3	0.055	0.270	0.3	0.55	3.8	0.074	0.3	0.22	458	21	444	25	400	110	458	21	NA
12JT23_49	84	5.1	0.058	0.430	0.2	0.62	5.5	0.075	0.4	0.13	467	22	483	35	440	150	467	22	NA
12JT23_45	117	3.8	0.058	0.370	0.3	0.60	4.7	0.075	0.4	0.12	467	22	475	31	470	130	467	22	NA
12JT23_6	857	2.0	0.058	0.270	0.2	0.59	3.9	0.075	0.4	0.33	467	21	469	26	510	110	467	21	NA
12JT23_8	650	2.4	0.057	0.280	0.2	0.58	3.9	0.076	0.4	0.27	469	21	461	25	480	110	469	21	NA
12JT23_14	253	2.2	0.055	0.310	0.3	0.56	4.0	0.076	0.4	0.08	472	21	450	27	420	120	472	21	NA
12JT23_70	407	1.7	0.056	0.280	0.3	0.58	4.0	0.076	0.4	0.24	472	21	466	26	420	110	472	21	NA
12JT23_85	627	2.9	0.055	0.270	0.3	0.56	3.8	0.076	0.4	0.26	474	21	454	25	430	110	474	21	NA
12JT23_38	654	1.6	0.057	0.280	0.2	0.59	4.0	0.077	0.4	0.31	475	21	472	26	490	110	475	21	NA
12JT23_61	629	1.6	0.057	0.280	0.3	0.58	4.0	0.077	0.4	0.26	476	21	464	25	480	110	476	21	NA
12JT23_15	193	2.9	0.058	0.320	0.3	0.58	4.3	0.077	0.4	0.15	477	22	470	27	510	120	477	22	NA
12JT23_13	201	3.4	0.057	0.330	0.3	0.59	4.3	0.077	0.4	0.18	477	22	469	27	480	120	477	22	NA
12JT23_54	466	2.0	0.055	0.280	0.2	0.58	4.0	0.077	0.4	0.27	478	22	465	26	400	110	478	22	NA

TABLE SM2.3: LA-ICPMS U-PB ISOTOPIC DATA (UC SANTA CRUZ LAB)

						Isotope ratios					Apparent ages (Ma)								
Analysis	U	U/Th	206Pb*	±	error	207Pb*	±	206Pb*	±	error	206Pb*	±	207Pb*	±	206Pb*	±	Best age	±	Conc
	(ppm)		207Pb*	(%)	corr.	235U*	(%)	238U	(%)	corr.	238U*	(Ma)	235U	(Ma)	207Pb*	(Ma)	(Ma)	(Ma)	(%)
12JT23_17	426	2.3	0.053	0.270	0.2	0.55	3.8	0.077	0.4	0.30	479	21	444	24	340	110	479	21	NA
12JT23_62	776	2.9	0.056	0.270	0.2	0.58	3.9	0.078	0.4	0.40	482	22	463	25	430	110	482	22	NA
12JT23_31	88	3.0	0.055	0.400	0.3	0.59	4.9	0.078	0.4	0.01	483	23	466	31	350	140	483	23	NA
12JT23_9	626	3.6	0.056	0.280	0.2	0.58	4.0	0.078	0.4	0.38	483	22	460	26	420	110	483	22	NA
12JT23_51	533	2.0	0.055	0.270	0.1	0.60	4.1	0.078	0.4	0.38	484	22	473	26	390	110	484	22	NA
12JT23_83	261	2.8	0.056	0.300	0.2	0.61	4.3	0.080	0.4	0.21	498	23	479	27	420	120	498	23	NA
12JT23_16	385	1.4	0.059	0.310	0.2	0.72	5.1	0.092	0.4	0.22	569	26	548	30	550	120	569	26	NA
12JT23_78	47	2.0	0.060	0.470	0.3	0.83	7.7	0.097	0.5	0.22	595	30	605	40	540	150	595	30	NA
12JT23_84	41	2.1	0.064	0.480	0.4	0.85	7.6	0.100	0.5	0.17	614	31	611	42	590	150	614	31	104
12JT23_93	475	2.1	0.063	0.300	0.2	0.95	6.5	0.105	0.5	0.26	644	29	675	34	700	100	644	29	92
12JT23_11	905	22.7	0.070	0.320	0.0	1.40	9.3	0.150	0.7	0.62	904	40	886	40	934	98	904	40	97
12JT23_86	892	30.0	0.078	0.350	0.1	1.98	13.0	0.188	0.9	0.80	1109	48	1105	46	1146	93	1146	93	97
12JT23_32	177	3.2	0.112	0.520	0.2	5.04	34.0	0.326	1.5	0.56	1817	73	1826	57	1827	85	1827	85	99
12JT23_47	30	0.6	0.187	0.910	0.3	13.82	95.0	0.533	2.6	0.56	2750	110	2738	67	2723	82	2723	82	101
>20% Discordance																			
12JT23_109	284	3.4	0.063	0.360	0.3	0.49	3.7	0.056	0.3	0.14	353	16	406	25	690	120	353	16	NA
12JT23_19	113	2.8	0.086	0.550	0.3	0.90	7.2	0.079	0.4	0.13	490	23	647	39	1280	130	490	23	NA
>5% Reverse Discordance																			
12JT23_52	44	1.6	0.061	0.450	0.3	0.87	7.5	0.101	0.5	0.22	621	31	626	41	540	150	621	31	115
12JT23_101	34	3.2	0.065	0.470	0.3	1.33	11.0	0.149	0.8	0.17	896	43	847	51	690	150	896	43	130
12JT23_76	208	0.8	0.100	0.470	0.1	4.28	29.0	0.303	1.4	0.66	1706	71	1692	55	1621	87	1621	87	105
>1000 U ppm																			
12JT23_71	1946	87.5	0.055	0.280	0.4	0.32	2.2	0.042	0.2	0.17	264	12	285	18	410	110	264	12	NA
12JT23_35	1737	3.6	0.078	0.370	0.4	0.48	3.2	0.046	0.2	0.49	288	14	396	22	1149	95	288	14	NA
12JT23_43	2721	6.2	0.055	0.260	0.2	0.45	3.0	0.059	0.3	0.52	368	17	378	21	420	100	368	17	NA

TABLE SM2.3: LA-ICPMS U-PB ISOTOPIC DATA (UC SANTA CRUZ LAB)

						Isotope ratios					Apparent ages (Ma)								
Analysis	U	U/Th	206Pb*	±	error	207Pb*	±	206Pb*	±	error	206Pb*	±	207Pb*	±	206Pb*	±	Best age	±	Conc
	(ppm)		207Pb*	(%)	corr.	235U*	(%)	238U	(%)	corr.	238U*	(Ma)	235U	(Ma)	207Pb*	(Ma)	(Ma)	(Ma)	(%)
12JT23_34	1261	2.0	0.055	0.270	0.3	0.49	3.3	0.065	0.3	0.46	407	19	401	23	380	110	407	19	NA
12JT23_4	1664	1.7	0.057	0.260	0.2	0.52	3.4	0.067	0.3	0.38	417	19	426	23	480	100	417	19	NA
12JT23_7	1136	2.2	0.055	0.260	0.2	0.52	3.5	0.070	0.3	0.36	434	19	424	23	420	110	434	19	NA
12JT24; Clarence River Group (N69.28, W141.75)																			
12JT24_8	328	1.7	0.116	0.300	-0.4	5.68	17.0	0.352	0.8	0.97	1941	36	1926	28	1898	47	1898	47	102
12JT24_17	135	0.8	0.117	0.310	0.3	5.43	15.0	0.338	0.7	0.62	1879	31	1889	24	1911	48	1911	48	98
12JT24_12	137	0.9	0.117	0.310	0.3	5.44	16.0	0.337	0.6	0.56	1872	31	1892	24	1912	47	1912	47	98
12JT24_6	215	1.1	0.118	0.310	0.3	5.66	16.0	0.349	0.7	0.55	1930	31	1925	25	1920	47	1920	47	101
12JT24_18	187	0.8	0.118	0.310	0.1	5.36	16.0	0.331	0.7	0.88	1843	34	1876	26	1921	47	1921	47	96
12JT24_25	95	0.9	0.120	0.330	0.1	5.07	16.0	0.309	0.6	0.61	1737	31	1830	26	1948	50	1948	50	89
12JT24_1	233	1.1	0.122	0.320	0.2	6.19	17.0	0.370	0.7	0.61	2029	33	2003	25	1978	47	1978	47	103
12JT24_15	87	1.0	0.126	0.340	0.2	6.28	18.0	0.364	0.7	0.53	2000	34	2016	26	2034	47	2034	47	98
12JT24_4	193	1.3	0.136	0.360	0.1	7.35	21.0	0.391	0.8	0.73	2126	35	2155	26	2181	46	2181	46	97
12JT24_14	430	1.0	0.151	0.390	0.2	9.40	26.0	0.452	0.8	0.72	2403	37	2377	26	2357	44	2357	44	102
12JT24_24	221	2.1	0.159	0.420	-0.2	9.33	28.0	0.425	0.9	0.89	2281	38	2370	28	2443	45	2443	45	93
12JT24_5	344	1.6	0.162	0.420	0.3	10.43	29.0	0.468	0.9	0.68	2476	38	2474	26	2474	44	2474	44	100
12JT24_2	382	2.0	0.168	0.440	0.0	11.04	32.0	0.477	1.0	0.92	2512	42	2525	27	2535	43	2535	43	99
12JT24_23	133	1.6	0.178	0.470	0.0	11.94	35.0	0.488	1.0	0.88	2560	42	2597	28	2633	44	2633	44	97
12JT24_11	183	1.3	0.186	0.480	0.3	13.75	39.0	0.538	1.0	0.75	2775	43	2733	26	2706	43	2706	43	103
12JT24_22	3	0.9	0.289	3.700	0.0	27.40	770.0	0.700	16.0	0.72	2960	510	2780	240	3230	210	3230	210	92
>20% Discordance																			
12JT24_9	945	2.1	0.147	0.380	-0.6	5.66	24.0	0.283	1.0	0.99	1602	50	1915	35	2308	44	2308	44	69
12JT24_20	749	0.7	0.161	0.430	0.8	5.58	16.0	0.252	0.6	0.85	1449	29	1914	25	2467	46	2467	46	59
12JT24_7	407	0.9	0.217	0.580	-0.8	12.60	64.0	0.419	1.8	0.99	2232	79	2606	49	2955	43	2955	43	76
>5% Reverse Discordance																			

TABLE SM2.3: LA-ICPMS U-PB ISOTOPIC DATA (UC SANTA CRUZ LAB)

						Isotope ratios					Apparent ages (Ma)								
Analysis	U	U/Th	206Pb*	±	error	207Pb*	±	206Pb*	±	error	206Pb*	±	207Pb*	±	206Pb*	±	Best age	±	Conc
	(ppm)		207Pb*	(%)	corr.	235U*	(%)	238U	(%)	corr.	238U*	(Ma)	235U	(Ma)	207Pb*	(Ma)	(Ma)	(Ma)	(%)
12JT24_13	89	0.3	0.111	0.300	0.2	5.33	16.0	0.350	0.7	0.64	1933	33	1874	25	1813	48	1813	48	107
>1000 U ppm																			
12JT24_3	1208	1.6	0.133	0.350	-0.6	3.09	11.0	0.167	0.4	0.98	994	23	1426	26	2139	45	994	23	46
12JT24_21	1136	1.8	0.114	0.300	-0.9	4.01	14.0	0.254	0.6	0.99	1456	34	1621	35	1857	48	1857	48	78
12JT24_16	1121	4.1	0.130	0.350	-0.9	4.47	24.0	0.248	1.1	1.00	1421	56	1705	47	2092	48	2092	48	68
12JT24_19	1022	6.8	0.139	0.360	-0.7	6.25	22.0	0.326	0.8	0.99	1818	40	2005	31	2211	46	2211	46	82
12JT24_10	1113	3.8	0.146	0.380	-0.8	5.70	19.0	0.284	0.7	0.99	1609	34	1934	29	2300	45	2300	45	70
12JT35; Clarence River Group (N69.47, W141.47)																			
12JT35_55	315	0.6	0.059	0.140	0.2	0.58	2.8	0.071	0.3	0.47	442	19	465	18	576	52	442	19	NA
12JT35_38	50	0.7	0.066	0.220	0.1	0.65	3.5	0.072	0.3	0.48	447	20	508	21	770	71	447	20	NA
12JT35_46	152	0.5	0.058	0.160	0.0	0.58	2.9	0.072	0.3	0.41	449	20	462	18	519	55	449	20	NA
12JT35_88	36	0.5	0.060	0.310	0.1	0.59	4.0	0.072	0.4	0.21	450	21	472	26	520	110	450	21	NA
12JT35_57	7	4.3	0.059	0.410	0.2	0.61	4.8	0.073	0.4	0.22	454	23	478	30	510	130	454	23	NA
12JT35_2	87	3.1	0.059	0.170	0.2	0.59	3.0	0.073	0.3	0.35	454	20	472	19	533	64	454	20	NA
12JT35_62	343	1.1	0.059	0.140	0.2	0.60	2.8	0.073	0.3	0.38	454	19	474	18	564	52	454	19	NA
12JT35_69	429	0.6	0.059	0.140	-0.3	0.60	2.8	0.073	0.3	0.65	456	19	476	18	548	50	456	19	NA
12JT35_34	142	0.3	0.059	0.180	0.2	0.59	3.3	0.075	0.4	0.66	468	24	471	21	542	66	468	24	NA
12JT35_26	547	1.3	0.059	0.140	0.3	0.61	2.9	0.076	0.3	0.40	469	20	485	18	549	53	469	20	NA
12JT35_44	155	3.6	0.056	0.140	0.0	0.59	2.9	0.076	0.3	0.49	471	20	471	18	455	57	471	20	NA
12JT35_89	31	2.8	0.060	0.250	0.3	0.64	3.7	0.076	0.4	0.23	474	21	500	23	569	86	474	21	NA
12JT35_43	585	0.3	0.059	0.130	0.3	0.63	3.0	0.077	0.3	0.45	479	20	498	18	571	49	479	20	NA
12JT35_42	375	0.8	0.057	0.130	0.2	0.62	2.9	0.078	0.4	0.40	483	21	490	18	497	50	483	21	NA
12JT35_15	67	0.8	0.062	0.190	0.2	0.66	3.4	0.078	0.4	0.25	484	21	515	21	655	68	484	21	NA
12JT35_85	221	1.2	0.058	0.140	0.1	0.63	3.1	0.079	0.4	0.42	488	21	498	19	517	52	488	21	NA
12JT35_41	295	2.6	0.058	0.140	0.3	0.64	3.0	0.079	0.4	0.28	490	21	500	19	538	51	490	21	NA
12JT35_12	42	0.0	0.059	0.230	0.2	0.64	3.7	0.079	0.4	0.30	492	22	498	22	515	86	492	22	NA

TABLE SM2.3: LA-ICPMS U-PB ISOTOPIC DATA (UC SANTA CRUZ LAB)

						Isotope ratios					Apparent ages (Ma)								
Analysis	U	U/Th	206Pb*	±	error	207Pb*	±	206Pb*	±	error	206Pb*	±	207Pb*	±	206Pb*	±	Best age	±	Conc
	(ppm)		207Pb*	(%)	corr.	235U*	(%)	238U	(%)	corr.	238U*	(Ma)	235U	(Ma)	207Pb*	(Ma)	(Ma)	(Ma)	(%)
12JT35_87	83	0.9	0.056	0.160	0.2	0.61	3.1	0.079	0.4	0.19	492	21	483	19	422	64	492	21	NA
12JT35_21	25	3.3	0.058	0.250	0.3	0.63	3.6	0.080	0.4	0.06	493	21	489	23	477	88	493	21	NA
12JT35_61	178	0.4	0.058	0.150	0.3	0.63	3.0	0.080	0.4	0.29	493	21	494	19	511	56	493	21	NA
12JT35_8	52	0.6	0.059	0.200	0.3	0.66	3.5	0.080	0.4	0.17	494	22	510	21	570	74	494	22	NA
12JT35_35	289	0.7	0.059	0.140	0.2	0.65	3.1	0.080	0.4	0.33	494	21	506	19	549	53	494	21	NA
12JT35_25	20	0.2	0.060	0.320	0.1	0.66	4.5	0.080	0.4	0.33	499	23	509	27	520	110	499	23	NA
12JT35_18	215	1.0	0.059	0.160	0.2	0.65	3.3	0.081	0.4	0.29	499	22	510	20	554	61	499	22	NA
12JT35_99	526	0.4	0.059	0.130	0.1	0.66	3.1	0.080	0.4	0.62	499	22	514	19	570	50	499	22	NA
12JT35_30	48	1.0	0.060	0.230	0.1	0.65	4.2	0.080	0.5	0.62	501	27	512	26	561	83	501	27	NA
12JT35_23	108	1.7	0.056	0.200	0.3	0.63	3.3	0.081	0.4	0.17	504	22	495	21	451	79	504	22	NA
12JT35_24	67	0.4	0.062	0.250	0.0	0.71	4.5	0.081	0.4	0.64	505	25	542	26	671	87	505	25	NA
12JT35_100	112	0.3	0.057	0.150	0.2	0.64	3.1	0.081	0.4	0.33	505	21	501	19	490	58	505	21	NA
12JT35_6	115	0.9	0.058	0.170	0.1	0.65	3.3	0.081	0.4	0.41	505	22	507	20	507	65	505	22	NA
12JT35_3	773	0.8	0.058	0.130	0.3	0.65	3.1	0.082	0.4	0.47	505	22	510	19	515	50	505	22	NA
12JT35_58	60	0.0	0.056	0.180	0.2	0.63	3.3	0.082	0.4	0.29	506	22	497	20	446	68	506	22	NA
12JT35_91	84	0.6	0.066	0.210	0.1	0.76	3.9	0.082	0.4	0.32	506	22	571	23	797	67	506	22	NA
12JT35_70	144	4.6	0.057	0.150	0.2	0.65	3.1	0.082	0.4	0.29	506	21	505	19	493	55	506	21	NA
12JT35_16	158	6.0	0.057	0.150	0.1	0.65	3.2	0.082	0.4	0.51	507	22	510	19	495	55	507	22	NA
12JT35_14	617	0.8	0.058	0.130	0.2	0.65	3.0	0.082	0.4	0.46	507	22	509	19	507	49	507	22	NA
12JT35_31	135	0.2	0.057	0.160	0.3	0.64	3.2	0.082	0.4	0.26	508	22	502	20	481	61	508	22	NA
12JT35_10	52	0.1	0.058	0.190	0.4	0.66	3.4	0.082	0.4	-0.01	509	22	512	21	505	71	509	22	NA
12JT35_93	62	0.1	0.061	0.190	0.2	0.68	3.6	0.082	0.4	0.53	509	23	527	21	608	65	509	23	NA
12JT35_78	14	2.9	0.059	0.370	0.1	0.64	4.8	0.082	0.4	0.28	510	25	499	30	470	120	510	25	NA
12JT35_11	322	0.5	0.060	0.140	0.0	0.68	3.3	0.082	0.4	0.51	510	22	529	19	601	52	510	22	NA
12JT35_77	35	0.2	0.058	0.230	0.3	0.66	3.7	0.082	0.4	0.28	511	23	516	23	526	81	511	23	NA
12JT35_73	54	0.0	0.056	0.250	0.0	0.65	4.1	0.082	0.4	0.35	511	23	506	25	475	96	511	23	NA
12JT35_52	189	0.7	0.060	0.150	0.2	0.69	3.3	0.083	0.4	0.31	511	22	533	20	608	52	511	22	NA
12JT35_27	8	2.1	0.059	0.390	0.2	0.68	5.3	0.082	0.4	0.18	512	25	511	32	470	130	512	25	NA

TABLE SM2.3: LA-ICPMS U-PB ISOTOPIC DATA (UC SANTA CRUZ LAB)

						Isotope ratios					Apparent ages (Ma)								
Analysis	U	U/Th	206Pb*	±	error	207Pb*	±	206Pb*	±	error	206Pb*	±	207Pb*	±	206Pb*	±	Best age	±	Conc
	(ppm)		207Pb*	(%)	corr.	235U*	(%)	238U	(%)	corr.	238U*	(Ma)	235U	(Ma)	207Pb*	(Ma)	(Ma)	(Ma)	(%)
12JT35_47	98	0.8	0.057	0.160	0.2	0.65	3.2	0.083	0.4	0.31	514	22	508	20	481	59	514	22	NA
12JT35_97	18	4.1	0.056	0.270	0.2	0.65	4.1	0.084	0.4	0.19	519	24	507	25	408	97	519	24	NA
12JT35_17	106	0.5	0.057	0.190	0.1	0.66	3.5	0.084	0.4	0.47	519	23	512	22	465	75	519	23	NA
12JT35_63	139	2.3	0.060	0.160	0.1	0.70	3.4	0.084	0.4	0.45	519	23	536	21	599	56	519	23	NA
12JT35_39	7	0.1	0.065	0.520	0.0	0.78	7.9	0.085	0.6	0.45	523	33	547	44	580	150	523	33	NA
12JT35_49	323	0.5	0.057	0.130	0.2	0.66	3.1	0.084	0.4	0.44	523	22	513	19	491	49	523	22	NA
12JT35_37	6	0.0	0.061	0.450	0.3	0.73	5.9	0.086	0.5	0.08	531	27	554	34	580	140	531	27	NA
12JT35_66	217	0.9	0.058	0.140	0.2	0.68	3.3	0.087	0.4	0.39	535	23	528	19	518	54	535	23	NA
12JT35_92	292	2.5	0.057	0.140	0.3	0.68	3.3	0.087	0.4	0.58	540	24	529	20	493	53	540	24	NA
12JT35_36	19	0.1	0.059	0.270	0.1	0.71	4.3	0.089	0.4	0.28	548	25	540	25	527	93	548	25	NA
12JT35_4	186	0.3	0.060	0.180	0.0	0.73	4.2	0.090	0.4	0.70	552	26	554	24	581	68	552	26	NA
12JT35_65	44	0.1	0.072	0.320	-0.1	0.88	5.4	0.090	0.4	0.40	554	24	634	29	900	89	554	24	NA
12JT35_90	106	1.0	0.068	0.290	0.1	0.86	5.5	0.091	0.5	0.65	560	31	628	31	909	85	560	31	NA
12JT35_28	31	2.0	0.057	0.260	0.2	0.69	4.8	0.092	0.6	0.43	561	36	527	29	474	94	561	36	NA
12JT35_71	34	0.3	0.060	0.230	0.0	0.76	4.7	0.092	0.5	0.54	565	27	569	26	589	80	565	27	NA
12JT35_60	39	1.4	0.056	0.210	-0.1	0.72	4.2	0.092	0.4	0.38	566	25	548	24	437	78	566	25	NA
12JT35_13	157	1.9	0.063	0.190	-0.3	0.89	7.0	0.101	0.7	0.91	621	39	643	39	717	63	621	39	87
12JT35_1	231	0.8	0.085	0.190	0.0	2.35	11.0	0.201	0.9	0.66	1182	48	1228	34	1304	44	1304	44	91
>20% Discordance																			
12JT35_83	347	0.1	0.070	0.220	0.4	0.61	3.2	0.064	0.3	0.43	398	18	484	20	910	64	398	18	NA
12JT35_74	277	1.2	0.060	0.180	0.2	0.53	2.7	0.064	0.3	0.50	400	18	431	18	597	64	400	18	NA
12JT35_56	406	0.9	0.068	0.170	-0.2	0.69	3.4	0.074	0.3	0.75	462	20	534	21	864	51	462	20	NA
12JT35_50	95	0.7	0.074	0.280	0.2	0.75	4.9	0.075	0.4	0.53	463	26	562	27	986	68	463	26	NA
12JT35_22	20	0.9	0.074	0.460	0.0	0.77	5.8	0.076	0.4	0.34	472	23	571	33	940	120	472	23	NA
12JT35_45	204	0.1	0.062	0.200	0.7	0.69	3.5	0.080	0.4	-0.27	495	21	534	21	655	64	495	21	NA
12JT35_68	8	0.2	0.088	0.620	0.1	1.07	9.2	0.090	0.5	0.42	553	31	708	43	1230	140	553	31	NA
12JT35_95	7	0.1	0.126	1.000	0.1	1.71	18.0	0.097	0.7	0.42	593	39	939	65	1820	160	593	39	NA

TABLE SM2.3: LA-ICPMS U-PB ISOTOPIC DATA (UC SANTA CRUZ LAB)

						Isotope ratios					Apparent ages (Ma)								
Analysis	U	U/Th	206Pb*	±	error	207Pb*	±	206Pb*	±	error	206Pb*	±	207Pb*	±	206Pb*	±	Best age	±	Conc
	(ppm)		207Pb*	(%)	corr.	235U*	(%)	238U	(%)	corr.	238U*	(Ma)	235U	(Ma)	207Pb*	(Ma)	(Ma)	(Ma)	(%)
12JT35_54	51	1.2	0.204	0.700	-0.1	2.79	19.0	0.098	0.6	0.82	603	33	1343	52	2842	57	603	33	21
12JT35_48	12	0.1	0.077	0.570	0.2	1.19	13.0	0.123	1.3	0.59	732	71	727	59	950	150	732	71	77
12JT35_20	4	0.1	0.093	0.610	0.4	1.89	15.0	0.150	0.9	0.35	900	52	1047	53	1380	140	900	52	65
>1000 U ppm																			
12JT35_84	1790	0.7	0.063	0.140	0.3	0.33	1.5	0.038	0.2	0.48	241	10	289	12	698	47	241	10	NA

1. Best age is chosen to be the 206Pb/238U age for analyses with 206Pb/238U age <1000 Ma otherwise the 206Pb/207Pb age is preferred for analyses with 206Pb/238Uage >1000 Ma.

2. Concordance is based on 206Pb/238U age / 206Pb/207Pb age. Value is not reported for 206Pb/238U ages <600 Ma because of large uncertainty in 206Pb/207Pb age and higher sensitivity to discordance; however, some ages were filtered out using graphical discordance on a concordia plot.

3. All uncertainties are reported at the 2-sigma level, and include measurement errors and an additional factor based on MSWD of sets of secondary standards to account for overdispersion of standard measurements

4. Systematic errors (at 2-sigma level) include contributions from U decay constants, composition of common Pb, true age of the standard, and scatter of measured age of the standards, and are as follows: 1.0% (206Pb/238U) & 0.9% (206Pb/207Pb)

6. U decay constants and composition as follows: 238U = 9.8485 x 10-10, 235U = 1.55125 x 10-10, 238U/235U = 137.88.

TABLE SM2.4: LA-ICPMS U-PB ISOTOPIC DATA (STOCKHOLM UNIVERSITY LAB)

						Isotope ratios					Apparent ages (Ma)								
Analysis	U	206Pb	U/Th	206Pb*	±	207Pb*	±	206Pb*	±	error	206Pb*	±	207Pb*	±	206Pb*	±	Best age	±	Conc
	(ppm)	204Pb		207Pb*	(%)	235U*	(%)	238U	(%)	corr.	238U*	(Ma)	235U	(Ma)	207Pb*	(Ma)	(Ma)	(Ma)	(%)
40LF13; Clarence River Group (N69.37, W142.91)																			
40LF13-87	6866	654.6	2.0	0.055	0.5	0.457	4.8	0.061	0.3	0.52	380	18	382	33	400	190	380	18	NA
40LF13-85	6988	1855.0	0.7	0.097	1.4	1.050	32.0	0.065	0.5	0.90	383	32	680	120	1490	210	383	32	NA
40LF13-76	136	304.4	2.9	0.058	0.5	0.530	5.0	0.067	0.2	0.52	415	11	428	31	520	180	415	11	NA
40LF13-49	7468	376.0	1.2	0.089	1.3	0.830	12.0	0.071	0.3	0.29	425	19	602	61	1290	260	425	19	NA
40LF13-51	37717	632.0	1.3	0.052	0.6	0.497	6.3	0.069	0.3	0.29	434	21	419	43	300	210	434	21	NA
40LF13-63	1501	187.0	2.6	0.060	0.6	0.640	7.0	0.076	0.3	0.18	468	16	499	45	600	240	468	16	NA
40LF13-9	13532	38.0	2.7	0.072	0.6	1.240	12.0	0.128	0.6	0.75	792	24	819	53	970	170	792	24	82
40LF13-57	13328	637.0	6.5	0.071	0.6	1.280	15.0	0.137	0.7	0.38	821	39	841	58	960	170	821	39	86
40LF13-119	1081	295.5	1.6	0.074	0.6	1.420	13.0	0.142	0.4	0.48	850	25	900	52	1030	170	850	25	83
40LF13-93	25064	248.1	12.0	0.074	0.6	1.440	13.0	0.145	0.5	0.71	863	29	903	54	1050	160	863	29	82
40LF13-37	24671	438.0	5.7	0.071	0.6	1.440	13.0	0.148	0.5	0.61	890	30	905	56	930	170	890	30	96
40LF13-78	832	117.3	1.6	0.075	0.6	1.570	14.0	0.150	0.4	0.33	896	26	958	55	1090	170	896	26	82
40LF13-36	4682	872.0	14.5	0.074	0.6	1.570	14.0	0.152	0.5	0.48	908	29	955	56	1040	170	908	29	87
40LF13-89	285	47.6	4.0	0.074	0.7	1.630	22.0	0.152	0.8	0.72	909	45	972	73	1020	190	909	45	89
40LF13-70	18726	191.0	1.4	0.072	0.6	1.490	14.0	0.153	0.7	0.41	916	41	926	58	950	170	916	41	96
40LF13-6	554	27.0	5.9	0.071	0.6	1.530	14.0	0.154	0.5	0.28	925	27	939	55	930	180	925	27	99
40LF13-62	13473	463.0	16.5	0.078	0.6	1.680	15.0	0.157	0.4	0.67	930	26	1000	56	1150	160	930	26	81
40LF13-61	1155	310.0	2.0	0.073	0.7	1.530	18.0	0.156	0.8	0.30	933	44	944	65	1000	170	933	44	93
40LF13-22	12937	215.0	2.2	0.075	0.7	1.610	16.0	0.157	0.7	0.46	936	43	975	61	1080	200	936	43	87
40LF13-118	1620	144.1	1.0	0.076	0.7	1.700	18.0	0.161	0.8	0.20	955	46	1003	69	1080	190	955	46	88
40LF13-24	2421	155.0	2.4	0.075	0.7	1.650	16.0	0.163	0.6	0.52	970	33	993	57	1040	170	970	33	93
40LF13-16	2040	771.0	3.2	0.072	0.7	1.620	16.0	0.163	0.5	0.38	971	31	979	65	940	200	971	31	103
40LF13-120	42	379.3	591.9	0.074	0.6	1.670	15.0	0.163	0.5	0.62	972	27	997	56	1040	170	972	27	94
40LF13-80	3079	87.8	2.0	0.077	0.7	1.710	16.0	0.164	0.5	0.29	973	32	1015	57	1110	170	973	32	88
40LF13-21	5883	179.0	1.6	0.076	0.7	1.650	17.0	0.165	0.6	0.42	979	37	1001	63	1090	190	979	37	90
40LF13-20	3505	334.0	3.4	0.072	0.6	1.650	17.0	0.164	0.7	0.50	979	43	985	65	980	190	979	43	100

TABLE SM2.4: LA-ICPMS U-PB ISOTOPIC DATA (STOCKHOLM UNIVERSITY LAB)

						Isotope ratios					Apparent ages (Ma)								
Analysis	U	206Pb	U/Th	206Pb*	±	207Pb*	±	206Pb*	±	error	206Pb*	±	207Pb*	±	206Pb*	±	Best age	±	Conc
	(ppm)	204Pb		207Pb*	(%)	235U*	(%)	238U	(%)	corr.	238U*	(Ma)	235U	(Ma)	207Pb*	(Ma)	(Ma)	(Ma)	(%)
40LF13-67	1362	100.0	1.6	0.074	0.7	1.650	16.0	0.165	0.5	0.20	985	28	989	62	1030	190	985	28	96
40LF13-91	17539	380.7	2.9	0.094	0.8	3.210	28.0	0.248	0.7	0.69	1429	37	1457	68	1510	150	1510	150	95
40LF13-68	15760	305.0	1.6	0.095	0.8	2.710	28.0	0.213	1.3	0.94	1243	68	1325	79	1530	150	1530	150	81
40LF13-74	11558	160.0	2.1	0.100	0.8	3.130	32.0	0.231	1.1	0.63	1340	56	1437	76	1610	150	1610	150	83
40LF13-114	1538	68.0	1.1	0.099	0.8	3.220	36.0	0.243	1.3	0.78	1405	67	1456	83	1610	150	1610	150	87
40LF13-23	5556	503.0	1.4	0.101	0.8	3.760	34.0	0.271	0.8	0.33	1543	38	1581	71	1620	160	1620	160	95
40LF13-71	5892	62.0	1.9	0.101	0.9	3.890	36.0	0.281	0.8	0.46	1596	40	1607	74	1630	150	1630	150	98
40LF13-59	3002	177.0	1.9	0.101	0.8	3.450	33.0	0.248	1.1	0.73	1427	55	1508	77	1650	170	1650	170	86
40LF13-88	14093	135.0	1.6	0.102	0.8	3.920	36.0	0.277	1.3	0.63	1573	64	1616	77	1670	150	1670	150	94
40LF13-4	9465	58.0	1.2	0.104	0.9	3.810	34.0	0.269	0.9	0.32	1533	45	1594	71	1680	160	1680	160	91
40LF13-90	3477	204.8	3.4	0.103	0.9	4.000	37.0	0.276	1.0	0.30	1571	49	1632	76	1680	160	1680	160	94
40LF13-115	1052	73.9	1.8	0.104	0.9	4.220	46.0	0.296	1.5	0.56	1679	79	1680	88	1680	160	1680	160	100
40LF13-104	99431	427.3	1.7	0.105	0.9	3.860	36.0	0.273	1.2	0.73	1556	60	1606	73	1700	150	1700	150	92
40LF13-56	2446	150.0	1.4	0.105	0.9	4.330	40.0	0.300	0.8	0.47	1691	42	1696	77	1720	160	1720	160	98
40LF13-86	16324	157.0	1.8	0.108	0.9	4.020	37.0	0.277	0.9	0.51	1574	47	1648	72	1750	160	1750	160	90
40LF13-54	14911	105.0	1.6	0.107	0.9	4.310	43.0	0.295	1.4	0.39	1664	68	1696	84	1750	150	1750	150	95
40LF13-43	2914	106.0	1.9	0.109	0.9	4.600	41.0	0.306	0.9	0.57	1718	43	1746	74	1790	150	1790	150	96
40LF13-82	3408	132.6	0.9	0.110	0.9	4.530	43.0	0.306	1.4	0.68	1722	69	1736	80	1790	150	1790	150	96
40LF13-58	7436	125.0	3.8	0.109	0.9	4.460	40.0	0.304	1.0	0.67	1711	49	1727	71	1790	140	1790	140	96
40LF13-8	993	1226.0	1.6	0.110	1.0	4.450	52.0	0.296	1.7	0.62	1686	74	1726	98	1800	170	1800	170	94
40LF13-44	7827	1050.0	4.8	0.111	0.9	4.770	46.0	0.316	1.5	0.68	1768	76	1778	82	1820	150	1820	150	97
40LF13-31	2183	1842.0	2.7	0.110	1.0	5.020	56.0	0.327	1.5	0.48	1825	71	1820	89	1830	150	1830	150	100
40LF13-42	4261	659.0	0.7	0.114	0.9	4.050	38.0	0.260	1.1	0.73	1487	54	1643	75	1850	150	1850	150	80
40LF13-81	1024	791.6	3.1	0.113	0.9	4.670	48.0	0.298	1.4	0.28	1679	67	1759	82	1850	150	1850	150	91
40LF13-69	4581	352.0	3.9	0.113	0.9	4.680	42.0	0.300	1.0	0.71	1691	48	1766	72	1850	150	1850	150	91
40LF13-100	3303	150.0	2.7	0.114	1.0	5.130	50.0	0.328	1.6	0.49	1828	78	1837	84	1850	160	1850	160	99
40LF13-10	14468	1092.0	5.4	0.114	1.0	4.720	44.0	0.299	1.0	0.09	1688	50	1767	79	1870	150	1870	150	90
40LF13-77	3604	108.4	1.1	0.116	1.0	4.870	43.0	0.303	0.8	0.46	1710	42	1793	75	1900	150	1900	150	90

TABLE SM2.4: LA-ICPMS U-PB ISOTOPIC DATA (STOCKHOLM UNIVERSITY LAB)

						Isotope ratios					Apparent ages (Ma)								
Analysis	U	206Pb	U/Th	206Pb*	±	207Pb*	±	206Pb*	±	error	206Pb*	±	207Pb*	±	206Pb*	±	Best age	±	Conc
	(ppm)	204Pb		207Pb*	(%)	235U*	(%)	238U	(%)	corr.	238U*	(Ma)	235U	(Ma)	207Pb*	(Ma)	(Ma)	(Ma)	(%)
40LF13-53	1739	93.0	1.6	0.117	1.0	4.810	50.0	0.308	1.4	0.44	1730	69	1789	82	1900	150	1900	150	91
40LF13-92	8736	414.0	2.4	0.117	1.0	5.240	47.0	0.330	1.0	0.36	1835	48	1856	75	1900	140	1900	140	97
40LF13-83	1480	1362.0	2.5	0.122	1.0	5.250	46.0	0.317	0.9	0.39	1776	46	1859	76	1980	150	1980	150	90
40LF13-3	10103	29.0	1.2	0.121	1.0	5.380	46.0	0.324	0.8	0.65	1808	41	1882	76	1980	150	1980	150	91
40LF13-107	39154	1328.0	2.3	0.129	1.1	6.050	56.0	0.345	1.0	0.48	1911	50	1978	80	2080	160	2080	160	92
40LF13-7	2913	29.0	4.0	0.179	1.4	11.800	100.0	0.475	1.2	0.69	2504	54	2590	82	2650	130	2650	130	94
40LF13-97	20514	65.7	4.1	0.185	1.6	11.900	130.0	0.467	2.5	0.70	2470	110	2602	88	2700	140	2700	140	91
40LF13-66	8549	133.1	0.9	0.185	1.5	12.500	110.0	0.492	1.4	0.60	2576	60	2638	82	2700	130	2700	130	95
40LF13-38	17683	62.8	1.6	0.188	1.5	13.500	130.0	0.526	2.5	0.61	2720	100	2714	93	2720	130	2720	130	100
40LF13-55	71268	59.3	5.0	0.190	1.5	10.700	110.0	0.408	2.2	0.96	2200	100	2484	97	2740	130	2740	130	80
40LF13-113	287	151.1	1.9	0.193	1.6	13.900	130.0	0.532	2.4	0.56	2750	99	2738	91	2760	140	2760	140	100
40LF13-65	946	76.0	1.5	0.207	1.6	12.600	120.0	0.446	1.7	0.75	2375	75	2644	87	2880	130	2880	130	82
40LF13-15	17648	159.0	1.4	0.219	1.7	13.800	120.0	0.460	1.4	0.86	2436	62	2735	85	2990	130	2990	130	81
>20% Discordance																			
40LF13-50	8354	418.5	8.3	0.143	1.5	3.410	52.0	0.166	0.8	0.81	898	49	1480	110	2230	180	898	49	40
40LF13-45	1126	572.0	0.8	0.097	0.8	1.800	17.0	0.137	0.6	0.79	796	37	1044	60	1560	150	796	37	51
40LF13-34	82558	1433.0	1.8	0.156	1.3	4.570	43.0	0.215	0.6	0.76	1255	33	1739	78	2390	100	2390	100	53
40LF13-102	10006	612.4	0.7	0.180	1.5	6.630	76.0	0.276	1.6	0.76	1572	78	2057	93	2650	140	2650	140	59
40LF13-84	4882	21.0	1.3	0.126	1.1	4.000	38.0	0.232	0.7	0.19	1345	38	1631	76	2030	160	2030	160	66
40LF13-101	436	329.0	4.8	0.080	0.7	1.480	13.0	0.137	0.4	0.36	812	23	923	55	1210	160	812	23	67
40LF13-11	392	297.6	4.6	0.080	0.7	1.250	15.0	0.117	0.7	0.71	792	24	819	64	1180	170	792	24	67
40LF13-46	1288	628.0	1.1	0.101	0.8	2.900	26.0	0.211	0.7	0.36	1234	36	1382	67	1630	160	1630	160	76
40LF13-48	2632	768.0	4.9	0.077	0.6	1.540	14.0	0.147	0.4	0.46	876	25	946	55	1120	160	876	25	78
40LF13-79	841	887.0	1.3	0.080	0.7	1.730	15.0	0.158	0.5	0.55	932	28	1017	57	1190	160	932	28	78
40LF13-64	1379	224.0	12.1	0.072	0.6	1.310	11.0	0.132	0.4	0.60	792	24	851	52	1000	160	792	24	79
>5% Reverse Discordance																			

TABLE SM2.4: LA-ICPMS U-PB ISOTOPIC DATA (STOCKHOLM UNIVERSITY LAB)

						Isotope ratios					Apparent ages (Ma)								
Analysis	U	206Pb	U/Th	206Pb*	±	207Pb*	±	206Pb*	±	error	206Pb*	±	207Pb*	±	206Pb*	±	Best age	±	Conc
	(ppm)	204Pb		207Pb*	(%)	235U*	(%)	238U	(%)	corr.	238U*	(Ma)	235U	(Ma)	207Pb*	(Ma)	(Ma)	(Ma)	(%)
40LF13-52	2199	160.1	1.4	0.069	0.6	1.460	14.0	0.155	0.7	0.51	929	42	919	61	880	180	929	42	106
40LF13-25	212531	321.6	2.0	0.068	0.6	1.450	15.0	0.154	0.7	0.50	924	42	917	63	860	170	924	42	107
40LF13-26	2091	150.4	1.3	0.064	0.9	1.080	14.0	0.126	1.0	0.08	792	24	754	57	680	290	792	24	116
40LF13-72	1393	503.4	4.2	0.062	0.6	0.990	11.0	0.117	0.6	0.52	792	24	694	55	650	190	792	24	122
40LF13-60	556	154.9	1.0	0.059	0.6	0.802	9.2	0.099	0.5	0.48	792	24	598	51	570	190	792	24	139
>10% uncertainty in 206Pb/238U or 207Pb/206Pb age																			
40LF13-94	72364	45.0	1.8	0.093	0.8	3.260	31.0	0.256	0.9	0.68	1467	47	1466	73	1490	150	1490	150	98
40LF13-39	1720	1056.0	2.7	0.092	0.8	2.590	24.0	0.204	0.8	0.85	1197	41	1296	67	1470	150	1470	150	81
40LF13-73	688	172.0	1.7	0.158	1.5	0.920	11.0	0.041	0.4	0.88	226	23	660	59	2420	160	226	23	NA
40LF13-47	42041	704.1	3.9	0.092	0.8	2.970	33.0	0.230	1.1	0.83	1332	57	1401	74	1460	150	1460	150	91
40LF13-95	2126	140.0	1.0	0.100	0.9	3.860	35.0	0.282	0.9	0.01	1608	48	1610	81	1620	170	1620	170	99
40LF13-32	11296	518.5	2.5	0.090	0.7	2.390	27.0	0.201	1.0	0.64	1184	53	1244	67	1420	150	1420	150	83
40LF13-40	17248	44.0	2.5	0.093	0.8	2.990	28.0	0.235	0.7	0.48	1361	38	1407	75	1500	160	1500	160	91
40LF13-17	8083	75.0	2.2	0.092	0.8	3.010	29.0	0.236	0.7	0.52	1365	38	1414	75	1470	160	1470	160	93
40LF13-14	6584	69.4	2.2	0.092	0.9	3.330	40.0	0.278	1.6	0.54	1581	79	1500	88	1460	160	1460	160	108
40LF13-19	6879	47.0	3.2	0.089	0.7	2.920	26.0	0.240	0.8	0.54	1384	40	1389	64	1420	160	1420	160	97
40LF13-5	1205	639.0	3.2	0.090	0.8	2.870	28.0	0.239	1.1	0.75	1378	58	1369	74	1410	160	1410	160	98
40LF13-1	2307	843.0	3.6	0.096	0.9	2.440	23.0	0.189	0.8	0.47	1114	45	1259	74	1560	180	1560	180	71
40LF13-35	9914	190.6	3.3	0.082	0.7	2.210	23.0	0.195	0.9	0.23	1150	47	1180	70	1260	150	1260	150	91
40LF13-41	20845	421.4	2.7	0.086	0.7	3.270	35.0	0.277	1.3	0.71	1576	65	1474	76	1340	160	1340	160	118
40LF13-33	15087	188.0	3.8	0.090	0.7	2.960	27.0	0.240	0.8	0.59	1385	42	1395	68	1420	170	1420	170	98
40LF13-13	3686	317.4	2.2	0.082	0.7	2.240	22.0	0.194	0.9	0.44	1144	48	1189	71	1250	150	1250	150	92
40LF13-30	10363	114.0	0.8	0.098	0.9	3.300	32.0	0.247	0.9	0.21	1439	45	1476	76	1580	190	1580	190	91
40LF13-18	6089	224.0	6.6	0.083	0.7	1.970	18.0	0.174	0.6	0.69	1036	31	1103	63	1270	160	1270	160	82
40LF13-2	4804	64.0	2.2	0.083	0.8	2.070	21.0	0.181	0.6	0.31	1074	35	1143	72	1320	170	1320	170	81
40LF13-99	7792	541.2	3.6	0.081	0.7	2.070	19.0	0.192	0.9	0.50	1132	48	1139	66	1220	160	1220	160	93
40LF13-75	1925	425.0	2.5	0.078	0.6	2.010	18.0	0.188	0.6	0.61	1110	31	1121	61	1140	150	1140	150	97

TABLE SM2.4: LA-ICPMS U-PB ISOTOPIC DATA (STOCKHOLM UNIVERSITY LAB)

						Isotope ratios					Apparent ages (Ma)								
Analysis	U	206Pb	U/Th	206Pb*	±	207Pb*	±	206Pb*	±	error	206Pb*	±	207Pb*	±	206Pb*	±	Best age	±	Conc
	(ppm)	204Pb		207Pb*	(%)	235U*	(%)	238U	(%)	corr.	238U*	(Ma)	235U	(Ma)	207Pb*	(Ma)	(Ma)	(Ma)	(%)
40LF13-96	3853	438.0	5.6	0.081	0.7	2.210	19.0	0.199	0.5	0.42	1172	29	1186	57	1210	160	1210	160	97
40LF13-108	15023	529.0	2.1	0.080	0.7	2.110	19.0	0.189	0.5	0.45	1117	27	1149	61	1190	160	1190	160	94
40LF13-98	2020	551.0	2.7	0.078	0.6	2.060	18.0	0.190	0.5	0.60	1121	29	1133	60	1160	160	1160	160	97
40LF13-103	4398	30.0	2.9	0.085	0.8	2.500	23.0	0.213	0.6	0.15	1244	32	1274	65	1300	180	1300	180	96
40LF13-112	2427	547.4	3.3	0.080	0.6	1.990	19.0	0.181	0.8	0.48	1069	44	1111	63	1220	170	1220	170	88
40LF13-109	732	55.0	1.1	0.114	1.4	0.770	18.0	0.047	0.7	0.94	275	39	572	99	1880	240	275	39	NA
40LF13-106	22516	351.0	3.2	0.078	0.7	1.860	17.0	0.175	0.5	0.42	1036	27	1068	62	1170	170	1170	170	89
40LF13-117	1465	84.0	1.0	0.083	0.8	1.900	18.0	0.168	0.5	0.33	1001	27	1079	67	1290	190	1290	190	78
40LF13-116	2257	244.0	1.4	0.078	0.6	1.880	18.0	0.174	0.8	0.51	1036	42	1070	65	1140	170	1140	170	91
40LF13-111	27467	132.0	2.4	0.077	0.7	1.870	18.0	0.179	0.5	0.30	1059	29	1081	62	1120	170	1120	170	95
40LF13-110	203	66.3	2.3	0.078	0.7	1.950	21.0	0.180	0.9	0.24	1071	45	1104	65	1160	180	1160	180	92
40LF13-105	886	40.0	1.9	0.077	0.7	1.950	20.0	0.181	0.7	0.33	1069	36	1088	69	1150	190	1150	190	93
40LF13-27	63	74.9	1.2	0.077	0.7	1.860	20.0	0.176	0.8	0.33	1042	44	1073	65	1110	190	1110	190	94
40LF13-28	206	542.6	5.3	0.070	0.6	1.660	18.0	0.171	0.8	0.60	1018	42	993	65	930	170	930	170	109
40LF13-12	409	70.6	2.5	0.072	0.7	1.690	19.0	0.179	0.8	0.59	1062	45	1010	69	960	190	960	190	111
40LF13-29	20218	123.0	2.2	0.099	0.8	3.120	29.0	0.228	0.8	0.73	1322	40	1433	72	1600	160	1600	160	83

1. Best age is chosen to be the 206Pb/238U age for analyses with 206Pb/238U age <1000 Ma otherwise the 206Pb/207Pb age is preferred for analyses with 206Pb/238Uage >1000 Ma.

2. Concordance is based on 206Pb/238U age / 206Pb/207Pb age. Value is not reported for 206Pb/238U ages <600 Ma because of large uncertainty in 206Pb/207Pb age and higher sensitivity to discordance; however, some ages were filtered out using graphical discordance on a concordia plot.

3. All uncertainties are reported at the 2-sigma level, and include measurement errors and an additional factor based on MSWD of sets of secondary standards to account for overdispersion of standard measurements

4. Systematic errors (at 2-sigma level) include contributions from U decay constants, composition of common Pb, true age of the standard, and scatter of measured age of the standards, and are as follows: 1.0% (206Pb/238U) & 0.9% (206Pb/207Pb)

6. U decay constants and composition as follows: 238U = 9.8485 x 10-10, 235U = 1.55125 x 10-10, 238U/235U = 137.88.

TABLE SM2.5: SIMS U-TH-PB ISOTOPIC DATA (NORDSIM-LAB, STOCKHOLM)

					Isotope ratios									Apparent ages (Ma)									
Analysis	U	Th/U	Pb	f206Pb	238U	±	207Pb	±	207Pb	±	206Pb	±	error	207Pb	±	207Pb	±	206Pb	±	206Pb*	±	Best age	±	Conc
	(ppm)		(ppm)	(%)	206Pb	(%)	206Pb	(%)	235U	(%)	238U	(%)	corr.	206Pb	(Ma)	235U	(Ma)	238U	(Ma)	238U	(Ma)	(Ma)	(Ma)	(%)
40LF13; Clarence River Group (N69.37, W142.91)																								
n5021-25	534	0.2	41.0	0.00	14.623	0.688	0.1	0.605	0.5	0.92	0.068	0.688	0.751	469	13	433	3	426	3	426	3	426	3	NA
n5021-14	420	1.0	41.2	0.18	14.224	0.683	0.1	0.693	0.5	0.97	0.070	0.683	0.702	469	15	443	3	438	3	438	3	438	3	NA
n5021-17	169	0.5	14.3	0.21	14.180	0.676	0.1	1.093	0.5	1.29	0.071	0.676	0.526	454	24	442	5	439	3	439	3	439	3	NA
n5021-16	252	0.2	19.8	0.07	14.162	0.677	0.1	0.885	0.5	1.11	0.071	0.677	0.608	467	19	444	4	440	3	439	3	439	3	NA
n5021-34	551	0.2	43.5	0.01	14.139	0.795	0.1	0.697	0.5	1.06	0.071	0.795	0.752	414	16	436	4	441	3	441	3	441	3	NA
n5021-06	258	0.1	45.6	0.10	6.203	0.718	0.1	0.519	1.6	0.89	0.161	0.718	0.811	982	11	969	6	964	6	963	7	963	7	98
n5021-04	148	0.3	28.1	0.00	6.179	0.686	0.1	0.779	1.6	1.04	0.162	0.686	0.661	941	16	959	6	967	6	968	6	968	6	103
n5021-19	369	0.1	67.1	0.00	6.134	0.676	0.1	0.433	1.6	0.80	0.163	0.676	0.842	964	9	971	5	974	6	974	6	974	6	101
n5021-02	166	0.2	30.9	0.00	6.109	0.725	0.1	0.749	1.6	1.04	0.164	0.725	0.696	1000	15	984	7	977	7	976	7	976	7	98
n5021-03	250	0.1	46.0	0.00	6.060	0.687	0.1	0.599	1.6	0.91	0.165	0.687	0.754	989	12	986	6	985	6	984	7	984	7	100
n5021-01	74	0.6	16.7	0.00	5.583	0.677	0.1	0.909	1.9	1.13	0.179	0.677	0.598	1075	18	1066	8	1062	7	1061	7	1061	7	99
n5021-04	175	0.5	40.0	0.72	5.453	1.080	0.1	1.231	2.1	2.10	0.182	1.074	0.512	1255	35	1139	14	1078	11	1069	12	1069	12	86
n5021-11	132	0.6	34.3	0.17	4.845	0.751	0.1	0.619	2.3	0.97	0.206	0.751	0.772	1195	12	1204	7	1209	8	--	--	1195	12	101
n5021-12	59	0.8	16.4	0.88	4.833	0.686	0.1	0.903	2.3	1.13	0.207	0.686	0.605	1235	18	1221	8	1212	8	--	--	1235	18	98
n5021-07	270	0.2	72.3	0.06	4.267	0.717	0.1	0.388	2.8	0.82	0.234	0.717	0.879	1333	7	1348	6	1357	9	--	--	1333	7	102
n5021-15	206	0.4	65.2	0.04	3.783	0.749	0.1	0.405	3.4	0.85	0.264	0.749	0.880	1496	8	1505	7	1512	10	--	--	1496	8	101
n5021-10	179	0.5	58.1	0.04	3.803	0.700	0.1	0.478	3.4	0.85	0.263	0.700	0.826	1513	9	1508	7	1505	9	--	--	1513	9	99
n5021-22	909	1.0	315.7	0.03	4.140	0.676	0.1	0.191	3.3	0.70	0.242	0.676	0.962	1610	4	1482	5	1395	8	--	--	1610	4	87
n5021-21	208	0.2	70.2	0.01	3.430	0.685	0.1	0.358	4.1	0.77	0.292	0.685	0.886	1647	7	1648	6	1649	10	--	--	1647	7	100
n5021-08	178	0.2	62.2	0.00	3.364	0.880	0.1	0.649	4.3	1.09	0.297	0.880	0.805	1726	12	1699	9	1678	13	--	--	1726	12	97
n5021-18	99	0.5	66.3	0.04	1.974	0.688	0.2	0.317	13.1	0.76	0.507	0.688	0.908	2727	5	2690	7	2642	15	--	--	2727	5	97
>20% Discordance																								
n5021-09	244	0.3	29.0	0.25	9.929	0.695	0.1	0.819	0.9	1.07	0.101	0.695	0.647	792	17	657	5	619	4	615	4	615	4	77
n5021-24c	173	0.6	29.6	0.07	7.834	1.326	0.1	0.860	1.3	1.58	0.128	1.326	0.839	1047	17	848	9	774	10	765	10	765	10	73
n5021-13	142	0.3	85.1	0.07	2.315	0.705	0.3	0.253	15.1	0.75	0.432	0.705	0.941	3207	4	2821	7	2315	14	--	--	3207	4	72

TABLE SM2.5: SIMS U-TH-PB ISOTOPIC DATA (NORDSIM-LAB, STOCKHOLM)

					Isotope ratios									Apparent ages (Ma)										
Analysis	U	Th/U	Pb	f206Pb	238U	±	207Pb	±	207Pb	±	206Pb	±	error	207Pb	±	207Pb	±	206Pb	±	206Pb*	±	Best age	±	Conc
	(ppm)		(ppm)	(%)	206Pb	(%)	206Pb	(%)	235U	(%)	238U	(%)	corr.	206Pb	(Ma)	235U	(Ma)	238U	(Ma)	238U	(Ma)	(Ma)	(Ma)	(%)
>10% uncertainty in 206Pb/238U or 207Pb/206Pb age																								
n5021-20	384	0.4	26.1	4.11	16.779	1.063	0.1	2.921	0.4	6.41	0.057	1.028	0.160	383	136	362	20	358	4	358	4	358	4	NA
>1000 U ppm																								
n5021-23	2051	0.3	181.1	2.50	13.197	2.028	0.1	1.266	0.6	3.80	0.074	1.980	0.520	672	68	497	15	459	9	456	9	456	9	NA

1. Age uncertainties are reported at the 1-sigma level.

2. 207-corrected 206Pb/238U age calculated using the 207Pb correction of Ludwig (2012), assuming an initial Pb composition of Stacey and Kramers (1975) two-stage model*

3. Best age is determind using a 1000 Ma cutoff between 207 corrected 206Pb/238U and 206Pb/207Pb ages

4. Concordance is based on 206Pb/238U age / 206Pb/207Pb age, with 100% = concordant.

5. Concordance is not reported for 206Pb/238U ages <600 Ma because of large uncertainty in 206Pb/207Pb age.

TABLE SM2.6: STEPWISE $^{40}Ar/^{39}Ar$ ISOTOPE COMPOSITIONS OF MUSCOVITE (UNIVERSITY OF ALASKA FAIRBANKS LAB)

L.Power	Cumulative	Age	±	$^{40}Ar/^{39}Ar$	±	$^{37}Ar/^{39}Ar$	±	$^{36}Ar/^{39}Ar$	±	%Atm.	Ca/K	±	Cl/K	±	$40^*/^{39}K$	±
(mW)	39Ar	(Ma)	(Ma)	meas.	abs.	meas.	abs.	meas.	abs.	^{40}Ar	meas.	abs.	meas.	abs.	meas.	abs.
12JT13A; Neruokpuk Formation (N69.23, W142.83)																
1250	0.020	320	10	53.41837	1.199	0.57285	0.01385	0.01104	0.00426	6.02322	1.05152	0.0254	0.00184	0.00029	50.19327	1.71
1500	0.051	384	9	62.93955	1.415	0.03971	0.00226	0.00547	0.00226	2.56597	0.07286	0.0042	0.00095	0.00019	61.29732	1.55
1750	0.311	403	7	65.19665	1.309	0.00639	0.0004	0.00156	0.0003	0.70754	0.01172	0.0007	0.00021	0.00006	64.70615	1.3
2000	0.343	398	8	64.46249	1.296	0.00668	0.00256	0.00212	0.00246	0.97176	0.01226	0.0047	0.00023	0.0002	63.80696	1.48
2500	0.435	406	10	65.26705	1.822	0.00285	0.00106	0.00019	0.00117	0.08444	0.00523	0.002	0.00021	0.00012	65.18239	1.85
3000	0.520	405	9	65.21331	1.642	0.00302	0.00168	0.00074	0.00099	0.33515	0.00554	0.0031	0.00063	0.00016	64.96528	1.67
4000	0.839	405	8	65.37231	1.365	0.00206	0.0003	0.00121	0.00024	0.54765	0.00378	0.0006	0.00047	0.00009	64.98485	1.36
5000	0.926	409	9	66.14311	1.622	0.00439	0.0011	0.00141	0.00095	0.62961	0.00806	0.002	0.00062	0.00015	65.69735	1.64
9000	1.000	406	10	66.05637	1.694	0.00474	0.00135	0.00287	0.00135	1.28225	0.0087	0.0025	0.00041	0.00011	65.18027	1.73
Integrated	NA	402	4	65.07973	0.625	0.01634	0.00036	0.00167	0.00026	0.75452	0.02998	0.0007	0.00043	0.00004	64.55996	0.63
Weighted average of J from standards = 3.869e-03 +/- 2.644e-05																
12JT12; Neruokpuk Formation (N69.21, W142.85)																
500	0.003	1620	800	603.566	412.6	-0.37142	1.51956	0.11062	0.59655	5.4211	-0.6813	2.7867	0.28427	0.23894	570.6683	427
750	0.009	6820	889	16910.1557	8534	-0.23958	0.82984	0.17091	0.39572	0.29878	-0.4395	1.5221	0.72563	0.37878	16856.75	8507
1000	0.015	5604	790	8346.9325	3831	-0.18762	0.58919	-0.14799	0.24816	-0.52374	-0.3442	1.0808	0.29422	0.15674	8389.507	3850
1250	0.023	4404	535	4049.13861	1315	-0.02915	0.46053	-0.24431	0.25612	-1.7829	-0.0535	0.845	0.07736	0.06763	4121.216	1340
1500	0.040	3138	282	1854.54956	350.4	0.13124	0.2669	0.03719	0.10986	0.59198	0.24083	0.4898	0.04556	0.03707	1843.712	350
1750	0.067	852	88	210.00748	20.17	-0.01861	0.13546	-0.09125	0.06946	-12.84136	-0.0342	0.2485	-0.01373	0.01616	236.9387	30.5
2000	0.110	372	68	85.66562	4.968	0.0349	0.10114	-0.01463	0.0587	-5.05189	0.06403	0.1856	-0.00707	0.01141	89.96437	18.1
2500	0.205	305	25	77.4225	2.522	0.02952	0.05007	0.01751	0.01988	6.6829	0.05416	0.0919	-0.00065	0.00514	72.22223	6.33
3000	0.328	342	18	84.31936	2.109	0.00769	0.02934	0.00854	0.0149	2.99216	0.01412	0.0538	0.00076	0.00403	81.76802	4.86
4000	0.546	423	13	102.40705	2.044	0.00933	0.02229	-0.00436	0.01038	-1.25882	0.01711	0.0409	-0.00193	0.00229	103.6668	3.7
5000	0.844	433	9	107.92189	1.251	-0.00008	0.01348	0.00527	0.00737	1.44445	-0.0002	0.0247	0.00215	0.00158	106.3337	2.5
9000	1.000	750	19	204.08624	5.418	0.02821	0.02564	0.00668	0.01	0.96556	0.05177	0.0471	-0.00019	0.00353	202.0903	6.13
Integrated	NA	1086	11	324.2262	3.513	0.00929	0.01466	0.00015	0.00685	0.0137	0.01705	0.0269	0.00767	0.00174	324.1542	4.05
Weighted average of J from standards = 2.552e-03 +/- 1.290e-05																

TABLE SM2.6: STEPWISE $^{40}Ar/^{39}Ar$ ISOTOPE COMPOSITIONS OF MUSCOVITE (UNIVERSITY OF ALASKA FAIRBANKS LAB)

L.Power	Cumulative	Age	±	$^{40}Ar/^{39}Ar$	±	$^{37}Ar/^{39}Ar$	±	$^{36}Ar/^{39}Ar$	±	%Atm.	Ca/K	±	Cl/K	±	$40^*/^{39}K$	±
(mW)	39Ar	(Ma)	(Ma)	meas.	abs.	meas.	abs.	meas.	abs.	^{40}Ar	meas.	abs.	meas.	abs.	meas.	abs.
37LF13; Neruokpuk Formation (N69.35, W142.92)																
300	0.003	965	306	338.35877	125	0.24518	0.32707	0.20635	0.18196	18.01676	0.44994	0.6003	-0.01132	0.03238	277.4212	114
500	0.011	1191	125	391.02303	50.97	0.09062	0.09897	0.08079	0.07466	6.10371	0.16629	0.1816	-0.01901	0.01225	367.1517	52.6
750	0.036	1680	47	626.61827	25.66	-0.01214	0.02922	0.07768	0.02752	3.66358	-0.0223	0.0536	-0.00788	0.00296	603.6278	26
1000	0.080	2174	28	918.59537	20.26	-0.00776	0.02178	0.00481	0.01458	0.15484	-0.0142	0.04	-0.0016	0.00162	917.1384	20.7
1250	0.148	2337	31	1048.55519	24.17	-0.1052	0.06373	0.02379	0.02024	0.6714	-0.193	0.1169	0.00061	0.00219	1041.408	24.7
1500	0.247	2470	20	1151.82654	16.98	0.00497	0.00816	0.00205	0.0053	0.05255	0.00911	0.015	-0.0003	0.0008	1151.196	17
1750	0.373	2544	13	1216.58198	11.26	0.00109	0.00471	0.00331	0.00399	0.08041	0.002	0.0087	-0.00135	0.00076	1215.575	11.3
2000	0.570	2542	11	1214.71634	10.05	-0.00203	0.00336	0.00092	0.00285	0.02232	-0.0037	0.0062	-0.00075	0.00062	1214.414	10.1
2500	0.642	2519	25	1192.11588	22.18	-0.00489	0.00982	-0.0042	0.00857	-0.10415	-0.009	0.018	-0.00165	0.00135	1193.324	22.4
3000	0.712	2520	25	1194.4757	21.76	0.05342	0.01025	-0.00026	0.00687	-0.0067	0.09802	0.0188	-0.00211	0.00229	1194.571	21.9
4000	0.763	2494	43	1168.81183	36.75	-0.00741	0.02052	-0.00999	0.01219	-0.2525	-0.0136	0.0377	-0.0041	0.00149	1171.727	37
5000	0.839	2498	27	1172.45674	23.66	0.01464	0.01924	-0.00957	0.0096	-0.24134	0.02687	0.0353	-0.0025	0.0014	1175.269	23.9
9000	1.000	2214	13	946.21915	9.873	-0.00959	0.00786	-0.00189	0.00364	-0.05883	-0.0176	0.0144	-0.00003	0.00101	946.7397	9.94
Integrated	NA	2418	9	1108.62244	5.424	-0.00362	0.0054	0.00397	0.00246	0.10581	-0.0066	0.0099	-0.00143	0.0004	1107.417	5.47
Weighted average of J from standards = 2.552e-03 +/- 1.290e-05																
J1355-67; Neruokpuk Formation (N69.22, W142.96)																
300	0.012	3459	122	2321.41507	184.5	0.01542	0.08792	0.14396	0.04093	1.83249	0.02829	0.1613	0.0609	0.0114	2278.871	181
500	0.029	2853	97	1551.10766	105	-0.09852	0.06385	0.11502	0.03779	2.19177	-0.1808	0.1171	0.05957	0.00788	1516.976	103
750	0.073	1150	26	368.3193	10.28	0.27838	0.03078	0.06314	0.01432	5.06017	0.51088	0.0565	0.03504	0.00288	349.7223	10.6
1000	0.137	805	13	227.39017	4.083	0.02439	0.01575	0.02287	0.00746	2.9716	0.04475	0.0289	0.01366	0.00193	220.608	4.53
1250	0.219	928	14	265.65263	4.96	-0.00247	0.01296	0.00545	0.00621	0.60668	-0.0045	0.0238	0.00656	0.00141	264.011	5.26
1500	0.348	1366	14	444.9106	6.422	0.00103	0.00735	0.00243	0.00347	0.16126	0.0019	0.0135	0.00169	0.00086	444.1638	6.49
1750	0.432	1197	13	368.05256	4.803	-0.00844	0.01578	-0.00566	0.00901	-0.45426	-0.0155	0.029	0.00252	0.00177	369.6924	5.51
2000	0.527	1483	13	498.45203	6.119	-0.00852	0.0098	-0.00709	0.00444	-0.4205	-0.0156	0.018	0.00151	0.00178	500.5152	6.28
2500	0.670	1607	14	562.31926	7.51	-0.00797	0.00734	-0.00596	0.00339	-0.31296	-0.0146	0.0135	0.00035	0.00078	564.0461	7.6
3000	0.762	1534	12	524.28648	5.99	0.00512	0.01032	-0.00523	0.00383	-0.29496	0.00939	0.0189	0.00045	0.00091	525.8051	6.11
4000	0.860	1513	13	513.88416	6.506	-0.00094	0.01141	-0.00552	0.00537	-0.31753	-0.0017	0.0209	-0.0011	0.00091	515.4857	6.72
5000	0.968	1748	13	642.36088	7.106	-0.0068	0.01095	0.00209	0.00425	0.09611	-0.0125	0.0201	0.00015	0.00105	641.7107	7.21

TABLE SM2.6: STEPWISE $^{40}Ar/^{39}Ar$ ISOTOPE COMPOSITIONS OF MUSCOVITE (UNIVERSITY OF ALASKA FAIRBANKS LAB)

L.Power	Cumulative	Age	±	$^{40}Ar/^{39}Ar$	±	$^{37}Ar/^{39}Ar$	±	$^{36}Ar/^{39}Ar$	±	%Atm.	Ca/K	±	Cl/K	±	$40^*/^{39}K$	±
(mW)	39Ar	(Ma)	(Ma)	meas.	abs.	meas.	abs.	meas.	abs.	^{40}Ar	meas.	abs.	meas.	abs.	meas.	abs.
9000	1.000	1661	49	597.54691	26.82	0.09344	0.03293	0.01428	0.0148	0.70475	0.17147	0.0604	0.0046	0.004	593.3454	27
Integrated	NA	1498	7	509.70986	2.456	0.01228	0.00392	0.00633	0.00187	0.36663	0.02254	0.0072	0.00541	0.00044	507.8159	2.51
Weighted average of J from standards = 2.552e-03 +/- 1.290e-05																
12JT24; Clarence River Group (N69.28, W142.75)																
300	0.009	2516	23	1201.69233	19.29	0.10832	0.02861	0.03768	0.0231	0.92585	0.19877	0.0525	0.01487	0.00263	1190.628	20.3
500	0.026	160	14	46.34279	0.846	0.12311	0.01746	0.03373	0.01083	21.49637	0.22591	0.0321	0.00735	0.00097	36.36062	3.26
750	0.066	176	6	41.26508	0.491	0.10065	0.00738	0.00391	0.00425	2.78203	0.1847	0.0135	0.00513	0.0007	40.09105	1.34
1000	0.132	266	3	64.24004	0.349	0.21559	0.00437	0.00628	0.00256	2.86456	0.39563	0.008	0.0041	0.00026	62.38049	0.83
1250	0.218	391	3	95.6962	0.414	0.50521	0.00611	0.00247	0.00186	0.71892	0.92731	0.0112	0.00164	0.00032	95.01265	0.69
1500	0.305	417	3	102.18777	0.597	0.88318	0.0107	0.00091	0.00207	0.19052	1.62153	0.0197	0.0017	0.0003	102.0271	0.85
1750	0.383	427	4	103.95041	0.815	1.22978	0.01418	-0.00244	0.003	-0.78995	2.25843	0.0261	0.00231	0.00037	104.8327	1.21
2000	0.452	421	4	103.34382	0.67	1.44857	0.01275	0.00175	0.00248	0.38469	2.66065	0.0234	0.00242	0.00032	103.0221	0.99
2500	0.528	422	4	103.69194	0.948	1.78087	0.01828	0.00177	0.0022	0.36371	3.27177	0.0336	0.00331	0.00025	103.4153	1.15
3000	0.604	411	3	100.85195	0.645	1.03541	0.00899	0.00203	0.00203	0.50922	1.90123	0.0165	0.00227	0.00024	100.3823	0.88
4000	0.702	515	3	129.51304	0.583	0.04882	0.00262	-0.00084	0.00164	-0.19508	0.08959	0.0048	0.00062	0.00018	129.7404	0.76
5000	0.798	531	3	134.13874	0.775	0.03375	0.00316	-0.00007	0.00196	-0.01841	0.06194	0.0058	0.00054	0.00029	134.1369	0.97
9000	1.000	585	2	150.78829	0.653	0.05422	0.00148	0.0013	0.0008	0.25188	0.09949	0.0027	0.001	0.00012	150.3846	0.69
Integrated	NA	484	2	121.24043	0.225	0.57079	0.00211	0.00217	0.00064	0.49026	1.04774	0.0039	0.00211	0.00008	120.6651	0.29
Weighted average of J from standards = 2.552e-03 +/- 1.290e-05																
09LF13; Clarence River Group (N69.27, W142.66)																
300	0.002	157	191	88.43796	19	0.43686	0.24279	0.17878	0.15593	59.71627	0.80183	0.4458	0.04587	0.02911	35.62514	45.4
500	0.003	354	185	414.00764	77.99	0.21412	0.3233	1.11284	0.26159	79.4311	0.39295	0.5934	0.00729	0.0377	85.16359	49
750	0.007	346	73	99.71511	8.496	0.59234	0.09498	0.05672	0.06041	16.76501	1.08732	0.1744	-0.00025	0.01128	83.00788	19.2
1000	0.015	318	90	113.28026	5.146	1.37815	0.08649	0.12801	0.07826	33.30012	2.53118	0.159	-0.00471	0.00714	75.6116	23.3
1250	0.032	462	16	115.4099	2.278	0.4475	0.02834	0.00323	0.01304	0.79557	0.82136	0.052	0.00328	0.00389	114.4985	4.47
1500	0.052	460	18	114.53848	2.788	0.01394	0.02396	0.0019	0.01421	0.49053	0.02557	0.044	0.00263	0.00325	113.9482	5.03
1750	0.085	464	10	115.93303	0.826	0.00412	0.01311	0.00303	0.00888	0.77111	0.00755	0.0241	0.0019	0.00156	115.0099	2.75
2000	0.149	465	6	115.92671	1.321	0.00679	0.00614	0.00181	0.00428	0.46128	0.01246	0.0113	0.00091	0.00083	115.363	1.83
2500	0.502	456	2	113.22081	0.663	0.00097	0.0018	0.00086	0.00076	0.2232	0.00179	0.0033	0.00068	0.00021	112.9386	0.7

TABLE SM2.6: STEPWISE $^{40}Ar/^{39}Ar$ ISOTOPE COMPOSITIONS OF MUSCOVITE (UNIVERSITY OF ALASKA FAIRBANKS LAB)

L.Power	Cumulative	Age	±	$^{40}Ar/^{39}Ar$	±	$^{37}Ar/^{39}Ar$	±	$^{36}Ar/^{39}Ar$	±	%Atm.	Ca/K	±	Cl/K	±	$40^*/^{39}K$	±
(mW)	39Ar	(Ma)	(Ma)	meas.	abs.	meas.	abs.	meas.	abs.	^{40}Ar	meas.	abs.	meas.	abs.	meas.	abs.
3000	0.633	462	3	114.65743	0.579	0.00343	0.00326	-0.00001	0.0019	-0.0023	0.0063	0.006	0.00083	0.0004	114.6307	0.81
4000	0.805	457	3	113.18677	0.728	-0.00033	0.00203	-0.00025	0.00187	-0.06408	-0.0006	0.0037	0.00038	0.00027	113.2296	0.92
5000	0.935	453	3	112.12498	0.658	-0.00107	0.00298	0.00021	0.00234	0.05523	-0.002	0.0055	0.00037	0.00035	112.0333	0.95
9000	1.000	452	5	113.31269	0.882	0.00756	0.00655	0.00556	0.00404	1.45038	0.01388	0.012	0.00051	0.00063	111.6406	1.48
Integrated	NA	456	3	113.9384	0.325	0.02393	0.00159	0.00414	0.00112	1.07193	0.04391	0.0029	0.00077	0.0002	112.6896	0.46
Weighted average of J from standards = 2.552e-03 +/- 1.290e-05																
40LF13; Clarence River Group (N69.27, W142.91)																
300	0.001	389	78	115.35378	17.54	-0.37574	0.18991	0.07085	0.05291	18.18179	-0.6893	0.3483	-0.06542	0.03118	94.33106	21
500	0.005	303	30	86.41989	4.833	-0.15123	0.0618	0.04968	0.02268	17.00843	-0.2775	0.1134	-0.02012	0.01331	71.68892	7.78
750	0.018	290	9	74.51792	1.481	-0.03504	0.0197	0.02058	0.00648	8.16893	-0.0643	0.0362	-0.00336	0.00413	68.40164	2.35
1000	0.048	341	5	85.61713	0.95	-0.01637	0.00803	0.01339	0.00336	4.62579	-0.03	0.0147	-0.00221	0.00134	81.62739	1.34
1250	0.089	402	3	97.69264	0.755	-0.01194	0.00653	-0.00044	0.00191	-0.13062	-0.0219	0.012	-0.0018	0.00099	97.78968	0.94
1500	0.151	420	3	102.92471	0.843	-0.01602	0.00359	0.00034	0.00148	0.09911	-0.0294	0.0066	-0.00098	0.00067	102.7919	0.95
1750	0.253	428	2	105.04168	0.506	-0.00367	0.0025	0.00003	0.00098	0.00747	-0.0067	0.0046	-0.00018	0.00042	105.0039	0.58
2000	0.387	437	1	107.48511	0.314	-0.00325	0.00174	0.00011	0.00062	0.03159	-0.006	0.0032	-0.00002	0.00031	107.4212	0.36
2500	0.583	436	2	107.59678	0.475	-0.00311	0.00113	0.00092	0.00044	0.25179	-0.0057	0.0021	0.00036	0.00023	107.296	0.49
3000	0.700	435	2	106.89616	0.489	-0.00443	0.00241	0.00001	0.00082	0.00181	-0.0081	0.0044	-0.00032	0.00035	106.8642	0.55
4000	0.795	436	3	107.84393	0.864	-0.00438	0.00293	0.00234	0.00102	0.64175	-0.008	0.0054	-0.00039	0.00048	107.122	0.91
5000	0.855	435	3	107.2692	0.58	-0.01161	0.00456	0.00108	0.00151	0.2998	-0.0213	0.0084	-0.00134	0.00069	106.9171	0.73
9000	1.000	437	2	107.66128	0.523	-0.00459	0.00165	-0.00009	0.00045	-0.02368	-0.0084	0.003	-0.00032	0.00031	107.6567	0.54
Integrated	NA	428	2	105.39693	0.19	-0.00722	0.0009	0.00143	0.00032	0.40131	-0.0132	0.0017	-0.00056	0.00016	104.9438	0.21
Weighted average of J from standards = 2.552e-03 +/- 1.290e-05																
14BJ27; Clarence River Group (N69.26, W142.66)																
300	0.000	54	959	114.84144	76.91	-0.53091	1.02887	0.35544	0.64215	91.5197	-0.9738	1.8864	0.03664	0.08129	9.73273	177
500	0.001	496	609	194.44896	116.9	-1.32435	1.07553	0.31223	0.4767	47.51183	-2.4277	1.9698	-0.01014	0.05384	101.9517	143
750	0.002	308	322	88.2614	29.13	-0.30494	0.44824	0.09532	0.2231	31.95326	-0.5594	0.8221	0.00615	0.02981	60.02586	68.2
1000	0.006	369	78	81.88084	5.858	-0.07164	0.09376	0.02946	0.05486	10.64424	-0.1315	0.172	0.00837	0.00688	73.13501	17
1250	0.017	498	33	103.40061	3.975	-0.0374	0.04099	0.0031	0.02234	0.88883	-0.0686	0.0752	0.00527	0.00303	102.4494	7.69
1500	0.036	482	20	98.72939	1.918	-0.01541	0.01932	0.00012	0.0143	0.03635	-0.0283	0.0355	0.00022	0.00175	98.66274	4.64

TABLE SM2.6: STEPWISE $^{40}Ar/^{39}Ar$ ISOTOPE COMPOSITIONS OF MUSCOVITE (UNIVERSITY OF ALASKA FAIRBANKS LAB)

L.Power	Cumulative	Age	±	$^{40}Ar/^{39}Ar$	±	$^{37}Ar/^{39}Ar$	±	$^{36}Ar/^{39}Ar$	±	%Atm.	Ca/K	±	Cl/K	±	$40^*/^{39}K$	±
(mW)	39Ar	(Ma)	(Ma)	meas.	abs.	meas.	abs.	meas.	abs.	^{40}Ar	meas.	abs.	meas.	abs.	meas.	abs.
1750	0.088	479	8	99.41472	1.239	-0.00833	0.00757	0.0044	0.00456	1.30772	-0.0153	0.0139	0.00083	0.00067	98.08477	1.82
2000	0.212	477	4	97.3561	0.671	-0.00184	0.00342	-0.00052	0.00198	-0.15654	-0.0034	0.0063	0.00029	0.00023	97.47862	0.89
2500	0.606	474	2	96.86885	0.295	0.00003	0.00126	-0.00002	0.00071	-0.0052	0.00006	0.0023	0.00037	0.0001	96.84419	0.36
3000	0.677	467	6	96.07133	1.025	-0.00207	0.00533	0.00249	0.00322	0.76496	-0.0038	0.0098	-0.00036	0.00047	95.30681	1.39
4000	0.772	469	4	95.69016	0.706	-0.0109	0.00471	-0.00023	0.00242	-0.071	-0.02	0.0086	-0.00015	0.00035	95.72764	1.01
5000	0.816	478	8	96.50584	0.942	-0.0121	0.00761	-0.00406	0.00522	-1.24123	-0.0222	0.014	0.00084	0.0007	97.67279	1.81
9000	1.000	471	3	96.23921	0.371	-0.00401	0.00171	-0.0002	0.00154	-0.06022	-0.0074	0.0031	0.00026	0.00021	96.26718	0.59
Integrated	NA	473	2	96.85517	0.217	-0.00531	0.00145	0.00065	0.00088	0.19958	-0.0097	0.0027	0.00038	0.00012	96.63186	0.34

Weighted average of J from standards = 3.107e-03 +/- 8.884e-06

TABLE SM2.7: SINGLE-GRAIN MUSCOVITE TOTAL FUSION $^{40}Ar/^{39}Ar$ ISOTOPE COMPOSITIONS (UNIVERSITY OF ALASKA FAIRBANKS LAB)

14BJ27; Clarence River Group (N69.27, W142.66)															
Grain #	Age	±	$^{40}Ar/^{39}Ar$	±	$^{37}Ar/^{39}Ar$	±	$^{36}Ar/^{39}Ar$	±	%Atm.	Ca/K	±	Cl/K	±	$40*/^{39}K$	±
	(Ma)	(Ma)	meas.	abs.	meas.	abs.	meas.	abs.	^{40}Ar	meas.	abs.	meas.	abs.	meas.	abs.
1	480	1	99.44526	0.19	-0.00156	0.002	0.00362	0.00019	1.07697	-0.00286	0.003	0.00053	0.00003	98.34477	0.196
2*	472	7	104.98345	1.216	-0.01182	0.024	0.02915	0.00369	8.2087	-0.02169	0.044	0.00221	0.00069	96.33761	1.558
3	481	1	99.48791	0.279	-0.00628	0.004	0.00335	0.00053	0.99688	-0.01152	0.007	0.00053	0.00011	98.4663	0.317
4*	473	4	107.26563	0.713	-0.02762	0.011	0.03622	0.00189	9.98271	-0.05068	0.021	0.00041	0.0003	96.52899	0.852
5*	468	6	101.70489	1.051	-0.02394	0.031	0.02068	0.00287	6.0113	-0.04392	0.057	0.00002	0.00059	95.56157	1.301
6	496	7	105.02431	0.567	-0.0089	0.027	0.00983	0.00552	2.76735	-0.01633	0.05	0.00113	0.00081	102.0884	1.722
7	481	2	100.69176	0.346	0.00195	0.002	0.00764	0.00056	2.24176	0.00357	0.003	0.00045	0.00017	98.40559	0.377
8	521	5	109.91415	0.899	-0.00517	0.009	0.00653	0.00248	1.7553	-0.00949	0.017	0.00171	0.00089	107.95525	1.148
9	490	2	105.17606	0.318	0.00146	0.006	0.01554	0.00165	4.36627	0.00268	0.012	0.00109	0.00042	100.55549	0.577
10	441	2	90.85636	0.36	-0.00846	0.01	0.0056	0.00144	1.82134	-0.01553	0.018	0.00054	0.00045	89.17186	0.554
11	464	2	95.82278	0.341	-0.00132	0.002	0.00405	0.00054	1.24955	-0.00243	0.005	0.00054	0.00015	94.59601	0.372
12	491	1	102.87943	0.269	0.00455	0.004	0.00708	0.00072	2.03427	0.00835	0.008	0.00067	0.00017	100.75781	0.339
13	462	4	97.28589	0.756	-0.00042	0.005	0.01081	0.00126	3.28414	-0.00077	0.008	0.00044	0.00029	94.06213	0.82
14*	475	7	105.39561	1.033	-0.0014	0.055	0.02828	0.00474	7.93031	-0.00258	0.102	0.00074	0.00266	97.00997	1.692

Weighted average of J from standards = 3.107e-03 +/- 8.884e-06

*Single-grain total fusion age used in weighted mean age calculation presented in manuscript (Fig. 7)

Chapter 3 (supplemental material): The Whale Mountain allochthon: a relic of the Iapetus Ocean preserved in the northeastern Brooks Range, Alaska

Benjamin G. Johnson[1], Justin V. Strauss[2], John F. Taylor[3], William P. Ward[4], Maurice Colpron[5], William C. McClelland[4], Jaime Toro[1]

[1]Department of Geology and Geography, West Virginia University, Morgantown, West Virginia, 26506 USA

[2]Department of Earth Sciences, Dartmouth College, Hanover, New Hampshire 03755, USA

[3]Department of Geoscience, Indiana University of Pennsylvania, Indiana, Pennsylvania 15705 USA

[4]Department of Earth and Environmental Sciences, University of Iowa, Iowa City, Iowa 52242, USA

[5]Yukon Geological Survey, Whitehorse, Yukon, Canada YIA 2C6

LA-ICPMS U-Pb Zircon Geochronology

U-Pb isotopic ratios for zircon from two volcaniclastic samples from the Whale Mountain allochthon were analyzed by LA-ICPMS at the University of Arizona LaserChron Center. Instrument setup, tuning, run parameters, standard-unknown bracketing, and data reduction followed that of Gehrels et al. (2006, 2008) and Gehrels and Pecha (2014). The separated zircon grains were ablated with a Photon Machines Analyte G2 excimer laser with a HelEx ablation cell using a spot diameter of 20 μm. The ablation pit was ~12 μm in depth using an energy density of ~5 J/cm^2, repetition rate of 8 hz, and an ablation time of 10 seconds. Each analysis included counting for 5 seconds with the laser off for backgrounds and 10 seconds with

the laser firing for peak intensities, followed by a 20 second delay to purge the previous sample and to save the files.

The measured intensities for each analysis were imported into the Arizona LaserChron Center's data reduction program, "agecalc," which reduces the data, alerts users to unusual analyses (e.g., large age uncertainty), calculates ages, and produces a publication ready data table (e.g., Table SM3.2). Three types of zircon grains with known ages were mounted along with unknown grains from our sample set. These were used as primary standards to assess reproducibility and analytical uncertainty of the unknown analyses from our sample set, and they include the Sri Lanka ($^{206}Pb/^{238}U$ age of 563.2 ± 4.8 Ma, 2, Gehrels et al., 2008), FC-52 ($^{206}Pb/^{207}U$ age of 1099.0 ± 0.6 Ma; Paces and Miller, 1993), and R33 ($^{206}Pb/^{238}U$ age of 420.53 ± 0.16 Ma, 2, Mattinson, 2010). For each analysis, the errors in determining $^{206}Pb/^{238}U$ and $^{206}Pb/^{204}Pb$ result in a measurement error of ~1%–2% (at the 2σ level) in the $^{206}Pb/^{238}U$ age. The errors in measurement of $^{206}Pb/^{207}Pb$ and $^{206}Pb/^{204}Pb$ also result in ~1%–2% (at the 2σ level) uncertainty in age for grains that are >900 Ma, but are substantially larger for younger grains due to the low intensity of the ^{207}Pb signal. For this reason, we report a "Best Age" in Table SM3.2, which selects from the either the $^{206}Pb/^{238}U$ or $^{206}Pb/^{207}Pb$ age using a cutoff of 900 Ma in the $^{206}Pb/^{238}U$ age. Analyses that are >20% discordant or >5% reverse discordant (by comparison of $^{206}Pb/238U$ and $^{206}Pb/^{207}Pb$ ages) were filtered out and rejected from any further interpretation.

Zircon Lu-Hf Isotopic Analysis

A subset of the zircon grains were analyzed for their Lu-Hf isotopic composition using a Nu Instruments HR-ICP-MS connected to a Photon Machines Analyte G2 excimer laser equipped with a HelEX cell at the Arizona LaserChron Center. Instrument setup, tuning, run parameters, standard-unknown bracketing, and data reduction followed that of Gehrels and

Pecha (2014). In each analysis, a 40 µm diameter ablation site is centered over the previously excavated U–Pb analysis pit. The analytical routine consists of a 40 second on-peak background measurement, a 60 second laser ablation measurement, and a 15 second washout time. Using a typical laser effluence of ~5 J/cm^2 and pulse rate of 7 Hz, the ablation rate is ~0.8 microns per second. Unknown analyses were bracketed by several standard, including R33, SL2, Plesovice, Temora-2, FC-52, 91500, and Mud Tank (Woodhead and Hergt 2005; Sláma et al. 2008; Bahlburg et al. 2010; Vervoort 2010).

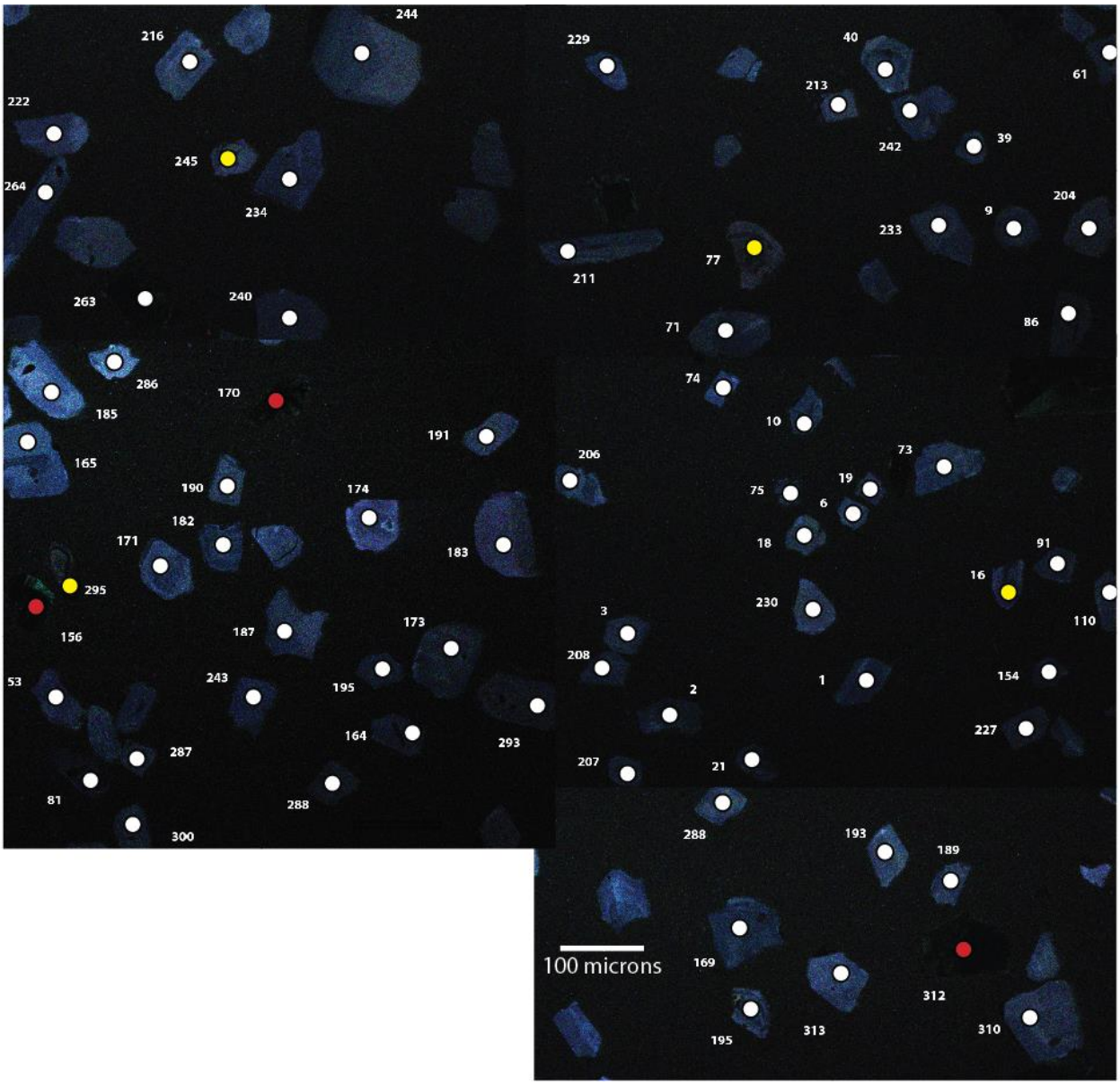

Figure SM3.1: Cathodoluminescence images of selected zircon grains from 15BJ06. White dots show the 20 µm ablation site of grains in Table SM3.2; Yellow dots show ablation site of potential contaminated grains, also shown in Table SM3.2; Red dots show ablation site of grains with spurious zircon chemistry that are not included in Table SM3.2.

References

Bahlburg, H., Vervoort, J.D., and DuFrane, S.A., 2010, Plate tectonic significance of Middle Cambrian and Ordovician siliciclastic rocks of the Bavarian facies, Armorican terrane assemblage, Germany–U-Pb and Hf isotope evidence from detrital zircons: Gondwana Research, v. 17, p. 223–235, doi:10.1016/j.gr.2009.11.007.

Gehrels, G.E., Valencia, V., and Pullen, A., 2006, Detrital zircon geochronology by Laser Ablation Multicollector ICP-MS at the Arizona LaserChron Center, *in* Loszewski, T., and Huff, W., eds., Geochronology: Emerging Opportunities, Paleontology Society Short Course: Paleontology Society Papers, v. 11, 10 p.

Gehrels, G.E., Valencia, V., and Ruiz, J., 2008, Enhanced precision, accuracy, efficiency, and spatial resolution of U-Pb ages by laser ablation–multicollector–inductively coupled plasma–mass spectrometry: Geochemistry Geophysics Geosystems, v. 9, Q03017, doi:10.1029/2007GC001805.

Gehrels, G.E., and Pecha, M., 2014, Detrital zircon U-Pb geochronology and Hf isotope geochemistry of Paleozoic and Triassic passive margin strata of western North America: Geosphere, v. 10, p. 49–65, doi:10.1130/GES00889.1.

Mattinson, J.M., 2010, Analysis of the relative decay constants of 235U and 238U by multi-step CA-TIMS measurements of closed-system natural zircon samples: Chemical Geology, v. 275, p. 186–198, doi:10.1016/j.chemgeo.2010.05.007.

Paces, J.B., and Miller, J.D., 1993, Precise U-Pb ages of Duluth Complex and related mafic intrusions, northern Minnesota: geochronological insights to physical, petrogenic, paleomagnetic, and tectonomagmatic processes associated with the 1.1 Ga midcontinent

rift system: Journal of Geophysical Research: Solid Earth, v. 98, p. 13,977–14,013, doi: 10.1029/9.

Sláma, J., Košler, J., Condon, D.J., Crowley, J.L., Gerdes, A., Hanchar, J.M., Horstwood, M.S., Morris, G.A., Nasdala, L., Norberg, N. and Schaltegger, U., 2008, Plešovice zircon—a new natural reference material for U–Pb and Hf isotopic microanalysis: Chemical Geology, v. 249, p. 1-35, doi: 10.1016/j.chemgeo.2007.11.005

Stacey, J.S., and Kramers, J.D., 1975, Approximation of terrestrial lead isotope evolution by a two-stage model: Earth and Planetary Science Letters, v. 26, p. 207–221, doi: 10.1016/0012-821X(75)90088-6.

Vervoort, J.D., 2010, Hf analysis in zircon by LA-MC-ICPMS: Promise and pitfalls: Geological Society of America Abstracts with Programs, v. 42, p. 667.

Woodhead, J.D., and Hergt, J.M., 2007, A preliminary appraisal of seven natural zircon reference materials for in situ Hf isotope determination: Geostandards and Geoanalytical Research, v. 29, p. 183–195.

Table SM3.1: SAMPLE LOCATIONS FROM THE WHALE MOUNTAIN ALLOCHTHON

Sample Number	Latitude	Longitude	Stratigraphic Unit	Analysis
Southern Belt				
14BJ22	N 69.117	W 143.173	Marsh Fork volcanic rocks	WR-Geochem
14BJ24	N 69.117	W 143.178	Marsh Fork volcanic rocks	WR-Geochem
15BJ08	N 69.069	W 143.907	Marsh Fork volcanic rocks	WR-Geochem
15BJ06	N 69.108	W 143.894	Marsh Fork volcanic rocks	U-Pb & Lu-hf
J1475	N 69.116	W 143.256	Egaksrak formation	Fossil location
Central Belt				
12JT13B	N 69.251	W 141.729	Whale Mountain volcanic rocks	WR-Geochem
12JT14	N 69.251	W 141.729	Whale Mountain volcanic rocks	WR-Geochem
12JT15	N 69.251	W 141.729	Whale Mountain volcanic rocks	WR-Geochem
12JT16	N 69.251	W 141.729	Whale Mountain volcanic rocks	WR-Geochem
12JT17	N 69.251	W 141.729	Whale Mountain volcanic rocks	WR-Geochem
12JT18	N 69.251	W 141.729	Whale Mountain volcanic rocks	WR-Geochem
12JT19	N 69.251	W 141.729	Whale Mountain volcanic rocks	WR-Geochem
12JT20	N 69.251	W 141.729	Whale Mountain volcanic rocks	WR-Geochem
12JT21	N 69.247	W 141.723	Whale Mountain volcanic rocks	WR-Geochem
17LF13	N 69.347	W 142.639	Whale Mountain volcanic rocks	WR-Geochem
18LF13	N 69.347	W 142.639	Whale Mountain volcanic rocks	WR-Geochem
19LF13	N 69.347	W 142.639	Whale Mountain volcanic rocks	WR-Geochem
20LF13	N 69.347	W 142.639	Whale Mountain volcanic rocks	WR-Geochem
21LF13	N 69.347	W 142.639	Whale Mountain volcanic rocks	WR-Geochem
22LF13	N 69.347	W 142.639	Whale Mountain volcanic rocks	WR-Geochem
23LF13	N 69.347	W 142.639	Whale Mountain volcanic rocks	WR-Geochem
13MC-062	N 69.176	W 140.924	Whale Mountain volcanic rocks	WR-Geochem
13MC-063	N 69.169	W 140.879	Whale Mountain volcanic rocks	WR-Geochem
13MC-065	N 69.169	W 140.882	Whale Mountain volcanic rocks	WR-Geochem
13JVS-362	N 69.184	W 140.921	Whale Mountain volcanic rocks	WR-Geochem
13WW23	N 69.182	W 140.924	Whale Mountain volcanic rocks	U-Pb & Lu-hf
J1352	N 69.184	W 140.917	Egaksrak formation	Fossil location
J1480	N 69.346	W 142.656	Egaksrak formation	Fossil location
Northern Belt				
12JT37	N 69.469	W 141.468	Ekaluakat formation	WR-Geochem
12JT39	N 69.456	W 141.451	Ekaluakat formation	WR-Geochem

Note: WR-Geochem stands for whole-rock geochemical analysis

TABLE SM3.2: LA-ICPMS U-Pb ISOTOPIC DATA

						Isotope ratios					Apparent ages (Ma)								
Analysis	U	206Pb	U/Th	206Pb*	±	207Pb*	±	206Pb*	±	error	206Pb*	±	207Pb*	±	206Pb*	±	Best age	±	Conc
	(ppm)	204Pb		207Pb*	(%)	235U*	(%)	238U	(%)	corr.	238U*	(Ma)	235U	(Ma)	207Pb*	(Ma)	(Ma)	(Ma)	(%)
13WW23; Whale Mountain volcanic rocks (central belt; N69182, W140.924)																			
13WW24-55	634	44178	1.0	17.344	2.1	0.6227	7.1	0.0783	6.8	0.96	486	32	492	28	517	45	486	32	94
13WW24-56	112	14897	1.2	17.526	3.4	0.6249	3.9	0.0794	2.0	0.51	493	10	493	15	494	74	493	10	100
13WW24-53	175	30946	1.7	17.308	2.1	0.6424	4.0	0.0806	3.5	0.86	500	17	504	16	521	46	500	17	96
13WW24-59	199	30104	1.7	16.896	1.9	0.6690	5.6	0.0820	5.2	0.94	508	26	520	23	574	41	508	26	89
13WW24-58	116	32355	1.2	17.091	3.0	0.6636	5.8	0.0823	5.0	0.85	510	24	517	24	549	66	510	24	93
13WW24-57	278	48440	1.7	17.231	2.0	0.6637	2.6	0.0829	1.7	0.63	514	8	517	11	531	45	514	8	97
>20% Discordance																			
13WW24-54	107	19777	1.2	13.238	9.7	0.8213	10.1	0.0789	2.5	0.25	489	12	609	46	1083	196	489	12	45
15BJ06; Marsh Fork volcanic rocks (southern belt; N69.108, W143.894)																			
15BJ06-202	163	93547	1.0	17.236	2.4	0.6100	3.3	0.0763	2.3	0.68	474	10	484	13	530	53	474	10	89
15BJ06-001	130	46589	0.8	17.308	2.2	0.6255	3.2	0.0785	2.3	0.73	487	11	493	12	521	47	487	11	93
15BJ06-278	106	97855	1.9	17.074	3.4	0.6383	3.9	0.0790	2.0	0.51	490	9	501	16	551	74	490	9	89
15BJ06-155	277	39032	0.9	17.141	1.8	0.6358	2.8	0.0790	2.1	0.76	490	10	500	11	542	39	490	10	90
15BJ06-248	97	28710	1.4	17.590	2.0	0.6270	2.7	0.0800	1.7	0.64	496	8	494	10	486	45	496	8	102
15BJ06-115	69	12511	1.1	17.574	4.2	0.6295	4.9	0.0802	2.6	0.52	497	12	496	19	488	93	497	12	102
15BJ06-260	254	40924	1.2	17.690	1.8	0.6258	2.8	0.0803	2.2	0.78	498	10	494	11	473	39	498	10	105
15BJ06-293	98	36533	1.9	16.884	2.6	0.6560	3.3	0.0803	2.0	0.61	498	10	512	13	576	56	498	10	87
15BJ06-080	68	26811	1.1	17.442	2.7	0.6355	3.5	0.0804	2.2	0.63	498	10	500	14	504	59	498	10	99
15BJ06-249	107	33981	1.3	16.918	2.0	0.6559	2.9	0.0805	2.1	0.73	499	10	512	11	571	42	499	10	87
15BJ06-206	146	174000	1.3	17.484	2.2	0.6347	3.0	0.0805	2.1	0.69	499	10	499	12	499	49	499	10	100
15BJ06-167	155	234322	1.8	17.520	2.0	0.6336	2.5	0.0805	1.6	0.64	499	8	498	10	495	43	499	8	101
15BJ06-291	286	81360	0.8	17.290	2.1	0.6421	2.9	0.0805	1.9	0.67	499	9	504	11	524	47	499	9	95
15BJ06-268	48	14287	1.7	16.593	4.0	0.6693	4.4	0.0806	1.9	0.42	499	9	520	18	613	86	499	9	81
15BJ06-227	64	21797	1.2	17.325	2.6	0.6415	3.3	0.0806	2.1	0.63	500	10	503	13	519	56	500	10	96
15BJ06-241	84	103733	1.6	16.983	2.6	0.6546	3.2	0.0806	1.9	0.58	500	9	511	13	563	56	500	9	89
15BJ06-266	199	37789	1.4	17.269	1.9	0.6441	2.8	0.0807	2.0	0.72	500	10	505	11	526	42	500	10	95
15BJ06-236	71	16377	1.7	17.672	2.8	0.6295	3.7	0.0807	2.3	0.64	500	11	496	14	475	63	500	11	105
15BJ06-270	91	48704	1.2	17.057	2.8	0.6524	3.6	0.0807	2.3	0.63	500	11	510	14	553	61	500	11	90
15BJ06-246	77	42754	1.6	16.916	2.7	0.6580	3.4	0.0807	2.1	0.62	500	10	513	14	571	58	500	10	88

TABLE SM3.2: LA-ICPMS U-Pb ISOTOPIC DATA

						Isotope ratios					Apparent ages (Ma)								
Analysis	U	206Pb	U/Th	206Pb*	±	207Pb*	±	206Pb*	±	error	206Pb*	±	207Pb*	±	206Pb*	±	Best age	±	Conc
	(ppm)	204Pb		207Pb*	(%)	235U*	(%)	238U	(%)	corr.	238U*	(Ma)	235U	(Ma)	207Pb*	(Ma)	(Ma)	(Ma)	(%)
15BJ06-276	113	59878	1.4	16.492	2.8	0.6764	3.4	0.0809	2.0	0.58	502	10	525	14	626	60	502	10	80
15BJ06-144	84	43418	1.6	17.257	3.4	0.6471	4.0	0.0810	2.1	0.53	502	10	507	16	528	75	502	10	95
15BJ06-275	43	17931	1.5	17.392	2.8	0.6423	3.4	0.0810	1.9	0.56	502	9	504	14	511	62	502	9	98
15BJ06-104	159	67233	1.5	17.198	2.0	0.6498	2.8	0.0811	2.0	0.72	502	10	508	11	535	43	502	10	94
15BJ06-222	27	20331	1.4	17.346	5.6	0.6445	6.0	0.0811	2.1	0.36	503	10	505	24	516	123	503	10	97
15BJ06-264	94	49399	1.5	16.948	2.1	0.6597	2.9	0.0811	1.9	0.67	503	9	514	12	567	47	503	9	89
15BJ06-239	201	62966	1.3	17.526	1.9	0.6384	2.6	0.0811	1.8	0.68	503	9	501	10	494	42	503	9	102
15BJ06-010	164	48694	1.9	17.136	2.3	0.6530	3.2	0.0811	2.3	0.70	503	11	510	13	543	50	503	11	93
15BJ06-137	84	36451	2.2	16.965	2.0	0.6598	2.7	0.0812	1.8	0.66	503	9	515	11	565	44	503	9	89
15BJ06-129	55	34203	1.4	16.987	3.3	0.6592	4.2	0.0812	2.6	0.61	503	13	514	17	562	73	503	13	90
15BJ06-294	96	164226	1.2	16.746	2.5	0.6687	3.0	0.0812	1.7	0.56	503	8	520	12	593	55	503	8	85
15BJ06-043	50	35947	2.0	17.214	2.4	0.6514	3.2	0.0813	2.1	0.66	504	10	509	13	533	52	504	10	95
15BJ06-084	93	26152	2.0	17.012	2.6	0.6591	3.5	0.0813	2.3	0.67	504	11	514	14	559	57	504	11	90
15BJ06-161	58	31078	1.9	16.881	3.5	0.6645	4.1	0.0814	2.2	0.54	504	11	517	17	576	75	504	11	88
15BJ06-212	115	58019	1.8	17.431	2.3	0.6436	3.5	0.0814	2.6	0.75	504	13	505	14	506	50	504	13	100
15BJ06-126	155	40541	2.0	16.542	1.9	0.6782	3.0	0.0814	2.3	0.77	504	11	526	12	620	42	504	11	81
15BJ06-243	50	51904	1.3	17.590	3.2	0.6379	4.0	0.0814	2.4	0.61	504	12	501	16	486	70	504	12	104
15BJ06-261	220	29833	0.9	17.497	1.8	0.6413	2.6	0.0814	1.9	0.74	504	9	503	10	497	39	504	9	101
15BJ06-238	225	212825	1.6	17.383	1.9	0.6457	2.8	0.0814	2.1	0.75	504	10	506	11	512	41	504	10	99
15BJ06-060	164	32024	1.2	17.387	2.1	0.6455	3.1	0.0814	2.3	0.75	504	11	506	12	511	46	504	11	99
15BJ06-117	31	27726	1.6	16.448	4.5	0.6831	4.9	0.0815	2.0	0.41	505	10	529	20	632	96	505	10	80
15BJ06-253	79	35365	1.5	17.595	3.0	0.6390	3.6	0.0815	2.0	0.56	505	10	502	14	485	65	505	10	104
15BJ06-013	91	16334	1.2	17.433	2.2	0.6449	3.1	0.0815	2.1	0.70	505	10	505	12	505	49	505	10	100
15BJ06-306	185	201949	1.4	17.381	2.0	0.6469	3.0	0.0816	2.2	0.74	505	11	507	12	512	44	505	11	99
15BJ06-285	55	16943	1.5	17.207	2.7	0.6535	3.6	0.0816	2.4	0.66	505	12	511	14	534	59	505	12	95
15BJ06-185	51	24721	1.3	17.506	3.4	0.6424	4.3	0.0816	2.7	0.62	505	13	504	17	496	75	505	13	102
15BJ06-190	179	27223	1.7	17.367	2.2	0.6478	2.8	0.0816	1.7	0.62	506	8	507	11	514	48	506	8	98
15BJ06-302	144	40501	1.3	17.398	2.0	0.6467	3.1	0.0816	2.3	0.75	506	11	506	12	510	45	506	11	99
15BJ06-228	125	50560	1.6	17.317	2.7	0.6498	3.3	0.0816	2.0	0.59	506	10	508	13	520	59	506	10	97
15BJ06-234	54	23957	1.3	17.489	3.2	0.6439	3.8	0.0817	2.1	0.54	506	10	505	15	498	70	506	10	102
15BJ06-078	71	28210	1.6	17.336	3.4	0.6499	4.3	0.0817	2.7	0.62	506	13	508	17	518	74	506	13	98
15BJ06-113	100	127931	1.7	17.263	2.1	0.6532	2.8	0.0818	1.8	0.64	507	9	510	11	527	47	507	9	96
15BJ06-182	217	134171	1.2	17.135	2.4	0.6582	3.1	0.0818	2.0	0.63	507	10	514	13	543	53	507	10	93

TABLE SM3.2: LA-ICPMS U-Pb ISOTOPIC DATA

						Isotope ratios					Apparent ages (Ma)								
Analysis	U	206Pb	U/Th	206Pb*	±	207Pb*	±	206Pb*	±	error	206Pb*	±	207Pb*	±	206Pb*	±	Best age	±	Conc
	(ppm)	204Pb		207Pb*	(%)	235U*	(%)	238U	(%)	corr.	238U*	(Ma)	235U	(Ma)	207Pb*	(Ma)	(Ma)	(Ma)	(%)
15BJ06-072	30	24608	2.2	17.628	4.2	0.6401	5.0	0.0818	2.6	0.53	507	13	502	20	481	93	507	13	105
15BJ06-191	43	21809	1.9	17.087	3.3	0.6606	3.9	0.0819	2.1	0.54	507	10	515	16	549	72	507	10	92
15BJ06-122	237	213323	0.9	17.432	1.5	0.6479	2.4	0.0819	1.9	0.77	507	9	507	10	506	34	507	9	100
15BJ06-232	117	87640	1.6	16.863	2.5	0.6700	4.0	0.0819	3.1	0.77	508	15	521	16	578	55	508	15	88
15BJ06-022	137	28775	1.2	17.162	2.8	0.6584	3.4	0.0819	1.9	0.55	508	9	514	14	540	62	508	9	94
15BJ06-231	191	70959	1.6	17.323	1.8	0.6526	2.5	0.0820	1.8	0.71	508	9	510	10	519	39	508	9	98
15BJ06-050	65	45598	1.9	17.049	2.7	0.6633	3.3	0.0820	1.9	0.56	508	9	517	13	554	60	508	9	92
15BJ06-175	46	11223	1.3	17.084	3.7	0.6620	4.4	0.0820	2.4	0.54	508	12	516	18	550	80	508	12	92
15BJ06-087	46	40117	1.3	16.812	3.6	0.6728	4.1	0.0820	2.0	0.49	508	10	522	17	585	78	508	10	87
15BJ06-089	303	40065	0.9	17.195	1.8	0.6579	2.9	0.0820	2.2	0.77	508	11	513	12	536	40	508	11	95
15BJ06-135	82	38302	1.7	17.092	2.8	0.6621	3.5	0.0821	2.0	0.58	508	10	516	14	549	61	508	10	93
15BJ06-058	45	84961	1.2	16.614	3.5	0.6812	4.2	0.0821	2.3	0.55	509	11	527	17	610	75	509	11	83
15BJ06-025	125	31844	1.4	17.257	2.4	0.6559	3.0	0.0821	1.8	0.60	509	9	512	12	528	53	509	9	96
15BJ06-225	152	69242	1.9	17.492	1.8	0.6472	2.8	0.0821	2.2	0.78	509	11	507	11	498	39	509	11	102
15BJ06-226	86	46602	1.6	17.119	2.9	0.6615	3.7	0.0821	2.2	0.61	509	11	516	15	545	63	509	11	93
15BJ06-012	117	30186	1.6	17.058	2.5	0.6639	3.3	0.0821	2.2	0.66	509	11	517	13	553	54	509	11	92
15BJ06-064	32	51667	1.4	16.593	3.0	0.6827	3.7	0.0822	2.2	0.59	509	11	528	15	613	64	509	11	83
15BJ06-136	98	146274	1.8	17.068	3.1	0.6637	3.7	0.0822	2.0	0.55	509	10	517	15	552	68	509	10	92
15BJ06-119	117	47855	2.1	17.501	1.9	0.6473	2.8	0.0822	2.0	0.72	509	10	507	11	497	42	509	10	102
15BJ06-194	121	122999	1.8	17.250	1.9	0.6573	2.9	0.0822	2.2	0.75	509	11	513	12	529	43	509	11	96
15BJ06-105	100	49968	1.7	16.974	2.1	0.6686	2.6	0.0823	1.5	0.59	510	8	520	11	564	46	510	8	90
15BJ06-014	98	46387	1.5	17.087	2.4	0.6644	3.3	0.0823	2.2	0.67	510	11	517	13	549	53	510	11	93
15BJ06-203	138	63878	1.9	17.113	2.6	0.6635	3.8	0.0824	2.8	0.74	510	14	517	15	546	56	510	14	93
15BJ06-171	74	42870	1.6	17.319	2.2	0.6557	3.0	0.0824	2.0	0.68	510	10	512	12	520	48	510	10	98
15BJ06-307	39	20744	2.0	17.500	4.4	0.6490	5.2	0.0824	2.8	0.53	510	14	508	21	497	97	510	14	103
15BJ06-301	85	25716	1.9	17.133	3.1	0.6630	4.0	0.0824	2.6	0.64	510	13	516	16	544	67	510	13	94
15BJ06-062	129	91579	1.2	17.406	2.3	0.6527	3.3	0.0824	2.4	0.72	510	12	510	13	509	50	510	12	100
15BJ06-229	270	39040	1.3	17.540	1.9	0.6477	2.9	0.0824	2.2	0.76	510	11	507	12	492	42	510	11	104
15BJ06-151	24	19320	1.3	17.536	4.1	0.6479	4.8	0.0824	2.5	0.52	510	12	507	19	493	91	510	12	104
15BJ06-124	81	49641	1.5	17.246	2.6	0.6588	3.2	0.0824	1.9	0.58	510	9	514	13	529	58	510	9	96
15BJ06-290	76	25694	1.9	17.440	2.6	0.6515	3.7	0.0824	2.6	0.71	510	13	509	15	505	57	510	13	101
15BJ06-065	152	28754	1.2	17.058	1.8	0.6660	2.9	0.0824	2.3	0.79	510	11	518	12	553	40	510	11	92
15BJ06-242	74	45814	1.5	17.204	2.4	0.6605	3.5	0.0824	2.4	0.71	510	12	515	14	535	54	510	12	96

TABLE SM3.2: LA-ICPMS U-Pb ISOTOPIC DATA

						Isotope ratios					Apparent ages (Ma)								
Analysis	U	206Pb	U/Th	206Pb*	±	207Pb*	±	206Pb*	±	error	206Pb*	±	207Pb*	±	206Pb*	±	Best age	±	Conc
	(ppm)	204Pb		207Pb*	(%)	235U*	(%)	238U	(%)	corr.	238U*	(Ma)	235U	(Ma)	207Pb*	(Ma)	(Ma)	(Ma)	(%)
15BJ06-073	87	26924	1.6	17.177	2.1	0.6615	3.2	0.0824	2.4	0.75	511	12	516	13	538	46	511	12	95
15BJ06-197	183	120634	1.2	17.069	2.1	0.6660	2.8	0.0824	1.8	0.65	511	9	518	11	552	47	511	9	93
15BJ06-311	100	42300	1.0	16.921	3.5	0.6720	4.0	0.0825	2.1	0.52	511	10	522	16	571	75	511	10	89
15BJ06-150	158	245577	1.9	17.297	2.3	0.6575	3.1	0.0825	2.0	0.65	511	10	513	12	523	52	511	10	98
15BJ06-289	179	64058	1.7	17.079	2.2	0.6659	2.5	0.0825	1.3	0.51	511	6	518	10	550	47	511	6	93
15BJ06-217	65	40825	2.0	17.356	2.7	0.6553	4.0	0.0825	3.0	0.74	511	15	512	16	515	60	511	15	99
15BJ06-096	42	236354	1.5	17.027	3.6	0.6681	4.2	0.0825	2.3	0.54	511	11	520	17	557	78	511	11	92
15BJ06-003	46	45551	2.1	17.197	2.8	0.6615	3.5	0.0825	2.2	0.62	511	11	516	14	535	60	511	11	95
15BJ06-032	190	66997	0.9	17.058	2.1	0.6671	2.9	0.0825	2.0	0.69	511	10	519	12	553	46	511	10	92
15BJ06-297	46	33227	1.7	17.359	3.6	0.6555	3.9	0.0825	1.4	0.36	511	7	512	15	515	79	511	7	99
15BJ06-145	58	29157	2.0	17.407	3.2	0.6537	3.6	0.0825	1.7	0.46	511	8	511	15	509	71	511	8	100
15BJ06-128	173	162542	1.4	17.541	1.4	0.6487	2.4	0.0825	1.9	0.81	511	9	508	10	492	31	511	9	104
15BJ06-187	41	36321	1.6	16.924	3.9	0.6725	4.4	0.0825	2.2	0.49	511	11	522	18	570	84	511	11	90
15BJ06-114	66	28763	1.3	17.389	3.4	0.6548	4.1	0.0826	2.2	0.54	511	11	511	16	511	75	511	11	100
15BJ06-160	96	25311	1.6	17.452	2.4	0.6525	2.9	0.0826	1.7	0.58	512	8	510	12	503	52	512	8	102
15BJ06-074	44	28434	1.1	17.240	4.2	0.6606	4.9	0.0826	2.5	0.51	512	12	515	20	530	92	512	12	97
15BJ06-298	243	132932	0.9	17.319	1.7	0.6577	2.8	0.0826	2.2	0.80	512	11	513	11	520	37	512	11	98
15BJ06-189	81	42627	1.4	16.909	2.4	0.6736	3.4	0.0826	2.3	0.69	512	11	523	14	572	53	512	11	89
15BJ06-002	215	158409	1.6	17.542	1.7	0.6493	3.0	0.0826	2.5	0.83	512	12	508	12	492	38	512	12	104
15BJ06-154	56	23730	1.4	17.029	2.5	0.6691	3.2	0.0826	2.0	0.63	512	10	520	13	557	54	512	10	92
15BJ06-257	91	195778	1.9	17.229	2.2	0.6615	2.8	0.0827	1.8	0.63	512	9	516	11	531	48	512	9	96
15BJ06-024	137	28151	1.3	17.249	2.3	0.6610	3.1	0.0827	2.1	0.68	512	10	515	13	529	50	512	10	97
15BJ06-034	71	41928	1.4	16.571	2.9	0.6880	3.6	0.0827	2.2	0.60	512	11	532	15	616	62	512	11	83
15BJ06-103	147	81165	0.9	17.200	1.7	0.6629	2.5	0.0827	1.8	0.72	512	9	516	10	535	38	512	9	96
15BJ06-284	280	28582	0.9	17.046	1.5	0.6690	2.6	0.0827	2.1	0.82	512	11	520	11	555	32	512	11	92
15BJ06-085	130	91408	1.3	17.209	2.4	0.6627	3.5	0.0827	2.6	0.73	512	13	516	14	534	53	512	13	96
15BJ06-211	282	143573	0.8	17.358	1.5	0.6572	2.6	0.0827	2.2	0.82	512	11	513	11	515	33	512	11	100
15BJ06-015	126	41323	1.2	17.335	2.5	0.6581	3.3	0.0827	2.2	0.67	512	11	513	13	518	54	512	11	99
15BJ06-169	178	39066	1.2	17.487	2.9	0.6525	3.8	0.0828	2.4	0.64	513	12	510	15	499	64	513	12	103
15BJ06-053	48	46801	1.3	16.991	3.4	0.6717	4.2	0.0828	2.4	0.57	513	12	522	17	562	75	513	12	91
15BJ06-180	45	223993	2.0	17.108	3.3	0.6671	3.9	0.0828	1.9	0.50	513	9	519	16	547	73	513	9	94
15BJ06-256	84	37321	2.0	17.416	2.7	0.6554	3.5	0.0828	2.2	0.62	513	11	512	14	508	60	513	11	101
15BJ06-230	27	41578	1.8	17.006	3.9	0.6713	4.3	0.0828	1.8	0.41	513	9	522	17	560	85	513	9	92

TABLE SM3.2: LA-ICPMS U-Pb ISOTOPIC DATA

						Isotope ratios					Apparent ages (Ma)								
Analysis	U	206Pb	U/Th	206Pb*	±	207Pb*	±	206Pb*	±	error	206Pb*	±	207Pb*	±	206Pb*	±	Best age	±	Conc
	(ppm)	204Pb		207Pb*	(%)	235U*	(%)	238U	(%)	corr.	238U*	(Ma)	235U	(Ma)	207Pb*	(Ma)	(Ma)	(Ma)	(%)
15BJ06-066	70	25105	1.1	17.529	2.5	0.6513	3.2	0.0828	2.1	0.64	513	10	509	13	493	55	513	10	104
15BJ06-305	145	93255	1.3	17.364	2.2	0.6581	3.0	0.0829	2.0	0.67	513	10	513	12	514	48	513	10	100
15BJ06-134	72	28534	1.5	17.475	3.4	0.6540	4.1	0.0829	2.3	0.55	513	11	511	16	500	75	513	11	103
15BJ06-035	72	45811	1.8	16.614	2.5	0.6880	3.0	0.0829	1.7	0.58	513	9	532	13	610	53	513	9	84
15BJ06-123	111	139781	1.2	17.364	2.4	0.6583	3.7	0.0829	2.8	0.76	513	14	514	15	514	53	513	14	100
15BJ06-100	29	17831	1.3	17.460	4.6	0.6549	5.2	0.0829	2.5	0.48	514	12	511	21	502	101	514	12	102
15BJ06-283	273	237236	0.8	17.371	1.8	0.6584	2.6	0.0829	1.9	0.72	514	9	514	10	513	40	514	9	100
15BJ06-005	88	192337	1.1	17.388	3.2	0.6579	4.3	0.0830	2.9	0.68	514	14	513	17	511	70	514	14	101
15BJ06-051	210	131258	1.6	17.434	2.0	0.6570	2.8	0.0831	1.9	0.68	514	9	513	11	505	45	514	9	102
15BJ06-204	35	38992	1.9	16.966	3.7	0.6752	4.3	0.0831	2.1	0.49	514	10	524	18	565	82	514	10	91
15BJ06-224	84	54550	1.9	17.501	2.5	0.6549	3.3	0.0831	2.1	0.64	515	10	511	13	497	56	515	10	104
15BJ06-127	56	138723	2.0	16.693	3.1	0.6867	4.0	0.0831	2.5	0.64	515	13	531	16	600	66	515	13	86
15BJ06-063	67	41444	1.2	17.192	2.4	0.6670	2.9	0.0832	1.7	0.58	515	9	519	12	536	52	515	9	96
15BJ06-299	40	78687	1.2	16.723	3.3	0.6858	3.7	0.0832	1.7	0.47	515	9	530	15	596	71	515	9	86
15BJ06-267	64	27766	1.4	17.558	3.2	0.6532	3.8	0.0832	2.1	0.56	515	11	510	15	490	70	515	11	105
15BJ06-147	86	66631	1.3	16.900	2.5	0.6787	3.5	0.0832	2.4	0.70	515	12	526	14	573	54	515	12	90
15BJ06-059	55	190792	1.5	17.356	3.1	0.6612	3.6	0.0832	1.9	0.53	515	10	515	15	515	68	515	10	100
15BJ06-199	179	42081	1.1	17.382	1.7	0.6604	2.6	0.0832	1.9	0.74	515	10	515	10	512	38	515	10	101
15BJ06-007	64	20658	1.6	17.350	3.0	0.6616	3.6	0.0833	2.1	0.58	516	10	516	15	516	65	516	10	100
15BJ06-075	128	185827	1.1	17.150	2.3	0.6694	3.1	0.0833	2.1	0.67	516	10	520	13	541	51	516	10	95
15BJ06-271	93	37691	1.9	17.159	2.9	0.6692	3.7	0.0833	2.3	0.62	516	12	520	15	540	64	516	12	95
15BJ06-031	60	20886	2.1	16.985	3.6	0.6764	4.4	0.0833	2.6	0.59	516	13	525	18	562	78	516	13	92
15BJ06-142	105	55153	1.9	17.406	2.4	0.6604	3.0	0.0834	1.9	0.61	516	9	515	12	509	53	516	9	101
15BJ06-157	163	42504	1.6	17.463	2.0	0.6583	3.1	0.0834	2.4	0.76	516	12	514	13	502	44	516	12	103
15BJ06-215	43	39103	1.6	17.453	2.9	0.6589	4.2	0.0834	2.9	0.71	516	15	514	17	503	64	516	15	103
15BJ06-037	50	27044	1.2	17.215	3.2	0.6685	4.1	0.0835	2.5	0.61	517	12	520	17	533	71	517	12	97
15BJ06-110	37	22228	2.1	17.291	3.7	0.6656	4.6	0.0835	2.7	0.58	517	13	518	19	523	82	517	13	99
15BJ06-168	222	63309	1.0	17.343	1.6	0.6642	2.5	0.0835	2.0	0.77	517	10	517	10	517	35	517	10	100
15BJ06-292	60	27158	1.4	17.470	2.9	0.6596	3.5	0.0836	2.0	0.57	517	10	514	14	501	64	517	10	103
15BJ06-108	123	46730	1.3	17.248	1.6	0.6681	2.5	0.0836	2.0	0.79	517	10	520	10	529	34	517	10	98
15BJ06-083	127	28747	1.9	17.427	2.1	0.6619	2.8	0.0837	1.8	0.65	518	9	516	11	506	46	518	9	102
15BJ06-164	71	148396	2.1	17.403	2.8	0.6628	3.2	0.0837	1.5	0.48	518	8	516	13	509	62	518	8	102
15BJ06-026	70	104685	2.0	17.301	2.7	0.6668	3.6	0.0837	2.3	0.66	518	12	519	15	522	59	518	12	99

TABLE SM3.2: LA-ICPMS U-Pb ISOTOPIC DATA

						Isotope ratios					Apparent ages (Ma)								
Analysis	U	206Pb	U/Th	206Pb*	±	207Pb*	±	206Pb*	±	error	206Pb*	±	207Pb*	±	206Pb*	±	Best age	±	Conc
	(ppm)	204Pb		207Pb*	(%)	235U*	(%)	238U	(%)	corr.	238U*	(Ma)	235U	(Ma)	207Pb*	(Ma)	(Ma)	(Ma)	(%)
15BJ06-023	111	35458	1.4	17.518	2.6	0.6595	3.5	0.0838	2.3	0.66	519	11	514	14	495	58	519	11	105
15BJ06-041	31	40414	2.0	16.988	3.2	0.6801	4.0	0.0838	2.4	0.61	519	12	527	17	562	70	519	12	92
15BJ06-196	88	32419	1.7	17.152	2.7	0.6743	3.2	0.0839	1.8	0.55	519	9	523	13	541	59	519	9	96
15BJ06-098	59	41799	1.7	16.523	3.1	0.7000	4.0	0.0839	2.5	0.63	519	12	539	17	622	67	519	12	83
15BJ06-109	27	21776	0.8	17.521	4.5	0.6605	5.0	0.0839	2.1	0.42	520	10	515	20	494	100	520	10	105
15BJ06-208	73	32267	1.4	17.112	3.1	0.6766	3.7	0.0840	1.9	0.52	520	10	525	15	546	69	520	10	95
15BJ06-056	63	44603	1.9	17.214	3.4	0.6729	3.9	0.0840	1.8	0.46	520	9	522	16	533	75	520	9	98
15BJ06-004	59	31709	2.1	17.234	3.5	0.6722	4.3	0.0840	2.4	0.56	520	12	522	18	531	78	520	12	98
15BJ06-106	293	131732	1.1	17.268	1.9	0.6709	2.7	0.0840	2.0	0.72	520	10	521	11	526	41	520	10	99
15BJ06-036	33	37219	1.0	17.350	4.2	0.6678	4.9	0.0840	2.6	0.52	520	13	519	20	516	93	520	13	101
15BJ06-091	112	134304	1.5	16.981	2.6	0.6823	3.3	0.0840	1.9	0.59	520	10	528	13	563	58	520	10	92
15BJ06-018	81	47044	2.0	17.262	2.8	0.6713	3.7	0.0840	2.3	0.64	520	12	521	15	527	62	520	12	99
15BJ06-310	26	29208	1.8	17.434	3.9	0.6650	4.4	0.0841	2.0	0.46	520	10	518	18	505	85	520	10	103
15BJ06-061	54	34669	1.4	16.887	2.6	0.6866	3.6	0.0841	2.5	0.68	520	12	531	15	575	57	520	12	91
15BJ06-287	84	93786	1.9	17.352	2.5	0.6682	3.2	0.0841	2.0	0.63	521	10	520	13	516	54	521	10	101
15BJ06-193	74	115381	2.3	17.352	2.6	0.6684	3.2	0.0841	1.8	0.57	521	9	520	13	516	57	521	9	101
15BJ06-033	135	62924	1.2	17.260	1.9	0.6724	3.0	0.0842	2.4	0.78	521	12	522	12	527	42	521	12	99
15BJ06-314	74	32933	2.0	17.105	3.1	0.6795	4.0	0.0843	2.5	0.62	522	12	526	17	547	69	522	12	95
15BJ06-216	42	10218	1.6	17.411	4.3	0.6677	4.9	0.0843	2.4	0.50	522	12	519	20	508	94	522	12	103
15BJ06-188	547	155902	0.6	17.500	1.4	0.6644	2.8	0.0843	2.4	0.87	522	12	517	11	497	31	522	12	105
15BJ06-055	115	754043	1.7	17.100	2.7	0.6803	3.4	0.0844	2.0	0.59	522	10	527	14	548	60	522	10	95
15BJ06-198	25	10815	1.5	16.925	4.1	0.6880	4.7	0.0845	2.3	0.49	523	11	532	19	570	90	523	11	92
15BJ06-121	175	68675	1.0	17.155	1.8	0.6790	2.5	0.0845	1.8	0.71	523	9	526	10	541	38	523	9	97
15BJ06-112	84	167171	1.7	17.282	2.5	0.6746	3.5	0.0846	2.4	0.69	523	12	524	14	525	55	523	12	100
15BJ06-186	84	24793	1.3	16.952	1.9	0.6879	2.8	0.0846	2.1	0.75	523	11	532	12	567	41	523	11	92
15BJ06-017	49	109121	1.7	17.113	3.1	0.6822	3.7	0.0847	2.1	0.57	524	11	528	15	546	67	524	11	96
15BJ06-132	107	55274	1.7	17.382	2.4	0.6717	3.0	0.0847	1.8	0.61	524	9	522	12	512	52	524	9	102
15BJ06-086	50	22011	1.7	17.498	2.6	0.6679	3.2	0.0848	1.9	0.59	525	10	519	13	497	57	525	10	105
15BJ06-179	63	31495	1.8	17.352	2.8	0.6741	3.7	0.0848	2.5	0.66	525	12	523	15	516	61	525	12	102
15BJ06-237	277	119454	0.8	17.360	1.7	0.6741	2.5	0.0849	1.8	0.71	525	9	523	10	515	38	525	9	102
15BJ06-006	35	13962	2.2	17.324	3.4	0.6769	3.8	0.0851	1.8	0.47	526	9	525	16	519	74	526	9	101
15BJ06-205	46	27020	1.9	16.373	3.7	0.7167	4.0	0.0851	1.6	0.40	527	8	549	17	642	79	527	8	82
15BJ06-090	149	78466	1.9	17.149	2.3	0.6843	3.2	0.0851	2.2	0.68	527	11	529	13	541	51	527	11	97

TABLE SM3.2: LA-ICPMS U-Pb ISOTOPIC DATA

						Isotope ratios					Apparent ages (Ma)								
Analysis	U	206Pb	U/Th	206Pb*	±	207Pb*	±	206Pb*	±	error	206Pb*	±	207Pb*	±	206Pb*	±	Best age	±	Conc
	(ppm)	204Pb		207Pb*	(%)	235U*	(%)	238U	(%)	corr.	238U*	(Ma)	235U	(Ma)	207Pb*	(Ma)	(Ma)	(Ma)	(%)
15BJ06-149	114	34808	1.7	17.164	2.3	0.6846	3.4	0.0852	2.5	0.74	527	13	530	14	540	50	527	13	98
15BJ06-102	49	40008	2.0	16.838	3.1	0.6981	3.7	0.0852	2.2	0.58	527	11	538	16	581	67	527	11	91
15BJ06-027	87	35345	1.6	17.277	2.2	0.6824	2.9	0.0855	2.0	0.68	529	10	528	12	525	47	529	10	101
15BJ06-213	38	28582	1.7	16.980	3.6	0.6954	4.3	0.0856	2.3	0.54	530	12	536	18	563	79	530	12	94
15BJ06-220	33	13865	0.9	17.262	3.2	0.6850	4.1	0.0858	2.6	0.63	530	13	530	17	527	70	530	13	101
15BJ06-181	37	34478	1.4	16.973	3.0	0.6968	3.5	0.0858	1.7	0.49	531	9	537	14	564	66	531	9	94
15BJ06-177	51	41861	1.3	17.206	2.2	0.6891	3.7	0.0860	2.9	0.79	532	15	532	15	534	49	532	15	100
15BJ06-195	109	154670	1.7	17.139	2.2	0.6924	3.6	0.0861	2.8	0.79	532	14	534	15	543	48	532	14	98
15BJ06-265	146	29612	1.5	17.329	1.7	0.6872	2.6	0.0864	1.9	0.74	534	10	531	11	519	38	534	10	103
15BJ06-045	44	28165	1.2	17.238	3.9	0.6927	4.6	0.0866	2.4	0.53	535	12	534	19	530	85	535	12	101
15BJ06-210	59	146544	1.5	17.375	3.6	0.6878	4.1	0.0867	2.0	0.48	536	10	531	17	513	79	536	10	104
15BJ06-049	32	13329	1.9	17.059	4.2	0.7007	4.7	0.0867	2.1	0.44	536	11	539	19	553	91	536	11	97
15BJ06-042	81	83826	1.8	17.269	2.0	0.6942	3.1	0.0869	2.3	0.74	537	12	535	13	526	45	537	12	102
15BJ06-099	67	25385	1.5	16.846	2.9	0.7130	3.4	0.0871	1.9	0.55	538	10	547	15	580	63	538	10	93
15BJ06-130	52	31116	1.4	17.080	2.7	0.7111	3.4	0.0881	2.1	0.61	544	11	545	15	550	59	544	11	99
15BJ06-046	68	200485	0.8	8.940	1.6	5.0788	2.4	0.3293	1.8	0.75	1835	29	1833	21	1830	29	1830	29	100
15BJ06-081	851	204103	0.6	5.810	1.2	9.6076	2.6	0.4048	2.4	0.90	2191	44	2398	24	2578	19	2578	19	85
>20% Discordance																			
15BJ06-159	379	119943	0.8	16.507	2.1	0.6610	2.6	0.0791	1.5	0.59	491	7	515	10	624	45	491	7	79
15BJ06-020	48	28854	1.7	16.241	3.1	0.6861	3.7	0.0808	2.1	0.56	501	10	530	15	659	67	501	10	76
15BJ06-028	32	84872	1.8	16.038	4.3	0.7022	4.9	0.0817	2.3	0.47	506	11	540	21	686	93	506	11	74
15BJ06-166	49	40597	1.6	16.077	3.7	0.7014	4.6	0.0818	2.8	0.61	507	14	540	19	681	79	507	14	74
15BJ06-118	96	59722	1.7	14.789	3.6	0.7653	3.9	0.0821	1.6	0.41	509	8	577	17	857	75	509	8	59
15BJ06-250	118	95334	1.9	16.082	2.4	0.7099	3.0	0.0828	1.8	0.61	513	9	545	13	680	51	513	9	75
15BJ06-125	162	50083	1.8	16.066	3.0	0.7191	3.4	0.0838	1.6	0.47	519	8	550	14	682	64	519	8	76
15BJ06-040	131	70295	1.4	15.841	2.5	0.7294	3.4	0.0838	2.3	0.68	519	12	556	15	713	53	519	12	73
15BJ06-139	72	42771	2.0	16.063	3.8	0.7231	4.5	0.0842	2.4	0.54	521	12	553	19	683	81	521	12	76
15BJ06-068	86	31193	1.2	15.239	2.6	0.7667	3.2	0.0847	1.8	0.57	524	9	578	14	794	55	524	9	66
15BJ06-071	42	67013	1.9	14.536	6.3	0.8218	7.0	0.0866	2.9	0.42	536	15	609	32	893	130	536	15	60
15BJ06-069	55	11947	1.8	13.509	8.0	0.8944	8.6	0.0876	3.1	0.36	542	16	649	41	1042	161	542	16	52
15BJ06-300	218	40136	0.7	9.763	2.6	3.0556	3.3	0.2164	2.0	0.61	1263	23	1422	25	1668	48	1668	48	76
15BJ06-038	961	64229	2.4	9.235	1.7	3.6215	2.7	0.2426	2.1	0.77	1400	26	1554	22	1771	32	1771	32	79

TABLE SM3.2: LA-ICPMS U-Pb ISOTOPIC DATA

						Isotope ratios					Apparent ages (Ma)								
Analysis	U	206Pb	U/Th	206Pb*	±	207Pb*	±	206Pb*	±	error	206Pb*	±	207Pb*	±	206Pb*	±	Best age	±	Conc
	(ppm)	204Pb		207Pb*	(%)	235U*	(%)	238U	(%)	corr.	238U*	(Ma)	235U	(Ma)	207Pb*	(Ma)	(Ma)	(Ma)	(%)
>5% Reverse Discordance																			
15BJ06-252	84	40335	1.4	17.718	2.6	0.6218	3.4	0.0799	2.2	0.65	496	10	491	13	470	57	496	10	106
15BJ06-308	56	18472	1.3	17.704	3.2	0.6282	4.0	0.0807	2.3	0.59	500	11	495	16	471	71	500	11	106
15BJ06-158	71	15673	1.6	17.800	3.1	0.6250	3.7	0.0807	2.0	0.53	500	9	493	14	459	70	500	9	109
15BJ06-162	77	33709	1.9	17.705	3.5	0.6320	3.9	0.0812	1.8	0.46	503	9	497	16	471	77	503	9	107
15BJ06-148	73	13500	1.9	17.794	2.3	0.6289	3.4	0.0812	2.5	0.74	503	12	495	13	460	51	503	12	109
15BJ06-244	61	25898	1.3	17.676	3.6	0.6339	4.3	0.0813	2.4	0.56	504	12	499	17	475	79	504	12	106
15BJ06-277	50	61628	1.5	17.961	3.2	0.6240	4.0	0.0813	2.4	0.59	504	11	492	16	439	72	504	11	115
15BJ06-019	57	33539	1.4	17.712	3.4	0.6338	4.2	0.0814	2.4	0.58	505	12	498	16	471	75	505	12	107
15BJ06-052	54	28509	2.3	17.652	3.0	0.6365	3.8	0.0815	2.3	0.60	505	11	500	15	478	67	505	11	106
15BJ06-280	57	26989	1.6	17.705	3.7	0.6364	4.2	0.0817	2.0	0.47	506	10	500	17	471	82	506	10	107
15BJ06-233	51	27352	1.7	17.665	3.6	0.6379	4.0	0.0817	1.9	0.47	506	9	501	16	476	79	506	9	106
15BJ06-258	109	28685	1.5	17.691	2.9	0.6377	3.9	0.0818	2.6	0.67	507	13	501	15	473	63	507	13	107
15BJ06-207	84	39013	0.9	17.984	2.4	0.6274	3.4	0.0818	2.4	0.71	507	12	494	13	437	54	507	12	116
15BJ06-163	274	27927	1.1	17.663	1.9	0.6398	2.7	0.0820	1.9	0.71	508	9	502	11	477	43	508	9	107
15BJ06-274	117	34347	1.6	17.733	2.4	0.6377	3.0	0.0820	1.9	0.63	508	9	501	12	468	52	508	9	109
15BJ06-221	36	20341	1.7	18.039	4.0	0.6274	4.7	0.0821	2.4	0.52	509	12	494	18	430	89	509	12	118
15BJ06-209	65	44772	1.4	17.687	2.7	0.6410	3.3	0.0822	1.9	0.58	509	9	503	13	474	59	509	9	108
15BJ06-008	52	20604	1.9	17.859	3.0	0.6351	4.1	0.0823	2.7	0.66	510	13	499	16	452	68	510	13	113
15BJ06-255	45	11939	1.7	17.741	3.3	0.6397	4.3	0.0823	2.7	0.63	510	13	502	17	467	73	510	13	109
15BJ06-088	60	23249	2.0	18.035	2.9	0.6296	3.6	0.0824	2.2	0.62	510	11	496	14	430	64	510	11	119
15BJ06-240	30	12590	1.4	18.002	4.0	0.6311	4.6	0.0824	2.2	0.48	510	11	497	18	434	90	510	11	118
15BJ06-146	39	26905	1.5	17.608	4.6	0.6457	5.1	0.0825	2.3	0.45	511	11	506	20	483	101	511	11	106
15BJ06-303	95	68710	1.3	17.643	2.9	0.6448	3.5	0.0825	1.9	0.55	511	9	505	14	479	64	511	9	107
15BJ06-116	85	35223	1.1	17.632	2.2	0.6458	2.9	0.0826	1.9	0.65	511	9	506	12	481	49	511	9	106
15BJ06-039	64	26846	1.7	17.672	3.9	0.6443	4.4	0.0826	2.0	0.45	512	10	505	17	475	86	512	10	108
15BJ06-176	70	215027	2.2	17.877	2.8	0.6371	3.5	0.0826	2.1	0.59	512	10	501	14	450	63	512	10	114
15BJ06-286	40	511982	1.8	17.946	3.6	0.6353	4.5	0.0827	2.6	0.58	512	13	499	18	441	81	512	13	116
15BJ06-201	138	31585	1.6	17.613	2.0	0.6476	2.7	0.0827	1.7	0.64	512	8	507	11	483	45	512	8	106
15BJ06-076	122	29197	1.4	17.686	2.4	0.6456	3.1	0.0828	2.1	0.65	513	10	506	13	474	53	513	10	108
15BJ06-313	65	52904	1.8	17.658	2.7	0.6467	3.4	0.0828	2.1	0.61	513	10	506	14	477	60	513	10	107
15BJ06-172	78	35662	1.9	17.814	2.3	0.6412	3.1	0.0828	2.1	0.66	513	10	503	12	458	52	513	10	112

TABLE SM3.2: LA-ICPMS U-Pb ISOTOPIC DATA

						Isotope ratios					Apparent ages (Ma)								
Analysis	U	206Pb	U/Th	206Pb*	±	207Pb*	±	206Pb*	±	error	206Pb*	±	207Pb*	±	206Pb*	±	Best age	±	Conc
	(ppm)	204Pb		207Pb*	(%)	235U*	(%)	238U	(%)	corr.	238U*	(Ma)	235U	(Ma)	207Pb*	(Ma)	(Ma)	(Ma)	(%)
15BJ06-214	103	36135	1.4	17.699	2.4	0.6456	3.0	0.0829	1.9	0.61	513	9	506	12	472	53	513	9	109
15BJ06-141	54	36631	1.7	17.815	3.7	0.6416	4.2	0.0829	2.1	0.50	513	10	503	17	458	81	513	10	112
15BJ06-219	55	35025	1.4	17.655	3.6	0.6477	4.3	0.0829	2.3	0.53	514	11	507	17	478	80	514	11	108
15BJ06-047	91	36516	1.1	17.570	2.5	0.6533	3.7	0.0833	2.7	0.74	516	13	511	15	488	55	516	13	106
15BJ06-165	157	84956	1.1	17.638	1.8	0.6509	3.0	0.0833	2.3	0.79	516	12	509	12	480	41	516	12	107
15BJ06-133	64	20564	1.8	17.811	2.6	0.6447	3.6	0.0833	2.5	0.70	516	13	505	14	458	58	516	13	113
15BJ06-079	32	8881	0.8	17.928	3.9	0.6409	4.8	0.0833	2.7	0.57	516	13	503	19	444	87	516	13	116
15BJ06-173	136	25282	1.6	17.636	1.6	0.6532	2.6	0.0835	2.0	0.77	517	10	510	10	480	36	517	10	108
15BJ06-309	65	39136	1.6	17.589	2.9	0.6555	3.8	0.0836	2.6	0.67	518	13	512	15	486	63	518	13	107
15BJ06-247	171	140436	1.7	17.604	2.3	0.6555	3.0	0.0837	2.0	0.65	518	10	512	12	484	51	518	10	107
15BJ06-094	64	63901	2.3	17.621	2.3	0.6552	3.1	0.0837	2.0	0.65	518	10	512	12	482	51	518	10	108
15BJ06-288	82	38733	1.6	17.758	3.1	0.6514	4.0	0.0839	2.5	0.63	519	13	509	16	465	68	519	13	112
15BJ06-070	38	15834	1.5	17.991	2.7	0.6433	4.1	0.0839	3.0	0.74	520	15	504	16	436	61	520	15	119
15BJ06-282	38	19400	2.1	17.588	4.8	0.6582	5.5	0.0840	2.7	0.48	520	13	514	22	486	106	520	13	107
15BJ06-200	75	26537	1.2	17.765	2.5	0.6530	3.2	0.0841	2.0	0.62	521	10	510	13	464	56	521	10	112
15BJ06-057	79	56052	2.0	17.679	2.5	0.6575	3.0	0.0843	1.7	0.57	522	8	513	12	475	54	522	8	110
15BJ06-304	75	20040	1.8	17.699	3.3	0.6574	4.0	0.0844	2.2	0.55	522	11	513	16	472	74	522	11	111
15BJ06-140	53	38819	1.9	17.549	2.5	0.6632	3.5	0.0844	2.4	0.69	522	12	517	14	491	56	522	12	106
15BJ06-296	49	24493	1.5	17.531	2.9	0.6659	3.5	0.0847	1.9	0.55	524	10	518	14	493	64	524	10	106
15BJ06-138	59	38203	1.6	17.932	2.9	0.6520	3.9	0.0848	2.7	0.68	525	14	510	16	443	64	525	14	118
15BJ06-009	49	14680	1.5	17.687	2.8	0.6614	3.6	0.0848	2.2	0.62	525	11	515	15	474	63	525	11	111
15BJ06-093	77	26297	1.4	17.767	3.0	0.6611	3.5	0.0852	1.9	0.54	527	10	515	14	464	66	527	10	114
15BJ06-315	216	8440759	1.8	17.505	1.9	0.6719	3.0	0.0853	2.3	0.78	528	12	522	12	496	42	528	12	106
15BJ06-030	160	122865	1.3	17.525	1.8	0.6713	2.7	0.0853	2.1	0.76	528	10	521	11	494	39	528	10	107
15BJ06-095	56	21416	1.0	17.645	2.8	0.6725	3.5	0.0861	2.1	0.60	532	11	522	14	479	62	532	11	111
15BJ06-048	88	41100	1.4	17.750	2.1	0.6721	2.7	0.0865	1.7	0.62	535	9	522	11	466	46	535	9	115
15BJ06-152	111	26487	0.9	17.445	2.3	0.6866	3.1	0.0869	2.1	0.69	537	11	531	13	504	50	537	11	107
15BJ06-178	28	22951	1.6	17.419	4.4	0.7279	5.2	0.0920	2.8	0.53	567	15	555	22	507	96	567	15	112
Contamination(?)																			
15BJ06-295	601	74913	3.2	20.730	2.6	0.0814	3.6	0.0122	2.6	0.70	78	2	79	3	111	61	78	2	NA
15BJ06-077	691	31702	1.2	21.059	2.4	0.0965	3.1	0.0147	2.0	0.65	94	2	94	3	74	57	94	2	NA

TABLE SM3.2: LA-ICPMS U-Pb ISOTOPIC DATA

						Isotope ratios					Apparent ages (Ma)								
Analysis	U	206Pb	U/Th	206Pb*	±	207Pb*	±	206Pb*	±	error	206Pb*	±	207Pb*	±	206Pb*	±	Best age	±	Conc
	(ppm)	204Pb		207Pb*	(%)	235U*	(%)	238U	(%)	corr.	238U*	(Ma)	235U	(Ma)	207Pb*	(Ma)	(Ma)	(Ma)	(%)
15BJ06-016	438	19822	1.6	21.438	2.8	0.1017	3.4	0.0158	1.9	0.57	101	2	98	3	31	67	101	2	NA
15BJ06-192	202	23558	2.2	21.215	4.2	0.1122	4.7	0.0173	2.2	0.46	110	2	108	5	56	100	110	2	NA
15BJ06-245	83	19745	3.3	19.689	3.9	0.1938	4.4	0.0277	2.1	0.48	176	4	180	7	231	90	176	4	NA
Pb loss(?)																			
15BJ06-131	706	117177	1.7	18.257	1.8	0.4272	2.7	0.0566	2.0	0.75	355	7	361	8	403	40	355	7	NA

1. Best age is chosen to be the 206Pb/238U age for analyses with 206Pb/238U age <900 Ma otherwise the 206Pb/207Pb age is preferred for analyses with 206Pb/238Uage >900 Ma.

2. Concordance is based on 206Pb/238U age / 206Pb/207Pb age. Value is not reported for 206Pb/238U ages <400 Ma because of large uncertainty in 206Pb/207Pb age and higher sensitivity to discordance.

3. All uncertainties are reported at the 1-sigma level, and include measurement errors and an additional factor based on MSWD of sets of secondary standards to account for overdispersion of standard measurements

4. Systematic errors (at 2-sigma level) include contributions from U decay constants, composition of common Pb, true age of the standard, and scatter of measured age of the standards, and are as follows: 1.0% (206Pb/238U) & 0.9% (206Pb/207Pb)

5. Common Pb correction is from measured 204Pb with common Pb composition interpreted from Stacey and Kramers (1975), and Common Pb composition assigned uncertainties of 1.5 for 206Pb/204Pb, 0.3 for 207Pb/204Pb, and 2.0 for 208Pb/204Pb.

6. U decay constants and composition as follows: 238U = 9.8485 x 10-10, 235U = 1.55125 x 10-10, 238U/235U = 137.88.

TABLE SM3.3: Hf ISOTOPIC DATA

Sample	(^{176}Yb + ^{176}Lu) / ^{176}Hf (%)	Volts Hf	^{176}Hf/^{177}Hf	± (1σ)	^{176}Lu/^{177}Hf	^{176}Hf/^{177}Hf (T)	E-Hf (0)	E-Hf (0) ± (1σ)	E-Hf (T)	Age (Ma)	± (1σ)
13WW23; Whale Mountain volcanic rock (central belt; N69.182, W140.924)											
13WW24-055	46.9	2.5	0.282638	0.000032	0.002581	0.282615	-5.2	1.1	4.8	486	32
13WW24-056	12.8	3.7	0.282709	0.000025	0.000735	0.282702	-2.7	0.9	8.1	493	10
13WW24-053	28.2	2.5	0.282622	0.000036	0.001634	0.282607	-5.8	1.3	4.9	500	17
13WW24-059	30.9	3.2	0.282685	0.000030	0.001699	0.282668	-3.6	1.1	7.2	508	26
13WW24-058	21.9	3.3	0.282779	0.000027	0.001445	0.282765	-0.2	1.0	10.7	510	24
13WW24-057	13.5	2.8	0.282628	0.000034	0.000797	0.282620	-5.6	1.2	5.6	514	8
15BJ06; Marsh Fork volcanic rocs (southern belt; N69.108, W143.894)											
15BJ06-297	14.7	3.1	0.282745	0.000029	0.000711	0.282738	-1.4	1.0	9.7	511	7
15BJ06-145	16.6	3.6	0.282721	0.000029	0.000775	0.282714	-2.2	1.0	8.9	511	8
15BJ06-257	13.4	3.7	0.282674	0.000024	0.000600	0.282668	-3.9	0.8	7.3	512	9
15BJ06-256	15.7	3.0	0.282707	0.000029	0.000681	0.282700	-2.8	1.0	8.4	513	11
15BJ06-063	20.4	1.3	0.282753	0.000047	0.001136	0.282742	-1.1	1.7	10.0	515	9

1. Hf fractionation is corrected by comparing measured 179Hf/177Hf against known 179/177 (line by line). Beta Hf is applied as a power law.

2. Yb fractionation is corrected by comparing measured 173Yb/171Yb against known 173/171 (line by line) if 171Yb intensity is more than ~1 mv. Beta Yb is applied as a power law.

a. If 171Yb intensity is less than can be measured reliably, Beta Hf is used to correct for Yb fractionation.

b. The actual cutoff used is determined from the analysis of standards during the same session

3. Data are filtered by intensity of Hf

4. Data are filtered by removing 1 max and 1 min value (out of 60).

5. Data are aflso filtered by 95% filter (rejected if outside of 2-sigma std dev of full set)

6. Uncertainties are standard error of the mean, expressed at 1-sigma